PO Box 2345, Beijing 100023, China
Fax: +86-10-85381893
E-mail: wjg@wjgnet.com www.wjgnet.com

World J Gastroenterol 2004;10(14):2003-2009
World Journal of Gastroenterology
 ISSN 1007-9327

• REVIEW •

L-arginine-induced experimental pancreatitis

Péter Hegyi, Zoltán Rakonczay Jr, Réka Sári, Csaba Góg, János Lonovics, Tamás Takács, László Czakó

Péter Hegyi, Zoltán Rakonczay Jr, Réka Sári, Csaba Góg, János Lonovics, Tamás Takács, László Czakó, First Department of Medicine, Faculty of Medicine, University of Szeged, Szeged, H6722, Hungary
Péter Hegyi, Zoltán Rakonczay Jr, School of Cell and Molecular Biosciences, Medical School, University of Newcastle, Newcastle upon Tyne, NE2 4HH, United Kingdom
Supported by The Wellcome Trust, Grant No. 022618, and by the Hungarian Scientific Research Fund, No. D42188, T43066 and T042589
Correspondence to: Péter Hegyi, M.D., Ph.D., University of Szeged, Faculty of Medicine, First Department of Medicine, PO Box 469, H-6701, Szeged, Hungary. hep@in1st.szote.u-szeged.hu
Telephone: +36-62-545-200 **Fax:** +36-62-545-185
Received: 2003-11-12 **Accepted:** 2003-12-23

Abstract

Despite medical treatment, the lethality of severe acute pancreatitis is still high (20-30%). Therefore, it is very important to find good animal models to characterise the events of this severe disease. In 1984, Mizunuma *et al*. developed a new type of experimental necrotizing pancreatitis by intraperitoneal administration of a high dose of L-arginine in rats. This non-invasive model is highly reproducible and produces selective, dose-dependent acinar cell necrosis. Not only is this a good model to study the pathomechanisms of acute necrotizing pancreatitis, but it is also excellent to observe and influence the time course changes of the disease. By writing this review we iluminate some new aspects of cell physiology and pathology of acute necrotizing pancreatitis. Unfortunately, the reviews about acute experimental pancreatitis usually did not discuss this model. Therefore, the aim of this manuscript was to summarise the observations and address some challenges for the future in L-arginine-induced pancreatitis.

Hegyi P, Rakonczay Jr Z, Sári R, Góg C, Lonovics J, Takács T, Czakó L. L-arginine-induced experimental pancreatitis. *World J Gastroenterol* 2004; 10(14): 2003-2009
http://www.wjgnet.com/1007-9327/10/2003.asp

EFFECT OF EXCESSIVE DOSES OF L-ARGININE ON DIFFERENT TISSUES

Mizinuma *et al*. were the first who studied the effect of an excessive dose of L-arginine (Arg) on different tissues in rats[1]. After a single intraperitoneal (ip.) injection of 500 mg/100 g body mass (bm) Arg, the liver cells showed slight vacuolar degeneration. The kidney contained eosinophilic compositions in some proximal convoluted tubules, but showed no degenerative changes. Adipose tissues around the pancreas showed fat necrosis. There were no changes in the weight of different organs (liver, kidney, spleen, thymus), except for the pancreas. Due to the effect of pancreatitis the weight of the pancreas nearly doubled by the end of the first 24 h. No evidence of pathophysiological lesions was observed in the lung, heart, intestine, testis, spleen and thymus[1]. After the first observation Kishino *et al*. examined the pancreas by electron microscopy[2]. They found that degeneration started with disorganization of the rough endoplasmic reticulum. The main changes in acinar cells after 24 h were partial distension of the endoplasmic reticulum. At this time large sequestered areas in the cytoplasm contained disarranged rough endoplasmic reticulum and degraded zymogen granules. Forty-eight hours after Arg-injection, dissociation and necrosis of acinar cells were noted. Subsequently, the necrotic cells were replaced by interstitial tissue composed of leucocytes and fibroblasts. The early morphological changes of the acinar cells may be related to metabolic alterations associated with the endoplasmic reticulum. The final conclusion was that an excessive dose of arginine was toxic to the rat pancreas when injected intraperitoneally[2]. Tani *et al*. continued this work by observing the effect of Arg on the pancreas[3]. They clearly proved that excessive doses of Arg could cause a severe acute necrotizing pancreatitis. On the other hand, Delaney and Weaver showed that long term administration of Arg caused pancreatic atrophy with insufficiency, therefore high doses of Arg were also suitable for the induction of chronic pancreatitis[4,5].

INDUCTION OF PANCREATITIS

Mizunuma *et al*. induced acute necrotizing pancreatitis by a high dose of Arg ip. (500 mg/100 g bm), which evoked selective pancreatic acinar cell damages without any morphological change in the Langerhans islets[1]. After this first observation, researchers investigating Arg-induced pancreatitis usually modified the method of pancreatitis induction. Tani *et al*. tried to use higher doses of Arg, but found that Arg at the dose of more than 500 mg/100 g bm killed most of the treated rats within a few hours[3]. When a single dose of 500 mg/100 g bm of Arg was injected, 70-80% of the pancreatic acinar cells were necrotized within 3 d[3]. When rats were given additional 3 injections of 250 mg/100 g bm over 10 d, there was up to 90% acinar destruction[4]. The longest treatment of Arg was performed by Weaver *et al*. Daily administration of 350 mg/100 g bm of Arg for 30 d resulted in severe pancreatic necrosis by wk 4, only isolated single acinar cells remained within a fibrous connective tissue matrix[5]. Most of the authors, who studied the pathomechanisms of this pancreatitis used 250 mg/100 g bm of Arg twice at an interval of one hour[6-8]. On the other hand, when the regenerative processes were studied after pancreatitis, a smaller dose of Arg (200 mg/100 g bm of Arg ip. twice at an interval of 1 h) was used[9,10].

All in all, the dose- and time-dependency of the effects of Arg gives an excellent opportunity to study the different phases of pancreatitis. A higher dose of Arg is suggested to study the pathomechanism of acute pancreatitis, while a smaller dose of Arg seems more suitable to characterize the regenerative processes. Long-term administration of Arg is suggested to study chronic pancreatitis (Table 1).

PATHOMECHANISM OF L-ARGININE INDUCED PANCREATITIS

The mechanism by which Arg causes pancreatitis is not fully known. Accumulating evidence suggests that oxygen free radicals[7,8,11-13], nitric oxide (NO)[14], inflammatory mediators[6,12,15,16] all have a key role in the development of the disease.

Changes in cytokine levels

We found that both serum tumor necrosis factor-α (TNF-α) and interleukin (IL)-6 level were already significantly increased

Table 1 Induction of pancreatitis: differences in methods

Dose of L-Arginine	Reference
Single dose	
500 mg/100 g bm ip.	Mizinuma *et al.* 1984, Kishino *et al.* 1984, Tani *et al.* 1990, Shields *et al.* 2000, Kihara *et al.* 2001, Tachibana *et al.* 1997, Tashiro *et al.* 2001
450 mg/100 g bm ip.	Tashiro *et al.* 2001
400 mg/100 g bm ip.	Tashiro *et al.* 2001, Rakonczay *et al.* 2002
300 mg/100 g bm ip.	Tashiro *et al.* 2001, Rakonczay *et al.* 2002
250 mg/100 g bm ip.	Pozsar *et al.* 1997
200 mg/100 g bm ip.	Tashiro *et al.* 2001
Double dose	
2×250 mg/100 g bm ip.	Takacs *et al.* 1996, Varga I. *et al.* 1997, Toma *et al.* 2000, Czako *et al.* 2000, Czako *et al.* 2000, Czako *et al.* 2000, Takacs *et al.* 2002, Toma *et al.* 2002
2×230 mg/100 g bm ip.	Takacs *et al.* 2002
2×200 mg/100 g bm ip.	Hegyi *et al.* 1997, Hegyi *et al.* 1999, Hegyi *et al.* 2000, Takacs *et al.* 2001
Multiple dose	
350 mg/100 g bm ip. daily from 1 to 4 wk	Weaver *et al.* 1994
a single 500 mg/100 g bm ip. and triple 250 mg/100 gbm ip. (d 4, 7, 10)	Delaney *et al.* 1993

Table 2 Changes of inflammatory mediator levels in Arg-induced acute pancreatitis

Mediator	Dose of Arg/100 g bm	Effect	Reference
MDA	2x250 mg	↑	Czakó *et al.*, 1998
NSG, MDA	300 mg	↑	Rakonczay *et al.*, 2003
Protein carbonyl	300 mg	↑	Rakonczay *et al.*, 2003
Mn-, Cu, Zn-SOD	2x250 mg	↓	Czakó *et al.*, 1998
Catalase	2x250 mg	↓	Czakó *et al.*, 1998
glutathione peroxidase	2x250 mg	↓ ↑	Czakó *et al.*, 1998
Serum TNF-α, IL-6	2x250 mg	↑	Czakó *et al.*, 2000
Serum TNF-α, IL-1, IL-6	2x230 mg	↑	Rakonczay *et al.*, 2002
Pancreatic IL-1β	300 and 400 mg	↑	Rakonczay *et al.*, 2003
Pancreatic TNF-α	300 and 400 mg	↑	Rakonczay *et al.*, 2003
Pancreatic cNOS	2x250 mg	↓ ↑	Takács *et al.*, 2002
Pancreatic iNOS	2x250 mg	↑	Takács *et al.*, 2002
CCK	2x250 mg	↑	Czakó *et al.*, 2000

↓: decreased activity, ↑: increased activity, Arg: L-arginine, MDA: malondialdehyde, NSG: nonprotein sulfhydryl group, SOD: superoxide dismuthase, TNF: tumor necrosis factor, IL: interleukin, CCK: cholecystokinin-octapeptide.

at 12 h after administration of 2×250 mg/100 g bm Arg, and remained elevated at 48 h in Arg-treated animals *vs* controls (Table 2)[6, 12]. Increased serum TNF-α, IL-6 and IL-1 levels were demonstrated at 24 h after the induction of pancreatitis with 2×230 mg/100 g bm Arg[15] (Table 2).

Later on, we showed that the pancreatic IL-1β level significantly decreased at 1 h after ip. administration of 300 or 400 g/100 g bm Arg[15]. The IL-1β levels increased significantly at 12 h after Arg injection, peaked at 24 h and decreased thereafter (Table 2). The pancreatic TNF-α content increased significantly at 6 h, peaked at 18 h, and then remained elevated at a relatively constant level during pancreatitis (Table 2). Pretreatment with antioxidant pyrrolidine dithiocarbamate (PDTC) or methylprednisolone (MP) significantly decreased the pancreatic levels of these proinflammatory cytokines, ameliorated pancreatic oedema and exerted a beneficial effect on pancreatic morphological damage[15]. It can be proposed that these cytokines are involved in the pathogenesis of Arg-induced acute pancreatitis.

Oxidative stress changes

In 1998, we demonstrated that the pancreatic malondialdehyde (MDA) level was significantly elevated at 24 h, and peaked at 48 h after administration of 2×250 mg/100 g bw Arg[8]. Among the endogenous scavengers Mn-superoxide dismutase (SOD) and catalase activities decreased significantly throughout the entire study *vs* the control. Cu, Zn-SOD activity decreased only at 12 h, while the glutathione peroxidase activity decreased at 6 and 12 h after Arg injection (Table 2). Pretreatment with the xanthine oxidase inhibitor allopurinol (100 and 200 mg/kg) prevented the generation of reactive oxygen metabolites and ameliorated the severity of Arg-induced pancreatitis.

We also showed that 300 mg/100 g bm Arg significantly increased the pancreatic non-protein sulfhydryl group content, malondialdehyde and the protein carbonyl levels *vs* the control (Table 2)[15]. Pretreatment with PDTC or MP significantly ameliorated these changes and reduced the severity of the disease.

These results suggest that generation of free radicals is an early and perhaps pivotal mechanism in the pathogenesis of Arg-induced acute pancreatitis.

Role of nitric oxide

NO, a highly reactive free radical, is generated from Arg by an enzymatic pathway (NO synthase: NOS) originally demonstrated in vascular endothelial cells[17]. Under physiologic conditions,

constitutive NO synthase (cNOS) results in a low level of NO, while in different inflammatory processes inducible NO synthase (iNOS) produces larger quantities of NO in various cell types. The activity of NOS is specifically inhibited by structural analogues of L-arginine such as N^G-nitro-L-arginine methyl ester (L-NAME)[17].

It was demonstrated that the cNOS activity was depleted at 6 h after onset of Arg-induced pancreatitis, it then gradually increased to a level significantly higher than that in controls and decreased thereafter at 48 h[13]. The iNOS activity was significantly increased at 24 and 48 h *vs* control (Table 2). Treatment with L-NAME significantly reduced the amylase activity, pancreatic oedema, pancreatic vascular permeability and cNOS activity in the pancreas at 24 h after the onset of pancreatitis as compared with those in the control. L-NAME treatment reduced the iNOS activity, but not significantly, and did not exert any beneficial effect on the histological score[14]. It can be concluded that both cNOS and iNOS play an important role in the development of Arg-induced acute pancreatitis in rats.

Endogenous cholecystokinin

Endogenous cholecystokinin (CCK) and CCK-A receptors have been suspected to play a role in the development of acute pancreatitis in rats[18,19]. No significant differences in plasma CCK bioactivity were found between the pancreatitic animals and the control group during the course of Arg-induced pancreatitis (Table 2). KSG-054, a CCK receptor antagonist did not exert any beneficial effect on the laboratory and morphologic changes observed in Arg-induced pancreatitis[12]. These results suggest that endogenous CCK is not involved in the pathogenesis of Arg-induced pancreatitis.

Effect of nuclear factor-kappa B activation

Recent studies have established the critical role played by inflammatory mediators in acute pancreatitis[14,20]. One of the most important transcription factors that control proinflammatory gene expression is nuclear factor kappa B (NF-κB)[21]. Therefore, we set out to investigate NF-κB activation and proinflammatory cytokine synthesis in the pancreas during Arg-induced acute pancreatitis in rats[15]. The dose-response (300 or 400 mg/ 100 g bm) and time-effect (0.5-96 h) curves related to the action of Arg on the pancreatic NF-κB activation and IL-1β, TNF-α, heat shock the protein (HSP) 60 and HSP72 synthesis were evaluated. Also we wanted to establish whether PDTC or MP pretreatment could block the activation of pancreatic NF-κB and their effects on the severity of Arg-induced acute pancreatitis. Our results showed that pancreatic NF-κB and proinflammatory cytokine expressions were activated dose-dependently during Arg-induced acute pancreatitis in rats, although at a later stage as compared with other models. We have established that PDTC and MP pretreatment specifically and dose-dependently can block this NF-κB activation in the pancreas. Furthermore, the inhibition of NF-κB activation and proinflammatory cytokine synthesis has been found to be clearly associated with a protective effect against pancreatic damage[15].

Apoptosis and gene expression of pancreatitis-associated protein

Pancreatitis-associated protein (PAP) is an acute phase secretory protein known to be overexpressed in acute pancreatitis[22]. Motoo *et al.* examined the effects of arginine (1.25, 2.5, 5 or 10 mg/mL) on cellular morphology, PAP expression and apoptosis in rat pancreatic acinar AR4-2J cells[23]. This *in vitro* experimental design allowed the study of acinar cells without the confounding effects of other cell types involved in acute pancreatitis (e.g. inflammatory cells). The growth of AR4-2J cells was inhibited by Arg in a dose-dependent manner. This inhibition was due to Arg-induced apoptosis of cells which was shown by fluorescence staining, and DNA fragmentation assay. The DNA fragmentation was most prominent at 24 h when the PAP mRNA level was low, whereas it was not seen when the level was high. The expression of PAP mRNA was detected at 2 h and peaked at 6 h, it was highest at a dose of 2.5 mg/mL Arg. Motoo *et al.* speculated that PAP might inhibit the induction of apoptosis[23].

Role of transforming growth factor beta 1

Mild acute pancreatitis is often followed by full recovery of pancreatic tissue structure and function once the primary cause is eliminated[24]. Transforming growth factor beta (TGF-β) and the extracellular matrix are believed to play an important part in this process[20]. TGF-β promotes regeneration in wounded tissues by attracting monocytes and leukocytes and inducing angiogenesis and fibroblast recruitment. Kihara *et al.* induced acute necrotizing pancreatitis by intraperitoneal injection of 500 mg/ 100 g bm Arg, and examined the expression of TGF-β1, extracellular matrix proteins and metalloproteinases (degradeing a variety of extracellular matrix components). TGF-β, protocollagen types I, III, IV, and fibronectin mRNA expression reached a peak value on d 2.5-3 and gradually decreased thereafter to reach control levels on d 7. Matrix metalloproteinase-2 mRNA levels peaked on d 5, whereas the immunoreactivity was maximal on d 7. TGF-β immunoreactivity was detected in disrupted acinar cells on d 3 and 5. Immunoreactivity for fibronectin was detected around disrupted acinar cells and interstitial spaces on d 3 and maximally on d 5. The authors believe that the results suggest an important role of TGF-β in extracellular matrix production during the early phase of acute pancreatitis[20].

Effect of endotoxaemia in Arg-induced pancreatitis

Systemic endotoxaemia is a common feature of severe acute pancreatitis[25]. The effect of *E. coli* endotoxin was investigated by Pozsár *et al.* on the mortality rates and pancreatic histology of Arg-induced (250 mg/ 100 g bm) acute pancreatitis in rats[26]. The mortality rates of rats treated with 5 and 10 mg/kg endotoxin were 10 % and 30%, respectively (no death was observed in the group with only Arg-induced pancreatitis). The extent of acinar cell necrosis, hemorrhage, oedema and leukocyte infiltration was significantly greater in the endotoxin-treated groups *vs* the control groups. The authors speculated that systemic endotoxemia might exert its effect by stimulating pro-inflammatory cytokine synthesis in granulocytes. The animal experiments were closely related to similar observations made in humans. It was found that high serum endotoxin levels showed a positive correlation with disease severity[26].

Expression of nerve growth factor

Nerve growth factor (NGF) is a known mediator of the inflammatory response[27]. It is believed to play an important role in the pathogenesis of pain. NGF expression was investigated after injection of 250 mg/100 g bm Arg twice intraperitoneally[28]. No significant differences in NGF mRNA levels were found between the Arg-injected and control rats before 3 d. However, NGF mRNA levels significantly increased On days 3 (10-18 fold) and 5 (3.2-6 fold). NGF protein levels were 2-fold higher than control levels on day 3, but this did not reach statistical significance. On d 5 there was a 4-fold increase in NGF protein levels. The cellular sites of increased NGF production were investigated by immunohistochemistry. In control rats NGF-immunoreactivity was localized to the islets of Langerhans. In Arg-induced pancreatitis, NGF was detected in the cytoplasm of exocrine pancreatic tissues, including acinar

and ductal cells at 2 and 6 h. On d of NGF was predominantely found in ductal cells. It was possible that this change in staining pattern represented a release of stored NGF from the islets to the parenchyma[28].

Effect of Arg-induced pancreatitis on the cytoskeleton

Disruption of the cytoskeleton seems to be a common prominent early feature in acute pancreatitis. Actin cytoskeleton was investigated using rhodamin phalloidin and epifluorescence microscopy combined with Normanski images[29]. In control tissue actin was primarily localised as an intense fluorescent band beneath the luminal membrane. Arg administration (200-500 mg/100 g bm) resulted in changes of the actin cytoskeleton, including reduced actin staning underneath the luminal and basolateral membranes and increased cytoplasmic staining in pancreatic acinar cells. Interestingly, the total actin content of cells was increased twofold at 24 h. The intermediate filaments were investigated by confocal microscopy. A single large dose arginine also induced the disruption of intermediate cytokeratin filaments, which were replaced by a few focal deposits or small aggregates. Sub-basolateral staining appeared with a lower intensity whereas cytoplasmic staining was not presenty[29].

Role of heat shock proteins

Heat shock proteins (HSPs) are highly conserved cytoprotective proteins that are present in all species and have essential functions in protein folding, transport, translocation, assembly and degradation. HSP families have been categorized by their molecular mass. HSPs can be induced by a wide variety of conditions. Interestingly, cerulein pancreatitis has been reported to increase[30-32] or decrease[33-35] the synthesis of pancreatic HSP60 and HSP72. Arg-induced pancreatitis was accompanied with large increases in HSP27 and HSP70 levels, peaking at 24 h and localized to acinar cells[36]. Moreover, HSP27 shifted to the phosphorylated forms during pancreatitis. There were smaller increases in HSP60 and HSP90, and no effect on GRP78. Interestingly, a lower dose of Arg induced less pancreatitis, but larger increases in HSP27 and HSP70 expression and phosphorylation of HSP27. The results of Tashiro *et al.* are in accordance with our findings[36]. The smaller increases in the quantity of HSPs following 400 mg/100 g bm Arg were probably due to tissue necrosis, protein degradation and decreased gene activation. We believe that the increased levels of HSPs most probably act to limit the severity of the disease. In a recent study, Tashiro *et al.* have shown that hyperthermia and possibly HSPs confer significant protection against Arg-induced (400 mg/100 g bm) pancreatitis[36]. More specifically, the degradation and disorganization of the actin cytoskeleton were prevented. These previous findings are in contrast with ours[16]. We could only demonstrate decreases in the serum proinflammatory cytokine (TNF-α, IL-1, IL-6) levels after hot-water (and also cold-water) immersion pretreatment of rats with Arg-induced pancreatitis (2×250 mg/100 g bm), but the biochemical and morphological parameters of the pancreas were not significantly different. The explanation of the discrepancies between the results of the two studies may lie in the different types of pretreatment and the differences in the dose of Arg and the strains of rats used.

Role of vacuole membrane protein 1

In vitro expression of vacuole membrane protein 1 (VMP1) promoted formation of cytoplasmic vacuoles which was followed by cell death[37]. In order to test if VMP1 expression was related to the cytoplasmic vacuolization of acinar cells during acute pancreatitis, Vaccaro *et al.* studied the *in vivo* expression of the VMP1 gene during Arg-induced (500 mg/100 g) acute pancreatitis[38]. Northern blot analysis showed that the maximal induction of VMP1 after 24 h remained high after 48 h of arginine administration. Significant increases in the number of apoptotic cells were found during those periods. Twenty-four and 48 h after arginine administration, light micrographs from thin plastic toluidine blue sections revealed numerous vacuoles in the cytoplasm of acinar cells. *In situ* hybridization studies showed a high expression of VMP1 in acinar cells with cytoplasmic vacuolization. VMP1 mRNA highly and significantly correlated with vacuole formation. The results suggest that VMP1 expression might be involved in the cytoplasmic vacuolization of acinar cells during the early stage of acute pancreatitis[38].

EXTRAPANCREATIC MANIFESTATIONS OF L-ARGININE INDUCED PANCREATITIS

Whereas the mortality of interstitial pancreatitis was close to zero, patients with necrotizing pancreatitis had a considerable mortality. The extrapancreatic manifestations, such as circulatory, pulmonary, renal and hepatic failure (multi-organ failure) contributed significantly to the morbidity and mortality of this disease[39-41]. This model seems to be an appropriate tool to study the extrapancreatic organ damage and its pathomechanisms.

We found that oxidative stress developed not only in the pancreas but also in remote organs during acute pancreatitis induced by 2×250 mg/100 g bm Arg[11]. The MDA concentration was significantly increased at 6 h after Arg treatment in the liver and at 24 h in the kidney. Among the endogenous scavengers, Mn-, and Cu, Zn-SOD and glutathione peroxidase were significantly reduced both in the liver and in the kidney during the course of Arg-induced pancreatitis. The catalase activity was significantly increased in the liver, whereas it was significantly decreased in the kidney. The prophylactic application of 200 mg/kg allopurinol significantly restrained the generation of free radicals in the liver. Histologic examination revealed vacuolar degeneration within hepatic cells and eosinophilic components in proximal convoluted tubules in the kidney.

Hypertonic saline (HTS) could restore the circulating volume in haemorrhagic shock by improving cardiac contractility and peripheral tissue perfusion[42]. The aim of Shields[43,44] was to investigate the effect of HTS resuscitation on the development of end-organ damage in Arg-induced pancreatitis. They demonstrated increased pulmonary endothelial permeability and increased myeloperoxidase activity at 72 h after pancreatitis induction by a single 500 mg/100 g bm Arg injection. Histological examination of the lung revealed marked interstitial congestion and hemorrhage. HTS injections (75 g/L NaCl, 2 mL/kg) were applied at 24 and 48 h after the administration of Arg. Pulmonary oedema, endothelial leak, enhanced neutrophil activity were all attenuated and the pancreatic and pulmonary histological scores were improved in animals treated with HTS.

REGENERATIVE PROCESS AFTER L-ARGININE-INDUCED PANCREATITIS

Time course changes

In the early phase of acute pancreatitis evoked by 200 mg/100 g bm Arg (d 1-3), the laboratory signs of acute pancreatic inflammation predominated in the Arg-treated rats[9]. Pancreatitis revealed an intercellular edema with the infiltration of leukocytes, dilatation of the capillaries, and microfocal necroses in the parenchyma on d 1 after pancreatitis induction. Interestingly, acinar cells surrounding the Langerhans islets remained intact (Figure 1). Following the early acinar cell necrosis, histological examinations revealed a marked adipose tissue deposition at the end of the first week. Accumulation of adipose tissue was a sign of atrophy. The rest of the pancreas (not involved in Arg-induced cell

destruction) could be the site of pancreatic hypertrophy and hyperplasia. The pancreatic content of enzymes (amylase, trypsinogen and lipase) was decreased by d 7 as a sign of pancreatic acinar cell damage. After the first week regenerative processes dominated. Furthermore, by the end of the fourth week the pancreatic content of enzymes was significantly elevated[9].

The mortality of this type of pancreatitis was 2.5%. The rats died between days 1-5 after pancreatitis induction. No mortality was found in the control group.

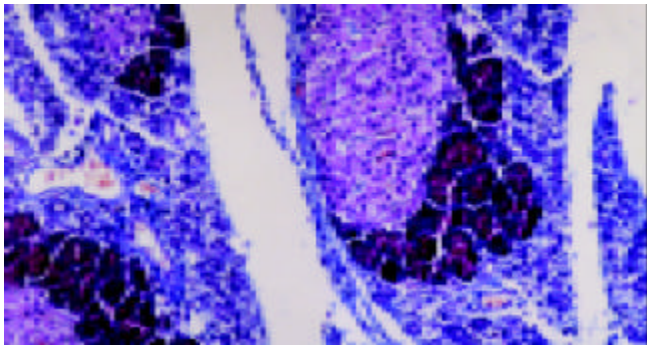

Figure 1 Histologic alterations in the pancreas following Arg-induced pancreatitis on d 3. The signs of acute inflammation and tubular complexes are visible. Segmental fibroses with blue stained fibroblast are observed. Intact pancreatic acinar cells are presented mainly around the Langerhans islets (Chrossmonn's trichrome staining ×100).

Effect of exogenous CCK on the regenerative process

In the early phase of pancreatitis, administration of low doses of CCK-8 further deteriorated the laboratory and histologic parameters of acute pancreatitis[9]. The mortality rate (15%) also demonstrated the harmful effect of CCK-8 in the early phase of this pancreatitis. Histologic sections demonstrated a more intense mitotic activity due to the effect of CCK-8 on d 7. Moreover, histologic examination revealed that the bulk of hypertrophized pancreatic acinar cells were found surrounding the enlarged Langerhans islets following CCK-8 administration. It appears that the closeness of the Langerhans islets protects acinar cells and accelerates the regenerative process during Arg-evoked pancreatic tissue damage. The reason for this might be the complex interaction of acinar and islet cells. The laboratory changes (such as pancreatic DNA and enzymes content) also proved the positive effect of CCK-8 during the recovery phase[9].

Secretory changes

Experimental studies have revealed that, suggesting that pancreatic enzyme secretion is reduced after the induction of acute pancreatitis[45-47]. We characterized the secretory changes in Arg-induced pancreatitis on d 1, 3, 7 and 14 following pancreatitis induction, when the rats were surgically prepared with pancreatic duct and femoral vein cannulae under urethane anesthesia[48].

In pancreatitic rats, both the basal and the maximal pancreatic volumes were significantly increased *vs* controls on d 1 following the induction of pancreatitis. The basal output was still significantly higher *vs* controls on d 3 and 7, but the maximal output was significantly decreased *vs* the controls on d 7. No change in basal pancreatic fluid secretion was observed in pancreatitic rats, but the maximal output was significantly decreased on d 14. These results proved that there was a conversion from the acute inflammatory phase to the late regenerative phase on d 7. As far as the pancreatic protein secretion was concerned, in pancreatitis-group the basal secretory protein level was significantly diminished throughout the experiment. The maximal pancreatic protein secretion was significantly decreased in a progressive manner on d 3, 7 and 14. In the pancreatitic rats, both the basal and the maximal pancreatic amylase secretion were significantly increased on d 1. The maximal output was significantly decreased only on d 14. Taken together, the pancreatic secretion in the early phase of Arg-induced pancreatitis is characterized by increases in the secretory volume and amylase level, with a simultaneous decrease in protein output. A progressive decrease in pancreatic secretory capacity was then detected confirming the acinar cell damage.

Effect of diabetes on Arg-induced pancreatitis

The interesting finding that periinsular acini remained intact during Arg-induced-pancreatitis prompted us to continue studies on the effects of diabetes in the process of pancreatic remodeling[9]. An insulo-acinar correlation was also indicated by the morphological evidence. Acinar cells around the islets could be distinguished from teleinsular acini by their staining characteristics. These periinsular cells were larger, contained larger nuclei and nucleoli, and had more abundant zymogen granules[49,50]. To achieve our aims, we used streptozotocin (STZ) to evoke diabetes[51]. STZ was specifically toxic to the β-cells of the islets of Langerhans, which was irreversible and dose-dependent[52]. When pancreatitis was induced in diabetic rats, the periinsular acini did not remain intact during Arg-induced-pancreatitis. We also found that in diabetic rats, the pancreatic regenerative processes (mitotic activity of acinar cells) in response to low doses of CCK-8 were markedly diminished. The lack of regenerative effect of CCK-8 may be due to the low insulin level. Furthermore, histological sections indicated no difference between the peri- and teleinsular acinar cell damage in diabetic rats. This is a morphological confirmation of the pivotal role of insulin in the regulation of the exocrine pancreatic structure. However, other islet cell hormones might also be involved in this process.

When Arg-induced pancreatitis was evoked in STZ-diabetic rats, the significant elevation in serum amylase level was not so obvious as that observed in pancreatitic rats. The explanation of this phenomenon is that a diabetic state (in rats without pancreatitis) appeared to shift the normal pancreatic enzyme content (decreased amylase and increased trypsinogen). These data are in accordance with those of Sofrankova *et al*., who demonstrated a similar pancreatic enzyme pattern in a secretory study[53].

Early increases were observed in the basal pancreatic fluid and amylase secretion in Arg-STZ-treated rats. However, no CCK-8-stimulated fluid secretory peak following pancreatitis induction was detected in diabetic animals, in contrast with the situation in non-diabetic rats, suggesting that diabetes could moderate the CCK-8-stimulated secretory changes in both the early and late phases of Arg-induced pancreatitis.

In order to clearly prove the effect of β-cells during the process of pancreatitis, we replaced the endogenous insulin with mixed exogenous insulin (2 IU s.c. twice daily, 30% short-acting and 70% intermediate-duration insulin), and found that simultaneous administration of exogenous insulin replaced the hypertrophic effect of low-doses of CCK-8[54].

Late recovery in normal and diabetic rats

Six months after Arg-induced pancreatitis without diabetes, a major restitution of the pancreatic enzyme content was found[55]. The lipase and trypsinogen contents of the pancreas were recovered, but amylase was significantly decreased *vs* the controls. In spite of this large-scale restitution of the pancreatic enzyme compositions, marked histologic alterations, periductal fibroses, adipose tissue and tubular complexes, were detected 6 mo following pancreatitis induction. No mitotic activity and centroacinar hyperplasia were observed at this time. When

pancreatitis was induced in STZ-diabetic rats, a very considerable recovery of the enzyme content was noted 6 mo following pancreatitis induction. Even at this time, however, the amylase content remained significantly decreased. This may be due to the combined effect of STZ-evoked decrease on amylase biosynthesis and the toxic damage caused by Arg to pancreatic acinar cells[56]. So far as the pancreatic histologic structure was concerned, the morphologic changes were similar to those seen in Arg-induced pancreatitic non-diabetic rats.

Effect of fibroblast growth factor-7 and fibroblast growth factor-10, and role of keratinocyte growth factor receptor

Keratinocyte growth factor (KGF) is a member of the rapidly growing fibroblast growth factor (FGF) family of mitogens[57]. FGF-7 and FGF-10 show high structural homology and similar biological characteristics. Both are mainly synthesized by mesenchymal cells and stimulate epithelial cells via KGF receptor (KGFR) which is a splice variant of FGF receptor-2[58].

In normal pancreas, FGF-7 is localized in alpha islet cells, but FGF-10 is not detected. KGFR is also localized in islet cells, ductal cells, and centroacinar cells in the normal pancreas. In the pancreatic tissues of rats with Arg-induced pancreatitis, FGF-7 was localized in alpha cells, whereas FGF-10 was expressed in vascular smooth muscle cells (VSMCs). KGFR was not expressed in centroacinar cells after Arg treatment. These findings suggest that FGF-7 and FGF-10 contribute to the regeneration and differentiation of acinar cells and angiogenesis in acute pancreatitis through KGFR[58].

Expression of lumican proteins

Lumican is a member of a small leucine-rich proteoglycan family[59]. It has been reported that lumican mRNA and its protein were ectopically and highly expressed in acinar cells in chronic pancreatitis (CP)-like lesions close to pancreatic cancer cells[60]. CP-like lesions are characterized by acinar and ductal-ductular cell proliferation with expanding fibrosis. Immunohistochemically, the lumican proteins are localized in ductules and a few centroacinar cells in normal pancreas.

After administration of an excessive dose of Arg, an immature fibrosis with fragmented and loose collagen fibers was observed on d 4 after pancreatitis induction. Moreover, lumican immunoreactivity was also detected in the collagen fibers on d 4. Lumican mRNA was barely detected in islet cells in the normal pancreas, but it was strongly expressed in acinar and islet cells on d 1 following the induction of pancreatitis. Lumican mRNA was expressed in many proliferating fibroblasts on d 4. These findings indicate that lumican is transiently synthesized by acinar cells and fibroblasts during Arg-induced acute pancreatitis. Lumican proteins may contribute to immature and transient fibrosis of acute pancreatitis.

CONCLUSIONS AND PERSPECTIVES

We are just starting to understand the pathophysiology of acute necrotizing pancreatitis. By this review we tried to illuminate new aspects of cell physiology and pathology of acute necrotizing pancreatitis. Firstly, we explored the effects of high doses of Arg on different tissues. Then, we concentrated on the pancreas showing that Arg could cause a necrotizing acute pancreatitis. Finally we characterized the early and late phases of this model of acute experimental pancreatitis.

We beleive that this review confirms the value of Arg-induced pancreatitis. In the past plenty of excellent observations were published on this necrotizing pancreatitis model. Many questions were answered concerning acute necrotizing pancreatitis using high doses of Arg. On the other hand, authors usually left the endocrine status of the pancreas unexamined. Using this model, we could highlight the importance of the insulo-acinar axis.

Despite our current knowledge, many hypotheses and questions remain unanswered concerning the effects of Arg. Therefore, it seems to be well worthwhile to continue to explore the pathomechanism of Arg-induced pancreatitis.

REFERENCES

1 **Mizunuma T**, Kawamura S, Kishino Y. Effects of injecting excess arginine on rat pancreas. *J Nutr* 1984; **114**: 467-471
2 **Kishino Y**, Kawamura S. Pancreatic damage induced by injecting a large dose of arginine. *Virchows Arch B Cell Pathol Incl Mol Pathol* 1984; **47**: 147-155
3 **Tani S**, Itoh H, Okabayashi Y, Nakamura T, Fujii M, Fujisawa T, Koide M, Otsuki M. New model of acute necrotizing pancreatitis induced by excessive doses of arginine in rats. *Dig Dis Sci* 1990; **35**: 367-374
4 **Delaney CP**, McGeeney KF, Dervan P, Fitzpatrick JM. Pancreatic atrophy: a new model using serial intra-peritoneal injections of L-arginine. *Scand J Gastroenterol* 1993; **28**: 1086-1090
5 **Weaver C**, Bishop AE, Polak JM. Pancreatic changes elicited by chronic administration of excess L-arginine. *Exp Mol Pathol* 1994; **60**: 71-87
6 **Takacs T**, Czako L, Jarmay K, Farkas G Jr, Mandi Y, Lonovics J. Cytokine level changes in L-arginine-induced acute pancreatitis in rat. *Acta Physiol Hung* 1996; **84**: 147-156
7 **Varga IS**, Matkovics B, Hai DQ, Kotorman M, Takacs T, Sasvari M. Lipid peroxidation and antioxidant system changes in acute L-arginine pancreatitis in rats. *Acta Physiol Hung* 1997; **85**: 129-138
8 **Czako L**, Takacs T, Varga IS, Tiszlavicz L, Hai DQ, Hegyi P, Matkovics B, Lonovics J. Involvement of oxygen-derived free radicals in L-arginine-induced acute pancreatitis. *Dig Dis Sci* 1998; **43**: 1770-1777
9 **Hegyi P**, Takacs T, Jarmay K, Nagy I, Czako L, Lonovics J. Spontaneous and cholecystokinin-octapeptide-promoted regeneration of the pancreas following L-arginine-induced pancreatitis in rat. *Int J Pancreatol* 1997; **22**: 193-200
10 **Takacs T**, Hegyi P, Jarmay K, Czako L, Gog C, Rakonczay Z Jr, Nemeth J, Lonovics J. Cholecystokinin fails to promote pancreatic regeneration in diabetic rats following the induction of experimental pancreatitis. *Pharmacol Res* 2001; **44**: 363-372
11 **Czako L**, Takacs T, Varga IS, Tiszlavicz L, Hai DQ, Hegyi P, Matkovics B, Lonovics J. Oxidative stress in distant organs and the effects of allopurinol during experimental acute pancreatitis. *Int J Pancreatol* 2000; **27**: 209-216
12 **Czako L**, Takacs T, Varga IS, Hai DQ, Tiszlavicz L, Hegyi P, Mandi Y, Matkovics B, Lonovics J. The pathogenesis of L-arginine-induced acute necrotizing pancreatitis: inflammatory mediators and endogenous cholecystokinin. *J Physiol Paris* 2000; **94**: 43-50
13 **Varga IS**, Matkovics B, Czako L, Hai DQ, Kotorman M, Takacs T, Sasvari M. Oxidative stress changes in L-arginine-induced pancreatitis in rats. *Pancreas* 1997; **14**: 355-359
14 **Takacs T**, Czako L, Morschl E, Laszlo F, Tiszlavicz L, Rakonczay Z Jr, Lonovics J. The role of nitric oxide in edema formation in L-arginine-induced acute pancreatitis. *Pancreas* 2002; **25**: 277-282
15 **Rakonczay Z**, Jarmay K, Kaszaki J, Mandi Y, Duda E, Hegyi P, Boros I, Lonovics J, Takacs T. NF-kappaB activation is detrimental in arginine-induced acute pancreatitis. *Free Radic Biol Med* 2003; **34**: 696-709
16 **Takacs T**, Rakonczay Z Jr, Varga IS, Ivanyi B, Mandi Y, Boros I, Lonovics J. Comparative effects of water immersion pretreatment on three different acute pancreatitis models in rats. *Biochem Cell Biol* 2002; **80**: 241-251
17 **Gross SS**, Wolin MS. Nitric oxide: pathophysiological mechanisms. *Annu Rev Physiol* 1995; **57**: 737-769
18 **Beglinger C**. Potential role of cholecystokinin in the development of acute pancreatitis. *Digestion* 1999; **60**(Suppl 1): 61-63
19 **Tachibana I**, Shirohara H, Czako L, Akiyama T, Nakano S, Watanabe N, Hirohata Y, Otsuki M. Role of endogenous cholecystokinin and cholecystokinin-A receptors in the development of acute pancreatitis in rats. *Pancreas* 1997; **14**: 113-121
20 **Kihara Y**, Tashiro M, Nakamura H, Yamaguchi T, Yoshikawa H, Otsuki M. Role of TGF-beta1, extracellular matrix, and matrix metalloproteinase in the healing process of the pancreas after

induction of acute necrotizing pancreatitis using arginine in rats. *Pancreas* 2001; **23**: 288-295
21 **Abraham E**. NF-kappaB activation. *Crit Care Med* 2000; **28** (4 Suppl): N100-N104
22 **Dusetti NJ**, Frigerio JM, Fox MF, Swallow DM, Dagorn JC, Iovanna JL. Molecular cloning, genomic organization, and chromosomal localization of the human pancreatitis-associated protein (PAP) gene. *Genomics* 1994; **19**: 108-114
23 **Motoo Y**, Taga K, Su SB, Xie MJ, Sawabu N. Arginine induces apoptosis and gene expression of pancreatitis-associated protein (PAP) in rat pancreatic acinar AR4-2J cells. *Pancreas* 2000; **20**: 61-66
24 **Takacs T**, Czako L, Jarmay K, Hegyi P, Pozsar J, Marosi E, Pap A, Lonovics J. Time-course changes in pancreatic laboratory and morphologic parameters in two different acute pancreatitis models in rats. *Acta Med Hung* 1994; **50**: 117-130
25 **Kivilaakso E**, Valtonen VV, Malkamaki M, Palmu A, Schroder T, Nikki P, Makela PH, Lempinen M. Endotoxaemia and acute pancreatitis: correlation between the severity of the disease and the anti-enterobacterial common antigen antibody titre. *Gut* 1984; **25**: 1065-1070
26 **Pozsar J**, Schwab R, Simon K, Fekete L, Orgovan G, Pap A. Effect of endotoxin administration on the severity of acute pancreatitis in two experimental models. *Int J Pancreatol* 1997; **22**: 31-37
27 **Dray A**. Inflammatory mediators of pain. *Br J Anaesth* 1995; **75**: 125-131
28 **Toma H**, Winston J, Micci MA, Shenoy M, Pasricha PJ. Nerve growth factor expression is up-regulated in the rat model of L-arginine-induced acute pancreatitis. *Gastroenterology* 2000; **119**: 1373-1381
29 **Tashiro M**, Schafer C, Yao H, Ernst SA, Williams JA. Arginine induced acute pancreatitis alters the actin cytoskeleton and increases heat shock protein expression in rat pancreatic acinar cells. *Gut* 2001; **49**: 241-250
30 **Bhagat L**, Singh VP, Song AM, van Acker GJ, Agrawal S, Steer ML, Saluja AK. Thermal stress-induced HSP70 mediates protection against intrapancreatic trypsinogen activation and acute pancreatitis in rats. *Gastroenterology* 2002; **122**: 156-165
31 **Ethridge RT**, Ehlers RA, Hellmich MR, Rajaraman S, Evers BM. Acute pancreatitis results in induction of heat shock proteins 70 and 27 and heat shock factor-1. *Pancreas* 2000; **21**: 248-256
32 **Weber CK**, Gress T, Muller-Pillasch F, Lerch MM, Weidenbach H, Adler G. Supramaximal secretagogue stimulation enhances heat shock protein expression in the rat pancreas. *Pancreas* 1995; **10**: 360-367
33 **Rakonczay Z Jr**, Ivanyi B, Varga I, Boros I, Jednakovits A, Nemeth I, Lonovics J, Takacs T. Nontoxic heat shock protein coinducer BRX-220 protects against acute pancreatitis in rats. *Free Radic Biol Med* 2002; **32**: 1283-1292
34 **Strowski MZ**, Sparmann G, Weber H, Fiedler F, Printz H, Jonas L, Goke B, Wagner AC. Caerulein pancreatitis increases mRNA but reduces protein levels of rat pancreatic heat shock proteins. *Am J Physiol* 1997; **273**(4 Pt 1): G937-G945
35 **Weber H**, Wagner AC, Jonas L, Merkord J, Hofken T, Nizze H, Leitzmann P, Goke B, Schuff-Werner P. Heat shock response is associated with protection against acute interstitial pancreatitis in rats. *Dig Dis Sci* 2000; **45**: 2252-2264
36 **Tashiro M**, Ernst SA, Edwards J, Williams JA. Hyperthermia induces multiple pancreatic heat shock proteins and protects against subsequent arginine-induced acute pancreatitis in rats. *Digestion* 2002; **65**: 118-126
37 **Dusetti NJ**, Jiang Y, Vaccaro MI, Tomasini R, Azizi Samir A, Calvo EL, Ropolo A, Fiedler F, Mallo GV, Dagorn JC, Iovanna JL. Cloning and expression of the rat vacuole membrane protein 1 (VMP1), a new gene activated in pancreas with acute pancreatitis, which promotes vacuole formation. *Biochem Biophys Res Commun* 2002; **290**: 641-649
38 **Vaccaro MI**, Grasso D, Ropolo A, Iovanna JL, Cerquetti MC. VMP1 expression correlates with acinar cell cytoplasmic vacuolization in arginine-induced acute pancreatitis. *Pancreatology* 2003; **3**: 69-74
39 **Steinberg W**, Tenner S. Acute pancreatitis. *N Eng J Med* 1994; **330**: 1198-1220
40 **Renner IG**, Savage WT, Pantoga JL, Renner VJ. Death due to acute pancreatitis. A retrospective analysis of 405 autopsy cases. *Dig Dis Sci* 1985; **10**: 1005-1008
41 **Karomgani I**, Porter KA, Langevin RE, Banks PA. Prognostic factors in sterile pancreatic necrosis. *Gastroenterology* 1992; **103**: 1636-1640
42 **Kramer GC**, Perron PR, Lindsey DC, Ho HS, Gunther RA, Boyle WA, Holcroft JW. Small-volume resuscitation with hypertonic saline dextran solution. *Surgery* 1986; **100**: 239-247
43 **Shields CJ**, Sookhai S, Winter DC, Dowdall JF, Kingston G, Parfrey N, Wang JH, Kirwan WO, Redmond HP. Attenuation of pancreatitis-induced pulmonary injury by aerosolized hypertonic saline. *Surg Infect* 2001; **2**: 215-224
44 **Shields CJ**, Winter DC, Sookhai S, Ryan L, Kirwan WO, Redmond HP. Hypertonic saline attenuates end-organ damage in an experimental model of acute pancreatitis. *Br J Surg* 2000; **87**: 1336-1340
45 **Saluja A**, Saito I, Saluja M, Houlihan MJ, Powers RE, Meldolesi J, Steer ML. *In vivo* rat pancreatic acinar cell function during supramaximal stimulation with cerulein. *Am J Physiol* 1985; **249**: G702-G710
46 **Manso MA**, San Roman JI, Dios I, Garcia LJ, Lopez MA. Cerulein-induced acute pancreatitis in the rat. Study of pancreatic secretion and plasma VIP and secretin levels. *Dig Dis Sci* 1992; **37**: 364-368
47 **Niederau C**, Niederau M, Luthen R, Strohmeyer G, Ferrell LD, Grendel JH. Pancreatic exocrine secretion in acute experimental pancreatitis. *Gastroenterology* 1990; **99**: 1120-1127
48 **Hegyi P**, Czako L, Takacs T, Szilvassy Z, Lonovics J. Pancreatic secretory responses in L-arginine-induced pancreatitis: comparison of diabetic and nondiabetic rats. *Pancreas* 1999; **19**: 167-174
49 **Hellman B**, Wallgren A, Petersson B. Cytological characteristics of the exocrine pancreatic cells with regard to their position in relation to the islets of Langerhans. *Acta endocrinol* 1962; **93**: 465-473
50 **Kramer MF**, Tan HT. The peri-insular acini of the pancreas of the rat. *Z Zellforsch* 1968; **86**: 163-170
51 **Rakieten N**, Rakieten LM, Nadkarni MV. Studies on the diabetogenic action of streptozotocin. *Cancer Chemother* 1963; **29**: 91
52 **Junod A,** Lambert AE, Orci L, Pictet R, Gonet AE, Renold AE. Studies on the diabetogenic action of streptozotocin. *Proc Soc Exp Biol Med* 1967; **126**: 201
53 **Sofrankova A**, Dockray GJ. Cholecystokinin- and secretin-induced pancreatic secretion in normal and diabetic rats. *Am J Physiol* 1983; **244**: G370-G374
54 **Hegyi P**, Rakonczay Z Jr, Sari R, Farkas N, Góg C, Nemeth J, Lonovics J, Takacs T. Insulin is necessary for the hypertrophic effect of CCK-8 following acute necrotizing experimental pancreatitis. *World J Gastroenterol* 2004; in press
55 **Hegyi P**, Takacs T, Tiszlavicz L, Czako L, Lonovics J. Recovery of exocrine pancreas six months following pancreatitis induction with L-arginine in streptozotocin-diabetic rats. *J Physiol Paris* 2000; **94**: 51-55
56 **Williams JA**, Goldfine ID. The insulin-acinar relationship. In: The Exocrine Pancreas: Biology, Pathobiology and Diseases. Edited by Go VLW *et al*. *Raven Press, New York* 1993; pp: 789-802
57 **Werner S**. Keratinocyte growth factor: a unique player in epithelial repair processes. *Cytokine Growth Factor Rev* 1998; **9**: 153-165
58 **Ishiwata T**, Naito Z, Lu YP, Kawahara K, Fujii T, Kawamoto Y, Teduka K, Sugisaki Y. Differential distribution of fibroblast growth factor (FGF)-7 and FGF-10 in L-arginine-induced acute pancreatitis. *Exp Mol Pathol* 2002; **73**: 181-190
59 **Greiling H.** Structure and biological functions of keratan sulfate proteoglycans. *Review EXS* 1994; **70**: 101-122
60 **Naito Z**, Ishiwata T, Lu YP, Teduka K, Fujii T, Kawahara K, Sugisaki Y. Transient and ectopic expression of lumican by acinar cells in L-arginine-induced acute pancreatitis. *Exp Mol Pathol* 2003; **74**: 33-39

Edited by Zhu LH and Wang XL **Proofread by** Xu FM

PO Box 2345, Beijing 100023, China
Fax: +86-10-85381893
E-mail: wjg@wjgnet.com www.wjgnet.com

World J Gastroenterol 2004;10(14):2010-2013
World Journal of Gastroenterology
 ISSN 1007-9327

• GASTRIC CANCER •

Preparation of magnetic polybutylcyanoacrylate nanospheres encapsulated with aclacinomycin A and its effect on gastric tumor

Hong Gao, Ji-Yao Wang, Xi-Zhong Shen, Yong-Hui Deng, Wei Zhang

Hong Gao, Ji-Yao Wang, Xi-Zhong Shen, Department of Gastroenterology, Zhongshan Hospital, Fudan University, Shanghai 200032, China
Yong-Hui Deng, Department of Macromolecular Sciences, Fudan University, Shanghai 200032, China
Wei Zhang, Department of Gastroenterology, Huadong Hospital, Shanghai 200040, China
Supported by the National High Technology Research and Development Program of China 863 Program, No. 2001AA218011
Correspondence to: Dr. Xi-Zhong Shen, Associate Chief of Department of Gastroenterology, Zhongshan Hospital, Fudan University, Shanghai 200032, China. shenxz@zshopital.net
Telephone: +86-21-64041990-2070 **Fax:** +86-21-34160980
Received: 2004-02-02 **Accepted:** 2004-02-21

Abstract

AIM: To evaluate the effect of aclacinomycin A-loaded magnetic polybutylcyanoacrylate nanoparticles on gastric tumor growth *in vivo* and *in vitro*.

METHODS: Magnetic polybutylcyanoacrylate (PBCA) nanospheres encapsulated with aclacinomycin A (MPNS-ACM) were prepared by interfacial polymerization. Particle size, shape and drug content were examined. Female BABL/c nude mice were implanted with MKN-45 gastric carcinoma tissues subcutaneously to establish human gastric carcinoma model. The mice were randomly divided into 5 groups of 6 each: ACM group (8 mg/kg bm); group of high dosage of MPNS-ACM (8 mg/kg bm); group of low dosage of MPNS-ACM (1.6 mg/kg bm); group of magnetic PBCA nanosphere (MPNS) and control group (normal saline). Magnets (2.5 T) were implanted into the tumor masses in all of the mice one day before the therapy. Above-mentioned drugs were administered intravenously to the mice of every group on the first day and sixth day. When the mice were sacrificed, tumor weight was measured, and the assay of granulocyte- macrophage colony forming-unit (CFU-GM) was performed on semi-solid culture. White blood cell, alanine aminotransferase and creatine were examined. 3-[4-dimethylthiazol-2-yl]-2,5-diphenyltetrazolium bromide (MTT) was used to examine the viability of MKN-45 cells after incubation with different concentrations of ACM, MPNS and MPNS-ACM suspension respectively for 48 h.

RESULTS: Content of ACM in MPNS-ACM was 12.0% and the average diameter of the particles was 210 nm. The inhibitory rates of ACM (8 mg/kg bm), high dosage of MPNS-ACM (8 mg/kg bm), low dosage of MPNS-ACM (1.6 mg/kg bm) and MPNS on human gastric carcinoma in nude mice were 22.63%, 52.55%, 30.66% and 10.22%, respectively. There was a significant decrease in the number of CFU-GM of bone marrow in ACM group compared with control group, whereas no obvious change was observed in that of the nanosphere groups. The values of 50% inhibition concentration (IC50) of ACM, MPNS and MPNS-ACM were 0.09, 97.78 and 1.07 μg/mL, respectively.

CONCLUSION: The tumor inhibitory rate of MPNS-ACM was much higher than that of ACM under magnetic field and the inhibition on bone marrow was alleviated significantly compared with ACM group.

Gao H, Wang JY, Shen XZ, Deng YH, Zhang W. Preparation of magnetic polybutylcyanoacrylate nanospheres encapsulated with aclacinomycin A and its effect on gastric tumor. *World J Gastroenterol* 2004; 10(14): 2010-2013
http://www.wjgnet.com/1007-9327/10/2010.asp

INTRODUCTION

Cytotoxic medicine has extensively been employed in cancer chemotherapy. However, the usage of these drugs has been limited by the non-targeting towards cancer and serious toxicity to normal cells in the body. To enhance the therapeutic efficacy of anticancer drugs and reduce the toxicity to normal tissue of the body, targeted drug delivery systems at solid tumors have been developed.

Magnetic targeted drugs are the fourth generation of targeted reagents. The advantage of the magnetic targeted drug delivery systems over other drug targeting techniques is their ability to minimize the uptake by reticuloendothelial system (RES)[1]. Some investigators have reported successful tumor remission in animal experiments upon the use of magnetically responsive anticancer drug carriers under magnetic fields, but in previous studies the majority of magnetically responsive drug carriers, which included magnetic albumin microspheres and magnetic liposomes had been administered intra-arterially to obtain highly efficient localized targeting during the first circulation passing through a strong magnetic field[2,3]. However intra-arterial administration of these carriers is not considered to be suitable for the treatment of multiple systemic lesions and is inconvenient to apply. Accordingly, the treatment of solid tumors requires the development of magnetically responsive carriers that can be effectively delivered to any systemic site via intravenous administration. Yet the therapeutic efficacy of intravenously administered magnetically responsive carriers has not been estalished maturely to date.

Polyalkylcyanoacrylates (PACAs) were not employed as polymers until the early 1980s. However the corresponding monomers, alkylcyanoacrylates, have been extensively used as tissue adhesives for the closure of skin wounds[4]. More recently, one application of the polymers is the use of PACAs as nanoparticulate drug carriers[5-9]. This very exciting area of research has gained increasing interest in therapeutics, especially for cancer treatments. Other molecules of interest, including poorly stable compounds such as peptides and nucleic acids, have been combined with PACAs nanoparticles for targeting purposes[10]. Today, PACAs nanoparticles are considered the most promising polymer colloidal for drug delivery system and are already in clinical development for cancer therapy[11-15]. The main attraction of PACAs nanoparticles is their ability of tissue targeting and enhanceing intracellular penetration of drugs[16]. Among the species, polybutylcyanoacrylate (PBCA), as a polymer with medium-

length alkyl side chain, is of lower toxicity, proper degradation time. PBCA carrying drugs could increase the antibacterial efficacy[17], elevate the anti-cancer effect[18], enhance the relative bioavailability of insulin[19] *etc*. So PBCA has recently been regarded as a kind of widely used, biocompatible, degradable, low-toxic drug carrier.

Employing supermagnetic iron oxide as the ferromagnetic material, aclacinomycin A (ACM) as the targeted fat soluble model drug and PBCA as the carrier, a kind of magnetically targeted polymer encapsulated with an anticancer drug, magnetic PBCA nanospheres encapsulated with ACM were designed and successfully prepared. The antiancer efficacy of the magnetically targeted system was investigated on gastric cancer *in vivo* and *in vitro*.

MATERIALS AND METHODS

Materials

Butylcyanoacrylate was supplied by Zhejiang Golden Roc. Chemicals Co. Inc. ACM was obtained from Shenzhen Main Luck Pharmaceuticals Inc. Human gastric cancer MKN-45 cell line and BALB/c nude mice (SPF, female) were kindly supplied by Shanghai Cancer Institute. Column NdFeB permanent magnets (surface field strength 2.5 T, diameter 1 mm, length 10 mm) were supplied by Shanghai Jieling Magnetic & Device Co. Ltd. Semi-solid methylcellulose M3545 and Iscove's Modified Dulbecco's Medium (IMDM) were purchased from Stemcell Company, Canada.

Methods

Synthesis of magnetic colloidal nanoparticles Magnetic colloidal iron oxide nanoparticles were prepared with the method of coprecipitation as described before[20]. Briefly, 10 mol/L sodium hydroxide was added into the mixture of solution of $FeCl_2$ and $FeCl_3$ (Fe^{2+}/Fe^{3+} molar ratio 1/2) in a nitrogen atmosphere. The solution was stirred for 1 h at 20 ℃, and heated at 90 ℃ for 1 h. The obtained iron oxide suspension was then stirred for 30 min at 90 ℃ with the addition of 100 mL trisodium citrate solution (0.3 mol/L). Subsequently, the iron oxide dispersion was cooled down to room temperature with continuous stir. The magnetic particles were washed with double distilled deionized water and collected with the help of a magnet. Finally, the ultrafine magnetic particles were redispersed in water and the suspensions were adjusted to 2.0% (w/w) for further use.

Preparation of ACM encapsulated magnetic PBCA nanoparticles (MPNS-ACM) Interfacial polymerization was applied to synthesize MPNS-ACM based on the methods used before[21,22]. Briefly, 20 mg ACM dispersed in diluted hydrochloric acid and 2 mL magnetic fluid were mingled, then the mixture was added to 100 g hexane including 2 g Span 80 and 0.6 g polysorbate 80 which was stirred at 600 r/min. The fluid was stirred for 0.5-1 h to make it uniform and emulsive. Then 2 mL butylcyanoacrylate was added dropwise with constant stir at room temperature. After 6 h polymerization the particles were separated with the help of a magnet and washed with methanol for several times. Then the particles were washed with deionized water for several times. The particles were lyophilized and ^{60}Co irradiation (15 kGy) was performed to sterilize them. The preparation of magnetic PBCA nanoparticles (MPNS) is similar to the synthesis of MPNS-ACM except no ACM in HCl solution.

Characterization and measurements Transmission electron microscopy (TEM) was performed for MPNS (Hitachi HU-11B). Scanning electron microscopy (SEM, Philips XL30) was used to determine the size and morphology of MPNS. Dynamic light scattering (DLS, Malvern 4700) was used to measure the hydrodynamic diameter of nanoparticles. The particles were treated with ammonia and then ACM was extracted with ethyl acetate. ACM concentration was determined with UV spectrophotometer at 259 nm. And then drug contents were calculated.

Human gastric carcinoma model of nude mice Human gastric carcinoma MKN-45 cells during exponential growth phase were adjusted to 5×10^7 /mL with RPMI 1640. Then 0.2 mL suspension of MKN-45 cells was inoculated subcutaneously near right forefoot in female BALB/c nude mice. Two weeks later, the solid tumors were taken out from the mice in which the tumors were well growing without necrosis. Tumor masses were cut into small pieces with the diameter of about 2 mm. One tiny piece was implanted into one mouse subcutaneously near right forefoot with a needle. The models were successfully produced after about 2 wk when the tumor grew up to 1 cm in diameter.

Tumor inhibition rate *in vivo* Thirty nude mice models were randomly divided into 5 groups of six each: ACM group (8 mg/kg bm), high dose of MPNS-ACM group (equivalent to ACM 8 mg/kg bm), low dose of MPNS-ACM group (equivalent to ACM 1.6 mg/kg bm), MPNS carrier group (equivalent to MPNS-ACM loaded with ACM 8 mg/kg bm) and control group (normal saline). Magnets (with surfacial field strength 2.5 T) were implanted into the center of the tumors one day before the administration. Above-mentioned agents were administrated intravenously on the first day and sixth day. The largest diameter (LD) and its vertical diameter (VD) of the tumors were measured with calipers every two days after the beginning of administration. The volume of tumor was equal to $LD\times VD^2/2$. The mice were sacrificed on the eleventh day after treatment. The tumors were taken out, weighed and the tumor inhibition rate (TIR) was calculated with the following formula: TIR(%)=(1-average tumor weight of experimental group/average tumor weight of control group)×100%.

Stem cells colony-forming unit assay of bone marrow was performed. White blood cell, serum alanine aminotransferase (ALT) and creatine of the mice were examined.

Assay of granulocyte-macrophage colony-forming unit (CFU-GM) of bone marrow The assay of CFU-GM was performed with semi-solid methylcellulose culture. The femoras of the mice were taken out under sterile condition. Both extremities of them were cut and the bones were immersed into Iscove's modified Dulbecco's medium (IMDM). The bone marrow was washed out and the concentration of the cells with nuclei was adjusted with IMDM to 2×10^5/mL. Cell suspension 0.2 mL was added to 2 mL M3534 semi-solid culture. The mixture was added to a 12-well cell culture plate. The cells were cultured for 7 d at 37 ℃ with 50 mL/L CO_2 in air and >95% humidity. The number of colonies (>30 cells) were counted under inverted microscope[23].

Anticarcinoma effect on gastric cancer cell line *in vitro* Gastric cancer cell line MKN-45 cells were trypsinized and suspended in RPMI 1640 with the concentration of 2×10^5/mL. The cells were seeded onto 96-well culture plates with 190 μL per well and then were cultured at 37 ℃ with 50 ml/L CO_2 in air and >95% humidity for 24 h. Different concentrations of ACM, MPNS and MPNS-ACM in RPMI 1640 were added to the wells and the final concentrations were 0.001, 0.01, 0.1, 1.0, 10 and 100 μg/mL, respectively. The cells were cultured for another 48 h. Then, 10 μL of 5 mg/mL 3-(4,5-dimethylthiazol-2-yl)-2,5-diphenylterazolium bromide (MTT) was added to each well and the cells were cultured for 4 h at 37 ℃. Then the culture medium was discarded, and 150 μL dimethylsulfoxide was added to each well and the absorbance at 570 nm (A_{570}) was measured with microplate reader.

Inhibition rate=(1-A_{570} in treatment group/A_{570} in control group) ×100%.

Statistical analysis

The data were presented as mean±SD. One-Way ANOVA analysis was used to perform single factor multiple comparison in animal tests. The level of significance was set at $P<0.05$. Logistic regression was applied to analyze the inhibition rate of ACM, MPNS and MPNS-ACM in the *in vitro* study.

RESULTS

Characteristics of MPNS-ACM

The average particle size was 210 nm and the size distribution range was 100-400 nm with the most frequent size around 210 nm (Figure 1). A typical core-shell structure is shown under TEM (Figure 2), it indicated black Fe_3O_4 was surrounded by white polymer. SEM photograph shows uniform sphere. The drug content of MPNS-ACM was 12.0%.

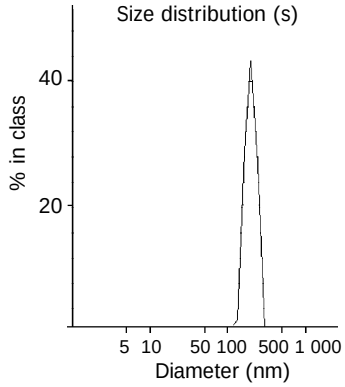

Figure 1 Size distribution of MPNS –ACM.

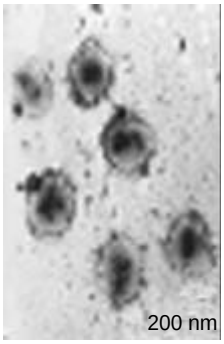

Figure 2 TEM photograph of MPNS-ACM.

Antitumor effect on human gastric carcinoma model of nude mice

The tumor mass and volume were significantly decreased in both ACM group and MPNS-ACM group than control group at the end of the therapy ($P<0.05$). The anti-tumor activity of high dosage of MPNS-ACM was higher than those of the other agents (Table 1).

Table 1 Tumor mass on the 11th day and TIR of the five groups (n=6, mean±SD)

Group	Tumor mass (g)	TIR (%)
ACM	1.06±0.27[a]	22.63
High dosage of MPNS-ACM	0.65±0.26[aceg]	52.55
Low dosage of MPNS-ACM	0.95±0.15[ag]	30.66
MPNS	1.23±0.25	10.22
Control	1.37±0.21	/ /

[a]$P<0.05$ *vs* control group; [c]$P<0.05$ *vs* ACM group; [e]$P<0.05$ *vs* group of low dosage MPNS-ACM; [g]$P<0.05$ *vs* MPNS group.

The TIR of ACM was 22.63%. The tumor mass of ACM group on the eleventh day (1.06±0.27 g) was much lower than that of control group (1.37±0.21 g) ($P<0.05$).

The TIR of high dosage of MPNS-ACM was 52.55%. The tumor mass on the eleventh day (0.65±0.26 g) was much lower than those of the same dosage of ACM group, low dosage of MPNS-ACM group (0.95±0.15 g), MPNS carrier group (1.23±0.25 g) and control group.

The TIR of low dosage of MPNS-ACM (1.6 mg/kg bm) group was 30.66%, which was higher than that of ACM group (8 mg/kg bm), but there was no statistical difference as to the tumor mass between the two groups ($P>0.05$). The tumor weight of low dosage of MPNS-ACM group was lower than those of MPNS group, and control group ($P<0.05$).

The TIR of MPNS carrier was 10.22%. The tumor weight (1.23±0.25 g) was similar to that of control group (1.37±0.21, $P>0.05$).

Side effects of the agents

The white blood cell counts, serum ALT and creatine of the mice in all the groups were similar ($P<0.05$) (Table 2). The number of CFU-GM of ACM group was much lower than those of the other four groups ($P<0.001$). The white blood cell counts in ACM group was lower than that in control group, yet the ones in MNPS carrier and MNPS-ACM groups were similar to that in control group ($P>0.05$, Table 2).

Anti-tumor effect on gastric cancer cell line in vitro

The IC50 of ACM, MPNS and MPNS-ACM was 0.09, 97.78 and 1.07 (Table 3).

Table 3 Inhibition concentration of the drugs (μg/mL)

Group	IC10	IC50	IC90
ACM	0.006	0.09	1.53
MPNS	10.34	97.8	925
MPNS-ACM	0.19	1.07	6.03

DISCUSSION

Selective targeting agents are the trend of antineoplastic chemotherapy. However the production of the biodegradable agents of proper size, high targeting ability and good

Table 2 White blood cells, marrow CFU-GM, serum ALT and creatine(n=6, mean±SD)

Group	White blood cells ($\times10^9$/L)	CFU-GM number (/10^4)	ALT (U/L)	Creatine (μmol/L)
ACM	76.67±17.32	74.75±21.91[b]	30.67±16.51	12.17±1.17
High dosage of MPNS-ACM	70.00±8.74	107.83±14.75	29.17±14.36	12.50±1.05
Low dosage of MPNS-ACM	74.67±9.71	115.25±12.53	23.83±3.55	13.00±2.19
MPNS	79.00±11.23	117.50±12.75	20.83±4.71	12.00±1.55
Control	74.83±6.08	117.00±12.48	37.83±35.13	12.67±1.51

[b]$P<0.001$ *vs* control group.

bioconsistency is an ongoing challenge. Small-sized magnetic particles(<400 nm) can be extravasated into the tumor interstitium and retained there, owing to the enhanced permeability and retention effect of the tumor[24]. Polymer carriers encapsulated with magnetite are difficult to prepare because of the different solubility of magnetite and polymers. Here, a kind of modified superparamagnetic iron oxide particles was introduced to prepare the magnetic targeting agents and the particle size could be controlled to 210 nm also, which was very important for the tolerance and efficacy of the agents.

There were two steps for preparation of MPNS-ACM: the preparation and modification of superparamagnetic iron oxide nanoparticles and the synthesis of magnetic polymer loaded with drug. Chemical coprecipitation was applied to synthesize the iron oxide nanoparticles. After modification with acid, well-suspended and stable magnetite fluid was successfully made. It can be stored as suspension for over one year at room temperature. The magnetite can be localized under magnetic field and redispersed when the magnetic force disappears. Interfacial polymerization was applied to the second step where the biodegradable macromolecular material butylcyanoacrylate reacted at the interface between oil and water. Magnetic nanoparticles and fat soluble ACM were encapsulated during the polymerization. The encapsulated ACM was more stable than the one by attachment. The lyophilization agent can be stored long-term at room temperature. After complete ultrasonication, the nanoparticles intravenously administered could locate at the tumor by magnetic force. ACM was slowly released to produce high efficacy and low toxicity with the degradation of ploymer.

The results showed that the anti-tumor effect of MPNS-ACM *in vitro* without magnetic field was similar to that of MPNS carrier group (considering the drug content was 12% approximately), yet the anti-tumor test *in vivo* showed higher inhibitory efficacy of the magnetic carrier encapsulated with ACM on the gastric cancer model under magnetic field, which was based on the high targeting capacity of the system. TIR of targeted agent was higher than that of five-fold dosage of non-targeted drug. On the other hand, no toxicity to marrow, liver function and kidney function was found from targeted agents. The results show the high therapeutic efficacy on the tumor and the low toxicity to other organs of the magnetic targeted drug delivery system. It is a kind of safe chemotherapeutic agent.

Due to the difference between fat soluble drugs and water soluble drugs, different methods have been applied to encapsulate the drugs to the biopolymer carrier system with or without magnetite. The attempt to load ACM in to the carrier benefits the studies on other drugs including fat soluble drugs and water soluble drugs.

In conclusion, the magnetic targeted chemotherapy using MPNS-ACM has better tumor targeting, therapeutic efficacy and lower toxicity.

ACKNOWLEDGEMENT

We are grateful to Ming Yao and Shi-Ming Fan of Shanghai Cancer Institute for their kind help with the animal experiments.

REFERENCES

1 **Gupta PK,** Hung CT. Magnetically controlled targeted micro-carrier systems. *Life Sci* 1989; **44:** 175-186
2 **Widder KJ,** Morris RM, Poore GA, Howard DP, Senyei AE. Selective targeting of magnetic albumin microspheres containing low-dose doxorubicin: total remission in Yoshida sarcoma-bearing rats. *Eur J Cancer Clin Oncol* 1983; **19:** 135-139
3 **Rudge S,** Peterson C, Vessely C, Koda J, Stevens S, Catterall L. Adsorption and desorption of chemotherapeutic drugs from a magnetically targeted carrier(MTC). *J Control Release* 2001; **74:** 335-340
4 **King ME**, Kinney AY. Tissue adhesives: a new method of wound repair. *Nurse Pract* 1999; **24:** 66-74
5 **de Verdiere AC,** Dubernet C, Nemati F, Soma E, Appel M, Ferte J, Bernard S, Puisieux F, Couvreur P. Reversion of multidrug resistance with polyalkylcyanoacrylate nanoparticles:towards a mechanism of action. *Br J Cancer* 1997; **76:** 198-205
6 **Zhang ZR,** He Q. Study on liver targeting and hepatocytes permeable valaciclovir polybutylcyanoacrylate nanoparticles. *World J Gastroenterol* 1999; **5:** 330-333
7 **Ravi Kumar MN.** Nano and microparticles as controlled drug delivery devices. *J Pharm Pharm Sci* 2000; **3:** 234–258
8 **Soppimath KS,** Aminabhavi TM, Kulkarni AR, Rudzinski WE. Biodegradable polymeric nanoparticles as drug delivery devices. *J Control Release* 2001; **70:** 1–20
9 **Couvreur P,** Barratt G, Fattal E, Legrand P, Vauthier C. Nanocapsule technology: a review. *Crit Rev Ther Drug Carrier Syst* 2002; **19:** 99–134
10 **Kattan J,** Droz JP, Couvreur P, Marino JP, Boutan-Laroze A, Rougier P, Brault P, Vranckx H, Grognet JM, Morge X, Sancho-Garnier H. Phase I clinical trial and pharmacokinetic evaluation of doxorubicin carried by polyisohexylcyanoacrylate nanoparticles, Invest. *New Drugs* 1992; **10:** 191–199
11 **Stella B,** Arpicco S, Peracchia MT, Desmaele D, Hoebeke J, Renoir M, D'Angelo J, Cattel L, Couvreur P. Design of folic acid-conjugated nanoparticles for drug targeting, *J Pharm Sci* 2000; **89:** 1452–1464
12 **Brigger I,** Chaminade P, Marsaud V, Appel M, Besnard M, Gurny R, Renoir M, Couvreur P. Tamoxifen encapsulation within polyethylene glycol-coated nanospheres. A new antiestrogen formulation. *Int J Pharm* 2001; **214:** 37–42
13 **Calvo P,** Gouritin B, Chacun H, Desmaele D, D'Angelo J, Noel JP, Georgin D, Fattal E, Andreux JP, Couvreur P. Long-circulating PEGylated polycyanoacrylate nanoparticles as new drug carrier for brain delivery. *Pharm Res* 2001; **18:** 1157–1166
14 **Li YP,** Pei YY, Zhou ZH, Zhang XY, Gu ZH, Ding J, Zhou JJ, Gao XJ, Zhu JH. Stealth polycyanoacrylate nanoparticles as tumor necrosis factor-alpha carriers: pharmacokinetics and anti-tumor effects. *Biol Pharm Bull* 2001; **24:** 662–665
15 **Vauthier C,** Dubernet C, Fattal E, Pinto-Alphandary H, Couvreur P. Poly(alkylcyanoacrylates) as biodegradable materials for biomedical applications. *Adv Drug Deliv Rev* 2003; **55:** 519-548
16 **Skidan IN,** Gel'perina SE, Severin SE, Guliaev AE. Enhanced activity of rifampicin loaded with polybutyl cyanoacrylate nanoparticles in relation to intracellularly localized bacteria. *Antibiot Khimioter* 2003; **48:** 23-26
17 **Zhang ZR,** He Q, Liao GT, Bai SH. Study on the anticarcinogenic effect and acute toxicity of liver-targeting mitoxantrone nanoparticles. *World J Gastroenterol* 1999; **5:** 511-514
18 **Zhang Q,** Shen Z, Nagai T. Prolonged hypoglycemic effect of insulin-loaded polybutylcyanoacrylate nanoparticles after pulmonary administration to normal rats. *Int J Pharm* 2001; **218:** 75-80
19 **Deng Y,** Wang L, Yang W, Fu S, Elaissari A. Preparation of magnetic polymeric particles via inverse microemulsion polymerization process. *J Magnetism Magnetic Materials* 2003; **257:** 69-78
20 **Kreuter J.** Evaluation of nanoparticles as drug-delivery systems I: perparation methods. *Pharm Acta Helv* 1983; **58**: 196-209
21 **Sommerfeld P**, Schroeder U, Sabel BA. Long-term stability of PBCA nanoparticle suspensions suggests clinical usefulness. *Int J Pharm* 1997; **155:** 201-207
22 **Kuwata T,** Wang IM, Tamura T, Ponnamperuma RM, Levine R, Holmes KL, Morse HC III, De Luca LM, Ozato K. Vitamin A deficiency in mice causes a systemic expansion of myeloid cells. *Blood* 2000; **95:** 3349-3356
23 **Matsumura Y**, Maeda H. A new concept for macromolecular therapeutics in cancer chemotherapy:mechanism of tumoritropic accumulation of proteins and the antitumor agent smancs. *Cancer Res* 1986; **46**(12 Pt 1): 6387-6392
24 **Yuan F,** Dellian M, Fukumura D, Leunig M, Berk DA, Torchilin VP, Jain RK. Vascular permeability in a human tumor xenograft: molecular size dependence and cutoff size. *Cancer Res* 1995; **55:** 3752-3756

Edited by Chen WW **Proofread by** Zhu LH and Xu FM

PO Box 2345, Beijing 100023, China
Fax: +86-10-85381893
E-mail: wjg@wjgnet.com www.wjgnet.com

World J Gastroenterol 2004;10(14):2014-2018
World Journal of Gastroenterology
 ISSN 1007-9327

• LIVER CANCER •

Clinical significance of serum vascular cell adhesion molecule-1 levels in patients with hepatocellular carcinoma

Joanna W. Ho, Ronnie T. Poon, Cindy S. Tong, Sheung Tat Fan

Joanna W. Ho, Ronnie T. Poon, Cindy S. Tong, Sheung Tat Fan, Centre for the Study of Liver Disease and Department of Surgery, University of Hong Kong, Pokfulam, Hong Kong, China
Supported by the Committee on Research and Conferences Grant of the University of Hong Kong 2002-2003 and Sun CY Research Foundation for Hepatobiliary and Pancreatic Surgery of the University of Hong Kong, China
Correspondence to: Dr. Ronnie T. Poon, University of Hong Kong Medical Centre, Department of Surgery, Queen Mary Hospital, 102 Pokfulam Road, Hong Kong, China. poontp@hkucc.hku.hk
Telephone: +852-28553635 **Fax:** +852-28175475
Received: 2004-02-06 **Accepted:** 2004-03-11

Abstract

AIM: To evaluate the correlation between serum vascular cellular adhesion molecule-1 (VCAM-1) levels and clinicopathological features in patients with hepatocellular carcinoma (HCC).

METHODS: Ninety-six patients who underwent HCC resection were recruited in the study. Preoperative serum levels of soluble VCAM-1 were measured by enzyme-linked immunosorbent assay.

RESULTS: Serum VCAM-1 level in HCC patients was inversely correlated with platelet count (r=-0.431, P<0.001) and serum albumin level (r=-0.279, P<0.001), and positively correlated with serum bilirubin level (r=0.379, P<0.001). Serum VCAM-1 level was not associated with tumor characteristics such as tumor size, venous invasion, presence of microsatellite nodules, tumor grade and tumor stage. Serum VCAM-1 level was significantly higher in HCC patients with cirrhosis compared with those without cirrhosis (median 704 *vs* 546 ng/mL, P<0.001). Furthermore, a significantly better disease-free survival was observed in HCC patients with low VCAM-1 level (P=0.019).

CONCLUSION: Serum VCAM-1 level appears to reflect the severity of underlying chronic liver disease rather than the tumor status in HCC patients, and low preoperative serum VCAM-1 level is predictive of better disease-free survival after surgery.

Ho JW, Poon RT, Tong CS, Fan ST. Clinical significance of serum vascular cell adhesion molecule-1 levels in patients with hepatocellular carcinoma. *World J Gastroenterol* 2004; 10 (14): 2014-2018
http://www.wjgnet.com/1007-9327/10/2014.asp

INTRODUCTION

Hepatocellular carcinoma (HCC) is a tumor characterized by a rich vasculature. The formation of rich vasculature depends on angiogenesis, which is a process that plays an important role in tumor progression, growth, and metastasis. Many angiogenic factors and mediators are involved in the control of angiogenesis.

Vascular cell adhesion molecule-1 (VCAM-1) is one of the adhesion molecules that have been implicated as a mediator of angiogenesis[1]. As one of the cell adhesion molecules in the immunoglobulin superfamily, human VCAM-1 is M_r 100 000-110 000, type 1 transmembrane glycoprotein[2-4]. VCAM-1 is transiently expressed on activated vascular endothelial cells in response to vascular endothelial growth factor (VEGF) and other cytokines, such as tumor necrosis factor α, interleukin 1β, and interferon γ[2,5-7]. Functionally, its expression plays a major role in adhesion of leukocytes to the endothelium in inflammed tissue and in the tumor site[2]. It also plays an important role in providing attachment to the developing endothelium during angiogenesis[8-10]. Furthermore, it may also exert its function as an adhesion molecule to facilitate metastasis[2]. A previous study showed that VCAM-1 expression was associated with the metastasis of melanoma[11].

VCAM-1 is a soluble molecule that can be detected in the circulation. Although the exact mechanism by which VCAM-1 is shredded into the bloodstream is unknown, it may involve both proteolytic processing and alternative splicing[12,13]. Because VCAM-1 can be identified in bloodstream, it is potentially useful as a non-invasive biomarker for the monitoring of disease progression in cancer and other diseases[14-16]. It has been reported that VCAM-1 is over-expressed in various diseases and cancers. Recent studies have demonstrated high serum levels of VCAM-1 in patients with colorectal cancer and gastric cancer[16-17]. One study demonstrated that a high serum VCAM-1 level was significantly associated with advanced disease stage and the presence of distant metastasis in gastric cancer[17]. A high serum VCAM-1 level has been shown to be associated with angiogenesis and poor prognosis in breast cancer[18]. A study has also found that serum VCAM-1 was an independent prognostic marker in patients with Hodgkin's lymphoma[19].

Up-regulated VCAM-1 expression in chronic liver disease has also been reported, suggesting that VCAM-1 may play a role in the pathogenesis of chronic hepatitis or cirrhosis[20-26]. Serum VCAM-1 levels higher than normal have been consistently reported in several studies of chronic liver disease of various etiologies[19-27]. However, the clinical significance of serum VCAM-1 in HCC patients has not yet been reported before. The majority of HCC patients have associated chronic hepatitis or cirrhosis. It is of interest to study serum VCAM-1 in HCC patients because VCAM-1 may be involved in the progression of both the tumor and the underlying chronic liver disease.

The objective of this study was to evaluate the levels of serum soluble VCAM-1 in HCC patients compared with cirrhotic patients without HCC and normal controls, and to analyze the correlation of serum VCAM-1 level with clinicopathological features in HCC patients.

MATERIALS AND METHODS

Patients

Ninety-six patients (71 men and 25 women; median age 55.5 years, range 16-79 years) who underwent resection of HCC in the Department of Surgery of the University of Hong Kong at Queen

Mary Hospital were studied. In the majority of cases (81%, *n*=78), HCC was related to hepatitis B viral infection. None of the 96 patients had received any preoperative treatment. The study was approved by the Ethics Committee of our institution and informed consent was obtained from the patients.

Preoperative serum was collected from the patients. Venous blood samples were drawn into a serum separator tube and centrifuged at 3 000 r/min for 10 min, then stored at -80 ℃ until VCAM-1 levels were determined. Serum samples were also obtained from 19 healthy controls without evidence of any active disease and 23 patients with cirrhosis but no evidence of HCC on ultrasonography and alpha fetoprotein (AFP) surveillance. The majority of the 23 cirrhotic patients (74%, *n*=17) had cirrhosis related to hepatitis B viral infection.

Measurement of serum VCAM-1 level

Serum VCAM-1 levels were quantified using an enzyme-linked immunosorbent assay kit designed to quantitatively measure human soluble VCAM-1 concentration in serum (Human sVCAM-1 Immunoassay; R&D systems, Minneapolis, MN). This assay contains recombinant human VCAM-1 and antibodies against the recombinant factor. The assay can recognize both recombinant and natural human VCAM-1. Briefly, 100 μL of diluted VCAM-1 conjugate (antibody to recombinant VCAM-1 conjugated to horse-radish peroxidase) was added to each well that was pre-coated with monoclonal antibody specific for VCAM-1, after which, 100 μL of serially diluted recombinant VCAM-1 standards and serum samples were added to the wells and incubated at room temperature for 1.5 h. After the wells were washed with wash buffer 6 times to clear any unbound substances, tetramethylbenzidine was added to the wells for color development. The intensity of the developed color was measured by reading absorbance at 450 nm. Each measurement was made in duplicate and the serum VCAM-1 level was determined by extrapolation from a standard curve generated for each set of samples assayed. The sensitivity of the assay was 2 ng/mL, and the coefficients of variation of intraassay and interassay determination were in the range given by the manufacturer (4.3-5.9% and 8.5-10.2%, respectively).

Clinicopathologic and follow-up data

All clinicopathologic and follow-up data were prospectively collected and entered into a computerized database. Detailed preoperative blood tests such as complete blood count, coagulation profile, liver biochemistry, indocyanine green retention at 15 min (ICG_{15}), serum AFP level, and hepatitis viral serology were assessed for all patients. Histopathologic data including Edmonson grade[28] (1-2 or 3-4), any venous invasion, tumor capsule, microsatellite lesion and pTNM stage[29] (I/II or III/IVA) were collected. All patients had a computed tomography (CT) scan 1 mo after the hepatic resection to detect any tumor, which was considered a residual disease. Patients who had a positive margin or residual tumors in the 1-month CT scan were considered having a palliative resection.

Postoperative follow-up included monitoring for tumor recurrence by monthly serum AFP level and chest X-ray detection together with ultrasonography or computed tomography (CT) scan every 3 mo. Recurrence of disease was diagnosed by the detection of any intrahepatic or extrahepatic tumor with a typical enhancement pattern of HCC in contrast CT scan and elevation of serum AFP level on serial measurements. Percutaneous fine-needle aspiration cytology was performed to confirm the diagnosis of recurrence in uncertain cases. Disease-free survival was calculated from the date of hepatic resection to the date when recurrence was diagnosed or, in the absence of detectable recurrence, to the date of death or last follow-up.

Statistical analysis

Continuous data were expressed as median with range in parenthesis. For comparison between groups, Mann-Whitney *U* test was used for analysis of continuous variables, and Chi-square test (or the Fisher's exact test, where appropriate) was used for analysis of discrete variables. Correlation analysis was performed using the Spearman rank correlation test. Cumulative disease-free survival was computed using the Kaplan-Meier method and compared between groups by the log-rank test. Serum VCAM level was entered into a multivariate Cox regression analysis together with 7 other variables that were demonstrated to be of prognostic importance in previous studies from our center and others, namely, serum AFP level, tumor size, presence of venous invasion, presence of microsatellite nodules, presence of underlying cirrhosis and pTNM stage[30,31]. All statistical analyses were performed using the SPSS statistical software (SPSS/PC+, SPSS Inc., Chicago, Illinois). $P<0.05$ was considered statistically significant.

RESULTS

Serum VCAM-1 levels

Figure 1 shows the distribution of serum VCAM levels in normal controls (*n*=19), patients with cirrhosis only (*n*=23) and HCC patients (*n*=96). The median serum VCAM-1 level in healthy individuals, patients with cirrhosis only, and patients with HCC was 631 ng/mL (449-1 103), 780 ng/mL (509-4 120), and 621 ng/mL (179-3 199), respectively. There was no significant difference in serum VCAM-1 levels between HCC patients and normal individuals ($P=0.447$). However, there were significant differences in serum VCAM-1 levels between cirrhotic patients without HCC and normal individuals ($P=0.010$), and between cirrhotic patients with and without HCC ($P<0.001$).

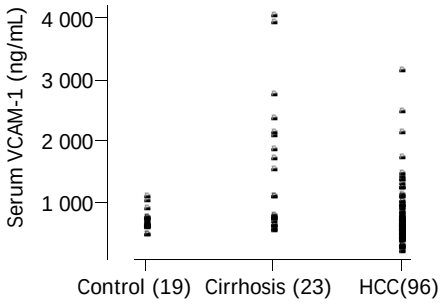

Figure 1 Scatter plot to illustrate the distribution of serum VCAM-1 level (ng / mL) in healthy control subjects (*n*=19), cirrhosis subjects without HCC (*n*=23), and HCC patients (*n*=96).

Correlation between serum VCAM-1 levels and clinicopathological features in HCC patients

Preoperative serum levels of VCAM-1 in the 96 patients with HCC were analyzed to identify any relationship with the clinicopathological parameters. When analyzed in relation to preoperative clinical parameters categorized as binary variables (Table 1), serum VCAM-1 level had no significant relationship with patients' sex, age, hepatitis B surface antigen status, serum AFP level or serum albumin level. However, serum VCAM-1 levels were significantly higher in patients with high ICG_{15} (>10%), which signifies impaired liver function, and in patients with thrombocytopenia, which signifies the presence of significant hypersplenism. When correlated as continuous variables, serum VCAM-1 levels were positively correlated with serum bilirubin level ($r=0.379$, $P<0.001$) and negatively correlated with white cell count ($r=-0.226$, $P=0.027$), platelet count ($r=-0.431$, $P<0.001$) and serum albumin level ($r=-0.279$, $P<0.001$).

Table 1 Preoperative serum VCAM-1 levels categorized by clinical and laboratory variables

Variables	Median serum VCAM-1 (ng/mL)	P^1
Gender		
Male (n=71)	623	0.381
Female (n=25)	594	
Age (yr)		
≤60 (n=56)	615	0.460
>60 (n=40)	639	
HBsAg		
Positive (n=78)	623	0.266
Negative (n=18)	592	
Serum AFP		
≤20 ng/mL (n=29)	608	0.737
>20 ng/mL (n=67)	623	
Serum albumin		
≤40 g/L (n=59)	614	0.228
>40 g/L (n=37)	634	
ICG_{15}		
≤10% (n=45)	531	<0.001
>10% (n=51)	667	
Platelet count		
≤150 $\times 10^9$/L (n=44)	728	<0.001
>150 $\times 10^9$/L (n=52)	547	

HBsAg: Hepatitis B surface antigen; AFP: alpha-fetoprotein; ICG_{15}: indocyanine green retention at 15 min. [1]By Mann-Whitney U test.

Table 2 Preoperative serum VCAM-1 levels categorized by pathological variables

Variables	Median serum VCAM-1 (ng/mL)	P^1
Background liver disease		
Normal (n=7)	462	
Chronic hepatitis (n=39)	548	0.084[2]
Cirrhosis (n=50)	704	<0.001[b]
Cirrhotic liver		
Absent (n=46)	546	<0.001
Present (n=50)	704	
Tumor size		
≤5 cm (n=35)	686	0.158
>5 cm (n=61)	609	
Tumor capsule		
Absent (n=66)	597	0.015
Present (n=30)	736	
Venous invasion		
Absent (n=49)	643	0.248
Present (n=47)	574	
Microsatellite nodules		
Absent (n=50)	643	0.359
Present (n=46)	626	
Edmonson grade		
I/II (n=49)	634	0.629
III/IV (n=47)	642	
pTNM stage		
I/II (n=43)	649	0.134
III/IV (n=53)	592	

pTNM: Pathological tumor-node-metastasis. [1]By Mann-Whitney U test; [2]Compared with normal nontumorous liver; [b]P<0.001 compared with both normal liver and chronic hepatitis.

Table 2 shows the relationship of serum VCAM-1 levels and histopathologic features of the resected HCC. There was no significant relationship with the tumor size (P=0.185), the presence of microsatellite tumor nodules (P=0.359) or venous invasion (P=0.248). Significantly higher serum VCAM-1 levels were observed with the presence of tumor capsule (P=0.015) and the presence of cirrhosis in adjacent non-tumor liver tissues (P<0.001). When categorized according to tumor pTNM staging or Edmonson grading, no significant differences in serum VCAM-1 levels were observed between different tumor stages or grades.

Serum VCAM-1 levels in HCC patients with or without cirrhosis

Fifty out of the 96 HCC patients had cirrhotic liver adjacent to the resected tumor. The median level of serum VCAM-1 in these cases of HCC with cirrhosis was 704 ng/mL (179-3 199), which was significantly higher than that in the HCC cases without cirrhosis (median 546 ng/mL, range 207-1 248, P<0.001), but it was significantly lower than that in the 23 patients with cirrhosis only (P=0.034). All patients with HCC and cirrhosis had Child's A liver function status, whereas among the 23 patients with cirrhosis only, 8 patients were Child's A, 7 patients were Child's B and 8 patients were Child's C. When compared with the healthy individuals, although the median level of serum VCAM-1 in HCC patients with cirrhosis was higher, the difference was not statistically different (P=0.271). In contrast, HCC patients without cirrhosis (n=46) had a significantly lower level of VCAM-1 when compared with healthy individuals (P=0.008). HCC patients with chronic hepatitis (n=39) had a higher serum VCAM-1 level than HCC patients with normal liver, but the difference was not statistically significant (P=0.084).

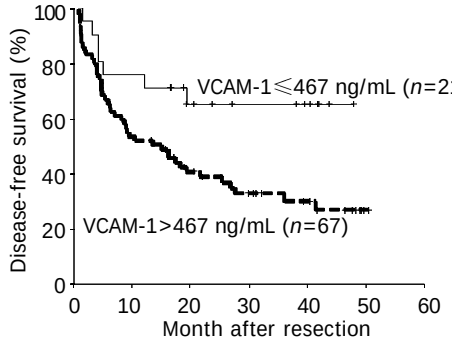

Figure 2 Disease-free survival analysis of HCC patients segregated into low (≤467 ng/mL, n=21) and high (>467 ng/mL, n=67) preoperative serum VCAM-1 levels (P=0.019).

Prognostic value of serum VCAM-1 levels on disease-free survival

Excluding 8 patients with hospital mortality or palliative resection, 88 patients were available for survival analysis to determine the prognostic influence of serum VCAM-1 levels. The median follow-up of the patients was 33 mo (range 15-52 mo). Because of the skewed distribution of serum VCAM-1 levels among the 88 patients, the 25 th percentile of VCAM-1 levels (467 ng/mL) was used as a cut-off point of high and low values of serum VCAM-1 levels in these patients[32]. At the time of analysis, 52 of the 88 HCC patients had postoperative recurrence. The disease-free survival was compared between two groups of patients who were segregated in low (n=21) and high (n=67) serum VCAM-1 levels. Patients with low levels of VCAM-1 had significantly better disease-free survival than those with high levels of VCAM-1 (3-year disease-free survival 66.7% *vs* 32.8%, P=0.019, Figure 2). The overall survival was also better in the group with low serum VCAM-1 levels than in the group with high levels, but the difference was not statistically significant (3-year overall survival 75.0% *vs* 54.2%, P=0.406).

Serum VCAM-1 was entered into a Cox regression analysis of disease-free survival together with serum AFP (> or ≤20 ng/mL), tumor size (> or ≤5 cm), presence of venous invasion, presence of microsatellite lesions, presence of cirrhosis and tumor pTNM stage. Only pTNM stage (risk ratio 1.409, 95% confidence interval 1.080-1.840, *P*=0.012) and serum VCAM-1 (risk ratio 2.329, 95% confidence interval 1.045-5.191, *P*=0.039) were significant prognostic factors for disease-free survival.

DISCUSSION

Evaluation of angiogenic factors has shown important clinical implications in many types of cancer. In particular, the measurement of various circulating angiogenic factors might provide important prognostic values independent of conventional pathological factors in cancer patients[33]. HCC is a highly vascularized malignancy, and angiogenesis has been known to be important for its development and metastasis[34]. Hence, it is of great interest to evaluate the clinical significance of circulating angiogenesis-related markers in HCC patients. Serum VCAM-1 appears to be a promising circulating marker that might have a prognostic value in several types of cancer[16-19]. To our knowledge, this is the first study that evaluated the clinical significance of serum VCAM-1 levels in HCC patients.

Although the median level of VCAM-1 in HCC patients appeared to be similar to that in normal subjects, within the group of HCC patients, those with underlying cirrhosis had a significantly higher VCAM-1 level than those with chronic hepatitis or normal nontumorous liver. Furthermore, high serum VCAM-1 levels in HCC patients correlated positively with serum bilirubin level and inversely with serum albumin level and platelet count. These findings suggested that high serum VCAM-1 levels were related to the severity of underlying chronic liver diseases. In contrast, there was no significant relationship between serum VCAM-1 levels and tumor size, pathological features of invasiveness or tumor stage. This finding in HCC patients was contrary to the findings of higher serum VCAM-1 levels associated with more advanced stage tumors in other cancers[16-19]. Analysis of serum VCAM-1 levels in HCC patients is complicated by the fact that most cases of HCC are associated with chronic liver disease, which could also contribute to the serum VCAM-1 levels. The source of VCAM-1 in the circulation of HCC patients could come from activated endothelial cells in both the tumor and chronic hepatitis or cirrhosis in the nontumorous liver. Our study suggested that serum VCAM-1 level in HCC patients could reflect the severity of underlying chronic liver disease rather than the tumor status. Unlike the case of some other cancers, VCAM-1 may play a less important role as a mediator of angiogenesis or related pathological processes in HCC. One of the main functions of endothelial adhesion molecules in tumor is to facilitate the adhesion of leukocytes into tumor endothelium, which in turn could promote angiogenesis[35]. Yoong *et al*.[36] demonstrated that vascular adhesion protein-1 and intercellular adhesion molecule-1, rather than VCAM-1, supported adhesion of tumor infiltrating lymphocytes to tumor endothelium in HCC. In fact, the serum VCAM-1 levels of the 46 patients with HCC and noncirrhotic liver were significantly lower than those of normal controls, suggesting that VCAM-1 expression may be down-regulated in HCC patients. While most studies in other types of cancer reported the expression of serum VCAM-1 levels was up-regulated, down-regulation of VCAM-1 has also been reported in node positive breast cancer patients[37].

The serum VCAM-1 levels in the 96 HCC patients in this study were significantly lower than those of 23 patients with cirrhosis only. Even when the 50 patients with HCC and background cirrhosis were separately analyzed, their serum VCAM-1 levels were still significantly lower than those of the 23 patients with cirrhosis only. This is probably attributable to the fact that all cirrhotic patients with HCC who underwent hepatic resection had Child's A cirrhosis, whereas the majority of patients in the group with cirrhosis only had Child's B or C cirrhosis. Several previous studies have demonstrated that serum VCAM-1 levels were elevated in cirrhotic patients compared with normal controls, and that serum VCAM-1 level was higher with more severe impairment of liver function or more severe portal hypertension[22,23,26,27]. Two studies demonstrated that serum VCAM-1 levels reflected the degree of fibrosis in hepatitis C related cirrhotic patients[24,25]. Our study suggested a similar relationship between serum VCAM-1 level and severity of cirrhosis in a group of patients with predominantly hepatitis B virus related cirrhosis. VCAM-1 appears to play an important role in liver inflammation and fibrosis, probably by mediating interaction between lymphocytes and endothelium. Further studies to clarify the role of VCAM-1 in chronic liver disease may lead to a better understanding of the pathogenesis of cirrhosis and may provide a novel target of intervention to prevent progression of cirrhosis.

Although serum VCAM-1 level was not related to tumor invasiveness or stage, we observed a significantly better disease-free survival in HCC patients with low level of serum VCAM-1. Our study demonstrated that preoperative circulating level of VCAM-1 had a prognostic value in patients undergoing resection of HCC independent of conventional prognostic factors. The exact mechanism underlying the survival differences between patients with low and high serum VCAM-1 levels is unclear. In view of the relationship between serum VCAM-1 levels and the severity of underlying chronic liver disease or cirrhosis found in this study and other studies[22-27], we speculate that the unfavorable prognostic influence of high serum VCAM-1 level is likely to be related to the underlying cirrhotic or fibrotic condition. The presence of cirrhosis or a higher degree of liver fibrosis has been shown to predispose to multicentric hepatocarcinogenesis and hence postoperative recurrence of HCC[30,31]. An alternative possibility is that HCC with significantly down-regulated VCAM-1 expression may be associated with more favorable prognosis after resection. However, the exact mechanism for the reduction in serum VCAM-1 level in the presence of HCC observed in some patients is far from clear, and such a possibility seems less likely in view of the lack of association between serum VCAM-1 and tumor characteristics. Further studies that correlate serum VCAM-1 level with the expression of VCAM-1 in HCC tumor tissues and adjacent nontumorous liver may help clarify the mechanism underlying the prognostic significance of serum VCAM-1 levels in HCC patients. Irrespective of the underlying mechanism, the predictive value of serum VCAM-1 level might have potential clinical application in selecting patients with a higher risk of postoperative recurrence for some adjuvant therapy to reduce recurrence.

In conclusion, our data demonstrated that serum VCAM-1 levels in HCC patients correlated with the impairment of liver function and the presence of cirrhosis but not tumor size or features of tumor invasiveness. Hence, serum VCAM-1 levels appear to reflect the severity of underlying liver disease rather than the tumor status in HCC patients. A low serum VCAM-1 level predicts better disease-free survival after tumor resection in HCC patients. Further studies are merited to investigate the exact mechanisms involved in these observations and to explore the potential use of serum VCAM-1 level as a novel prognostic marker in HCC patients.

REFERENCES

1 **Koch AE,** Halloran MM, Haskell CJ, Shah MR, Polverini PJ.

Angiogenesis mediated by soluble forms of E-selectin and vascular cell adhesion molecule-1. *Nature* 1995; **376**: 517-519
2 **Osborn L,** Hession C, Tizard R, Vassallo C, Luhowskyj S, Chi-Rosso G, Lobb R. Direct expression cloning of vascular cell adhesion molecule 1, a cytokine-induced endothelial protein that binds to lymphocytes. *Cell* 1989; **59**: 1203-1211
3 **Cybulsky MI,** Fries JW, Williams AJ, Sultan P, Eddy R, Byers M, Shows T, Gimbrone MA Jr, Collins T. Gene structure, chromosomal location, and basis for alternative mRNA splicing of the human VCAM1 gene. *Proc Natl Acad Sci U S A* 1991; **88**: 7859-7863
4 **Hession C,** Tizard R, Vassallo C, Schiffer SB, Goff D, Moy P, Chi-Rosso G, Luhowskyj S, Lobb R, Osborn L. Cloning of an alternate form of vascular cell adhesion molecule-1 (VCAM1). *J Biol Chem* 1991; **266**: 6682-6685
5 **Doukas J,** Pober JS. IFN-gamma enhances endothelial activation induced by tumor necrosis factor but not IL-1. *J Immunol* 1990; **145**: 1727-1733
6 **Thornhill MH,** Wellicome SM, Mahiouz DL, Lanchbury JS, Kyan-Aung U, Haskard DO. Tumor necrosis factor combines with IL-4 or IFN-gamma to selectively enhance endothelial cell adhesiveness for T cells. The contribution of vascular cell adhesion molecule-1-dependent and -independent binding mechanisms. *J Immunol* 1991; **146**: 592-598
7 **Fox SB,** Turner GD, Gatter KC, Harris AL. The increased expression of adhesion molecules ICAM-3, E- and P-selectins on breast cancer endothelium. *J Pathol* 1995; **177**: 369-376
8 **Imhof BA,** Dunon D. Leukocyte migration and adhesion. *Adv Immunol* 1995; **58**: 345-416
9 **Watt SM,** Gschmeissner SE, Bates PA. PECAM-1: its expression and function as a cell adhesion molecule on hemopoietic and endothelial cells. *Leuk Lymphoma* 1995; **17**: 229-244
10 **Patey N,** Vazeux R, Canioni D, Potter T, Gallatin WM, Brousse N. Intercellular adhesion molecule-3 on endothelial cells. Expression in tumors but not in inflammatory responses. *Am J Pathol* 1996; **148**: 465-472
11 **Langley RR,** Carlisle R, Ma L, Specian RD, Gerritsen ME, Granger DN. Endothelial expression of vascular cell adhesion molecule-1 correlates with metastatic pattern in spontaneous melanoma. *Microcirculation* 2001; **8**: 335-345
12 **Pigott R,** Dillon LP, Hemingway IH, Gearing AJ. Soluble forms of E-selectin, ICAM-1 and VCAM-1 are present in the supernatants of cytokine activated cultured endothelial cells. *Biochem Biophys Res Commun* 1992; **187**: 584-589
13 **Terry RW,** Kwee L, Levine JF, Labow MA. Cytokine induction of an alternatively spliced murine vascular cell adhesion molecule (VCAM) mRNA encoding a glycosylphosphatidylinositol-anchored VCAM protein. *Proc Natl Acad Sci U S A* 1993; **90**: 5919-5923
14 **Matsuda M,** Tsukada N, Miyagi K, Yanagisawa N. Increased levels of soluble vascular cell adhesion molecule-1 (VCAM-1) in the cerebrospinal fluid and sera of patients with multiple sclerosis and human T lymphotropic virus type-1-associated myelopathy. *J Neuroimmunol* 1995; **59**: 35-40
15 **Sudhoff T,** Wehmeier A, Kliche KO, Aul C, Schlomer P, Bauser U, Schneider W. Levels of circulating endothelial adhesion molecules (sE-selectin and sVCAM-1) in adult patients with acute leukemia. *Leukemia* 1996; **10**: 682-686
16 **Alexiou D,** Karayiannakis AJ, Syrigos KN, Zbar A, Kremmyda A, Bramis I, Tsigris C. Serum levels of E-selectin, ICAM-1 and VCAM-1 in colorectal cancer patients: correlations with clinicopathological features, patient survival and tumour surgery. *Eur J Cancer* 2001; **37**: 2392-2397
17 **Alexiou D,** Karayiannakis AJ, Syrigos KN, Zbar A, Sekara E, Michail P, Rosenberg T, Diamantis T. Clinical significance of serum levels of E-selectin, intercellular adhesion molecule-1, and vascular cell adhesion molecule-1 in gastric cancer patients. *Am J Gastroenterol* 2003; **98**: 478-485
18 **O'Hanlon DM,** Fitzsimons H, Lynch J, Tormey S, Malone C, Given HF. Soluble adhesion molecules (E-selectin, ICAM-1 and VCAM-1) in breast carcinoma. *Eur J Cancer* 2002; **38**: 2252-2257
19 **Christiansen I,** Sundstrom C, Enblad G, Totterman TH. Soluble vascular cell adhesion molecule-1 (sVCAM-1) is an independent prognostic marker in Hodgkin's disease. *Br J Haematol* 1998; **102**: 701-709
20 **Adams DH,** Burra P, Hubscher SG, Elias E, Newman W. Endothelial activation and circulating vascular adhesion molecules in alcoholic liver disease. *Hepatology* 1994; **19**: 588-594
21 **Haruta I,** Tokushige K, Komatsu T, Ikeda I, Yamauchi K, Hayashi N. Clinical implication of vascular cell adhesion molecule-1 and very late activation antigen-4 interaction, and matrix metalloproteinase-2 production in patients with liver disease. *Can J Gastroenterol* 1999; **13**: 721-727
22 **Lim AG,** Jazrawi RP, Levy JH, Petroni ML, Douds AC, Maxwell JD, Northfield TC. Soluble E-selectin and vascular cell adhesion molecule-1 (VCAM-1) in primary biliary cirrhosis. *J Hepatol* 1995; **22**: 416-422
23 **Pirisi M,** Fabris C, Falleti E, Soardo G, Toniutto P, Vitulli D, Gonano F, Bartoli E. Serum soluble vascular-cell adhesion molecule-1 (VCAM-1) in patients with acute and chronic liver diseases. *Dis Markers* 1996; **13**: 11-17
24 **Kaplanski G,** Farnarier C, Payan MJ, Bongrand P, Durand JM. Increased levels of soluble adhesion molecules in the serum of patients with hepatitis C. Correlation with cytokine concentrations and liver inflammation and fibrosis. *Dig Dis Sci* 1997; **42**: 2277-2284
25 **Lo Iacono O,** Garcia-Monzon C, Almasio P, Garcia-Buey L, Craxi A, Moreno-Otero R. Soluble adhesion molecules correlate with liver inflammation and fibrosis in chronic hepatitis C treated with interferon-alpha. *Aliment Pharmacol Ther* 1998; **12**: 1091-1099
26 **Yamaguchi N,** Tokushige K, Haruta I, Yamauchi K, Hayashi N. Analysis of adhesion molecules in patients with idiopathic portal hypertension. *J Gastroenterol Hepatol* 1999; **14**: 364-369
27 **Kobayashi H,** Horikoshi K, Long L, Yamataka A, Lane GJ, Miyano T. Serum concentration of adhesion molecules in postoperative biliary atresia patients: relationship to disease activity and cirrhosis. *J Pediatr Surg* 2001; **36**: 1297-1301
28 **Edmonson HA,** Steiner PE. Primary carcinoma of the liver: a study of 100 among 48 900 necropsies. *Cancer* 1954; **7**: 462-503
29 **Hermanek P,** Sobin LH, eds. TNM classification of malignant tumors. 4th ed. *Berlin, Springer Verlag* 1987
30 **Tung-Ping Poon R,** Fan ST, Wong J. Risk factors, prevention, and management of postoperative recurrence after resection of hepatocellular carcinoma. *Ann Surg* 2000; **232**: 10-24
31 **Lauwers GY,** Vauthey JN. Pathological aspects of hepatocellular carcinoma: a critical review of prognostic factors. *Hepatogastroenterology* 1998; **45**(Suppl 3): 1197-1202
32 **Kaplan EL,** Meier P. Nonparametric estimation from incomplete observations. *J Am Stat Assoc* 1958; **53**: 457-481
33 **Tung-Ping Poon R,** Fan ST, Wong J. Clinical implications of circulating angiogenic factors in cancer patients. *J Clin Oncol* 2001; **19**: 1207-1225
34 **Poon RT,** Fan ST, Wong J. Clinical significance of angiogenesis in gastrointestinal cancers: a target for novel prognostic and therapeutic approaches. *Ann Surg* 2003; **238**: 9-28
35 **Jain RK,** Koenig GC, Dellian M, Fukumura D, Munn LL, Melder RJ. Leukocyte-endothelial adhesion and angiogenesis in tumors. *Cancer Metastasis Rev* 1996; **15**: 195-204
36 **Yoong KF,** McNab G, Hubscher SG, Adams DH. Vascular adhesion protein-1 and ICAM-1 support the adhesion of tumor-infiltrating lymphocytes to tumor endothelium in human hepatocellular carcinoma. *J Immunol* 1998; **160**: 3978-3988
37 **Madhavan M,** Srinivas P, Abraham E, Ahmed I, Vijayalekshmi NR, Balaram P. Down regulation of endothelial adhesion molecules in node positive breast cancer: possible failure of host defence mechanism. *Pathol Oncol Res* 2002; **8**: 125-128

Edited by Wang XL **Proofread by** Chen WW and Xu FM

PO Box 2345, Beijing 100023, China
Fax: +86-10-85381893
E-mail: wjg@wjgnet.com www.wjgnet.com

World J Gastroenterol 2004;10(14):2019-2023
World Journal of Gastroenterology
 ISSN 1007-9327

• LIVER CANCER •

Effects of KAI1 gene on growth and invasion of human hepatocellular carcinoma MHCC97-H cells

Sui-Hai Si, Jian-Min Yang, Zhi-Hong Peng, Yuan-Hui Luo, Ping Zhou

Sui-Hai Si, Jian-Min Yang, Zhi-Hong Peng, Yuan-Hui Luo, Ping Zhou, Gastroenterology Research Center, Southwest Hospital, Third Military Medical University, Chongqing 400038, China
Supported by the National Natural Science Foundation of China, No. 30070348
Co-correspondents: Dr. Sui-Hai Si
Correspondence to: Professor Jian-Min Yang, Gastroenterology Research Center, Southwest Hospital, Third Military Medical University, Chongqing 400038, China. jianminyang@hotmail.com
Telephone: +86-23-68754678 **Fax:** +86-537-2903067
Received: 2003-08-06 **Accepted:** 2003-10-12

Abstract

AIM: To study the effects of sense and antisense KAI1 genes on the growth and invasion of human hepatocellular carcinoma (HCC) cell line MHCC97-H.

METHODS: KAI1 sense and antisense eukaryotic expression plasmids were constructed using subclone technique and transfected into MHCC97-H cells respectively by DOTAP liposome. After successful transfection was confirmed, *in vitro* growth curve, cell cycles, plate clone formation efficiency, invasive ability in Boyden Chamber assay and ultrastructural morphology were studied.

RESULTS: KAI1 sense and antisense genes had no significant effects on the cell growth curve and cell cycles. After transfection with sense KAI1 gene, decreased invasive ability in Boyden Chamber assay and decreased amount of mitochondria, but no significant changes of plate clone formation efficiency were observed in MHCC97-H-S cells. The plate clone formation efficiency and invasive ability in Boyden Chamber assay were significantly increased in MHCC97-H-AS cells, after transfection with antisense KAI1 gene. Furthermore, increased amount of mitochondria, rough endoplasmic reticulum, Golgi apparatus and expanded endoplasmic reticulum were also noted in MHCC97-H-AS cells.

CONCLUSION: Changes of KAI1 expression in HCC cells may alter their invasive and metastasis ability of the tumor.

Si SH, Yang JM, Peng ZH, Luo YH, Zhou P. Effects of KAI1 gene on growth and invasion of human hepatocellular carcinoma MHCC97-H cells. *World J Gastroenterol* 2004; 10 (14): 2019-2023
http://www.wjgnet.com/1007-9327/10/2019.asp

INTRODUCTION

Hepatocellular carcinoma (HCC) is one of the most common malignant tumors in China. Metastasis and recurrence are the most principal factors for the prognosis of patients with the tumor[1]. KAI1 gene, isolated from human metastatic prostate tumor in 1995, was regarded as a new metastasis suppressor gene. Up to now, many researches on the relationship between KAI1 gene and invasion, metastasis of malignant tumors have been reported, but most of them were made by histopathological and molecular pathological methods[2-16]. In the present research, we studied the effects of KAI1 gene on the growth and invasion of human hepatocellular carcinoma (HCC) by subclone, gene transfection and antisense technology.

MATERIALS AND METHODS

Plasmid and vector

Plasmid pCMV-KAI1, with a full length of 8.2 kb, containing human a full-length of KAI1 structural cDNA gene, was a generous gift from Professor J.Carl Barrett and Dr. Dong of National Institute of Health of USA[2]. Eukaryotic expression plasmid vector pCI-neo, with a full length of 4.7 kb, was purchased from Promega Corporation.

Gene recombination and identification

Sense and antisense KAI1 eukaryotic expression plasmids constructed by subclone technique, were confirmed and identified by restriction endonuclease *Sal* I and *Xba* I analysis.

Cell line and culture

MHCC97-H, a hepatocellular carcinoma cell line with highly metastatic potential[17], purchased from Liver Cancer Institute, Zhongshan Hospital,Shanghai Fudan University, was used as target cells of gene transfection in the present study. The cell line was cultured in Dulbecco minimum essential medium (Hyclone, USA) containing 100 mL/L fetal calf serum (Hyclone, USA), 100 kU/L penicillin and 100 kU/L streptomycin at 37 ℃ in a 50 mL/L CO_2 incubator.

Gene transfection

Sense and antisense KAI1 eukaryotic expression plasmids were transfected into MHCC97-H cells respectively by DOTAP (Roche, USA) liposome transfection system similar to our previous report[18]. Forty-eight hours after transfection, the cells were transfer-selection-cultured for two weeks under the pressure of 800 mg/L G418 (Pierces, USA) in the culture medium. Then the positive cell clones were mixed and the resistance cells were expanded to be cultured under the pressure of 250-600 mg/L G418. Enhanced culture, passaging and storage were performed until few cells were killed by G418.

Integration and expression of transfected genes

Gene integration was identified with amplification of neo genes[19] by polymerase chain reaction (PCR). The primers, designed to amplify the neo genes in vector pCI-neo: forward (P1): 5' -CAA GAT GGA TTG CAC GCA GG-3' , reverse (P2): 5' -CCC GCT CAG AAG AAC TCG TC -3' , were synthesized by Shanghai Bioenginering Company, China. Theoretical length of PCR product was 790 bp. Western blot and immunocytochemistry were also performed to understand whether transfection was successful and the effects of transfected genes on KAI1 expression in MHCC97-H cells.

Ultrastructural morphology

Ultrastructural changes of the cells transfected with sense or antisense KAI1 gene were observed with transmission electron microscope.

Cell growth curve

Cells in exponential growth phase were trypsinized to develop single-cell suspension. Four $\times 10^4$ viable cells in 1 mL of medium were added to each well of the 24-well culture plates, which were incubated at 37 ℃ with 50 mL/L CO_2. Cell numbers in 4 wells were counted and averaged with blood counting chamber every 24 h for 10 consecutive days, and cell growth curve was plotted based on these results.

Cell cycles

Cell cycle analyses were performed by flow cytometry, and each group was examined for 3 times.

Plate clone formation test

Cells cultured (2×10^3) for 48 h were added to each well containing 1mL of culture medium of a 6-well culture plate, each cell group contained 4 wells. Then the culture plate was gently swayed to disperse cells. The cells were incubated at 37 ℃ with 50 mL/L CO_2 for 12 d. Then the cells were washed twice with warm PBS, and stained with Giemsa solution. The number of colonies containing 50 cells or more was counted under a microscope.

In vitro invasion assay

In vitro invasive ability was tested by Boyden Chamber assay[20,21] according to the kit directions. Invasion Chamber inserts (BD Biosciences, USA) with 8 μm-pores in their PET membrane had been coated by matrigel. Before invasion assay, the invasion chambers were rehydrated with DMEM (serum-free) for 2 h in a humidified tissue culture incubator at 37 ℃ with 50 mL/L CO_2 atmosphere. DMEM with 100 mL/L fetal bovine serum was added to the lower compartment, and 1.5×10^5 tumor cells in serum-free DMEM were added to the upper compartment of the chamber. Each cell group was plated in 3 duplicate wells. After 48 h incubation, the matrigel was removed, and the filter was washed, cells were fixed and stained in Giemsa solution. Then the cells having migrated to the lower sides of the PET membrane in 5 random visual fields (200×) were counted under a light microscope.

Statistical analysis

Statistical analysis software package SPSS (V10.0) was used for data processing, and $P<0.05$ was considered statistically significant.

RESULTS

KAI1 gene recombination and identification

Two fragments of 3 kb and 5.2 kb appeared after pCMV-KAI1 was digested by *Xba* I. According to the plasmid pCMV-KAI1 map, the 3 kb fragment containing human full-length structural KAI1 cDNA gene was extracted. The cleaved vector pCI-neo after digestion by *Xba* I and dephosphorylation by CIP was linked up with the 3 kb fragment. Two recombinant plasmids were extracted and digested by *Sal* I, the plasmid appearing 2 fragments of 2.25 kb and 6.22 kb after digestion was consistent with the expected sense KAI1 expression plasmid, and the other appearing two fragments of 0.75 kb and 7.72 kb was consistent with the expected antisense KAI1 expression plasmid (Figure 1A). Then the 2 recombinants were digested by *Xba* I to further confirm the insertion of target fragment into the vector. The results showed the two recombinants were respectively cleaved into the same two fragments 3kb, 5.4 kb (Figure 1B), and suggested subclone reconstruction was successfully performed.

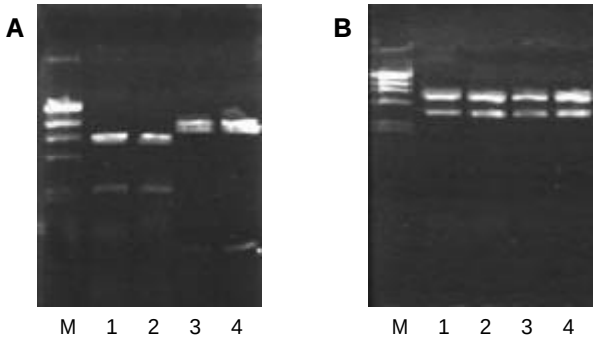

Figure 1 Identification of KAI1 recombinant plasmids digested by *Sal* I and *Xba* I. M: λDNA / Hind III marker (23.13, 9.42, 6.56, 4.36, 2.32 and 2.02 kb), 1, 2: pCI-KAI1, 3, 4: pCI-anti-KAI1.

KAI1 gene transfection and identification

The recombinants containing sense or antisense KAI1 cDNA were respectively transfected into MHCC97-H cells by DOTAP liposome system. After stable cell clones were screened by G418, the cells transfected with sense KAI1 gene were renamed as MHCC97-H-S, the cells transfected with antisense KAI1 gene were renamed as MHCC97-H-AS, and the cells transfected with vector pCI-neo (vacant vector) were renamed as MHCC97-H-pCI. With amplification of the neo genes by PCR, a specific fragment with a length of 790 bp could be produced from MHCC97-H-S, MHCC97-H-AS and MHCC97-H-pCI cells, but none from MHCC97-H cells (Figure 2). It suggested that the recombinant genes were integrated into genomes of the target cells respectively.

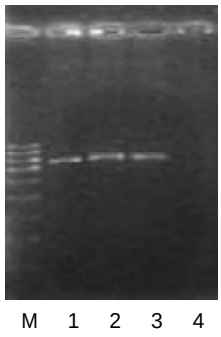

Figure 2 Identifications of gene integration by neo gene amplification. M: Ladder marker (1.0, 0.9, 0.8, 0.7, 0.6, 0.5, 0.4 and 0.3 kb), 1: MHCC97-H-S (790 bp), 2: MHCC97-H-AS (790 bp), 3: MHCC97-H-pCI (790 bp), 4: MHCC97-H.

Western blot and immunocytochemistry staining showed KAI1 protein expression was enhanced in MHCC97-H-S, but decreased in MHCC97-H-AS, and no obvious difference in MHCC97-H-pCI as compared with MHCC97-H cells (Figures 3, 4).

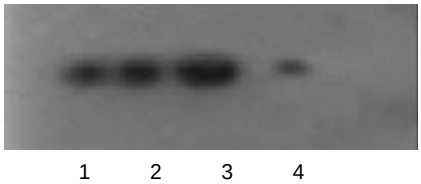

Figure 3 KAI1 protein expressions in different cells revealed by Western blot. 1: MHCC97-H, 2: MHCC97-H-pCI, 3: MHCC97-H-S, 4: MHCC97-H-AS.

Ultrastrucrtural changes in transfected cells

Under electron microscope, the amount of mitochondria was decreased in MHCC97-H-S cells, but increased in MHCC97-H-AS cells. Furthermore, increased amount of rough endoplasmic reticulum (RER), Golgi apparatus, expanded endoplasmic reticulum and myelin-sheath-like changes of mitochondria were also noted in MHCC97-H-AS cells (Figure 5). However, there were no obvious differences in cell shape, superficial microvilli, karyotype and karyokinesis among MHCC97-H-S, MHCC97-H-AS and MHCC97-H cells.

Table 1 Cell cycle distribution of different cells revealed by flow cytometer (%)

Cell	G_0/G_1	S	G_2/M
MHCC97-H-S	69.8±6.7	19.7±6.4	10.5±0.9
MHCC97-H-AS	72.1±7.2	19.0±6.3	8.9±0.9
MHCC97-H	73.1±2.0	16.4±1.4	10.5±1.5

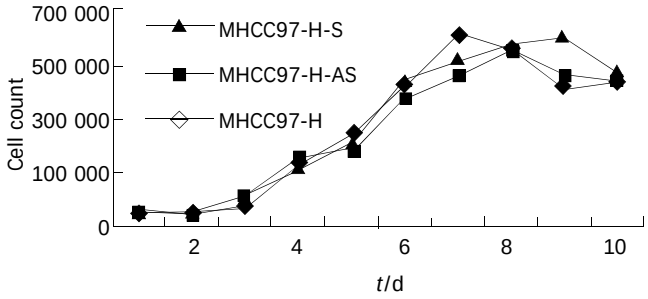

Figure 6 Growth curves of different cells.

Growth curve and cell cycles

No significant differences in growth curve and cell cycles were observed among MHCC97-H-S, MHCC97-H-AS, and MHCC97-H cells in 10 consecutive days (Figure 6, Table 1). The results demonstrated that KAI1 gene had no obvious effect on cell proliferation ability.

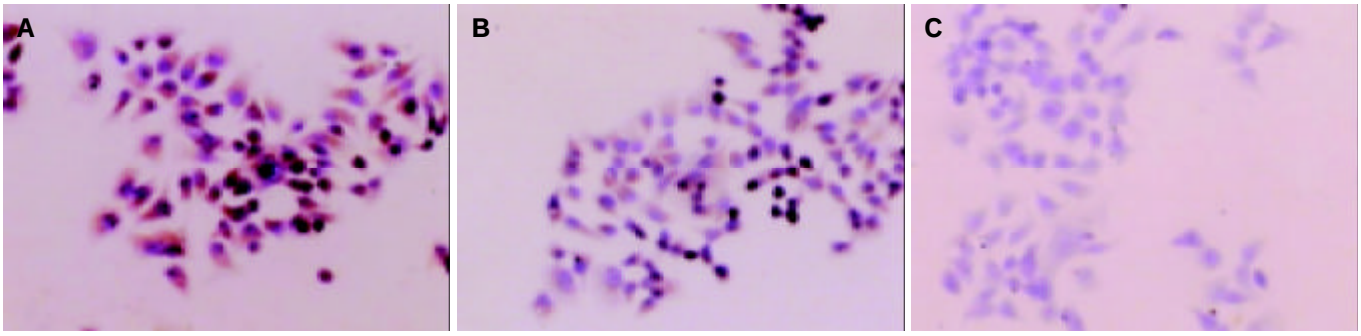

Figure 4 KAI1 protein expression in different cells revealed by immunocytochemistry (SP×400). A: MHCC97-H-S, B: MHCC97-H, C: MHCC97-H-AS.

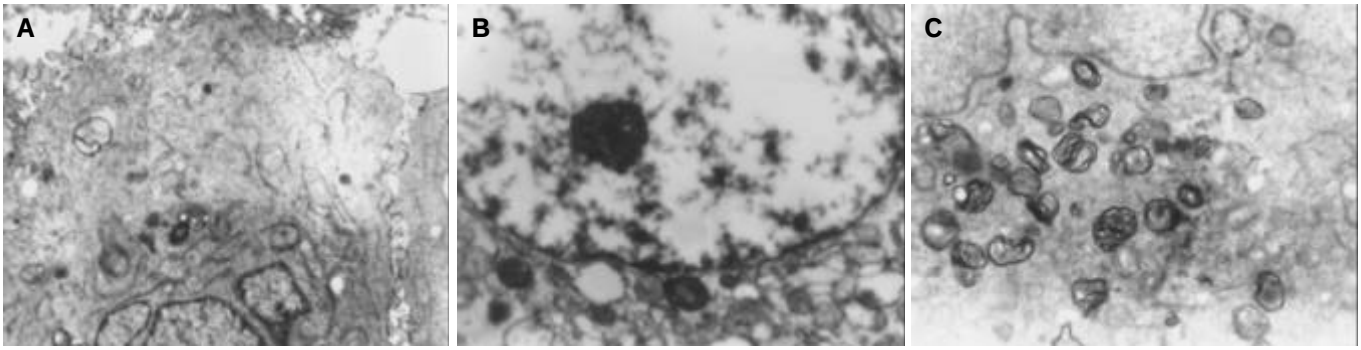

Figure 5 Ultrastrucrtural changes in transfected cells. ×6 200. A: MHCC97-H-S cells, fewer RER and mitochondria, B: MHCC97-H-AS cells, more mitochondria, expanded endoplasmic reticulum, C: MHCC97-H-AS cells, myelin-sheath-like changes of mitochondria.

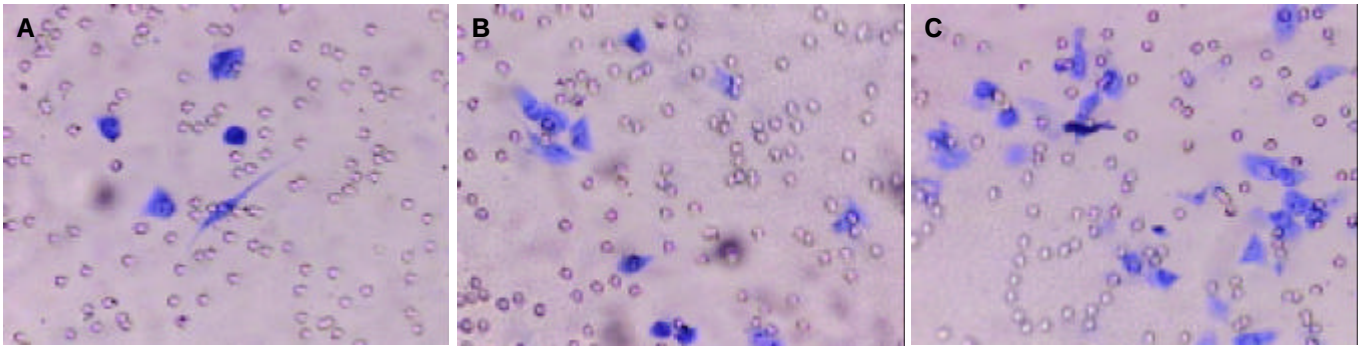

Figure 7 Penetrated cells (blue) in Boyden Chamber test. Giemsa×400. A: MHCC97-S, B: MHCC97-H, C: MHCC97-H-AS.

Plate clone formation efficiency

After two weeks of culture, the results of plate clone formation test showed no statistical difference in clone formation number between MHCC97-H-S (36.2±3.3) and MHCC97-H (38.5±1.9) (P>0.05). However, MHCC97-H-AS (132.5±2.9) showed more clone formation number (P<0.01).

Cell invasive ability

Boyden Chamber assay showed that the cells penetrated the artificial basement membrane in MHCC97-H-S (59.7±3.5) were fewer than in MHCC97-H (92.7±1.5) (P<0.01). However, more penetrated cells in MHCC97-H-AS (188.00±4.5) were noted as compared with those in MHCC97-H (P<0.01). These results suggested that sense KAI1 gene could decrease the invasive ability of MHCC97-H, while, antisense KAI1 gene could increase the invasive ability of MHCC97-H (Figure 7).

DISCUSSION

KAI1 is a newly discovered metastasis suppressor gene in human prostate cancer, which was mapped to chromosome 11p11.2 by Dr. Dong *et al*.[2] of National Institute of Health, USA in 1995. KAI1 specifies a leukocyte surface glycoprotein of 267 amino acids with molecular mass of 29 610 u. KAI1 protein has been recognized as a structurally distinct family of membrane glycoproteins, transmembrane 4 superfamily[22]. Recent researches showed the expression of KAI1 was down-regulated not only in human prostate cancer but also in a variety of human malignant tumors[3,16], and these suggested KAI1 might be a broad-spectrum metastasis suppressor gene for human tumors.

Previous studies on the relationship between KAI1 gene and tumor invasion, metastasis were mostly based on the detection of KAI1 protein, DNA or RNA in tissue samples from surgical resections with immunopathological and molecular pathological methods in combination with analysis of clinical data. In the present study, we transfected full-length structural sense and antisense KAI1 genes from subclone recombinants into hepatocellular carcinoma MHCC97-H cell line with highly metastatic potential respectively. By observation of the changes of cell growth, invasion and ultrastructures of MHCC97-H before and after KAI1 transfection, we hoped to understand the effects of KAI1 gene on the capability of growth and invasion of hepatocellular carcinoma and to provide experimental evidences for the prevention and treatment of invasion and metastasis of this malignant tumor.

Restriction endonuclease analysis showed KAI1 full-length cDNA was respectively inserted into plasmid vector pCI-neo by two different directions, indicating that sense and antisense KAI1 genes eukaryon expression plasmids were successfully reconstructed. After KAI1 gene transfected into MHCC97-H by DOTAP liposome system, amplification of the neo gene in transfected cells was performed by PCR to confirm whether KAI1 gene was integrated into genomes of target MHCC97-H cells. Neo is a screening marker gene in the vector pCI-neo, and no sequence of this gene exists in the genomes of mammal cells, but it could stably exist in the genomes of mammal cells after transfection. Therefore, if the sequence could be amplified from the genomes of transfected cells by PCR, it could confirm the exogenous genes were integrated into genomes of MHCC97-H cells. PCR results showed sense and antisense KAI1 genes eukaryon expression plasmids were successfully integrated into genomes of MHCC97-H. Western blot and immunocytochemical staining were made to determine if the recombinant plasmids could expectantly express in the transfected cells. The results showed that sense KAI1 could up regulate the expression of KAI1 protein in MHCC97-H as compared with the control parental cells, but antisense KAI1 could down regulate the expression of KAI1 protein, and no obvious difference between the cells transfected with pCI-neo and the control parental cells was noted. These results showed the transfected genes could produce expected effects, and vector pCI-neo itself had no obvious effects on the expression of KAI1.These suggested that the above cells transfected with genes could be used to explore the effects of KAI1 on the biological behaviors of HCC cells.

In the present study, our data indicated that KAI1 gene had no obvious effects on the *in vitro* cell growth and proliferation of hepatocellular carcinoma MHCC97-H cell line. These results were consistent with the studies in prostatic cancer, colon cancer cells by Dong and Takaoka *et al*.[2,23]. In contrast with MHCC97-H control parent cells, the plate clone formation ability had no obvious reduction in MHCC97-H-S, but had obvious enhancement in MHCC97-H-AS cells. These data suggested down regulated expression of KAI1 could enhance motoricity and aggregative abilities of MHCC97-H. Though the cells transfected with sense KAI1 expressed more KAI1 protein revealed by Western blot and immunocytochemical staining, their plate clone formation ability had no obvious reduction. This may be attributed to the small amount of KAI1 protein expression in MHCC97-H cells.

Invasion has been found to be one of the important and necessary properties for tumor metastasis formation[24-29]. Boyden chamber assay, which imitates the invasion process of *in vivo* tumor cells, has also been found to be an ideal method for evaluating the invasive and metastatic abilities of tumor cells[20,22]. Our data suggested that the invasive ability of HCC cells transfected with antisense KAI1 gene was increased, but the invasive ability of HCC cells transfected with sense KAI1 gene was partly inhibited. These indicated that different levels of KAI1 protein expression in HCC cells could affect their invasive and metastatic ability and that it might be an effective route to up regulate KAI1 expression for inhibiting the metastasis of HCC.

Under transmission electron microscope, we found that though KAI1 gene had no obvious effects on cell shape, superficial microvillus, karyotype and karyokinesis of MHCC97-H, sense KAI1 gene transfected into MHCC97-H resulted in reduction of the amount of mitochondria, however antisense KAI1 gene transfection resulted in increase of the amount of mitochondria, RER and Golgi apparatus with expanded endoplasmic reticulum and myelin-sheath-like changes of mitochondria. The biological function of these changes was unknown. It is still necessary to further study whether increased expression of KAI1 can inhibit invasion and metastasis of tumor cells by decreasing products of some organelles.

Though present researches have suggested KAI1 gene is important in preventing the development of metastases in a wide variety of human tumors, the mechanism of KAI1-mediated metastasis suppression remains unclear. The molecular structure of KAI1 protein indicates KAI1 functions in cell-cell interactions and cell-extracellular matrix interactions. These suggest that KAI1 may affect cell-cell adhesion and cell-extracellular matrix adhesion through some signaling pathways to inhibit tumor metastasis[30,31].

REFERENCES

1 **Qin LX,** Tang ZY. The prognostic significance of clinical and pathological features in hepatocellular carcinoma. *World J Gastroenterol* 2002; **8**: 193-199

2 **Dong JT,** Lamb PW, Rinker-Schaeffer CW, Vukanovic J, Ichikawa T, Isaacs JT, Barrett JC. KAI1, a metastasis suppressor gene for prostate cancer on human chromosome 11p11.2. *Science* 1995; **268**: 884-886

3 **Huang CI,** Kohno N, Ogawa E, Adachi M, Taki T, Miyake M. Correlation of reduction in MRP-1/CD9 and KAI1/CD82 ex-

pression with recurrences in breast cancer patients. *Am J Pathol* 1998; **153**: 973-983
4 **White A,** Lamb PW, Barrett JC. Frequent downregulation of the KAI1(CD82) metastasis suppressor protein in human cancer cell lines. *Oncogene* 1998; **16**: 3143-3149
5 **Adachi M,** Taki T, Konishi T, Huang CI, Higashiyama M, Miyake M. Novel staging protocol for non-small-cell lung cancers according to MRP-1/CD9 and KAI1/CD82 gene expression. *J Clin Oncol* 1998; **16**: 1397-1406
6 **Yu Y,** Yang JL, Markovic B, Jackson P, Yardley G, Barrett J, Russell PJ. Loss of KAI1 messenger RNA expression in both high-grade and invasive human bladder cancers. *Clin Cancer Res* 1997; **3**: 1045-1049
7 **Houle CD,** Ding XY, Foley JF, Afshari CA, Barrett JC, Davis BJ. Loss of expression and altered localization of KAI1 and CD9 protein are associated with epithelial ovarian cancer progression. *Gynecol Oncol* 2002; **86**: 69-78
8 **Liu FS,** Chen JT, Dong JT, Hsieh YT, Lin AJ, Ho ES, Hung MJ, Lu CH. KAI1 metastasis suppressor gene is frequently down-regulated in cervical carcinoma. *Am J Pathol* 2001; **159**: 1629-1634
9 **Liu FS,** Dong JT, Chen JT, Hsieh YT, Ho ES, Hung MJ, Lu CH, Chiou LC. KAI1 metastasis suppressor protein is down-regulated during the progression of human endometrial cancer. *Clin Cancer Res* 2003; **9**: 1393-1398
10 **Wu DH,** Liu L, Chen LH, Ding YQ. Expression of KAI1/CD82 in human colorectal tumor. *Diyi Junyi Daxue Xuebao* 2003; **23**: 714-715
11 **Ito Y,** Yoshida H, Uruno T, Nakano K, Takamura Y, Miya A, Kobayashi K, Yokozawa T, Matsuzuka F, Kuma K, Miyauchi A. KAI1 expression in thyroid neoplasms: its linkage with clinicopathologic features in papillary carcinoma. *Pathol Res Pract* 2003; **199**: 79-83
12 **Lee HS,** Lee HK, Kim HS, Yang HK, Kim WH. Tumour suppressor gene expression correlates with gastric cancer prognosis. *J Pathol* 2003; **200**: 39-46
13 **Yang JL,** Jackson P, Yu Y, Russell PJ, Markovic B, Crowe PJ. Expression of the KAI1 metastasis suppressor gene in non-metastatic versus metastatic human colorectal cancer. *Anticancer Res* 2002; 22: 3337-3342
14 **Tozawa K,** Akita H, Kawai N, Okamura T, Sasaki S, Hayashi Y, Kohri K. KAI1 expression can be a predictor of stage A prostate cancer progression. *Prostate Cancer Prostatic Dis* 2001; **4**: 150-153
15 **Imai Y,** Sasaki T, Shinagawa Y, Akimoto K, Fujibayashi T. Expression of metastasis suppressor gene (KAI1/CD82) in oral squamous cell carcinoma and its clinico-pathological significance. *Oral Oncol* 2002; **38**: 557-561
16 **Muneyuki T,** Watanabe M, Yamanaka M, Shiraishi T, Isaji S. KAI1/CD82 expression as a prognosic factor in sporadic colorectal cancer. *Anticancer Res* 2001; **21**: 3581-3587
17 **Li Y,** Tang ZY, Ye SL, Liu YK, Chen J, Xue Q, Chen J, Gao DM, Bao WH. Establishment of cell clones with different metastatic potential from the metastatic hepatocellular carcinoma cell line MHCC97. *World J Gastroenterol* 2001; **7**: 630-636
18 **Yang JM,** Chen WS, Liu ZP, Luo YH, Liu WW. Effects of insulin-like growth factors-IR and -IIR antisense gene transfection on the biological behaviors of SMMC-7721 human hepatoma cells. *J Gastroenterol Hepatol* 2003; **18**: 296-301
19 **Poggiali P,** Scoarughi GL, Lavitrano M, Donini P, Cimmino C. Construction of a swine artificial chromosome: a novel vector for transgenesis in the pig. *Biochimie* 2002; **84**: 1143-1150
20 **Nawrocki-Raby B,** Gilles C, Polette M, Bruyneel E, Laronze JY, Bonnet N, Foidart JM, Mareel M, Birembaut P. Upregulation of MMPs by soluble E-cadherin in human lung tumor cells. *Int J Cancer* 2003; **105**: 790-795
21 **Vehvilainen P,** Hyytiainen M, Keski-Oja J. Latent transforming growth factor-beta-binding protein 2 is an adhesion protein for melanoma cells. *J Biol Chem* 2003; **278**: 24705-24713
22 **Dong JT,** Isaacs WB, Barrett JC, Isaacs JT. Genomic organization of the human KAI1 metastasis-suppressor gene. *Genomics* 1997; **41**: 25-32
23 **Takaoka A,** Hinoda Y, Satoh S, Adachi Y, Itoh F, Adachi M, Imai K. Suppression of invasive properties of colon cancer cells by a metastasis suppressor KAI1 gene. *Oncogene* 1998; **16**: 1443-1453
24 **Kurokawa H,** Katsube K, Podyma KA, Ikuta M, Iseki H, Nakajima M, Akashi T, Omura K, Takagi M, Yanagishita M. Heparanase and tumor invasion patterns in human oral squamous cell carcinoma xenografts. *Cancer Sci* 2003; **94**: 277-285
25 **Wernicke M,** Pineiro LC, Caramutti D, Dorn VG, Raffo MM, Guixa HG, Telenta M, Morandi AA. Breast cancer stromal myxoid changes are associated with tumor invasion and metastasis: a central role for hyaluronan. *Mod Pathol* 2003; **16**: 99-107
26 **Katayama M,** Sanzen N, Funakoshi A, Sekiguchi K. Laminin gamma2-chain fragment in the circulation: a prognostic indicator of epithelial tumor invasion. *Cancer Res* 2003; **63**: 222-229
27 **Wells A,** Kassis J, Solava J, Turner T, Lauffenburger DA. Growth factor-induced cell motility in tumor invasion. *Acta Oncol* 2002; **41**: 124-130
28 **Patarroyo M,** Tryggvason K, Virtanen I. Laminin isoforms in tumor invasion, angiogenesis and metastasis. *Semin Cancer Biol* 2002; **12**: 197-207
29 **Nabeshima K,** Inoue T, Shimao Y, Sameshima T. Matrix metalloproteinases in tumor invasion: role for cell migration. *Pathol Int* 2002; **52**: 255-264
30 **Jee B,** Jin K, Hahn JH, Song HG, Lee H. Metastasis-suppressor KAI1/CD82 induces homotypic aggregation of human prostate cancer cells through Src-dependent pathway. *Exp Mol Med* 2003; **35**: 30-37
31 **Shibagaki N,** Hanada K, Yamashita H, Shimada S, Hamada H. Overexpression of CD82 on human T cells enhances LFA-1 / ICAM-1-mediated cell-cell adhesion: functional association between CD82 and LFA-1 in T cell activation. *Eur J Immunol* 1999; **29**: 4081-4091

Edited by Xu CT and Wang XL **Proofread by** Pan BR and Xu FM

PO Box 2345, Beijing 100023, China
Fax: +86-10-85381893
E-mail: wjg@wjgnet.com www.wjgnet.com

World J Gastroenterol 2004;10(14):2024-2028
World Journal of Gastroenterology
 ISSN 1007-9327

• LIVER CANCER •

Growth inhibition and apoptosis induction of tanshinone II-A on human hepatocellular carcinoma cells

Shu-Lan Yuan, Yu-Quan Wei, Xiu-Jie Wang, Fei Xiao, Sheng-Fu Li, Jie Zhang

Shu-Lan Yuan, Yu-Quan Wei, Xiu-Jie Wang, Fei Xiao, Sheng-Fu Li, Jie Zhang, Key Laboratory of Biotherapy of Human Diseases, Ministry of Education of China and Cancer Center, West China Hospital, West China Medical School, Sichuan University, Chengdu 610041, Sichuan Province, China
Supported by the Science Foundation of the Ministry of Health of China, No. 96-1-240 and the Applied Basic Research Programs of Science and Technology Commission Foundation of Sichuan Province, No.2000-135
Correspondence to: Shu-Lan Yuan, Key Laboratory of Biotherapy of Human Diseases, Ministry of Education of China and Cancer Center, West China Hospital, 37 Guo Xue Xiang, Chengdu 610041, Sichuan Province, China. tuyuan@mail.sc.cninfo.net
Telephone: +86-28-85423039 **Fax:** +86-28-85503246
Received: 2003-12-19 **Accepted:** 2004-01-08

Abstract

AIM: To evaluate the effects of tanshinone II-A on inducing growth inhibition and apoptosis of human hepatocellular carcinoma (HCC) cells.

METHODS: The human hepatocellular carcinoma cell line SMMC-7721 was used for the study. The cells were treated with tanshinone II-A at different doses and different times. Cell growth and proliferation were measured by MTT assay, cell count and colony-forming assay. Apoptosis induction was detected by microscopy, DNA ladder electrophoresis and flow cytometry.

RESULTS: In MTT assay, the inhibitory effect became gradually stronger with the passage of time, 24, 48, 72 and 96 h after treatment with tanshinone II-A, and the most significant effect was observed at 72 h. On the other hand, the increase of doses (0.125, 0.25, 0.5, 1.0 mg/L tanshinone II-A) resulted in enhanced inhibitory effect. The growth and proliferation of SMMC-7721 cells were obviously suppressed in a dose- and time-dependent manner. The results of cell count were similar to that of MTT assay. In colony-forming assay, the colony-forming rates were obviously inhibited by tanshinone II-A. In tanshinone II-A group, the morphology of cellular growth inhibition and characteristics of apoptosis such as chromatin condensation, crescent formation, margination and apoptotic body were observed under light and transmission electron microscopes. DNA ladder of cells was presented in electrophoresis. The apoptosis index (AI) was 16.9% (the control group was 4.6%) in flow cytometry. The cells were arrested in G_0/G_1 phase, and the expressions of apoptosis-related genes *bcl-2* and *c-myc* were down-regulated and *fas, bax, p53* up-regulated.

CONCLUSION: Tanshinone II-A could inhibit the growth and proliferation of HCC cell effectively *in vitro* by apoptosis induction, which was associated with up-regulation of *fas, p53, bax,* expression and down-regulation of *bcl-2* and *c-myc*.

Yuan SL, Wei YQ, Wang XJ, Xiao F, Li SF, Zhang J. Growth inhibition and apoptosis induction of tanshinone II-A on human hepatocellular carcinoma cells. *World J Gastroenterol* 2004; 10(14): 2024-2028
http://www.wjgnet.com/1007-9327/10/2024.asp

INTRODUCTION

Hepatocarcinoma is one of the most common causes of malignancy-related death in China. Its therapy in clinic is a big challenge. New remedial method would possibly depend on advances in basic research[1]. Recent evidence suggests that apoptosis of cell is closely related to occurrence, progress and metastasis of tumor[2]. Study on induced apoptosis of tumor cells is an important field of tumor therapy and tumor molecular biology at present. Inducing apoptosis is a new therapeutic target of cancer research. New and promising anticancer drugs could be discovered by studies on apoptosis induction[3-5]. Tanshinone II-A is an alcohol-extracted product from the root of the traditional Chinese medicine-*Salvia miltiorrhiza Bunge*, which is known to have anti-inflammatory, anti-oxidative and cytotoxic activities[6-9]. Traditional Chinese medicines considered as potential drug in cancer treatment. Previous studies confirmed that tanshinone II-A could induce differentiation of human cervical carcinoma cell line (ME180) and leukemia cells (NB4, HL60 and K562), reverse malignant phenotype of human hepatocarcinoma cell line (SMMC-7721)[10-16]. However, there were no studies about growth inhibition and apoptosis induction of tanshinone II-A in hepatocarcinoma cell. In this *in vitro* study, human hepatocarcinoma cell line SMMC-7721 was used. The growth inhibition and apoptosis induction of tanshinone II-A on SMMC-7721 cell were obviously exhibited. We conclude that the effect of growth inhibition of tanshinone II-A on hepatocarcinoma might be related to induction of cellular apoptosis through regulation of apoptosis-associated genes.

MATERIALS AND METHODS

Cell line culture and reagents

Human hepatocellular carcinoma SMMC-7721 cell line was provided by Shanghai Institute of Cancer Research[17]. The cells were grown in RPMI 1640 (Gibco) supplemented with 100 ml/L fetal bovine serum (Huamei, Chengdu, China), penicillin (100 mg/L) and streptomycin (100 mg/L) in a humidified atmosphere of 50 mg/L CO_2 at 37 ℃. Anti-*p53, fas, c-myc, bax* and *bcl-2* antibodies were obtained from Sigma. Other special chemicals were purchased from Sigma (St Louis, MO, USA).

Drugs and treatment

Tanshinone II-A (Tan II-A) was provided by Institute of Traditional Chinese Medicine (concentration 96%). It was dissolved in DMSO (final concentration 0.2 mL/L). The solution was filtered through a 0.22 μm micropore filter and stored at 4 ℃.

SMMC-7721 cells were seeded in flasks or dishes. The Tan II-A group was treated with Tan II-A of different doses (0.125, 0.25, 0.5, 1.0 mg/L) for 24, 48, 72 and 96 h, respectively. The control group was added with equal concentration of DMSO

for negative control. The cells were measured after successive 96-h treatment.

MTT assay

SMMC-7721 cells were seeded in 96-well microtitre plates with 1×10^3 per well and incubated for 24 h in 100 μL culture media. Then the cells were treated with 0.125, 0.25, 0.5, 1.0 mg/L of Tan II-A in the experimental group for 24, 48, 72, and 96 h respectively. MTT 100 μL (5 g/L) was added to the cells and cultivated for another 4 h. After the supernatant fluid was removed, DMSO 100 μL per well was added to the cells and shaken for 15 min. The absorbance at 570 nm was measured by an ELISA reader. At the same time, the SMMC-7721 cells without treatment were served as control. Each assay was repeated three times.

Cell count

SMMC-7721 cells were treated with Tan II-A (0.125, 0.25, 0.5, 1.0 mg/L) for 96 h, respectively, then condition of the cell growth was observed under an inverse and light microscope. Number and viability of the cells were assessed by trypan blue exclusion.

Cell colony-forming assay

Cells were seeded in a 6-well plate with 300 cells per well. After 24 h, the cells were treated with Tan II-A (0.125, 0.25, 0.5, 1.0 mg/L), and cultured in routine medium for 10 days continually. Then the cells were fixed by methanol, Giemsa staining. Finally, the sum of colony per group was counted. The inhibiting rate of colony-formation was calculated.

Light and transmission electron microscopy

SMMC-7721 cells were treated with DMSO (control group) or 0.5, 1.0 mg/L Tan II-A for 48 h. The cells were gently washed with serum-free medium, and observed by inverse and light microscopy after Giemsa staining. On the other hand, some other cells were fixed with 25 g/L glutaraldehyde in 0.1 mol/L of sodium cacodylate buffer, osmicated with 10 g/L osmium tetroxide. then cell block was stained, dehydrated in graded ethanol, infiltrated with propylene oxide, and embedded overnight and incubated in a 60 ℃ oven for 48 h. Silver sections were cut with an Ultracut E microtome, collected on a formvar and carbon-coated grid, stained with uranyl acetate and Reynold's lead citrate, and examined under a transmission electron microscope to identify the morphological changes of apoptosis.

DNA ladder detection

After induction of apoptosis, the cells (1×10^6/group, both attached and detached cells) were washed by PBS, and fixed in ice-cold 700 mg/L ethanol for 24 h. After the ethanol was removed, the cells were rinsed in 0.2 mol/L Na_2HPO_4 and 0.1 mol/L citric acid (192:8, pH 7.8) for 60 min at room temperature. After being centrifuged (10 000 *g*), the supernatant was collected in Eppendorf tubes, 2.5 g/L NP-40 and 10 g/L RNase A were added at 37 ℃ for 30 min, then Protein K (1 g/L, Promega) was added at 50 ℃ for 30 min. Equal quantity of DNA was electrophoresed in 15 g/L agarose gels and stained with ethidium bromide (5 mL/L) for 2 h at 80 V. Ladder formation of oligonucleosomal DNA fragmentation was detected under ultraviolet light.

Flow cytometry measurement

The sample preparation and measurement followed the method described in reference[15]. The cells were harvested, counted and fixed. The cell concentration was adjusted to 10^6/mL. According to the routine method, cell frequency distribution of each phase in cell cycle was measured. Cellular *fas*, *p53*, *bax*, *bcl-2* and *myc* gene expressions were detected by immunohistochemical method on FACS-420 FCM. The results were shown with scanning figure and date.

Statistical analysis

Data were presented as the mean±SD error of the mean. Student's *t* test was used for comparison among different groups. A *P* value of less than 0.05 is considered statistically significant.

RESULTS

Cell growth and proliferation

Tan II-A exhibited a statistically significant dose-dependent growth-inhibitory effect on SMMC-7721 cell evaluated by MTT assay. The inhibiting rates of cell growth were 12.2%, 30.6%, 52.4% and 82.5%, respectively when treated with Tan II-A of different doses (0.125, 0.25, 0.5, 1.0 mg/L) for 96 h (Figure 1A). Moreover, the growth-inhibitory effect of Tan II-A on the cells was found to be time-dependent. The inhibiting rates were 12.5%, 38.2%, 47.6% and 58.7%, respectively when treated separately for 24, 48, 72 and 96 h with 0.5 mg/L of Tan II-A (Figure 2B). The inhibitory effect became gradually stronger with the passage of time after treatment, and the most significant effect was observed at 72 h. The cell growth and proliferation were obviously inhibited in a dose- and time-dependent manner. The same inhibitory effect was found by cell count. In colony-forming assay, the colony-forming rates of SMMC-7721 cell were 11.6%, 22.5%, 38.5%, 42.2% in Tan II-A group and 68.2% in control group, respectively, suggesting the obviously inhibiting effect of Tan II-A on cell proliferation.

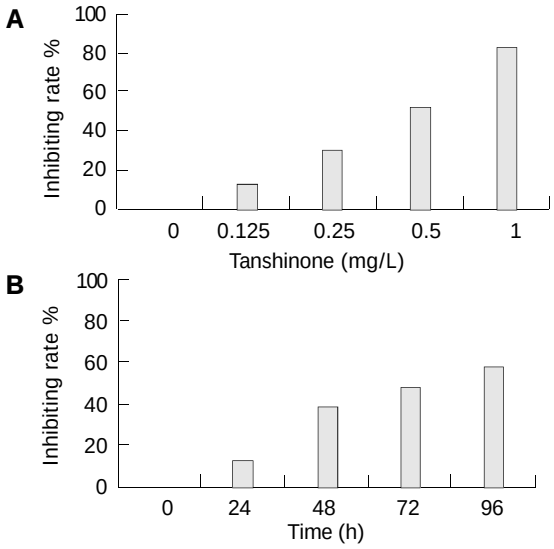

Figure 1 Growth-inhibitory effect of Tan II-A on SMMC-7721 cells detected by MTT. A: In a dose-dependent manner detected by MTT; B: In a time-dependent manner detected by MTT.

Morphological changes of apoptosis

As shown in Figure 2, Tan II-A-induced morphological changes were evident by 72 h of treatment in SMMC-7721 cell. Roundish, large and serried cells (in control group, Figure 2A) became polygonal, small, detached or sparse, membranous frothed and wizened (Tan II-A group, Figure 2B) in the dishes under light microscope. The ultrastructural characteristics of apoptosis such as chromatin condensation, crescent formation, margination and apoptotic bodies were observed by electron microscopy in the Tan II-A group (Figure 3), which were more obvious in the given experimental period than that in the control group.

DNA fragments

Agarose gel electrophoresis exhibited DNA ladder formation in SMMC-7721 cell after exposed to different concentration of Tan II-A for 96 h. Compared with control, the DNA ladder was

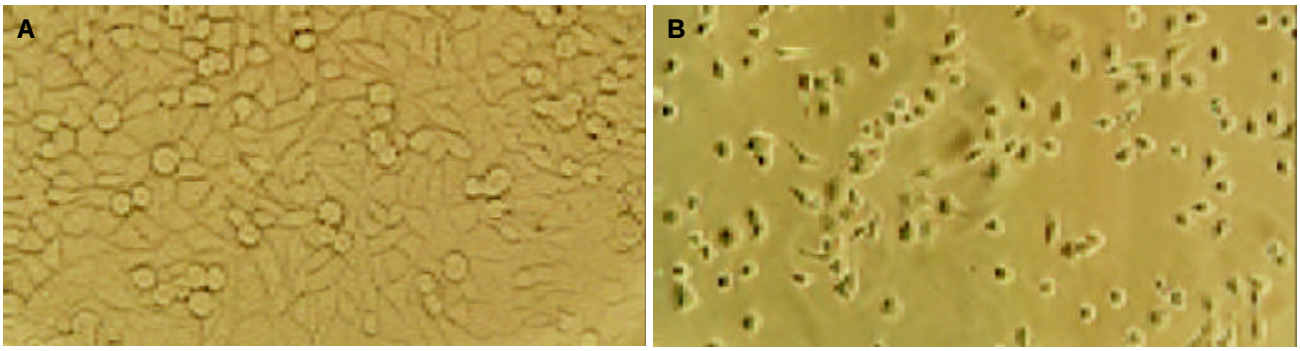

Figure 2 Morphological characteristics of SMMC-7721 cells before and after Tan II-A treatment. A: Roundish, large and serried SMMC-7721cells (in control group); B: Polygonal, small, detached or sparse, membranous frothed and wizened SMMC-7721cells (in Tan II A group).

more clearly observed by treatment with 0.5, 1.0 and 2.0 mg/L Tan II-A, while the DNA fragment induced by 0.125, 0.25 mg/L Tan II-A was not clear (Figure 4).

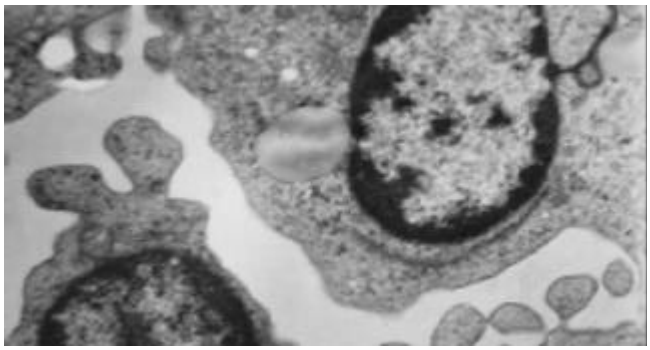

Figure 3 Ultrastructural changes of SMMC-7721 cells with 1.0 mg/L Tan II-A treatment for 96 h under TEM (×10 000). The chromatin condensation, original margination were observed.

Figure 4 DNA agarose gel electrophoresis of SMMC-7721 cells with Tan II-A treatment for 96 h. Lane 1: Marker, Lane 2: Control, Lane 3: 2.0 mg.L^{-1}, Lane 4: 1.0 mg.L^{-1}, Lane 5: 0.5 mg.L^{-1}.

Cell cycle effect

In order to determine the effect of Tan II-A on proliferation and apoptosis in SMMC-7721 cell, the cells were exposed to 0.5 mg/L Tan II-A for 96 h. Cell cycle distribution, cell proliferation and apoptotic damage of DNA were determined on a flow cytometer. The result showed the accumulation of cells in G_0/G_1 and a corresponding reduction in percentages of cells in S and G_2/M phase, and decreased proliferation index (PI). The cells in sub-G_1 phase were increased. An apoptotic peak was detected (Table 1, Figure 5)

Table 1 Effect of Tan II-A on cell cycle distribution and apoptosis in SMMC-7721

Group	Cell cycle distribution (%)			PI %	AI %
	G_0/G_1	S	G_2/M		
Control	71.3±2.3	9.8±0.6	18.9±1.6	28.7±2.6	4.9±0.4
Tan II-A	77.8±3.8^b	7.2±0.5^b	15.0±1.2^b	22.2±2.2^b	16.9±1.2

χ^2 test. $^bP<0.01$ *vs* control group.

Table 2 Effect of Tan II-A on apoptosis associated gene expression of SMMC-7721

Group	Positive rate of protein expression (%)				
	fas	p53	bax	bcl-2	c-myc
Control	19.7±0.5	21.4±1.6	20.2±1.6	27.9±2.4	23.8±1.8
Tan II A	28.4±2.5^b	39.1±3.1^b	31.5±2.7^b	16.3±1.3^b	14.6±1.1^b

χ^2 test, $^bP<0.01$ *vs* control group.

Apoptosis-associated genes expression

The expressions of apoptosis associated genes *fas, bax, p53* were up-regulated. The expressions of *bcl-2* and *c-myc* were

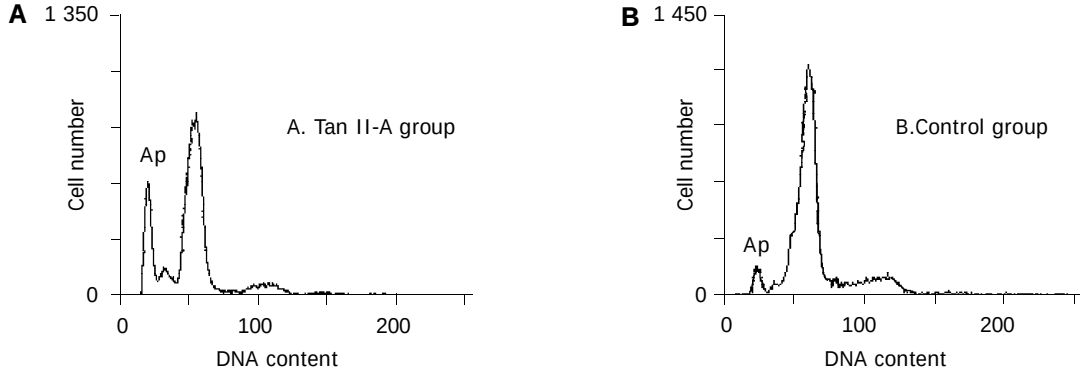

Figure 5 Flow cytometry analysis of apoptosis in SMMC-7721 cells treated with Tan II-A (A) and DMSO (B).

down-regulated (Table 2). The tabulated percentages were an average calculated on the results of three separate experiments. The values were presented as mean±SE (n=3).

DISCUSSION

Cellular proliferation and apoptosis in normal tissue maintain a balance. Unlimited growth and proliferation, but blocked apoptosis are main characteristics of malignant tumor cell. So inhibiting proliferation by apoptosis induction of cancer cell is a new method for cancer control and therapy[18-20].

On the basis of previous studies, we chose different concentrations of non-cytotoxic Tan II-A to study Tan II-A induced-apoptosis *in vitro*. MTT, cell count assay and colony-forming assay showed that 0.25, 0.5, 1.0 mg/L Tan II-A obviously inhibited the growth and proliferation of SMMC-7721, and the inhibiting effect was in a dose- and time-dependent manner. The most significant effect was observed at 72 h by 1.0 mg/L Tan II-A. Flow cytometer showed that Tan II-A produced significant cell cycle arrest in G_0/G_1, decreased proliferation index (PI) as evidence of an antiproliferation effect. The cellular growth and inhibition could be observed by morphology. The morphological characteristics of cellular growth inhibition were also observed under light microscope. Our results demonstrated that Tan II-A inhibited growth and proliferation of SMMC-7721 cells[21,22].

Apoptosis, or programmed cell death, has an essential role in controlling cell number in many developmental and physiological settings and in chemotherapy-induced tumour-cell killing. The execution of apoptosis may be initiated by many different signals, either from within or outside the cell involving ligand-receptor interactions, as has been shown for Fas/Fas-ligand, or potentially by more unspecific signals such as DNA damage. During the modulation phase of apoptosis many different genes such as *p53*, *c-myc* or *Bcl-2*/*Bax* have been shown to be able to shift the balance either to cellular proliferation or death. Cellular growth and proliferation are closely related to apoptosis[23-25].

The detection of apoptotic cell by microscopy is based on several well-established morphological features. These features include condensation of chromatin and cytoplasm as well as fragmentation of the cells that lead to the appearance of membrane bound apoptotic bodies[26]. Those ultrastructural characteristics apoptosis, the DNA ladder and increased cells in sub-G_1 phase were observed in SMMC-7721 cells treated with 0.5, 1.0 mg/L Tan II-A.

Apoptosis-associated genes play a major role in apoptosis, participating in the initiation and progress of programmed cell death. *Bcl-2* has been identified as an apoptosis inhibitor, and shown to cooperate with *c-myc* in immortalizing cells. Under certain conditions, constitutive expression of *c-myc* induces apoptosis and can be suppressed by *bcl-2*. It appears that the *c-myc* cooperating oncogenic activity of *bcl-2* is related to its inhibition of apoptotic pathways[26]. Bax protein inhibits the function of *bcl-2* leading to increased apoptosis.

The tumor suppressor gene *p53*, a transcription factor, has been identified as a participant in the cellular DNA damage response. Upon DNA damage, *p53* up-regulation causes G1 arrest. The apoptosis promoting capacity of *p53* is presumably due to its ability to activate *bax*, a gene that encodes an inhibitor of *bcl-2*. Fas (CD95/APO-1) is a death-promoting receptor that belongs to the tumor necrosis factor (TNF) receptor family, and induces apoptosis through different ways[27].

In the present study, we observed down-regulation of *bcl-2* and *c-myc* expression, which is in keeping with the role of *bcl-2* in blocking apoptosis and *c-myc* in promoting proliferation. At the same time, the expressions of apoptosis associated genes *fas*, *bax*, *p53* were up-regulated. These suggested that *Bcl-2*, *c-myc*, *fas*, *bax* and *p53* were involved in apoptosis of hepatocarcinoma cells induced by Tan II-A. Parts of these mechanisms were related to inhibition of cell growth. Some results of our study on inducing apoptosis in human hepatocellular carcinoma cell are consistent with other researches[28].

Tan II-A inhibits growth and proliferation of hepatocarcinoma cells by inducing apoptosis. Tan II-A might have different mechanisms in inducing apoptosis and inhibiting proliferation of cancer cells. Other possible mechanisms of the action of Tan II-A need to be further investigated. We consider that Tan II-A could be a new prospective, highly effective and low toxic anticancer drug.

REFERENCES

1 **Kanzler S,** Galle PR. Apoptosis and the liver. *Semin Cancer Biol* 2000; **10**: 173-184
2 **Carson DA,** Ribeiro JM. Apoptosis and disease. *Lancet* 1993; **341**: 1251-1254
3 **Kerr JF,** Winterford CM, Harmon BV. Apoptosis. Its significance in cancer and cancer therapy. *Cancer* 1994; **73**: 2013-2026
4 **Thompson CB.** Apoptosis in the pathogenesis and treatment of disease. *Science* 1995; **267**: 1456-1462
5 **Lee SM,** Li ML, Tse YC, Leung SC, Lee MM, Tsui SK, Fung KP, Lee CY, Waye MM. Paeoniae Radix, a Chinese herbal extract, inhibit hepatoma cells growth by inducing apoptosis in a p53 independent pathway. *Life Sci* 2002; **71**: 2267-2277
6 **Li ZT,** Yang BJ, Ma GE. Chemical studies of Salvia miltiorrhiza f. alba. *Yaoxue Xuebao* 1991; **26**: 209-213
7 **Lin TJ.** Antioxidation mechanism of schizandrin and tanshinonatic acid A and their effects on the protection of cardiotoxic action of adriamycin. *Shengli Kexue Jinzhan* 1991; **22**: 342-345
8 **Liang Y,** Yang YM, Yuan SL. Studies on Pharmic mechanism and clinic application of Tanshinone. *Traditional Herbal Drugs* 2000; **31**: 304-306
9 **Wu WL,** Chang WL, Chen CF. Cytotoxic activities of tanshinones against human carcinoma cell lines. *Am J Chin Med* 1991; **19**: 207-216
10 **Yuan S,** Huang G, Wang X. The differentiation-inducing effect of tanshinone and retinoic acid on human cervical carcinoma cell line *in vitro*. *Zhonghua Zhongliu Zazhi* 1995; **17**: 422-424
11 **Liang Y,** Yang Y, Yuang S, Liu T, Jia Y, Xu C, Niu T, Qin H, Qin P. Terminal differentiation of human acute promyelocytic leukemia (APL) cells induced by Tanshinone II A in primary culture. *Huaxi Yike Daxue Xuebao* 2000; **31**: 207-210
12 **Yoon Y,** Kim YO, Jeon WK, Park HJ, Sung HJ.Tanshinone IIA isolated from Salvia miltiorrhiza BUNGE induced apoptosis in HL60 human premyelocytic leukemia cell line. *J Ethnopharmacol* 1999; **68:** 121-127
13 **Sung HJ,** Choi SM, Yoon Y, An KS. Tanshinone IIA, an ingredient of Salvia miltiorrhiza BUNGE, induces apoptosis in human leukemia cell lines through the activation of caspase-3. *Exp Mol Med* 1999; **31:** 174-178
14 **Wang X,** Yuan S, Wang C. A preliminary study of the anticancer effect of tanshinone on hepatic carcinoma and its mechanism of action in mice. *Zhonghua Zhongliu Zazhi* 1996; **18:** 412-414
15 **Yuan S,** Wang Y, Chen X, Song Y, Yang Y. A study on apoptosis of nasopharyngeal carcinoma cell line induced by Tanshinone II A and its molecular mechanism. *Huaxi Yike Daxue Xuebao* 2002; **33:** 84-86
16 **Yuan SL,** Huang RM, Wang XJ, Song Y, Huang GQ. Reversing effect of Tanshinone on malignant phenotypes of human hepatocarcinoma cell line. *World J Gastroenterol* 1998; **4:** 317-319
17 **Ai ZW.** Reversing effect of retinoic acid on some phenotypes of human hepatocarcinoma cell line. *Zhonghua Zhongliu Zazhi* 1991; **13:** 9-12
18 **Marx J.** Cell death studies yield cancer clues. *Science* 1993; **259:**

760-761

19 **Sakuma H,** Yamamoto M, Okumura M, Kojima T, Maruyama T, Yasuda K. High glucose inhibits apoptosis in human coronary artery smooth muscle cells by increasing bcl-xL and bfl-1/A1. *Am J Physiol Cell Physiol* 2002; **283:** C422-428

20 **Tsuda H,** Sata M, Ijuuin H, Kumabe T, Uchida M, Ogou Y, Akagi Y, Shirouzu K, Hara H, Nakashima Y. A novel strategy for remission induction and maintenance in cancer therapy. *Oncol Rep* 2002; **9:** 65-68

21 **Hu W,** Kavanagh JJ. Anticancer therapy targeting the apoptotic pathway. *Lancet Oncol* 2003; **4:** 721-729

22 **Giridharan P,** Somasundaram ST, Perumal K, Vishwakarma RA, Karthikeyan NP, Velmurugan R, Balakrishnan A. Novel substituted methylenedioxy lignan suppresses proliferation of cancer cells by inhibiting telomerase and activation of c-myc and caspases leading to apoptosis. *Br J Cancer* 2002; **87:** 98-105

23 **Fimognari C,** Nusse M, Cesari R, Iori R, Cantelli-Forti G, Hrelia P. Growth inhibition, cell-cycle arrest and apoptosis in human T-cell leukemia by the isothiocyanate sulforaphane. *Carcinogenesis* 2002; **23:** 581-586

24 **Altieri DC.** Survivin, versatile modulation of cell division and apoptosis in cancer. *Oncogene* 2003; **22:** 8581-8589

25 **Suda T,** Takahashi T, Golstein P, Nagata S. Molecular cloning and expression of the Fas ligand, a novel member of the tumor necrosis factor family. *Cell* 1993; **75:** 1169-1178

26 **Barnhart BC,** Lee JC, Alappat EC, Peter ME. The death effector domain protein family. *Oncogene* 2003; **22:** 8634-8644

27 **Lyu SY,** Choi SH, Park WB. Korean mistletoe lectin-induced apoptosis in hepatocarcinoma cells is associated with inhibition of telomerase via mitochondrial controlled pathway independent of p53. *Arch Pharm Res* 2002; **25:** 93-101

28 **Rahman MA,** Dhar DK, Masunaga R, Yamanoi A, Kohno H, Nagasue N. Sulindac and exisulind exhibit a significant antiproliferative effect and induce apoptosis in human hepatocellular carcinoma cell lines. *Cancer Res* 2000; **60:** 2085-2089

Edited by Chen WW **Proofread by** Zhu LH and Xu FM

PO Box 2345, Beijing 100023, China
Fax: +86-10-85381893
E-mail: wjg@wjgnet.com www.wjgnet.com

World J Gastroenterol 2004;10(14):2029-2033
World Journal of Gastroenterology
 ISSN 1007-9327

• LIVER CANCER •

Prokaryotic expression and renaturation of engineering chimeric Fab antibody against human hepatoma

Jin-Liang Xing, Xiang-Min Yang, Xi-Ying Yao, Fei Song, Zhi-Nan Chen

Jin-Liang Xing, Xiang-Min Yang, Xi-Ying Yao, Fei Song, Zhi-Nan Chen, Cell Engineering Research Center, Faculty of Preclinical Medicine, Fourth Military Medical University, Xi' an 710032, Shaanxi Province, China
Supported by the National High Technology Research and Development Program of China (863 Program), No. 2001AA215101 and the National Natural Science Foundation of China, No. 3020330
Correspondence to: Professor Zhi-Nan Chen, Cell Engineering Research Center, Faculty of Preclinical Medicine, Fourth Military Medical University, Xi' an 710032, Shaanxi Province, China. chcerc2@fmmu.edu.cn
Telephone: +86-29-3374545 **Fax:** +86-29-3293906
Received: 2003-11-13 **Accepted:** 2004-01-15

Abstract

AIM: To express chimeric Fd (cFd) and chimeric light chain (cL) in *E.coli* respectively and refold them into chimeric Fab (cFab) antibody.

METHODS: cFd and cL genes were respectively inserted into the prokaryotic expression vector pET32a to construct recombinant vectors pET32a/cFd and pET32a/cL. Then, the competent *E.coli* cells were transformed by the recombinant vectors and induced by IPTG. Moreover, a large quantity of cFd and cL expression products were prepared and mixed with equal molar to refold into cFab by gradient dialysis. The refolded products were identified and analyzed by sodium SDS-PAGE, Western blotting, ELISA and HPLC.

RESULTS: High efficient prokaryotic expressions of both cFd and cL in the form of non-fusion protein were obtained with the expression levels of 28.3% and 32.3% of total bacteria proteins, respectively. Their relative molecular masses were all 24 ku or so, and both of them mainly existed in the form of inclusion bodies. In addition, cFd and cL were successfully refolded into cFab by gradient dialysis, with about 59.45% of recovery when the starting total protein concentration was 100 μg/mL. The renatured cFab could specifically bind to related antigen with high affinity.

CONCLUSION: The cFab antibody against human hepatoma was highly and efficiently expressed and refolded, which laid a solid foundation for studying its application in the treatment of hepatoma.

Xing JL, Yang XM, Yao XY, Song F, Chen ZN. Prokaryotic expression and renaturation of engineering chimeric Fab antibody against human hepatoma. *World J Gastroenterol* 2004; 10(14): 2029-2033
http://www.wjgnet.com/1007-9327/10/2029.asp

INTRODUCTION

The advent of monoclonal antibody (mAb) greatly promotes application of antibodies in various fields[1]. However, due to immunogenicity and comparatively high molecular mass, mouse derived complete antibody was more or less limited in the application of disease diagnosis and treatment[2]. The cFab antibody is about 50 ku, only 1/3 of full-length IgG. Because of good penetrating ability, better characteristics of pharmaceutical kinetics and good antigen-binding activity, cFab antibody has been used more and more widely[3-5]. Compared with complete antibody, the cFab has no Fc fragment so that non-specific binding is decreased greatly. In addition, the cFab could not produce antibody-dependent cellular cytotoxicity (ADCC) and complement-dependent cytotoxicity (CDC), so it was mostly used as the carrier for targeted delivery of drugs[6]. It could also be further reconstructed into engineering $cF(ab)_2$ antibody[7]. In this paper, based on cloned V_H and V_L genes of mAb HAb18 against human hepatoma[8], we expressed cFd and cL in *E.coli* in the form of non-fusion protein and refolded them into cFab antibody. It was expected that a practical protocol could be established for the preparation of a large quantity of cFab against human hepatoma, which would lay a solid foundation for further studies of its application in hepatoma treatment.

MATERIALS AND METHODS

Materials

The pComb3/cFab vector containing cFd and cL genes of mAb HAb18 was previously constructed in our laboratory. Prokaryotic expression vector pET32a (+) and competent *E. coli JM109(DE3)* were purchased from Novagen Inc (USA). T vector, PCR reagents, restriction endonucleases and T4 DNA ligase were from Takara Inc. (DaLian, China). The mAb HAb18, chimeric IgG antibody chHAb18 and HRP-HAb18 were previously prepared in our laboratory. IPTG, FITC-labeled and HRP-labeled goat anti-human IgG were from SABC Inc. (Luo Yang, China). Protein G affinity column was purchased from Pharmacia Inc (USA). Hepatoma cell line HHCC was from ATCC (Shanghai, China).

Primer design and synthesis

According to gene sequences of HAb18 cFd and cL which were previously constructed in our laboratory, PCR primers were designed by computer software Primer Premier 5.0, and relative restriction endonuclease sites were introduced into primers for the construction of prokaryotic non-fusion expression vectors of cFd and cL. All PCR primers were synthesized by Shenggong Inc. (Shanghai, China), and their sequences were as follows: cFd back: 5' GCGGAATTCATATGGTTAAG CTTGAAGAGTCTGGAGGAGGCTT 3' ; cFd forward: 5' GGGGTCGACTCATTAACTAGTTTTGTCACAAGATTT GGGCT3' ; cL back: 5' GCGGAATTCATATGAGTATTGTGA TGACCCAGACTCCCA3' ; cL forward: 5' GGGCCTCGAG TCATTAACATTCACCTCTGTTGAAGCTCT3' . Underlined sequences are restriction sites *Nde* I, *Sal* I and *Xho* I.

Construction of expression vectors

With the vector pComb3/cFab as template, cFd and cL genes were amplified using related primers. The PCR products were

purified by gel extraction. Then, the plasmid pET32a (+) and PCR amplified cFd or cL gene were digested by a pair of restriction endonucleases *Nde* I and *Sal* I or *Nde* I and *Xho* I. After the corresponding target fragments were purified by gel extraction, ligation, transformation and screening of the positive clones containing the recombinant vector pET32a/cFd or pET32a/cL were sequentially conducted. Finally, recombinant vectors were identified by restriction endonucleases digestion and DNA sequencing was completed by Shenggong Inc. (Shanghai, China).

Small-scale expression by IPTG induction

The *E.coli* cells containing pET32a/cFd or pET32a/cL or pET32a (+) were respectively inoculated with 1:100 into 5 mL LB medium containing ampicillin (100 μg/mL). When absorbance of $A_{600\,nm}$ was up to 0.8 or so, 1 mL *E.coli* cultures were obtained for further assay. Then, IPTG was added to left cultures with 1 mmol/L of final concentration and another 10 h induction of expression (250 r/min, 37 ℃) was conducted. After being treated by boiling and centrifugation, all *E.coli* samples after and before induction were loaded onto 120 g/L SDS-PAGE gel for further analysis. At the same time, Western blotting was done by HRP-labeled goat anti-human IgG (H+L). In addition, *E.coli* cells containing pET32a/cFd and pET32a/cL after induction were collected and treated by repeated freezing and thawing. Then, the location of expression products was investigated by SDS-PAGE.

Renaturation of cFab antibody

A total of 500 mL cultures of *E.coli* containing pET32a/cFd or pET32a/cL were induced for the protein expression under the same condition as mentioned above. Inclusion body was isolated and solubilized by 8 mol/L urea[9]. The total protein concentration was determined by bicinchoninic acid (BCA) assay[10] and the expression percentages of cFd and cL were evaluated by SDS-PAGE. cFd and cL dissolved in urea were mixed with equal molar, and the total protein concentration was adjusted to 100 μg/mL by adding the lysis solution. Renaturation was conducted by gradient dialysis as described by Lee *et al*.[11]. The renatured products were centrifuged, and the supernatant was collected, then the precipitation was dissolved in the lysis solution again. Protein recovery was determined by BCA assay. Single cFd and single cL were set as control at the same refolding condition when cFab was renatured. All samples above were detected by SDS-PAGE, Western blotting and HPLC.

Effect of total protein concentration on renaturation of cFab antibody

After the total protein concentration was respectively adjusted to 200 μg/mL and 400 μg/mL, cFab antibody was renatured according to the method described above. The protein concentration of all samples was detected by BCA assay and protein recovery was evaluated. In addition, all samples were loaded onto SDS-PAGE gel for further analysis.

Purification of renatured cFab antibody

After dialysis in PBS overnight at 4 ℃, renatured cFab was purified by protein G affinity chromatography according to manufacturer's protocol.

Detection of antigen-binding activity of purified cFab antibody

Indirect ELISA GST-HAb18GE, GST-fusion expression product of extracellular region of HAb18G[12] was the antigen of mAb HAb18, and the purified GST expression products were coated on the ELISA plates for detecting the antigen-binding activity of purified cFab antibody. Detailed protocol was described by Yan *et al*.[13].

Competitive binding assay GST-HAb18GE was coated on ELISA plates overnight at 4 ℃. After blocking, the mixture of HRP-HAb18 (0.1 mg/L) and gradiently diluted cFab was added into ELISA plates. After incubation for 1 h at 37 ℃, the unbound antibody was washed away by PBST, followed by TMB staining. Finally, A_{450} was detected by an ELISA plate reader (Bio-Rad, USA), and inhibition rate and comparative affinity were determined according to the following method: Inhibition rate (%)=[(A_{450} of control group-A_{450} of experimental group)/A_{450} of control group]×100%; comparative affinity (%)=[concentration of cFab when inhibition rate is 50%/concentration of HRP-HAb18(0.1 mg/L)]×100%.

FACS detection The single-cell suspension of hepatoma cell line HHCC overexpressing HAb18G was prepared. The cell density was adjusted to 5×10^9-1×10^{10}/L. HAb18 cFab diluted with horse serum was added into 50 μL HHCC single-cell suspension. Then, the mixture was incubated for 30 min at 4 ℃. After washed twice by PBS, FITC-labeled rabbit anti-human IgG was added and the reaction mixture was incubated for 30 min at 4 ℃. Then, washing and detecting were performed. In this assay, human IgG was set as negative control and PBS was set as blank control.

RESULTS

Construction of recombinant expression vectors

cFd and cL genes were successfully amplified using designed primers. Agarose gel electrophoresis showed that the sizes of cFd and cL genes were about 700 bp and 680 bp, respectively (lanes 2,5, Figure 1), which was in accordance with their expected sizes. The recombinant vectors pET32a/cFd and pET32a/cL digested by restrictive endonucleases (Figure 1) indicated that cFd and cL genes were correctly inserted into corresponding cloning sites. The results of DNA sequencing (results not provided) proved that cFd and cL genes inserted in expression vector had no base mutation and the codon reading frame was completely exact.

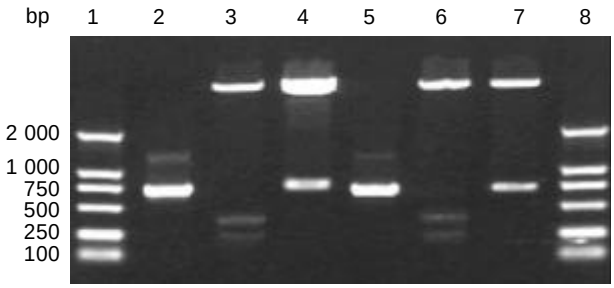

Figure 1 Analysis of recombinant non-fusion expression vectors pET32a/cFd and pET32a/cL digested by restrictive endonucleases. 1: DNA marker; 2: cFd; 3: pET32a/ *Nde* I+*Sal* I; 4: pET32a/ cFd/ *Nde* I+*Sal* I; 5: cL; 6: pET32a/*Nde* I+*Xho* I; 7: pET32a/ cL /*Nde* I+*Xho* I; 8: DNA marker.

Expression induction and identification of cFd and cL

SDS-PAGE (Lanes 1-7, Figure 2) showed that a 21-ku new protein was expressed in *E.coli* transformed by control vector after induction, which is in accordance with the expression characteristics of the control vector, and that the recombinant cFd and cL with the same molecular weight of 24 ku were also successfully expressed after induced by IPTG. Scanning analysis by Smartview software indicated that the quantities of expressed cFd and cL were about 28.3% and 32.3% of the total bacterial protein, respectively. Western blotting (Lanes A-D, Figure 2) identified that both expressed cFd and cL were able to bind to anti-human IgG and the staining bands were at 24 ku. In addition, SDS-PAGE showed that the interested expression products existed in the form of insoluble inclusion body (Figure 3).

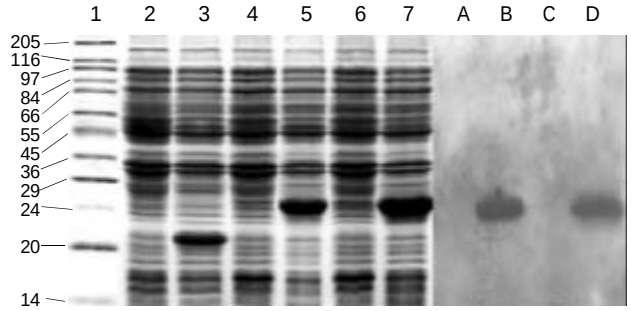

Figure 2 SDS-PAGE and Western blotting of the expressed products of cFd and cL. 1: High molecular mass marker; 2: Uninduced pET32a; 3: Induced pET32a; 4: Uninduced pET32a / cFd; 5: Induced pET32a / cFd; 6: Uninduced pET32a / cL; 7: Induced pET32a / cL; A: Uninduced pET32a / cFd; B: Induced pET32a / cFd; C: Uninduced pET32a / cL; D: Induced pET32a / cL.

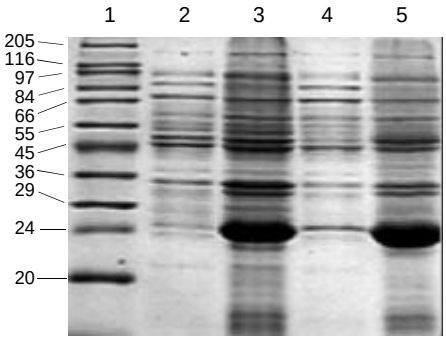

Figure 3 Location analysis of cFd and cL expression products on SDS-PAGE. 1: High molecular mass marker; 2: Supernatant of induced pET32a / cFd; 3: Inclusion body of induced pET32a / cFd; 4: Supernatant of induced pET32a / cL; 5: Inclusion body of induced pET32a / cL.

Renaturation of cFab antibody

The total protein concentrations of inclusion body solution in 8 mol/L urea containing cFd or cL determined by BCA assay were respectively 12.04 mg/mL and 9.66 mg/mL. The results (not provided) of SDS-PAGE analysis indicated that cFd and cL were up to 49.8% and 58.3% in the total protein of inclusion body solution, respectively. SDS-PAGE (Figure 4, lanes 1-7) also showed that the new 45-ku protein band appeared under nonreduced condition after cFd and cL were mixed to refold. Western blotting (lanes A, B, Figure 4) also identified that the new protein bands could bind to anti-human IgG under reduced and nonreduced conditions. The recovery rate was about 75% when the starting concentration of total protein was 100 μg/mL. In addition, when the starting total protein concentration was separately increased to 200 μg/mL and 400 μg/mL, recovery rate was respectively decreased to 70.5% and 61%. SDS-PAGE (Figure 5) demonstrated that precipitation rose rapidly with the increase of starting total protein concentration, and the percentage of elevated precipitation was more than that of increased starting total protein concentration. HPLC analysis (Figure 6) showed that two new elution peaks (1) and (2) emerged after cFd and cL were mixed to refold in comparison with single refolded cFd and cL. The largest absorbance value of elution peak (2) was at 260 nm, so it was possible that elution peak (2) was not protein peak. In addition, the position of elution peak (3) was the same as elution peak (4) of refolded cFd and elution peak (5) of refolded cL. ELISA(result not provided) demonstrated that only elution peak (1) had specific antigen-binding activity. The peak areas of elution peak (1) and (3) were 33.49% and 17.75%, respectively. Renaturation yield of cFab antibody was about 49% determined by the method described previously.

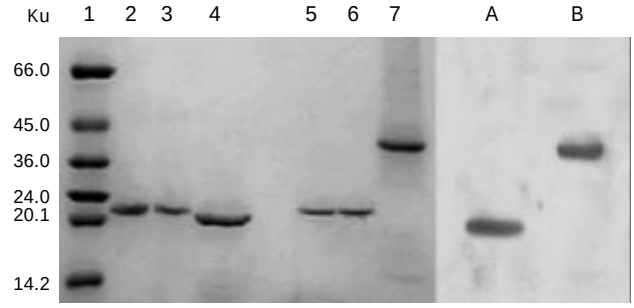

Figure 4 SDS-PAGE and Western blotting of renaturation of cFab antibody. 1: High molecular mass marker; 2: Reduced cFd; 3: Reduced cL; 4: Reduced cFab; 5: Unreduced cFd; 6: Unreduced cL; 7: Unreduced cFab; A: Western blotting of reduced cFab; B: Western blotting of unreduced cFab.

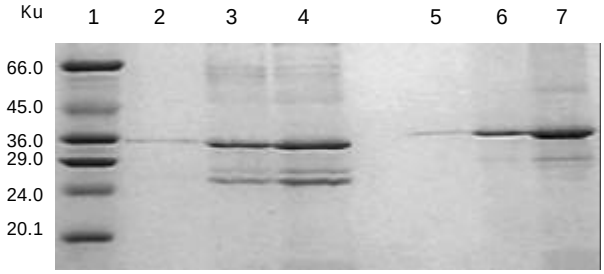

Figure 5 Relationship between the starting total protein concentration and denaturation analyzed by SDS-PAGE. 1: High molecular mass marker; 2, 3, 4: Precipitated proteins under reduced condition at starting total protein concentrations of 100, 200, 400 μg / mL, respectively; 5, 6, 7: Precipitated proteins under unreduced condition at starting total protein concentrations of 100, 200, 400 μg / mL, respectively.

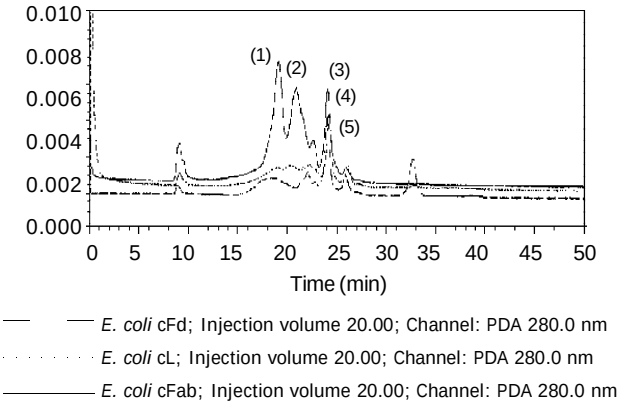

Figure 6 HPLC of cFd, cL and cFab after renaturation.

Analysis of antigen-binding activity of purified cFab antibody

cFab 1 mL (80 μg/mL) was purified by protein G affinity chromatography. Indirect ELISA (Figure 7) showed that cFab was capable of specific binding to HAb18GE and the antigen-binding activity became higher with increasing concentration of cFab antibody. Competitive ELISA (Figure 8) indicated that the refolded cFab could competitively bind to the same antigen epitope as parental mouse antibody HAb18 and the binding ability improved with the increase of cFab antibody concentration. The affinity of cFab was evaluated to be 10% of parental mouse antibody HAb18 according to the concentration ratio of cFab and HAb18 when inhibition rate was 50%. FACS detection (Figure 9) demonstrated that cFab could bind specifically to hepatoma cell line HHCC and the binding capacity increased with the elevation of cFab antibody concentration.

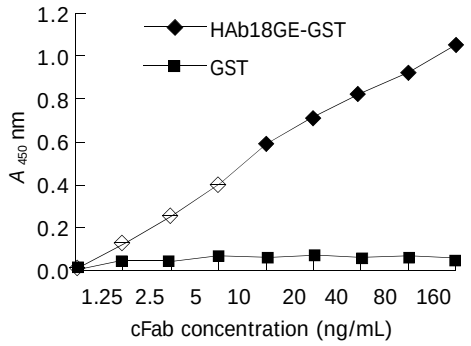

Figure 7 Detection of antigen-binding specificity of cFab by indirect ELISA.

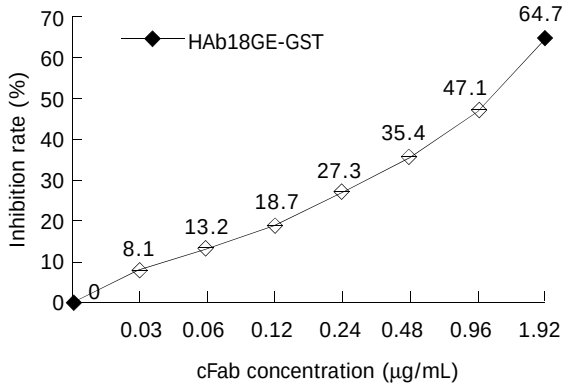

Figure 8 Detection of antigen-binding activity of cFab and HAb18 by competitive ELISA.

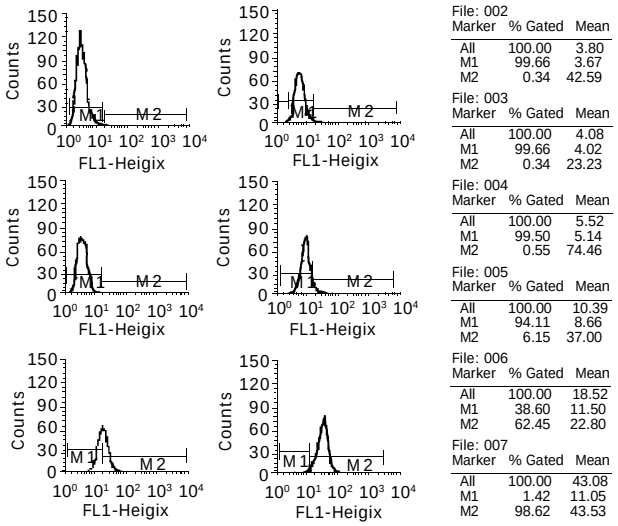

Figure 9 Detection of antigen-binding activity of cFab by FACS. 002: Negative control; 003: 0.008 μg / mL; 004: 0.04 μg / mL; 005: 0.2 μg / mL; 006: 1 μg / mL; 007: 5 μg / mL.

DISCUSSION

In a previous study, we successfully expressed cFab antibody gene in the periplasmic compartment of *E.coli*. However, the productivity was rather low. So, we tried to improve the expression level of cFab. We separately expressed cFd and cL without signal peptide in cytoplasm of *E.coli* in the form of inclusion body. The expression levels of different fragment of antibody genes in *E.coli* were greatly diverse, which mainly depended on the design of translation initiation site, the type of antibody fragment, antibody gene sequence, sensitivity to proteases of expression products and the class of host bacterium, *etc*[14]. But high efficient expression of antibody genes was relatively easy to be obtained using prokaryotic expression vector. We successfully constructed recombinant vectors pET32a/cFd and pET32a/cL by cloning cFd and cL genes into the pET32a expression vector, and achieved high expression level of cFd and cL in *E.coli*. The expression products mainly existed in the form of the inclusion body, with 28.3% and 32.3% of expression percentages of total bacterial protein, respectively. Expression proteins in inclusion body could avoid being digested by proteases and were easy to be isolated and purified. cFd and cL must be refolded together in order to get active cFab.

As we know, effectively promoting the correct formation of intramolecular or intermolecular disulfide bond and inhibiting the formation of aggregation were key to protein renaturation[15]. In order to promote the refolded protein to form the correct disulfide bond, some reducers, such as β-sulfhydryl ethanol and DTT, were added into detergent solution to unfold wrong disulfide bonds of expression proteins in inclusion body. These wrong disulfide bonds might be formed during the lysis of host bacterium or during the resolving process of expression protein. When the protein was renatured, correct disulfide bonds could be reformed only by air oxidation[16]. In most cases, iron can promote the process of air oxidation[17]. In addition, the repeated formation and unclosing of the disulfide bonds may increase the probability of obtaining protein with correct conformation. This process could be facilitated by some enzymes (such as disulfide isomerase)[18] or oxidation-reduction response caused by the oxidation- and reduction-type sulfhydryl mixture[17](such as glutathione). During the renaturation, the formation of aggregation was the most common reason resulting in lower renaturation efficiency. However, the mechanism of aggregation formation is still unclear. De Bern ardez Clark *et al*.[19] suggested that the hydrophobic action among protein molecules was the most likely explanation for the aggregation formation facilitated by the formation of wrong disulfide bonds. In the experiment of mixed protein renaturation involving two or more proteins, small aggregation was first caused by the hydrophobic action, and then by the disulfide bonds formation from unpaired cystines that resulted in the formation of big heterogeneous aggregation. The formation of large quantities of aggregation would result in more protein precipitation, therefore, renaturation efficiency decreased greatly[11]. The previous study on renaturation also showed that arginine, a kind of stable reagent promoting protein dissolving during renaturation, could facilitate the correct folding of proteins possibly by inhibiting the formation of bigger aggregation[20].

In this study, we mixed cFd and cL with equal molar. The detergent was slowly removed from the mixture by gradient dialysis in the presence of a given concentration of arginine, while glutathione was added into the mixture to delete wrong reduced disulfide bonds. The results showed that this strategy for renaturation was successful. At the starting total protein concentration of 100 μg/mL, cFd and cL were refolded into cFab with 75% of protein recovery rate. Protein loss was mainly due to protein precipitation and adsorption onto dialysis belt. Replacing dialysis materials could reduce the latter loss. We identified the renatured cFab by SDS-PAGE, Western blotting and ELISA. The results proved that cFd and cL were successfully refolded into cFab. SDS-PAGE indicated that the molecular weight of renatured cFab was about 45 ku under the unreduced condition, less than 48 ku (cFd+cL), which revealed that the formation of intramolecular disulfide bond happened in the renatured protein[15]. HPLC of renatured products revealed that the renatured cFab produced two very different elution peaks. ELISA demonstrated that only elution peak (1) had antigen-binding activity. In addition, the biggest absorbance value of elution peak (2) was at 260 nm, which

revealed that elution peak (2) might be nuclear acid existing in inclusion body. It was estimated by HPLC that the renaturation efficiency was up to 49%, which was quite desirable in comparison with the generally 10-40% of renaturation efficiency for antibody protein. The desirable renaturation efficiency was mainly explained by good renaturation strategy and special antibody sequences, which are in accordance with the viewpoint of Wibbenmeyer *et al*.[21]. It was also estimated that dozens of milligrams of active cFab could be gained from 1 L of *E.coli* cultures under the experimental condition described above. Therefore, further optimizing the preparation protocol can increase the yield.

When preparing a large quantity of active protein by dialysis renaturation method, another important influence factor must be taken into consideration, namely the volume of renaturation protein solution. The speed of protein aggregating and precipitating was positively correlated with the protein concentration, so protein precipitation would be predominant course when protein concentration was up to the highest point. As a result, the starting total protein concentration was generally very low, which would inevitably result in excessively large sample volume to be dealt with otherwise more troubles would arise. In this study, in order to explore the optimal renaturation condition of preparing a large quantity of cFab antibody, we increased the starting total protein concentration for renaturation to 200 μg/mL and 400 μg/mL, respectively, and investigated the renaturation efficiency after the protein concentration was increased. The results revealed that protein precipitation promptly increased with the increase of starting protein concentration, and increased percentage was more than that of protein concentration increase, which indicated that a part of renaturation efficiency was surely sacrificed in order to reduce the treatment volume and increase the speed of preparation during the large-scale production of cFab.

In conclusion, we successfully obtained cFab antibody with good activity by prokaryotic expression technique, followed by dialysis, which laid a solid foundation for further application in hepatoma treatment. In addition, based on this achievement, we are planning to modify cFab genes to produce another kind of more useful engineering antibody, bivalent chimeric F (ab')$_2$[22]. It is expected to replace murine-derived F (ab')$_2$ antibody produced by protease digestion, and reduce clinical cost and improve therapeutic efficacy.

REFERENCES

1 **Chen ZN,** Bian HJ, Jiang JL. Recent progress in anti-hepatoma monoclonal antibody and its application. *Huaren Xiaohua Zazhi* 1998; **6**: 461-462

2 **Hasholzner U,** Stieber P, Meier W, Lamerz R. Value of HAMA–determination in clinical practice-an overview. *Anticancer Res* 1997; **17**: 3055-3058

3 **Quinn MJ,** Plow EF, Topol EJ. Platelet glycoprotein IIb/IIIa inhibitors: recognition of a two-edged sword? *Circulation* 2003; **107**: E39-E39

4 **Lai ZZ,** Xiong DS, Fan DM, Peng H, Xu YF, Zhu ZP, Yang YZ. High expression of the chimeric antibody Fab against-CD_{20} in *E coli* and bioactivity determination. *Zhongguo Mianyixue Zazhi* 2000; **16**: 521-524

5 **Xia L,** Gu J, Zhang X, Liu Y, Wan H, Li P, Ruan C. Preparation of an antifibrin thrombus-specific murine/human chimeric monoclonal antibody Fab fragment in *Escherichia coli*. *Thromb Res* 1996; **8**: 477-484

6 **Better M,** Bernhard SL, Lei SP, Fishwild DM, Lane JA, Carroll SF, Horwitz AH. Potent anti-CD5 ricin A chain immunoconjugates from bacterially produced Fab' and F(ab')2. *Proc Natl Acad Sci U S A* 1993; **90**: 457-461

7 **Humphreys DP**, Vetterlein OM, Chapman AP, King DJ, Antoniw P, Suitters AJ, Reeks DG, Parton TA, King LM, Smith BJ, Lang V, Stephens PE. F (ab')$_2$ molecules made from Escherichia coli produced Fab' with hinge sequences conferring increased serum survival in an animal model. *J Immunol Methods* 1998; **217**: 1–10

8 **Lou C,** Chen ZN, Bian HJ, Li J, Zhou SB. Pharmacokinetics of radioimmunotherapeutic agent of direct labeling mAb 188Re-HAb18. *World J Gastroenterol* 2002; **8**: 69-73

9 **Wu JY,** Jiang YH, Wang J, Zhang HB, Li M. Purification of recombinant human angiogenin. *Guangdong Yixue* 1999; **20**: 85

10 **Guo YJ,** Wu D, Chen RW, Sun SH. Purification and expression and cloning of porcine INF γ gene. *Shengwu Gongcheng Xuebao* 2001; **17**: 183-186

11 **Lee MH,** Kwak JW. Expression and functional reconstitution of a recombinant antibody (Fab') specific for human apolipoprotein B-100. *J Biotechnol* 2003; **101**: 189-198

12 **Xing JL,** Chen ZN, Mi L, Li Y, Feng Q. Establishment of CHO cell strain that can highly efficiently express hepatoma associate antigen HAb18G. *Zhongliu* 2001; **21**: 4-7

13 **Yan ZY,** Wang HL. Jingbian Fenzishengwuxue Shiyan Zhinan [M]. *Beijing: Science Press* 1998

14 **Laden JC,** Philibert P, Torreilles F, Pugniere M, Martineau P. Expression and folding of an antibody fragment selected *in vivo* for high expression levels in Escherichia coli cytoplasm. *Res Microbiol* 2002; **153**: 469-474

15 **Middelberg AP.** Preparative protein refolding. *Trends Biotechnol* 2002; **20**: 437-443

16 **Anfinsen CB,** Haber E, Sela M, White FH Jr. The kinetics of formation of native ribonuclease during oxidation of the reduced polypeptide chain. *Proc Natl Acad Sci U S A* 1961; **47**: 1309-1314

17 **Saxena VP,** Wetlaufer DB. Formation of three-dimensional structure in proteins. I. Rapid nonenzymic reactivation of reduced lysozyme. *Biochemistry* 1970; **9**: 5015-5023

18 **Carmichael DF,** Morin JE, Dixon JE. Purification and characterization of a thiol: protein disulfide oxidoreductase from bovine liver. *J Biol Chem* 1977; **252**: 7163-7167

19 **De Bernardez Clark E,** Hevehan D, Szela S, Maachupalli-Reddy J. Oxidative renaturation of hen egg-white lysozyme. Folding *vs* aggregation. *Biotechnol Prog* 1998; **14**: 47-54

20 **Timasheff SN,** Arakawa T. Stabilization of protein structure by solvents. In: Creighton TE. Ed. Protein Structure: A Practical Approach, 2nd ed. Oxford: *IRL Press* 1997

21 **Wibbenmeyer JA,** Xavier KA, Smith-Gill SJ, Willson RC. Cloning, expression, and characterization of the Fab fragment of the anti-lysozyme antibody HyHEL-5. *Biochim Biophys Acta* 1999; **1430**: 191-202

22 **Rodrigues ML,** Snedecor B, Chen C, Wong WL, Garg S, Blank GS, Maneval D, Carter P. Engineering Fab' fragments for efficient F (ab) 2 formation in *Escherichia coli* and for improved *in vivo* stability. *J Immunol* 1993; **151**: 6954-6961

Edited by Chen WW **Proofread by** Zhu LH and Xu FM

PO Box 2345, Beijing 100023, China
Fax: +86-10-85381893
E-mail: wjg@wjgnet.com www.wjgnet.com

World J Gastroenterol 2004;10(14):2034-2038
World Journal of Gastroenterology
 ISSN 1007-9327

• LIVER CANCER •

Expression of cancer-testis antigens in hepatocellular carcinoma

Li Zhao, Dong-Cheng Mou, Xi-Sheng Leng, Ji-Run Peng, Wan-Xiang Wang, Lei Huang, Shu Li, Ji-Ye Zhu

Li Zhao, Xi-Sheng Leng, Ji-Run Peng, Wan-Xiang Wang, Lei Huang, Shu Li, Ji-Ye Zhu, Center of Hepatobiliary Surgery, People' s Hospital, Peking University, Beijing 100044, China
Dong-Cheng Mou, Department of General Surgery, First Affiliated Hospital of TsingHua University, Beijing 100016, China
Supported by the National Natural Science Foundation of China, No. 30200271, and the National Key Technologies Research and Development Program of China during the 9th Five-Year Plan Period, No. 2001BA703B04, and the Clinical Program of Ministry of Health of China (2001) and Center for Human Disease Genomics of Peking University (2001-6)
Co-first-authors: Li Zhao and Dong-Cheng Mou
Correspondence to: Dr. Xi-Sheng Leng, Center of Hepatobiliary Surgery, People' s Hospital, Peking University, 11 XiZhimen Nandajie, West District, Beijing 100044, China. lengxs2003@yahoo.com.cn
Telephone: +86-10-68314422-3500
Received: 2004-02-02 **Accepted:** 2004-02-21

Abstract

AIM: To investigate the expression of cancer-testis (CT) antigens *MAGE-1, SSX-1 ,CTp11* and *HCA587* genes in hepatocellular carcinoma (HCC) and the possibility of applying these antigens as targets for specific immunotherapy for HCC.

METHODS: Expression levels of *MAGE-1, SSX-1, CTp11* and *HCA587* mRNA were detected with reverse transcription polymerase chain reaction (RT-PCR) in HCC tissues and corresponding adjacent non-cancerous tissues from 105 HCC patients, 40 samples of cirrhosis and normal liver tissues. Genes of five samples with positive PCR results were sequenced.

RESULTS: Of 105 HCC tissues, *MAGE1, SSX-1 ,CTp11* and *HCA587* mRNA expressions were detectable in 75.2%(79/105), 72.4%(76/105), 62.9%(66/105) and 56.2%(59/105) of HCC samples, respectively. About 93.3%(98/105), 72.4%(76/105), 48.6%(51/105) and 37.1%(39/105) of HCC tissues positively expressed at least one, two, three, and four members of CT antigens, respectively. Conversely, only *SSX-1* could be detectable in 2.9%(3/105) of the corresponding adjacent non-HCC tissues in which no metastatic lesion was found. Of the latter 3 patients, biopsy samples far from tumor were obtained in 2 patients and RT-PCR indicated no expression of S*SX-1* mRNA in these two samples. In addition, none of 40 samples of cirrhotic and normal liver tissues expressed CT antigen gene mRNA. DNA sequences confirmed that the RT-PCR products were true target cDNA. No relationship was found between expression of CT antigens and clinico pathological indicators such as age, gender, tumor size, degree of tumor differentiation, serum α-fetoprotein level and infection of hepatitis B virus or hepatitis C virus (P>0.05).

CONCLUSION: CT antigens genes (*MAGE-1*, *SSX-1*, *CTp11* and *HCA587*) are expressed with high percentage and specificity in HCC and their products are promising targets for antigen-specific immunotherapy of HCC. High frequent co-expression of multiple members of CT antigens in HCC provides possibility of polyvalent vaccinations for HCC.

Zhao L, Mou DC, Leng XS, Peng JR, Wang WX, Huang L, Li S, Zhu JY. Expression of cancer-testis antigens in hepatocellular carcinoma. *World J Gastroenterol* 2004; 10(14): 2034-2038
http://www.wjgnet.com/1007-9327/10/2034.asp

INTRODUCTION

Hepatocellular carcinoma (HCC) is a common tumor with a poor prognosis, irrespective of a variety of treatment options[1,2]. So, there is a need to develop additional therapeutic approaches for the management of this disease. A proposed strategy is immunotherapy, which has the potency to eradicate systemic tumor cells in multiple sites in the body and the specificity to discriminate between neoplastic and non-neoplastic cells[3,4]. Genes or antigens, which are either exclusively or preferentially expressed in malignant tissues, are a prerequisite for antigen-specific cancer immunotherapy[4,5].

Recently, the integration of molecular and immunological techniques has led to the identification of a new category of tumor-specific antigens called cancer-testis (CT) antigens, such as MAGE superfamily, SSX family, GAGE, BAGE, SCP-1, NY-ESO-1, CTp11 and HCA587[6,7]. The CT antigens share several distinct features including: (1) CT antigen mRNA is expressed predominantly in tumors of different origins with various frequencies but not in normal tissues except for testis; and (2) the genes encoding CT antigens locate at the X chromosome[8,9]. The combination of CT antigen peptides and human leukocyte antigen (HLA), when efficiently presented by antigen presenting cells to cytotoxic T lymphocytes (CTL), is capable of eliciting cellular immune responses in cancer patients[10,11]. Also, some members of CT antigens are capable of inducing humoral immunity[12,13]. Both cellular and humoral immune response can kill tumor cells specifically. The testis is an immune privileged organ because spermatogenic cells do not express HLA class I antigen at their surface. Concomitantly, the testis has a so-called blood-testis barrier, which limits contact between testicular and immune cells, in the seminiferous tubuli generated by the Sertoli cells[7,14]. Because of these features, CT antigens have the potential to provide specific antitumor immunity directly to malignant cells without harm to normal cells. At present, the application of tumor antigenic peptide vaccine based on CT antigens for cancer immunotherapy has become a hot spot[15,16].

The screening of tumor antigens recognized by autologous cytotoxic T cells led to the isolation of *MAGE-1*, which has been identified as a member of *MAGE-A* genes family[17]. Clinical trials targeting MAGE-1 antigen are in progress for malignant melanoma and have shown favorable curative effect[18,19]. *SSX* genes and *HCA* genes were originally identified using serological analysis of recombinant cDNA expression libraries (SERAX). SEREX was to define B cell epitopes in antigens that were specifically recognized by antibodies in cancer sera, suggesting that SSX and HCA antigens were immunogenic and capable of inducing an antibody response[6,20]. In a recent report, Li *et al*. have proved HCC patients were able to develop humoral immune response to HCA587 antigen. Based on representational difference analysis of cDNA, Zendman *et al*.[21]

first identified the expression of *CTp11* in melanoma cell lines. In another study (unpublished data), our group predicted HLA-A2-restricted CTL epitopes of *CTp11* by peptide supermotif prediction combined with quantitative motif [22,23] and found the potential HLA-A2-restricted CTL epitopes of CTp11 antigen (*HLA-A2* is the most common *HLA-A* allele in Asian population, especially in Chinese, with an estimated frequency of more than 50%[24,25]), suggesting the possibility of CTP11 antigen to trigger cellular immunity and a new potential vaccine candidate for HCC immunotherapy.

Several studies reported high frequent expression of CT antigens in the HCC tissues, such as MAGE-1[26,27] and SSX-1[4,28]. However, the expression of CT antigens is heterogenous in a variety of human tumors, which may be a way for malignant cells to evade from immunosurveillance[7,29-31]. Screening highly and specifically expressed multiple CT antigens in tumors and using them as targets for immunotherapy are promising means to overcome the heterogenous expression of tumor cells, thus expanding patients' opportunities for cancer specific immunotherapy and establishing the basis of polyvalent vaccinations[29].

In an effort to improve the efficiency of tumour vaccines and prevent immune escape, we investigated the expression of CT antigens MAGE1, SSX-1, CTp11 and HCA587 in HCC tissues.

MATERIALS AND METHODS

Data of patients

From October 2000 to September 2003, 105 patients receiving operation for HCC, including hepatectomy or orthotopic liver transplantation, at the 2nd Hospital of Peking University Health Science Center, were enrolled in this study. There were 90 men and 15 women with a mean age of 47.2±8.4 years (range 18-75). The hepatitis B surface antigen was positive in 98 cases. Among 105 cases, anti-HCV was positive in 5 cases. The serum α-fetoprotein (α-FP) level was normal (<20 ng/mL) or elevated slightly (<40 ng/mL) in 35 patients. Histopathological examination indicated that 18 HCC samples were well differentiated, 61 moderately and 26 samples poorly differentiated, respectively. According to TNM classification of the International Union Against Cancer[32], there were 13 cases at stage I, 30 at stage II, 12 at stage III and 50 at stage IV, respectively. Seventy-nine patients had large-sized tumors (>5 cm), while the tumor size of the other 26 patients was equal to or less than 5 cm (≤5 cm). The control samples included 20 tissues from cirrhosis patients and 20 normal liver tissues from patients without liver disease by surgical biopsy. Testis tissues (kindly provided by Urological Department of the 2nd Hospital of Peking University Health Science Centre) were used as the positive control. Each sample was immediately frozen in liquid nitrogen after a surgical resection and stored at -80 ℃ until the extraction of total RNA. Informed consent was obtained from each patient before the study was conducted. The Ethic Committee of Peking University approved the study protocol.

Total RNA extraction and synthesis of cDNA

Total RNA was extracted from frozen tissue specimens (50-100 mg) using TRIzol reagent (GIBCOL BRL) according to the protocol provided by the manufacturer. Total RNA (2.5 μg) was primed with an Oligo (dT) 15 oligonucleotide (Promega) and reverse-transcribed according to manufacturer's instructions.

PCR amplification of CT antigens

The amplification reaction contained 5 μL of a 1:5 dilution of reverse-transcribed products, 1 μL each of 10 μmol/L specific primers, 1 μL 10 mmol/L dNTP mixture (dATP, dGTP, dCTP, dTTP), 2.5 U *Taq* DNA polymerase (Gibco BRL) and PCR-buffer solution. The total volume was brought to 50 μL using water. The PCR amplifications were performed in a UNO II thermocycler (Perkin-Elmer, USA) under the following conditions: After an initial denaturation for 5 min at 94 ℃, samples were subjected to 35 cycles of amplification, followed by a final extension of 8 min at 72 ℃. The length of PCR products was 421 base pair (bp) (*MAGE-1*), 422 bp (*SSX-1*), 297 bp (*CTp11*) and 238 bp (*HCA587*), respectively. To verify that the RNA had not degraded, a PCR assay with specific primers for the gene β_2-microglobin (B_2-*MG*) was performed on each cDNA sample under the following conditions: After an initial heating for 2 min at 94 ℃, samples were subjected to 30 cycles of amplification, followed by a final extension of 8 min at 72 ℃. The product size was 335 bp. The PCR conditions and specific primer sets for *MAGE-1*[33], *SSX-1*[4], *CTp11*[21], *HCA587*[34] and B_2-*MG*[26] used in this study are shown in Table 1.

At last, 10 μL of reaction product was analyzed by electrophoresis on a 20 g/L agarose gel (Promega, USA), followed by ethidium bromide staining and digital camera photographing (Korda D3.5, USA).

Sequence analysis of PCR products

To confirm the specificity of the RT-PCR products of the CT antigen genes, we performed the sequence analysis. In brief, purified PCR products were cloned into pGEM-T Easy Vector (Promega) by *T4* DNA ligase and amplified in *E. coli*, JM109. Five cases of positive colonies were selected and assessed using *Eco*RI digestion of mini-prepared DNA. The putative *MAGE-1*, *SSX-1*, *CTp11* and *HCA587* cDNA samples were sequenced with T7 sequencing primers in Sangon Co, Shanghai, China.

Statistical analysis

The statistical analysis was assessed using the chi-square test and the Fisher's exact test, and the significant level was set at $P<0.05$.

RESULTS

Expression of CT antigen genes

Among the 105 HCC tissues investigated, *MAGE1*, *SSX-1*, *CTp11* and *HCA587* mRNA was expressed in 75.2%(79/105), 72.4%(76/105), 62.9%(66/105) and 56.2%(59/105) of tumor samples from HCC patients, respectively. At least one CT antigen mRNA was positive in 93.3%(98/105) of HCC tissues. Conversely, only *SSX-1* could be detected in 2.9%(3/105) of the corresponding adjacent non-HCC tissues in which no metastatic lesions were found. Of the latter 3 patients, biopsy samples far from tumor were obtained in 2 patients and RT-PCR indicated no expression of *SSX-1* mRNA was detectable in these 2 samples. No expression of *MAGE-1*, *CTP11* and *HCA587* was detected in the samples of corresponding adjacent non-cancerous tissues. In addition, none of 40 samples of cirrhosis and normal liver tissue expressed each CT antigen mRNA. In consistent with Chen *et al.*'s findings[4], the electrophoretogram analysis revealed the intensities of PCR products varied considerably among different samples, indicating HCC cells expressing tumor antigens at mRNA level are heterogeneous. The typical electrophoresis of RT-PCR products amplified from cDNA of tissue samples of some HCC patients is shown in Figure 1.

Highly synchronous expression of multiple CT antigens in HCC samples

Highly frequent co-expression of multiple members of CT antigens was observed in HCC samples, with synchronous expression of at least two, three, and four of these gene in

Table 1 PCR amplification program

Gene	Temperature, duration of denaturation, annealing, extension	Primer sequence	Product size (bp)
MAGE-1	94 ℃, 45 s	f: 5'-CGGCCGAAGGAACCTGACCCAG-3'	
	65 ℃, 45 s	s r: 5'-GCTGGAACCCTCACTGGGTTGCC-3'	421
	72 ℃, 45 s		
SSX-1	94 ℃, 60 s	f: 5'-CTAAAGCATCAGAGAAGAGAAGC-3'	
	57 ℃, 60 s	r: 5'-AGATCTCTTATTAATCTTCTCAGAAA-3'	422
	72 ℃, 60 s		
CTp11	94 ℃, 45 s	f: 5'-CTGCCCCAGACATTGAAGAA-3'	
	57 ℃, 60 s	r: 5'-TCCATGAATTCCTCCTCCTC-3'	297
	72 ℃, 90 s		
HCA587	94 ℃, 30 s	f: 5'-AGGCGCGAATCA AGTTAG-3'	
	60 ℃, 30 s	r: 5'-CTCCTCTGCTGTGCTGAC-3'	238
	72 ℃, 30 s		
B_2-MG	94 ℃, 45 s	f: 5'-CTCGCGCTACTCTCTCTTTCTGG-3'	
	55 ℃, 45 s	r: 5'-GCTTACATGTCTCGATCCCACTTA-3'	335
	72 ℃, 45 s		

f: Forward primer, r: Reverse primers.

Table 2 Expression of CT antigens and clinico pathological indicators

Group	n^1	MAGE-1		SSX-1		CTp11		HCA587		CT^2(+)	
		+	-	+	-	+	-	+	-	+	-
Total number	105	79	26	76	29	66	39	59	46	98	7
Gender											
Male	90	70	20	66	24	57	33	48	42	85	5
Female	15	9	6	10	5	9	6	11	4	13	2
Tumor diameter											
≤5 cm	26	18	8	16	10	14	12	15	11	22	4
>5 cm	79	61	18	60	19	52	27	44	35	76	3
TNM stage											
I+II	43	29	14	31	12	27	16	22	21	39	4
III+IV	62	50	12	45	17	39	23	37	25	59	3
Hepatitis B virus											
HBV (+)	98	74	24	71	27	62	36	55	43	91	7
HBV (-)	7	5	2	5	2	4	3	4	3	7	0
Hepatitis C virus											
HCV (+)	5	5	0	4	1	4	1	4	1	5	0
HCV (-)	100	74	26	72	28	62	38	55	45	93	7
AFP (ng/mL)											
<40	35	28	7	22	13	20	15	18	17	32	3
≥40	70	51	19	54	16	46	24	41	29	66	4
Differentiation											
Well	18	13	5	12	6	12	6	9	9	16	2
Moderately	61	44	17	44	17	39	22	34	27	58	3
Poorly	26	22	4	20	6	15	11	16	10	24	2

n^1 : Number of samples ; CT^2: At least one of these 4 CT antigen genes; No relationship is found between the expression of CT antigens and clinical indicators such as age, gender, degree of tumour differentiation, serum α-FP level, TNM classification, tumor size, infection of hepatitis B virus or hepatitis C virus (P>0.05).

72.4%(76/105), 48.6%(51/105) and 37.1%(39/105) of HCC tissues, respectively. We also analysed the cases with expression of neither *MAGE-1* nor *SSX-1* genes to determine targets for cancer immunotherapy other than *MAGE-1* and/or *SSX-1*. Among 18 HCC patients with expression of neither *MAGE-1* nor *SSX-1*, 61.1% (11/18) of HCC samples expressed *CTp11* and/or *HCA587*.

Sequence analysis of PCR products

Sequence analysis of PCR products verified the nucleotide sequences of *MAGE-1*, *SSX-1*, *CTp11* and *HCA587* cDNA fragments were identical to that in the database of the GenBank. It confirmed that the RT-PCR products were true *MAGE-1*, *SSX-1*, *CTp11* and *HCA587* cDNA (data not shown).

Expression of CT antigens and clinical indicators

No relationship was found between the expression of CT antigens and clinico pathological indicators such as age, gender, differentiation degree of tumour, serum α-FP level, TNM classification, tumor size, infection of hepatitis B virus or

hepatitis C virus (P>0.05). However, among 35 patients with the normal (<20 ng/mL) or slightly elevated (<40 ng/mL) serum α-FP level, 32 patients had *MAGE-1*, *SSX1*, *CTp11* or *HCA587* gene transcripts detected in their HCC tissues. The results are demonstrated in Table 2.

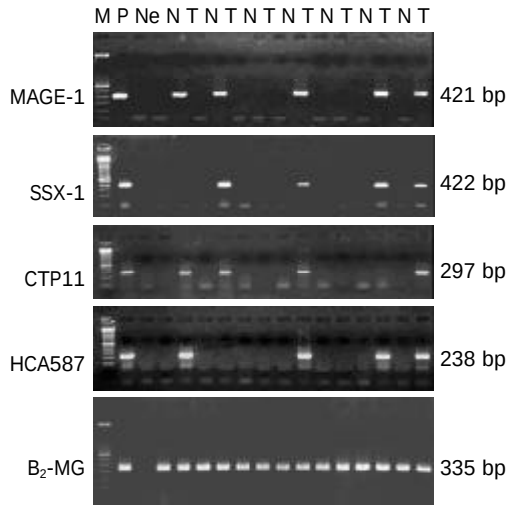

Figure 1 Electrophoresis of RT-PCR products amplified from cDNA of HCC tissues. M: Molecular marker, 100-bp DNA ladder (Gibco); P: Positive control, testis tissues; Ne: Negative control, PCR amplification in the absence of template; B_2-MG: 335-bp cDNA quality control; T: HCC tissues, arrows indicate the RT-PCR products of CT antigens; N: Corresponding adjacent non-tumor tissues. All the samples shown here except for the negative control are positive.

DISCUSSION

Tumor antigens should demonstrate high frequency expression in the tumor tissues and restricted expression in normal tissues, which is the prerequisite for being an ideal candidate antigen for antigen-specific cancer immunotherapy[35]. The growing class of CT antigens is of particular interest for antitumor immunotherapy because of their specific expression on tumor cells. It has demonstrated high frequent expression of *MAGE-1* and *SSX-1* in HCC tissues, but little in nontumor tissues[4,26-28]. However, the heterogeneous expression of MAGE-1 and SSX-1 antigens may cause problems for immunotherapy targeting these antigens, as tumor cases with a low percentage or negative expression of MAGE-1 and/or SSX-1 antigens may be less suitable for immunotherapy targeting these antigens. Furthermore, to our knowledge, so far little information is available on the *CTp11* and *HCA587* expression in HCC tissues. Therefore, we investigated the expression of CT antigens MAGE1, SSX-1, CTp11 and HCA587 in HCC tissues.

In the present study, we found highly positive rate of *MAGE-1, SSX-1, CTp11* and *HCA587* transcripts in HCC tissues (56.2-75.2%). No expression of *MAGE-1, CTP11* and *HCA587* was detected in the samples of corresponding adjacent non-cancerous tissues, while *SSX-1* mRNA could be detected in 2.9%(3/105) of the corresponding adjacent non-HCC tissues where no metastatic lesions were found, similar to Chen *et al.*' s findings[4]. Of these 3 patients, biopsy samples far from tumor were obtained in 2 patients and RT-PCR indicated expression of SSX-1 mRNA was not detectable in these two samples. The sensitivity of RT-PCR assay was much higher than that of conventional methods[36], such as histochemistry and cytology, so we speculate that there might be micrometastasis in the adjacent non-tumor liver tissue. In addition, none of 40 samples of cirrhosis and normal liver tissues expressed each of these 4 CT antigen mRNAs. As *MAGE-1*, *SSX-1*, *CTp11* and *HCA587* were expressed with a high percentage and specificity in HCC, their products might be ideal antigen targets for HCC immunotherapy. A high proportion (93.3%, 98/105) of the HCC tissue samples was positive for at least one of these 4 CT antigen genes, indicating using multiple CT antigens as targets will greatly increase the number of candidates for CT antigen-based HCC immunotherapy.

In the present study, we found relatively high frequency of expression of *CTp11* and *HCA587* mRNA, being 62.9%(66/105) and 56.2%(59/105) of tumor samples from HCC patients, respectively, while no expression of *CTP11* and *HCA587* was detected in the samples of corresponding adjacent non-cancerous tissues and control liver tissues, indicating their products may also be ideal antigen targets for HCC immunotherapy. Though frequency of expression of *CTp11* and *HCA587* mRNA was relative lower than that of *MAGE-1* and *SSX-1*, being 75.2%(79/105) and 72.4%(76/105), respectively, we found that samples with negative expression of *MAGE-1* and *SSX-1* showed expression of *CTp11* and *HCA587*. With respect to these HCC patients, vaccines based on *CTp11* and *HCA587* should be a desirable choice.

We also found a high frequency of synchronous expression of multiple CT antigens in HCC samples, with synchronous expression of at least two, three, and four of these genes in 72.4%(76/105), 48.6%(51/105) and 37.1%(39/105) of HCC tissues, respectively. High frequent co-expression of multiple members of CT antigens in HCC provides possibility of polyvalent vaccinations for HCC. The polyvalent vaccinations with multiple antigens, which avoid the heterogenous expression of tumor cells, might obtain better clinical results than a single antigen-based vaccination in cancer immunotherapy. Patients' opportunities for cancer specific immunotherapy can thus be expanded[37]. However, our results showed no expression of CT antigens in 6.7%(7/105) of HCC tissues. For these patients, it is necessary to screen other CT antigens or tumor specific antigens serving as immune targets for HCC immunotherapy.

Concerning the issues of heterogenous expression of CT antigens and possibility of polyvalent vaccinations for HCC, Tahara *et al*.[27] investigated the 10 CT antigens expression in HCC with RT-PCR and found that 86%(19/22) of HCC tissue samples expressed at least one CT antigen gene. Comparably, Luo *et al*.[28] showed that 81%(17/21) of HCC tissue samples expressed at least one of the 10 CT genes. While in our present study, selecting just 4 CT antigens, we proved that 93.3%(98/105) of HCC patients were detectable of at least one positive CT antigen expression. Notably, the sample number of our study is 105, which is much more than the case number in the study of Tahara *et al*.[27] (22 cases) or Luo *et al*.[28] (22 cases), therefore our results should be more convincing.

Our previous report showed the prognostic value of *MAGE-1* and *MAGE-3* as tumor specific markers to detect blood dissemination of HCC cells after hepatectomy[33]. In this study, our results indicated *SSX-1, CTp11* and *HCA587* were also expressed in HCC tissues with high percentage and sensitivity, and some cases with negative *MAGE* expression were positive for *SSX-1, CTp11* and/or *HCA587* transcripts. Therefore, we can combine *SSX-1, CTp11* and *HCA587* genes with *MAGE* genes and apply them as multiple-markers to detect hepatoma cells in circulation, which may improve the sensitivity of the assay.

In this study, the serum α-FP was normal (<20 ng/mL) or slightly elevated (<40 ng/mL) in 30.0%(35/105) of HCC patients. In these 35 patients, 32 had *MAGE-1, SSX1, CTp11* or *HCA587* transcripts in their HCC tissues, suggesting applying their mRNAs as tumour-specific markers to detect HCC cells in circulation might be an adjuvant diagnostic tool. This assay combined with the examination of serum α-FP level may improve the diagnosis of HCC patients.

REFERENCES

1 **Lai YC**, Shih CY, Jeng CM, Yang SS, Hu JT, Sung YC, Lin HT, Hou SM, Wu CH, Chen TK. Hepatic arterial infusion chemotherapy for hepatocellular carcinoma with portal vein tumor thrombosis. *World J Gastroenterol* 2003; **9**: 2666-2670

2 **Zhou Q**, He Q, Liang LJ. Expression of p27, cylin E and cylin A in hepatocellular carcinoma and its clinical significance. *World J Gastroenterol* 2003; **9**: 2450-2454

3 **Liu CL**, Fan ST. Nonresectional therapies for hepatocellular cacinoma. *Am J Surg* 1997; **173**: 358-365

4 **Chen CH**, Chen GJ, Lee HS, Huang GT, Yang PM, Tsai LJ, Chen DS, Sheu JC. Expressions of cancer-testis antigens in human hepatocellular carcinomas. *Cancer Lett* 2001; **164**: 189-195

5 **Tureci O**, Chen YT, Sahin U, Gure AO, Zwick C, Villena C, Tsang S, Seitz G, Old LJ, Pfreundschuh M. Expression of SSX genes in human tumors. *Int J Cancer* 1998; **77**: 19-23

6 **Wang Y**, Han KJ, Pang XW, Vaughan HA, Qu W, Dong XY, Peng JR, Zhao HT, Rui JA, Leng XS, Cebon J, Burgess AW, Chen WF. Large scale identification of human hepatocellular carcinoma-associated antigens by autoantibodies. *J Immunol* 2002; **169**: 1102-1109

7 **dos Santos NR**, Torensma R, de Vries TJ, Schreurs MW, de Bruijn DR, Kater-Baats E, Ruiter DJ, Adema GJ, van Muijen GN, van Kessel AG. Heterogeneous expression of the SSX cancer/testis antigens in human melanoma lesions and cell lines. *Cancer Res* 2000; **60**: 1654-1662

8 **Tajima K**, Obata Y, Tamaki H, Yoshida M, Chen YT, Scanlan MJ, Old LJ, Kuwano H, Takahashi T, Takahashi T, Mitsudomi T. Expression of cancer/testis (CT) antigens in lung cancer. *Lung Cancer* 2003; **42**: 23-33

9 **Yakirevich E**, Sabo E, Lavie O, Mazareb S, Spagnoli GC, Resnick MB. Expression of the MAGE-A4 and NY-ESO-1 cancer-testis antigens in serous ovarian neoplasms. *Clin Cancer Res* 2003; **9**: 6453-6460

10 **Sahin U**, Tureci O, Pfreundschuh M. Serological identication of human tumor antigens. *Curr Opin Immunol* 1997; **9**: 709-716

11 **Stockert E,** Jager E, Chen YT, Scanlan MJ, Gout I, Karbach J, Arand M, Knuth A, Old LJ. A survey of the humoral immune response of cancer patients to a panel of human tumor antigens. *J Exp Med* 1998; **187**: 1349-1354

12 **Chaux P**, Luiten R, Demotte N, Vantomme V, Stroobant V, Traversari C, Russo V, Schultz E, Cornelis GR, Boon T, van der Bruggen P. Identification of five MAGE-A1 epitopes recognized by cytolytic T lymphocytes obtained by *in vitro* stimulation with dendritic cells transduced with MAGE-A1. *J Immunol* 1999; **163**: 2928-2936

13 **Graff-Dubois S**, Faure O, Gross DA, Alves P, Scardino A, Chouaib S, Lemonnie FA, Kosmatopoulos K. Generation of CTL recognizing an HLA-A*0201-restricted epitope shared by MAGE-A1, -A2, -A3, -A4, -A6, -A10 and -A12 tumor antigens: implication in a broad-spectrum tumor immunotherapy. *J Immunol* 2002; **169**: 575-580

14 **Wang Z**, Zhang Y, Liu H, Salati E, Chiriva-Internati M, Lim SH. Gene expression and immunologic consequence of SPAN-Xb in myeloma and other hematologic malignancies. *Blood* 2003; **101**: 955-960

15 **Scanlan MJ**, Gure AO, Jungbluth AA, Old LJ, Chen YT. Cancer/testis antigens: an expanding family of targets for cancer immunotherapy. *Immunol Rev* 2002; **188**: 22-32

16 **Rosenberg SA**. Progress in human tumour immunology and immunotherapy. *Nature* 2001; **411**: 380-384

17 **van der Bruggen P,** Traversari C, Chomez P, Lurquin C, De Plaen E, Van den Eynde B, Knuth A, Boon T. A gene encoding an antigen recognized by cytolytic T lymphocytes on a human melanoma. *Science* 1991; **254**: 1643-1647

18 **Thurner B,** Haendle I, Roder C, Dieckmann D, Keikavoussi P, Jonuleit H, Bend A, Maczek C, Schreiner D, von den Driesch P, Brocker EB, Steinman RM, Enk A, Kampgen E, Schuler G. Vaccination with mage-3A1 peptide-pulsed mature, monocyte-derived dendritic cells expands specific cytotoxic T cells and induces regression of some metastases in advanced stage IV melanoma. *J Exp Med* 1999; **190**: 1669-1678

19 **Hu X,** Chakraborty NG, Sporn JR, Kurtzman SH, Ergin MT, Mukherji B. Enhancement of cytolytic T lymphocyte precursor frequency in melanoma patients following immunization with the MAGE-1 peptide loaded antigen presenting cell-based vaccine. *Cancer Res* 1996; **56**: 2479-2483

20 **Gure AO**, Tureci O, Sahin U, Tsang S, Scanlan MJ, Jager E, Knuth A, Pfreundschuh M, Old LJ, Chen YT. SSX: a multigene family with several members transcribed in normal testis and human cancer. *Int J Cancer* 1997; **72**: 965-971

21 **Zendman AJ,** Cornelissen IM, Weidle UH, Ruiter DJ, van Muijen GN. CTp11, a novel member of the family of human cancer/testis antigens. *Cancer Res* 1999; **59**: 6223-6229

22 **Parker KC**, Bednarek MA, Coligan JE. Scheme for ranking potential HLA-A2 binding peptides based on independent binding of individual peptide side-chains. *J Immunol* 1994; **152**: 163-175

23 **Zhu B**, Chen Z, Cheng X, Lin Z, Guo J, Jia Z, Zou L, Wang Z, Hu Y, Wang D, Wu Y. Identification of HLA-A*0201-restricted cytotoxic T lymphocyte epitope from TRAG-3 antigen. *Clin Cancer Res* 2003; **9**: 1850-1857

24 **Shieh DC**, Lin DT, Yang BS, Kuan HL, Kao KJ. High frequency of HLA-A*0207 subtype in Chinese population. *Transfusion* 1996; **36**: 818-821

25 **Dong HL**, Sui YF, Ye J, Li ZS, Qu P, Zhang XM, Chen GS, Lu SY. Prediction synthesis and identification of HLA-A2-restricted cytotoxic T lymphocyte epitopes of the tumor antigen MAGE-n. *Zhonghua Yixue Zazhi* 2003; **83**: 1080-1083

26 **Chen H**, Cai S, Wang Y, Zhao H, Peng J, Pang X, Zhu J, Cong X, Rui J, Leng X, Du R, Wang Y, Vaughan H, Cebon J, Burgess AW, Chen W. Expression of the MAGE-1 gene in human hepatocellular carcinomas. *Chin Med J* 2000; **113**: 1112-1128

27 **Tahara K,** Mori M, Sadanaga N, Sakamoto Y, Kitano S, Makuuchi M. Expression of the MAGE gene family in human hepatocellular carcinoma. *Cancer* 1999; **85**: 1234-1240

28 **Luo G**, Huang S, Xie X, Stockert E, Chen YT, Kubuschok B, Pfreundschuh M. Expression of cancer-testis genes in human hepatocellular carcinomas. *Cancer Immun* 2002; **2**: 11-16

29 **Mashion K**, Sadanaga N, Tanaka F, Yamaguchi H, Nagashima H, Inoue H, Sugimachi K, Mori M. Expression of multiple cancer-testis antigen genes in gastrointestinal and breast carcinomas. *Br J cancer* 2001; **85**: 713-720

30 **Jungbluth AA,** Stockert E, Chen YT, Kolb D, Iversen K, Coplan K, Williamson B, Altorki N, Busam KJ, Old LJ. Monoclonal antibody MA454 reveals a heterogeneous expression pattern of MAGE-1 antigen in formalin-fixed paraffin embedded lung tumours. *Br J cancer* 2000; **83**: 493-497

31 **Dhodapkar MV**, Osman K, Teruya-Feldstein J, Filippa D, Hedvat CV, Iversen K, Kolb D, Geller MD, Hassoun H, Kewalramani T, Comenzo RL, Coplan K, Chen YT, Jungbluth AA. Expression of cancer/testis (CT) antigens MAGE-A1, MAGE-A3, MAGE-A4, CT-7, and NY-ESO-1 in malignant gammopathies is heterogeneous and correlates with site, stage and risk status of disease. *Cancer Immun* 2003; **3**: 9-14

32 **Peck-Radosavljevic M,** Pidlich J, Bergmann M, Ferenci P, Seelos C, Wichlas M, Lipinski E, Gnant M, Gangl A, Muhlbacher F**.** Preoperative TNM-classification is a better prognostic indicator for recurrence of hepatocellular carcinoma after liver transplantation than albumin mRNA in peripheral blood. Liver Transplant Oncology Group. *J Hepatol* 1998; **28**: 497-503

33 **Mou DC,** Cai SL, Peng JR, Wang Y, Chen HS, Pang XW, Leng XS, Chen WF. Evaluation of MAGE-1 and MAGE-3 as tumour-specific makers to detect blood dissemination of hepatocellular carcinoma cells. *Br J Cancer* 2002, **86**: 110-116

34 **Lucas S**, De Plaen E, Boon T. MAGE-B5, MAGE-B6, MAGE-C2, and MAGE-C3: four new members of the MAGE family with tumor-specific expression. *Int J Cancer* 2000; **87**: 55-60

35 **Odunsi K**, Jungbluth AA, Stockert E, Qian F, Gnjatic S, Tammela J, Intengan M, Beck A, Keitz B, Santiago D, Williamson B, Scanlan MJ, Ritter G, Chen YT, Driscoll D, Sood A, Lele S, Old LJ. NY-ESO-1 and LAGE-1 cancer-testis antigens are potential targets for immunotherapy in epithelial ovarian cancer. *Cancer Res* 2003; **63**: 6076-6083

36 **Paterlini-Brechot P,** Vona G, Brechot C. Circulationg tumorous cells in patients with hepatocellular carcinoma. Clinical impact and future directions. *Semin Cancer Biol* 2000; **10**: 241-249

37 **Sahin U**, Tureci O, Chen YT, Seitz G, Villena-Heinsen C, Old LJ, Pfreundschu M. Expression of multiple cancer/testis (CT) antigens in breast cancer and melanoma: basis for polyvalent CT vaccine strategies. *Int J Cancer* 1998; **78**: 387-389

Edited by Chen WW **Proofread by** Zhu LH and Xu FM

PO Box 2345, Beijing 100023, China
Fax: +86-10-85381893
E-mail: wjg@wjgnet.com www.wjgnet.com

World J Gastroenterol 2004;10(14):2039-2044
World Journal of Gastroenterology
 ISSN 1007-9327

• LIVER CANCER •

A DNA vaccine against extracellular domains 1-3 of flk-1 and its immune preventive and therapeutic effects against H22 tumor cell *in vivo*

Fan Lü, Zhao-Yin Qin, Wen-Bin Yang, Yin-Xin Qi, Yi-Min Li

Fan Lü, Zhao-Yin Qin, Wen-Bin Yang, Yin-Xin Qi, Yi-Min Li, Department of General Surgery, Second Hospital of Xi' an Jiaotong University, Xi' an 710004, Shaanxi Province, China
Supported by the Natural Science Foundation of Shaanxi Province, No. 2003$C_2$54
Correspondence to: Yi-Min Li, Department of General Surgery, Second Hospital of Xi' an Jiaotong University, Xi' an 710004, Shaanxi Province, China. liyiming@yahoo.com.cn
Telephone: +86-29-7679246
Received: 2004-02-06 **Accepted:** 2004-02-26

Abstract

AIM: To construct a DNA vaccine against extracellular domains 1-3 of fetal liver kinase-1 (flk-1), and to investigate its preventive and therapeutic effect against H22 cell *in vivo*.

METHODS: Flk-1 DNA vaccine was produced by cloning extracellular domains 1-3 of flk-1 and by inserting the cloned gene into pcDNA3.1 (+). Fifteen mice were divided into 3 groups and inoculated by vaccine, plasmid and saline respectively to detect specific T lymphocyte response. Thirty Mice were equally divided into preventive group and therapeutic group. Preventive group was further divided into V, P, and S subgroups, namely immunized by vaccine, pcDNA3.1 (+) and saline, respectively, and attacked by H22 cell. Therapeutical group was divided into 3 subgroups of V, P and S, and attacked by H22, then treated with vaccine, pcDNA3.1 (+) and saline, respectively. The tumor size, tumor weight, mice survival time and tumor latency period were compared within these groups. Furthermore, intratumoral microvessel density (MVD) was assessed by immunohistochemistry.

RESULTS: DNA vaccine pcDNA3.1 (+) flk-1-domains 1-3 was successfully constructed and could raise specific CTL activity. In the preventive group and therapeutic group, tumor latency period and survival time were significantly longer in vaccine subgroup than that in P and S subgroups ($P<0.05$); the tumor size, weight and MVD were significantly less in vaccine subgroup than that in P and S subgroups ($P<0.05$). The survival time of therapeutic vaccine subgroup was significantly shorter than that of preventive vaccine subgroup ($P<0.05$); the tumor size, and MVD of therapeutic vaccine subgroup were significantly greater than that of preventive vaccine subgroup ($P<0.05$).

CONCLUSION: DNA vaccine against flk-1 domains 1-3 can stimulate potent specific CTL activity; and has distinctive prophylactic effect on tumor H22; and also can inhibit the tumor growth *in vivo*. This vaccine may be used as an adjuvant therapy because it is less effective on detectable tumor.

Lü F, Qin ZY, Yang WB, Qi YX, Li YM. A DNA vaccine against extracellular domains 1-3 of flk-1 and its immune preventive and therapeutic effects against H22 tumor cell *in vivo*. *World J Gastroenterol* 2004; 10(14): 2039-2044
http://www.wjgnet.com/1007-9327/10/2039.asp

INTRODUCTION

Extensive studies by many investigators established that angiogenesis has a central role in the invasion, growth and metastasis of solid tumors[1-3]. The inhibition of tumor growth by attacking the tumor' s vascular supply offers a primary target for anti-angiogenic intervention. There are several advantages of targeting proliferating endothelial cells in the tumor vasculature rather than directly to tumor cells. First, endothelial cells are genetically stable and do not down regulate MHC-class I and II antigens. Second, the therapeutic target is tumor-independent. Thus, killing of proliferating endothelial cells in the tumor microenvironment can be effective against a variety of malignancies and clones[3,4]. Vascular endothelial growth factor (VEGF) plays a center role in tumor angiogenesis, while fetal liver kinase-1 (flk-1), which expressed exclusively on the endothelial cells, is the key receptor that binds VEGF[5,6]. Blocking the VEGF-flk-1 pathway may inhibit tumor angiogenesis. Hence, we constructed a DNA vaccine to target the extracellular domain 1-3 of flk-1 and tested its preventive and therapeutic effect against H22 cell *in vivo* with the hope that the vaccine might be able to inhibit angiogenesis via targeting flk-1 and flk-1 expressing endothelial cell. This research has no parallel reports at home.

MATERIALS AND METHODS

Materials

Cell line Tumor cell H22 cell line, constructed by Dalian Medical University from the mouse ascite, was heterogeneous cells with higher declination to spread by lymph vessel. COS7 cell is derived from African green monkey kidney and preserved by our laboratory. Endothelial cells were primarily cultured from mouse vessel by our laboratory.

Animal BALB/c mice were bought from Laboratory Animal Center of the Fourth Military Medical University. All mice were male, specific pathogen free animals, with age of 6-8 wk and weight of 15-20 g.

Main reagents pcDNA3.1(+) was purchased from Invitrogen (U.S). CD31 antibody was a product of Santa Cruz (U.S). pMDT- 18 Vector, T4 DNA ligase, Taq^{EX} DNA polymerase, *Hin*d III, *Ecro*R I, and dNTP were products of TaKaRa (Japan). *M- MLV* reverse transcriptase was purchased from Promega (U.S). E.Z.N.A^R gel extraction kit was purchased from Omega Bio-tek (U.S). Trizol, lipofectamine 2000, DMEM and G418 were purchased from Gibco (U.S). Western blot luminescence kit was purchased from NEN (Britain). Micro BCA protein assay was purchased from Pierce (U.S).

Methods

Culture of cells H22 cell was transferred in abdomen cavity of

BALB/c mouse. The ascites were taken from the mouse in the super clean bench and then diluted with DMEM to 1×10^7/mL. A total of 0.2 mL of 1×10^7 H22 cells were inoculated subcutaneously at the right armpit of mouse to establish a tumor model. The interval between the ascites taking and the last mouse inoculation was less than 2 h. COS7 cell was cultured in DMEM containing 100 mL/L FCS and 50 mL /L CO_2 at 37 ℃. Primary culture of endothelial cells (ECs) were performed as follow: the mouse thoracic aorta was sterile dissociated, and sheared into small pieces about 0.5 cm×0.5 cm, washed with Hank's fluid, its EC surface was sticked to 1.5% gelatin culture medium, and then DMEM containing 100 mL/L FCS and benzylpenicillin (100 U/mL) and streptomycin (100 U/mL) was slowly added, then cultured at 37 ℃ under humidified atmosphere containing 50 mL/L CO_2 until the cells form a single layer. Transfer of cell culture was performed (≤3 generations).

Construction of the expression vector encoding murine flk-1 domain 1-3 Total cellular RNA of mouse liver tissue was extracted using TRIZOL reagent and cDNA was prepared by random priming from 2 μg of total RNA using M-MLV according to the manufacturers' instructions. PCR was performed for 35 cycles as follows: denaturation at 94 ℃ for 30 s, annealing at 60 ℃ for 30 s and extension at 72 ℃ for 80 s. Oligonucleotide primers to amplify flk-1 domain 1-3 transcripts were designed on the mouse sequence: upstream primer:5' -CGGATAACC TGGCTGACC-3' ; and downstream primer 5' -AGGGATT CGGACTTGACTGC-3. Then the cloned gene was inserted into the pMDT-18 vector, followed by cut out from pMDT-18 by *Eco*R I and *Hin*d III and insertion into the pcDNA3.1 vector between the restriction sites *Eco*R I and *Hin*d III generating pcDNA3.1 (+)-flk-1-Domain1-3. Reading frame and sequence were proved right by DNA sequencing.

Expression of the pcDNA3.1 (+)-flk-1-domain 1-3 in the COS7 cell COS7 cells were plated in antibiotic free growth medium and cultured until about 90% confluence at the time of transfection. A 4 μg of pcDNA3.1 (+)-flk-1-Domain1-3 was diluted and mixed in 250 μL of DMEM, 10 μL of lipofectamine™ 2000 was diluted and mixed in 250 μL of DMEM respectively. They were mixed together after 5 min of incubation at room temperature, and incubated for 20 min then poured into 35 mm wells plated with COS7. Mixed gently and incubated at 37 ℃ in 50 mL/L CO_2 incubator for 48 h. Cultured cells were incubated for 20 min and sonicated twice for 5 s in cold lysis buffer. Total extracts were cleared by centrifugation for 3 0 min at 4 ℃ at 14 000 *g*. Protein levels were quantified with Micro BCA protein assay. Samples were resolved by 120 g/L SDS-polyacrylamide gel electrophoresis (SDS-PAGE). In all gels, 80 μg of protein dissolved in sample buffer was loaded per lane. Immunoblotting was performed by electroblotting onto nitrocellulose membrane (0.2 mm) at 32 mA for 1 h using a semidry immunoblotter. Membranes were blocked for 2 h at room temperature with blocking buffer and subsequently incubated for 1 h at room temperature with anti-flk-1 polyclonal antibody at a 1:200 dilution with blocking buffer. The enhanced chemiluminescence system was used for the detection of bound antibody. Primary antibody-antibody-bound membranes were incubated for 1 h at room temperature with horseradish peroxidase conjugated antirabbit or antimouse IgG at a 1:1 000 dilution with blocking buffer. After washing with TBS and TBST, the membranes were treated with enhanced chemiluminescence reagents according to the manufacturer's protocol. The membranes were exposed to X-ray film for 2 min.

Analysis of specific cytolytic T lymphocyte (CTL) activity Fifteen mice were classified to three groups: vaccine group, plasmid group, and saline group, each group had 5 mice. Mice were injected with 100 μg of vaccine, 100 μg of plasmid, and 100 μg of saline respectively, at the concentration of 1 μg/μL once every 10 d. All the mice were killed on day 10 after the last immunization and the spleen lymphocytes were separated and cultured in complete culture medium with interleukin-2 (1×10^5U/L) and 100 mL/L FCS at saturated humidified atmosphere containing 50 mL/L CO_2 at 37 ℃ to induce the CTL. CTL and mouse ECs was mixed at 100:1 and 50:1 effector/target rate, respectively. In addition, there were a CTL control group, an ECs control group and a culture medium control group. The specimens of each group had 3 parallel wells on a 96-well culture plate and were cultured under conditions of saturated humidity at 37 ℃ containing 50 mL/L CO_2 for 48 h. Cell-mediated cytotoxicity was determined by using a standard ^{51}Cr release assay. Briefly, target cells were pelleted and resuspended in 3.7 GBq of ^{51}Cr per 10^6 cells and incubated at 37 ℃ in a humidified 50 mL/L CO_2 incubator for 1 h. They were washed three times with media, resuspended to 5×10^4/mL, and 0.1 mL was added to round-bottomed microtiter wells. Varying numbers of effector cells were added in 0.1-mL volume to achieve the desired E/T ratios. For a spontaneous ^{51}Cr-release control, 0.1 mL of media was substituted for effector cells. Maximum release was determined by adding 0.1 mL of 1% NP-40 to the target cells. After 6 h at 37 ℃, the plates were centrifuged at 1 200 r /min for 5 min, and 0.1 mL of supernatant was taken from each well and counted on a gamma counter. Data are presented as percent specific 51Cr-release=100×[(experimental group counts per minute (cpm)-spontaneous group cpm)/(maximum release cpm - spontaneous cpm)].

Preventive effect of pcDNA3.1 (+)-flk-1-domain1-3 against H22 Thirty BALB/c mice were randomly divided into V, P, and S subgroups, 10 mice in each subgroup, and immunized by 100 μg vaccine, plasmid, and saline, respectively, at concentration of 100 μg /μL, once every 10 d by intramuscular injection at left hip. Five days after the last immunization, all mice were injected with 1×10^7 of H22 cells at the right armpit subcutaneously. The mice weight, tumor formation, tumor size and mice survival time were recorded. Tumor volume was measured in 2 dimensions and calculated as follows: length/2×width^2. After mice death, tumor tissue was routinely fixed and embedded in paraffin and then performed CD31 staining. All mice were kept observation until death.

Therapeutic effect of pcDNA3.1 (+)-flk-1-domain1-3 against H22 Thirty BALB/c mice were randomly divided into V, P, and S subgroups, ten mice in each subgroup. All mice were injected with 1×10^7 of H22 tumor cell subcutaneously at right armpit. Four days later, tumor was formed in all mice, which demonstrated the successful construction of tumor model. Mice in different groups were treated with 100 μg of vaccine, plasmid, and saline, respectively, at the concentration of 1 μg/μL, two times every 5 d by intramuscular injection at left hip. The tumor weight and size were recorded each day. The mice weight, tumor formation, tumor size and survival period of mice were recorded. After mice death, tumor tissue was routinely fixed and embedded in paraffin for CD31 staining. All mice were kept observation until death.

Counting of microvessel density in H22 solid tumor Tumor tissue was washed with cold PBS, then fixed in 40 g/L buffered fomaldehyde solution and embedded in paraffin. Tissue sections (4 μm thick) were preincubated for 30 min with PBS containing 3 mL/L hydrogen peroxide and then blocked with blocking solution containing 50 mL/L goat serum. CD3 staining was performed with a polyclonal rabbit anti-rat CD31 antibody diluted in PBS (1:50) supplemented with blocking solution for 24 h at 4 ℃. Finally, sections were incubated with the biotinylated secondary antibody followed by streptavidin-horse-radish-peroxidase complex. Antibody binding was visualized with diaminobenzidine (DAB). Vessel counts within the tumor were assessed by light microscopy after CD31 staining. Based on the criteria of Weidner *et al*.[7], a vessel lumen was not required for the identification of a microvessel.

The five areas with the highest number of discrete microvessels in each slide were identified by scanning tumor sections at low power. Then the number of microvessels were counted in these areas at 200 magnification (0.75 mm^2 area) to obtain accurate microvessel density. The average value of the five areas was counted as MVD.

Statistical analysis

Results were expressed as mean±SD. Data were analyzed by the method of ANOVA using SPSS 10.0 software. $P<0.05$ was considered statistically significant.

RESULTS

Cloning of flk-1 domain1-3 and construction of pcDNA3.1 (+)-flk-1-domain1-3

A 1 250 bp gene part was cloned from mouse liver tissue using RT-PCR technique (Figure 1). DNA sequencing showed that pcDNA3.1 (+) flk-1-domain1-3 was the right reading frame and sequence. Western blotting of the lipotransfected COS7 cell showed that the expression of a M_r 44 000 protein in the cell after transfection of the pcDNA3.1 (+)-flk-1-domain1-3 (Figures 2, 3).

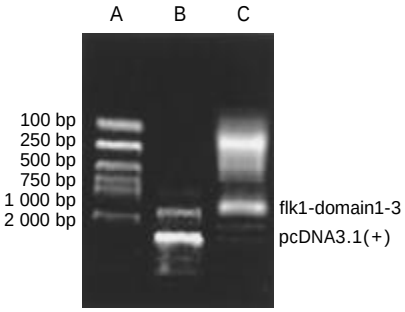

Figure 1 Clone of flk-1-domain1-3 and construction of expressing vector. A: DNA marker; B: PCR results.

Activity of spleen CTL

CTL activity of mice in vaccine subgroup was significantly higher than that of plasmid and saline subgroup (Figure 4, $P<0.05$).

Protective effect of pcDNA3.1 (+)-flk-1-domain 1-3 against H22 in different subgroup

Observation of carcinogenesis Mice of different subgroups in immune preventive group were injected with H22 cells after 3 times inoculation, the tumor latent time, survival time of the vaccine subgroup were longer than that of plasmid subgroup and saline subgroup ($P<0.05$); The tumor weight and tumor volume of vaccine subgroup was the lowest among the 3 subgroups ($P<0.05$, Table1, Figure 5). The tumor latent time, survival time, tumor volume and tumor weight of plasmid subgroup and saline subgroup have no statistical significance compared with each other.

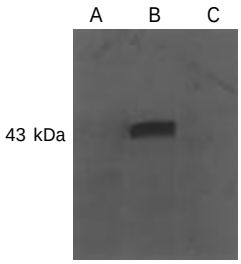

Figure 2 Functionality of the flk-1-domain 1-3 expressing vector. A: Western blotting of protein extracted from COS7 cell; B: Western blotting of protein from COS7 transfected with vaccine; C: Western blotting of protein from COS7 transfected with pcDNA3.1 (+).

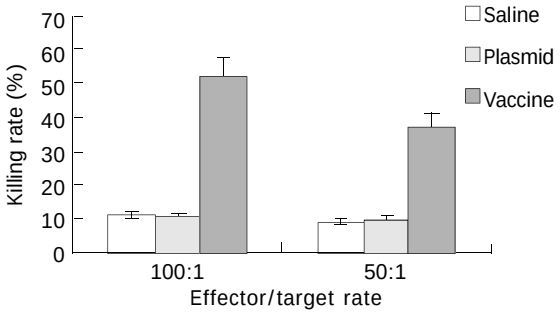

Figure 4 CTL activity of each group at different effector / target rate.

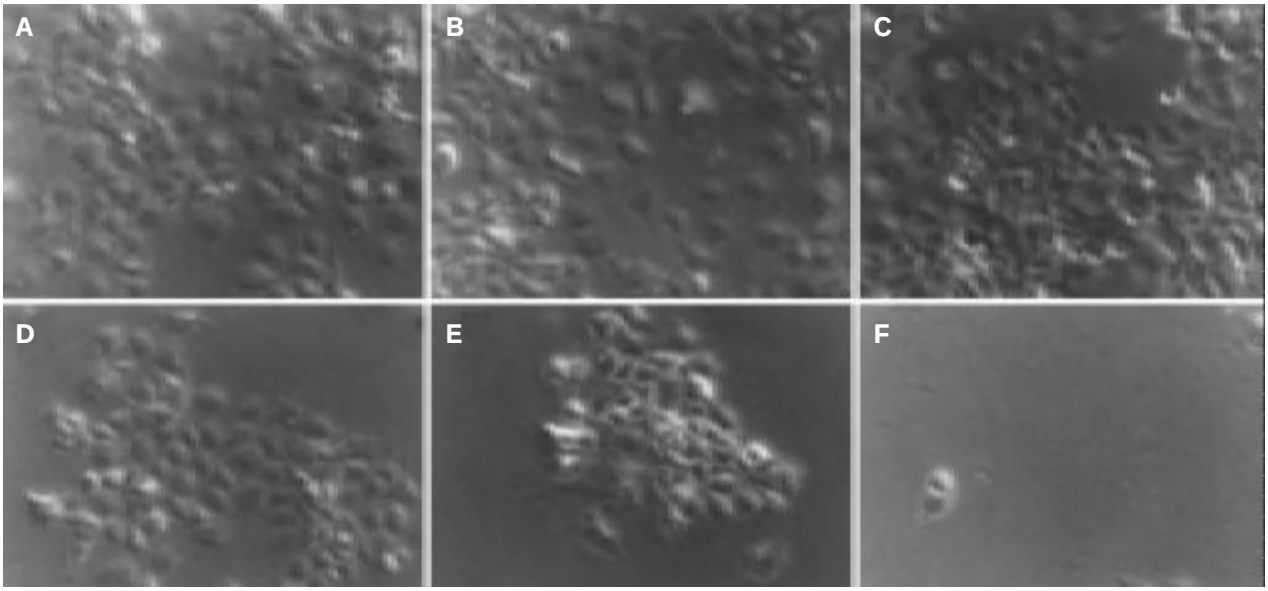

Figure 3 COS 7 cell before and after transfection with vaccine, plasmid and saline, respectively. A, D: One day before and 2 wk after transfection with vaccine; B, E: One day before and 2 wk after transfection with plasmid; C, F: One day before and 2 wk after transfection with saline.

Table 1 Protective effect of DNA vaccine against H22 tumor cell *in vivo* (mean±SD)

Group	*n*	Tumor latency time (d)	Survival time (d)	Microvessel density	Tumor weight (g)
Vaccine	10	5.20±0.86[a]	24.47±3.23[c]	10.10±1.66[e]	1.41±0.13[g]
Plasmid	10	4.00±0.67	14.70±2.63	27.30±3.34	1.79±0.16
Saline	10	3.80±0.63	14.30±2.00	25.30±4.64	1.82±0.16

[a]$P<0.05$, [c]$P<0.05$, [e]$P<0.05$, [g]$P<0.05$ *vs* plasmid group and saline group.

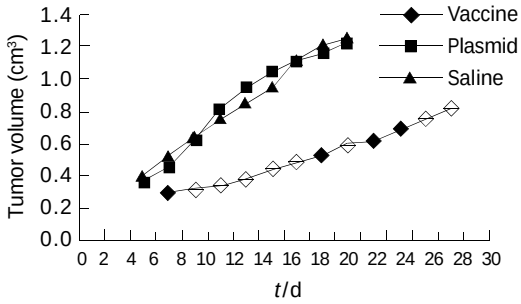

Figure 5 Curve of tumor growth in preventive group.

MVD of different subgroups Macroscopic structure showed the tumor tissue was hard and adhered to the surrounding tissue. MVD of vaccine subgroup was the lowest among the three subgroups ($P<0.05$). MVD of the plasmid subgroup and saline subgroup have no statistical significance compared with each other ($P>0.05$). This indicates that V subgroup has the lowest micro vessel density (Figure 6).

Therapeutic effect of pcDNA3.1 (+)-flk-1-domain1-3 against H22

Inhibitory effect of pcDNA3.1 (+)-flk-1-domain1-3 in carcinogenesis Treated with DNA vaccine pcDNA3.1 (+)-flk-1-domain1-3, plasmid and saline, The survival time of the vaccine subgroup were longer than that of plasmid subgroup and saline subgroup ($P<0.05$); The tumor weight and tumor volume of vaccine subgroup was the lowest among the 3 subgroups ($P<0.05$, Table 2, Figure 7). The survival time, tumor volume and tumor weight of plasmid subgroup and saline subgroup have no statistical significance compared with each other. But the survival times of therapeutic vaccine subgroup were significantly shorter than that of preventive vaccine subgroup ($P<0.05$); the tumor size, and MVD of therapeutic vaccine subgroup were significantly greater than that of preventive vaccine subgroup (Table 3).

MVD of different subgroups Macroscopic structure showed the tumor tissue was hard and adhered to the surrounding tissue. MVD of vaccine subgroup was the lowest among the 3 subgroups ($P<0.05$). MVD of the plasmid subgroup and saline subgroup had no statistical significance compared with each other (Figure 8).

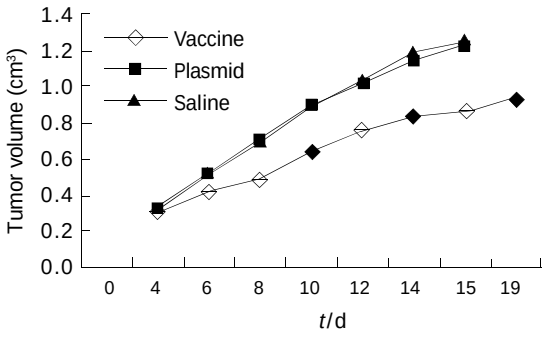

Figure 7 Curve of tumor growth in therapeutic group.

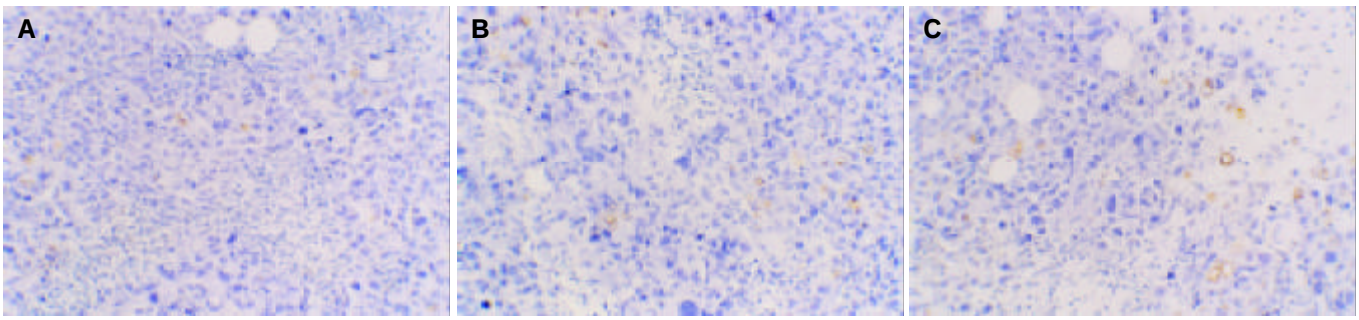

Figure 6 Microvessel staining by anti-CD31 antibody in preventive Group (Original magnification: ×200). A: Vaccine subgroup; B: Plasmid control group; C: Saline control group.

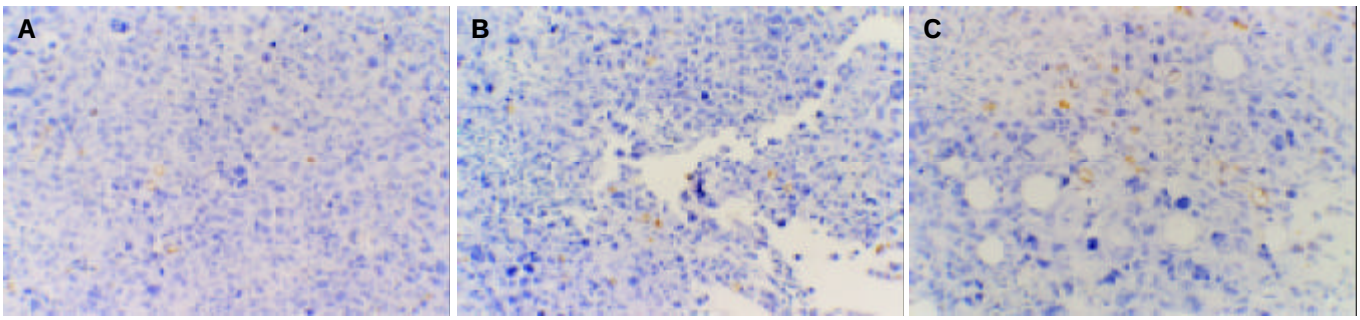

Figure 8 Microvessel staining by anti-CD31 antibody in therapeutic group. A: Vaccine subgroup; B: Plasmid control group; C: Saline control group.

Table 2 Therapeutic effects of DNA vaccine against H22 tumor cell *in vivo* (mean±SD)

Group	*n*	Survival time (d)	Microvessel density	Tumor weight (g)
Vaccine	10	19.17±1.72[a]	18.60±3.47[c]	1.57±0.12[e]
Saline	10	13.52±1.89	26.90±3.41	1.85±0.09
Plasmid	10	13.67±2.94	25.50±4.43	1.82±0.06

[a]$P<0.05$, [c]$P<0.05$, [e]$P<0.05$ *vs* plasmid group and saline group.

Table 3 Comparison of therapeutic and preventive effects of DNA vaccine (mean±SD)

Group	*n*	Survival time (d)	Microvessel density	Tumor weight (g)
Protective vaccine subgroup	10	24.47±3.23[a]	10.10±1.66[c]	1.41±0.13[e]
Therapeutic vaccine subgroup	10	19.17±1.72	18.60±3.47	1.57±0.12

[a]$P<0.05$, [c]$P<0.05$, [e]$P<0.05$ *vs* therapeutic vaccine subgroup.

DISCUSSION

We successfully cloned the domains 1-3 of extracellular parts of flk-1, constructed the DNA vaccine pcDNA3.1 (+) flk-1-domains 1-3, which induced the immune response against endothelial cell, and finally blocked the growth of H22 tumor cells by blocking angiogenesis.

DNA sequencing and blast showed that the cloned gene completely matched the DNA sequence listed in GenBank. Western blot of lipotransfected COS7 showed that the cell transfected with vaccine could express a M_r 44 000 specific protein, which had no corresponding band in the control group, indicating that flk-1 could be expressed by the vaccine in eukaryotic cells. Standard 4-h ^{51}Cr release test showed that the vaccine against domains 1-3 could generate specific immune response in mice through breaking tolerance to self-flk-1 antigen.

In the immune preventive group, mice were first inoculated with the vaccine and then challenged with tumor cells. The results showed that compared with the control group, the inoculated mice had a longer survival time, longer tumor latent period, lower tumor weight at death time and slower tumor growth rate. Furthermore, tumor in inoculated mice had low MVD. So we concluded that the vaccine inhibited tumor growth by its anti-angiogenic effects. In the therapeutic group, effects of the vaccine were supposed to investigate in the clinical conditions. The H22 cells were first injected to the mice and waited until tumor was well constructed, then the mice were treated with the vaccine. We found that, similar to the preventive group, the survival time, tumor weight at death time of mice and tumor growth rate all had significant difference compared with the control group. But compared with that of the preventive group, the vaccine was less effective in the therapeutic group, The MVD, survival time had significant difference between the vaccine subgroup of these groups, indicating that the vaccine might be less effective against well-structured tumors.

Recent advances in the understanding of the molecular control of angiogenesis have shown that this process is essential for tumor development and spread. VEGF is a highly specific mitogen for vascular endothelial cells, which can induce endothelial cell proliferation, promotes cell migration, and inhibits cell apoptosis and immune response against cancer[8-11], and plays a central role in the tumor angiogenesis[12-14].

Flk-1 is the main receptor though which VEGF could modulate tumor growth and metastasis[15-18]. Flk-1 belongs to receptor tyrosine kinases (RTKs) family and are expressed almost exclusively in endothelial cells and on various types of tumor cells[19,20]. Flk-1 has a typical tyrosine kinase receptor structure with 7 immunoglobulin (Ig)-like domains in the extracellular region, as well as a long kinase insert in the tyrosine kinase domain[20]. Evidence shows that IgG-like domains 2-3 are sufficient for tight binding, domain 1 is necessary for tight binding and domains 4-7 are not essential for signaling, and the residues within this region of domain 3 are critical for VEGF binding[21, 22]. Various studies have shown that VEGF and flk-1 expression are significantly associated with advanced stage, high incidence of distant metastases after surgery, and less favorable prognosis in a number of malignancies[23-28]. As it directly involved in tumor angiogenesis, flk-1 is an appropriate target for suppression of solid tumor growth[6].

Several approaches have been used to block flk-1, including dominant-negative receptor mutants, germ-line disruption of VEGFR genes, monoclonal antibodies, dendritic cell vaccine, and a series of synthetic RTK inhibitors[29-33]. They all achieved the goal of blocking VEGF-flk-1 signaling pathway and inhibiting angiogenesis, but they all have some common defects, such as requiring constant drug injection, only blocking VEGF pathway and high cost. Our strategy was to construct DNA vaccine target flk-1 in order to inhibit angiogenesis by blocking VEGF-flk-1 pathway and destructing endothelial cell that expresses flk-1. Compared with strategies mentioned above, DNA vaccines against flk-1 could achieve similar results and are simpler and cheaper to produce and can induce very long-lasting immune responses[34,35]. Furthermore, the immune response not only blocks VEGF-flk-1 pathway, but also blocks other angiogenesis pathway by destruction of endothelial cells[33]. Also it has been reported that liver cancer cells and various types of other tumor cells could express flk-1 receptor, but in our study we could not amplify flk-1 gene from cultured H22 tumor cells, so we could not evaluate whether or not the vaccine had direct effect on the tumor cells. Our research showed that the vaccine was less effective against well-formed tumors. This may be contributed to the immune escaping capacity of well-structured tumors. This result was in consistent with previous reports at home and abroad[33, 36-38]. So we propose that the vaccine should be combined with other therapies, such as surgery, to prevent primary site from recurring and metastasis. Further research is needed in this direction.

In short, we constructed DNA vaccine against extracellular domain1-3 of flk-1, and evaluated its immune preventive and immune therapeutic effects against H22 tumor cell, suggesting that the vaccine could inhibit tumor growth through its anti-angiogenic effect. Further research is needed to increase the effectiveness of this vaccine.

REFERENCES

1 **Bikfalvi A**, Bicknell R. Recent advances in angiogenesis, anti-angiogenesis and vascular targeting. *Trends Pharmacol Sci* 2002; **23:** 576-582

2 **Shibuya M.** Angiogenesis,anti-angiogenesis, and tumor suppression. *Nippon Yakurigaku Zasshi* 2002; **120**: 285-294

3 **Matter A.** Tumor angiogenesis as a therapeutic target. *Drug Discov Today* 2001; **6**: 1005-1024

4 **Bisacchi D**, Benelli R, Vanzetto C, Ferrari N, Tosetti F, Albini A. Anti-angiogenesis and angioprevention: mechanisms, problems and perspectives. *Cancer Detect Prev* 2003; **27**: 229-238

5 **Shibuya M.** Structure and function of VEGF/VEGF-receptor system involved in angiogenesis. *Cell Struct Funct* 2001; **26**: 25-35

6 **Shibuya M.** Vascular endothelial growth factor receptor-2: its unique signaling and specific ligand, VEGF-E. *Cancer Sci* 2003; **94**: 751-756

7 **Weidner N**, Folkman J, Pozza F, Bevilacqua P, Allred EN, Moore DH, Meli S, Gasparini G. Tumor angiogenesis: a new

significant and independent prognostic indicator in early-stage breast carcinoma. *J Natl Cancer Inst* 1992; **84**: 1875-1887

8 **Graff BA**, Bjornaes I, Rofstad EK. Microvascular permeability of human melanoma xenografts to macromolecules: relationships to tumor volumetric growth rate, tumor angiogenesis, and VEGF expression. *Microvasc Res* 2001; **61**: 187-198

9 **Baek JH**, Jang JE, Kang CM, Chung HY, Kim ND, Kim KW. Hypoxia-induced VEGF enhances tumor survivability via suppression of serum deprivation-induced apoptosis. *Oncogene* 2000; **19**: 4621-4631

10 **Ohm JE**, Gabrilovich DI, Sempowski GD, Kisseleva E, Parman KS, Nadaf S, Carbone DP. VEGF inhibits T-cell development and may contribute to tumor-induced immune suppression. *Blood* 2003; **101**: 4878-4886

11 **Ohm JE**, Carbone DP. VEGF as a mediator of tumor-associated immunodeficiency. *Immunol Res* 2001; **23**: 263-272

12 **Yoshida S**, Amano H, Hayashi I, Kitasato H, Kamata M, Inukai M, Yoshimura H, Majima M. COX-2/VEGF-dependent facilitation of tumor-associated angiogenesis and tumor growth *in vivo*. *Lab Invest* 2003; **83**: 1385-1394

13 **Verheul HM**, Pinedo HM. The role of vascular endothelial growth factor (VEGF) in tumor angiogenesis and early clinical development of VEGF-receptor kinase inhibitors. *Clin Breast Cancer* 2000; **1**(Suppl 1): S80-84

14 **Werther K**, Nielsen HJ. Significance of vascular endothelial growth factor-VEGF-in tumor angiogenesis. Therapeutic possibilities in solid tumors. *Ugeskr Laeger* 2000; **162**: 4916-4920

15 **Yoshiji H,** Kuriyama S, Hicklin DJ, Huber J, Yoshii J, Miyamoto Y, Kawata M, Ikenaka Y, Nakatani T, Tsujinoue H, Fukui H. KDR/Flk-1 is a major regulator of vascular endothelial growth factor-induced tumor development and angiogenesis in murine hepatocellular carcinoma cells. *Hepatology* 1999; **30**: 1179-1186

16 **Brekken RA**, Overholser JP, Stastny VA, Waltenberger J, Minna JD, Thorpe PE. Selective inhibition of vascular endothelial growth factor (VEGF) receptor 2 (KDR/Flk-1) activity by a monoclonal anti-VEGF antibody blocks tumor growth in mice. *Cancer Res* 2000; **60**: 5117-5124

17 **Neufeld G**, Cohen T, Gengrinovitch S, Poltorak Z. Vascular endothelial growth factor (VEGF) and its receptors. *FASEB J* 1999; **13**: 9-22

18 **Xiang F**, Tanaka J, Takahashi J, Fukuda T. Expression of vascular endothelial growth factor (VEGF) and its two receptors in diffusely infiltrating astrocytomas and relationship to proliferative activity of tumor cells. *Brain Tumor Pathol* 2001; **18**: 67-71

19 **Kanno S,** Oda N, Abe M, Terai Y, Ito M, Shitara K, Tabayashi K, Shibuya M, Sato Y. Role of two VEGF receptors, Flt-1 and KDR, in the signal transduction of VEGF effects in human vascular endothelial cells. *Oncogene* 2000; **19**: 2138-2146

20 **McMahon G.** VEGF receptor signaling in tumor angiogenesis. *Oncologist* 2000; **5**(Suppl 1): 3-10

21 **Shinkai A**, Ito M, Anazawa H, Yamaguchi S, Shitara K, Shibuya M. Mapping of the sites involved in ligand association and dissociation at the extracelluar domain of the kinase insert domain-containing receptor of vascular endothelial growth factor. *J Biol Chem* 1998; **273**: 31283-31288

22 **Lu D**, Kussie P, Pytowski B, Persaud K, Bohlen P, Witte L, Zhu Z. Identification of the residues in the extracellular region of KDR important for interaction with vascular endothelial growth factor and neutralizing anti-KDR antibodies. *J Biol Chem* 2000; **275**: 14321-14330

23 **Ryden L,** Linderholm B, Nielsen NH, Emdin S, Jonsson PE, Landberg G. Tumor specific VEGF-A and VEGFR2/KDR protein are co-expressed in breast cancer. *Breast Cancer Res Treat* 2003; **82**: 147-154

24 **Mukherjee T,** Kumar A, Mathur M, Chattopadhyay TK, Ralhan R. Ets-1 and VEGF expression correlates with tumor angiogenesis, lymph node metastasis, and patient survival in esophageal squamous cell carcinoma. *J Cancer Res Clin Oncol* 2003; **129**: 430-436

25 **Stockhammer G**, Obwegeser A, Kostron H, Schumacher P, Muigg A, Felber S, Maier H, Slavc I, Gunsilius E, Gastl G. Vascular endothelial growth factor (VEGF) is elevated in brain tumor cysts and correlates with tumor progression. *Acta Neuropathol* 2000; **100**: 101-105

26 **Wang S**, Xia T, Zhang Z, Kong X, Zeng L, Mi P, Xue Z. Expression of VEGF and tumor angiogenesis in bladder cancer. *Zhonghua Waike Zazhi* 2000; **38**: 34-36

27 **Tamura M,** Ohta Y, Kajita T, Kimura K, Go T, Oda M, Nakamura H, Watanabe G. Plasma VEGF concentration can predict the tumor angiogenic capacity in non-small cell lung cancer. *Oncol Rep* 2001; **8:** 1097-1102

28 **Karademir S**, Sokmen S, Terzi C, Sagol O, Ozer E, Astarcioglu H, Coker A, Astarcioglu I. Tumor angiogenesis as a prognostic predictor in pancreatic cancer. *J Hepatobiliary Pancreat Surg* 2000; **7**: 489-495

29 **Becker CM,** Farnebo FA, Iordanescu I, Behonick DJ, Shih MC, Dunning P, Christofferson R, Mulligan RC, Taylor GA, Kuo CJ, Zetter BR. Gene therapy of prostate cancer with the soluble vascular endothelial growth factor receptor Flk1. *Cancer Biol Ther* 2002; **1**: 548-553

30 **Li Y**, Wang MN, Li H, King KD, Bassi R, Sun H, Santiago A, Hooper AT, Bohlen P, Hicklin DJ. Active immunization against the vascular endothelial growth factor receptor flk1 inhibits tumor angiogenesis and metastasis. *J Exp Med* 2002; **195**: 1575-1584

31 **Zhang W**, Ran S, Sambade M, Huang X, Thorpe PE. A monoclonal antibody that blocks VEGF binding to VEGFR2 (KDR/Flk-1) inhibits vascular expression of Flk-1 and tumor growth in an orthotopic human breast cancer model. *Angiogenesis* 2002; **5**: 35-44

32 **Shibuya M**. VEGF-receptor inhibitors for anti-angiogenesis. *Nippon Yakurigaku Zasshi* 2003; **122**: 498-503

33 **Li Y,** Wang MN, Li H, King KD, Bassi R, Sun H, Santiago A, Hooper AT, Bohlen P, Hicklin DJ. Active immunization against the vascular endothelial growth factor receptor flk1 inhibits tumor angiogenesis and metastasis. *J Exp Med* 2002; **195**: 1575-1584

34 **Haupt K,** Roggendorf M, Mann K. The potential of DNA vaccination against tumor-associated antigens for antitumor therapy. *Exp Biol Med* 2002; **227**: 227-237

35 **Henke A.** DNA immunization–a new chance in vaccine research? *Med Microbiol Immunol* 2002; **191**: 187-190

36 **Muehlbauer PM.** Anti-angiogenesis in cancer therapy. *Semin Oncol Nurs* 2003; **19**: 180-192

37 **Zogakis TG,** Libutti SK. General aspects of anti-angiogenesis and cancer therapy. *Expert Opin Biol Ther* 2001; **1:** 253-275

38 **Takahashi Y,** Mai M. Significance of angiogenesis and clinical application of anti-angiogenesis. *Nippon Geka Gakkai Zasshi* 2001; **102**: 381-384

Edited by Kumar M and Chen WW **Proofread by** Xu FM

PO Box 2345, Beijing 100023, China
Fax: +86-10-85381893
E-mail: wjg@wjgnet.com www.wjgnet.com

World J Gastroenterol 2004;10(14):2045-2049
World Journal of Gastroenterology
 ISSN 1007-9327

Identification of 5' capped structure and 3' terminal sequence of hepatitis E virus isolated from Morocco

Guo-Bing Chen, Ji-Hong Meng

Guo-Bing Chen, Ji-Hong Meng, Department of Microbiology and Immunology, Southeast University School of Medicine, Nanjing 210009, Jiangsu Province, China
Supported by the Natural Scientific Foundation, No. 30271231; and the Natural Scientific Foundation of Jiangsu Province, No. BK2002053
Correspondence to: Professor Ji-Hong Meng, Department of Microbiology and Immunology, Southeast University School of Medicine, Nanjing 210009, Jiangsu Province, China. jihongmeng @263.net
Telephone: +86-25-3272454
Received: 2003-12-17 **Accepted:** 2004-01-08

Abstract

AIM: To examine 5' and 3' terminal sequences of hepatitis E virus (HEV) isolated from Morocco, to confirm 5' methylated cap structure of the genome, and to investigate whether the 3' UTR can be used to distinguish HEV genotypes instead of HEV complete genome sequence.

METHODS: RNA ligase-mediated rapid amplification of cDNA ends (RLM-RACE) was employed to obtain the 5' and 3' terminal sequences of HEV Morocco strain. The 3' UTR sequence of the Morocco strain was compared with that of the other 29 HEV strains using the DNAStar software.

RESULTS: The 5' PCR product was obtained only from the RLM-RACE based on the capped RNA template. The 5' UTR of the Morocco strain had 26 nucleotides, and the 3' UTR had 65 nucleotides upstream to the polyA. The 5' UTR between HEV strains had only point mutations of nucleotides. The phylogenetic tree based on the sequences of 3' UTR was not the same as that based on the complete sequences.

CONCLUSION: The genome of HEV Morocco strain was methylated cap structure. The 3' terminal sequence can not be used for distinguishing HEV genotype for all HEV strains in place of the whole HEV genome sequence.

Chen GB, Meng JH. Identification of 5' capped structure and 3' terminal sequence of hepatitis E virus isolated from Morocco. *World J Gastroenterol* 2004; 10(14): 2045-2049
http://www.wjgnet.com/1007-9327/10/2045.asp

INTRODUCTION

Hepatitis E virus (HEV) is an enterically transmitted agent that causes epidemic and sporadic cases of hepatitis predominantly in developing countries of Asia, Africa and North America[1]. The disease generally affects young adults and has a high mortality rate, up to 20%, in infected pregnant women. Success in cloning and sequencing of the HEV genome allowed the elucidation of the HEV genetic organization[2]. The HEV genome is a positive-sense, single-stranded, polyadenylated RNA of approximately 7.2 kb containing three open reading frames (ORFs). ORF1, located at the 5' end of the genome, is about 5 kb in length and encodes for a putative nonstructural polyprotein that contains motifs characteristic for methyltransferase, papain-like protease, RNA helicase, and RNA-dependent RNA polymerase domains. ORF2 is about 2 kb in length and encodes for the structural protein(s). The small ORF3 of only 369 nucleotides overlaps ORF1 and ORF2 and encodes for a protein of unknown function[3].

The genomes of several HEV strains from Asia and North America have been sequenced in their entirety[4]. Partial sequences are also available for other strains from some of these geographic regions. In Africa, the HEV virus has been identified from Morocco, Tunis, Algeria, Chad, Egypt, Nigeria and Namibia[5-10]. However, only a few short isolated nucleotide sequences from African strains of HEV were available for analysis. In 1997, Chatterjee *et al.* isolated an HEV strain in Morocco[5]. In 1999, Meng *et al.* obtained the nucleotide sequences of HEV Morocco strain that spanned the extreme 3' terminal region of ORF1, full length ORF2 and ORF3, and a part of the 3' noncoding region[11,12]. Although more similar to the Asian strains than to the Mexico strain, partial HEV sequences from Morocco strains were, nonetheless, distinct from all known Asian strains. It is urgent to obtain the complete sequence of the Morocco strain to elucidate its biological function.

Although the genomic coding regions of several HEV strains have been sequenced completely, the sequence of the 5' UTR has been reported only for a limited number of HEV strains[13]. The 5' UTR of HEV strains were usually determined either by cDNA cloning and sequencing or by classical 5' rapid amplification of cDNA ends (RACE)[13]. However, there still exists the possibility that the 5' UTR sequences are not complete because neither method has a control to detect premature termination of cDNA synthesis. Furthermore, by coupling a reverse transcription polymerase chain reaction (RT-PCR) assay with immune-capture of genomic RNA based on the ability of a monoclonal antibody to recognize 7-methylguanosine showed that the genomic RNA of HEV is capped[14]. It is not clear how this structure will have affected previous assays used to determine the 5' terminal nucleotides. For getting the complete sequence of HEV Morocco strain, we employed a RLM-RACE technique to obtain the 5' and 3' terminal sequences in our study, and confirmed that the genome of Morocco strain was capped.

Furthermore, how to distinguish the genotypes of HEV is still an issue. Based on the complete sequence analysis, Burma-1, Burma-2, China-1 to -6, Pak-1, Pak-2, India-1 to -4, Nepal and Morocco strains are included in genotype I; Mexico strain belongs to genotype II; Genotype III holds US-1, US-2, US-SW, Japan-1 to -7, Japan-SW and Canada-SW; China-T1 belongs to genotype IV[15-17]. Considering the difficulties in obtaining the complete sequences of each strain, we attempted to evaluate whether the 3' UTR can be used to analyze the HEV genotype in this study.

MATERIALS AND METHODS

Sample

The sample was obtained from Professor Pillot, Pasteur Institute, France, and treated as described in references 16 and

17. Aliquots of virus stock were prepared and stored at -70 ℃.

Reagents

HEV RNA was extracted with TRIzol (GIBCO, USA). The 5' and 3' RLM-RACE was carried out with the GeneRacer kit (Invitrogen, USA). The nested PCR was carried out with high fidelity system DNA polymerase (Roche, USA). PCR products were purified with QIAquick PCR purification kit (Qiagen, German).

Primers

5' RACE primers: Two RNA 5' -adaptor primers supplied in the GenRacer kit were used as forward primers. The sequences of the reverse primers were: 5' -AGA AAA GGC CTA ACC ACC ACA GCA TTC G-3' (outer reverse primer) and 5' -CTA AAG CAG CCT GCT CAA TAG CAG TAG-3' (inner reverse primer).

3' RACE primers: Sequences of the forward primers were: 5' -GTT GTC TCA GCC AAT GGC GAG C-3' (outer forward primer) and 5' -AAG ATG AAG GTG GGT AAA ACT CGG GAG-3' (inner forward primer). Two RNA 3' -adaptor primers supplied in the GenRacer kit were used as reverse primers.

GenBank accession number and software

The GenBank accession number of 3' UTR sequence of HEV Morocco strain was AY220474. The 5' and 3' UTR sequence of Morocco strain were compared with that of other 29 strains, respectively, by the MegAlign in DNAStar software (DNASTAR Inc, USA). The phylogenetic trees of 3' and complete HEV sequences were also made with MegAlign in DNASTAR. The GenBank accession numbers of these sequences were: Jap-SW (AB073912)[18], Japan-1 (AB074918), Japan-2 (AB074920)[19], Japan-3 (AB089824)[20], Japan-4 (AP003430)[21], Japan-5 (AB074915), Japan-6 (AB074917)[19], Japan-7 (AB080575)[22], Nepal (AF051830)[23], US-1 (AF060668), US-2 (AF060669)[24,25], US-SW (AF082843)[26], Canada-SW (AY115488)[27], India-1 (X98292), India-2 (AF459438)[28], India-3 (AF076239)[29], India-4 (X99441), Pak-1 (M80581)[30], Pak-2 (AF185822)[31], Burma-1 (M73218)[3], Burma-2 (D10330)[32], China-1 (L25547), China-2 (L25595)[33], China-3 (L08816), China-4 (M94177)[34], China -5 (D11092)[35], China-6 (D11093), Mexico (M74506)[4] and China-T1 (AJ272108)[36]. The RNA secondary structure was reconstructed with RNAstructure software (Isis Pharmaceuticals).

Extraction of HEV RNAs

One hundred microliters of the filtered supernatant of the Morocco strain was mixed with 400 μL of TRIzol reagent. The mixture was homogenized and incubated for 5 min at room temperature. One hundred microliters of chloroform was added and the mixture was vigorously shaken for 15 s and incubated at room temperature for 3 min. After centrifugation at 12 000 *g* for 15 min at 4 ℃, the aqueous phase was transferred to a fresh microfuge tube. The RNA from the aqueous phase was precipitated by incubating with an equal volume of isopropyl alcohol and 1 μL of glycogen (20 mg/mL) at room temperature for 15 min, and centrifuging at 12 000 *g* at 4 ℃ for 15 min. After removing the supernatant, the RNA pellet was washed once with 800 μL of 750 mL/L ethanol and centrifuged again, dried, and then dissolved in 20 μL of diethylpyrocarbonate treated water.

5' RLM-RACE

The 5' RACE was carried out with the GeneRacer kit following the manufacture' s instructions. Briefly, 14 μL of extracted RNA was treated with calf intestinal phosphatase (CIP) in a total 20 μL reaction mixture containing 2 μL of 10× CIP buffer and 2 μL of CIP for 1 h at 50 ℃. After extracted with phenol/chloroform, RNA was resuspended in 6 μL of nuclease-free water. The 6 μL of CIP-treated RNA was treated with tobacco acid pyrophosphatase (TAP) in a 10 μL of reaction mixture containing 1 μL of 10× TAP buffer and 2 μL of TAP for 1 h at 37 ℃. Again after extracted with phenol/chloroform, the CIP/TAP-treated RNA was resuspended in 6 μL of nuclease-free water and ligated to 250 ng of RNA adaptor by T4 RNA ligase in a 10 μL reaction mixture for 1 h at 37 ℃. Then the CIP/TAP/Ligated-RNA was extracted with phenol/chloroform and resuspended in 20 μL nuclease-free water and reserved at -70 ℃. Another 6 μL non-treated RNA was ligated to 250 ng of RNA adaptor directly by T4 RNA ligase as a control. Ten microliters of the ligated RNA or control RNA was used as a template to synthesize cDNA with AMV reverse transcriptase for 1 h at 42 ℃. The outer reverse primer was used to prime the cDNA synthesis. The cDNA was then amplified by nested PCR with high fidelity system DNA polymerase. The PCR reaction mixture was incubated for 2 min at 94 ℃ followed by 35 amplification cycles, comprising denaturation at 94 ℃ for 30 s, annealing at 65 ℃ for 30 s and extension at 72 ℃ for 30 s. The reaction was extended for another 7 min at 72 ℃ to insure the full extension. Based on our former work (data not shown), the expected size of the final PCR product was 100 bp or greater. PCR products were analyzed on 20 g/L agarose gel.

3' RACE

The 3' RACE was carried out with the GeneRacer kit following the manufacture' s instructions. Ten microliters of the HEV RNA was used as a template to synthesize cDNA with AMV reverse transcriptase for 1 h at 42 ℃. The oligo (dT)-adaptor primer supplied with the kit was used to prime the cDNA synthesis. The cDNA was then amplified by nested PCR with high fidelity system DNA polymerase. The PCR reaction mixture was incubated for 2 min at 94 ℃, followed by 35 amplification cycles comprising denaturation at 94 ℃ for 30 s, annealing at 65 ℃ for 30 s, and extension at 72 ℃ for 30 s. The reaction was extended for another 7 min at 72 ℃ to ensure the full extension. Based on our former work (data not shown), the expected size of the final PCR product was 98 bp or greater. PCR products were analyzed on 20 g/L agarose gel.

Sequence analysis and comparison

PCR products were purified with QIAquick PCR purification kit and sequenced. The 5' and 3' UTR sequence of Morocco strain were compared with that of other 29 strains, respectively, using DNAStar software. The RNA secondary structure was reconstructed with RNAstructure software. The phylogenetic trees of 3' and complete HEV sequences were also made with DNASTAR.

RESULTS

5' UTR

As shown in Figure 1A, bands of the expected size were obtained. The band was obtained in 5' RLM-RACE reactions only when the template was CIP/TAP treated RNA.

The 5' terminus of Morocco had 26 nucleotides preceding the predicted start codon, including the 7-methylguanosine. The sequence of PCR product was: GGC AGA CCA CAT ATG TGG TCG ATG CC. A comparison of the 5' UTR sequence of 30 HEV strains was made as shown in Figure 2: there was a "T" at the position 4 preceding the predicted start codon in Morocco and other 25 strains while a "C" was found in other four strains; a "G" at the position 9 in the Morocco and other 28 strains turn out to be a "T" in US-SW strain; an "A" at the position 16 in Morocco and other 20 strains was replaced by a "G" or "C" in other nine strains; an additional

"A" at the terminus of eight strains except Morocco strain; and additional 9 nucleotides in the US-2 terminus.

As shown in Figure 3, the 26 nucleotides of 5' terminus could form a putative stem-loop structure. All single-nucleotide differences occurred within that loop structure.

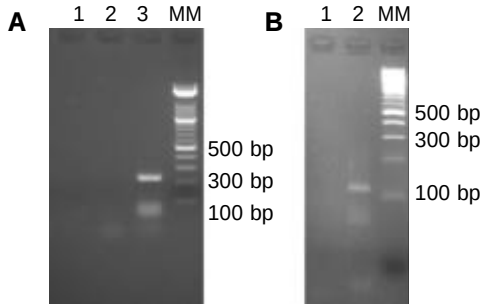

Figure 1 RT-PCR products of 5' and 3' RNA of HEV Morocco strain. A: Products of 5' RLM-RACE; Lane 1: negative control without template RNA; Lane 2: RNA template without CIP/TAP treated; Lane 3: RNA template treated with CIP and TAP. B: Products of 3' RACE; Lane 1: negative control without template RNA; Lane 2: products of 3' RACE; MM: 100 bp ladder.

Sequence Name		< Pos = 35 30 25 20 15 10 5 1
Burma-1	[1]	--------AGGCAGACCACATATGTGGTCGATGCCATG
Burma-2	[1]	--------AGGCAGACCACATATGTGGTCGATGCCATG
Canada-3W	[3]	---------GGCAGACCACGTATGTGGTCGATGCCATG
China-1	[1]	---------GGCAGACCACATATGTGGTCGATGCCATG
China-2	[1]	---------GGCAGACCACATATGTGGTCGATGCCATG
China-3	[1]	----------------------------------GCCATG
China-4	[1]	--------AGGCAGACCACATATGTGGTCGATGCCATG
China-5	[1]	--------AGGCAGACCACATATGTGGTCGATGCCATG
China-6	[1]	--------AGGCAGACCACATATGTGGTCGATGCCATG
China-T1	[4]	----------GCAGACCACGTATGTGGTCGACGCCATG
India-1	[1]	---------GGCAGACCACCTATGTGGTCGATGCCATG
India-2	[1]	--------AGGCAGACCACATATGTGGTCGATGCCATG
India-3	[1]	--------AGGCAGACCACATATGTGGTCGATGCCATG
India-4	[1]	--------AGGCAGACCACATATGTGGTCGATGCCATG
Japan-1	[3]	----------GCAGACCACGTATGTGGTCGATGCCATG
Japan-2	[3]	--------------------------GTCGATGCCATG
Japan-3	[3]	----------GCAGACCACGTATGTGGTCGATGCCATG
Japan-4	[3]	---------GGCAGACCACGTATGTGGTCGATGCCATG
Japan-5	[4]	--------------------------GTCGACGCCATG
Japan-6	[4]	--------------------------GTCGACGCCATG
Japan-7	[4]	----------GCAGACCACGTATGTGGTCGACGCCATG
Jap-3W	[3]	----------GCAGACCACGTATGTGGTCGATGCCATG
Mexico	[2]	----------GCAGACCACATTGTGGTCGATGCCATG
MOROCCO	[1]	---------GGCAGACCACATATGTGGTCGATGCCATG
Nepal	[1]	--------AGGCAGACCACATATGTGGTCGATGCCATG
Pak-1	[1]	----------GCAGACCACATATGTGGTCGATGCCATG
Pak-2	[1]	------------------------------------ATG
US-1	[3]	------------------------------------ATG
US-2	[3]	TCGACAGGGGGCAGACCACGTATGTGGTCGATGCCATG
US-3W	[3]	--------------------------TTCGATGCCATG

Figure 2 Comparison of sequence in the 5' UTR of different HEV strains. The translation initiation codon is underlined. The number in brackets following the strain name is the genotype designation. Changes from the consensus sequence are boxed.

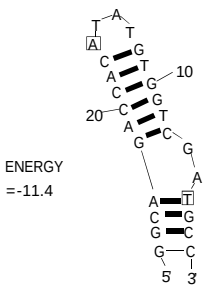

Figure 3 RNA secondary structure of HEV 5' terminal sequence. Changes among HEV strains are boxed.

3'UTR

As shown in Figure 1B, 3' RACE bands of the expected size were obtained. The 3' terminus of Morocco had 65 nucleotides upstream of the polyA (the GenBank accession is AY220474). The sequence of 3' UTR was: TTT ATT TGC TTG TGC CCT CCT TCT TTC TGT TGC TTA TTT CTC TTT TCT GCG TTT CGC GCT CCC TG. The comparison of the 3' UTR sequence with the corresponding regions of other 29 HEV strains from different parts of the world revealed that the Morocco strain was most similar to the genotype 1 strains (92.3-97.4%) (Table 1). The 3' UTR nucleotide sequences of the HEV genotypes II, III and IV strains shared a lower similarity with that of Morocco strain: 80%, 65.6-83.1% and 84.6-89.2%, respectively. The phylogenetic trees also showed that the HEV Morocco strain was grouped together with all genotype I strains as a separate branch (Figures 4 and 5). Based on the 3' UTR analysis, Japan-5, -6, -7 belonged to genotype III. But according to the complete sequence analysis, they were included in genotype IV.

Table 1 Percent identity of 3' UTR of HEV genotypes (%)

	I	II	III	IV
Mor	92.3-97.4	80	65.6-83.1	84.6-89.2
I	92.3-100	74.4-81.5	25.6-84.6	79.5-90.8
II	-	100	37.5-71.8	55.1-83.8
III	-	-	75.9-94.4	41.4-80.0
IV	-	-	-	77.9-94.3

I, II, III, IV: HEV Genotype; Mor: HEV Morocco strain; -: blank well.

DISCUSSION

Variations in the length of the 5' UTR have been observed. The Burma strain was reported to have 27 nucleotides in its 5' UTR, compared with 35 nucleotides in the 5' UTR of US-2 and 26 nucleotides in the most of other strains[13]. It remains to be determined if the extra nucleotides are really present in functional genomes. Maybe they just represented artifacts generated because the presence of a cap structure was not recognized at the time some of those strains were sequenced, or because of the additional "A" with the non-proofreading DNA polymerase in the PCR action. What was more interesting, the US-2 strain had additional nine nucleotides at the 5' terminus. They were included in the GenBank sequence but had not been discussed elsewhere, so they were difficult to evaluate. Except the US-2, all HEV strains had a comparable 5' UTR sequence with only point change from each other, and the single-nucleotide differences occurred within the loop structure. This structure may play a very important role either in replication or translation. It needs to be verified experimentally.

The 5' UTR sequences obtained by the methods of cDNA cloning/sequencing or classical 5' rapid amplification of cDNA ends (RACE) may be incomplete because neither method has a control to detect premature termination of cDNA synthesis. The finding of a 7mGpppG cap allowed reevaluation of 5' UTR sequences with a modified RACE technique called RNA ligase-mediated RACE (RLM-RACE). In RLM-RACE, an RNA sample was first treated with calf intestinal phosphatase (CIP) to remove the 5' -phosphate from all RNA species except those with a cap structure. Tobacco acid pyrophosphatase (TAP) was then used to remove the cap structure from RNA, leaving a 5' -phosphate. Next, a synthetic RNA adaptor was ligated to the CIP/TAP treated RNA. Because the adaptor ligates only to RNA containing a 5' -phosphate, RLM-RACE ensures that cDNA was amplified from decapped RNA predominantly, starting at the ultimate 5' terminus. In 2001,

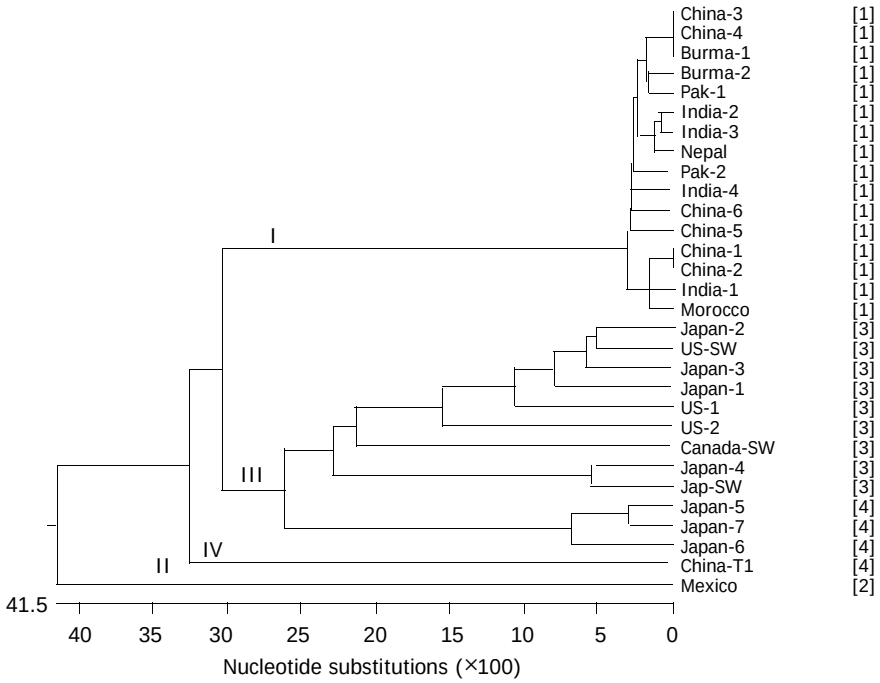

Figure 4 Proposed phylogenetic trees using 3' UTR sequences of Morocco and other 29 HEV strains. The Roman number in the tree represents the genotype designation based on the 3' UTR sequence. The number in brackets following the strain name represents the genotype designation based on the full genome sequence.

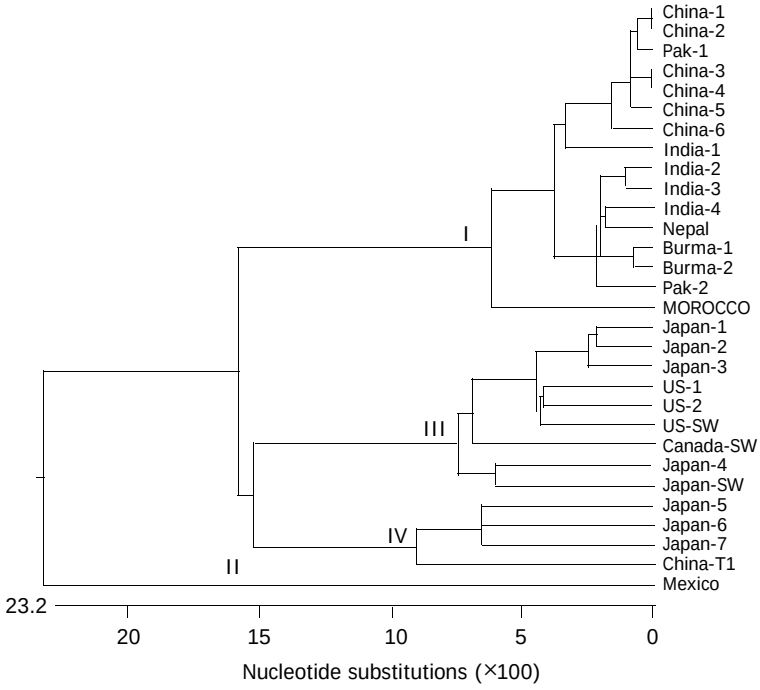

Figure 5 Proposed phylogenetic trees using full sequences of 30 HEV strains. The Roman number in the tree represents the genotype designation.

Zhang *et al.* used the RLM-RACE method to confirm the capped HEV genome and extended the 5' terminal sequence of Mexico and Pak-1 strains[13]. In the current study to obtain the complete sequence of HEV Morocco strain, we used a sequence amplification procedure that required the presence of an internal pyrophosphatase sensitive linkage in the 5' termini of HEV genome. The results indicated that the Morocco strain was capped.

The comparison of the 3' UTR sequence with the corresponding regions of other 29 HEV strains and the phylogenetic trees of those complete sequences of 30 HEV strains revealed that the HEV Morocco strain was grouped together with all genotype I strains as a separate branch. The distribution of 3' UTR of genotypes I, II and IV was as same as that obtained by the comparison of the complete genome sequence. However, three strains isolated from Japan, Japan-5, -6, -7, which were included in genotype IV according to complete sequences analysis, clustered together with the genotype III strains based on the 3' UTR sequences analysis. This suggests that the comparison of HEV 3' UTR sequence can not represent the divergence of complete genome sequence perfectly, although this region is regarded as containing the majority of genotype-specific nucleotide positions, and easily and efficiently to amplify. So, the 3' terminal sequence upstream the polyA can not be used

for phylogenetic genotyping analysis of the HEV genome optionally. Because of the difficulties to get the complete sequences, many scientists preferred to analyze the HEV genotypes based on the partial sequences they obtained. It remains uncertain whether the partial sequences can replace the complete genome in distinguishing the HEV genotypes. So, it is prudent to analyze the HEV genotypes based on complete sequences to date.

REFERENCES

1 **Worm HC**, van der Poel WH, Brandstatter G. Hepatitis E: an overview. *Microbes Infect* 2002; **4**: 657–666

2 **Reyes GR**, Purdy MA, Kim JP, Luk KC, Young LM, Fry KE, Bradley DW. Isolation of a cDNA from the virus responsible for enterically transmitted non-A, non-B hepatitis. *Science* 1990; **247**: 1335-1339

3 **Tam A W**, Smith MM, Guerra ME, Huang CC, Bradley DW, Fry KE, Reyes GR. Hepatitis E virus (HEV): molecular cloning and sequencing of the full-length viral genome. *Virology* 1991; **185**: 120-131

4 **Huang CC**, Nguyen D, Fernandez J, Yun KY, Fry KE, Bradley DW, Tam AW, Reyes GR. Molecular cloning and sequencing of the Mexico isolate of hepatitis E virus (HEV). *Virology* 1992; **191**: 550-558

5 **Chatterjee R**, Tsarev S, Pillot J, Coursaget P, Emerson SU, Purcell RH. African strains of Hepatitis E Virus that are distinct from Asian strains. *J Med Virol* 1997; **53**: 139-144

6 **Benjelloun S**, Bahbouhi B, Bouchrit N, Cherkaoui L, Hda N, Mahjour J, Benslimane A. Seroepidemiological study of an acute hepatitis E outbreak in Morocco. *Res Virol* 1997; **148**: 279-287

7 **Cuyck-Gandre H**, Zhang HY, Tsarev SA, Clements NJ, Cohen SJ, Caudill JD, Buisson Y, Coursaget P, Warren RL, Longer CF. Characterization of Hepatitis E virus (HEV) from Algeria and Chad by partial genome sequence. *J Med Viro*l 1997; **53**: 340-347

8 **Tsarev SA**, Binn LN, Gomatos PJ, Arthur RR, Monier MK, Cuyck-Gandre H, Longer CF, Innis BL. Phylogenetic analysis of hepatitis E virus isolates from egypt. *J Med Virol* 1999; **57:** 68–74

9 **Buisson Y,** Grandadam M, Nicand E, Cheval P, Cuyck-Gandre H, Innis B, Rehel P, Coursaget P, Teyssou R, Tsarev S. Identification of a novel hepatitis E virus in Nigeria. *J Gen Virol* 2000; **81**: 903-909

10 **Maila HT,** Bowyer SM, Swanepoel R. Identification of a new strain of hepatitis E virus from an outbreak in Namibia in 1995. *J Gen Virol* 2004; **85**: 89-95

11 **Meng J**, Cong M, Dai X, Pillot J, Purdy MA, Fields HA, Khudyakov YE. Primary structure of open reading frame 2 and 3 of the Hepatitis E Virus isolated from Morocco. *J Med Virol* 1999; **57**: 126-133

12 **Meng J**, Pillot J, Dai X, Fields HA, Khudyakov YE. Neutralization of different geographic strains of the hepatitis E virus with anti-hepatitis E virus-positive serum samples obtained from different sources. *Vorology* 1998; **249**: 316-324

13 **Zhang M**, Purcell RH, Emerson SU. Identification of the 5' terminal sequence of the SAR-55 and MEX-14 strains of Hepatitis E Virus and confirmation that the genome is capped. *J Med Virol* 2001; **65**: 293-295

14 **Kabrane-Lazizi Y**, Meng XJ, Purcell RH, Emerson SU. Evidence that the genomic RNA of hepatitis E virus is capped. *J Virol* 1999; **73**: 8848-8850

15 **Schlauder GG**, Mushahwar IK. Genetic Heterogeneity of Hepatitis E Virus. *J Med Virol* 2001; **65**: 282-292

16 **Meng J**, Guinet R, Pillot J. Infection of PLC / PRF / 5 cells with the hepatitis E virus. IN :Buisson Y, Coursaget P, Kane M, editors. Enterically-transmitted hepatitis viruses. Joue-les-Tours, *France: La Simarre* **1996**: P336-345

17 **Meng J**, Dubreuil P, Pillot J. A new PCR-based seronrutralization assay in cell culture for diagnosis of hepatitis E. *J Clin Microbiol* 1997; **35**: 1373-1377

18 **Okamoto H**, Takahashi M, Nishizawa T, Fukai K, Muramatsu U, Yoshikawa A. Analysis of the complete genome of indigenous swine hepatitis E virus isolated in Japan. *Biochem Biophys Res Commun* 2001; **289**: 929-936

19 **Takahashi K**, Kang JH, Ohnishi S, Hino K, Mishiro S. Genetic heterogeneity of hepatitis E virus recovered from Japanese patients with acute sporadic hepatitis. *J Infect Dis* 2002; **185**: 1342-1345

20 **Tokita H**, Harada H, Gotanda Y, Takahashi M, Nishizawa T, Okamoto H. Molecular and serological characterization of sporadic acute hepatitis E in a Japanese patient infected with a genotype III hepatitis E virus in 1993. *J Gen Virol* 2003; **84**: 421-427

21 **Takahashi K**, Iwata K, Watanabe N, Hatahara T, Ohta Y, Baba K, Mishiro S. Full-genome nucleotide sequence of a hepatitis E virus strain that may be indigenous to Japan. *Virology* 2001; **287**: 9-12

22 **Takahashi M**, Nishizawa T, Yoshikawa A, Sato S, Isoda N, Ido K, Sugano K, Okamoto H. Identification of two distinct genotypes of hepatitis E virus in a Japanese patient with acute hepatitis who had not travelled abroad. *J Gen Virol* 2002; **83**: 1931-1940

23 **Gouvea V**, Snellings N, Popek MJ, Longer CF, Innis BL. Hepatitis E virus: complete genome sequence and phylogenetic analysis of a Nepali isolate. *Virus Res* 1998; **57**: 21-26

24 **Schlauder GG**, Dawson GJ, Erker JC, Kwo PY, Knigge MF, Smalley DL, Rosenblatt JE, Desai SM, Mushahwar IK. The sequence and phylogenetic analysis of a novel hepatitis E virus isolated from a patient with acute hepatitis reported in the United States. *J Gen Virol* 1998; **79**: 447-456

25 **Erker JC**, Desai SM, Schlauder GG, Dawson GJ, Mushahwar IK. A hepatitis E virus variant from the United States: molecular characterization and transmission in cynomolgus macaques. *J Gen Virol* 1999; **80**: 681-690

26 **Meng XJ**, Purcell RH, Halbur PG, Lehman JR, Webb DM, Tsareva TS, Haynes JS, Thacker BJ, Emerson SU. A novel virus in swine is closely related to the human hepatitis E virus. *Proc Natl Acad Sci U S A* 1997; **94**: 9860-9865

27 **Pei Y,** Yoo D. Genetic characterization and sequence heterogeneity of a canadian isolate of swine hepatitis E virus. *J Clin Microbiol* 2002; **40**: 4021-4029

28 **Jameel S**, Zafrullah M, Chawla YK, Dilawari JB. Reevaluation of a North India isolate of hepatitis E virus based on the full-length genomic sequence obtained following long RT-PCR. *Virus Res* 2002; **86**: 53-58

29 **Panda SK**, Ansari IH, Durgapal H, Agrawal S, Jameel S. The *in vitro*-synthesized RNA from a cDNA clone of hepatitis E virus is infectious. *J Virol* 2000; **74**: 2430-2437

30 **Tsarev SA**, Emerson SU, Reyes GR, Tsareva TS, Legters LJ, Malik IA, Iqbal M, Purcell RH. Characterization of a prototype strain of hepatitis E virus. *Proc Natl Acad Sci U S A* 1992; **89**: 559-563

31 **van Cuyck-Gandre H**, Zhang HY, Tsarev SA, Warren RL, Caudill JD, Snellings NJ, Begot L, Innis BL, Longer CF. Short report: phylogenetically distinct hepatitis E viruses in Pakistan. *Am J Trop Med Hyg* 2000; **62**: 187-189

32 **Aye TT**, Uchida T, Ma X, Iida F, Shikata T, Ichikawa M, Rikihisa T, Win KM. Sequence and gene structure of the hepatitis E virus isolated from Myanmar. *Virus Genes* 1993; **7**: 95-109

33 **Yin S**, Purcell RH, Emerson SU. A new Chinese isolate of hepatitis E virus: comparison with strains recovered from different geographical regions. *Virus Genes* 1994; **9**: 23-32

34 **Bi SL**, Purdy MA, McCaustland KA, Margolis HS, Bradley DW. The sequence of hepatitis E virus isolated directly from a single source during an outbreak in China. *Virus Res* 1993; **28**: 233-247

35 **Aye TT**, Uchida T, Ma XZ, Iida F, Shikata T, Zhuang H, Win KM. Complete nucleotide sequence of a hepatitis E virus isolated from the Xinjiang epidemic (1986-1988) of China. *Nucleic Acids Res* 1992; **20**: 3512

36 **Wang Y**, Zhang H, Ling R, Li H, Harrison TJ. The complete sequence of hepatitis E virus genotype 4 reveals an alternative strategy for translation of open reading frames 2 and 3. *J Gen Virol* 2000; **81**: 1675-1686

Edited by Kumar M and Zhu LH **Proofread by** Xu FM

PO Box 2345, Beijing 100023, China
Fax: +86-10-85381893
E-mail: wjg@wjgnet.com www.wjgnet.com

World J Gastroenterol 2004;10(14):2050-2054
World Journal of Gastroenterology
 ISSN 1007-9327

• VIRAL HEPATITIS •

Inhibition of human La protein by RNA interference downregulates hepatitis B virus mRNA in 2.2.15 cells

Qin Ni, Zhi Chen, Hang-Ping Yao, Zheng-Gang Yang, Ke-Zhou Liu, Ling-Ling Wu

Qin Ni, Zhi Chen, Hang-Ping Yao, Zheng-Gang Yang, Ke-Zhou Liu, Institute of Infectious Diseases, First Affiliated Hospital, School of Medicine, Zhejiang University, Hangzhou 310003, Zhejiang Province, China
Ling-Ling Wu, Department of Clinical Medicine, Medical College, Zhejiang University, Hangzhou 310031, Zhejiang Province, China
Supported by the Major Programs of Health Bureau of Zhejiang Province, No. 2002ZD007 and the National Natural Science Foundation of China, No. 30371270 and the Major Programs of Department of Science and Technology of Zhejiang Province, No. 2003C13015
Correspondence to: Dr. Zhi Chen, Institute of Infectious Diseases, First Affiliated Hospital, School of Medicine, Zhejiang University, Hangzhou 310003, Zhejiang Province, China. chenzhi@zju.edu.cn
Telephone: +86-571-87236579 **Fax:** +86-571-87068731
Received: 2004-02-20 **Accepted:** 2004-03-06

Abstract

AIM: To investigate the role of human La protein in HBV mRNA expression.

METHODS: Three human La protein (hLa) specific siRNA expression cassettes (SECs) containing U6+1 promoter were prepared via one-step overlapping extension PCR. After transfection with SECs into HepG2 cells, inhibition effects on hLa expression were analyzed by semi-quantitative RT-PCR and Western blotting. Then, effective SECs were screened out and transfected into 2.2.15 cells, a stable HBV-producing cell line. HBV surface antigen (HBsAg) and e antigen (HBeAg) secretions into culture media were detected by microparticle enzyme immunoassay (MEIA) and HBs and HBe mRNA levels were analyzed by semi-quantitative RT-PCR.

RESULTS: SEC products containing U6+1 snRNA promoter, and 3 sites of hLa mRNA specific siRNA were obtained successfully by one-step overlapping extension PCR and could be directly transfected into HepG2 cells, resulting in inhibition of La protein expression in both mRNA and protein levels, among which U6+1-hLa833 was the most efficient, which reduced 18.6-fold mRNA and 89% protein level respectively. In 2.2.15 cells, U6+1-hLa833 was also efficient on inhibition of hLa expression. Furthermore, semi-quantitative RT-PCR showed that HBs and HBe mRNA levels were significantly decreased by 8- and 66-fold in U6+1-hLa833 transfected cells compared to control. Accordingly, HBsAg and HBeAg secretions were decreased partly posttransfection with SECs.

CONCLUSION: PCR-based SECs can be used to mediate RNAi in mammalian cells and provide a novel approach to study the function of La protein. The inhibition of La protein expression can result in a significant decrease of HBV mRNA, which implies that the hLa protein is also involved HBV RNA metabolism as one of the HBV RNA-stabilizing factors in human cells.

Ni Q, Chen Z, Yao HP, Yang ZG, Liu KZ, Wu LL. Inhibition of human La protein by RNA interference downregulates hepatitis B virus mRNA in 2.2.15 cells. *World J Gastroenterol* 2004; 10(14): 2050-2054
http://www.wjgnet.com/1007-9327/10/2050.asp

INTRODUCTION

Human La protein is a 47-ku phosphoprotein predominantly localized in nuclei. La protein is a member of RNA-binding proteins containing RNA recognition motifs (RRM) and interacts with RNA polymerase III transcripts such as pre-tRNA by binding to a small stretch of uridines at the 3' -end common to these transcripts and might be necessary for proper processing of these precursors[1-3]. In addition, La protein is known to interact with a variety of viral RNAs for stabilizing various RNAs[4-7], and is required for viral internal ribosomal entry site (IRES) -mediated translation[8-12].

La protein has been identified as a host factor potentially involved in the cytokine-induced post-transcriptional down-regulation of hepatitis B virus (HBV) RNA[13]. A strong correlation between cytokine-mediated disappearance of HBV RNA and cytokine-induced processing of full-length mouse La protein (mLa) was observed. The mLa binding site was mapped to a predicted stem-loop structure within a region located at the 5' -end of the post-transcriptional regulatory element of HBV shared by all HBV RNAs[5,6]. In addition, HBV RNA was accessible to endoribonucleolytic cleavage near this mLa binding site and HBV RNA substrates were more efficiently cleaved after induction of mLa processing[7]. All these findings indicate that La protein might be an HBV RNA-stabilizing factor. Determination of the high affinity interaction between human La protein (hLa) and HBV RNA *in vitro*[14], which is similar to that of mLa-HBV RNA interaction, implied that hLa might be involved in HBV RNA metabolism. But the role of human La protein (hLa) in HBV RNA metabolism *in vivo* is still unknown at present.

RNA interference (RNAi) is a process of sequence-specific post-transcriptional gene silencing via double-stranded RNA (dsRNA) present in plants and invertebrates[15]. With the increasing findings that 21-23 nt RNA duplexes known as small interfering RNA (siRNA) can also specifically and effectively knock down target gene expression in mammalian cells but short enough to evade host response[16], RNAi has been promptly developed into a powerful tool for studying protein function.

In this report, we utilized PCR-based siRNA strategy[17-19] to obtain several hLa-specific siRNA expression cassettes (SECs) containing U6+1 snRNA promoter and to deplete the hLa expression by transfection with SECs into human cells. In a stable HBV-producing cell line 2.2.15 cells[20], the inhibition of hLa expression resulted in a significant decrease of HBV mRNA and partly reduction of HBV antigen secretion. This result suggests that human La protein also plays an important role in HBV expression.

MATERIALS AND METHODS

Reagents and materials

Pyrobest DNA polymerase was obtained from Takara Biotech (Japan). TaqPlus DNA polymerase was purchased from Dingguo (China). QIAquick PCR purification kit was obtained from Qiagen (Germany). M-MuLV reverse transcriptase was obtained from MBI fermentas (Lithuania). G418 was from

Clontech (USA). Fetal calf serum was from Hyclone (USA). Trizol reagent and Lipofectamine 2000 were obtained from Invitrogen Lifetechnology (USA). Mouse monoclonal antibody against human La protein was purchased from BD Biosciences (USA). Rabbit polyclonal antibody against actin was from Wuhan Boster Biological Technology (China). Donkey anti-mouse and goat anti-rabbit horseradish peroxidase (HRP)-IgG were from SantaCruz (USA). *Re-Blot Plus* Western blot recycling kit was obtained from Chemicon (USA). SuperSignal west dura extended duration substrate ECL kit and CL-Xposure film were obtained from Pierce Biotech (USA). AxSYM and detective kits of HBsAg and HBeAg were purchased from ABBOTT (USA). Polyvinylidene difluoride (PVDF) membranes were obtained from Millipore (USA). All PCR primers were synthesized by Shanghai Sangon Biological Company (China).

Plasmids and cell lines

Plasmid pAVU6+27 was a gift of Dr. Paul D. Good (Engelke Laboratory, Department of Biological Chemistry). Plasmid pcDNA3.1 was obtained from Clontech (USA). HepG2, a human hepatoblastoma cell line, and 2.2.15 cells derived from HepG2 cells and stably transfected with HBV DNA[20] were maintained in our laboratory.

Selection of siRNA and shRNA design

Target sites of siRNA were determined by using on-line tool from Ambion Company. Three sites for hLa located downstream of the start codon were selected, their sequences are as follows: coding region 347-357 (5'-AAGGCTTCCC AACTGATGC AA-3') for hLa347, 833-843 (5'-AAGCCAAG GAAGCAT TGGGTA-3') for hLa833, 911-921 (5'-AAGTACTAGAA GGAGAGGTGG-3') for hLa911. 5'-AAGGGCGAGG AGCTGTTCACC-3' for EGFP10 siRNA site was used as control for studying the effect of hLa siRNA. Using 5'-TTCAAGAGA-3' as 9-nt loop, all short hairpin RNAs (shRNA) were designed according to the structure of siRNA sense strand-loop-siRNA antisense strand.

Preparation of SECs

U6+1 promoter was obtained from plasmid pAVU6+27 containing human U6 promoter. Oligonucleotides coding hairpin shRNA antisense were synthesized and used for PCR reaction as 3' specific extension primers. All extension primers have the 5' end 21-nt containing additional adaptor sequence and a stretch of 6 deoxyadenosines as transcription terminator. The 5' universal primer is complementary to 18 nt at the 5' end of the U6 snRNA promoter (bold italics) 5'-GGAAGA TCTGGATCCAAGGTCGGG-3' and the 3' universal primer is complementary to the first 21-nt at the 5' end of all extension primers 5'-CGGCT CTAGAGTTCAAAAAAG-3'. Both universal primers were 5'-phosphorylated and could be used for all PCR reactions. SEC was constructed by using one specific extension primer and two universal primers via overlapping extension one-step PCR as depicted in Figure 1. Using Pyrobest polymerase 30 cycles of PCR reactions were carried out, each at 94 ℃ for 30 s, at 58 ℃ for 30 s, and at 72 ℃ for 30 s. The PCR products were purified using QIAquick PCR purification kit (Qiagen) and stored at -20 ℃ prior to use.

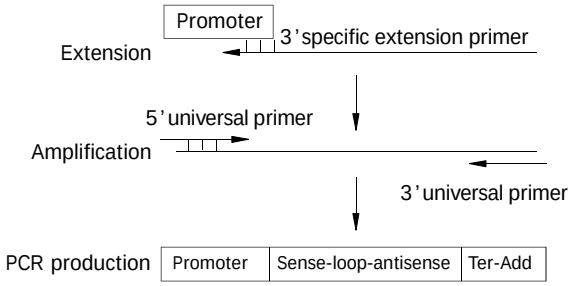

Figure 1 Schematic representation of one-step overlapping extension PCR strategy used to yield SECs.

Cell culture and cotransfection

HepG2 cells were maintained in Dulbecco's modified Eagle's minimal essential medium (DMEM) supplemented with 100 mL/L FCS, streptomycin (100 μg/mL) and penicillin (100 IU/mL) at 37 ℃ in a humidified atmosphere containing 50 mL/L CO_2. 2.2.15 cells were grown in DMEM with 100 mL/L FCS, 400 μg/mL G418. HepG2 and 2.2.15 cells were seeded into 24-well plates 24 h or 48 h prior to transfection. HepG2 cells at 50% confluence and 2.2.15 cells at 70% were prepared for transfection. For all co-transfections, a total of 0.05 μg pcDNA3.1+ (used as carrier DNA) and 0.2 μg SEC was delivered using Lipofectamine 2 000 according to the manufacturer's instructions. HepG2 cells were harvested for analysis of La mRNA and protein expression. 2.2.15 cells and supernatants were harvested for detection of HBV mRNA and antigen.

RNA extraction and semi-quantitative RT-PCR analysis

Total RNA was extracted from cells with Trizol reagent according to the manufacturer's instructions, 1.0 μg of total RNA was reverse transcribed to cDNA using oligo (dT) 18 as primer and Mu-MLV reverse transcriptase, and 0.5 μL of the cDNA template was separately used to amplify different mRNA. Information of primers is shown in Table 1. The PCR conditions for different target were as follows. A total of 28 cycles for GAPDH were performed, each at 94 ℃ for 30 s, at 60 ℃ for 30 s, and at 72 ℃ for 30 s. A total of 26 cycles for hLa were performed, each at 94 ℃ for 30 s, at 58 ℃ for 30 s, and at 72 ℃ for 30 s. A total of 26 cycles for HBs were performed, each at 94 ℃ for 30 s, at 56 ℃ for 30 s, and at 72 ℃ for 30 s. A total of 30 cycles for HBe were performed, each at 94 ℃ for 30 s, at 46 ℃ for 30 s, and at 72 ℃ for 45 s. After electrophoresis and scanning, all PCR product bands were analyzed by using the software Gel Pro analyzer32 and relative mRNA expression was estimated by normalization with GAPDH.

Table 1 PCR primers for amplification

Primer	GenBank accession No	Sequence of primer pair
GAPDH	BC023632 (26-260)	Sense: 5'-TGGGGAAGGTGAAGGTCGGA-3'
		Antisense: 5'-GGGATCTCGCTGCTCGAAGA-3'
hLa	BC001289 (871-1313)	Sense: 5'-GGATAGACTTCGTCAGAGGAGCA-3'
		Antisense: 5'-CTGGTCTCCAGCACCATTTTCTG-3'
HBs	U95551 (232-681)	Sense: 5'-CTCACAATACCGCAGAGTC-3'
		Antisense: 5'-TAAACTGAGCCAGGAGAAA-3'
HBe	U95551 (1816-2452)	Sense: 5'-ATGCAACTTTTTCACCTC-3'
		Antisense: 5'-AACATTGAGGTTCCCGAG-3'

Western blot analysis

Cells were harvested and lysed in lysis buffer (0.1 mol/L Tris, pH 7.6, containing 0.15 mol/L NaCl, 2 mmol/L EDTA, 5 g/L Nonidet P-40, 5 g/L Triton X-100, 100 μmol/L sodium vanadate, 10 μg/mL aprotinin, and 20 μg/mL soybean trypsin inhibitor). The cell lysate (10-15 μg protein) was separated by sodium dodecyl sulfate-polyacrylamide (SDS-PAGE) gel electrophoresis and electrophoretically transferred onto PVDF membrane. After non-specific binding sites were blocked with 50 g/L non-fat milk, the membrane was incubated with mouse anti-hLa monoclonal antibody (1:600 dilution) overnight at 4 ℃. After washed, the blot was incubated with HRP-conjugated anti-mouse IgG for 1 h at room temperature, and immunoreactive bands were visualized with the ECL reagent. After the blot was stripped with stripping solution, the blot was reprobed with rabbit anti-actin polyclonal antibody for comparison of protein load in each lane. Densitometric scanning of the X-ray film following chemiluminescence was done and La protein expression level was estimated after normalization with actin.

Microparticle enzyme immunoassay (MEIA) analysis

Supernatants of 2.2.15 cells were harvested on days 1, 2, 3, 6 and 9 postransfection respectively in same wells. Each experiment well was performed in triplicate. A microparticle enzyme immunoassay (MEIA) method was applied for the detection of HBsAg and HBeAg according to the kit's instructions. Sample with S/N values great than or equal to 2.0 for HBsAg, and S/CO values great than or equal to 2.1 for HBeAg were considered reactive as described previously[21].

RESULTS

RNAi inhibited hLa protein expression in cultured HepG2 cells

To determine whether siRNA specific to the hLa gene sequence could inhibit hLa expression, we screened the activity of three sites of hLa-specific siRNA by semi-quantitated RT-PCR of hLa mRNA in HepG2 cells 36 h posttransfection with SECs. Two of them, SEC U6+1-hLa347 and U6+1-hLa833 siginificantly decreased hLa mRNA levels by about 8.8- and 17.6-fold respectively as compared with the control (Figure 2A). However, SEC U6+1-hLa911 only slightly affected hLa mRNA expression (1.3-fold reduction). No significant inhibition of hLa mRNA expression was detected in cells transfected with SEC U6+1-EGFP10 (Figure 2A). Furthermore, we performed Western blot analysis to verify the inhibitory effects on hLa protein expression levels 72 h posttransfection with SEC U6+1-hLa347 and U6+1-hLa833. As shown in Figure 2B, hLa protein expression almost could not be detected in cells transfected with U6+1-hLa833. After normalized to actin, the level of hLa protein expression was reduced to approximately 11% and 49% of the control cells for U6+1-hLa833 and U6+1-hLa347 respectively, and no reduction was found for U6+1-EGFP10. These data demonstrated that SEC-mediated RNAi could effectively inhibit human La protein expression in cultured HepG2 cells and the down-regulation in hLa was sequence-specific and highly site-dependant.

RNAi inhibited hLa mRNA expression in cultured 2.2.15 cells

As SEC U6+1-hLa833 could greatly specific inhibit hLa mRNA and protein expressions in HepG2 cells, we then assessed its inhibitory effects on 2.2.15 cells derived from HepG2. As shown in Figure 3A, inhibition of hLa mRNA levels was detected with the reduction of about 22- and 3.4-fold on days 1 and 2 posttransfection, but no inhibitory effects were observed from days 3 to 9 posttransfection. In addition, no significant inhibition of hLa mRNA levels was detected in cells posttransfection with the SEC U6+1-EGFP-10 (Figure 3A). This result indicates that SEC-mediated RNAi could also effectively inhibit hLa mRNA expression in cultured 2.2.15 cells, but the inhibitory effects could last only for a short time.

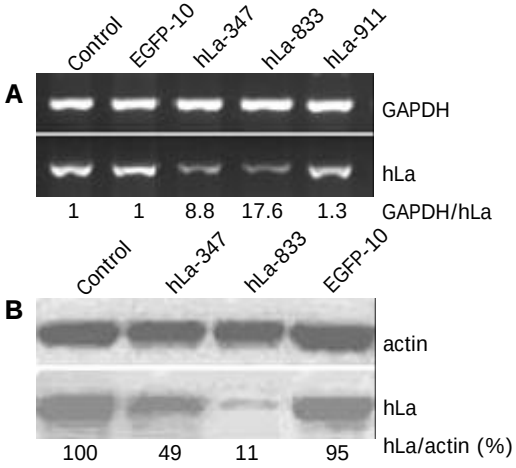

Figure 2 Effect of RNAi on hLa expression in HepG2 cells. A: Total RNA isolated from HepG2 cells transfected with various SECs for hLa and EGFP. The number was the ratio between the signal intensity for GAPDH and hLa mRNA amplified in parallel. B: Western blotting of total cell lysates harvested from SECs-transfected HepG2 cells 72 h posttransfection. Actin was used as loading control. The number was the percentage of the signal intensity of hLa and actin protein (%).

Inhibition of hLa expression led to reduction of HBV mRNA levels in cultured 2.2.15 cells

In order to investigate the relationship between hLa mRNA and HBV RNA expression, using the same samples, the levels of HBs and HBe mRNA expression in SEC-transfected 2.2.15 cells were detected by semi-quantitative RT-PCR. The HBs mRNA levels were also decreased about 8- and 2.8-fold in the first 2 d posttransfection, which were associated with a parallel reduction of hLa mRNA levels (Figure 3B). Moreover, HBe mRNA decreased dramatically, and almost could not be detected in the first 2 d and the inhibitory effect could last for at least 9 d (Figure 3C). In contrast, no significant changes in HBs and HBe mRNA levels were observed in cells posttransfection with SEC U6+1-EGFP-10 (Figures 3B and 3C). These results demonstrated that RNAi against hLa could lead to reduction of HBV mRNA levels in 2.2.15 cells.

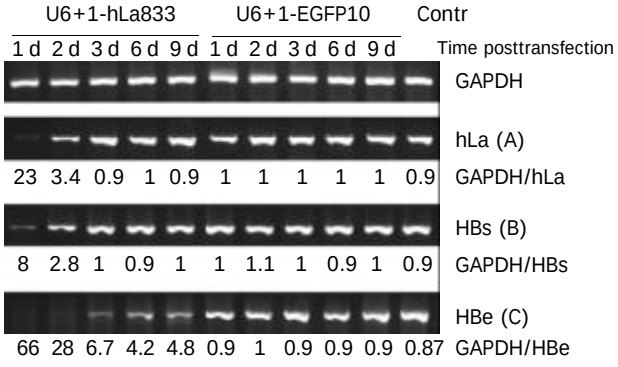

Figure 3 Effect of RNAi on hLa mRNA expression and levels of HBV mRNA expression in 2.2.15 cells. The number was the ratio between the signal intensity for hLa, HBs, HBe, and GAPDH mRNA amplified in parallel.

Inhibition of hLa expression affected HBsAg and HBeAg secretion in 2.2.15 cells

If the inhibition of hLa expression could affect HBs and HBe

mRNA expressions in 2.2.15 cells, HBsAg and HBeAg secretion would be affected accordingly. Supernatant of SEC-transfected and control cells was harvested in the same period of posttransfection, HBsAg and HBeAg concentrations in the culture media were measured by MEIA method. Figure 4A shows that transfection with SEC U6+1-hLa833 inhibited the secretion of HBsAg in 2.2.15 cells from days 3 to 9 posttransfection in comparison with that of SEC U6+1-EGFP10 (P<0.05). The maximal inhibitory effect on day 6 posttransfection was 40%, and returned to 26% on d 9. HBeAg secretion was inhibited 38% on d 3 posttransfection with SEC U6+1-hLa833 and remained 46% and 51% on d 6 and 9 respectively (Figure 4B). There was a significant difference (P<0.05) in HBeAg secretion between SEC U6+1-hLa833- and U6+1-EGFP10-transfected cells on d 3, 6 and 9 posttransfection.

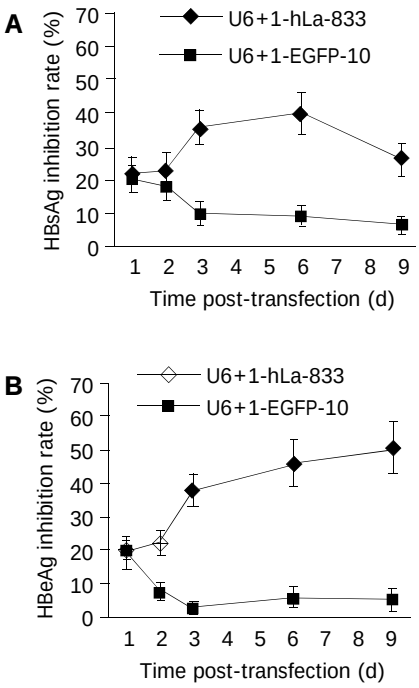

Figure 4 Time-efficiency inhibition course of SECs on HBsAg and HBeAg in 2.2.15 cells. The inhibition rate (IR) was calculated according to the following formula:

$$IR=\frac{X \text{ of wells for control- } X \text{ of wells for thansfection}}{X \text{ of wells for control-N}} \times 100\%$$

X represents S/N or S/CO for HBsAg or HBeAg, and n=2.0 for HBsAg and 2.1 for HBeAg respectively.

DISCUSSION

Results showed here from studies in 2.2.15 cells using siRNA against human La protein revealed a significant reduction in hLa expression, that resulted in HBV mRNA level reduction simultaneously, especially the expression of HBe mRNA, which was markedly decreased in the first 3 d and maintained at a lower level on the 9th d after inhibition of hLa expression. Following HBV mRNA reduction, HBsAg and HBeAg secretions were decreased accordingly though reduction of HBV antigen was less significant than that of corresponding mRNA. The relevance of RNAi-mediated knockdown of hLa towards reduction of HBV mRNA level suggested that human La protein might also be involved in HBV RNA metabolism. Based on the previous findings of the high affinity interaction between human La protein (hLa) and HBV RNA *in vitro*[14], and mouse La protein might be an HBV RNA-stabilizing factor in HBV-transgenic mouse model[5,7]. Our results invited a presumption that La protein might also play a role in stabilizing HBV RNA in human cells. However, HBsAg and HBeAg secretions could be affected slightly by hLa expression level, indicating that La protein is not a unique factor, and additional factors could contribute to viral RNA stability or HBV expression regulation. Therefore, using only hLa as targets for a novel antiviral strategy[14] would not be practical. Experiments to investigate the role of other RNA-binding proteins in HBV RNA metabolism might gain better insights into this problem.

We also observed that downregulation of HBe seemed more significant than HBs, implying more abundant HBs mRNA could generate HBsAg than HBe in 2.2.15 cells, which was in accord with the redundant HBsAg expression and secretion from patients with HBV infection. So HBs might be poorly susceptible to interfering factors. In addition, the feature of overlapping reading frames made entire 2.1-kb mRNA sequence encode HBs that was contained in 3.5-kb mRNA sequence encoding Hbe[22,23]. In fact, HBs mRNA level detected by RT-PCR in our experiments represented the total transcript level containing HBe and HBs. Therefore, instead of RT-PCR, Northern blot analysis should reflect the truth of all HBV transcripts in more detail.

As to siRNA application in RNAi technology, besides chemically synthesized 21-nt siRNA duplexes[16], some approaches could generate siRNA for various needs, such as *in vitro* transcribed siRNA[24,25], plasmid DNA expression vector-based siRNA[26, 27], viral vector-based siRNA[28-30], and PCR-based siRNA expression cassette (SEC)[17-19] which was proved to be a rapid, facile and cheap approach for identification of optimal siRNA-targets. In this report, we attempted to simplify the commonly used two-step PCR into overlapping-extension one-step PCR reaction by using three primers: a long specific extension primer and two universal primers, and also successfully prepared SECs targeting three sites of hLa mRNA. After transfection with these SECs into HepG2 cells, SEC U6+1-hLa833 demonstrated that strong RNAi effect was promptly screened out as optimal SEC to be used for further study. As a 347-bp in length of SEC DNA, it is often difficult to transfect them into mammalian cells, but using plasmid as carrier DNA, the efficiency of transfection seemed to be improved significantly (data not shown). On the other hand, stability of SEC DNA in cells should be considered. Despite SECs were phosphorylated for enhancing resistance to nuclease in cells, but target mRNA level still returned to normal on day 3 posttransfection, which maintained RNAi effect not as long as reported in application of vector–based siRNA[26], indicating that SEC strategy should be just adapted to transient gene silencing at present and the better modification strategies should be developed for its stability.

To our knowledge, this is the first report that describes the role of human La protein in HBV expression in cultured human cells. Elucidating the mechanism of human La protein affecting HBV expression and replication will allow a deeper understanding of the interaction between host factors and HBV during HBV infection and clearance, and will provide useful clues for controlling HBV infection.

ACKNOWLEDGEMENTS

We thank Dr. Paul D. Good (Engelke Laboratory) for supplying plasmid pAVU6+27. We also thank Dr. Jian-Er Wo, Dr. Yu Chen and Dr. Jun-Bin Shao for technological support, and Dr. Edward Zumbika for English revision of this paper.

REFERENCES

1 **Chakshusmathi G,** Kim SD, Rubinson DA, Wolin SL. A La protein requirement for efficient pre-tRNA folding. *EMBO J* 2003;

22: 6562-6572
2 **Wolin SL**, Cedervall T. The La protein. *Annu Rev Biochem* 2002; **71**: 375-403
3 **Maraia RJ**. La Protein and the trafficking of nascent RNA polymerase iii transcripts. *J Cell Biol* 2001; **153**: F13-F18
4 **Spangberg K**, Wiklund L, Schwartz S. Binding of the La autoantigen to the hepatitis C virus 3' untranslated region protects the RNA from rapid degradation *in vitro*. *J Gen Virol* 2001; **82**(Pt 1): 113-120
5 **Heise T**, Guidotti LG, Cavanaugh VJ, Chisari FV. Hepatitis B virus RNA-binding proteins associated with cytokine-induced clearance of viral RNA from the liver of transgenic mice. *J Virol* 1999; **73**: 474-481
6 **Heise T**, Guidotti LG, Chisari FV. La autoantigen specifically recognizes a predicted stem-loop in hepatitis B virus RNA. *J Virol* 1999; **73**: 5767-5776
7 **Heise T**, Guidotti LG, Chisari FV. Characterization of nuclear RNases that cleave hepatitis B virus RNA near the La protein binding site. *J Virol* 2001; **75**: 6874-6883
8 **Pudi R**, Abhiman S, Srinivasan N, Das S. Hepatitis C virus internal ribosome entry site-mediated translation is stimulated by specific interaction of independent regions of human La autoantigen. *J Biol Chem* 2003; **278**: 12231-12240
9 **Ali N**, Pruijn GJ, Kenan DJ, Keene JD, Siddiqui A. Human La antigen is required for the hepatitis C virus internal ribosome entry site-mediated translation. *J Biol Chem* 2000; **275**: 27531-27540
10 **Cheung P**, Zhang M, Yuan J, Chau D, Yanagawa B, McManus B, Yang D. Specific interactions of HeLa cell proteins with Coxsackievirus B3 RNA: La autoantigen binds differentially to multiple sites within the 5' untranslated region. *Virus Res* 2002; **90**: 23-36
11 **Ray PS**, Das S. La autoantigen is required for the internal ribosome entry site-mediated translation of Coxsackievirus B3 RNA. *Nucleic Acids Res* 2002; **30**: 4500-4508
12 **De Nova-Ocampo M**, Villegas-Sepulveda N, del Angel RM. Translation elongation factor-1alpha, La, and PTB interact with the 3' untranslated region of dengue 4 virus RNA. *Virology* 2002; **295**: 337-347
13 **Tsui LV**, Guidotti LG, Ishikawa T, Chisari FV. Posttranscriptional clearance of hepatitis B virus RNA by cytotoxic T lymphocyte-activated hepatocytes. *Proc Natl Acad Sci U S A* 1995; **92**: 12398–12402
14 **Horke S**, Reumann K, Rang A, Heise T. Molecular characterization of the human La protein / hepatitis B virus RNA.B interaction *in vitro*. *J Biol Chem* 2002; **277**: 34949-34958
15 **Hannon GJ**. RNA interference. *Nature* 2002; **418**: 244-251
16 **Elbashir SM**, Harborth J, Lendeckel W, Yalcin A, Weber K, Tuschl T. Duplexes of 21-nucleotide RNAs mediate RNA interference in cultured mammalian cells. *Nature* 2001; **411**: 494-498
17 **Castanotto D**, Li H, Rossi JJ. Functional siRNA expression from transfected PCR products. *RNA* 2002; **8**: 1454-1460
18 **Gou D,** Jin N, Liu L. Gene silencing in mammalian cells by PCR-based short hairpin RNA. *FEBS Lett* 2003; **548**: 113-118
19 **Zheng L**, Liu J, Batalov S, Zhou D, Orth A, Ding S, Schultz PG. An approach to genomewide screens of expressed small interfering RNAs in mammalian cells. *Proc Natl Acad Sci U S A* 2004; **101**: 135-140
20 **Sells MA**, Chen ML, Acs G. Production of hepatitis B virus particles in HepG2 cells transfected with cloned hepatitis B virus DNA. *Proc Natl Acad Sci U S A* 1987; **84**: 1005-1009
21 **Chen Y**, Wu W. Determination of low-level HBsAg in serum by microparticle enzyme immunoassay. *Hepatobiliary Pancreat Dis Int* 2002; **1**: 262-264
22 **Moolla N**, Kew M, Arbuthnot P. Regulatory elements of hepatitis B virus transcription. *J Viral Hepat* 2002; **9**: 323-331
23 **Seeger C**, Mason WS. Hepatitis B Virus Biology. *Microbiol Mol Biol Rev* 2000; **64**: 51-68
24 **Anderson J**, Banerjea A, Planelles V, Akkina R. Potent suppression of HIV type 1 infection by a short hairpin anti-CXCR4 siRNA. *AIDS Res Hum Retroviruses* 2003; **19**: 699-706
25 **Myers JW**, Jones JT, Meyer T, Ferrell JE Jr. Recombinant Dicer efficiently converts large dsRNAs into siRNAs suitable for gene silencing. *Nat Biotechnol* 2003; **21**: 324-328
26 **Paul CP**, Good PD, Winer I, Engelke DR. Effective expression of small interfering RNA in human cells. *Nat Biotechnol* 2002; **20**: 505-508
27 **Brummelkamp TR**, Bernards R, Agami R. A system for stable expression of short interfering RNAs in mammalian cells. *Science* 2002; **296**: 550-553
28 **Liu CM**, Liu DP, Dong WJ, Liang CC. Retrovirus vector-mediated stable gene silencing in human cell. *Biochem Biophys Res Commun* 2004; **313**: 716-720
29 **Rubinson DA**, Dillon CP, Kwiatkowski AV, Sievers C, Yang L, Kopinja J, Rooney DL, Ihrig MM, McManus MT, Gertler FB, Scott ML, Van Parijs L. A lentivirus-based system to functionally silence genes in primary mammalian cells, stem cells and transgenic mice by RNA interference. *Nat Genet* 2003; **33**: 401-406
30 **Zhao LJ**, Jian H, Zhu H. Specific gene inhibition by adenovirus-mediated expression of small interfering RNA. *Gene* 2003; **316**: 137-141

Edited by Wang XL **Proofread by** Chen WW and Xu FM

PO Box 2345, Beijing 100023, China
Fax: +86-10-85381893
E-mail: wjg@wjgnet.com www.wjgnet.com

World J Gastroenterol 2004;10(14):2055-2059
World Journal of Gastroenterology
 ISSN 1007-9327

Helicobacter pylori lipopolysaccharide: Biological activities *in vitro* and *in vivo*, pathological correlation to human chronic gastritis and peptic ulcer

Yi-Hui Luo, Jie Yan, Ya-Fei Mao

Yi-Hui Luo, Jie Yan, Ya-Fei Mao, Department of Medical Microbiology and Parasitology, College of Medical Science, Zhejiang University, Hangzhou 310031, Zhejiang Province, China
Supported by the Foundation of Ministry of Education of China for Distinguished Young Scholars
Correspondence to: Professor Jie Yan, Department of Medical Microbiology and Parasitology, College of Medical Science, Zhejiang University, 353 Yan An Road, Hangzhou 310031, Zhejiang Province, China. yanchen@mail.hz.zj.cn
Telephone: +86-571-87217385 **Fax:** +86-571-87217044
Received: 2003-12-23 **Accepted:** 2004-01-12

Abstract

AIM: To determine the biological activity of *Helicobacter pylori* (*H pylori*) lipopolysaccharide (H-LPS) and understand pathological correlation between H-LPS and human chronic gastritis and peptic ulcer.

METHODS: H-LPS of a clinical *H pylori* strain and LPS of *Escherichia coli* strain O55:B5 (E-LPS) were extracted by phenol-water method. Biological activities of H-LPS and E-LPS were detected by limulus lysate assay, pyrogen assay, blood pressure test and PBMC induction test in rabbits, cytotoxicity test in NIH 3T3 fibroblast cells and lethality test in NIH mice. By using self-prepared rabbit anti-H-LPS serum as the first antibody and commercial HRP-labeled sheep anti-rabbit sera as the second antibody, H-LPS in biopsy specimens from 126 patients with chronic gastritis (68 cases) or gastric ulcer (58 cases) were examined by immunohistochemistry.

RESULTS: Fibroblast cytotoxicity and mouse lethality of H-LPS were weaker than those of E-LPS. But the ability of coagulating limulus lysate of the two LPSs was similar (+/0.5 ng/mL). At 0.5 h after H-LPS injection, the blood pressures of the 3 rabbits rapidly declined. At 1.0 h after H-LPS injection, the blood pressures in 2 of the 3 rabbits fell to zero causing death of the 2 animals. For the other one rabbit in the same group, its blood pressure gradually elevated. At 0.5 h after E-LPS injection, the blood pressures of the three rabbits also quickly declined and then maintained at low level for approximately 1.0 h. At 0.5 h after injection with H-LPS or E-LPS, PBMC numbers of the rabbits showed a remarkable increase. The total positivity rate of H-LPS from 126 biopsy specimens was 60.3%(76/126). H-LPS positivity rate in the biopsy specimens from chronic gastritis (50/68, 73.5%) was significantly higher than that from gastric ulcer (26/58, 44.8%) (χ^2=10.77, P<0.01). H-LPS positivity rates in biopsy specimens from chronic superficial gastritis (38/48, 79.2%) and chronic active gastritis (9/10, 90.0%) were significantly higher than that of the patients with atrophic gastritis (3/10, 30.0%) (χ^2=7.50-9.66, P<0.01).

CONCLUSION: The biological activities of H-LPS were weaker than those of E-LPS, the activities of H-LPS of lowering rabbit blood pressure and inducing rabbit PBMC were relatively stronger. H-LPS may play a critical role in inducing inflammatory reaction in human gastritis.

Luo YH, Yan J, Mao YF. *Helicobacter pylori* lipopolysaccharide: Biological activities *in vitro* and *in vivo*, pathological correlation to human chronic gastritis and peptic ulcer. *World J Gastroenterol* 2004; 10(14): 2055-2059
http://www.wjgnet.com/1007-9327/10/2055.asp

INTRODUCTION

Gastritis and peptic ulcer are the most prevalent gastric diseases. Gastric cancer is one of the malignant tumors with high morbidities in China[1]. *Helicobacter pylori* (*H pylori*) is recognized as a human-specific gastric pathogen that colonizes the stomachs of at least half of the world' s populations[2]. Most infected individuals are asymptomatic. However, in some subjects, the infection causes acute, chronic gastritis or peptic ulceration, and plays an important role in the development of peptic ulcer and gastric adenocarcinoma, mucosa-associated lymphoid tissue lymphoma and primary gastric non-Hodgkin' s lymphoma[3-7].

H pylori is a microaerophilic Gram-negative bacillus. It is well known that lipopolysaccharide (LPS) is a common and essential component in outer membrane of most Gram-negative bacteria responsible for the toxicity of endotoxin. Some literatures revealed *H pylori* possesses LPS (H-LPS) with a lower virulence compared to the typical bacterial endotoxins such as *Escherichia coli* LPS (E-LPS)[8-12]. However, some biological activities such as regulating blood pressure and inducing peripheral blood mononuclear cell (PBMC), which are clinically important in local tissue inflammation and injury, and pathological importance of H-LPS in human gastric diseases are still little understood. Besides, some previously published data demonstrated that different strains of the same bacterium and different extraction methods would significantly affect the biological activity of LPS[13,14].

For measurement of the biological activities of H-LPS *in vivo* and *in vitro* compared to a typical LPS from *E. coli*, we used phenol-water method to extract LPS from a clinical isolated *H pylori* strain and applied routine assays for determining the endotoxin activity of H-LPS such as limulus lysate agglutination, rabbit pyrogenicity and mouse lethality. Furthermore, we also examined H-LPS activities on blood pressure regulation and PBMC inducement. To obtain direct evidence for the correlation of H-LPS and human chronic gastritis and peptic ulcer, we detected H-LPS in gastric biopsy specimens from patients with different gastric diseases.

MATERIALS AND METHODS

Bacterial strains and culture

A clinical *H pylori* strain named as Y06 was isolated from a

biopsy specimen of a male patient with chronic superficial gastritis and duodenal ulcer by using selected Columbia agar (bioMérieux) supplemented with 80 mL/L sheep blood, 5 g/L cyclodextrin, 5 mg/L trimethoprime, 10 mg/L vancomycin, 2.5 mg/L amphotericin B and 2 500 U/L cefsulodin. This strain was identified as *H pylori* based on its typical Gram staining morphology, positivity for both urease and oxidase, and agglutination with a commercial rabbit antibody against whole cell of *H pylori* (DAKO). *E. coli* strain O55:B5 was offered by the National Institute for the Control of Pharmaceuticals and Biological Products of China (NICPBP) and cultured with BL agar.

LPS extraction

H-LPS from *H pylori* strain Y06 and E-LPS from *E. coli* strain O55:B5 were extracted by phenol-water method. Briefly, the two bacteria collected from Columbia agar and BL agar were ultrasonically broken, respectively. Each of the broken bacterial solutions was added with an equal volume of pre-warmed phenol-water (9:1, V:V) and then vibrated for 30 min at 68-70 ℃. The aqueous phase was collected after centrifugation at 3 000 r/min for 30 min. This extraction step was repeated for 3 times. All the aqueous phases were combined and then dialyzed against distilled water for 48 h. This rough LPS extract was concentrated to 1/6 of the original volume and then digested with RNase H and DNase I (Sigma) to both the final concentration of 50 μg/mL at 37 ℃ for 4 h. The digested extract was bathed in boiling-water for 15 min and then placed at 4 ℃ overnight. The supernatant obtained after centrifugation at 3 000 r/min for 30 min was dialyzed against distilled water for 48 h and then precipitated with 6-fold volumes of anhydrous alcohol at 4 ℃ for 12 h. The precipitate was collected by centrifugation at 5 000 r/min for 30 min and then re-suspended with distilled water and dialyzed against distilled water for 24 h to remove residual alcohol. The LPS extract was ultra-centrifuged at 110 000 *g* for 3 h (4 ℃) and the pellet was dialysed in distilled water and freeze-dried. The purified H-LPS and E-LPS were dissolved in pyrogen-free water or normal saline prepared with pyrogen-free water just before different uses.

Limulus lysate assay

Limulus lysate assay was applied by using E-TOXATE Reagent Kit (Sigma) to detect the H-LPS and E-LPS preparations according to the manufacturer's instruction (Sensitivity = +, 1 ng/mL *E. coli* O55:B5 LPS). In this assay, *E. coli* O55:B5 LPS (Sigma) and pyrogen-free water were used as the positive and negative controls, respectively.

Rabbit pyrogen assay

Anal temperatures of normal New Zealand rabbits with 3.0±0.2 kg of body mass were detected for3 times at an interval of 30 min before performing the test. A rabbit was suitable for the test if the fluctuant range of the three detected temperatures was ≤0.2 ℃. The qualified rabbits were randomly divided into three groups and each group contained three animals. Each of the three rabbits in one group was injected with 0.5 mL normal saline containing H-LPS or E-LPS at the same dosage of 100 μg/kg through ear vein. Each of the three rabbits in the 3rd group was injected with an equal volume of pyrogen-free normal saline as a negative control. Anal temperature in each of the tested rabbits was detected at an interval of 30 min for 5 h after injection. The positive standard for rabbit pyrogen assay was described as following: body temperature for any one of the three rabbits in one group showed ≥0.6 ℃ elevation, or the total elevated body temperature for the three rabbits in one group was ≥1.4 ℃.

Rabbit blood pressure regulation test

Normal New Zealand rabbits with 3.0±0.2 kg of body mass were ear-intravenously injected with 0.5 mL pyrogen-free normal saline. Then blood pressures of the animals were observed for three times at an interval of 30 min. A rabbit was suitable for this test if its blood pressure fluctuation was within 0.2 kPa. The qualified rabbits were divided into three groups and each contained three animals. Each of the three rabbits in one group was ear-intravenously injected with pyrogen-free saline containing H-LPS or E-LPS at the same dosage of 100 μg/kg and each of the three rabbits in the 3rd group were ear-intravenously injected with an equal volume of pyrogen-free saline as a negative control. The changes of blood pressure in the tested rabbits were observed.

PBMC inducement test

PBMC numbers in blood from ear vein of normal New Zealand rabbits with 3.0±0.2 kg of body mass were counted with hemacytometer twice at an interval of 30 min before performing the test. These rabbits were randomly divided into three groups and each contained 5 animals. Each of the five rabbits in one group was ear-intravenously injected with pyrogen-free saline containing H-LPS or E-LPS at the same dosage of 100 μg/kg and each of the five rabbits in the 3rd group were ear-intravenously injected with an equal volume of pyrogen-free saline as a negative control. The change of PBMC numbers for each of the tested rabbits was counted at an interval of 30 min after injection.

Cytotoxicity test

Microtiter plates were inoculated with 1×10^4 mouse 3T3 fibroblast cells in RPMI 1640 medium containing 100 mL/L bovine serum per well and then incubated at 37 ℃ overnight in 50 mL/L CO_2 atmosphere. The medium in the plates was discarded and then added with 200 μL of fresh medium containing H-LPS or E-LPS with different double dilutions. For each of the dilutions, 3 wells were repeated and then incubated for 48 h under the same conditions as mentioned above. In this test, the other 5 wells added with the same volume of LPS-free medium were set up as a negative control. ^{3}H-TdR per well (37 kBq) was added and then continuously incubated for 24 h. CPM value for each of the wells was detected by using ^{3}H-TdR incorporation method to compare the cytotoxicity of H-LPS and E-LPS.

Mouse lethality test

NIH mice weighing 20±2 g were randomly divided into 7 groups and each contained 8 animals. For 6 of the 7 groups, each of the mice in one group was intraperitoneally injected with 0.2 mL pyrogen-free normal saline containing H-LPS or E-LPS at the different dosages of 0.25, 0.50 and 1.0 mg, respectively. Each of the mice in the last group was intraperitoneally injected with 0.2 mL pyrogen-free saline as a negative control. All the tested animals were observed for 7 d.

Detection of H-LPS in biopsy specimens from patients with chronic gastritis and gastric ulcer

Biopsy specimens with positive urease from 126 patients (86 male, 40 female, mean age: 40±18 years) with gastric diseases during January to September of 2003 were collected from three hospitals in Hangzhou. Among these patients, 68 suffered from chronic gastritis (48 cases with chronic superficial, 10 active and 10 atrophic gastritis) and 58 cases suffered from gastric ulcer (12 cases with gastric, 40 duodenal and 6 complex ulcer). The biopsy specimens were fixed with 50 g/L glutaraldehyde. Rabbit anti-H-LPS serum was prepared by using routine subcutaneous immunization. By using the

rabbit anti-H-LPS serum (1∶200 dilution, self-prepared) as the first antibody and HRP-labeled sheep anti-rabbit serum (1∶3 000 dilution, ImmunoResearch) as the second antibody, H-LPS in the biopsy specimens was detected by routine immunohistochemistry. Cells with at least one whole gastric gland in a biopsy section showing exactly brown color could be considered as positive.

RESULTS

Limulus lysate coagulation

The ability of coagulating limulus lysate of H-LPS was as low as 0.5 ng/mL, which was similar to E-LPS (Table 1).

Table 1 Results of limulus lysate assay of H-LPS and E-LPS

Group	LPS (ng/mL)							
	10.0	5.0	2.5	1.0	0.5	0.25	0.1	0.05
H-LPS	+	+	+	+	+	-	-	-
E-LPS	+	+	+	+	+	-	-	-
Pyrogen-free water	negative in two repeated samples							

Pyrogenic response

The rabbits injected with H-LPS or E-LPS showed a similar biphasic fever but E-LPS could induce a stronger pyrogenic response. The animal temperature reached a peak at 1.5 h after injection and then showed a slight fall. At 3 h after injection, the second fever peak occurred (Figure 1).

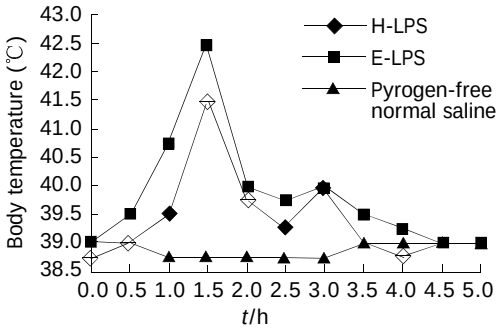

Figure 1 Fever curves of rabbits after injection with H-LPS or E-LPS.

Regulation of rabbit blood pressure

At 0.5 h after H-LPS injection, the blood pressures of the three rabbits rapidly declined from originally 11.331±0.152 kPa to 5.999±1.855 kPa. At 1.0 h after H-LPS injection, the blood pressures in two of the three rabbits fell to zero causing death of the two animals. For the other one rabbit in the same group, its blood pressure gradually elevated. At 0.5 h after E-LPS injection, the blood pressures of the three rabbits also quickly declined from originally 11.197±0.163 kPa to 8.531±2.424 kPa and then maintained the similar low blood pressure levels for approximately 1.0 h. At 2.5 h after injection, the blood pressures in all the three rabbits began to rise and returned to the original levels gradually.

PBMC inducement

At 0.5 h after injection with H-LPS or E-LPS, PBMC numbers of the rabbits showed a remarkable increase. From 1.0 h after injection with H-LPS or E-LPS, the PBMC numbers gradually and continuously decreased to low levels (Table 2).

Cytotoxicity to mouse fibroblast

Very low dosage of H-LPS or E-LPS (1 μg/mL) could show an obvious cytotoxicity to NIH 3T3 fibroblast. According to the counting per minute (CPM) of scintillation at the same concentrations, cytotoxicity of H-LPS seemed to be a little weaker than that of E-LPS (Table 3).

Table 2 PBMC number changes in the rabbits injected with H-LPS or E-LPS

Time (h)	PBMC (mean±SD, $\times10^9$/L)		
	H-LPS	E-LPS	Saline
Before injection	4.52±1.28	4.38±1.35	4.05±1.42
After injection			
0.5	12.51±0.54	8.22±0.68	4.25±1.28
1.0	2.55±0.87	2.23±1.32	4.40±1.19
1.5	1.56±1.33	1.58±1.27	4.08±1.24
2.0	1.62±0.93	1.64±0.89	4.05±1.06
2.5	1.65±1.12	1.60±1.34	4.35±1.17
3.0	1.56±1.45	1.52±1.10	4.16±1.22

Table 3 Cytotoxicity of H-LPS and E-LPS to mice fibroblast

Group	LPS (μg/mL)	CPM (mean±SD)	*t*	*P*
H-LPS	1.0	7 722±819	3.74	<0.05
	5.0	4 724±726	7.29	<0.01
	10.0	4 328±1 194	6.56	<0.01
	50.0	3 618±434	9.27	<0.001
	100.0	2 963±764	9.20	<0.001
E-LPS	1.0	6 813±1 183	4.17	<0.05
	5.0	4 290±474	8.37	<0.005
	10.0	3 516±645	8.96	<0.001
	50.0	3 224±534	9.55	<0.001
	100.0	2 513±630	10.72	<0.001
Control	0	11 083±1 324		

Mouse lethality

H-LPS showed a significantly weaker virulence to mice than E-LPS. Although the injecting dosage was as high as 1 mg H-LPS per mouse, 2 of the 8 mice survived (Table 4).

Table 4 Toxicity test results in mice injected with H-LPS or E-LPS

Group	Number (*n*)	Dosage (mg/mouse)	Death/Survival (*n*/*n*)	Mortality (%)
H-LPS	8	0.25	0/8	0
	8	0.50	4/4	50.0
	8	1.00	6/2	75.0
E-LPS	8	0.25	2/6	25.0
	8	0.50	7/1	87.5
	8	1.00	8/0	100
	8	/	0/8	0

Positivity rate of H-LPS in biopsy specimens

The total positivity rate of H-LPS in the 126 biopsy specimens was 60.3% (Table 5). Totally 73.5% of the biopsy specimens from chronic gastritis patients (50/68) were H-LPS positive, which was significantly higher than that (44.8%) from gastric ulcer patients (26/58) (χ^2=10.77, P<0.01). H-LPS positivity rate in biopsy specimens of the patients with chronic superficial gastritis (38/48, 79.2%) was similar to that of the patients with chronic active gastritis (9/10, 90.0%) (χ^2=0.63, P>0.05), but both positivity rates were much higher than that of the patients with atrophic gastritis (3/10, 30.0%) (χ^2=7.50-9.66, P<0.01). Among the biopsy specimens from patients with any one of

the three types of gastric ulcer, the H-LPS positive rates were similar to each other (χ^2=0.11-1.25, P>0.05). A H-LPS positive biopsy specimen is shown in Figure 2.

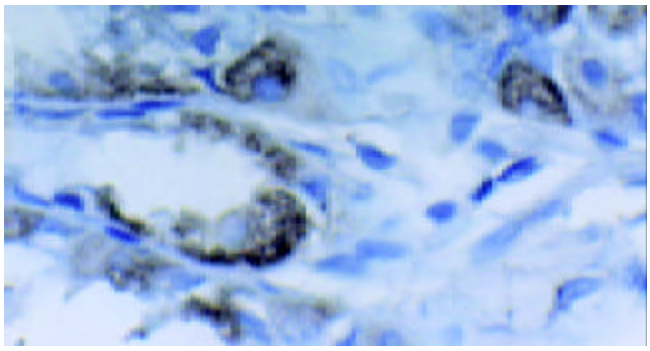

Figure 2 H-LPS positive biopsy specimen (Original magnification: ×600).

Table 5 H-LPS detection rates in the biopsy specimens from patients with chronic gastritis and gastric ulcer

Group	Number (*n*)	Positivity (*n*)	Positive rate (%)
Chronic gastritis			
Superficial	48	38	79.2
Active	10	9	90.0
Atrophic	10	3	30.0
Gastric ulcer			
Gastric	12	7	58.3
Duodenal	40	16	40.0
Complex	6	3	50.0
Total	126	76	60.3

DISCUSSION

Bacterial endotoxin possesses broad biological activities and its toxicity is mainly dependent on lipid A[15]. Among the biological activities of LPS, limulus amoebocyte lysate coagulation, rabbit pyrogen and mouse lethality are most typical and important[16,17]. In some of the previously published data, H-LPS showed much lower activities of coagulating limulus lysate, pyrogenic response in rabbit and lethal potential in mice[8,9]. In our study, we found that the effect of H-LPS on causing fever in rabbits, death in mice and its cytotoxicity to NIH 3T3 fibroblast were less compared to the LPS from *E. coli*. However, the ability of coagulating limulus lysate of H-LPS (+/0.5 ng/mL) was similar to that of E-LPS based on several repeated results. As mentioned in Introduction, LPS preparations might have various biological activities if different extraction methods were used[13,14]. The result in limulus lysate assay of this study differed from the previously reported probably due to H-LPS from different strains and the distinction in LPS extraction methods.

Salgado *et al*. revealed that H-LPS from different strains could be divided into two types: One of low biological activity and one of high biological activity of inducing the mitogenicity and TNF-α synthesis of cells. And the strains with the high activity were demonstrated belonging to the low virulence genotypes with *cagA*$^-$ and s1bm2 or s2m2 for *vacA*[18]. To our surprise, at the same injected dosage (100 μg/kg· b.w.) in our study, H-LPS caused death in two of the three tested rabbits in blood pressure regulation test but E-LPS did not. In addition, the ability of H-LPS of inducing PBMC at 0.5 h after injection ($12.51\pm0.54\times10^9$/L) was also stronger than that of E-LPS [$(8.22\pm0.68)\times10^9$/L]. These data, including the results reported by Salgado *et al.*, indicated that the role of the LPS as a virulence factor from some *H pylori* strains should be re-evaluated.

It was reported that H-LPS acted as a modulator of host-dependent gastritis through inducing both gastric epithelial cells and macrophages to secrete IL-1, TNF and IL-8[19-21]. In this study, a high frequency of H-LPS in the biopsy specimens from chronic gastritis patients (73.5%) was found. However, the positivity rate of H-LPS in the biopsy specimens from gastric ulcer patients (44.8%) was relatively lower (χ^2=10.77, P<0.01). Furthermore, the biopsy specimens from chronic superficial gastritis (79.2%) and chronic active gastritis (90.0%) showed significantly higher H-LPS positive rates compared to those from chronic atrophic gastritis (30.0%) (χ^2=7.50-9.66, P<0.01). These data indicated that H-LPS might play a more important role in inducing human gastric inflammation than previously considered. It is well known that PBMC are a mixture of neutrophilic granulocytes, mononuclear macrophages and lymphocytes[22-24]. Mononuclear macrophages and lymphocytes are the major cells to produce IL-1, TNF and IL-8[25-27]. The result from our study showed that H-LPS had a stronger ability of inducing PBMC than E-LPS, suggesting the critical effect of H-LPS on inducing inflammatory reaction in human gastritis.

REFERENCES

1 **Zhang Z**, Yuan Y, Gao H, Dong M, Wang L, Gong YH. Apoptosis, proliferation and p53 gene expression of *H pylori* associated gastric epithelial lesions. *World J Gastroenterol* 2001; **7**: 779-782

2 **Michetti P**, Kreiss C, Kotloff KL, Porta N, Blano JL, Bachmann D, Herranz M, Saldinger PF, Corthesy-Theulaz I, Losonsky G, Nichols R, Simon J, Stolte M, Acherman S, Monath TP, Blum AL. Orla immunization with urease and *Escherichia coli* heat-labile enterotoxin is safe and immunogenic in *Helicobacter pylori*-infected adults. *Gastroenterology* 1999; **116**: 804-812

3 **Suganuma M**, Kurusu M, Okabe S, Sueoka N, Yoshida M, Wakatsuki Y, Fujiki H. *Helicobacter pylori* membrane protein 1: a new carcinogenic factor of *Helicobacter pylori*. *Cancer Res* 2001; **61**: 6356-6359

4 **Nakamura S**, Matsumoto T, Suekane H, Takeshita M, Hizawa K, Kawasaki M, Yao T, Tsuneyoshi M, Iida M, Fujishima M. Predictive value of endoscopic ultrasonography for regression of gastric low grade and high grade MALT lymphomas after eradication of *Helicobacter pylori*. *Gut* 2001; **48**: 454-460

5 **Uemura N**, Okamoto S, Yamamoto S, Matsumura N, Yamaguchi S, Yamakido M, Taniyama K, Sasaki N, Schlemper RJ. *Helicobacter pylori* infection and the development of gastric cancer. *N Engl J Med* 2001; **345**: 8298-8332

6 **Morgner A**, Miehlke S, Fischbach W, Schmitt W, Muller-Hermelink H, Greiner A, Thiede C, Schetelig J, Neubauer A, Stolte M, Ehninger G, Bayerdorffer E. Complete remission of primary high-grade B-cell gastric lymphoma after cure of *Helicobacter pylori* infection. *J Clin Oncol* 2001; **19**: 2041-2048

7 **Kate V**, Ananthakrishnan N, Badrinath S. Effect of *Helicobacter pylori* eradication on the ulcer recurrence rate after simple closure of perforated duodenal ulcer: retrospective and prospective randomized controlled studies. *Br J Surg* 2001; **88**: 1054-1058

8 **Muotiala A**, Helander IM, Pyhala L, Kosunen TU, Moran AP. Low biological activity of *Helicobacter pylori* lipopolysaccharide. *Infect Immun* 1992; **60**: 1714-1716

9 **Ogawa T,** Suda Y, Kashihara W, Hayashi T, Shimoyama T, Kusumoto S, Tamura T. Immunobiological activities of chemically defined lipid A from *Helicobacter pylori* LPS in comparison with Porphyromonas gingivalis lipid A and *Escherichia coli*-type synthetic lipid A (compound 506). *Vaccine* 1997; **15**: 1598-1605

10 **Matsuyama N,** Kirikae T, Kirikae F, Hashimoto M, Amanot K, Hayashi S, Hirai Y, Kubota T, Nakano M. Non-standard biological activities of lipopolysaccharide from *Helicobacter pylori*. *J Med Microbiol* 2001; **50**: 865-869

11 **Suda Y,** Kim YM, Ogawa T, Yasui N, Hasegawa Y, Kashihara W, Shimoyama T, Aoyama K, Nagata K, Tamura T, Kusumoto S. Chemical structure and biological activity of a lipid A compo-

nent from *Helicobacter pylori* strain 206. *J Endotoxin Res* 2001; **7**: 95-104

12 **Ogawa T,** Asai Y, Sakai Y, Oikawa M, Fukase K, Suda Y, Kusumoto S, Tamura T. Endotoxic and immunobiological activities of a chemically synthesized lipid A of *Helicobacter pylori* strain 206-1. *FEMS Immunol Med Microbiol* 2003; **36**: 1-7

13 **Venter P,** Lues JF. Extraction methods for lipopolysaccharides from *Escherichia coli* ATCC 25922 for quantitative analysis by capillary electrophoresis. *Int J Food Microbiol* 2003; **84**: 245-250

14 **Zherebylo OIe,** Moroz SM, Hvozdiak RI. Characteristics of bacterial lipopolysaccharides depending on extraction method. *Ukr Biokhim Zh* 2000; **72**: 51-55

15 **Mattsby-Baltzer I,** Mielniczuk Z, Larsson L, Lindgren K, Goodwin S. Lipid A in *Helicobacter pylori*. *Infect Immun* 1992; **60**: 4383-4387

16 **Skurnik M.** Molecular genetics, biochemistry and biological role of Yersinia lipopolysaccharide. *Adv Exp Med Biol* 2003; **529**: 187-197

17 **Luchi M,** Morrison DC. Comparable endotoxic properties of lipopolysaccharides are manifest in diverse clinical isolates of gram-negative bacteria. *Infect Immun* 2000; **68**: 1899-1904

18 **Salgado F,** Garcia A, Onate A, Gonzalez C, Kawaguchi F. Increased *in-vitro* and *in-vivo* biological activity of lipopolysaccharide extracted from clinical low virulence vacA genotype *Helicobacter pylori* strains. *J Med Microbiol* 2002; **51**: 771-776

19 **Pece S,** Giuliani G, Di Leo A, Fumarola D, Antonaci S, Jirillo E. Role of lipopolysaccharide and related cytokines in *Helicobacter pylori* infection. *Recenti Prog Med* 1997; **88**: 237-241

20 **Sakagami T,** Vella J, Dixon MF, O'Rourke J, Radcliff F, Sutton P, Shimoyama T, Beagley K, Lee A. The endotoxin of *Helicobacter pylori* is a modulator of host-dependent gastritis. *Infect Immun* 1997; **65**: 3310-3316

21 **Slomiany BL,** Slomiany A. Suppression of gastric mucosal inflammatory responses to *Helicobacter pylori* lipopolysaccharide by peroxisome proliferator-activated receptor gamma activation. *IUBMB Life* 2002; **53**: 303-308

22 **Valente JF,** Alexander JW, Li BG, Noel JG, Custer DA, Ogle JD, Ogle CK. Effect of *in vivo* infusion of granulocyte colony-stimulating factor on immune function. *Shock* 2002; **17**: 23-29

23 **Tsitsilonis OE,** Tsavaris NB, Kosmas C, Gouveris P, Papalambros E. Immune changes in patients with colorectal cancer treated by adjuvant therapy with monoclonal antibody 17-1A: a pilot study. *J Chemother* 2003; **15**: 387-393

24 **Yamamoto T,** Kimura T, Ueta E, Tatemoto Y, Osaki T. Characteristic cytokine generation patterns in cancer cells and infiltrating lymphocytes in oral squamous cell carcinomas and the influence of chemoradiation combined with immunotherapy on these patterns. *Oncology* 2003; **64**: 407-415

25 **Zhao D,** Pothoulakis C. Rho GTPases as therapeutic targets for the treatment of inflammatory diseases. *Expert Opin Ther Targets* 2003; **7**: 583-592

26 **Meeuwsen S,** Persoon-Deen C, Bsibsi M, Ravid R, Noort JM. Cytokine, chemokine and growth factor gene profiling of cultured human astrocytes after exposure to proinflammatory stimuli. *Glia* 2003; **43**: 243-253

27 **Xing L,** Remick DG. Relative cytokine and cytokine inhibitor production by mononuclear cells and neutrophils. *Shock* 2003; **20**: 10-16

Edited by Zhu LH and Chen WW **Proofread by** Xu FM

PO Box 2345, Beijing 100023, China
Fax: +86-10-85381893
E-mail: wjg@wjgnet.com www.wjgnet.com

World J Gastroenterol 2004;10(14):2060-2062
World Journal of Gastroenterology
 ISSN 1007-9327

Gene distribution of *cagII* in *Helicobacter pylori*-infected patients of Zhejiang Province

Hai-Yan Liu, Ping-Chu Fang, Yun-Shui Jiang, Ran Tao, Jin Chen

Hai-Yan Liu, Ping-Chu Fang, Yun-Shui Jiang, Ran Tao, Jin Chen, Department of Medical Microbiology and Parasitology, School of Medicine, Zhejiang University, Hangzhou 310031, Zhejiang Province, China
Supported by the Project of China Medical Board, No.96-628, and the Natural Science Foundation of Zhejiang Province, No.302023
Correspondence to: Ping-Chu Fang, Department of Medical Microbiology and Parasitology, School of Medicine, Zhejiang University, 353 Yanan Road, Hangzhou 310031, Zhejiang Province, China. fangpc@cmm.zju.edu.cn
Telephone: +86-571-87217403
Received: 2003-12-19 **Accepted:** 2004-01-15

Abstract

AIM: To determine the prevalence of genotypes of *cagII* in *Helicobacter pylori* (*H pylori*)-infected patients in Zhejiang Province and investigate the relationship between these genotypes and the types of gastroduodenal diseases.

METHODS: One hundred and seventy one clinical isolates were collected from 70 chronic superficial gastritis, 31 chronic atrophic gastritis, 41 gastric ulcer, 21 duodenal ulcer, 3 gastric and duodenal ulcer, and 5 gastric adenocarcinoma patients. Polymerase chain reaction assays were performed for analysis of *cagT, ORF13* and *ORF10* genes in the *cagII* region.

RESULTS: Of 171 *H pylori* isolates from Zhejiang patients, 159(93.0%) were positive for all the three loci. One isolate (0.6%) was negative for all the three loci, and 11(6.4%) were partially deleted in *cagII*. The positive rates of *cagT, ORF13* and *ORF10* genes were 97.1%, 94.7% and 99.4%, respectively. In the strains isolated from the patients with diseases including chronic superficial gastritis, chronic atrophic gastritis, gastric ulcer and duodenal ulcer, the sitive rates of *cagT* were 95.7%, 100.0%, 95.1% and 100.0%, respectively. The positive rates of *ORF13* were 94.3%, 93.5%, 95.1% and 100.0%, respectively. The sitive rates of *ORF10* were 98.6%, 100.0%, 100.0% and 100.0%, respectively. The three genes were all positive in the three *H pylori* strains isolated from the patients with both gastric and duodenal ulcer. In the five strains isolated from the patients with gastric adenocarcinoma, only one isolate was negative for *ORF13*. There were no significant differences of the *cagT*, *ORF13* and *ORF10* genes among the different gastroduodenal diseases including chronic superficial gastritis, chronic atrophic gastritis, gastric ulcer, duodenal ulcer, both gastric and duodenal ulcer and gastric adenocarcinoma (χ^2=3.098, P>0.05 for *cagT*; χ^2=3.935, P>0.05 for *ORF13* and χ^2=6.328, P>0.05 for *ORF10*).

CONCLUSION: The *cagII* is not a uniform and conserved entity. Although the genes in *cagII* are highly associated with the gastroduodenal diseases, the clinical outcome of *H pylori* infection is not reliably predicted by the three genes in *cagII* in patients from Zhejiang Province.

Liu HY, Fang PC, Jiang YS, Tao R, Chen J. Gene distribution of *cagII* in *Helicobacter pylori*-infected patients of Zhejiang Province. *World J Gastroenterol* 2004; 10(14): 2060-2062
http://www.wjgnet.com/1007-9327/10/2060.asp

INTRODUCTION

Although more than 50% of the world population are infected with *Helicobacter pylori* (*H pylori*), most of the carriers are asymptomatic[1,2]. Only a minority of infected persons may develop serious gastroduodenal diseases. Though the pathogenesis of *H pylori* infection is not well understood, there are several putative virulence factors that may contribute to mucosal damage by *H pylori* infection such as the cytotoxin associated gene (*cag*) pathogenicity island (*PAI*)[3]. The *cag PAI* was reported to be a major virulence factor of *H pylori*[4, 5]. The *cagII* is located on the left of *cag PAI*. There is growing evidence that genetic differences among strains determine the clinical outcome of infection[6, 7]. Some of the genes in *cagII* are believed to encode proteins that have similarities to recognized virulence factors in other bacteria. However in mainland China the distribution of these genes in *cagII* of *H pylori* and their relationship with gastroduodenal diseases remain unclear. In this work, we attempted to determine the structure of *cagII* of *H pylori* isolated from Zhejiang Province and the relationship between the genes in *cagII* and the types of the gastroduodenal diseases. The genes of *cagT*, *ORF13* and *ORF10* that have representative spacing sequences along the *cagII* were selected and amplified by polymerase chain reaction (PCR) to evaluate the *cagII* distribution in 171 isolates from *H pylori*-infected patients with different gastroduodenal diseases in Zhejiang Province.

MATERIALS AND METHODS

H pylori isolates

A total of 171 *H pylori* isolates were obtained from *H pylori*-infected adults who had undergone upper gastrointestinal endoscopy at the Second Affiliated Hospital of Zhejiang University and the Hospital of Daishan County in Zhejiang Province. The patients consisted of 115 men and 56 women with a mean age of 42.9 years (ranging from 16 to 71 years). The patients were classified into 6 groups of chronic superficial gastritis (n=70), chronic atrophic gastritis (n=31), gastric ulcer (n=41), duodenal ulcer (n=21), both gastric and duodenal ulcer (n=3) and gastric adenocarcinoma (n=5). The classification of patients was based on the results of endoscopic and histological examinations.

Culture of H pylori

Biopsy specimens were cultured on ECY-selective agar plates at 37 ℃ for 5 d under 100% humidity and microaerophilic conditions (50 mL/L O_2, 100 mL/L CO_2, and 850 mL/L N_2). *H pylori* was identified by the following criteria: characteristic of colony, rapid urease test, catalase test and morphology on Gram staining.

Genomic DNA extraction

H pylori genomic DNA was extracted by phenol/chloroform method.

Detection of cagT, ORF13 and ORF10 with PCR

For the detection of *cagT*, *ORF13* and *ORF10* genes, PCR was performed in a volume of 25 μL containing 2.5 μL of 10×buffer, 2 μL of 25 mmol/L $MgCl_2$, 2.5 μL of 2 mmol/L dNTPs, 0.2 μL of *Taq* DNA polymerase, 0.5 μL of 20 μmol/L primer sets (Table 1), 1 μL of genomic DNA, 15.8 μL of water. The primers for *cagT*, *ORF13* and *ORF10* were synthesized as described in Table 1. The PCR amplification of *cagT*, *ORF13* and *ORF10* genes was as follows: initial denaturation at 95 ℃ for 3 min; 30 cycles of at 94 ℃ for 30 s, at 56 ℃ for 30 s and at 72 ℃ for 45 s; and a final extension at 72 ℃ for 7 min. PCR was performed in a thermal cycle (GeneAmp PCR system 9 600; Perkin-Elmer, Norwalk, Conn, USA). After amplification, 5 μL of PCR products was electrophoresed on 17 g/L agarose gel and examined under UV illumination.

Table 1 PCR primers for amplification of *cagT*, *ORF13* and *ORF10*

Gene	Strand	Primer sequence	Length (bp)
cagT	+	5' TCTAAAAAGATTACGCTCATAGGCG 3'	490
	-	5' CTTTGGCTTGCATGTTCAAGTTGCC 3'	
ORF13	+	5' CGTTCATGTTCCATACATCTTTGGC 3'	617
	-	5' GATTTATAGCGATCTAAGAAACCGC 3'	
ORF10	+	5' AATAGTGCTTTCTTTAGGATTAGCG3'	658
	-	5' CCGATTTAATCCTTTCGCTTATGTG 3'	

Statistical analysis

Statistical analysis was performed using the χ^2 test. Values of $P<0.05$ were considered to be statistically significant.

RESULTS

Amplification of cagT, ORF13 and ORF10 genes

After PCR amplification of the *cagT*, *ORF13* and *ORF10* genes, the products were electrophoresed on 1.7% agarose gels, and stained with ethidium bromide (Figure 1).

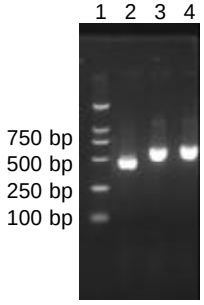

Figure 1 Electrophoresis of *cagT*, *ORF13* and *ORF10* after PCR. Lane 1:100 bp DNA ladder; Lane 2: *cagT* (490 bp); Lane 3: *ORF13*(617 bp); Lane 4: *ORF10*(658 bp).

Distribution of selected genes within cagII in H pylori isolates from patients with gastroduodenal diseases

Of 171 *H pylori* isolates from Zhejiang Province, 159(93.0%) were positive for all the three loci. One isolate (0.6%) from a patient with chronic superficial gastritis was negative for all the three loci, and 11(6.4%) were partially deleted in *cagII*. Among the latter 11 isolates, 6 were from chronic superficial gastritis, 2 from chronic atrophic gastritis, 3 from gastric ulcer and 1 from gastric adenocarcinoma. The positivity rates of *cagT*, *ORF13* and *ORF10* gene expression and their relationship with gastroduodenal diseases are listed in Table 2. There were no significant differences among the three selected genes in different gastroduodenal diseases (χ^2=3.098, $P>0.05$ for *cagT*; χ^2=3.935, $P>0.05$ for *ORF13* and χ^2=6.328, $P>0.05$ for *ORF10*).

DISCUSSION

H pylori is a Gram-negative, spiral-shaped, microaerophilic bacterium that infects human gastric mucosa and is recognized as a major cause of chronic active gastritis and most peptic ulcer diseases[8,9]. It is also closely related with gastric adenocarcinoma, gastric mucosa-associated lymphoid tissue lymphoma and primary gastric non-Hodgkin's lymphoma[10]. The *cag PAI* is an approximately 40-kb cluster of genes on the *H. pylori* chromosome[3,11] and divided into two regions, *cagI* and *cagII*. There are 14 open reading frames in *cagII*. Some of the genes within *cagII* are believed to encode proteins, which have homologue of recognized virulence factors in other bacteria by amino acid database search and analysis. The protein encoded by *cagT* gene is similar to *Shigella flexnerii* 42-kDa surface antigen IPAC. It was reported that IPAC of *Shigella* was essential for initial bacterial entry into epithelial cells by interacting with beta-catenin and destabilizing the cadherin-mediated cell adhesion complex[12], thus the epithelial cell-cell tight adhesion was disrupted. These events might facilitate the further basolateral invasion of bacteria through the disrupted space and/or modulate the cell-to-cell spread of *Shigella*. We propose that *cagT* may play a similar role in the pathogenesis of *H pylori*. Moreover the proteins encoded by *cagT*, *ORF13* and *ORF10* are similar to *virB7*, *virB10* and *virD4* of *Agrobacterium tumefaciens* that are needed for the transferring of the Ti plasmid DNA from the bacterium to the nucleus of the plant cell[1, 13]. The products of the *virB7, virB10* and *virD4* genes are considered to be important components in type IV secretion system[14]. Several lines of evidence suggest that the type IV secretion system encoded by the *cag PAI* of *H pylori* is recognized as a major virulence determinant, governing the translocation of the CagA protein to eukaryotic cells and inducing strongly the expression and secretion of IL-8 in gastric epithelial cells[2,15,16]. Deletion of the *cag*II segment from strain 26695 reduced IL-8 synthesis to about 10-20% of the wild-type control. Inactivation of *ORF13* or *cagT* also caused similar reduction in IL-8 synthesis after infection. In addition, the products of *cagT, ORF13* and *ORF10* were absolutely essential for the translocation of CagA and tyrosine phosphorylation[13,17,18]. IL-8, a potent neutrophil and T-cell chemoattractant and activator, is believed to play a key role in the pathogenesis of *H pylori*-induced tissue damage[19,20]. These

Table 2 Relationship between *cagT, ORF13, ORF10* gene expression and clinical diagnosis in patients of Zhejiang Province

Group	*n*	cagT *n*	%	*ORF*13 *n*	%	*ORF*10 *n*	%
Chronic superficial gastritis	70	67	95.7	66	94.3	69	98.6
Chronic atrophic gastritis	31	31	100.0	29	93.5	31	100.0
Gastric ulcer	41	39	95.1	39	95.1	41	100.0
Duodenal ulcer	21	21	100.0	21	100.0	21	100.0
Both gastric and duodenal ulcer	3	3	-	3	-	3	-
Gastric adenocarcinoma	5	5	-	4	-	5	-
Total	171	166	97.1	162	94.7	170	99.4

results indicate that the genes in *cagII* participate in the translocation of CagA and induction of IL-8 synthesis and then a resultant severe inflammatory response. The presence of *cagII* is highly associated with the gastroduodenal diseases[21].

In the present study, we have shown that the overall prevalence of the *cagT*, *ORF13* and *ORF10* is 97.1%, 94.7% and 99.4%, respectively. Although the genes in *cagII* are highly associated with the gastroduodenal diseases, the clinical outcome of *H pylori* infection is not reliably predicted by the genes of *cagT*, *ORF13* and *ORF10* in the *cag II* in Zhejiang Province. These results are in agreement with those of studies in Japanese and Taiwanese. The distribution of presence of *cagT*, *ORF13* and *ORF10* in Japan has been shown to be about 94%, 98.4% and 98.4%, respectively[16]. In Taiwanese, all strains were positive for *cagT* and *ORF13* genes[22]. However, in South Africa the overall positivity rate of *cagT* in clinical isolates was 81.7%, lower than our report. And the prevalence of *cagT* in patients with peptic ulceration and gastric adenocarcinoma was significantly higher than that in gastritis[21]. In Europe the prevalence of *cagT*, *ORF13* and *ORF10* in clinical isolates was 79.5%, also lower than the one of our report[23]. These results indicate that *H pylori* isolated from Asia is different from the ones isolated from South Africa and Europe. In the present study, of 171 *H pylori* isolates from Zhejiang patients, 159(93.0%) were positive for all the three loci. One isolate (0.6%) from a patient with chronic superficial gastritis was negative for all the three loci, and 11(6.4%) were partially deleted in *cagII*. It appears that the *cagII* is not a uniform, conserved entity.

In conclusion, we speculate that the distribution of *cagT*, *ORF13* and *ORF10* in Zhejiang Province is in accordance with those in other Asian countries. The clinical outcome of *H pylori* infection can not be reliably predicted by the genes of *cagT*, *ORF13* and *ORF10* in *cag II*. Many factors such as the genetic factors of both *H pylori* and the host cell and the circumstance may contribute to the clinical outcome of *H pylori* infection. Nevertheless, Further work is required to illustrate pathogenesis of *cagII* in *H pylori* associated gastroduodenal diseases.

REFERENCES

1 **Covacci A,** Telford JL, Del Giudice G, Parsonnet J, Rappuoli R. *Helicobacter pylori* virulence and genetic geography. *Science* 1999; **284**: 1328-1333

2 **Bhattacharyya A,** Pathak S, Datta S, Chattopadhyay S, Basu J, Kundu M. Mitogen-activated protein kinases and nuclear factor-kappaB regulate *Helicobacter pylori*-mediated interleukin-8 release from macrophages. *Biochem J* 2002; **368**(Pt 1): 121-129

3 **Censini S**, Lange C, Xiang Z, Crabtree JE, Ghiara P, Borodovsky M, Rappuoli R, Covacci A. cag, a pathogenicity island of *Helicobacter pylori*, encodes type I-specific and disease-associated virulence factors. *Proc Natl Acad Sci U S A* 1996; **93**: 14648-14653

4 **Ko JS**, Seo JK. cag pathogenicity island of *Helicobacter pylori* in Korean children. *Helicobacter* 2002; **7**: 232-236

5 **Mizushima T**, Sugiyama T, Kobayashi T, Komatsu Y, Ishizuka J, Kato M, Asaka M. Decreased adherence of cagG-deleted *Helicobacter pylori* to gastric epithelial cells in Japanese clinical isolates. *Helicobacter* 2002; **7**: 22-29

6 **Dubois A**, Berg DE, Incecik ET, Fiala N, Heman-Ackah LM, Perez-Perez GI, Blaser MJ. Transient and persistent experimental infection of non-human primates with *Helicobacter pylori*: implications for human disease. *Infect Immun* 1996; **64**: 2885-2891

7 **Atherton JC**, Peek RMJ, Tham KT, Cover TL, Blaser MJ. Clinical and pathological importance of heterogeneity in vacA, the vacuolating cytotoxin gene of *Helicobacter pylori*. *Gastroenterology* 1997; **112**: 92-99

8 **Zhang H**, Fang DC, Wang RQ, Yang SM, Liu HF, Luo YH. Effect of *Helicobacter pylori* infection on expression of Bcl-2 family members in gastric adenocarcinoma. *World J Gastroenterol* 2004; **10**: 227-230

9 **Bai Y**, Zhang YL, Wang JD, Lin HJ, Zhang ZS, Zhou DY. Conservative region of the genes encoding four adhesins of *Helicobacter pylori*: cloning, sequence analysis and biological information analysis. *Diyi Junyi Daxue Xuebao* 2002; **22**: 869-871

10 **Morgner A**, Miehlke S, Stolte M, Neubauer A, Alpen B, Thiede C, Klann H, Hierlmeier FX, Ell C, Ehninger G, Bayerdorffer E. Development of early gastric cancer 4 and 5 years after complete remission of *Helicobacter pylori* associated gastric low grade marginal zone B cell lymphoma of MALT type. *World J Gastroenterol* 2001; **7**: 248-253

11 **Tomb JF**, White O, Kerlavage AR, Clayton RA, Sutton GG, Fleischmann RD, Ketchum KA, Klenk HP, Gill S, Dougherty BA, Nelson K, Quackenbush J, Zhou L, Kirkness EF, Peterson S, Loftus B, Richardson D, Dodson R, Khalak HG, Glodek A, McKenney K, Fitzegerald LM, Lee N, Adams MD, Hickey EK, Berg DE, Gocayne JD, Utterback TR, Peterson JD, Kelley JM, Cotton MD, Weidman JM, Fujii C, Bowman C, Watthey L, Wallin E, Hayes WS, Borodovsky M, Karp PD, Smith HO, Fraser CM, Venter JC. The complete genome sequence of the gastric pathogen *Helicobacter pylori*. *Nature* 1997; **338**: 539-547

12 **Shaikh N**, Terajima J, Watanabe H. IpaC of Shigella binds to the C-terminal domain of beta-catenin. *Microb Pathog* 2003; **35**: 107-117

13 **Akopyants NS**, Clifton SW, Kersulyte D, Crabtree JE, Youree BE, Reece CA, Bukanov NO, Drazek ES, Roe BA, Berg DE. Analyses of the cag pathogenicity island of *Helicobacter pylori*. *Molecular Microbiogy* 1998; **28**: 37-53

14 **Krall L**, Wiedemann U, Unsin G, Weiss S, Domke N, Baron C. Detergent extraction identifies different VirB protein subassemblies of the type IV secretion machinery in the membranes of Agrobacterium tumefaciens. *Proc Natl Acad Sci U S A* 2002; **99**: 11405-11410

15 **Rohde M**, Puls J, Buhrdorf R, Fischer W, Haas R. A novel sheathed surface organelle of the *Helicobacter pylori* cag type IV secretion system. *Mol Microbiol* 2003; **49**: 219-234

16 **Maeda S**, Yoshida H, Ikenoue T, Ogura K, Kanai F, Kato N, Shiratori Y, Omata M. Structure of cag pathogenicity island in Japanese *Helicobacter pylori* isolates. *Gut* 1999; **44**: 336-341

17 **Fischer W,** Puls J, Buhrdorf R, Gebert B, Odenbreit S, Haas R. Systematic mutagenesis of the *Helicobacter pylori* cag pathogenicity island: essential genes for CagA translocation in host cells and induction of interleukin-8. *Mol Microbiol* 2001; **42**: 1337-1348

18 **Selbach M,** Moese S, Meyer TF, Backert S. Functional analysis of the *Helicobacter pylori* cag pathogenicity island reveals both VirD4-CagA-dependent and VirD4-CagA-independent mechanisms. *Infect Immun* 2002; **70**: 665-671

19 **Ogura K**, Maeda S, Nakao M, Watanabe T, Tada M, Kyutoku T, Yoshida H, Shiratori Y, Omata M. Virulence factors of *Helicobacter pylori* responsible for gastric diseases in Mongolian gerbil. *J Exp Med* 2000; **192**: 1601-1609

20 **Yamaoka Y**, Kita M, Kodama T, Sawai N, Tanahashi T, Kashima K, Imanishi J. Chemokines in the gastric mucosa in *Helicobacter pylori* infection. *Gut* 1998; **42**: 609-617

21 **Kidd M**, Lastovica AJ, Atherton JC, Louw JA. Conservation of the cag pathogenicity island is associated with vacA alleles and gastroduodenal disease in South African *Helicobacter pylori* isolates. *Gut* 2001; **49**: 11-17

22 **Sheu SM**, Sheu BS, Yang HB, Li C, Chu TC, Wu JJ. Presence of iceA1 but not cagA, cagC, cagE, cagF, cagN, cagT, or orf13 genes of *Helicobacter pylori* is associated with more severe gastric inflammation in Taiwanese. *J Formos Med Assoc* 2002; **101**: 18-23

23 **Jenks PJ**, Megraud F, Labigne A. Clinical outcome after infection with *Helicobacter pylori* does not appear to be reliably predicted by the presence of any of the genes of the cag pathogenicity island. *Gut* 1998; **43**: 752-758

Edited by Chen WW and Zhu LH **Proofread by** Xu FM

PO Box 2345, Beijing 100023, China
Fax: +86-10-85381893
E-mail: wjg@wjgnet.com www.wjgnet.com

World J Gastroenterol 2004;10(14):2063-2066
World Journal of Gastroenterology
 ISSN 1007-9327

Effects of fucosylated milk of goat and mouse on *Helicobacter pylori* binding to Lewis b antigen

Hong-Tao Xu, Yao-Feng Zhao, Zheng-Xing Lian, Bao-Liang Fan, Zhi-Hui Zhao, Shu-Yang Yu, Yun-Ping Dai, Li-Li Wang, Hui-Ling Niu, Ning Li, Lennart Hammarström, Thomas Borén, Rolf Sjöström

Hong-Tao Xu, Zhi-Hui Zhao, Shu-Yang Yu, Yun-Ping Dai, Li-Li Wang, Hui-Ling Niu, Ning Li, State Key Laboratories for Agrobiotechnology, China Agriculture University, Beijing 100094, China
Yao-Feng Zhao, Lennart Hammarström, Center for Biotechnology, Karolinska Institute, Sweden
Zheng-Xing Lian, College of Animal Science and Technology, China Agriculture University, Beijing 100094, China
Bao-Liang Fan, Bio-tech Research Center of Shandong Academy of Agricultural Sciences, Jinan 250100, Shandong Province, China
Thomas Borén, Department of Odontology and Oral Microbiology, Umeå University, Sweden
Rolf Sjöström, Department of Odontology, Umeå University, Sweden
Correspondence to: Professor Ning Li, State Key Laboratories for Agrobiotechnology, China Agriculture University, Beijing 100094, China. ninglbau@public3.bta.net.cn
Telephone: +86-10-62893323 **Fax:** +86-10-62893904
Received: 2003-12-23 **Accepted:** 2004-01-08

Abstract

AIM: To evaluate the effects of animal milk containing fucosylated antigens on *Helicobacter pylori* (*H pylori*) binding to Lewis b antigen.

METHODS: A mammary gland expression vector containing human α1-3/4-fucosyltransferase cDNA sequences was constructed. Transient expression of human α1-3/4-fucosyltransferase cDNA in goat mammary cell and establishment of transgenic mice were performed. The adhesion inhibitory properties of milk samples were analyzed by using *H pylori*.

RESULTS: Goat milk samples were found to inhibit bacterial binding to Lewis b antigen. The highest inhibition was observed 42 h after injection of the plasmid. The binding activity of *H pylori* to Lewis b antigen reduced mostly, by 83%, however milk samples from transgenic mice did not inhibit *H pylori* binding to Lewis b antigen.

CONCLUSION: The use of "humanized" animal milk produced by the transgenic introduction of fucosylated antigen can perhaps provide an alternative therapy and preventive measure for *H pylori* infection.

Xu HT, Zhao YF, Lian ZX, Fan BL, Zhao ZH, Yu SY, Dai YP, Wang LL, Niu HL, Li N, Hammarström L, Borén T, Sjöström R. Effects of fucosylated milk of goat and mouse on *Helicobacter pylori* binding to Lewis b antigen. *World J Gastroenterol* 2004; 10(14): 2063-2066
http://www.wjgnet.com/1007-9327/10/2063.asp

INTRODUCTION

Helicobacter pylori (*H pylori*), a human specific gastric pathogen, was first isolated in 1983[1]. Twenty years of research has found that *H pylori* infection is one of the major causes of upper gastrointestinal tract diseases, such as chronic active gastritis and peptic ulcer disease[2-6]. In chronic active gastritis, gastric ulcer and gastroduodenal ulcer, the incidences of *H pylori* infection are 71-94%, 72-100% and 73-100% respectively. In addition, *H pylori* infection has been linked with the development of gastric adenocarcinoma and mucosa-associated lymphoid tissue (MALT)[7-13]. It has been defined as a Class I carcinogen by WHO[14,15].

H pylori colonize human gastric mucosa by adhering both to the mucous epithelial cells and to the mucus layer[16]. Specific receptor structures in combination with the unique tissue-specific distribution of receptors can restrict microbial colonization to a limited number of hosts, tissues and cell lineages[17]. *H pylori* can bind tightly to epithelial cells using various bacterial surface components[18-20]. The best characterized adhesin, BabA, is a 78-kD outer-membrane protein that binds to the fucosylated Lewis b (Le^b) blood group antigen[21]. Accumulating evidence in animal models suggests that BabA is relevant to *H pylori*-associated diseases[22]. Le^b antigen is one of the most important receptors, governing adhesion of *H pylori* to gastric mucosa. Boren *et al.* found that the fucosylated Lewis blood group antigens Le^b and H-1 were the carbohydrate structures that specifically mediated the adherence of *H pylori* to human gastric epithelial cells *in situ*.

Le^b antigen is a human blood group antigen. In human cells, the synthesis of Lewis antigens is regulated by a series of glycosyltransferases that act sequentially upon a precursor molecule. The fucosyltransferases are responsible for the final step in this process. Their function is to add a fucose residue to precursor molecules to form human blood antigens, such as Le^a, Le^b and H1 antigen (Figure1). Addition of fucose to the terminal galactose residue of the lacto series core chain oligosaccharide results in the H1 antigen. Le^b antigen is formed by the addition of a "branched" fucose residue to H1-antigen, catalyzed by α1-3/4-fucosyltransferase. The fucosylated blood group antigens, typically found on erythrocytes, are also expressed on the gastro-intestinal epithelium. Le^b is the dominant fucosylated blood group antigen expressed on the gastric surface mucous cells in the gastric epithelial lining. The fucosylated blood group antigens are also present in the mucins of the gastric mucus layer and, in addition, as natural "scavengers" or clearance factors in secretions such as saliva, tears, and human milk.

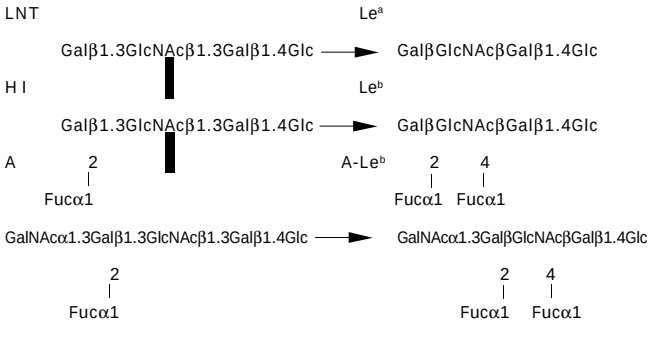

Figure 1 Formation of fucosylated blood group antigens.

H pylori infection is one of the most common infections in humans. Epidemiological data show that it affects about half of the human population. Without specific therapy, *H pylori* infection can persist for decades or even the host's lifetime. But only about 15% of *H pylori*-infected individuals actually have *H pylori*-associated diseases. It is likely to be associated with other additional factors such as genetic predisposition, age of infection, and the genotype of infective strain. The prevalence varies greatly among countries and among population groups within the same country. The overall prevalence of *H pylori* infection is strongly correlated with socioeconomic conditions. Eighty-five percent of *H pylori* can be eradicated by combination therapy in clinic, however, using antibiotics for several weeks may bring about other problems such as bacterial resistance. So many researchers are looking for other methods to prevent *H pylori* infection, such as preventing *H pylori* binding to or colonizing the gastric mucosa.

If we can add some *H pylori* specific receptor, for example, Le^b blood antigen or its analog to food, then *H pylori* binding to the human gastric mucosa may be prevented or reduced, and the bacteria will be excreted by the alimentary tract or destroyed by human antibody. Flak *et al.* reported that the α1-3/4-fucosyltransferase was expressed in the gastric mucosa of mice and that *H pylori* could bind to the mice gastric mucosa. At present, there are no reports of α1-3/4-fucosyltransferase being expressed in animal galactophore. Therefore, our aim was first to introduce human α1-3/4-fucosyltransferase into animals and get them expressed in the animal mammary gland and thus produce Le^b antigen in milk. This kind of milk does not only have nutritional value, it is also a natural source of lectin, a molecule that can block *H pylori* binding to the human gastric mucosa, and therefore prevent *H pylori* infection and reduce the severity of the infectious process. In this way, people can prevent *H pylori* infection by drinking this kind of milk daily.

This paper describes the transient expression of human α1-3/4-fucosyltransferase gene in goat mammary gland and the establishment of transgenic mouse model. A new test to prevent and cure *H pylori* infection and gastrointestinal diseases associated with *H pylori* infection is put forward in our study.

MATERIALS AND METHODS

Experimental animals

Kunming white mice were purchased from Beijing Laboratory Animal Research Center. Laoshan goats were provided by Beijing Sangao Corporation.

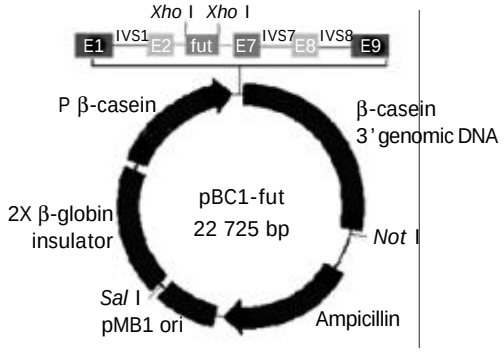

Figure 2 Map of expression vector: pBC1-fut.

Construction of expression vectors

A 1 115-bp α1-3/4-fucosyltransferase cDNA encompassing the entire 1 086-nt coding region specifying the 361-AA transmembrane glycoprotein, containing an upstream Kozak consensus sequence and *Xho*I site, a downstream *Xho*I site, was generated by PCR from a Fut/pCDM8 plasmid. The PCR product was then purified and digested by *Xho*I, and the digestion product was subcloned into pBC1 vector, which had been treated previously with *Xho*I, and transformed into *E. coli* DH5α. pBC1 is a specific milk expression vector which contains the goat β-casein promoter and other proprietary DNA sequences. The positive transfected clone containing the properly oriented α1-3/4-fucosyltransferase cDNA was screened by colony PCR. The expression vector, named pBC1-fut, allowed the α1-3/4-fucosyltransferase cDNA to be placed in its downstream of the β-casein promoter (Figure 2).

Transient expression

pBC1-fut was purified using Qiagen Plasmid Maxi kit. About 1 mg pBC1-fut was injected into a lactating goat's right and left mammary glands from the goat glandular duct. Milk samples at different times were then collected over a 100-h (4 d) period from both right (R) and left (L) udders. Then, milk samples were analyzed in a dilution series (25-, 50-, 100- and 200-fold) for adhesion inhibition properties.

Transgenic mice production

The 16-kb DNA fragment inserted was isolated by agarose gel electrophoresis and recovered by electro-elution. To remove any contamination, products were spot dialyzed against 40 mL TE (10 mmol/L Tris, 0.1 mmol/L EDTA, pH7.4) for 30 min (VSWP02 500 membrane, Millipore). Purified DNAs were diluted to 2-3 ng/μL in TE buffer and microinjected into the pronuclei of fertilized eggs of Kunming white mice.

Genomic DNAs were isolated from the tails of transgenic mice using a standard method. A pair of primers was designed to screen for transgenic mice: upper primer: 5' - GATTGACAA GTAATACGCTGTTTCCTC-3' and downstream primer: 5' - CATCAGAAGTTAAACAGCACAGTTAG-3' . PCR reactions using genomic DNAs as template were performed under the following condition: 30 cycles of 94 ℃ for 1 min, 58 ℃ for 1 min, and 74 ℃ for 1 min. After PCR screening, transgenic mice were confirmed by Southern hybridization. The probe was created by ^{32}P labeling α1-3/4-fucosyltransferase cDNA. Genomic DNA from transgenic mice and negative mouse as well as expression vector DNA were digested by *Bam*HI. Copies of the transgene were estimated by comparing the band density of the vector control with that in transgenic mice. Hybridizations were at 65 ℃ in Church (10 g/L BSA, 70 g/L SDS, 1 mmol/L EDTA, 0.5 mol/L sodium phosphate, pH 7.2). Final washes were in 2×SSC, 0. 5×SDS at 65 ℃. Signal from the membrane was detected using a Phosphor Screen (Molecular Dynamics, US).

Analysis of adhesion inhibitory properties of the milk

Goat milk was collected at different time points for 100 h from both right (R) and left (L) udders. The transgenic milk was collected at the 7 th day of lactation. The milk was centrifuged at 18 000 r/min for 1 h at 4 ℃. The fat on the surface was removed and the clear part of the supernatant was put in a new tube and used as the sample. Le^b antigen was labeled with ^{125}I by the chloramine T method. Milk samples were analyzed in dilution series (25-, 50-, 100- and 200-fold). The samples were mixed with an *H pylori* strain (CCUG17875), which bound bind Le^b antigen efficiently, on a cradle for 17 h at room temperature. After this period, ^{125}I radioactivity in bacterial pellet was measured with a gamma counter.

Western blotting

After electrophoresis on 80 g/L SDS-PAGE, proteins were transferred to a nitrocellulose extra blotting membrane (Sartorius, Germany). Le^b monoclonal antibodies (Immucor, GA) and HRP-conjugated goat anti-rabbit-IgG (Cappel Laboratories, US) were used to detect Le^b antigen.

Table 1 Blocking effect on *H pylori* binding to Lewis b antigen by goat milk

Time	Bind / Free Le^{b*} (%)				Sample	Bind / Free Le^{b*} (%)			
	25×	50×	100×	200×		25×	50×	100×	200×
R 6 h	32.5	43.4	49.6	53.9	L 6 h	36.9	47.1	52.1	55.1
R 12h	28.2	41.7	49.4	53.0	L 12 h	34.7	45.3	51.3	53.4
R 18 h	25.5	40.5	49.4	53.1	L 18 h	29.4	42.3	49.2	53.2
R 23 h	16.8	32.3	43.9	50.6	L 23 h	22.1	37.3	46.5	51.7
R 30 h	15.0	31.0	43.1	49.4	L 30 h	25.6	37.1	46.3	51.9
R 36 h	11.9	28.7	41.2	48.3	L 36 h	20.0	35.4	45.1	50.8
R 42 h	11.2	27.0	40.1	48.0	L 42 h	17.2	33.3	43.6	49.7
R 54 h	16.6	32.3	43.4	49.5	L 54 h	20.3	35.1	44.9	50.4
R 60 h	20.2	35.9	45.1	50.5	L 60 h	25.9	38.7	47.6	51.7
R 66 h	24.6	38.3	45.8	51.0	L 66 h	22.6	36.2	44.9	50.6
R 78 h	35.2	45.6	51.6	54.2	L 78 h	31.9	43.1	50.2	53.3
R 84 h	37.8	46.2	51.7	56.0	L 84 h	36.3	45.9	51.1	54.0
R 90 h	37.1	46.5	51.9	54.8	L 90 h	38.5	46.3	51.3	54.8
R 102 h	42.6	49.4	54.1	57.1	L 102 h	38.8	46.3	51.3	55.0
Control 1	61.2	61.2	61.5	61.5	Control 2	61.0	60.8	61.1	61.2

R: Right udders; L: Left udders; Control 1: Milk from right udders of unimmunized goats; Control 2: Milk from left udders of unimmunized goats.

RESULTS

Transient expression

As shown in Table 1 and Figure 3, milk samples from experimental goats inhibited *H pylori* binding to Le^b antigen, and the time of the highest inhibition efficacy was at 42 h after DNA immunization. Furthermore, milk collected from both right (R) and left (L) udders had inhibitory effect on *H pylori* binding to Le^b. Unimmunized goat (the negative controls) did not inhibit bacterial binding. The binding activity of *H pylori* to Le^b antigen reduced mostly, 83 % in the 25-fold diluted milk samples.

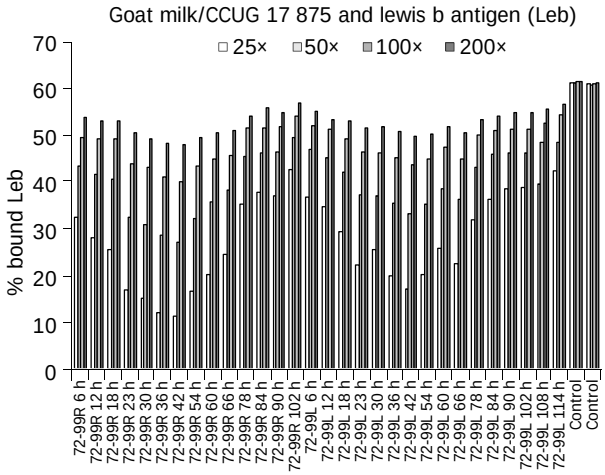

Figure 3 Blocking effect on *H pylori* binding to Lewis b antigen by goat milk. Abscissa: Goat milk collected at different time points and control milk. Ordinate: Rate of *H pylori* binding to Lewis b antigen.

Production of transgenic mice

Five of 84 mice including 2 males and 3 females were identified as being transgenic mice by PCR (Figure 4). The serial numbers of the positive mice were 15, 42, 47, 63 and 71. Efficiency of microinjection was about 6%, within the usual range of 5-20%. These transgenic mice were confirmed by using human α1-3/4-fucosyltransferase cDNA as a probe in Southern blotting (Figure 5). Transgene copy numbers were also determined by Southern blotting. We analyzed three female's milk for the blocking effect on binding of *H pylori* to Le^b antigen, but no inhibitory activity was detected by our experimental system.

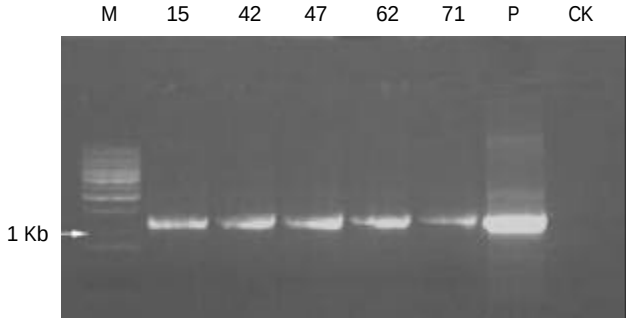

Figure 4 PCR results of transgenic mice. M: DNA ladder; P: pBC1-fut plasmid; CK: Non-transgenic mouse. 15, 42, 47, 62 and 71: Serial numbers of gene positive mice.

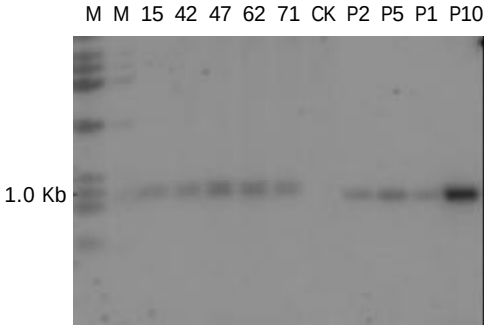

Figure 5 Southern blotting of transgenic mice. M: DNA ladder; CK: Non-transgenic mouse; P1, P2, P5 and P10: pBC1-fut plasmid equivalent to 1, 2, 5 and 10 gene copies, respectively. 15, 42, 47, 62 and 71: Serial numbers of gene positive mice.

Western blotting

We performed Western blotting and stained the membranes of the goat and transgenic mice milk protein with Le^b monoclonal antibody. The goat milk sample blot showed a beautiful, time-dependent induction of the blood group antigens secreted into milk (Figure 6). The band densities at different time points were consistent with the results of the transient expression described above. The band density was strongest at the 42 h after DNA immunization. But the transgenic mice milk did not give a positive signal, suggesting that this milk did not contain Le^b antigen or its analog.

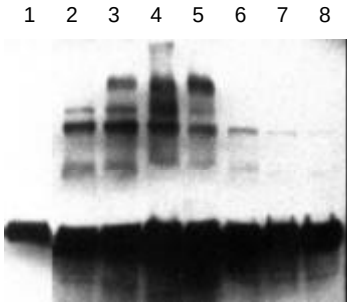

Figure 6 Western blotting of the transient expression milk of goat. Lanes 1-8: Milk collected at different time points of 6, 18, 30, 42, 60, 78, 90, 100 h postinjection, respectively.

DISCUSSION

In our experiment, goat milk could block *H pylori* binding to Le^b antigen, which is one of the most important receptors governing adhesion of *H pylori* to gastric mucosa. The activity of *H pylori* binding to Le^b antigen reduced as much as 83% in some samples. The result showed that some milk proteins might be fucosylated and structurally similar to human Le^b blood group antigen, so they were able to bind the bacteria. Goat milk fucosylated protein can bind *H pylori in vitro*. So "humanized" goat milk, in which human α1-3/4-fucosyltransferase has been introduced into goat mammary gland, may be an alternative therapy and a prevention method for *H pylori* infection.

Unfortunately, the transgenic mice milk collected did not block *H pylori* binding to Le^b antigen. The reasons might be as follows: (1) Level of α1-3/4-fucosyltransferase gene expression in mammary gland of mice was very low. Thus the quantity of Le^b antigen in the milk was so low that the milk could not effectively block *H pylori* binding to Le^b antigen. One way to increase the expression of α1-3/4-fucosyltransferase would be to introduce the complete genomic sequence of the α1-3/4-fucosyltransferase gene to mammary gland of mice. (2) There is no precursor of Le^b antigen in mice milk, so, even if α1-3/4-fucosyltransferase was expressed in mouse galactophore, the transgenic glycosylation patterns that were generated by the activity of α1-3/4-fucosyltransferase did not form epitopes that were recognized by the *H pylori* Le^b-binding adhesions. Therefore the milk could not block *H pylori* binding to Le^b antigen. Since other results have shown that α1-3/4-fucosyltransferase expression in the gastric mucosa of mice can block the binding of *H pylori* to mouse gastric mucosa, it is possible that there might be differences between the carbohydrate core chains of the Le^b antigen in milk glands and gastric mucosa in mice.

Although the results for the transgenic mice were not positive, the successful introduction of α1-3/4-fucosyltransferase cDNA into goat mammary cell and expression of Le^b antigen analog were an important finding. The "humanized" milk by the transgenic introduction of fucosylated antigens can be an alternative therapy and a prevention method for *H pylori* infection.

REFERENCES

1 **Warren JR**, Marshall B. Unidentified curved bacilli on gastric epithelium in active chronic gastritis. *Lancet* 1983; **8336**: 1273-1275

2 **Parsonnet J**, Hansen S, Rodriguez L, Gelb AB, Warnke RA, Jellum E, Orentreich N, Vogelman JH, Friedman GD. *Helicobacter pylori* infection and gastric lymphoma. *N Engl J Med* 1994; **330**: 1267-1271

3 **Hansson LE**, Nyren O, Hsing AW, Bergstrom R, Josefsson S, Chow WH, Fraumeni JF Jr, Adami HO. The risk of stomach cancer in patients with gastric or duodenal ulcer disease. *New Engl J Med* 1996; **335**: 242-249

4 **Dooley CP**, Cohen H, Fitzgibbons PL, Bauer M, Appleman MD, Perez-Perez GI, Blaser MJ. Prevalence of *Helicobacter pylori* infection and histologic gastritis in asymptomatic persons. *N Engl J Med* 1989; **321**: 1562-1566

5 **Eck M**, Schmausser B, Haas R, Greiner A, Czub S, Muller-Hermelink HK. MALT-type lymphoma of the stomach is associated with *Helicobacter pylori* strains expressing the CagA protein. *Gastroenterology* 1997; **112**: 1482-1486

6 **Wang RT**, Wang T, Chen K, Wang JY, Zhang JP, Lin SR, Zhu YM, Zhang WM, Cao YX, Zhu CW, Yu H, Cong YJ, Zheng S, Wu BQ. *H pylori* infection and gastric cancer: evidence from a retrospective cohort study and nested case-control study in China. *World J Gastroenterol* 2002; **8**: 1103-1107

7 **Eid R**, Moss SF. *Helicobacter pylori* infection and the development of gastric cancer. *N Engl J Med* 2002; **346**: 65-67

8 **Parsonnet J**, Isaacson PG. Bacterial infection and MALT lymphoma. *N Engl J Med* 2004; **350**: 213-215

9 **Forman D**, Newell DG, Fullerton F, Yarnell JW, Stacey AR, Wald N, Sitas F. Association between infection with *Helicobacter pylori* and risk of gastric cancer: evidence from a prospective investigation. *BMJ* 1991; **302**: 1302-1305

10 **Fox JG**. Helicobacter species and *in vivo* models of gastrointestinal cancer. *Aliment Pharmacol Ther* 1998; **12**(Suppl 1): 37-60

11 **Uemura N**, Okamoto S, Yamamoto S, Matsumura N, Yamaguchi S, Yamakido M, Taniyama K, Sasaki N, Schlemper RJ. *Helicobacter pylori* infection and the development of gastric cancer. *N Engl J Med* 2001; **345**: 784-789

12 **Wotherspoon AC**. *Helicobacter pylori* infection and gastric lymphoma. *Br Med Bull* 1998; **54**: 79-85

13 **Wotherspoon AC**. Gastric lymphoma of mucosa-associated lymphoid tissue and *Helicobacter pylori*. *Annu Rev Med* 1998; **49**: 289-299

14 **International Agency for Research on Cancer**. Schistosomes, liver flukes and *Helicobacter pylori*. IARC Working Group on the Evaluation of Carcinogenic Risks to Humans. Lyon, 7-14 June 1994. *IARC Monogr Eval Carcinog Risks Hum* 1994; **61**: 1-241

15 **Bayerdorffer E**, Neubauer A, Rudolph B, Thiede C, Lehn N, Eidt S, Stolte M. Regression of primary gastric lymphoma of mucosa-associated lymphoid tissue type after cure of *Helicobacter pylori* infection. MALT Lymphoma Study Group. *Lancet* 1995; **345**: 1591-1594

16 **Karlsson KA**. Animal glycosphingolipids as membrane attachment sites for bacteria. *Annu Rev Biochem* 1989; **58**: 309-350

17 **Boren T**, Falk P, Roth KA, Larson G, Normark S. Attachment of *Helicobacter pylori* to human gastric epithelium mediated by blood group antigens. *Science* 1993; **262**: 1892-1895

18 **Mahdavi J**, Sonden B, Hurtig M, Olfat FO, Forsberg L, Roche N, Angstrom J, Larsson T, Teneberg S, Karlsson KA, Altraja S, Wadstrom T, Kersulyte D, Berg DE, Dubois A, Petersson C, Magnusson KE, Norberg T, Lindh F, Lundskog BB, Arnqvist A, Hammarstrom L, Boren T. *Helicobacter pylori* SabA adhesin in persistent infection and chronic inflammation. *Science* 2002; **297**: 573-578

19 **Marshall B**. *Helicobacter pylori*: 20 years on. *Clin Med* 2002; **2**: 147-152

20 **Odenbreit S**, Faller G, Haas R. Role of the alpAB proteins and lipopolysaccharide in adhesion of *Helicobacter pylori* to human gastric tissue. *Int J Med Microbiol* 2002; **292**: 247-256

21 **Linden S**, Nordman H, Hedenbro J, Hurtig M, Boren T, Carlstedt I. Strain- and blood group-dependent binding of *Helicobacter pylori* to human gastric MUC5AC glycoforms. *Gastroenterology* 2002; **123**: 1923-1930

22 **Guruge JL**, Falk PG, Lorenz RG, Dans M, Wirth HP, Blaser MJ, Berg DE, Gordon JI. Epithelial attachment alters the outcome of *Helicobacter pylori* infection. *Proc Natl Acad Sci U S A* 1998; **95**: 3925-3930

Edited by Chen WW and Zhu LH **Proofread by** Xu FM

PO Box 2345, Beijing 100023, China
Fax: +86-10-85381893
E-mail: wjg@wjgnet.com www.wjgnet.com

World J Gastroenterol 2004;10(14):2067-2071
World Journal of Gastroenterology
 ISSN 1007-9327

• BASIC RESEARCH •

Microencapsulated hepatocytes and islets as *in vivo* bioartificial liver support system

Yue Gao, Jun Xu, Bei Sun, Hong-Chi Jiang

Yue Gao, Jun Xu, Bei Sun, Hong-Chi Jiang, Department of General Surgery, First Clinical Hospital, Harbin Medical University, Harbin 150001, Heilongjiang Province, China
Supported by the Natural Science Research Fund of Heilongjiang Province, D9746
Correspondence to: Dr. Yue Gao, Department of General Surgery, First Clinical Hospital of Harbin Medical University, 23 Youzheng Street, Nangang District, Harbin 150001, Heilongjiang Province, China. gaoyueee@163.com
Telephone: +86-451-88601563 **Fax:** +86-451-53600286
Received: 2004-01-15 **Accepted:** 2004-02-28

Abstract

AIM: To confirm the xenotransplantation of microencapsulated hepatocytes and islets as a temporary bioartificial liver support system for mice with acute liver failure (ALF).

METHODS: Mice were rendered ALF by a single intra-peritoneal injection of D-galactosamine (D-gal) and their tail blood was sampled to examine differences in blood ALT, albumin (ALB), total bilirubin (TB) and glucose (GLU) between 4 experimental groups. Rat hepatocytes and islets were collected and microencapsulated referring to both Sun's and Fritschy's methods. Mice were grouped into control group (CG), free hepatocyte group (FHG), microencapsulated hepatocyte group (MHG) and microencapsulated hepatocyte plus islet group (HIG). Tissue samples were subjected to microscopic and electron microscopic (EM) examinations.

RESULTS: The highest survival was observed in HIG, surprisingly at 100%(16/16), while the lowest was in CG at 12.5%(2/16), with inter-group statistical difference $P<0.05$. ALT levels revealed no statistical difference between groups but the ALB level of HIG descended by the slightest margin $\{q=(0.54, 0.24, 1.33), P<0.05\}$ at the time when it reached the lowest point in all groups. TB of HIG returned to normal reference range (NRR) statistically sooner than that of others after a fierce elevation. No statistical inter-group difference was observed in GLU levels. Fusion between hepatocytes and beta cells was demonstrated giving rise to theoretical assumptions.

CONCLUSION: Hepatocytes to be microencapsulated together with islets should be a preferred *in vivo* hepatic functional supporting system, which can dramatically prolong survival and improve living status.

Gao Y, Xu J, Sun B, Jiang HC. Microencapsulated hepatocytes and islets as *in vivo* bioartificial liver support system. *World J Gastroenterol* 2004; 10(14): 2067-2071
http://www.wjgnet.com/1007-9327/10/2067.asp

INTRODUCTION

Currently, temporary liver support is crucial to medical treatment for acute liver failure[1,2]. In this point, hepatocyte transplantation as a kind of bioartificial liver holds a bright prospect, but how to enhance graft functional status and neutralize immune rejection remains unsettled. Several authors have reported the "mutual benefit" between hepatocytes and pancreatic islets at co-transplantation[3-5], whereas Lim and Sun's[6] microencapsulating technique for immunoisolation opened a new era for cell transplantation. We suppose that hepatocytes and islets can be co-microencapsulated and transplanted to act as a bioartificial liver support system (BALSS), thus taking advantages of both the "mutual benefit" and the immunoisolation, simultaneously. If succeeded, this method would be a valuable alternative for *en bloc* organ transplantation and alleviate the donor shortage dilemma.

MATERIALS AND METHODS

Animals and ALF induction

Male Wistar rats weighing 150 g (as donor of hepatocytes) or 250 g (as donor of islets) and Kunming mice weighing 30-36 g served as donors and recipients, respectively. D-gal (Sigma) was dissolved in bacteriostatic normal saline and adjusted to pH 7.4 with 1 mol/L NaOH. The final concentration of the solution was 0.1 g/mL. Acute liver failure (ALF) mice was induced by a single intra-peritoneal injection of D-gal at a dose of 2 500 mg/kg without anesthesia, after which free access to aseptic water containing 100 g/L glucose was provided and models were fed on standard mouse chow.

Hepatocyte isolation

Donor hepatocytes were isolated by Seglen's *in situ* collagenase perfusion technique. Under pentobarbital anesthesia (35 mg/kg), the portal vein and the before-liver inferior *vena cava* (IVC) were cannulated and after liver IVC was ligated. The liver was perfused *in situ* first with 4 ℃ D-Hanks solution for 3 min and then with 37 ℃ Hanks solution containing 200 U/mL collagenase *IV* (Sigma) for 10 min at a flow rate of 20 mL/min until the effluent turned opaque. The perfusion route began at the portal vein and ended before liver IVC. The liver was removed, softly shattered and filtered through a hepatocyte dispersing instrument (containing a 105 μm stainless steel mesh) to produce a homogenous suspension. The hepatocytes were washed 3 times in 4 ℃ D-Hanks solution and centrifuged at 50 r/min for 2 min between washes, $(3.5\text{-}5.0)\times10^8$ hepatocytes were obtained through this process. After the cell viability (82-93%) was determined by trypan blue exclusion test, the hepatocytes were cultured in 100 g/L fetal calf serum (FCS, Hyclone) enriched RPMI-1640 medium containing 10^{-7} mol/L insulin, 0.1 mg/mL streptomycin sulfate and 100 U/mL penicillin G at 37 ℃ in a humidified atmosphere (950 mL/L O_2 and 50 mL/L) awaiting transplantation.

Islet isolation

Donor islets of Langerhans were extracted by Sutton's method. The common bile duct (CBD) was cannulated and the rat was killed by a heart incision before the whole pancreas was distended uniformly with 4 mL 4 ℃ Hanks solution (buffered by 20 mmol/L HEPES at pH 7.8). The pancreas was removed, further distended by 16 mL 4 ℃ Hanks solution containing

2 mg/mL collagenase *V* (Sigma) and then put in an incubator at 38 ℃ for 8 min before the tissue was dispersed. The pelleted tissue was filtered through a steel mesh with 40 pores per inch and washed twice in 4 ℃ Hanks solution with centrifugation at 50 r/min for 1 min between washes. The last centrifugation was performed at 350 r/min for 2 min before the tissue was re-suspended in 25% Ficoll solution, on which 23%, 20% and 11% Ficoll densities were layered in sequence. The discontinuous density gradient containing the tissue pellets was spun at 800 r/min for 15 min at 4 ℃. Islets from 20-23% interface were collected, 721±153 islets could be isolated through this procedure with a purity higher than 87% and the ones with a diameter of 50-250 μm were handpicked and cultured in 100 g/L FCS enriched RPMI 1640 medium containing 0.1 mg/mL streptomycin sulfate and 100 U/mL penicillin G at 37 ℃ in a humidified atmosphere (950 g/L O_2 and 50 mL/L CO_2).

Microencapsulating procedure

Cells were microencapsulated according to Sun's and Fritschy's methods. The cells were centrifuged before re-suspension in 30 g/L alginate (ALG)-normal saline solution (pH 7.4) at a concentration of 1×10^7/mL (according to hepatocytes). Then the mixture was put into the container of a bi-nozzle air-jet droplet generator and sprayed into 100 mmol/L calcium chloride solution (HEPES buffered, pH 7.4) under the disturbance of a co-axial oxygen flow at 4 L/min to form round droplets, which were then washed in 4 ℃ D-Hanks solution and reacted in sequence with 2 g/L poly-L-lysine (PLL) for 8 min, 2 g/L ALG for 4 min and 30 mmol/L sodium citrate for 8 min, all were kept at 4 ℃ and adjusted to pH 7.4. The microcapsules (MCs) with a diameter of 0.3-0.5 mm were cultured in aforementioned medium for 24 h. Every mouse received MCs equal to 3×10^6 hepatocytes and the ratio of hepatocytes to islets was 10^6/40 at co-transplantation[7]. Through a 12 G needle, the MCs were injected into the recipient's abdomen through a 3 mm incision under light ether anesthesia. All mice underwent the same procedure.

Experimental design

Sixty-four mice with ALF were randomly divided into 4 groups, 16 mice in each: CG, FHG, MHG and HIG. Each mouse in a certain group received only 1 mL sterilized normal saline in CG, 3×10^6 free hepatocytes transplantation in FHG, 3×10^6 microencapsulated hepatocytes in MHG, MCs containing 3×10^6 hepatocytes together with 120 islets in HIG.

Each group was randomly divided into 4 subgroups, 4 mice in each: ALT group, ALB group, TB group and GLU group so that every index was observed in 4 mice and documented by their average. Blood samples were collected from tail veins and indexes were recorded before and every 12 h after administration of D-gal (time "0") until the 4th d, then once on the 7th d and finally once on the 14th d. The body mass was measured daily.

Histological studies

All animals that died after D-gal injection were autopsied and those alive were sacrificed weekly until the 2nd mo. Then all the remaining ones were cervically dislocated to collect samples from livers, MC aggregates and floating MCs, which were fixed either in 100 g/L phosphate-buffered formaldehyde and stained with hematoxylin/eosin for histological examination or in 2.5% osmium tetroxide for transmission EM examination.

Statistical analysis

One-way *ANOVA*, *q* test and χ^2 test were used to establish inter-group difference and data were expressed as mean±SD.

RESULTS

Survival

Mice still alive after 72 h secured unlimited survival. Compared with CG, the survival rates of FHG, MHG and HIG were statistically higher ($P<0.05$), while FHG held a survival rate significantly lower than MHG and HIG ($P<0.05$), between which no statistical difference was observed ($P>0.05$) (Figure 1A).

Biochemical findings

ALT in 4 groups similarly elevated to a peak of 1 912±344 U/L in 12 h, then dropped quickly to NRR (50.04±7.72 U/L) in 48 to 72 h. The sub-group of ALT in CG had only one mouse (1/4)

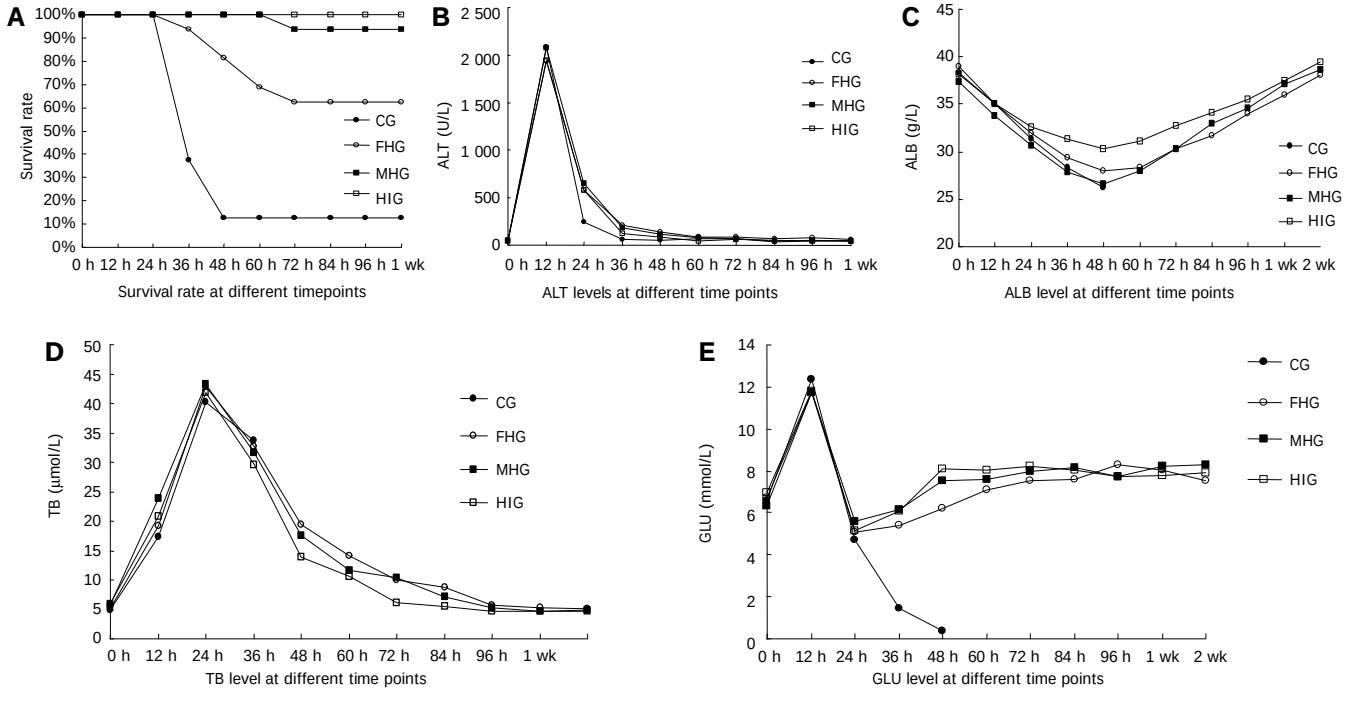

Figure 1 Survival rate, levels of ALT, ALB, TB and GLU at different time points. A: Survival rate; B: ALT level; C: ALB level; D: TB level; E: GLU level.

alive after 36 h. No relevant statistical difference was observed (Figure 1B).

Serum ALB gradually decreased after D-gal administration and reached the lowest point in 48 h, then stably returned to NRR of 38.19±1.68 g/L in 96 h (Figure 1C). The maximum decrease in ALB of HIG was 7.85±1.10 g/L, statistically smaller than that of other groups (P<0.05). No statistical difference was found in ALB reduction between CG, FHG and MHG (P>0.05).

TB in all groups ascended quickly after D-gal administration to the maximum of 36.64±5.08 μmol/L (P>0.05) in 24 h, then began to descend. All the 4 mice in TB sub-group of CG died in 36 h bringing its curve to a stop, while TB of other groups continued to descend to NRR (5.42±0.68 μmol/L) at different intervals. TB of HIG fell into NRR in 72 h, while FHG and MHG in 96 h (Figure 1D).

The non-fasting blood glucose of ALF mice temporarily elevated by 5.27±1.56 mmol/L in 12 h after D-gal administration, then fell down to 5.14±0.48 mmol/L at the 24th hour, when the mice underwent scheduled treatments. After 24 h, when the GLU of other groups began to increase, that of CG kept decreasing until all the four responsible mice died. The GLU of HIG ascended to NRR (8.31±0.93 mmol/L) in 48 to 60 h, while that of FHG and MHG normalized after 72 h (Figure 1E). No statistical inter-group difference was observed at any time point (P>0.05).

Liver destruction

Massive degenerative changes, ballooning and necrosis of the hepatic cells with vanishing nuclei were apparent under optical microscopy accompanied with closing sinusoids, widened Disse space and distorted hepatic lobules in tissue samples from mice died after administration of D-gal. Numerous bulbs, slightly distended mitochondria, shrinkage of nuclei and pigmentation of heterochromatin came under EM with cholangitis, exfoliation of microvilli and disappearance of tight conjunctions between adjacent hepatocytes dominating the view, as reported by Takenaka[8] (Figure 2).

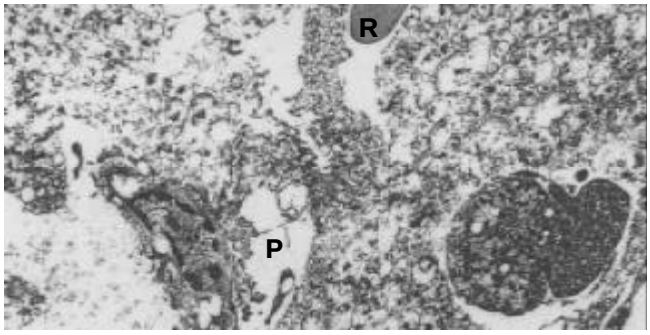

Figure 2 Transmigration of platelets (P) and red cells (R) into the Disse space.

Gross or microscopic microcapsules

Up to 90% of microcapsules remained free floating in 1 to 2 wk posttransplantation. Histological examination revealed smooth surface of most MCs, but mild fibroblasts were also observed on some MCs. Few hepatocytes were still alive inside the MCs from MHG, which were still free floating in the 4th week. Fewer free-floating MCs were observed in the HIG, blood vessels originated from the portal vein or the liver surface were easily seen with naked eyes polarizing huge aggregates of MCs attached to them. Till the 8th week, red aggregates of MCs were easily found in the vicinity of the portal vein in 67.5% (7/8) mice from HIG group. Though not abundant, aggregates attached to the diaphragmatic side of the liver, spleen or other organs were also seen. Smaller aggregates of MCs were seen on samples from MHG but without visible vascularization.

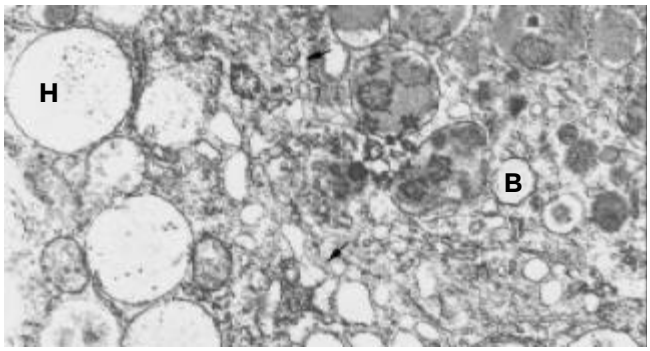

Figure 4 Connection of hepatocytes (H) and beta cells (B) by a network of plasmatic "bridges" formed by adjacent membranes of a string of vesicles (→) lining up along their original border.

EM findings

Generally, the wall of the MCs was 6-8 μm thick and could be divided into 3 layers, but hepatocytes were always embedded in it de-homogenizing the thickness and disarranging the layers. Mostly, a very thin feather-like structure with a medium density formed the outer layer, inside was a section with a very high density and a thickness of approximately 0.5 μm, then a flocculent low density structure formed the inner layer. There was no clear boundary between the later two layers, instead, the density of the middle layer lowered until it changed into the inner one, to which the encapsulated hepatocytes attached with their microvilli. A small number of hepatocytes of MHG group survived inside the MCs until the 8th week but their microvilli shortened or disappeared and mitochondria distended. The MCs from HIG attached to the liver surface were totally covered by fibroblasts in the 8th week, but capillaries originated from the liver were seen encircling the MCs or entering them. Inside these MCs, living beta cells were found surrounded by transformed hepatocytes, whose many microvilli thrust deeply into the former and the membranes of

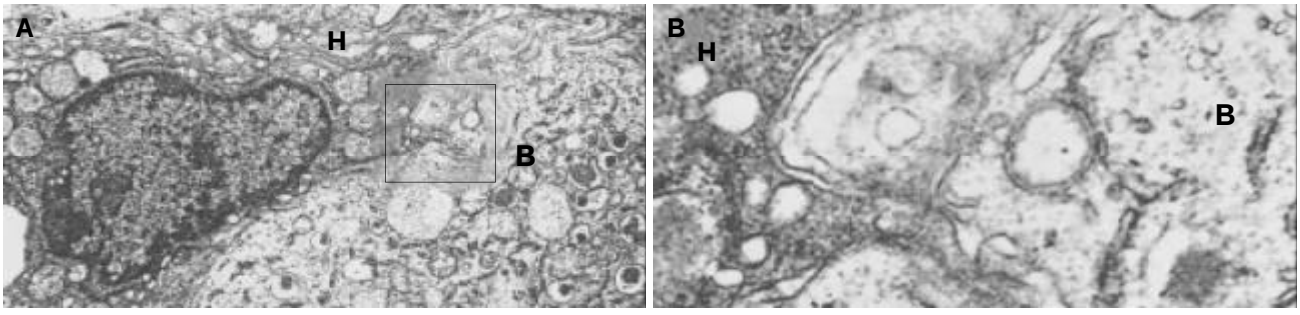

Figure 3 Association between hepatocytes (H) and a beta cells (B), and microvilli of hepatocytes (H) in beta cells (B). A: "Intimate association" between hepatocytes (H) and beta cells (B); B: Microvilli of hepatocytes (H) in beta cells (B).

both cells morphologically vanished at some places where two plasmas mixed (Figures 3A, 3B). Some hepatocyte-like cells recognized by their big round mitochondria and glycogen had well formed insulin granules inside their plasma but with a smaller size (Figure 4). No desmosome mentioned by Ricordi was found. Several ball-shaped hepatocytes with long microvilli and normal organella were seen attached to the MC wall in distance of the aggregates of hepatocytes and beta cells.

DISCUSSION

Life sustaining is of the greatest importance to patients with ALF during life threatening period and patients with end stage chronic liver failure (CLF) awaiting proper donors, so liver function support in a limited period is crucial to the management of both ALF and CLF.

Based on this principle, many kinds of artificial liver were developed such as charcoal hemoperfusion or high porosity hemodialysis, but optimistically speaking, these methods could only partially substitute for the original liver because besides functioning living hepatocytes, any man-made device could provide but an incomplete liver function support[9].

Artificial liver based on living hepatocytes has become a hot point of current researches aimed at substitution for liver function by hepatocytes. There are two kinds of BALSS currently in research: *ex vivo* bio-hemodialysis system and *in vivo* hepatocyte transplantation strategy. In recent years, great progress has been made in the *ex vivo* systems. Chen *et al*.[10] demonstrated the successful application of BALSS to canine liver failure and Ding *et al*. reported their initial success on human patients. But, unfortunately, the viability of hepatocytes was hard to sustain extracorporeally and they gradually lost their original functions and de-differentiated in 1 to 2 wk *in vitro*[11], so that frequent refreshing of the working hepatocytes is necessary to secure satisfactory efficiency, which adds extra-cost to the BALSS besides its already expensive electromechanical system. As for hepatocyte transplantation strategy, rejection aggressively reduced hepatocytic viability to almost zero in 1 wk[12] after allo-transplantation. Great attention has been paid to the mechanism of hepatocytic rejection and a recent study showed that recombinant ribonuclease P remarkably reduced the expression of MHC-II molecules on transplanted hepatocytes, thus obviously alleviating rejection and prolonging hepatocytic survival. But before the entire truth of human genome is unveiled, no induction of gene or genetic products into human body would be ethically accepted and clinically approved. Genetic interference with transplantation may be preserved for far future. The microencapsulating technique initiated by Lim and Sun brought a bright new hope for artificial liver and hepatocyte transplantation. The microcapsules act as a selective barrier between the hepatocytes inside and the killing molecules such as antibodies outside, reserving the permeability of nutrients and small active cellular products such as albumin and insulin, so that cell transplantation under immunoisolation is realized. In addition, it has been proved that through some uncertain pathways islets could enhance the viability and function of isolated hepatocytes[13,14]. We deem that microencapsulated hepatocytes and islets can be xenotransplanted to act as an *in vivo* BALSS, thus taking advantages of both the "mutual benefit" and the immunoisolation simultaneously. If succeeded, this method would be a valuable alternative for *en bloc* organ transplantation and alleviate the donor shortage dilemma.

In this work, we initially studied the feasibility of xeno-transplantation of co-microencapsulated hepatocytes and islets between closely related species (Wistar rats to Kunming mice) and its therapeutic effects on D-gal induced ALF. Drug-induced ALF could better imitate clinical ALF, mostly toxic, than surgically induced ALF, since it presented with similar pathological development[15].

ALT is a sensitive index to hepatocytic destruction, which sharply ascended after administration of D-gal and peaked at the 12th hour but the amplitude greatly varied between individual mice. No significant influence upon ALT curve by cell transplant was observed in this study indicating that ALT could reflect the extent of cell destruction instead of the therapeutic effect of different interventions, as confirmed by Yu' s studies[16]. Anti-apoptotic agent etoposide was given prior to the administration of D-gal in Nakama' s study[17], which would possibly have changed the metabolism of D-gal in hepatocytes and the pathological process of hepatocytic destruction, preventing a considerable proportion of hepatocytes from apoptosis, so that a lowered ALT peak was documented. In fact, to give hepatocytic protective agents prior to the establishment of ALF model could only demonstrate the protecting effects of such agents instead of their therapeutic attributes, which has attracted much more attention from medical community since ALF patients would not take liver protective medications before they got trapped in ALF.

ALB is not a frequently used index to hepatic failure, but it changes with a steady pace giving concrete confirmation to the status of hepatic anabolism. In this study, ALB levels in HIG group decreased by a margin significantly smaller than those in other groups after administration of D-gal, indicating that under the influence of xenografted islets, at least the production of ALB of the remaining liver cells of the model mouse or the transplanted hepatocytes was improved. Wang *et al*.[18] also confirmed the enhanced ALB synthesis in hepatocirrhotic rats after combined hepatocyte-islet transplantation.

TB level reflects the metabolic and detoxicating abilities of hepatocytes. It descended into NRR much earlier in HIG than in other groups, demonstrating a sooner recovery of hepatocellular metabolism in the existence of islets as stated by Wang *et al*.[19].

Temporary increase of blood glucose after D-gal administration, was rarely reported because most researchers took rats as subjects and kept an interval between blood samplings as long as 24 h or more, missing this phenomenon. It might have resulted from the release of a great amount of glycogens at massive hepatocytic destruction, which was absent in studies adopting 90% partially hepatectomized models as in Demetriou' s[20]. Though curves in Figure 1E show a sooner extrication from hypoglycemia in HIG group than in MHG group, no statistical difference in GLU was noticed between experimental groups, which might have been the result of inadequate samples or large scale fluctuation of non-fasting blood glucose of ALF mice.

All mice in HIG group survived and the survival rate in MHG group was 93.75%, astonishingly higher than that in other reports, which used rat models. The first reason for such a high survival might be a larger amount of hepatocytes transplanted, say, 3×10^6 hepatocytes were nearly 3-5% of total hepatocytes per mouse liver and the second reason might be a much shorter hepatocytic regeneration cycle in mouse, which resulted in a quicker recovery of liver function and a shorter life threatening period. In this point of view, it may be conjectured that the shorter the hepatocytic regeneration cycle is, the better the therapeutic effect of bio-artificial liver can be expected, thus to shorten the regeneration cycle of liver cells by means of some genetic method may further enhance the survival rate after ALF.

A close functional relation between hepatocytes and islets has been proved both experimentally and clinically. An "intimate association" between hepatocytes and beta cells was discovered by Ricordi[21] and then confirmed by others[22]. In this study, an even closer relationship was proved morphologically inside the microcapsules 2 mo after hepatocyte-islet co-transplantation.

Under EM, 1the hepatocytes were easily recognized with their wheel-shaped mitochondria, smooth reticulum, rose-petal-

shaped glycogens and Golgi complexes while beta cells with their homogeneous eyeball-like insulin granules, which accommodated high-density crystalloids at the center with a wide vacuum space around. The hepatocytes abandoned their original hexagon or cubic shape and flattened to wrap on the beta cells thrusting numerous finger-like microvilli deeply into the latter. No matter how complicatedly the microvilli wound in three-dimensional space on a cross-section, we should see two layers of complete membrane separating these "fingers" from the plasma of the victim beta cells, but discontinuous membranes were noticed where direct exchange of cellular content was suspected. Much more interestingly, the boundary between some hepatocytes and beta cells was replaced by a complicated network of plasmatic "bridges" formed by adjacent membranes of a string of vesicles lining up along the original border. Meanwhile morphologically intact beta granules were found inside such hepatocytes in direct contact with their plasma, seemingly having been swallowed. Generally, this was a kind of "hybridization" between these two kinds of cells, as mentioned by Cossel[23]. No desmosomes were found connecting these cells as mentioned by Ricordi. They might have functioned as anchors in the earlier stage (in 7 d as said by Ricordi) to immobilize cells giving rise to further interactions, then disappeared together with part of the membrane initiating hybridization in the later stage as found in our study. Direct plasmatic connection must be the best way for intercellular communication and exchange of substances, so contacting cells, which have close functional ties like hepatocytes and beta cells, would eventually establish such connections though neither the underlying mechanism nor its prognosis is clear. On the other hand, this phenomenon urges us to take good care of transplanted cells since it is still unknown whether such a "hybridization" produces pathogenic outcomes, say malignancies, or whether it undermines long-term effects of transplanted cells, though the outcome of such an association was fairly acceptable in our study. So that to separate transplanted cells by way of micro- or macro-encapsulation may be a good choice, which deprives them of direct contact with host cells and at the same time realizes functional support under immunoisolation.

In this study, we observed the hybridization between hepatocytes and beta cells inside microcapsules after co-transplantation. Better therapeutic effect of hepatocyte-islet co-transplantation than hepatocytes alone was also evidenced both histologically and biochemically. Though operative principles have not been fully established, co-transplantation of hepatocytes and islets by way of microencapsulation as a kind of BALSS holds a bright prospect.

ACKNOWLEDGEMENT

We are gratefulness to Wei Liu, Center of Scientific Research, 2nd Hospital of Harbin Medical University for sharing her expertise in cell bioengineering and to Wen-Jie Dai, National Center of Experimental Cell Transplantation for his administrative help during this project.

REFERENCES

1 **Fritschy WM,** Wolters GH, Van Schilfgaarde R. Effect of alginate-polylysine-alginate microencapsulation on *in vitro* insulin release from rat pancreatic islets. *Diabetes* 1991; **40**: 37-43
2 **Strain AJ,** Neuberger JM. A bioartificial liver–state of the art. *Science* 2002; **295**: 1005-1009
3 **Ricordi C,** Callery MP, Lacy PE, Flye MW. Pancreatic islets enhance hepatocellular survival in combined hepatocyte-islet-cell transplantation. *Transplant Proc* 1989; **21**(1 Pt 3): 2689-2690
4 **Genin B,** Andereggen E, Rubbia-Brandt L, Birraux J, Morel P, Le Coultre C. Improvement of the effect of hepatocyte isograft in the Gunn rat by cotransplantation of islets of Langerhans. *J Pediatr Surg* 1999; **34**: 321-324
5 **Kaufmann PM,** Sano K, Uyama S, Breuer CK, Organ GM, Schloo BL, Kluth D, Vacanti JP. Evaluation of methods of hepatotrophic stimulation in rat heterotopic hepatocyte transplantation using polymers. *J Pediatr Surg* 1999; **34**: 1118-1123
6 **Lim F,** Sun AM. Microencapsulated islets as bioartificial endocrine pancreas. *Science* 1980; **210**: 908-910
7 **Kaufmann PM,** Kneser U, Fiegel HC, Pollok JM, Kluth D, Izbicki JR, Herbst H, Rogiers X. Is there an optimal concentration of cotransplanted islets of langerhans for stimulation of hepatocytes in three dimensional matrices? *Transplantation* 1999; **68**: 272-279
8 **Takenaka K,** Sakaida I, Yasunaga M, Okita K. Ultrastructural study of development of hepatic necrosis induced by TNF-α and D-galactosamine. *Dig Dis Sci* 1998; **43**: 887-892
9 **Dixit V,** Darvasi R, Arthur M, Brezina M, Lewin K, Gitnick G. Restoration of liver function in Gunn rats without immunosuppression using transplanted microencapsulated hepatocytes. *Hepatology* 1990; **12**: 1342-1349
10 **Chen XP,** Xue YL, Li XJ, Zhang ZY, Li YL, Huang ZQ. Experimental research on TECA-I bioartificial liver support system to treat canines with acute liver failure. *World J Gastroenterol* 2001; **7**: 706-709
11 **Cai ZH,** Shi ZQ, Sherman M, Sun AM. Development and evaluation of a system of microencapsulation of primary rat hepatocytes. *Hepatology* 1989; **10**: 855-860
12 **Zhang YD,** Xu YM, Peng J. Viability and histological changes of encapsulated rat hepatocyte after transplantation. *Zhonghua Qiguan Yizhi Zazhi* 2001; **22**: 161-163
13 **Kaufmann PM,** Sano K, Uyama S, Schloo B, Vacanti JP. Heterotopic hepatocyte transplantation using three-dimensional polymers: evaluation of the stimulatory effects by portacaval shunt or islet cell cotransplantation. *Transplant Proc* 1994; **26**: 3343-3345
14 **Kaufmann PM,** Fiegel HC, Kneser U, Pollok JM, Kluth D, Rogiers X. Influence of pancreatic islets on growth and differentiation of hepatocytes in co-culture. *Tissue Eng* 1999; **5**: 583-596
15 **Papalois A,** Arkadopoulos N, Papalois B, Pataryas T, Papadimitriou J, Golematis B. Comparison of two experimental models for combined hepatocyte-islet transplantation. *Transplant Proc* 1994; **26**: 3473
16 **Yu CH,** Leng XS, Peng JR, Wei YH, Du RL. Morphology, structure and function of microencapsulated hepatocytes after intraperitoneal transplantation and its liver function support in acute hepatic failure rats. *Zhonghua Shiyan Waike Zazhi* 1998; **15**: 441-443
17 **Nakama T,** Hirono S, Moriuchi A, Hasuike S, Nagata K, Hori T, Ido A, Hayashi K, Tsubouchi H. Etoposide prevents apoptosis in mouse liver with D-galactosamine/lipopolysaccharide-induced fulminant hepatic failure resulting in reduction of lethality. *Hepatology* 2001; **33**: 1441-1450
18 **Wang Y,** Xue J, Zhang Z, Zhou Y. The influence of intrahepatic transplantation of hepatocytes and insular cells on liver cirrhosis. *Zhonghua Waike Zazhi* 1998; **36**: 179-181
19 **Wang XD,** Ar'Rajab A, Ahren B, Andersson R, Bengmark S. Improvement of the effects of intrasplenic transplantation of hepatocytes after 90% hepatectomy in the rat by cotransplantation with pancreatic islets. *Transplantation* 1991; **52**: 462-466
20 **Demetriou AA,** Reisner A, Sanchez J, Levenson SM, Moscioni AD, Chowdhury JR. Transplantation of microcarrier-attached hepatocytes into 90% partially hepatectomized rats. *Hepatology* 1988; **8**: 1006-1009
21 **Ricordi C,** Lacy PE, Callery MP, Park PW, Flye MW. Trophic factors from pancreatic islets in combined hepatocyte-islet allografts enhance hepatocellular survival. *Surgery* 1989; **105**(2 Pt 1): 218-223
22 **De Paepe ME**, Keymeulen B, Pipeleers D, Kloppel G. Proliferation and hypertrophy of liver cells surrounding islet grafts in diabetic recipient rats. *Hepatology* 1995; **21**: 1144-1153
23 **Cossel L**, Wohlrab F, Blech W, Hahn HJ. Morphological findings in the liver of diabetic rats after intraportal transplantation of neonatal isologous pancreatic islets. *Virchows Arch B Cell Pathol Incl Mol Pathol* 1990; **59**: 65-77

Edited by Wang XL **Proofread by** Chen WW and Xu FM

PO Box 2345, Beijing 100023, China
Fax: +86-10-85381893
E-mail: wjg@wjgnet.com www.wjgnet.com

World J Gastroenterol 2004;10(14):2072-2077
World Journal of Gastroenterology
 ISSN 1007-9327

• BASIC RESEARCH •

Contribution of C3d-P28 repeats to enhancement of immune responses against HBV-preS2/S induced by gene immunization

Li-Xin Wang, Wei Xu, Qing-Dong Guan, Yi-Wei Chu, Ying Wang, Si-Dong Xiong

Li-Xin Wang, Wei Xu, Qing-Dong Guan, Yi-Wei Chu, Ying Wang, Si-Dong Xiong, Department of Immunology, Shanghai Medical College of Fudan University, 138 Yi Xue Yuan Road, Shanghai 200032, China
Li-Xin Wang, Department of Microbiology and Immunology, School of Basic Medical Science of Southeast University, 87 Ding Jia Qiao Road, Nanjing 210009, Jiangsu Province, China
Supported by the Major State Basic Research Development Program of China, No. 2001CB510006; National Science Found for Distinguished Young Scholars from NSFC, No. 39925031 and Key Research Program of STCSM, No. 03DZ19229
Correspondence to: Dr. Si-Dong Xiong, Department of Immunology, Shanghai Medical College of Fudan University, 138 Yi Xue Yuan Road, Shanghai 200032, China. sdxiong@shmu.edu.cn
Telephone: +86-21-54237749 **Fax:** +86-21-54237749
Received: 2003-12-10 **Accepted:** 2004-02-01

Abstract

AIM: To investigate whether P28 derived from C3d can enhance the immune response to HBV-preS2/S induced by directly injection of naked plasmids containing variable repeats of P28 and HBV-preS2/S in fusion form.

METHODS: One to four copies of C3d-P28 coding gene, amplified by PCR and modified by restriction endonucleases digestion, were subcloned into a eukaryotic expression vector pVAON33 to construct pVAON33-P28, pVAON33-P28.2, pVAON33-P28.3 and pVAON33-P28.4 (pVAON33-P28.[1-4]). HBV-preS2/S coding sequence was then introduced into the pVAON33-P28.[1-4] and identified by both PCR and DNA sequencing. BALB/c mice were primed by intramuscular gene immunization with 100 μg different recombinant plasmids on day 0 and were boosted by subcutaneous inoculation with HBsAg protein (1 μg) 12 wk post-priming. The levels and avidity of specific IgG in sera collected at the indicated times from each group were determined by ELISA and NaSCN-displacement ELISA, respectively.

RESULTS: HBsAg specific antibody response was elicited in groups primed with plasmids pVAON33-S2/S-P28.[1-4] and pVAON33-S2/S. However, the response against HBsAg in the groups primed with pVAON33-S2/S-P28.[1-4] was significantly higher than that in pVAON33-S2/S group, the highest level of the specific antibody response was observed in the groups primed with pVAON33-S2/S-P28.4 ($P<0.01$). After secondary immunization with specific antigen, the acceleration of antibody levels was significantly higher and faster in the mice primed with DNA expressing preS2/S-P28 fusions than that with DNA expressing preS2/S only ($P<0.05$). Interestingly, mice primed with DNA expressing preS2/S-P28.4 fusions maintained the highest levels of anti-HBs antibodies in all animals. The avidity assay showed that the avidity index (AI) collected at 18 wk from mice primed with pVAON33-S2/S-P28.3 and pVAON33-S2/S-P28.4 were significantly higher than that from preS2/S-DNA vaccinated mice ($P<0.01$).

CONCLUSION: Different repeats of C3d-P28 can enhance both humoral immune response and avidity maturation of specific antibodies induced by gene immunization, in which four copies of C3d-P28 may be necessary to achieve the most modest antibody response.

Wang LX, Xu W, Guan QD, Chu YW, Wang Y, Xiong SD. Contribution of C3d-P28 repeats to enhancement of immune responses against HBV-preS2/S induced by gene immunization. *World J Gastroenterol* 2004; 10(14): 2072-2077
http://www.wjgnet.com/1007-9327/10/2072.asp

INTRODUCTION

The third complement protein (C3) plays a major role in the complement activation pathway, the critical role of the cleavage fragments of C3 in the humoral immune response for both T-dependent and T-independent antigens was reported in studies performed over a quarter of a century ago[1,2]. Complement' s potential use as an adjuvant in vaccines was first suggested when Dempsey *et al*.[2] demonstrated that mice, vaccinated with a genetically engineered construct containing three copies of mouse C3d fused to a model antigen, hen egg lysozyme, increased the efficiency of immunizations by more than 1 000-fold. Subsequent studies by Test *et al*.[3] showed that covalent conjugates of C3d and the capsular polysaccharide of serotype 14 s*treptococcus pneumoniae* (PPS14) elicited higher titers to PPS14 in mice than PPS14 only, and furthermore induced a class switch in anti-PPS14 from predominantly IgM to IgG1, which extended the adjuvant effects of C3d to T-independent antigen as well as T-dependent antigen. Recently, studies have further shown that gene immunization with C3d is an effective molecular adjuvant for inducing antibody responses to a range of viral pathogens, including influenza virus[4,5], human immunodeficiency virus[6], and measles virus[7]. The mechanism, by which C3d increases antibody responses, has been hypothesized to reflect the binding of C3d to cluster of differentiation 21 (CD21) on the surface of B-cells or follicular dendritic cells (FDC)[4,5,8,9].

The complement receptor 2 (CR2)-binding site on C3d was located, using chemical fragmentation and peptide mapping studies, between residues 1 199 and 1 210 of the complement C3 sequence (mature C3 numbering)[10]. A synthetic peptide corresponding to the CR2-binding site on C3d, P28 ($C3^{K1,187\text{-}A1,214}$: ^{1187}KFLTTAKDKNRWEDPGKQLYNVEATSYA^{1214}), as well as other C3d homologous, specifically binds to CR2 expressed on B cell lines, such as Raji cells[10,11]. Binding of P28 stimulates the proliferation of peripheral resting B lymphocytes or CR2-positive B cell lines[11-13]. In addition, the binding of CR2 to P28 peptides and the proliferative response of B cells by these peptides were dose dependent and could be inhibited by soluble C3d or anti-CR2 mAb[12,14]. Furthermore, when a P16 peptide (equivalent to residues 1 195-1 210 of C3) was coupled to anti-idiotype antibody, it induced a strong idiotype and antigen-specific response in mice[15].

In present study, we selected this active C3d-P28 peptide as a molecular adjuvant according to its binding-ability to CR2

on the B-cells or FDC[10-13,15], and HBV-preS2/S as a model antigen, to seek an enhanced anti-preS2/S antibody response following vaccination with DNA expressing fusions of HBV-preS2/S to variable copies of C3d-P28. Our results showed that immunizations with the preS2/S-P28 fusions DNA not only induced higher primary humoral responses as well as a faster and stronger memory reaction, but also accelerated the avidity maturation of anti-HBs compared with that resulting from immunization with preS2/S only. Our findings argue that four or more repeats of C3d-P28 may be necessary for efficient enhancement of antigen-specific immune responses.

MATERIALS AND METHODS

Plasmid

A eukaryotic expression vector pVAON33 was reconstructed from pVAX1, a kind gift from professor Zhongming Li (Food and Drug Administration, Bethesda, MD, USA). It contained the cytomegalovirus immediate-early (CMV-IE) promoter for initiating transcription of eukaryotic inserts and the bovine growth hormone polyadenylation signal [BGH poly(A)] for termination of transcription. It also contained pMB1 origin of replication for prokaryotic replication as well as the kanamycin resistance gene (*Kan*^{r}) for selection in antibiotic media. Moreover, a synthetic oligonucleotide (ON33) containing the Kozak' s translation initiation sequence was inserted into pVAX1 for the convenience of cloning four tandem repeats of the C3d-P28 in-frame with the gene encoding HBV-preS2/S (Figure 1). Plasmid pTG825 (tPA-C3d$_3$) containing the encoding gene of C3d was a gift from Dr. Ted M. Ross (University of Pittsburgh, Pittsburgh, PA, USA). Plasmid pcDNA-preS2/S containing the encoding gene of HBV-preS2/S was constructed and conserved by our laboratory. pGEM-T vector was purchased from Huashun Biotechnology (Shanghai, China).

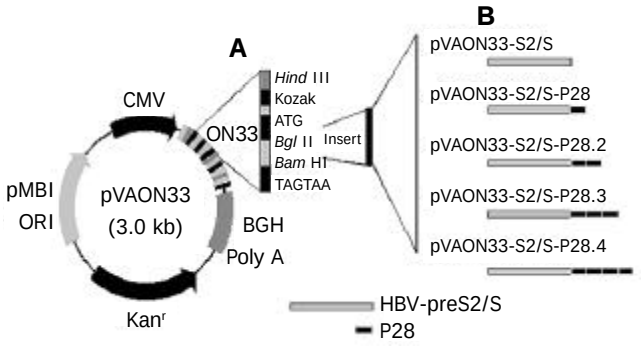

Figure 1 Schematic illustration representation of vector DNA vaccine constructs. A: A synthetic oligonucleotide (ON33) was inserted into the pVAX1 vector by the *Hind*III and *Bam*HI restriction endonuclease sites. Inserts were cloned into the vector using the *Bgl*II and *Bam*HI sites. B: The scheme represents constructs expressing fusions of HBV-preS2 / S to variable copies of C3d-P28.

Cell lines

Human hepatocellular carcinoma cell lines SMMC-7721 was obtained from the Department of Biochemistry and Moleculr Biology, Shanghai Medical College, Fudan University (Shanghai, China). SMMC-7721 cells were grown in RPMI 1640 medium (Gibco BRL) supplemented with 100 mL/L calf bovine serum (CBS), 100×10^3 U/L penicillin and 100×10^3 U/L streptomycin sulfate. *Eschrichia coli* strain, DH5 α. was kept in our laboratory and maintained in LB medium.

Animals

Female BALB/c mice (H_2d, 6 to 8-week-old) were purchased from the Center of Experimental Animal, Fudan University (Shanghai, China). They were randomly divided into 6 groups (6 mice per group) and fed with a standard laboratory diet under a specific pathogen-free (SPF) condition.

Main reagents

AMV reverse trancriptase, dNTP, Taq polymerase and PCR production-purified kits were purchased from Shanghai Biostar Co.. *Hind*III, *Bam*HI and *Bgl*II restriction endonuclease, T4 DNA ligase, DNA marker 2000 and RNase-free DNase I were purchased from MBI Co. (Ukraine). Horseradish peroxidase-labeled goat anti-mouse IgG were purchased from Southern Biotech (USA). Lipofectamine was purchased from the Invitrogen Co. (USA). The anion-exchange resin columns were purchased from Qiagen (Germany). The synthetic oligonucleotide (ON) and the PCR primers used were as follows: ON33, 5' -AGCTT GCCAC CATGA GATCT GGATC CTAGT AAG-3' (sense) and 5' -GATCT TACTA GGATC CAGAT CTCAT GGTGG CA-3' (antisense), which was used for reconstruction of the pVAX1 palsmid; C3d-P28, 5' -GAAGA TCTAA GTTTC TGAAC ACAGC-3' (sense) and 5' -CGGGA TCCGG CCTAG GATGT G-3' (antisense), which permitted the amplification of a 84-bp cDNA of C3d-P28; HBV-preS2/S, 5' -GGAAG ATCTC AGTGG AATTC CACAA C-3' (sense, bases 3 082 to 3 100) and 5' -GGAAG ATCTA ATGTA TACCC AAAGA CAA-3' (antisense, bases 706 to 688), which permitted the amplification of the entire coding region of HBV-preS2/s cDNA; T7 primers, 5' -CGATG AAGAT CTCT-3' (sense) and 5' -CGATG AAGAT CTCT-3' (antisense), which were used for identification of recombinant plasmids by PCR; GAPDH primers, 5' -CTGCA CCACC AACTG CTTAG-3' (sense) and 5' -CCACT GACAC GTTGG CAGTG-3' (antisense), which permitted the amplification of a 275-bp band corresponding to human GAPDH transcripts as described previously.

Construction of plasmid

The HBV-preS2/S gene was amplified by PCR from plasmid pcDNA-preS2/S. The gene encoding C3d-P28 amplified from plasmid pTG825 by PCR was cloned into the cloning vector-pGEM-T. Each gene was inserted into pVAON33 genetic immunization vector using standard molecular biological technology (Figure 1). Briefly, a 858 bp PCR-amplified preS2/S fragment was digested with *Bgl*II and ligated into the *Bgl*II restriction enzyme sites in the pVAON33. The vector expressing preS2/S-P28-fusion proteins was constructed by cloning four tandem repeats of the P28-encoding gene in-frame with preS2/S fragment and was designed based upon Dempsey *et al*[2]. Potential proteolytic cleavage sites between the junctions of HBV-preS2/S and P28 and the junction of P28 were mutated by ligating *Bam*HI and *Bgl*II restriction endonuclease sites to replace an arginine codon with a glycine codon. All recombinant plasmids amplified in *Eschrichia coli*, DH5α, were verified by PCR, restricted endonucleases digestion and DNA sequencing, and then were purified using anion-exchange resin columns. Purity of DNA preparations was determined by optical density reading at 260 nm and 280 nm. All the plasmid DNA were stored at -20 ℃ in sterile saline at 1 mg/mL for experimental use.

Cell transfection and plasmid gene expression analysis

SMMC-7721 cells (5×10^5 cells), a human hepatocellular carcinoma cell line, were transfected with 2 μg of the different plasmids DNA mixed with 100 g/L lipofectamine according to the manufacturer' s guidelines. Semiquantitative RT-PCR was used to analyze the transcription of HBV-preS2/S or preS2/S-P28 fusions and ensure the correct size of fusions containing variable copies of C3d-P28. Total RNA was extracted from the transfected cells (1×10^6 cells) using

guanidinium isothiocyanate-based buffer system according to the manufacturer' s instructions and then treated by RNase-free DNase I. First-strand cDNA was synthesized from 5 μL of total cellular RNA with a GeneAmp PCR system 2400 cycler (Perkin Elmer company, USA) using the following protocol: one cycle at 42 ℃ for 60 min and 70 for 10 min[16]. The cDNA was subjected to 30 cycles of amplification using the appropriate primers: (1) sense and antisense of HBV-preS2/S, which permitted the amplification of the HBV-preS2/S cDNA; (2) HBV-preS2/S sense and C3d-P28 antisense, which permitted the amplification of the preS2/S-P28 fusions cDNA; (3) sense and antisense of GAPDH, which permitted the amplification of the GAPDH cDNA. After initiate denaturation at 94 ℃ for 5 min, the amplification conditions were as follows: denaturation at 94 ℃ for 1 min, primers annealing at 58 ℃ for 1 min, and extension at 72 ℃ for 2 min. Final PCR products were analyzed on 10 g/L agarose gel electrophoresis and the intensity of the preS2/S and GAPDH PCR products was assessed by densitometry and quantitated by using UV-2000 (Tanon Science and Technology Ltd., China); preS2/S mRNA expression was calculated as the ratio of the intensity of the preS2/S band to the GAPDH band. At the same time, direct PCR reaction was performed to exclude the contamination of potential plasmid DNA in the RNA extracted from the transfected cells.

Immunization

The quadriceps of mice were first injected with a total of 100 μL of 2.5 g/L bupivacaine to enhance the cellular uptake of plasmid DNA one day before the first immunization. Then 100 μg of each plasmid DNA dissolved in 100 μL of normal saline was injected into the same region. Twelve weeks later, each mouse was boosted by subcutaneous injection with 1.0 μg of purified HBsAg protein diluted in 100 μL of sterile PBS. Sera were collected at 2-week intervals after primary immunization for antibody analysis.

Measurement of anti-HBs antibody levels

The anti-HBs antibody response elicited in mice was evaluated by ELISA. In brief, microtiter plates were coated with purified HBsAg protein (0.5 μg/well). After incubation with 100 mL/L FBS in PBS for 60 min at 37 ℃ to prevent nonspecific binding, 1:10 dilution of mouse serum were added to the plates and incubated at 37 ℃ for an additional 60 min. After the samples were washed with PBS containing 0.5 g/L Tween-20, a horseradish peroxidase-labeled goat anti-mouse antibody was added at a dilution 1:5 000. After 60 min incubation, plates were washed, and substrate was added for color development. Absorbance (A_{490}) of each plate wells was read at 490 nm that indicated the levels of specific antibody.

Measurement of anti-HBs antibody avidity

Relative antibody avidity was determined by a modified elution ELISA that was similar to serum antibody determination ELISAs up to the addition of samples as previously described[11,12]. Plates were washed 3 times with 0.5 g/L PBS-Tween 20. Sodium thiocyanate (NaSCN), a chaotropic compound that interferes with the antigen-antibody reaction, was added subsequently in concentrations ranging from 0.5 mol/L to 3.5 mol/L. Plates were allowed to left for 15 min at room temperature and then washed six times with PBS-Tween 20. Subsequent steps were performed similarly to the serum antibody determination ELISA. The avidity index (AI) corresponded to the effective concentration of NaSCN required to give a 50% reduction in absorbance at 490 nm.

Statistical analysis

Data were expressed as mean±SD. Experimental results were analyzed by variance analysis or *t* test with SPSS software. $P<0.05$ were considered statistically significant.

RESULTS

Construction and identification of the recombinant plasmids

To test for an effect of C3d-P28 on the immune responses to a DNA vaccine, we selected plasmids encoding HBV envelope proteins as a model system. Then the genes encoding middle (preS2 plus S) HBV envelope proteins (858 bp) were cloned into a eukaryotic expression vector pVAON33. One to four tandem repeats of the C3d-P28 fragment were inserted into pVAON33 plasmid to construct the recombinant plasmids pVAON33-P28, pVAON33-P28.2, pVAON33-P28.3 and pVAON33-P28.4 (pVAON33-P28.[1-4]), respectively. HBV-preS2/S coding sequence was then introduced into the pVAON33-P28.[1-4], respectively. The results of identification by both PCR and DNA sequencing showed that the coding-codon of HBV-preS2/S coding gene, repeats of the P28-coding gene and their junctions were correct (data not shown).

Expression of plasmids

SMMC-7721 cells were transiently transfected with preS2/S and preS2/S-P28.4 protein expression vectors, with the plasmid pVAON33 serving as a negative control. At 2 d after transfection, the preS2/S mRNA could be detected in SMMC-7721 cells transfected with both plasmid pVAON33-S2/S and pVAON33-S2/S-P28.4, but not in mock plasmid (Figure 2). However, mRNA representing fusions of preS2/S to various copies of P28 could only be detected in SMMC-7721 cells transfected with pVAON33-S2/S-P28.4 plasmid. Digested with DNase I, RNA samples extracted from the cells transfected with both pVAON33-S2/S and pVAON33-S2/S-P28.4 were confirmed the exclusion of potential plasmid DNA contamination (Figure 2). These results suggested that various copies of P28 had fused with the HBV-preS2/S. Semiquantitative RT-PCR analysis showed that preS2/S expressed by pVAON33-S2/S-P28.4-DNA was 29.61% lower than that expressed by pVAON33-S2/S-DNA.

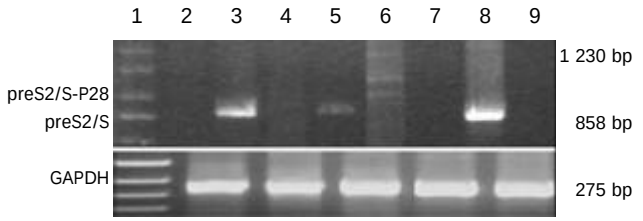

Figure 2 Semiquantitative RT-PCR for expression of the preS2/S-P28 fusion proteins. Lane 1: DNA marker; Lanes 2,3 and 5: RT-PCR with preS2/Ss and preS2/Sa primers that amplified an entire coding region (858 bp) of preS2/S, using RNA extracted from pVAON33, pVAON33-S2/S and pVAON33-S2/S-P28.4 transfected-cells, respectively; Lanes 4 and 6: RT-PCR with preS2/Ss and P28a primers that amplified a 1 230 bp cDNA fragment of preS2/S-P28.4 fusion cDNA (the ladder showed the RT-PCR production due to 4 copies of P28), using RNA extracted from pVAON33-S2/S and pVAON33-S2/S-P28.4 transfected-cells, respectively; Lanes 7 and 9: RNA extracted from pVAON33-S2/S and pVAON33-S2/S-P28.4 transfected-cells was founded to exclude the potential contamination of potential plasmid DNA by PCR with preS2/Ss and preS2/Sa primers, respectively; and Lane 8: pVAON33-S2/S plasmid DNA was taken as positive control.

Anti-HBs IgG levels after primary immunization

The preS2/S-P28-expressing DNA plasmids showed higher levels of anti-HBs antibody than the preS2/S-expressing DNA (Figure 3). When sera were assayed on HBsAg-coated plates, there were various degrees of enhancement of anti-HBs IgG antibody levels in the mice with DNA expressing fusions of HBV-preS2/S to variable copies of P28 compared to the mice

primed with DNA expressing HBV-preS2/S only (Figure 3). Interestingly, at 12 wk after the primary immunization, the highest level of the specific antibody response (A_{490}, 1.049±0.186) was observed in the groups primed with DNA expressing fusions of HBV-preS2/S to four copies of P28, which was not only significant higher than the level of antibody response from the group primed with preS2/S-expressing DNA (A_{490}, 0.621±0.064; P<0.01), but also obviously higher than the level of antibody response from the groups primed with preS2/S-P28.1-expressing DNA (A_{490}, 0.764±0.143; P<0.01), preS2/S-P28.2-expressing DNA (A_{490}, 0.915±0.275; P<0.05) and preS2/S-P28.3-expressing DNA (A_{490}, 0.696±0.091; P<0.01), respectively. It was suggested that P28, when fused with HBV-preS2/S, could enhance the specific antibody response against HBsAg following primary DNA immunization. Differences in the enhancement of the antibody levels raised by the fusions of preS2/S-P28 to variable repeats of P28 appeared to be determined by the different repeats of P28, in which four copies of P28 might be necessary to achieve the most modest antibody response.

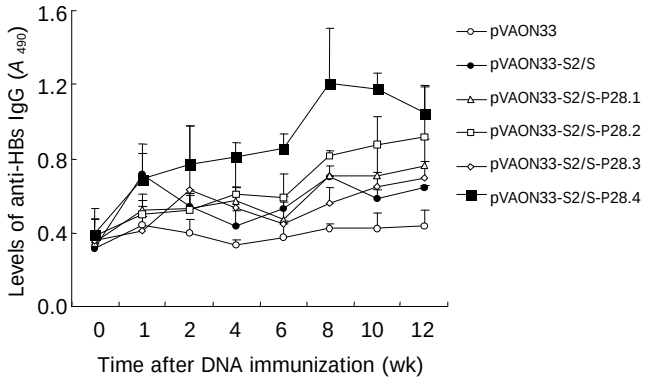

Figure 3 Determination of anti-HBs IgG of sera from mice primed by the plasmid vectors containing different copies of C3d-P28. BALB/c mice (6 animals per group) were primed im at week 0 with 100 μg of mock DNA (O), pVAON33-S2/S plasmid (●), pVAON33-S2/S-P28 plasmid (△), pVAON33-S2/S-P28.2 plasmid (□), pVAON33-S2/S-P28.3 plasmid (◇) and pVAON33-S2/S-P28.4 plasmid (■), separately. Sera collected at the indicated weeks from each group were diluted 1:10 for determination of specific IgG levels by ELISA. Data were represented as the average for each group of mice. Error bars were represented as 95% *CI* of the geometric mean for each group of sera.

Anti-HBs IgG levels after secondary vaccination

To further observe the effects of P28 peptides on the memory responses against HBsAg, mice from each group were boosted subcutaneously with 1 μg of HBsAg purified at the twelfth week after the primary immunization. The results showed that the mice of the groups vaccinated primarily with preS2/S-expressing DNA produced an increased levels of anti-HBs antibody compared to the mice immunized primarily with mock DNA after the second immunization with specific antigen (Figure 4). However, the acceleration of antibody levels was significantly higher and faster in the mice immunized with DNA expressing preS2/S-P28 fusions than that in the mice immunized with DNA expressing preS2/S only (P<0.05). Interestingly, at the eighteenth week after the primary immunization, mice immunized primarily with DNA expressing preS2/S-P28.4 fusions maintained the highest levels of anti-HBs antibodies in all animals (A_{490}, 1.273±0.106). It was suggested that the mice immunized with DNA expressing preS2/S-P28 fusions not only enhanced primary humoral responses against HBsAg, but also produced a quicker and stronger memory responses than that with DNA expressing preS2/S only, in which four copies of P28 might also be necessary to obtain the most modest antibody memory reaction.

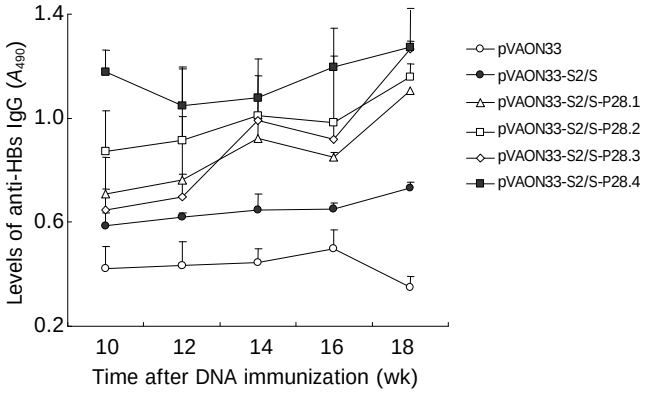

Figure 4 Determination of anti-HBs IgG of sera from mice primed by the different plasmid DNAs and boosted with HBsAg protein. Each group of mice (n=6) was primed im at week 0 with 100 μg of mock DNA (O), pVAON33-S2/S plasmid (●), pVAON33-S2/S-P28 plasmid (△), pVAON33-S2/S-P28.2 plasmid (□), pVAON33-S2/S-P28.3 plasmid (◇) and pVAON33-S2/S-P28.4 plasmid (■), separately. And then boosted sc at week 12 with HBsAg (1 μg per mouse). Sera collected at the indicated times from each group were diluted 1:10 for determination of specific IgG levels by ELISA.

Avidity of anti-HBs IgG

To observe whether P28 enhances the avidity maturation of the antibody response after immunization with P28-preS2/S fusions, NaSCN-displacement ELISA, a well-accepted approach, was used to evaluate the avidity of the anti-HBs antibodies[11-13]. The results demonstrated that the AI collected at 18 weeks from mice immunized primarily with preS2/S-P28.3 and preS2/S-P28.4 expressing DNA, separately was significantly higher than that from preS2/S-DNA vaccinated mice (Figure 5, P<0.01). However, no significant increases in the AI were found in either preS2/S-P28.1 expressing or preS2/S-P28.2 expressing DNA vaccinated mice compared to the mice immunized with DNA expressing preS2/S only. These results suggested that C3d-P28 could enhance the avidity maturation of antibodies against HBsAg following gene immunization with DNA expressing fusions of HBV-preS2/S to three or four repeats of C3d-P28.

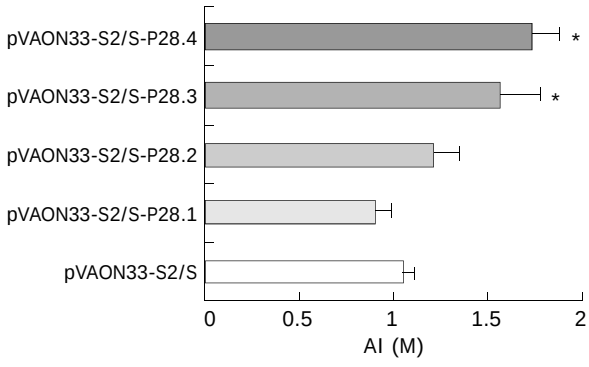

Figure 5 Determination of avidity of anti-HBs IgG of sera from immunized mice. Mice (six mouse per group) were primed im at week 0 with 100 μg of different plasmid DNAs and then boosted sc at week 12 with HBsAg (1 μg per mouse). Sera were obtained at week 18. The pooled serum samples from each mouse group were diluted 1:10 for determination of avidity of the anti-HBs IgG by an HBsAg–specific NaSCN–displacement ELISA. Data were represented as the average of three independent experiments plus standard errors (mean±SD).

DISCUSSION

Recently, several studies demonstrated that DNA vaccines encoding the small or middle viral envelope proteins of HBV elicited higher titer antibody, as well as cell-mediated immune responses compared with HBV subunit vaccines[17-19]. Moreover, DNA immunization was able to break immune tolerance in the HBV transgenic mouse model[20] and induces protective antibody responses in human non-responders to conventional vaccination[17], indicating that DNA vaccines might be beneficial for immunotherapy for individuals with chronic HBV infections. DNA vaccines for HBV infection are efficacious, as well as inexpensive, and therefore, may be a promising tool in controlling the viral infections and liver diseases[21].

However, one of the drawbacks that prevents the wide spread use of DNA vaccines is slower rise in humoral immunity compared with other vaccine strategies for HBV infection. This may be due to the low levels of antigen expression and presentation by inoculated DNA plasmids compared to the inoculation of HBsAg[22]. In order to enhance the efficacy of antigens expression and presentation in the DNA immunization, several studies have shown that three copies of C3d, as a molecular adjuvant when fused to an antigen, could enhance the immune responses and accelerate the antibody avidity maturation[2-7]. However, Suradhat *et al*.[23] reported that fusions of one or two copies of C3d with either bovine rotavirus VP7 or bovine herpesvirus type 1 glycoprotein D inhibited the specific humoral response following DNA immunization, and suggested that using three or more copies of C3d molecule may be necessary for efficient enhance of antigen-specific immune responses following DNA immunization. These results indicated that different repeats of C3d in the fusions of target antigen to C3d might influence efficient enhancement of antigen specific immune response following DNA immunization[2-7,23].

HBsAg is encoded by a single gene which is divided into S, preS2 and preS1 regions. preS vaccines have been most extensively applied in humans and shown to confer certain protective immunity. Recently more researches indicated that addition of the preS2 sequence could enhance the immunogenicity of the vaccines in human[24,25]. Therefore in this study, we selected HBV-preS2/S as a model antigen and different repeats of P28 peptide, an active peptide corresponding to the CR2-binding site on C3d[10-13], as a molecular adjuvant to explore enhancing effects on the immune response. As expected, mice vaccinated with DNA expressing fusions of preS2/S to P28 (one, two, three or four repeats) elicited a higher level of primary humoral response compared to mice vaccinated with DNA expressing only the preS2/S protein. Moreover, the mice immunized with DNA expressing preS2/S-P28 fusions produced a quicker and stronger memory responses than that with DNA expressing preS2/S only after second immunization. Interestingly, the results showed that the enhancing effect of various repeats of P28 in fusions of preS2/S to P28 on primary response as well as memory reaction was different, in which four copies of P28 might be necessary to achieve the most modest antibody response. It was indicated that the most modest antibody response appeared to be determined by the different repeats of P28. These results acquired here further explained the conflict between reports by Ross *et al*.[4] and by Suradhat *et al*.[23]. The increase in antibody response elicited by four copies of P28, similar to previous studies using antigen-C3d3 fusions[3-7], was even more intriguing, since the preS2/S-expression at the mRNA level by preS2/S-P28.4-expressing plasmid was 29.61% lower than the expression by plasmid expressing HBV-preS2/S only. The most likely mechanism by which P28 increases antibody responses is similar to C3d, which has been hypothesized to reflect the binding of C3d to CD21 on the surface of B-cells or follicular dendritic cells (FDC)[3,4,8].

Surprisingly, immunization with the preS2/S-P28 fusions also resulted in enhanced avidity maturation of anti-HBs antibody. The results demonstrated that the AI of sera collected from mice immunized primarily with preS2/S-P28.3 and preS2/S-P28.4 expressing DNA, separately, was significantly higher than that from preS2/S-DNA vaccinated mice. Avidity is a term used to describe the strength of interaction between multivalent antigens and antibodies in serum and is dependent on the individual affinities of the polyclonal antibodies[3]. Avidity maturation occurs in germinal centers where the somatic hypermutation of immunoglobulin results in a large repertoire of Ag-specific B cells that undergo inducing or selection for high-affinity B cell receptors by T helper cells or follicular dendritic cells (FDC)[8,9,26-28]. The most likely mechanism by which P28 enhanced the avidity maturation of anti-HBs antibodies might relate to multiple interactions of cells responsible for humoral immunity, including B cells, T helper cells, and FDC. These interactions, coupled with the enhancing effects of CR2 ligation on germinal center formation[29] and the enhancing effects of specific Th cells on somatic hypermutations of B cells[30], could promote the selection of antigen-specific B cells with high-affinity B cell receptors, resulting in the avidity maturation of anti-HBs antibodies and the development and maintenance of memory B cells[31].

Taken together, this is the first report to demonstrate that immunization with DNA expressing antigen-P28 fusions results in enhancing antibody response and enhancing antibody avidity maturation. These findings argue that four or more repeats of C3d-P28 may be necessary for efficient enhancement of antigen-specific immune responses, and thus C3d-P28, a short, active peptide derived from the CR2-binding site on complement C3d, may be another promising molecular adjuvant and may assist the future design of vaccines for health-threatening pathogens.

ACKNOWLEDGEMENTS

We sincerely thank Dr. T.M. Ross from University of Pittsburgh School of Medicine for helpful advice in this study and for providing the plasmid. We also thank Jin-Ping Zhang, Cong-Feng Xu, Huan-Bin Xu for their technical assistance.

REFERENCES

1 **Pepys MB.** Role of complement in induction of antibody production *in vivo*. Effect of cobra venom factor and other C3-reactive agents on thymus-dependent and thymus-independent antibody responses. *J Exp Med* 1974; **140**: 126-145

2 **Dempsey PW,** Allison MED, Akkaraju S, Goodnow CC, Fearon DT. C3d of complement as a molecular adjuvant: bridging innate and acquired immunity. *Science* 1996; **271:** 348–350

3 **Test ST**, Mitsuyoshi J, Connelly CC, Lucas AH. Increased immunogenicity and induction of class switching by conjugation of complement C3d to pneumococcal serotype 14 capsular polysaccharide. *Infect Immun* 2001; **69:** 3031–3040

4 **Ross TM,** Xu Y, Bright RA, Robinson HL. C3d enhancement of antibodies to Hemagglutinin accelerates protection against influenza virus challenge. *Nat Immunol* 2000; **1:** 127–131

5 **Mitchell JA,** Green TD, Bright RA, Ross TM. Induction of heterosubtypic immunity to influenza A virus using a DNA vaccine expressing hemagglutinin-C3d fusion proteins. *Vaccine* 2003; **21:** 902–914

6 **Ross TM,** Xu Y, Green TD, Montefiori DC, Robinson HL. Enhanced avidity maturation of antibody to human immunodeficiency virus envelope: DNA vaccination with gp120-C3d fusion proteins. *AIDS Res Hum Retroviruses* 2001; **17:** 829–835

7 **Green TD,** Newton BP, Rota PA, Xu Y, Robinson HL, Ross TM. C3d enhancement of neutralizing antibodies to measles

hemagglutinin. *Vaccine* 2001; **20:** 242–248
8 **Tew JG,** Wu J, Qin D, Helm S, Burton GF, Szakal AK. Follicular dendritic cells and presentation of antigen and costimulatory signals to B cells. *Immunol Rev* 1997; **156**: 39-52
9 **Yellin MJ,** Sinning J, Covey LR, Sherman W, Lee JJ, Glickman-Nir E, Sippel KC, Rogers J, Cleary AM, Parker M, Chess L, Lederman S. T lymphocyte T cell-B cell-activating molecule / CD40-L molecules induce normal B cells or chronic lymphocytic leukemia B cells to express CD80 (B7 / BB-1) and enhance their costimulatory activity. *J Immunol* 1994; **153:** 666-674
10 **Lambris JD,** Ganu VS, Hirani S, Müller-Eberhard HJ. Mapping of the C3d receptor (CR2)-binding site and a neoantigenic site in the C3d domain of the third component of complement. *Proc Natl Acad Sci U S A* 1985; **82:** 4235-4239
11 **Esparza I,** Becherer JD, Alsenz J, De la Hera A, Lao Z, Tsoukas CD, Lambris JD. Evidence for multiple sites of interaction in C3 for complement receptor type 2 (C3d / EBV receptor, CD21). *Eur J Immunol* 1991; **21:** 2829-2838
12 **Servis C,** Lambris JD. C3 synthetic peptides support growth of human CR2-positive lymphoblastoid B cells. *J Immunol* 1989; **142:** 2207-2212
13 **Frade R,** Hermann J, Barel M. A 16 amino acid synthetic peptide derived from human C3d triggers proliferation and specific tyrosine phosphorylation of transformed CR2-positive human lymphocytes and of normal resting lymphocytes-B. *Biochem Biophys Res Commun* 1992; **188:** 833-842
14 **Sarrias MR,** Franchini S, Canziani G, Argyropoulos E, Moore WT, Sahu A, Lambris JD. Kinetic analysis of the interactions of complement receptor 2 (CR2, CD21) with its ligands C3d, iC3b, and the EBV glycoprotein gp350 / 220. *J Immunol* 2001; **167**: 1490-1499
15 **Lou D,** Kohler H. Enhanced molecular mimicry of CEA using photoaffinity crosslinked C3d peptide. *Nat Biotechnol* 1998; **16:** 458-462
16 **Chow YH,** Chiang BL, Lee YL, Chi WK, Lin WC, Chen YT, Tao MH. Development of Th1 and Th2 populations and the nature of immune responses to hepatitis B virus DNA vaccines can be modulated by codelivery of various cytokine genes. *J Immunol* 1998; **160**: 1320-1329
17 **Rottinghaus ST,** Poland GA, Jacobson RM, Barr LJ, Roy MJ. Hepatitis B DNA vaccine induces protective antibody responses in human non-responders to conventional vaccination. *Vaccine* 2003; **31:** 4604-4608
18 **Kim SJ,** Suh D, Park SE, Park JS, Byun HM, Lee C, Lee SY, Kim I, Oh YK. Enhanced immunogenicity of DNA fusion vaccine encoding secreted hepatitis B surface antigen and chemokine RANTES. *Virology* 2003; **1:** 84-91
19 **Davis HL,** Mancini M, Michel ML, Whalen RG. DNA-mediated immunization to hepatitis B surface antigen: longevity of primary response and effect of boost. *Vaccine* 1996; **14:** 910-915
20 **Mancini M,** Hadchouel M, Davis HL, Whalen RG, Tiollais P, Michel ML. DNA-mediated immunization in a transgenic mouse model of the hepatitis B surface antigen chronic carrier state. *Proc Natl Acad Sci U S A* 1996; **93:** 12496-12501
21 **Hassett DE,** Whitton JL. DNA immunization. *Trends Microbiol* 1996; **4:** 307-312
22 **Robinson HL,** Pertmer TM. DNA vaccines for viral infections: basic studies and applications. *Adv Virus Res* 2000; **55:** 1–74
23 **Suradhat S,** Braun RP, Lewis PJ, Babiuk LA, Little-van den Hurk SD, Griebel PJ, Abca-Estrada ME. Fusion of C3d molecule with bovine rotavirus VP7 or bovine herpesvirus type 1 glycoprotein D inhibits immune responses following DNA immunization. *Vet Immunol Immunopathol* 2001; **83:** 79-92
24 **Davis HL,** Brazolot Millan CL. DNA-based immunization against hepatitis B virus. *Springer Semin Immunopathol* 1997; **19**: 195-209
25 **Jilg W**. Novel hepatitis B vaccines. *Vaccine* 1998; **16**: S65-S68
26 **Berek C,** Berger A, Apel M. Maturation of the immune response in germinal centers. *Cell* 1991; **67:** 1121–1129
27 **Jacob J,** Kelsoe G, Rajewsky K, Weiss U. Intraclonal generation of antibody mutants in germinal centres. *Nature* 1991; **354:** 389–392
28 **Fang Y,** Xu C, Fu YX, Holers VM, Molina H. Expression of complement receptors 1 and 2 on follicular dendritic cells is necessary for the generation of a strong antigen-specific IgG response. *J Immunol* 1998; **160**: 5273-5279
29 **Griffioen AW,** Rijkers GT, Janssens-Korpela P, Zegers BJM. Pneumococcal polysaccharides complexed with C3d bind to human B lymphocytes via complement receptor type 2. *Infect Immun* 1991; **59**: 1839-1845
30 **Razanajaona D,** van Kooten C, Lebecque S, Bridon JM, Ho S, Smith S, Callard R, Banchereau J, Briere F. Somatic mutations in human Ig variable genes correlate with a partially functional CD40-ligand in the X-linked hyper-IgM syndrome. *J Immunol* 1996; **157:** 1492-14928
31 **Fischer MB,** Goerg S, Shen L, Prodeus AP, Goodnow CC, Kelsoe G, Carroll MC. Dependence of germinal center B cells on expression of CD21 / CD35 for survival. *Science* 1998; **280**: 582-585

Edited by Kumar M **Proofread by** Xu FM

PO Box 2345, Beijing 100023, China
Fax: +86-10-85381893
E-mail: wjg@wjgnet.com www.wjgnet.com

World J Gastroenterol 2004;10(14):2078-2081
World Journal of Gastroenterology
 ISSN 1007-9327

• BASIC RESEARCH •

Expression and *in vitro* cleavage activity of anti-caspase-7 hammerhead ribozymes

Wei Zhang, Qing Xie, Xia-Qiu Zhou, Shan Jiang, You-Xin Jin

Wei Zhang, Qing Xie, Xia-Qiu Zhou, Shan Jiang, Department of Infectious Disease, Ruijin Hospital, Shanghai Second Medical University, Shanghai 200025, China
You-Xin Jin, Shanghai Institute of Biochemistry, Chinese Academy of Sciences, Shanghai 200025, China
Supported by the National Natural Science Foundation of China, No. 30170850
Co-correspondents: Dr. You-Xin Jin
Correspondence to: Dr. Qing Xie, Department of Infectious Disease, Ruijin Hospital, Shanghai Second Medical University, Shanghai 200025, China. xieqing@sh163.net
Telephone: +86-21-64311242
Received: 2003-09-23 **Accepted:** 2004-01-12

Abstract

AIM: To prepare hammerhead ribozymes against mouse caspase-7 and identify their cleavage activity *in vitro*, in order to select a ribozyme with specific cleavage activity against mouse caspase-7 as a potential gene therapy for apoptosis-related diseases.

METHODS: Anti-caspase-7 ribozymes targeting sites 333 and 394 (named Rz333 and Rz394) were designed by computer software, and their DNA sequences encoding ribozymes were synthesized. Caspase-7 DNA sequence was acquired by RT-PCR. Ribozymes and caspase-7 DNA obtained by *in vitro* transcription were cloned into pBSKneo U6' and pGEM-T vectors, respectively. The cleavage activity of ribozymes against mouse caspase-7 was identified by cleavage experiments *in vitro*.

RESULTS: Rz333 and Rz394 were designed and their DNA sequences were synthesized respectively. The expression vector of caspase-7 and plasmids containing Rz333 and Rz394 were reconstructed successfully. Ribozymes and caspase-7 mRNA were expressed by *in vitro* transcription. *In vitro* cleavage experiment showed that 243-nt and 744-nt segments were produced after caspase-7 mRNA was mixed with Rz333 in equivalent, and the cleavage efficiency was 67.98%. No cleaved segment was observed when caspase-7 mRNA was mixed with Rz394.

CONCLUSION: Rz333 can site-specific cleave mouse caspase-7 mRNA, and it shows a potential for gene therapy of apoptosis-related diseases by down-regulating gene expression of caspase-7.

Zhang W, Xie Q, Zhou XQ, Jiang S, Jin YX. Expression and *in vitro* cleavage activity of anti-caspase-7 hammerhead ribozymes. *World J Gastroenterol* 2004; 10(14): 2078-2081
http://www.wjgnet.com/1007-9327/10/2078.asp

INTRODUCTION

Apoptosis, or programmed cell death, is characterized by a series of morphological features such as chromatin condensation, nuclear fragmentation, and the appearance of membrane-enclosed apoptotic bodies, *etc*.[1,2], most of which are caused by the activation of caspases, a family of aspartate-specific cysteine proteases[3,4]. Caspases are constitutively present in cells as inactive zymogens and require proteolytic cleavage into the catalytic active heterodimer[5]. All activated caspases are comprised of a large subunit with M_r 17 000-20 000 that contains a redox-sensitive cysteine at the active site and a small subunit with M_r 10 000 approximately. According to their function and sequence of activation, caspases can be grouped into three categories: Caspases that function primarily in cytokine maturation (such as caspases-1, -4, and -5); initiator caspases involved in the early steps of apoptotic signaling (caspases-8, -9, and -10) and effector proteases in the execution phase of apoptosis (caspases-3, -6, and -7). The initiator caspases lead to the activation of executioner caspases following characteristic apoptotic stimuli. The substrates of executioner caspases include many proteins, the cleavage of which causes the characteristic morphology of apoptosis[6,7]. Because apoptosis is a regulated cellular process, it offers some opportunities for therapeutic intervention[8,9]. Indeed, eliminating caspase activity, either through mutation or the use of small pharmacological inhibitors, will slow down or even prevent apoptosis.

Ribozymes are small RNA molecules that hybridize to the target RNA around the cleavage site, and catalyze site-specific cleavage of substrate. Cleaved mRNA is rapidly degraded, allowing ribozyme to react with new targets. Various ribozymes have been used to down-regulate gene expression in a sequence-specific manner. Among them the hammerhead ribozyme, composed of only 30 to 40 nucleotides, is the smallest and simplest one, and has been used extensively to down-regulate gene expression[10-13].

Caspase-3 and caspase-7 are both important executioner caspases[14]. Expression pattern of caspase-7 is distinguishable from that of caspase-3, suggesting that they may regulate apoptosis in disparate tissues, although they share strong homology. In the past years, many researches have been concentrated on interfering with the activity or expression of caspase-3 so as to intervene in apoptosis[15-17]. Following its activation, caspase-7 was translocated into the microsomal and mitochondrial fractions, where it was responsible for the cleavage of specific substrates in those distinct subcellular compartments[18]. Recent results suggested that as one of important executioner caspases, caspase-7 is also essential in apoptotic signaling[19,20]. In this study, we designed and synthesized two hammerhead ribozymes against mouse caspase-7 at sites 333 and 394 (named Rz333 and Rz394), studied their *in vitro* transcription and cleavage activity, and selected the one that could site-specifically cleave caspase-7 mRNA as a hopeful gene therapy tool for apoptosis-related diseases.

MATERIALS AND METHODS

Materials

TRIzol reagent was product of Gibco. RT-PCR kit, T4 DNA ligase and restriction endonucleases were Takara products. *In vitro* transcription kit and pGEM-T vector were purchased from

Promega. pBSK neo-U6' was kindly donated by Dr. Youxin Jin. Plasmid extraction kit and gel purification kit were products of Shanghai Sangon Biotechnology Co.

Methods

Target mRNA secondary structure analysis and design of anti-caspase-7 ribozymes Caspase-7 gene sequence of BALB/c mouse searched in GenBank (gi: 6680849) was analyzed, and its secondary structure was simulated in computer. Ribozymes against caspase-7 mRNA were designed by software and DNA sequences encoding ribozymes were synthesized. A restriction site of *Xba*I was introduced into 5' end of sense strand. And a *Bam*H I restriction site was introduced into the 5' end of antisense strand. Two DNA strands were mixed at equal molar ratio after synthesis, and annealed by cooling to room temperature naturally after placed in boiling water for 2 min, then double strand DNA encoding ribozymes was obtained.

Ribozyme gene cloning Double-strand ribozyme DNAs designed by computer were inserted into pBSKneo U6' with T4 DNA ligase after pBSKneo U6' was cleaved by *Bam*H I and *Xba*I (Figure 1). The reconstructed plasmids containing ribozyme genes were identified by Sal I digestion and sequencing.

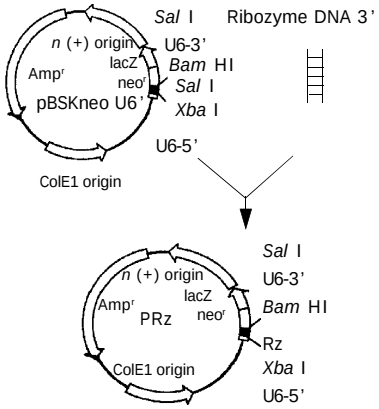

Figure 1 Ribozyme gene cloning.

Construction of caspase-7 expression vector Total RNA was extracted with TRIzol reagent from Balb/c mouse liver. Caspase-7 gene segment (841 bp) was amplified by RT-PCR with specific primers. The segment was cloned into pGEM-T vector downstream from T7 promoter, and the transformed clones selectively grew at 37 ℃ overnight in LB plate (Ampicillin resistance) containing IPTG and X-gal on plate's surface. Clones in blue were selected for sequencing. Caspase-7 primers were: P1 5'-GGATCCGAACGATGACCGATGATCAG-3', P2 5'-AAGCTTGTGAGCATGGACACCATAC-3'.

***In vitro* transcription of ribozyme and caspase-7 cDNAs** Constructed caspase-7 plasmid was linearized with *Hin*d III. Reconstructed ribozyme plasmid was considered as PCR template and a pair of primers containing T7 promotor was designed. P1 5'-TCTAGA*GTAATACGACTCACTATAGG GC*CTTCGGCAGCACATATAC-3', P2 5'-TATGGAACG CTTCAGGAT-3' (The italic is T7 promotor sequence). Both caspase-7 linearized plasmid and pRz PCR product were phenol-chloroform extracted, and ethanol precipitated. *In vitro* transcription was performed using T7 RNA polymerase. Transcript of caspase-7 labeled with α-^{32}P-UTP was heated (2 min, 95 ℃) before loading and electrophoresed on 6% polyacrylamide gel denatured by 8 mol/L urea. Transcript band was observed after autoradiography. *In vitro* transcription of ribozyme was not labeled with isotope. After electrophoresis on 60 g/L polyacrylamide gel, the transcript bands were observed under ultraviolet. All transcript bands in gel, labeled with isotope or not, were cut and dipped into nucleic acid (0.5 mol/L NH_4Ac, 1 mmol/L EDTA, 1 g/L SDS), precipitated in ethanol and dissolved in DEPC-H_2O. Concentrations of substrate and ribozyme were calculated through cpm counting and A_{260} measurement, respectively.

***In vitro* ribozyme cleavage assays** Ribozymes and caspase-7 mRNA were incubated at equal molar ratio at 37 ℃ for 90 min in a system of 5–10 μL containing 50 mmol/L Tris-HCl pH 7.5, 20 mmol/L $MgCl_2$, 20 mmol/L NaCl and 2 mmol/L EDTA. The products after cleavage were electrophoresed on 10% polyacrylamide gel, and the cleavage results were analyzed by autoradiography. Cleavage efficiency may be estimated according to cpm of both substrates (S) and cleaved products (P).

Cleavage ratio=[P/(S+P)]×100%

RESULTS

Design of ribozymes

According to the results of computer simulation, triplet GUC at site 333 and GUA at site 394 of caspase-7 mRNA were chosen as the cleavage sites of ribozyme. So ribozymes targeting site 333 and site 394 (named Rz333 and Rz394) were designed to cleave the target mRNA. Both designed ribozymes were comprised of a catalytic core and two flanking sequences (Figure 2).

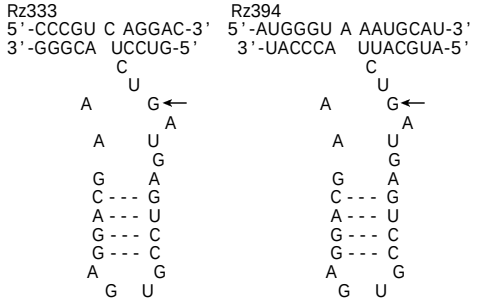

Figure 2 Sequences, structures and targets of ribozymes against caspase-7. Hammerhead ribozymes (bottom strand) binding to their targets (top strand) to form a typical three-stem structure that leads to the cleavage of caspase-7 RNA at the targets of GUC (Rz333) and GUA (Rz394).

Identification of reconstructed plasmid containing ribozyme

Reconstructed plasmids pU6Rz333 and pU6Rz394 were both incubated with *Sal*I at 37 ℃ for 2 h and then electrophoresed on 12 g/L agarose gel (Figure 3). Clones without 200 bp segment were sent for sequencing, and the results indicated that clones 2, 4 were correctly constructed.

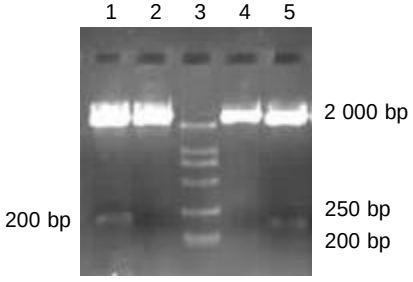

Figure 3 Restriction enzyme cleavage of reconstructed ribozyme plasmid. Lanes 1, 2: pU6Rz333 digested by *Sal* I; lanes 4, 5: pU6Rz394 digested by *Sal* I; lane 3: Marker (DL2000).

Caspase-7 DNA and its clone

Extracted total RNA was amplified by RT-PCR and a 891-bp caspase-7 DNA segment was seen on 20 g/L agarose gel (Figure 4).

It was cloned into pGEM-T vector, and white and blue monoclones were seen in LB medium after incubated at 37 ℃ overnight. Blue clones were selected and sent for sequencing.

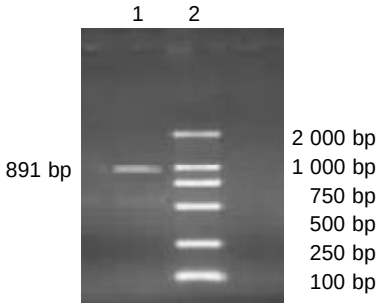

Figure 4 Agarose gel electrophoresis of RT-PCR products. Lane 1: A 891-bp caspase-7 gene segment; lane 2: Marker (DL2000).

In vitro transcription of target mRNA and ribozymes

Transcript of target mRNA was electrophoresed on 60 g/L polyacrylamide gel. After autoradiography, a black band of 987 nt was observed, including 891-nt caspase-7 mRNA and 96-nt U6 segment (Figure 5). *In vitro* transcripts of the two ribozymes were not labeled with isotope. The results of transcription were analyzed under ultraviolet. Black bands of 47 nt (Rz333) and 50 nt (Rz394) could be seen.

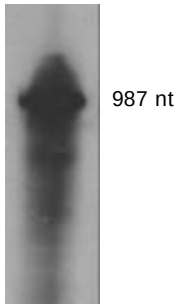

Figure 5 *In vitro* transcription of target RNA. The transcript is 987 nt.

In vitro cleavage of ribozymes

Products of cleavage assays were electrophoresed on 100 g/L polyacrylamide gel, and analyzed by autoradiography. Rz333 cleaved caspase-7 mRNA and produced two cleaved segments of 243 nt and 744 nt, with a cleavage efficiency of 67.98%. Rz394 could not cleave target RNA (Figure 6).

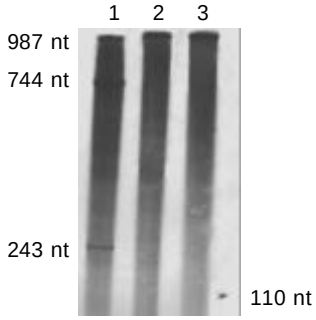

Figure 6 *In vitro* cleavage experiments of anti-caspase-7 ribozymes. Lane 1: Caspase-7 mRNA was mixed with Rz333 and two segments of 243 nt and 744 nt produced by cleavage reaction. Lane 2: Caspase-7 mRNA was mixed with Rz394 and no segment was seen after cleavage. Lane 3: Caspase-7 mRNA was mixed with neither Rz333 nor Rz394. The 110-nt marker is indicated by a short arrow.

DISCUSSION

RNA catalysis was first described by Altman and Cech with the discovery of RNase P and the group I intron, respectively[21,22]. This makes RNA the only molecule with an information-carrying capacity and inherent catalytic activity. So far, several natural ribozyme motifs have been identified and their physical structure, biological and biochemical properties have been the subject of reviews[23,24]. In general, however, natural ribozymes have been divided into groups based on their specialized catalytic properties. As the smallest one, the hammerhead ribozyme, with its capability of self-cleavage of a particular phosphodiester bond, has been studied extensively to understand the structure-activity relationship[25-29]. It provides a very valuable tool for genetic therapy through its RNA-mediated inhibition of gene expression. Hammerhead ribozyme has been used extensively to down-regulate cellular and viral gene expression[30,31], and recognized as a novel molecular therapeutic drug in the treatment of cancer or viral infection.

Apoptosis is essential to the normal development of multicellular organisms as well as physiologic cell turnover. In pathologic states, a failure to undergo apoptosis may cause abnormal cell overgrowth and malignancy, while excessive apoptosis may lead to organ injury. Apoptosis involves the activation of the caspases, which are hallmarks of apoptosis. Central to the execution phase of apoptosis are the two closely related caspase-3 and caspase-7, which share common substrate specificity and structure. Many cellular proteins are cleaved during the execution phase of apoptosis at a D*XX*D motif by the effector caspases-3 and -7. Caspase-3 has been extensively studied as gene therapeutic target. Caspase-7, as another crucial executioner caspase, has been chosen to be the gene therapy target of ribozyme.

In our experiment, we only discovered two sites (333 and 394) in caspase-7 gene suitable for hammerhead ribozymes to cleave, so Rz333 and Rz394 were synthesized and cloned. Caspase-7 gene segment (891 bp) was amplified by RT-PCR from total RNA of mouse liver, and was cloned into an expression plasmid. Ribozymes and substrate were both gained by *in vitro* transcription. The results of cleavage assays indicated that Rz333 could catalyze site-specific cleavage of caspase-7 mRNA, and produced 243-nt and 744-nt cleaved segments, but Rz394 could not cleave the substrate. This might be because the secondary structures of ribozymes and substrate simulated by computer could not reflect the real situation. Rz333 could site-specifically cleave caspase-7 mRNA with a cleavage efficiency of 67.98%. It may prevent apoptosis solely or in association with anti-caspase-3 ribozyme synthesized and selected in our previous study. Rz333 may become a candidate for gene therapy of apoptosis-related diseases.

REFERENCES

1 **Kuida K**, Zheng TS, Na S, Kuan CY, Yang D, Karasuyama H, Rakic P, Flavell RA. Decreased apoptosis in the brain and premature lethality in CPP32-deficient mice. *Nature* 1996; **384**: 368-372

2 **Woo M**, Hakem R, Soengas MS, Duncan GS, Shahinian DK, Hakem A, McCurrach M, Khoo W, Kaufman SA, Senaldi G, Howard T, Lowe SW, Mak TW. Essential contribution of caspase 3/CPP32 to apoptosis and its associated nuclear changes. *Genes Dev* 1998; **12**: 806-809

3 **Zimmermann KC**, Bonzon C, Green DR. The machinery of programmed cell death. *Pharmacol Ther* 2001; **92**: 57-70

4 **Xie Q**, Khaoustov VI, Chung CC, Sohn J, Krishnan B, Lewis DE, Yoffe B. Effect of tauroursodeoxycholic acid on endoplasmic reticulum stress-induced caspase-12 activation. *Hepatology* 2002; **36**: 592-601

5 **Hengartner MO**. The biochemistry of apoptosis. *Nature* 2000; **407**: 770-776

6 **Tozser J**, Bagossi P, Zahuczky G, Specht SI, Majerova E, Copeland TD. Effect of caspase cleavage-site phosphorylation on proteolysis. *Biochem J* 2003; **372**(Pt 1): 137-143

7 **Creagh EM**, Martin SJ. Caspases: cellular demolition experts. *Biochem Soc Trans* 2001; **29**(Pt 6): 696-702

8 **Katoch B**, Sebastian S, Sahdev S, Padh H, Hasnain SE, Begum R. Programmed cell death and its clinical implications. *Indian J Exp Biol* 2002; **40**: 513-524

9 **Ranganath RM**, Nagashree NR. Role of programmed cell death in development. *Int Rev Cytol* 2001; **202**: 159-242

10 **Lin JS**, Song YH, Kong XJ, Li B, Liu NZ, Wu XL, Jin YX. Preparation and identification of anti-transforming growth factor beta1 U1 small nuclear RNA chimeric ribozyme *in vitro*. *World J Gastroenterol* 2003; **9**: 572-577

11 **Langlois MA**, Lee NS, Rossi JJ, Puymirat J. Hammerhead ribozyme-mediated destruction of nuclear foci in myotonic dystrophy myoblasts. *Mol Ther* 2003; **7**(5 Pt 1): 670-680

12 **Hubinger G**, Wehnes E, Xue L, Morris SW, Maurer U. Hammerhead ribozyme-mediated cleavage of the fusion transcript NPM-ALK associated with anaplastic large-cell lymphoma. *Exp Hematol* 2003; **31**: 226-233

13 **Wang H,** Chen XP, Qiu FZ. Overcoming multi-drug resistance by anti-MDR1 ribozyme. *World J Gastroenterol* 2003; **9**: 1444-1449

14 **Sgorbissa A**, Benetti R, Marzinotto S, Schneider C, Brancolini C. Caspase-3 and caspase-7 but not caspase-6 cleave Gas2 *in vitro*: implications for microfilament reorganization during apoptosis. *J Cell Sci* 1999; **112**(Pt 23): 4475-4482

15 **Xu R**, Liu J, Zhou X, Xie Q, Jin Y, Yu H, Liao D. Activity identification of anti-caspase-3 mRNA hammerhead ribozyme in both cell-free condition and BRL-3A cells. *Chin Med J* 2001; **114**: 606-611

16 **Rajpal A**, Turi TG. Intracellular stability of anti-caspase-3 intrabodies determines efficacy in retargeting the antigen. *J Biol Chem* 2001; **276**: 33139-33146

17 **Xu R**, Liu J, Chen X, Xu F, Xie Q, Yu H, Guo Q, Zhou X, Jin Y. Ribozyme-mediated inhibition of caspase-3 activity reduces apoptosis induced by 6-hydroxydopamine in PC12 cells. *Brain Res* 2001; **899**: 10-19

18 **Chandler JM**, Cohen GM, MacFarlane M. Different subcellular distribution of caspase-3 and caspase-7 following Fas-induced apoptosis in mouse liver. *J Biol Chem* 1998; **273**: 10815-10818

19 **Germain M**, Affar EB, D'Amours D, Dixit VM, Salvesen GS, Poirier GG. Cleavage of automodified poly(ADP-ribose) polymerase during apoptosis. Evidence for involvement of caspase-7. *J Biol Chem* 1999; **274**: 28379-28384

20 **Sanceau J**, Hiscott J, Delattre O, Wietzerbin J. IFN-beta induces serine phosphorylation of Stat-1 in Ewing's sarcoma cells and mediates apoptosis via induction of IRF-1 and activation of caspase-7. *Oncogene* 2000; **19**: 3372-3383

21 **Guerrier Takada** C, Altman S. Catalytic activity of an RNA molecule prepared by transcription *in vitro*. *Science* 1984; **223**: 285-286

22 **Cech TR**, Zaug AJ, Grabowski PJ. *In vitro* splicing of the ribosomal RNA precursor of Tetrahymena: involvement of a guanosine nucleotide in the excision of the intervening sequence. *Cell* 1981; **27**(3 Pt 2): 487-496

23 **Cech TR**. The chemistry of self-splicing RNA and RNA enzymes. *Science* 1987; **236**: 1532-1539

24 **Symons RH**. Self-cleavage of RNA in the replication of small pathogens of plants and animals. *Trends Biochem Sci* 1989; **14**: 445-450

25 **Maniotis D**, Wood MJ, Phylactou LA. Hammerhead ribozymes reduce central nervous system (CNS)-derived neuronal nitric oxide synthase messenger RNA in a human cell line. *Neurosci Lett* 2002; **329**: 81-85

26 **Feng Y**, Kong YY, Wang Y, Qi GR. Intracellular inhibition of the replication of hepatitis B virus by hammerhead ribozymes. *J Gastroenterol Hepatol* 2001; **16**: 1125-1130

27 **Koizumi M**, Ozawa Y, Yagi R, Nishigaki T, Kaneko M, Oka S, Kimura S, Iwamoto A, Komatsu Y, Ohtsuka E. Design and anti-HIV-1 activity of hammerhead and hairpin ribozymes containing a stable loop. *Nucleosides Nucleotides* 1998; **17**: 207-218

28 **Hormes R**, Sczakiel G. The size of hammerhead ribozymes is related to cleavage kinetics: the role of substrate length. *Biochimie* 2002; **84**: 897-903

29 **Pley HW**, Flaherty KM, McKay DB. Three-dimensional structure of a hammerhead ribozyme. *Nature* 1994; **372**: 68-74

30 **Scott WG**, Finch JT, Klug A. The crystal structure of an all-RNA hammerhead ribozyme: a proposed mechanism for RNA catalytic cleavage. *Cell* 1995; **81**: 991-1002

31 **Fritz JJ**, Lewin A, Hauswirth W, Agarwal A, Grant M, Shaw L. Development of hammerhead ribozymes to modulate endogenous gene expression for functional studies. *Methods* 2002; **28**: 276-285

Edited by Chen WW **Proofread by** Zhu LH and Xu FM

PO Box 2345, Beijing 100023, China
Fax: +86-10-85381893
E-mail: wjg@wjgnet.com www.wjgnet.com

World J Gastroenterol 2004;10(14):2082-2086
World Journal of Gastroenterology
 ISSN 1007-9327

• BASIC RESEARCH •

Effects of octreotide on acute necrotizing pancreatitis in rabbits

László Czakó, Péter Hegyi, Tamás Takács, Csaba Góg, András Farkas, Yvette Mándy, Ilona Sz. Varga, László Tiszlavicz, János Lonovics

László Czakó, Péter Hegyi, Tamás Takács, Csaba Góg, János Lonovics, First Department of Internal Medicine, University of Szeged, Szeged, Hungary
András Farkas, Second Department of Internal Medicine and Cardiological Center, University of Szeged, Szeged, Hungary
Yvette Mándy, Department of Microbiology, University of Szeged, Szeged, Hungary
Ilona Sz. Varga, Biological Isotope Laboratory, Attila József University, Szeged, Hungary
László Tiszlavicz, Department of Pathology, University of Szeged, Szeged, Hungary
Supported by the grant from the Hungarian Scieutigic Research Found (OTKA No. D34004) the Hungarian Academy of Sciences (BÖ5/2003) and ETT SK503
Correspondence to: Dr. László Czakó M.D.,Ph.D., First Department of Medicine, University of Szeged, Szeged, PO Box 469, H-6701, Hungary. czal@in1st.szote.u-szeged.hu
Telephone: +36-62-545201 **Fax:** +36-62-545185
Received: 2003-12-11 **Accepted:** 2004-01-17

Abstract

AIM: To assess the role of oxygen-derived free radicals and cytokines in the pathogenesis of taurocholic acid-induced acute pancreatitis, and to evaluate the preventive effects of octreotide towards the development of acute pancreatitis.

METHODS: Acute pancreatitis was induced in male New Zealand white rabbits by retrograde injection of 0.8 mL/kg·b.m. of 50 g/L sodium taurocholate (NaTC) in the pancreatic duct. Sham-operated animals served as control. Octreotide 1 mg/kg·b.m. was administered subcutaneously before the induction of pancreatitis. Blood was taken from the jugular vein before and at 1, 3, 6, 12 and 24 h after pancreatitis induction. Serum activities of amylase, IL-6 and TNF-α and levels of malonyl dialdehyde (MDA), glutathione (GSH), glutathione peroxidase (GPx), catalase and superoxide dismutase (Mn-, Cu-, and Zn-SOD) in pancreatic tissue were measured.

RESULTS: Serum TNF-α and IL-6 levels increased significantly 3 h after the onset of pancreatitis, and then returned to control level. The tissue concentration of MDA was significantly elevated at 24 h, while the GSH level and GP-x, catalase, Mn-SOD, Cu-, Zn-SOD activities were all significantly decreased in animals with pancreatitis as compared to the control. Octreotide pretreatment significantly reversed the changes in cytokines and reactive oxygen metabolites. Octreotide treatment did not alter the serum amylase activity and did not have any beneficial effects on the development of histopathological changes.

CONCLUSION: Oxygen-derived free radicals and proinflammatory cytokines are generated at an early stage of NaTc-induced acute pancreatitis in rabbits. Prophylactic octreotide treatment can prevent release of cytokines and generation of reactive oxygen metabolites, but does not have any beneficial effects on the development of necrotizing pancreatitis.

Czakó L, Hegyi P, Takács T, Góg C, Farkas A, Mándy Y, Varga IS, Tiszlavicz L, Lonovics J. Effects of octreotide on acute necrotizing pancreatitis in rabbits. *World J Gastroenterol* 2004; 10(14): 2082-2086
http://www.wjgnet.com/1007-9327/10/2082.asp

INTRODUCTION

Acute pancreatitis is clinically classified into mild and severe forms. Mild or edematous acute pancreatitis is a self-limiting disease with a low complication and mortality rate. However, severe necrotizing pancreatitis has an unacceptably high morbidity and mortality rate. Multiple therapeutic modalities have been suggested for acute pancreatitis, but none has been unambiguously proven to be effective yet. The major problem is that the pathophysiology of the disease is not fully understood and hence, there is no specific casual treatment yet. The treatment of acute pancreatitis to date is essentially supportive[1-3].

Theories on the pathogenesis of acute pancreatitis suggest that autodigestion of the gland and peripancreatic tissues by activated digestive enzymes is a key component[4,5]. Furthermore, stimulation of exocrine pancreatic secretion in experimental acute pancreatitis has been demonstrated to worsen the disease. Prevention of release and activation of enzymes by inhibition of pancreatic exocrine secretion has been therefore suggested as a specific treatment. Somatostatin and its long-acting analogue octreotide are potent inhibitors of pancreatic secretion[6, 7]. The efficacy of somatostatin and octreotide in the management of acute pancreatitis has been studied for decades, yet the data still remain inconclusive. Some experimental[8,9] and clinical[10] studies have shown beneficial results, but others[11-14] demonstrated no benefit[15,16].

Somatostatin and octreotide increase the tone of the sphincter of Oddi, which can be reversed by administration of glyceryl trinitrate[17,18]. Furthermore, octreotide may trigger acute pancreatitis and worsen the disease[19].

We studied the effects of octreotide on necrotizing pancreatitis in rabbits. In these animals the pancreatic duct enters the duodenum at its distal part, and is completely separated from the common bile duct. Therefore, we can exclude the effect of octreotide on the sphincter of Oddi. The present study was to assess the roles of oxygen-derived free radicals and cytokines in the pathogenesis of taurocholic acid-induced acute pancreatitis, and to evaluate the preventive effects of octreotide on the development of acute pancreatitis.

MATERIALS AND METHODS

Animals

New Zealand white rabbits weighing 2.5-3.5 kg were used. The animals were kept at a constant room temperature of 27 ℃, and had free access to water and a standard laboratory chow [LATI, Gödöllö, Hungary]. The experimental protocol followed the principles of Laboratory Animal Care of the National Institute of Health, USA.

Experimental protocol

Overnight fasted animals were anesthetized with an intravenous

injection of pentobarbital 20 mg/kg and urethane 1 g/kg, and supplemented when needed. Four groups of animals were prepared through a midline incision; the pancreatic duct was cannulated transduodenally with a polyvinyl catheter. Acute pancreatitis was induced by retrograde intraductal infusion of 0.8 ml/kg· b.m. of 50 g/L sodium taurocholate (NaTc) (Reanal, Budapest) dissolved in 0.15 mol/L NaCl under steady manual pressure over a period of 30 s (Group I)[20]. After infusion the catheter was removed, and the abdomen was closed in two layers. In control animals, laparotomy was performed with visualization of the pancreatic duct before closure of the abdomen [Group II]. Animals in which pancreatitis was induced by administration of NaTc were injected subcutaneously with 1 mg/kg· b.m. octreotide (SANDOSTATIN Novartis, Basel, Switzerland) before pancreatitis induction (Group III). In Group IV animals were treated with saline before induction of pancreatitis. The body temperatures and weights of the animals were measured every 6 h. Blood was taken from the jugular vein before and at 1, 3, 6, 12 and 24 h after pancreatitis induction. Physiologic saline was injected into the jugular vein during the experiment in order to avoid severe hypovolemia. Twenty-four hours after the abdominal operation, the animals were sacrificed by aorta exsanguination. The pancreas was removed.

Assays

Serum amylase activity was measured by the Phadebas test method[21]. TNF-α levels were titrated in a bioassay on the WEHI-164 cell line[22]. IL-6 concentrations were measured via their proliferative action on the IL-6-dependent mouse hybridoma cell line B-9[23]. The activities were calibrated against recombinant TNF [Genzyme, Cambridge, UK] and recombinant IL-6 [Sigma-Aldrich, Munich, Germany].

The pancreata were homogenized. The homogenates were centrifuged at 3 000 r/min for 10 min and the supernatants were used for measurements.

Lipid peroxide MDA level was measured after reaction with thiobarbituric acid, according to the method of Placer *et al*.[24], and was corrected for the protein content of the tissue.

Superoxide dismutase (SOD) activity was determined on the basis of the inhibition of epinephrine-adrenochrome autoxidation[25]. Mn-SOD activity was measured by the autoxidation method in the presence of 5×10^{-3} mol/L KCN[26]. Cu-, Zn-SOD activity resulted from the deduction of Mn-SOD from SOD activity.

Catalase activity was determined spectrophotometrically at 240 nm by the method of Beers *et al*.[27] and expressed in Bergmeyer units (BU) (1 BU=decomposition of 1 g H_2O_2/min at 25 ℃).

Glutathione (GSH) level was measured spectrophotometrically with Ellman' s reagent from the supernatant, and was corrected for the protein content of the tissue[28]. Glutathione peroxidase (GPx) activity was determined according to the ' chemical' method, using cumene hydroperoxide and reduced GSH as substrates of GPx[29].

Protein concentration of the pancreatic tissue was determined by the method of Lowry *et al*.[30].

Histologic examination

A portion of the pancreas was fixed overnight in a 6% neutral formaldehyde solution and embedded in paraffin. Tissue slices were subjected to hematoxylin and eosin staining and histologic study by light microscopy. Slides were coded and examined blind by the pathologist for the grading of histologic alterations. Grading of intestinal edema, vacuolization, inflammation, hemorrhage and acinar cell necrosis was performed on a scale of 1 to 4.

Statistical analysis

Results are expressed as mean±SE. Experiments were evaluated statistically with two-way analysis of variance (ANOVA). *P* value less than 0.05 was statistically significant.

RESULTS

Seven animals died (2 within 1 h, 3 at 1 h, and 2 at 6 h after pancreatitis induction). Two of them were in the octreotide pretreatment (Group III), 2 in the saline pretreatment (Group IV), and 3 in the acute pancreatitis group (Group I). Thus, the results were the data on the surviving 32 animals (8 rabbits in each group). The results of Group III did not statistically differ from those of Group IV, therefore they were not depicted in figures and tables.

The body weights of the animals in the 3 groups did not change significantly during the experiments, indicating that the parenteral fluid supplementation during the observation period was sufficient.

The serum amylase activity was already increased significantly at 1 h, and increased gradually up to 24 h after the induction of pancreatitis in Group I as compared with the control group (5 678±881 *vs* 517±99 U/L) (Figure 1). Pretreatment of pancreatitic animals with octreotide (Group III) did not alter the serum amylase activity as compared with Group I at any time point. Since the amylase, TNF-α and IL-6 levels in Group IV did not differ significantly from those in Group III, they were not shown.

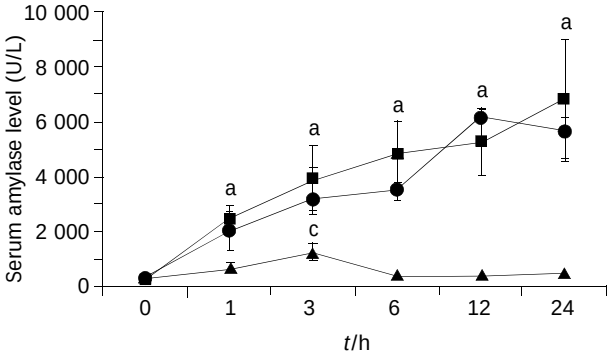

Figure 1 Effects of octreotide on serum amylase levels in rabbits with NaTc-induced acute pancreatitis. Group I: ●; Group II as control: ▲; Group III treated with octreotide: ■. $^aP<0.05$ *vs* Group II; $^cP<0.05$ *vs* Group I.

The serum TNF-α level increased significantly 3 h after the onset of pancreatitis in Group I (3 120±340 *vs* 85±15 U/L in Group II), and returned to the control level by 6 h (Figure 2). There was no significant serum TNF-α level elevation in the octreotide treated group.

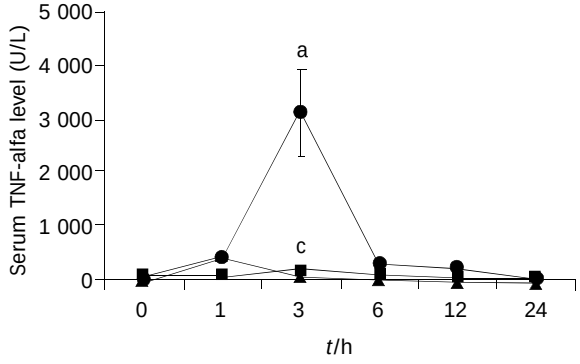

Figure 2 Effects of octreotide on serum TNF-α levels in rabbits with NaTc-induced acute pancreatitis. Group I:●; Group II as control: ▲; Group III treated with octreotide: ■. $^aP<0.05$ *vs* Group II; $^cP<0.05$ *vs* Group I.

Table 1 Effects of octreotide on pancreatic level of MDA and endogenous scavengers in rabbits with NaTc-induced acute pancreatitis

	Control	NaTc	NaTc+octreotide
MDA (nmol / mg protein)	2.24±0.51	7.52±1.05[a]	4.14±0.86[a,c]
GSH (nmol / mg protein $\times 10^{-2}$)	2.76±0.45	1.68±0.24[a]	2.23±0.48[a,c]
GPx (U / mg protein $\times 10^{-2}$)	1.18±0.34	0.53±0.08[a]	0.82±0.16[a,c]
Catalase (U / mg protein $\times 10^{-4}$)	3.08±0.54	2.79±0.41[a]	3.16±0.14[a,c]
Mn-SOD (U / mg protein)	1.03±0.22	0.43±0.08[a]	0.53±0.08[a]
Zn-,Cu-SOD (U / mg protein)	4.96±0.76	3.34±0.56[a]	4.12±0.84[a,c]

[a]$P<0.05$ *vs* control group; [c]$P<0.05$ *vs* NaTc treated group.

Table 2 Effects of octreotide on histologic score in rabbits with NaTc-induced acute pancreatitis

Group	Vacuolization	Edema	Necrosis	Inflammation	Congestion
Control	0	0	0	0	0
NaTc	1.12±0.16	2.00±0.35	2.37±0.42	3.15±0.48	1.57±0.33
NaTc+ somatostatin	1.57±0.45	2.14±0.32	2.43±0.58	3.05±0.36	1.50±0.25

The serum IL-6 level increased significantly 3 h after the onset of pancreatitis in Group I (690±88 *vs* 25±15 U/L in Group II), and returned to the control level by 24 h (Figure 3). Octreotide pretreatment attenuated the increase in IL-6 level throughout the study.

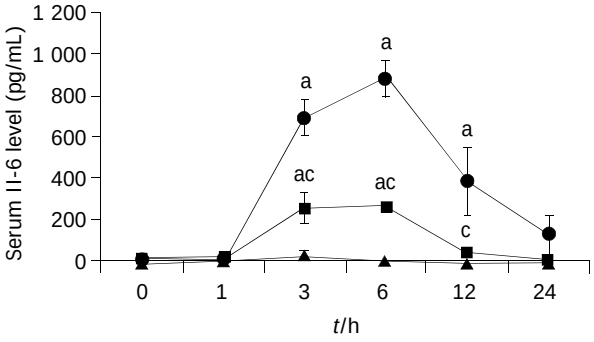

Figure 3 Effects of octreotide on serum IL-6 levels in rabbits with NaTc-induced acute pancreatitis. Group I: ●; Group II as control: ▲; Group III treated with octreotide: ■. [a]$P<0.05$ *vs* Group II; [c]$P<0.05$ *vs* Group I.

The tissue concentration of MDA was elevated significantly at 24 h as compared to the control. Octreotide pretreatment prevented the increase in MDA level. The GSH level and the activities of endogenous scavengers (GPx, catalase, Mn-SOD and Cu-, Zn-SOD) were all decreased significantly in pancreatitis animals in comparison with the control. Octreotide treatment significantly reversed the decrease of GPx, catalase and Cu-, Zn-SOD, but not Mn-SOD activity in comparison with Group I (Table 1).

Histological examination revealed acinar cell necrosis, hemorrhage, inflammatory cell infiltration and edema. Octreotide pretreatment did not exert any beneficial effect on the histological score (Table 2).

DISCUSSION

The results of our study can be summarized as follows. In our model, a short-lasting infusion of taurocholic acid in the pancreatic duct of rabbits produced a rapidly evolving necrotizing pancreatitis with mortality, as described earlier[20]. Proinflammatory cytokines were generated early in NaTc-induced acute pancreatitis. Tissue imbalance of the offense system represented by MDA and the defense system represented by GSH, SOD, GPx and catalase was observed. Prophylactic octreotide treatment prevented the release of cytokines, the increase in MDA and the decrease in GSH, SOD, GPx and catalase activities, but did not reduce the serum amylase level, and did not have beneficial effects on the development of histopathological changes.

Oxygen-derived free radicals have been reported to play an important role in the pathogenesis of acute pancreatitis[31,32]. In the present study, oxidative stress was assessed by measuring the MDA, a product of lipid peroxidation, the intracellular antioxidant GSH, and the endogenous scavengers SOD, GPx and catalase in pancreatic tissues, in order to elucidate the participation of free radicals in the process of NaTc-induced pancreatitis in rabbits. In agreement with previous studies made in other animals[31,32], this study revealed that the elevation of MDA as an offense system, and lowered GSH, SOD, GPx and catalase activities as a defense system, might be one cause of pancreatic injury induced by NaTc in rabbits.

Published data suggest that activated pancreatic macrophages can release proinflammatory cytokines in response to local tissue damages. These cytokines may act locally to aggravate acute pancreatitis, and both locally and systemically to increase the capillary permeability and to promote leukocyte adherence and extravasation[33, 34]. TNF-α, a major proinflammatory cytokine, is considered to be important in orchestrating the early events in the inflammatory cascade and contributes to the induction of systemic inflammatory response syndrome (SIRS) which is responsible for multiple organ failure in severe acute pancreatitis. IL-6 is the most potent inductor of acute-phase protein synthesis in the liver, and it has been shown that its level reflects the severity of acute pancreatitis[35]. This study confirmed the observations of others in rabbits that TNF-α and IL-6 were released in the early phase of NaTc-induced pancreatitis.

There is a growing evidence that somatostatin could inhibit the production of different cytokines, especially TNF-α and IL-6[36-38] and reduce the local generation of free radicals[39]. Nuclear factor-κB (NF-κB) plays a pivotal role in inducing the expression of multiple genes involved in immune and inflammatory responses, such as cytokines. NF-κB transcription pathway has been found to be activated by reactive oxygen species[39]. Therefore, somatostatin may also reduce indirectly the production of cytokines by inhibiting the generation of reactive oxygen metabolites. Furthermore, somatostatin could exert a direct cyto- and organoprotective

action in several models of toxic organ injury and stimulate on the reticulo-endothelial system[40-43].

In our study, octreotide completely reversed the pancreatitis-induced changes in cytokines, MDA, GSH, SOD, GPx and catalase activities. However, we were unable to detect a significant improvement both in the serum amylase level and in the histologic score in octreotide-treated group. This could be explained by severe chemical and mechanical destruction of the pancreatic gland induced by taurocholic acid. The severity of this local injury exceeded the pancreatic damage induced by inflammatory mediators. Overproduction of cytokines can lead to the development of SIRS, which is responsible for the mortality of the disease. However, reduction of cytokine production in octreotide-treated group did not result in a significant decrease in the morbidity or mortality. This suggests that liberation of other vasoactive and toxic mediators [e.g. phospholipase A2, platelet activating factor, nitric oxide, leukotrienes *etc*] by the necrotizing process plays an essential role in the development of SIRS. Therefore, blockade of one particular part of this complex inflammatory process is not beneficial.

Octreotide has been suggested for the treatment of acute pancreatitis on the basis of its inhibitory effect on pancreato-biliary secretion. However, a number of experimental studies have demonstrated that pancreatic enzyme secretion is almost abolished after induction of acute pancreatitis[44-46]. Therefore, the use of drugs inhibiting exocrine pancreatic secretion does not have a beneficial effect on the progression and outcome of the disease. In contrast, the basal pancreatic fluid secretion was greatly increased during the early stages of acute experimental pancreatitis[45, 46]. This fluid hypersecretion was resistant to cholecystokinin, secretin and cholinergic antagonists, and was probably caused by acinar cell proliferation[46]. Fluid hypersecretion can wash out inflammatory mediators and activated pancreatic enzymes from the pancreas, thereby serving as a natural host protective mechanism after a pancreatic injury. Accordingly, it seems unnecessary to attempt to suppress the basal pancreatic enzyme secretion further since it is already blocked. If the fluid hypersecretion is interrupted after the onset of acute pancreatitis, this might exacerbate the inflammatory process.

Furthermore, somatostatin could reduce splanchnic blood flow and the impairment of pancreatic microcirculation could lead to further deterioration in acute pancreatitis[47, 48].

Octreotide might worsen acute pancreatitis and even cause the disease by increasing the contractility of the sphincter of Oddi[18,19]. The most commonly used animals to study the effects of octreotide in acute pancreatitis were rats, whereas rabbits have never been used. However, rabbits seem to be the excellent animals for this research. Since the pancreatic duct enters the duodenum at its distal part, and is completely separated from the common bile duct, we may avoid the harmful effect of octreotide on the sphincter of Oddi. However, we can not exclude the effect of octreotide on pancreatic sphincter.

In conclusion, proinflammatory cytokines are generated early in NaTc-induced acute pancreatitis in rabbits. Tissue imbalance of the offense system represented by MDA and the defense system represented by GSH, SOD, GPx and catalase was detected in the pancreas. Prophylactic octreotide treatment can prevent the release of cytokines, the increase in MDA and the decrease in GSH, SOD, GPx and catalase activities, but does not have any beneficial effects on the development of necrotizing pancreatitis. The pancreatic duct injection model in rabbit is a useful model to exclude the effect of sphincter of Oddi on the course of acute pancreatitis.

REFERENCES

1 **Yousaf M,** McCallion K, Diamond T. Management of severe acute pancreatitis. *Br J Surg* 2003; **90**: 407-420

2 **Banks PA.** Practice guidelines in acute pancreatitis. *Am J Gastroenterol* 1997; **92**: 377-386

3 Conservative therapeutic concepts in acute pancreatitis. In: Büchler MW, Uhl W, Friess H, Malfertheiner P eds. Acute pancreatitis. Novel concepts in biology and therapy. *Berlin: Blackwell* 1999: 291-344

4 **Saluja AK**, Steer MLP6. Pathophysiology of pancreatitis. Role of cytokines and other mediators of inflammation. *Digestion* 1999; **60**(Suppl 1): 27-33

5 Primary events in the initiation of acute pancreatitis. In: Büchler MW, Uhl W, Friess H, Malfertheiner P eds. Acute pancreatitis. Novel concepts in biology and therapy. *Berlin Blackwell* 1999: 1-48

6 **Robberecht P**, Deschodt-Lanckman M, De Neef P, Christophe J. Effects of somatostatin on pancreatic exocrine function. Interaction with secretin. *Biochem Biophys Res Commun* 1975; **67**: 315-323

7 **Guan D**, Maouyo D, Sarfati P, Morisset J. Effects of SMS 201-995 on basal and stimulated pancreatic secretion in rats. *Endocrinology* 1990; **127**: 298-304

8 **Baxter JN**, Jenkins SA, Day DW, Roberts NB, Cowel DC, Mackie CR, Shields R. Effects of somatostatin and a long-acting somatostatin analogue on the prevention and treatment of experimentally induced acute pancreatitis in the rat. *Br J Surg* 1985; **72**: 382-385

9 **Kaplan O**, Kaplan D, Casif E, Siegal A, Paran H, Graf E, Skornick Y. Effects of delayed administration of octreotide in acute experimental pancreatitis. *J Surg Res* 1996; **62**: 109-117

10 **Choi TK**, Mok F, Zhan WH, Fan ST, Lai EC, Wong J. Somatostatin in the treatment of acute pancreatitis: a prospective randomised controlled trial. *Gut* 1989; **30**: 223-227

11 **Lankisch PG**, Koop H, Winckler K, Folsch UR, Creutzfeldt W. Somatostatin therapy of acute experimental pancreatitis. *Gut* 1977; **18**: 713-716

12 **Murayama KM**, Drew JB, Joehl RJ. Does somatostatin analogue prevent experimental acute pancreatitis? *Arch Surg* 1990; **125**: 1570-1572

13 **McKay C**, Baxter J, Imrie C. A randomized, controlled trial of octreotide in the management of patients with acute pancreatitis. *Int J Pancreatol* 1997; **21**: 13-19

14 **Uhl W**, Buchler MW, Malfertheiner P, Beger HG, Adler G, Gaus W. A randomised, double blind, multicentre trial of octreotide in moderate to severe acute pancreatitis. *Gut* 1999; **45**: 97-104

15 **Greenberg R**, Haddad R, Kashtan H, Kaplan O. The effects of somatostatin and octreotide on experimental and human acute pancreatitis. *J Lab Clin Med* 2000; **135**: 112-121

16 **Uhl W**, Anghelacopoulos SE, Friess H, Buchler MW. The role of octreotide and somatostatin in acute and chronic pancreatitis. *Digestion* 1999; **60**(Suppl 2): 23-31

17 **Di Francesco V**, Angolini G, Bovo P, Casarini MB, Filippini M, Vaona B, Frulloni L, Rigo L, Brunori MP, Cavallini G. Effects of octreotide on sphincter of Oddi motility in patients with acute recurrent pancreatitis: a manometric study. *Dig Dis Sci* 1996; **41**: 2392-2396

18 **Velosy B**, Madácsy L, Szepes A, Pavics L, Csernay L, Lonovics J. The effects of somatostatin and octreotide on the human sphincter of Oddi. *Eur J Gastroenterol Hepatol* 1999; **11**: 897-901

19 **Bodemar G**, Hjortswang H. Octreotide-induced pancreatitis: an effect of increased contractility of Oddi sphincter. *Lancet* 1996; **348**: 1668-1669

20 **Gyongyosi M**, Takacs T, Czako L, Jambrik Z, Boda K, Farkas A, Forster T, Csanady M. Noninvasive monitoring of hemodynamic changes in acute pancreatitis in rabbits. *Dig Dis Sci* 1997; **42**: 955-961

21 **Ceska M,** Birath K, Brown B. A new and rapid method for the clinical determination of alpha-amylase activities in human serum and urine optimal conditions. *Clin Chem Acta* 1969; **26**: 437-444

22 **Espevik T**, Niessen-Meyer J. A highly sensitive cell line, WEHI 164 clone 13, for measuring cytotoxic factor / tumor necrosis factor from human monocytes. *J Immunol Methods* 1986; **95**: 99-105

23 **Aarden LA**, De Groot ER, Schaap OL, Lansdorp PM. Production of hybridoma growth factor by human monocytes. *Eur J Immunol* 1987; **17**: 1411-1416

24 **Placer ZA**, Cushman L, Johnson BC. Estimation of product of lipid peroxidation [malonyl dialdehyde] in biochemical systems. *Anal Biochem* 1966; **16**: 359-364

25 **Misra HP**, Fridovich I. The role of superoxide anion in the autoxidation of epinephrine and a simple assay for superoxide dismutase. *J Biol Chem* 1972; **247**: 3170-3175

26 **Beauchamp C**, Fridovich I. Superoxide dismutase: Improved assays and an assay applicable to acrylamide gels. *Anal Biochem* 1971; **44**: 276-287

27 **Beers RF Jr**, Sizer IW. A spectrophotometric method for measuring the breakdown of hydrogen peroxide by catalase. *J Biol Chem* 1952; **195**: 133-140

28 **Sedlak J**, Lindsay RH. Estimation of total, protein-bound, and nonprotein sulfhydryl groups in tissue with Ellman's reagent. *Anal Biochem* 1968; **25**: 192-205

29 **Chiu DT**, Stults FH, Tappel AL. Purification and properties of rat lung soluble glutathione peroxidase. *Biochim Biophys Acta* 1976; **445**: 558-566

30 **Lowry OH**, Rosenbrough NJ, Farr AL, Randall RJ. Protein measurement with the folin phenol reagent. *J Biol Chem* 1951; **193**: 265-275

31 **Schoenberg MH**, Birk D, Beger HG. Oxidative stress in acute and chronic pancreatitis. *Am J Clin Nutr* 1995; **62**(6 Suppl): 1306S-1314S

32 **Sweiry JH**, Mann GE. Role of oxidative stress in the pathogenesis of acute pancreatitis. *Scand J Gastroenterol Suppl* 1996; **219**: 10-15

33 **Norman JG**, Fink GW, Denham W, Yang J, Carter G, Sexton C, Falkner J, Gower WR, Franz MG. Tissue-specific cytokine production during experimental acute pancreatitis. A probable mechanism for distant organ dysfunction. *Dig Dis Sci* 1997; **42**: 1783-1788

34 **Norman J**. The role of cytokines in the pathogenesis of acute pancreatitis. *Am J Surg* 1998; **175**: 76-83

35 **Leser HG**, Gross V, Scheibenbogen C, Heinisch A, Salm R, Lausen M, Ruckauer K, Andreesen R, Farthmann EH, Scholmerich J. Elevation of serum interleukin-6 concentration precedes acute-phase response and reflects severity in acute pancreatitis. *Gastroenterology* 1991; **101**: 782-785

36 **Peluso G**, Petillo O, Melone MA, Mazzarella G, Ranieri M, Tajana GF. Modulation of cytokine production in activated human monocytes by somatostatin. *Neuropeptides* 1996; **30**: 443-451

37 **Karalis K**, Mastorakos G, Chrousos GP, Tolis G. Somatostatin analogues suppress the inflammatory reaction *in vivo*. *J Clin Invest* 1994: **93**: 2000-2006

38 **Balibrea JL**, Arias-Diaz J, Garcia C, Vara E. Effect of pentoxifylline and somatostatin on tumour necrosis factor production by human pulmonary macrophages. *Circ Shock* 1994: **43**: 51-56

39 **Arias-Diaz J**, Vara E, Torres-Melero J, Garcia C, Hernandez J, Balibrea JL. Local production of oxygen free radicals and nitric oxide in rat diaphragm during sepsis: effects of pentoxifylline and somatostatin. *Eur J Surg* 1997; **163**: 619-625

40 **Kim H**, Seo JY, Roh KH, Lim JW, Kim KH. Suppression of NF-kappaB activation and cytokines production by N-acetylcysteine in pancreatic acinar cells. *Free Radic Biol Med* 2000; **29**: 674-683

41 **Usadel KH**, Schwedes U, Wdowinski JM. Pharmacological effects of somatostatin in acute organ lesions. *Inn Med* 1982; **9**: 204-209

42 **Baxter JN**, Jenkins SA, Day DW, Shields R. Effects of a somatostatin analogue (SMS 201-995) on hepatic and splenic reticuloendothelial function in the rat. *Br J Surg* 1985; **72**: 1005-1008

43 **Eliakim R**, Karmeli F, Okon E, Rachmilewitz D. Octreotide effectively decreases mucosal damage in experimental colitis. *Gut* 1993; **34**: 264-269

44 **Niederau C**, Niederau M, Luthen R, Strohmeyer G, Ferrell LD, Grendell JH. Pancreatic exocrine secretion in acute experimental pancreatitis. *Gastroenterology* 1990; **99**: 1120-1127

45 **Manso MA**, San Roman JI, de Dios I, Garcia LJ, Lopez MA. Cerulein-induced acute pancreatitis in the rat. Study of pancreatic secretion and plasma VIP and secretin levels. *Dig Dis Sci* 1992; **37**: 364-368

46 **Czako L**, Yamamoto M, Otsuki M. Pancreatic fluid hypersecretion in rats after acute pancreatitis. *Dig Dis Sci* 1997; **42**: 265-272

47 **Sonnenberg GE**, Keller U, Purruchud A, Burckhardt D, Gyr K. Effect of somatostatin on splanchnic hemodynamics in patients with cirrhosis of the liver and in normal subjects. *Gastroenterology* 1981; **80**: 526-532

48 **Schroder T**, Millard RW, Nakajima Y, Gabel M, Joffe SN. Microcirculatory effects of somatostatin in acute pancreatitis. *Eur Surg Res* 1988; **20**: 82-88

Edited by Wang XL and Chen WW **Proofread by** Xu FM

PO Box 2345, Beijing 100023, China
Fax: +86-10-85381893
E-mail: wjg@wjgnet.com www.wjgnet.com

World J Gastroenterol 2004;10(14):2087-2090
World Journal of Gastroenterology
 ISSN 1007-9327

• BASIC RESEARCH •

Changes of gut flora and endotoxin in rats with D-galactosamine-induced acute liver failure

Lan-Juan Li, Zhong-Wen Wu, Dang-Sheng Xiao, Ji-Fang Sheng

Lan-Juan Li, Zhong-Wen Wu, Dang-Sheng Xiao, Ji-Fang Sheng, Department of Infectious Diseases, First Affiliated Hospital, College of Medicine, Zhejiang University, Hangzhou 310003, Zhejiang Province, China
Supported by the Foundation for Medical Research of Zhejiang Educational Bureau, No. 491010-G20252 and partially by National Basic Research Program of China, No. 2003CB515506
Correspondence to: Dr. Lan-Juan Li, Department of Infectious Diseases, First Affiliated Hospital, College of Medicine, Zhejiang University, 79 Qingchun Road, Hangzhou 310003, Zhejiang Province, China. ljli@mail.hz.zj.cn
Telephone: +86-571-87709001 **Fax:** +86-571-87236755
Received: 2003-11-17 **Accepted:** 2004-01-08

Abstract

AIM: To investigate the changes of gut microflora and endotoxin levels in rats with acute liver failure (ALF) induced by D-galactosamine (GalN).

METHODS: Flora and endotoxin levels in the jejunum, ileum and colon in normal rats (group A) and rats with GalN - induced ALF were determined at 24 h (group B) or 48 h (group C) after GalN injection, as well as the endotoxin level in portal venous blood (PVB) and right ventricle blood (RVB) were determined by chromogenic limulus amoebocyte assay.

RESULTS: Intestinal (jejunum, ileum, colon) *lactobacillus* count was statistically reduced in group B compared with those in group A (3.4±0.3 *vs* 4.9±0.3, 6.1±0.4 *vs* 8.0±0.3, 8.1±0.2 *vs* 9.3±0.2, $P<0.001$, $P<0.001$ and $P<0.001$ respectively) and recovered partially in the group C compared with those in the group B, whereas the count of *Enterobacteriaceae* in the jejunum, ileum and colon in group B was increased markedly compared with those in the group A (5.1±0.3 *vs* 3.6±0.2, 6.9±0.5 *vs* 5.3±0.3, 8.7±0.2 *vs* 7.6±0.1, $P<0.001$, $P<0.05$ and $P<0.05$ respectively) and restored partially in the group C compared with those in the group B. The endotoxin level in ileum was increased in the group B compared with those in the group A (111.3±22.8 *vs* 51.5±8.9, $P<0.05$). In addition, the endotoxin level in PVB was obviously increased in group B compared with that in the group A (76.8±9.1 *vs* 40.6±7.3, $P<0.01$) and reduced to the baseline at 48 h (group C).

CONCLUSION: Severely disturbed gut flora in rats with GalN-induced acute liver failure plays an important role in the elevation of endotoxin level in PVB.

Li LJ, Wu ZW, Xiao DS, Sheng JF. Changes of gut flora and endotoxin in rats with D-galactosamine-induced acute liver failure. *World J Gastroenterol* 2004; 10(14): 2087-2090
http://www.wjgnet.com/1007-9327/10/2087.asp

INTRODUCTION

Patients with acute liver failure are prone to occurrence of endotoxemia[1], which is usually associated with Gram-negative infection. However, previous studies have showed that some patients with acute liver failure have a high level of endotoxin without clinical evidences of Gram-negative bacterial infection[1,2]. Recent studies have proposed that the elevation of plasma endotoxin is related to the translocation of endotoxin from the gut[3,4].

Gut contains numerous endotoxin, about 90% of which is released by aerobic Gram-negative bacteria, especially the family of enterobacteriaceae[5]. Normally, intestinal anaerobic flora such as *Bifidobacterium* and *Bacteriodes* can prevent the adherence of potential pathogenic enteric bacilli and limit bacterial overgrowth by occupying the space closest to intestinal epithelial cells[6], which is called microbial colonization resistance[7]. Disrupted gut flora observed in severely disease, such as hepatic cirrhosis and hemorrhagic shock, resulted in decrease of microbial colonization resistance and subsequent bacterial overgrowth[8,9]. Wang *et al*.[10] showed the *Escherichia coli* overgrowth in the distal small intestine from 1 h onward after hepatectomy. Researchers suggested that impaired components of the gut barrier, including normal intestinal microflora, could translocate both endotoxin and bacteria from lumen to circulation or other distant organs[6]. Moreover, manipulating gut contents with lactulose or neomycin sulfate with cefazolin could reduce the level of endotoxemia and enhance the survival of rat receiving partial hepatectomy[11]. But to the author's knowledge, the relationship between the changes of gut flora and the fluctuations of the endotoxin levels both in intestine and plasma in rats with GalN-induced acute liver failure has not been reported. In the present study, the changes of gut flora and endotoxin level in the jejunum, ileum and colon, as well as the levels of endotoxin in PVB and RVB of rats with GalN-induced ALF were estimated at various time points.

MATERIALS AND METHODS

Animals and treatment

Male Sprague-Dawley rats weighing about 200-300 g provided by Zhejiang Academy of Medical Sciences, Hangzhou, China, were acclimated to the animal laboratory for 5 d before experiments. They were fed with standard rat chow and water *ad libitum*. All procedures were approved by the Institutional Review Board according to the Animal Protection Act of China.

Acute liver failure in the rats was induced according to the protocol described previously[12]. Briefly, GalN (Chongqing Medical University, Chongqing, China) was dissolved in 0.5 mL of saline and adjusted to pH 6.8 with 1 mol/L NaOH. Then, 20 rats were intraperitoneally given 1.4 g/kg GalN twice at a 12-h interval, and fed with food and water after injection. Since the highest mortality of GalN-induced acute liver failure in rat is between 24 h and 48 h after drug administration[12], and we ensure that the number of survival rat is more than 9[13] at various time points after GalN administration, 40 rats were randomly divided into 3 groups according to the reported mortality[12]: group A with 10 rats without administration of GalN was chosen as normal control, group B with 12 rats that were sacrificed 24 h after GalN injection and group C with 18 rats that were killed at

48 h after injection. Under light ether anesthesia and aseptic conditions, plasma was separated from the portal vein and right ventricle at various time points after laparotomy, then stored immediately at –80 ℃ for analysis of endotoxin. The rats were killed by anaesthetic overdose after blood sampling, the segments of the jejunum, ileum and colon were removed as described by Wang *et al*[10]. Briefly, the segments of the jejunum (5 cm in length, including intestinal wall) and ileum including intestinal wall 5 cm long as well as colon contents were immediately collected from the proximal intestine (5 cm distal of the ligament of Treitz), distal small intestine (5 cm proximal to the ileocecal valve), and descending colon, respectively. After weighting, the samples were placed in pyrogen-free saline (1:9 w/v) in an anaerobic chamber (Forma Scientific Co, USA), mixed by a vortex mixer, and aliquots of 1 mL of mixture were subsequently put into anaerobic solution A (1:9 v/v, decimal dilutions up to 10^{-8}). The remnant was kept at -80 ℃ for detecting endotoxin.

Gut flora analysis

The specimens were cultured within 30 min after collection by modified Mitsuoka's method [14]. A total volume of 50 μL of the serial dilution (10^{-1}, 10^{-3}, 10^{-5}, 10^{-6}, 10^{-7}, 10^{-8}) was spread on 3 non-selective agar media: glucose blood liver (BL) (Nissui Pharmcy Co., Tokyo, Japan) agar with 60 mL/L defibrinated sheep blood for all lactic acid-producing bacteria; Eggerth Gagnon (EG) (Nissui Pharmcy Co.) agar with 60 mL/L defibrinated sheep blood for most obligate and facultative anaerobes; and trypticase soy (TS) agar (BioMerieux, Paris, France) with 60 mL/L defibrinated sheep blood for all aerobes and facultative anaerobes, and 4 selective agar media: neomycin sulfate-brilliant green-taurocholate-blood (NBGT) agar prepared with EG agar at our laboratory for members of the family *Bacteriodaceae*; MRS with vancomycin and bromocresol green (LAMVAB) medium [15] for *Lactobacillus sp*.; eosin methylene blue (EMB) agar (Hangzhou microbiological Co., Hangzhou, China) for members of the family of *Enterobacteriaceae*; and *Enterococcus* (Ec) agar prepared at our laboratory for *Enteroococcus sp*. The plates for the recovery of obligate anaerobes were incubated in an anaerobic chamber (N_2:CO_2:H_2=8:1:1) at 37 ℃ for 48-72 h. The media used for the isolation of aerobes and facultative species were incubated in air for 48 h at 37 ℃. After incubation, morphologically distinct colonies were enumerated, isolated and identified. Identification was performed in most cases at family or genus levels using standard bacteriologic techniques [16]. In our study, the lowest detection limit was 2×10^2 organisms per gram of the samples. The results were expressed as the log10 of the number of bacteria per gram weight of the samples.

Chromogenic limulus amoebocyte assay for detecting endotoxin

Intestinal specimens were prepared for endotoxin detection according to the described method[5]. The frozen specimens were thawed at room temperature. Limulus quantitative azo color (LQAC) test[17] with limulus lysate reagent (Eihua Medical Co, Shanghai, China) was used.

Statistical analysis

Data were expressed as the mean±SE. One-way ANOVA was used to compare gut flora data among individual groups. Frequency data were compared using Chi-square test or the Fisher's exact test when necessary. $P<0.05$ was considered statistically significant.

RESULTS

Degree of hepatic injury and mortality

To study the alterations in intestinal microflora and its relationship with plasma endotoxin, ALF model of rat was successfully established by GalN administration as mentioned previously[12]. The concentrations of alanine aminotransferase (ALT), aspartate aminotransferase (AST) and total bile acid (TBA) were increased significantly at 24 h and gradually decreased at 48 h, whereas those of alkaline phosphatase (AKP) and total bilirubin (TBiL) were increased continuously after GalN injection (Table 1). At the same time, the levels of serum total protein (TP) and albumin at 24 h after GalN administration were lowered markedly compared with those in control group ($P<0.01$, respectively) (Table 1), and increased at 48 h without significance compared with those at 24 h. The mortality rate of group C was higher than group B ($P<0.01$) (Table1). The general conditions, such as activity and appetite, in survivors were restored partially after 48 h.

Table 1 Degree of hepatic injury and mortality in ALF rats at various time points after injection of GalN

	Group A (n=10)	Group B (n=11)	Group C (n=10)
TP (g/L)	62.6±1.3	48.9±1.2[d]	51.0±3.1[d]
Albumin (g/L)	34.3±0.7	27.8±0.7[d]	30.3±1.1[d]
Globulin (g/L)	28.6±0.8	21.1±1.1[d]	21.5±2.6[d]
ALT (U/L)	60.6±3.3	4 798±1 114[d]	3 183±1 257[d]
AST (U/L)	138.0±7.5	5 032±1 067[d]	2 928±843[d]
AKP (U/L)	272.0±18.6	639±60[d]	747±133[d]
TBA (μmol/L)	11.8±2.6	425±33[d]	262±58[da]
TBiL(μmol/L)	7.0±0.4	40.6±8.2[d]	63.2±18.4[d]
Mortality	NO	8.33% (1/12)	44.44% (8/18)[b]

Values are expressed as mean±SE or frequency of occurrence (%). [a]$P<0.05$, [b]$P<0.01$ *vs* group B, [d]$P<0.01$ *vs* group A.

Table 2 Alterations in gut flora in rats with ALF at various time points after GalN administration

Flora	Group A (n=10)	Group B (n=11)	Group C (n=10)
Bacteriodaceae			
Jejunum	ND	ND	ND
Ileum	4.0±0.3	5.0±0.5	4.6±0.7
Colon	9.3±0.3	9.5±0.3	9.7±0.4
Lactobacillus			
Jejunum	4.9±0.3	3.4±0.3[d]	4.8±0.4[a]
Ileum	8.0±0.3	6.1±0.4[f]	6.2±0.3[f]
Colon	9.3±0.2	8.1±0.2[f]	8.5±0.2[d]
Enterobacteriaceae			
Jejunum	3.6±0.2	5.1±0.3[f]	4.3±0.3[b]
Ileum	5.3±0.3	6.9±0.5[c]	6.3±0.5
Colon	7.6±0.1	8.7±0.2[c]	7.9±0.3[a]
Enterococcus			
Jejunum	3.8±0.2	3.9±0.2	3.6±0.2
Ileum	4.9±0.3	5.8±0.3	5.2±0.5
Colon	6.8±0.2	5.8±0.4[c]	6.7±0.3

Data are expressed as mean±SE. ND: Not detected; [a]$P<0.05$, [b]$P<0.01$ *vs* group B, [c]$P<0.05$, [d]$P<0.01$, [f]$P<0.001$ *vs* group A.

Intestinal microflora analysis

To explore the variability in intestinal flora under ALF condition, we analyzed the microbiota from different intestinal segments including jejunum, ileum and colon of the rats at different time points. The count of *Enterobacteriaceae* in the jejunum, ileum and colon was significantly higher in the group A than that in control group ($P<0.001$, $P<0.05$, and $P<0.05$, respectively), whereas the count of *Lactobacillus* in the jejunum, ileum and colon, and that of *Enterococcus* in colon were greatly decreased

(P<0.01, P<0.001, P<0.001, and P<0.05, respectively) (Table 2). The count of *Enterobacteriaceae* in the jejunum and colon was lower in the group C than in the group B (P<0.01 and P<0.05, respectively), but the count of *Lactobacillus* in the jejunum in the group C was significantly elevated (P<0.05) (Table 2). The count of *Lactobacillus* in the ileum and colon in the group C was decreased more evidently than that in the group A (P<0.001 and P<0.01, respectively). These results indicated that the disturbed gut flora existed in rat with ALF, and the extent of changes in flora was correlated with the severity of liver injury.

Changes of endotoxin in intestine, portal venous and right ventricle blood

Gut endotoxin is usually translocated into the portal vein. To determine the relations of the levels of endotoxin in blood and in gut in rats with ALF, we measured the endotoxin levels of the intestine, PVB and RVB at various time points after GalN by LQAC test (Table 3). The levels of endotoxin in the ileum and PVB in group B after administration of GalN were increased more significantly than those in the group A (P<0.05 and P<0.01, respectively). At the same time, the level of endotoxin in the colon was increased, but not significantly. The levels of endotoxin in the ileum and colon in the group C were increased more significantly than those in the group B, and higher than those in the group A (P<0.01, respectively). The level of endotoxin in PVB in the group C was decreased significantly compared with those in the group B (P<0.05). Although there was an increase of endotoxin level in RVB after GalN, no statistically significant difference was observed.

Table 3 Levels of endotoxin in intestine, PVB and RVB in rats with ALF at different time points after injection of GalN

	Group A (n=10)	Group B (n=11)	Group C (n=10)
Jejunum (ng/g)	67.8±13.0	56.7±18.6	88.1±15.2
Ileum (ng/g)	51.5±8.9	111.3±22.8[a]	146.7±27.0[b]
Colon (ng/g)	1 022±179	1 841±363	2 444±349[b]
PVB (ng/L)	40.6±7.3	76.8±9.1[b]	45.0±5.3[c]
RVB (ng/L)	34.9±6.0	37.5±12.3	37.1±6.6

Data are expressed as mean±SE. [a]P<0.05, [b]P<0.01 *vs* group A; [c]P<0.05 *vs* group B. PVB: Portal venous blood; RVB: Right ventricle blood.

DISCUSSION

The present study showed that the count of *Enterobacteriaceae* at 24 h after injection of GalN was significantly increased, whereas that of *Lactobacillus* was markedly lowered. The whole intestinal microflora trended to recover at 48 h after GalN administration. These results indicated that there were intestinal microbial disturbance and overgrowth of *Enterobacteriaceae* in the rats with ALF. The tendency of changes in flora from the jejunum and ileum was consistent with that from the colon, and the extent of imbalance of intestinal microflora was correlated with the severity of liver injury. The alterations of intestinal bacterial flora might be due to the diminished bile secretion and the impaired intestinal motility, which were usually observed in rats with acute liver failure[18]. But the exact mechanisms need further study.

The level of endotoxin in the portal vein reflects the extent of translocation of endotoxin from gut[19]. Our findings showed that the levels of endotoxin in the ileum and colon increased continuously after administration of GalN, and the level of endotoxin in the portal vein was significantly elevated at 24 h, but lowered to the baseline value at 48 h. Interestingly, the elevation of the endotoxin in PVB was accompanied by the imbalance of intestinal flora and the overgrowth of *Enterobacteriaceae*, whereas a decrease of the level of endotoxin in PVB was paralleled with the partial restoration of disturbed flora. The present findings showed that an increase of endotoxin in PVB was closely related to the imbalance of intestinal flora in rats with ALF, and implied that ecological imbalance and bacterial overgrowth in ALF rats might play important roles in dysfunction of gut barrier, which could lead to translocation of endotoxin from gut. Our findings are supported by the previous study[20] that gut bacterial overgrowth is one of the etiological factors of bacteria and endotoxin translocation from gut. Moreover, it has been reported that an increase in gut permeability is related to histamine released by intestinal mast cell in rat with GalN-induced acute liver injury[21]. In addition, effect of bacterial proteases on microvillus membrane proteins contributes to the breakdown of the intestinal barrier[22]. Another reason that should be considered is that edema of intestinal wall resulting from digestive congestion and hypoproteinemia in ALF can injure the function of gut barrier[23]. In the present study, the levels of endotoxin in intestine increased continuously after GalN administration; this might be associated with the *Enterobacteriaceae* overgrowth[5]. Nevertheless, our findings indicated that enlargement of gut endotoxin pool had no impact on endotoxin translocation. In addition, the present data suggested that restoration of the disturbed gut flora might play an important role in inhibiting the endotoxin translocation from gut.

The present data showed there was no significant change of the concentrations of endotoxin in RVB after GalN administration, which was in agreement with Nakao *et al.*[24]. In contrast, the results by van Leeuwen *et al.*[11] showed that arterial plasma endotoxin levels increased in rats with hepatic failure induced by two-third partial hepatectomy. The discrepancy between two types of ALF seemed that the count of Kupffer cell in the latter reduced significantly because of hepatectomy. Plasma endotoxin is removed primarily by the Kupffer cells. Then, GalN exerted a minor effect on the function of kupffer cells, because the nucleotide contents of Kupffer cells were smaller than that those of hepatocytes[25]. Logically, Kupffer cells in rats after GalN administration can phagocytose the gut-derived endotoxin.

At present, we could not measure the pretreatment effect of probiotics on endotoxin translocation for lack of *Lactobacillus* preparation suitable for rats. However, it was demonstrated that administration of the probiotics *Lactobacillus plantarum* could reduce the circulating antibody to endotoxin in patients with ulcerative colitis[26]. Adawi *et al.*[27] showed that administration of *Lactobacillus* could reduce bacterial translocation and hepatocellular damage in rats with acute liver injury. Moreover, our previous work demonstrated that administration of probiotics *Bifidobacterium* (DM8504) could decrease significantly the levels of plasma endotoxin in patients with chronic hepatitis B[28].

In conclusion, severely disturbed intestinal flora disorders are observed in rats with GalN-induced acute liver failure, and related to the extent of injury of liver. Ecological imbalance of intestinal flora is one of the main causes of the translocation of endotoxin from lumen. Additionally, the present study implies that modulation of the intestinal flora using probiotics may be the optional treatment in preventing gut endotoxin translocation in patients with ALF.

ACKNOWLEDGEMENTS

We thank Dr. MH Wang (University of Colorado School of Medicine, USA) for revision the manuscript.

REFERENCES

1 **Rolando N**, Philpott-woward J, Williams R. Bacterial and fun-

gal infection in acute liver failure. *Semin Liver Dis* 1996; **16**: 389-402
2 **Han DW**. Intestinal endotoxemia as a pathogenetic mechanism in liver failure. *World J Gastroenterol* 2002; **8**: 961-965
3 **van Leeuwen PA**, Boermeester MA, Houdijk AP, Ferwerda CC, Cuesta MA, Meyer S, Wesdorp RI. Clinical significance of translocation. *Gut* 1994; **35**(1 Suppl): S28-S34
4 **Camara DS**, Caruana JA Jr, Schwartz KA, Montes M, Nolan JP. D-galactosamine liver injury: absorption of endotoxin and protective effect of small bowel and colon resection in rabbits. *Proc Soc Exp Biol Med* 1983; **172**: 255-259
5 **Goris H**, de Boer F, van der Waaij D. Kinetics of endotoxin release by gram-negative bacteria in the intestinal tract of mice during oral administration of *Bacitracin* and during *in vitro* growth. *Scand J Infect Dis* 1988; **20**: 213-219
6 **Swank GM**, Deitch EA. Role of the gut in multiple organ failure: bacterial translocation and permeability changes. *World J Surg* 1996; **20**: 411-417
7 **van der Waaij D**, Berghuis-de Vries JM, Lekkerkerk Lekkerkerk-v. Colonization resistance of the digestive tract in conventional and antibiotic-treated mice. *J Hyg* 1971; **69**: 405-411
8 **Gunnarsdottir SA**, Sadik R, Shev S, Simren M, Simren M, Sjovall H, Stotzer PO, Abrahamsson H, Olsson R, Bjornsson ES. Small intestinal motility disturbances and bacterial overgrowth in patients with liver cirrhosis and portal hypertension. *Am J Gastroenterol* 2003; **98**: 1362-1370
9 **Gordon DM**, Diebel LN, Liberati DM, Myers TA. The effects of bacterial overgrowth and hemorrhagic shock on mucosal immunity. *Am Surg* 1998; **64**: 718-721
10 **Wang XD**, Ar'Rajab A, Andersson R, Soltesz V, Wang W, Svensson M, Bengmark S. The influence of surgically induced acute liver failure on the intestine in the rat. *Scand J Gastroenterol* 1993; **28**: 31-40
11 **van Leeuwen PA**, Hong RW, Rounds JD, Rodrick ML, Wilmore D. Hepatic failure and coma after liver resection is reversed by manipulation of gut contents: the role of endotoxin. *Surgery* 1991; **110**: 169-174
12 **Shito M**, Balis UJ, Tompkins RG, Yarmush ML, Toner M**.** A fulminant hepatic failure model in the rat: involvement of interleukin-1beta and tumor necrosis factor-alpha. *Dig Dis Sci* 2001; **46**: 1700-1708
13 **Salminen S**, Salminen E. Lactulose, lactic acid bacteria, intestinal microecology and mucosal protection. *Scand J Gastroenterol Suppl* 1997; **222**: 45-48
14 **Ohkusa T**, Ozaki Y, Sato C, Mikuni K, Ikeda H. Long-term ingestion of lactosucrose increases *Bifidobacterium sp.* in human fecal flora. *Digestion* 1995; **56**: 415-420
15 **Hartemink R,** Rombouts FM. Comparison of media for the detection of bifidobacteria, lactobacilli and total anaerobes from faecal samples. *J Microbiol Methods* 1999; **36**: 181-192
16 **Benno Y**, Endo K, Mizutani T, Namba Y, Komori T, Mitsuoka T. Comparison of fecal microflora of elderly persons in rural and urban areas of Japan. *Appl Environ Microbil* 1989; **55**: 1100-1105
17 **Li LJ**, Shen ZJ, Lu YL, Fu SZ. The value of endotoxin concentrations in expressed prostatic secretions for the diagnosis and classification of chronic prostatitis. *BJU Int* 2001; **88**: 536-539
18 **Wang XD**, Soltesz V, Andersson R. Cisapride prevents enteric bacterial overgrowth and translocation by improvement of intestinal motility in rats with acute liver failure. *Eur Surg Res* 1996; **28:** 402-412
19 **Deitch EA**. Bacterial translocation or lymphatic drainage of toxic products from the gut: what is important in human beings? *Surgery* 2002; **131**: 241-244
20 **Barber AE**, Jones WG 2nd, Minei JP, Fahey TJ 3rd, Lowry SF, Shires GT. Bacterial overgrowth and intestinal atrophy in the etiology of gut barrier failure in the rat. *Am J Surg* 1991; **161**: 300-304
21 **Stachlewitz RF**, Seabra V, Bradford B, Bradham CA, Rusyn I, Germolec D, Thurman RG. Glycine and uridine prevent D-galactosamine hepatotoxicity in the rat: role of Kupffer cells. *Hepatology* 1999; **29**: 737-745
22 **Riepe SP**, Goldstein J, Alpers DH. Effect of secreted Bacteroides proteases on human intestinal brush border hydrolases. *J Clin Invest* 1980; **66**: 314-322
23 **Hashimoto N**, Ohyanagi H. Effect of acute portal hypertension on gut mucosa. *Hepatogastroenterology* 2002; **49**: 1567-1570
24 **Nakao A**, Taki S, Yasui M, Kimura Y, Nonami T, Harada A, Takagi H. The fate of intravenously injected endotoxin in normal rats and in rats with liver failure. *Hepatology* 1994; **19**: 1251-1256
25 **Hofmann F**, Wagle SR, Decker K. Effect of d-galactosamine administration on nucleotide and protein metabolism in isolated rat Kupffer cells. *Hoppe Seylers Z Physiol Chem* 1976; **357**: 1395-1400
26 **Garcia- Lafuente A**, Antolin M, Guarner F, Crespo E, Malagelada JR. Modulation of colonic barrier function by the composition of the commensal flora in the rat. *Gut* 2001; **48**: 503-507
27 **Adawi D**, Ahrne S, Molin G. Effects of different porbiotix strains of *Lactobacillus* and *Bifidobacterium* on bacterial translocation and liver injury in an acute liver injury model. *Int J Food Microbiol* 2001; **70**: 213-220
28 **Li LJ**, Sheng JF. Effect of probiotics bifidobacterium (DM8504) on the plasma endotoxin in patients with chronic hepatitis B. *Chin J Microecol* 1996; **8**: 20-22

Edited by Kumar M and Chen WW **Proofread by** Xu FM

PO Box 2345, Beijing 100023, China
Fax: +86-10-85381893
E-mail: wjg@wjgnet.com www.wjgnet.com

World J Gastroenterol 2004;10(14):2091-2094
World Journal of Gastroenterology
 ISSN 1007-9327

• BASIC RESEARCH •

Effect of extracts of trichosanthes root tubers on HepA-H cells and HeLa cells

Chang-Ming Dou, Ji-Cheng Li

Chang-Ming Dou, Ji-Cheng Li, Institute of Cell Biology, Zhejiang University, Hangzhou 310031, Zhejiang Province, China
Supported by the Science and Technology Department of Zhejiang Province, No.2003C30057
Correspondence to: Dr. Ji-Cheng Li, Institute of Cell Biology, Zhejiang University, Department of Lymphology, Department of Histology and Embryology, Zhejiang University Medical College, Hangzhou 310031, Zhejiang Province, China. lijc@mail.hz.zj.cn
Telephone: +86-571-87217139 **Fax:** +86-571-87217139
Received: 2003-10-28 **Accepted:** 2003-12-08

Abstract

AIM: To investigate the cytotoxic activity of extracts of trichosanthes root tubers (EOT) on HepA-H cells and HeLa cells compared with trichosanthin (TCS), and to explore the possible mechanism of growth inhibitory effect of EOT on HeLa cells.

METHODS: Tumor cells were cultured *in vitro*, and then microculture tetrzoalium assay (MTT) was used to investigate drugs' cytotoxic activity. Scanning electron microscopy (SEM) and transmission electron microscopy (TEM) were used to observe ultrastructural changes of cells, and electrophoresis was performed to detect changes of biochemical characteristics of intercellular DNA.

RESULTS: TCS and EOT had no obvious effects on HepA-H cells ($P>0.05$), but had remarkable effects on HeLa cells in a time and dose dependent manner ($r>0.864$, $P<0.05$ or $P<0.01$). The inhibitory rate of EOT was much higher than that of TCS ($P<0.01$). Median inhibitory rates (IC50) of TCS and EOT on HeLa cells were 610.9 mg/L and 115.6 mg/L for 36 h, and 130.7 mg/L and 33.4 mg/L for 48 h respectively. Marked morphologic changes were observed including microvillus disappearance or reduction, cell membrane bledding, cell shrinkage, condensation of chromosomes and apoptotic bodies with complete membranes. Meanwhile, apoptosis of HeLa cells was confirmed by DNA ladder formation on gel electrophoresis.

CONCLUSION: TCS and EOT have no obvious effects on HepA-H cells, but have significant inhibitory effects on HeLa cells, indicating that EOT is superior to TCS in anti-tumor activity.

Dou CM, Li JC. Effect of extracts of trichosanthes root tubers on HepA-H cells and HeLa cells. *World J Gastroenterol* 2004; 10(14): 2091-2094
http://www.wjgnet.com/1007-9327/10/2091.asp

INTRODUCTION

Trichosanthes Kirilowii Maximowii is a kind of liana of the Cucurbitaceae family, whose root tuber was a Chinese herbal medicine Tianhuafen (THF) that has been used to reset menstruation and expel retained placenta[1]. In the 1980 s, Trichosanthin (TCS) was isolated from the root tuber and proved to be the active component, a type I ribosome-inactivating protein (RIP) with 247 amino acids which inactivates eukaryotic ribosomes *via* its N-glycosidase activity. TCS has been used to induce mid-term abortion and to treat ectopic pregnancies, hydatidiform and trophoblastic moles in China[2]. In recent years, TCS has also been found to posses various pharmacological properties including immunomudulatory, anti-tumor and anti-HIV activities[3-6]. Clinical trials have also been performed. TCS has aroused extensive attention.

In the present study, we were interested in its anti-tumor activity *in vitro*. TCS has already been regarded as an effective anti-tumor agent highly specific to choriocarcinoma cells from trophoblasts[7]. However, researches and clinical application about TCS on tumor are mainly on gastrointestinal tumor and seldom on others[8]. TCS is an active anti-tumor component of Trichosanthes, yet there is no report of extracts of trichosanthes root tubers (EOT) on tumor cells. So in this study, we chose two tumor cell lines, HepA-H cells and HeLa cells, to investigate the growth inhibitory effect of EOT and TCS on the two cell lines and further compared their anti-tumor activity.

In recent years, screening of anti-tumor drugs from natural resource, especially from traditional Chinese medicines, has drawn worldwide research interest, and many exciting goals have been achieved[9]. As a research focus of life science and medicine, apoptosis has revealed its promising future[10-12]. Nowadays apoptosis has been considered as the most ideal path to conquer tumors. Therefore, in our study, we initially investigated the induction of apoptosis of HeLa cells by EOT. The present study may provide experimental bases for further researches and seeking novel anti-tumor agents.

MATERIALS AND METHODS

Drugs

TCS (1.2 mg/mL) was purchased from Jinshan Pharmacy Ltd, Shanghai. EOT was extracted from fresh root tubers of *Trichosanthes kirlowii* Maxim collected in Hangzhou[13], Zhejiang Province in November 2002. SDS-PAGE (100 g/L) was performed to detect the components of EOT samples in comparison with TCS and protein marker. Gel was stained by Coomassie brilliant blue. After decolored, the gel was visualized and photographed under gel imaging assay apparatus. Then straps in the gel were scanned to evaluate the content of relative proteins. Drugs were diluted with culture medium and sterilized before use.

Reagents and apparatus

RPMI-1640 and fetal calf serum (FCS) were from GIBCO, USA. 3-(4,5-dimethylthiazol-2-yl) -2,5-diphenyltetrazolium bromide (MTT), DMSO and all electrophoresis reagents were from Sigma Co., USA. Animal cell PCD ladder isolation kit was purchased from Dingguo Biological Products Ltd, Beijing. CO_2 incubator was the product of FORMA Company. TECNAI 10 TEM was from PHILIPS and STEREOSCAN 260 was from CAMBRIDGE Company. Electrophoresis apparatus was made by E-C Apparatus Corporation. Mini gel electrophoresis system was the product of Bio-Rad Company. Image analysis system was

purchased from Shanghai Tianneng Science and Technology Ltd.

Cell lines and cell culture

HepA-H and HeLa cells were preserved in our laboratory. The cell line of high lymphatic metastasis ascitic liver cancer was established and cultivated by professor Li and Yang[14]. Cells were grown in RPMI-1640 culture medium containing 100 mL/L FCS, 100 U/mL penicillin and 100 U/mL streptomycin at 37 ℃ in a humidified atmosphere of 50 mL/L CO_2.

Cytotoxic activity

Growth inhibitory effects of HepA-H and HeLa cells with various treatments were determined by MTT assay. Cells at exponential phase were seeded into 96-well plates, 100 μL (1×10^5/mL) per well. Then different concentrations of EOT and TCS in 100 μL culture medium were added and the final concentration in each well was 0.1 mg/L, 1 mg/L, 10 mg/L, 100 mg/L, and 500 mg/L respectively. Each treatment was tested in tetrad wells and the control group was given only culture medium containing no drug. All the above plates were placed in a 50 mL/L CO_2 humidified-atmosphere incubator at 37 ℃ for 24, 36 and 48 h. At the end of exposure, 20 μL MTT (5 g/L) was added to each well and the plates were incubated at 37 ℃ for 4 h. Then all culture medium supernatant was removed from wells and replaced with 100 μL DMSO. The plates were shaken for 15 min so that all the production of formazan reduced by MTT could be dissolved out from cells. Following thorough formation dissolved, the absorbance of each well was measured by standard enzyme-linked immunosorbant assay at 492 nm. The inhibition of tumor cell growth was calculated by the equation: Growth inhibitory rate=$(1-A_{492\ treated}/A_{492\ control})\times100\%$.

Based on the growth inhibitory rates of each group of drugs on cells, SPSS software was used to calculate 50% inhibitory concentrations (IC50).

Specimens for electron microscope

HeLa cells at exponential phase were used and cultivated with various concentrations of EOT for 24 h. Then cells were harvested and fixed with 25 g/L glutaraldehyde in 0.1 mol/L phosphate buffer (pH 7.4) for 2 h at 4 ℃. For TEM examination, the specimens were postfixed in 10 g/L osmium tetroxide in 0.1 mol/L phosphate buffer (pH 7.4) for 1 h at 4 ℃. After dehydration in a graded series of ethanol and infiltration in propylene oxide, they were embedded in Epson 812. Fine sections were cut with an LKB 2088 ultramicrotome and stained with uranyl acetate and lead citrate. The sections were examined with a PHILIPS TECNAI 10 TEM at 60 kV. For SEM examination, the specimens were postfixed for 1 h in 10 g/L O_SO_4, dehydrated in a graded series of alcohol, CO_2 critical-point dried, mounted on aluminum stubs and sputter-coated with gold. Specimens were examined with a STEREOSCAN 260 SEM at 25 kV.

Agarose gel electrophoresis of DNA

HeLa cells at exponential phase were exposed to different concentrations of EOT for 24, 36 and 48 h respectively. Then cells were harvested, washed twice with PBS, and DNA was extracted according to the directions of the kit. DNA was analyzed by electrophoresis at 75 mA on 8 g/L agarose gel containing 0.5 mg/L ethidium bromide. After about 1.5 h, the gel was visualized and photographed under transmission UV light.

Statistical analysis

Data were expressed as mean±SD. Statistics software package SPSS 11.5 was employed to process the data. Differences between groups were described by Student t test. *P* values less than 0.05 were considered statistically significant.

RESULTS

Protein electrophoresis of EOT and TCS

1 kg fresh trichosanthes root tubers was used in the present study and we got 0.83 g EOT. As the result of SDS-PAGE showed, sample EOT had an obvious major strap and several other minor straps. All the straps were scanned, sample EOT had a content of 70.93% of TCS and other unknown proteins. However, sample TCS had only a minor strap and its purity was 99.81%. Protein marker further conformed to protein TCS (Figure 1).

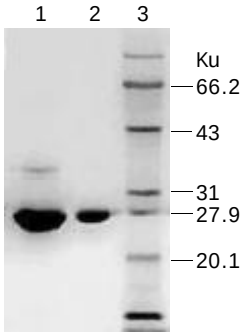

Figure 1 Analysis of EOT and TCS by SDS-PAGE. Lane 1: EOT, Lane 2: TCS, Lane 3: Protein Marker.

Cytotoxic activity of EOT and TCS in HepA-H and HeLa cells

After exposure to EOT and TCS, HepA-H cells had no growth arrest of significant importance. After 24 h, most growth of HepA-H cells was promoted, but the effect did not depend on the dose ($P>0.05$). After 36 h, all the cells were led to growth arrest, which also had no statistical relation with the dose. After 48 h, some were promoted, while the others were inhibited, and the relationship between the effect and dose was not found. All the three groups of data showed no statistical significance ($P>0.05$), suggesting HepA-H cells were not susceptible to EOT and TCS (Table 1).

Table 1 Cytotoxic activity of EOT and TCS in HepA-H cells (n=4, mean±SD)

Drug	Concentration (mg/L)	Inhibitory rate (%)		
		24 h	36 h	48 h
EOT	0.1	-3.1±2.9	19.1±2.6	15.7±0.8
	1.0	-3.6±8.1	7.9±11.5	5.1±2.6
	10	-25.0±1.7	6.8±0.1	3.8±3.6
	100	9.6±3.3	21.0±2.2	16.2±6.3
	500	7.6±7.6	17.0±3.0	13.4±0.7
TCS	0.1	-19.9±6.7	6.9±5.2	-3.7±4.9
	1.0	-6.1±6.4	4.7±0.6	7.4±2.7
	10	-16.1±19.1	0.7±2.4	-11.4±4.7
	100	-6.8±1.0	11.9±4.1	2.6±2.3
	500	-3.4±3.3	10.8±5.2	5.9±3.8

EOT and TCS had good effects on HeLa cells in a time and dose dependant manner ($r>0.864$). When the concentration of drugs was increased and the time was prolonged, the growth inhibitory rate increased gradually ($P<0.01$). EOT was superior to TCS in the effect on HeLa cells when the time and concentration were identical ($P<0.01$). The median inhibitory rates (IC50) of TCS and EOT for HeLa cells were 610.9 mg/L and 115.6 mg/L after 36 h, and 130.7 mg/L and 33.4 mg/L after 48 h, respectively. The results suggested that EOT and TCS could inhibit the growth of HeLa cells, while EOT had much stronger cytotoxic activity (Table 2).

Table 2 Cytotoxic activity of EOT and TCS in HeLa cells (n=4, mean±SD)

Drug	Concentration (mg/L)	Inhibitory rate (%)		
		24 h	36 h	48 h
EOT	0.1	3.4±4.1	9.7±7.0	9.9±3.1
	1.0	4.5±3.7	11.1±2.0	11.3±1.9
	10	16.3±3.2	20.9±6.8	29.4±4.1
	100	36.7±4.0	44.2±1.7	54.6±3.0
	500	57.9±3.4	71.8±3.9	89.4±1.9
TCS	0.1	2.2±1.7	2.9±2.7	4.4±3.1
	1.0	2.9±2.0	5.5±1.2	6.0±2.7
	10	16.4±4.1	6.7±2.4	13.0±3.3
	100	26.3±2.5	29.3±3.9	47.9±5.2
	500	39.6±4.8	53.8±4.0	70.2±2.9

Morphological observation

After exposure to EOT for 24 h, HeLa cells were observed under SEM, typical apoptotic characteristics were found, including cell membrane bledding, microvilli disappearance or reduction, and separated apoptotic bodies (Figure 2, A-B). Also treated HeLa cells were observed under TEM, and shrinkage of cells, condensation of chromosomes and apoptotic bodies with complete membrane were found (Figure 2, C-D).

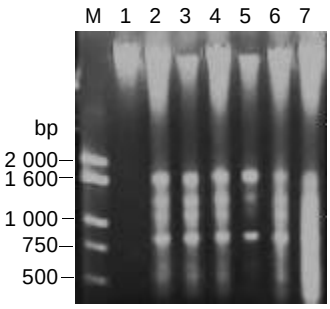

Figure 3 Analysis of DNA fragments of HeLa cells treated with EOT. M: DNA marker, lane 1: normal control, lane 2: 500 mg/L for 24 h, lane 3: 100 mg/L for 24 h, lane 4: 50 mg/L for 48 h, lane 5: 50 mg/L for 24 h, lane 6: 100 mg/L for 48 h, lane 7: 500 mg/L for 48 h.

DNA fragmentation

After HeLa cells were exposed to EOT 50 mg/L, 100 mg/L, 500 mg/L respectively for 24 h, DNA agarose gel electrophoresis showed the typical "DNA ladder" pattern of apoptosis. With time delayed, 48 h later, DNA ladder was much more obvious in the cells treated with EOT 50 mg/L, 100 mg/L, but DNA of cells treated with high concentration, 500 mg/L, took on a shape of smear, suggesting that cells underwent secondary necrosis (Figure 3). Results of DNA agarose gel electrophoresis further confirmed that EOT could induce HeLa cell apoptosis.

DISCUSSION

To our knowledge, researches of the effects of TCS on liver cancer arrived different conclusions, while studies on HeLa cells were scarcely reported[15,16]. In the present work, we investigated and analyzed the effect of EOT and TCS on HepA-H and HeLa cells. We found that TCS and EOT had no significant effect on HepA-H cells but had remarkable effect on HeLa cells in a time and dose dependant manner. The data suggested EOT had a much higher anti-tumor effect on HeLa cells than TCS. After 48 h, the growth inhibitory rate of HeLa cells exposed to EOT and TCS (500 mg/L) was 89.4% and 70.2%, respectively. The median inhibitory rates (IC50) were 610.9 mg/L and 115.6 mg/L after 36 h, and 130.7 mg/L and 33.4 mg/L after 48 h, respectively. SDS-PAGE showed, EOT contains 70.93% TCS and several other components. In contrast, TCS had a higher purity almost to 100%. It is generally believed TCS, a type I RIP, is the active component. So the results make us consider why EOT has a better inhibitory effect on the growth of tumor cells than TCS. Whether the good anti-tumor activity of EOT is correlated with the cooperation of other proteins or any other factors. As was reported, cytotoxicity of TCS was dependent on its intracellular concentration, and variation of cytotoxicity in different cells might be related to the mechanisms affecting its internalization[17]. So there might be some active factors in EOT that promote internalization of TCS. Of course, the actual mechanism needs further researches to clarify.

It has been reported that TCS has strong effects on cytotoxicity and induction of apoptosis of gastric cancer cells, human choriocarcinoma cells and leukemia cells[8,18,19]. Also relative genes inducing apoptosis have been isolated with their mechanism elucidated[20]. In this study, we investigated

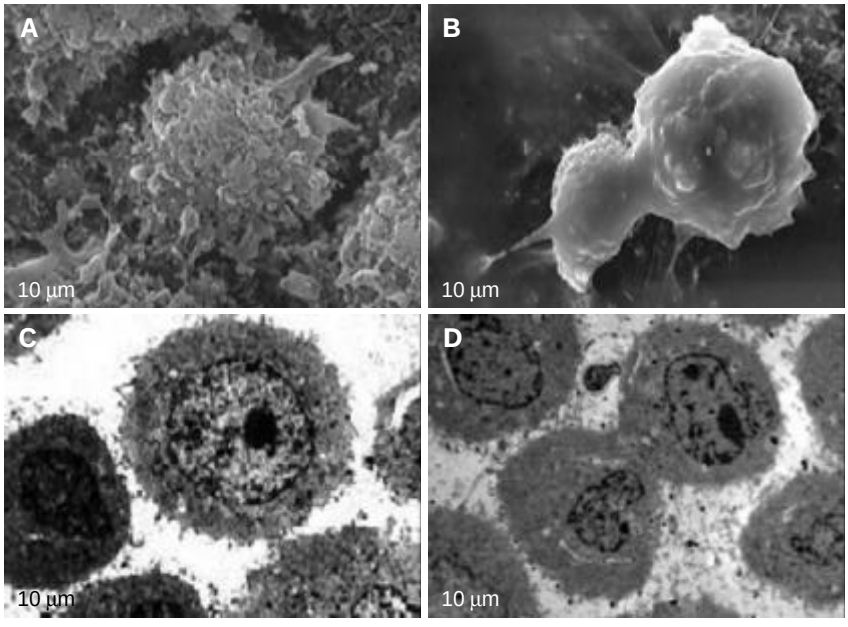

Figure 2 HeLa cells under SEM and TEM. A: HeLa cells under SEM in control group. B: HeLa cells under SEM treated with EOT (100 mg/L) for 24 h. C: HeLa cells under TEM in control group. D: HeLa cells under TEM treated with EOT (100 mg/L) for 24 h.

apoptosis of HeLa cells induced by EOT. Experiments on morphology and biochemistry revealed typical apoptotic characteristics, such as microvilli disappearance, cell membrane bledding, apoptotic body and DNA ladder pattern. The results suggested that the anti-tumor effect of EOT on HeLa cells was related with the induction of apoptosis.

In conclusion, EOT has stronger anti-tumor effects and can induce apoptosis of HeLa cells. EOT would have a bright future in the treatment of tumors and further work may lead to relative anti-tumor agents to be used in clinic.

REFERENCES

1 **Chan SH,** Hung FS, Chan DS, Shaw PC. Trichosanthin interacts with acidic ribosomal proteins P0 and P1 and mitotic checkpoint protein MAD2B. *Eur J Biochem* 2001; **268:** 2107-2112

2 **Lu PX**, Jin YC. Trichosanthin in the treatment of hydatidiform mole. Clinical analysis of 52 cases. *Chin Med J* 1990; **103:** 183-185

3 **Chan SH,** Shaw PC, Mulot SF, Xu LH, Chan WL, Tam SC, Wong KB. Engineering of a mini-trichosanthin that has lower antigenicity by deleting its C-terminal amino acid residues. *Biochem Biophys Res Commun* 2000; **270:** 279-285

4 **Wang JH,** Nie HL, Huang H, Tam SC, Zheng YT. Independency of anti-HIV-1 activity from ribosome-inactivating activity of trichosanthin. *Biochem Biophys Res Commun* 2003; **302:** 89-94

5 **Wang JH,** Nie HL, Tam SC, Huang H, Zheng YT. Anti-HIV-1 property of trichosanthin correlates with its ribosome inactivating activity. *FEBS Lett* 2002; **531:** 295-298

6 **Cai X,** Yao G, Xu G, Yang C, Xu H, Lin Y, Yu J, Sun B. Identification of the amino acid residues in trichosanthin crucial for IgE response. *Biochem Biophys Res Commun* 2002; **297:** 510-516

7 **Chan WY,** Huang H, Tam SC. Receptor-mediated endocytosis of trichosanthin in choriocarcinoma cells. *Toxicology* 2003; **186:** 191-203

8 **Tu SP,** Jiang SH, Qiao MM, Cheng SD, Wang LF, Wu YL, Yuan YZ, Wu YX. Effect of trichosanthin on cytotoxicity and induction of apoptosis of multiple drugs resistance cells in gastric cancer. *Shijie Huanren Xiaohua Zazhi* 2000; **8:** 150-152

9 **Liu ZS,** Tang SL, Ai ZL. Effects of hydroxyapatite nanoparticles on proliferation and apoptosis of human hepatoma BEL-7402 cells. *World J Gastroenterol* 2003; **9:** 1968-1971

10 **Kerr JF.** History of the events leading to the formulation of the apoptosis concept. *Toxicology* 2002; **181:** 471-474

11 **Levy RR,** Cordonier H, Czyba JC, Guerin JF. Apoptosis in preimplantation mammalian embryo and genetics. *Ital J Anat Embryol* 2001; **106**(2 Suppl 2): 101-108

12 **Thatte U,** Bagadey S, Dahanukar S. Modulation of programmed cell death by medicinal plants. *Cell Mol Biol* 2000; **46:** 199-214

13 **Wang Q.** Trichosanthin. 2nd ed. Beijing: *Sci Pub* 2000: 21-28

14 **Yang ZR,** Li JC. Establishment and biological characteristics of two murine hepatocarcinoma substrains with different lymphatic metastatic ability. *Shiyan Shengwu Xuebao* 2003; **36:** 99-104

15 **Ru QH,** Luo GA, Liao JJ, Liu Y. Capillary electrophoretic determination of apoptosis of HeLa cells induced by trichosanthin. *J Chromatogr A* 2000; **894:** 165-170

16 **Wang Q.** Trichosanthin. 2nd ed. Beijing: *Sci Pub* 2000: 298-319

17 **Chan WL,** Zheng YT, Huang H, Tam SC. Relationship between trichosanthin cytotoxicity and its intracellular concentration. *Toxicology* 2002; **177:** 245-251

18 **Zhang C,** Gong Y, Ma H, An C, Chen D, Chen ZL. Reactive oxygen species involved in trichosanthin-induced apoptosis of human choriocarcinoma cells. *Biochem J* 2001; **355**(Pt 3): 653-661

19 **Kong M,** Ke YB, Zhou MY, Ke XY, Lu B, Nie HL. Study on Trichosanthin induced apoptosis of leukemia K562 cells. *Shiyan Shengwu Xuebao* 1998; **31:** 233-243

20 **Li XY,** Wang GQ, Ge HL, Wang Y, Li NL, Zhu Q, Chen YL, Chou GY. Isolation of a gene related to trichosanthin-induced apoptosis (GRETA). *Shiyan Shengwu Xuebao* 2000; **33:** 81-84

Edited by Wang XL and Xu CT **Proofread by** Xu FM

PO Box 2345, Beijing 100023, China
Fax: +86-10-85381893
E-mail: wjg@wjgnet.com www.wjgnet.com

World J Gastroenterol 2004;10(14):2095-2098
World Journal of Gastroenterology
 ISSN 1007-9327

• BASIC RESEARCH •

Role of COX-2 in microcirculatory disturbance in experimental pancreatitis

Wen-Wei Yan, Zong-Guang Zhou, You-Dai Chen, Hong-Kai Gao

Wen-Wei Yan, III Department of General Surgery, West China Hospital, Sichuan University, Chengdu 610041, Sichuan Province, China & Department of Organ Transplantation of Tianjin First Central Hospital, Tianjin 300052, China
Zong-Guang Zhou, III Department of General Surgery, West China Hospital, Sichuan University, Chengdu 610041, Sichuan Province, China
You-Dai Chen, Hong-Kai Gao, Institute of Degestive Surgery, West China Hospital, Sichuan University, Chengdu 610041, Sichuan Province, China
Supported by the National Natural Science Foundation of China, No. 39770722
Correspondence to: Dr. Zong-Guang Zhou, III Department of General Surgery, West China Hospital, Sichuan University, Chengdu 610041, Sichuan Province, China. zhou767@21cn.com
Telephone: +86-28-85422525 **Fax:** +86-28-85422484
Received: 2004-02-11 **Accepted:** 2004-02-18

Abstract

AIM: To elucidate the role of COX-2 in the development of capillary leakage in rats with acute interstitial pancreatitis.

METHODS: Rats with acute interstitial pancreatitis were induced by caerulein subcutaneous injection. Reverse transcription–polymerase chain reaction (RT-PCR) was used to determine the gene expression of COX-2 in pancreatic tissues, spectrophotometry was used to assay the parameters of acute pancreatitis such as the serum amylase and plasma myeloperoxidase, and determination of capillary permeability in the pancreas by quantifying the permeability index (PI) assisted response of pancreatic microvascular via intravital fluorescence microscope video image analysis system.

RESULTS: A significant increase of COX-2 expression, elevation of serum amylase, and plasma myeloperoxidase were detected in rats with acute edematous pancreatitis compared with control rats. The changes of pancreatic microvascular after caerulein injection were as following: (a) the decrease of pancreatic capillary blood flow (4th h, 0.56±0.09 nL/min, $P<0.05$; 8 th h, 0.34±0.10 nL/min, $P<0.001$); (b) reduction of functional capillary density (4 th h, 381±9 cm^{-1}, $P>0.05$; 8th h, 277±13 cm^{-1}, $P<0.001$); (c) irregular and intermittent capillary perfusion was observed at the 8th h and these vessels were also prone to permeation.

CONCLUSION: COX-2 plays an important role in mediating capillary permeability in pancreatitis, thereby contributing to capillary leakage.

Yan WW, Zhou ZG, Chen YD, Gao HK. Role of COX-2 in microcirculatory disturbance in experimental pancreatitis. *World J Gastroenterol* 2004; 10(14): 2095-2098
http://www.wjgnet.com/1007-9327/10/2095.asp

INTRODUCTION

Pancreatic microcirculatory disturbance has been considered as one of the possible and important causative factors for the development of acute pancreatitis (AP)[1-5], although the underlying mechanism is unclear. COX-2, known as prostaglandin endoperoxide synthase-2, is a rate-limiting enzyme in the production of prostaglandins and an important regulator of vascular function[8,9]. Under resting conditions, the level of COX-2 was undetectable. COX-2 expression can be inducible by a wide range of extracellular and intracellular stimuli, including lipopolysaccharide, forskolin, interleukin-1 (IL-1), tumor necrosis factor (TNF), epidermal growth factor, interferon-γ, platelet activating factor and endothelin, suggesting that COX-2 plays a critical role in inflammatory disorder[6,7]. Previous studies demonstrated that COX-2 was a classic example of immediate early or primary response gene activation and generally considered as a proinflammatory enzyme[10-15], suggesting COX-2 may serve as one of triggering factors of inflammation. Studies showed that inducible cyclooxygenase (COX-2) might indirectly involve in the regulation of human vascular endothelial cells (HUVEC) inflammation[16,17]. However, no further studies examined it. For the purpose of verification of the result, reverse transcription polymerase chain reaction (RT-PCR) and intravital fluorescence microscopy with fluorescein isothiocyanate (FITC) labeled erythrocytes were used to study COX-2 gene expression and pancreatic microvasculature, with the aim of consolidating the relevance between the gene expression of COX-2 and dysfunction of pancreatic local microvasculature during acute edematous pancreatitis (AEP).

MATERIALS AND METHODS

Animal

A total of 96 male Wistar rats (250-350 g) were starved 15 h prior to the experiments with water *ad libitum* and randomly divided into 2 groups: (1) AEP group (n=72), 24 rats for extraction of total RNA from pancreatic tissue and 3 mL blood samples of portal venous for assay of serum amylase (AMS) and plasma myeloperoxidase (MPO); 24 rats for studying pancreatic microvasculature by intravital fluorescence microscope with fluorescein FITC-RBC; 24 rats for accessing the pancreatic microvasculature permeability and water content. (2) Normal control group (n=24). The model of AEP was established by subcutaneous injection of caerulein (Sigma) as previously described[1]. 1 h and 2 h after the beginning of experiment all experimental groups were injected caerulein 5.5 μg/kg and 7.5 μg/kg respectively, while control group received the same volume of 9 g/L sodium chloride.

Total RNA extraction from pancreatic tissue

After 2, 4, 8, 16 and 24 h of caerulein injection, the rats were anesthetized with intraperitoneal injection of 30 g/L barbitone sodium (35 mg/kg) and the sacrificed for extraction of total RNA. The isolation of total RNA was prepared from 100 mg pancreatic tissue, using Trizol reagent Kit (Gibco BRL). Yield and purity of RNA preparations were checked spectrophotometrically at 260 nm and 280 nm and quality was inspected visually on 13 g/L agarose gels after ethidium bromide staining.

Semi-quantitative RT-PCR analysis for COX-2 mRNA

RT-PCR was performed in combined one-tube reaction kits (Takara™) according to the manufacture' s suggestions. β-actin was used as an internal control. The primers for control and COX-2 were as follows: β-actin (sense) 5' -GAT GGT GGG TAT GGG TCA GAA-3' , (antisense) 5' -CTA GGA GCC AGG GCA GTA ATC-3' ; COX-2 (sense) 5' -CTG TAT CCC GCC CTG CTG GT-3' , (antisense) 5' -GAG GCA CTT GCG TTG ATG GT-3' . All the primers were synthesized by Life Technology (HongKong, China). RT-PCR was run in GeneAmp 9600 (Perkin-Elmer), following procedures: 50 ℃ for 30 min,1 cycle; 94 ℃ for 2 min, 1 cycle; 94 ℃ for 30 s, 55 ℃ for 30 s, 72 ℃ for 40 s, 30 cycles; 72 ℃ for 10 min, 1 cycle. 5 μL PCR products was placed onto 13 g/L agarose gels with ethidium bromide staining, using an ultrailluminator, and the level of COX-2 mRNA was expressed as the quotient (Q) of the integrated optical density values (IOD) for the COX-2 and the β-actin bands (Q=IOD COX-2 band / β-actin band).

Assay of plasma myeloperoxidase (MPO)

The activity of MPO, an index of tissue leukocyte recruitment, is a marker of inflammation of tissue. The activity of MPO in the pancreatic tissues was determined following the method described by Calkins[23] with minor modifications.

Response of pancreatic local microvessel

For studying response of pancreatic microvasculature we adopted erythrocytes (RBC) labeled by FITC using the approach as previously described. Briefly, washed RBC obtained from an experimental rat was incubated with PBS (137 mmol/L NaCl, 6.4 mmol/L Na_2HPO_4, 2.7 mmol/L KCl, 1.5 mmol/L KH_2PO_4, pH 7.8) solution containing 1 mg/mL FITC. The labeled cells were then washed twice with a saline solution containing 10 g/L bovine serum albumin (Sigma) to remove unconjugated fluorescent dye. The final volume percentage of the labeled cells was adjusted approximately to 50% by adding an isotonic saline solution, and an aliquot 91 mL/kg of these suspensions was injection through a tail vein of the rats to observe density and capillary perfusion by intravital fluorescence microscope (OLYMPUS X-70).

Assay for microvascular permeability

Half an hour before caerulein injection, the rats were given an intravenous injection of Evans blue (20 mg/kg) via a tail vein. Briefly, the lungs and pancreas were excised, weighted, and placed in 5 mL of formaldehyde solution and homogenized for 1 min. After incubated at room temperature for 16 h, the pancreas and lungs were measured at 650 nm in Beckman spectrophotometer. The concentration of Evans blue (EB) was determined by calculation against a standard curve. The blood was centrifuged at 600 r/min for 10 min and the concentration of EB in the serum was determined as described above. The permeability index (PI)=$^{[Evans\ blue]}$tissue/$^{[Evans\ blue]}$serum. Water mass fractions in the pancreas were used as a parameter of organ water accumulation after panceatitis induction. The tissues were removed in a humidity chamber and the wet mass was measured immediately. The tissue was dried at 70 ℃ to a constant mass for the determination of dry mass. Organ edema was determined by calculating tissue water content according to the following formula: Water mass fraction (%)=(1-dry mass/wet mass)×100%.

Statistics analysis

All results were represented as mean±SD. The significance of changes were evaluated by means of a *F* test in comparisons of the same time point in two groups or by analysis of variance (Newman-Keuls) when different time points in the same group were compared. Differences were considered significant when the $P<0.05$.

RESULTS

RT-PCR detection of COX-2 in the pancreas

COX-2 transcription remained at a low level in normal control (Figure 1). Whereas, after injection of caerulein, the expression of COX-2 mRNA in AEP was increased, with peaked at the 8th h, and kept at high level within 24 h. Setting the level of COX-2 expression at 2nd h as baseline, COX-2 expressions of the 4th h and 8th h in AIP were significant higher (2nd h, 0.23±0.03, $P<0.05$; 4 h, 1.55±0.93, 8th h, 4.04±1.05, 16th h, 3.73±0.15 and 24th h, 3.37±0.23, $P<0.01$ respectively). Compared with controls, this increase was also significant ($P<0.01$).

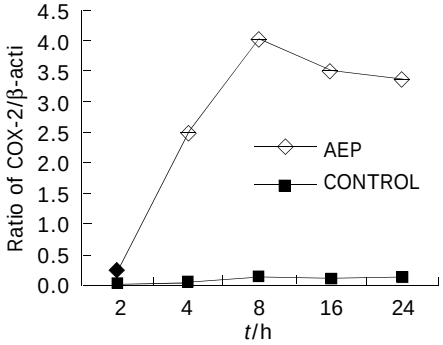

Figure 1 Time course of COX-2 gene expression in pancreas. After induction by caerulein, the expression of COX-2 mRNA in AEP was increased, which peaked at the 8th h and remained at a high level.

Inflammatory indicators for pancreatitis

The activity of serum AMS and MPO in AEP and controls are shown in Table 1.

Table 1 Levels of amylase (AMS) and myeloperoxidase (MPO) in AEP and control groups (mean±SD)

Group	*n*	MPO (U/mL)	AMS (U/dL)
Control (0 h)	24	0.32±0.13	40±37
AEP 2nd h	6	0.60±0.20	313±130[a]
4th h	6	0.74±0.39[b]	391±96[a]
8th h	6	0.85±0.56[b]	255±92[a]
16th h	6	0.88±0.29[b]	291±73[a]
F		4.542	12.322

[a]$P<0.05$, [b]$P<0.01$ *vs* control.

In vivo fluorescent microscopy

Compared with the control, the pancreatic microvasculature changes at the 4th, 6th and 8th h after caerulein were as follows: (a) the reduction of the density and velocity of FITC-RBC (4, 6 and 8th h $P<0.001$); (b) the decrease of the pancreatic capillary blood flow (4, 6, and 8th h, $P<0.001$); (c) diminution of functional capillary density (4th h, $P>0.05$; 6th h, $P<0.05$; 8th h, $P<0.001$) and arteioles diameter (4th h, $P>0.05$; 6th h and 8th h, $P<0.05$); (d) insufficient capillary perfusion appeared at the 8th h; (e) arterioles of pancreatic lobules and capillary density at the 6th h experienced significant changes, while the calibers of venules and capillaries shown no marked change (Table 2).

Microvascular permeability in pancreas and lungs

The PI from rats of control were shown little changes before and after injection of 0.9% sodium chloride, while both pancreas and lungs showed a significant increase in microvasculature from the 4th h to 16th h in rats of AEP and the increase in the lungs was higher than that in the pancreas (Lungs, 8th and 16th h, $P<0.001$, respectively; pancreas 8th and 16th h, $P<0.01$,

Table 2 Response of pancreatic local microvascular in AEP and controls (mean±SD)

	4th h		6th h		8th h	
	NC	AIP	NC	AIP	NC	AIP
[1]Density of RBC /(±10[9]cell/L)	113±5	85±9[a]	104±4	68±7[a]	96±6	59±9[a]
[2]Velocity of RBC /(cell/min)	86±3	43±2[a]	81±4	36±5[a]	84±5	30±5[a]
[3]RBC flow (nL/L)	0.28±0.01	0.12±0.03[a]	0.31±0.02	0.09±0.03[a]	0.29±0.04	0.07±0.03[a]
[4]Blood flow	0.88±0.06	0.56±0.09[a]	0.99±0.07	0.45±0.12[a]	0.91±0.06	0.34±0.10[a]
[5]Diameter (arteriod)/μm	23.5±8.0	20.2±5.1[a]	24.1±8.0	16.4±3.1[a]	23.2±5.5	18.2±3.5[a]
[6]Diameter (venule)/μm	28±3.0	29.1±2.0[a]	28±2.7	27.5±3.0[a]	27.4±1.6	29±1.5[a]
[7]Diameter (capillary)/μm	6.7±1.5	7.0±1.4[a]	6.9±1.5	6.0±0.3[a]	7.3±1.0	5.2±0.3[a]
[8]Density (capillary)/cm	394±7	381±9[a]	400±6	291±16[a]	349±8	277±13[a]

[1]F=109.68, P<0.01 ; [2]F=478.8, P<0.01 ; [3]F=185.2, P<0.01; [4]F=1.99, P<0.01; [5]F=3.52, P<0.001; [6]F=1.12, P>0.05; [7]F=5.71, P<0.001; [8]F=312.12, P<0.01; [a]P<0.05 *vs* control.

respectively) (Figure 2). The water mass fractions in the pancreas were increased after caerulein injection compared with controls (2nd h, 19.18±2.10; 4th h, 24.81±1.31; 8th h, 25.86±1.97; 16th h, 30.71±5.80, P<0.05), while the water mass fraction in normal remained relative stable.

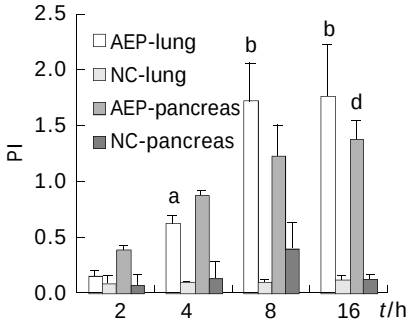

Figure 2 Microvascular permeability index (PI) in the pancreas and lungs in AEP and control group. The figures indicate the increase of PI in the lungs is higher than that in the pancreas [a]P<0.05 *vs* control; [b]P<0.001 *vs* control; [d]P<0.01 *vs* control.

DISCUSSION

Previous studies have discovered that COX-2 is the principal isoform of cyclooxygenase that participates in inflammation, while there is little COX-2 activity present in the stomach, kidney, or platelet. COX-2 is usually barely detectable during normal physiologic conditions. However, in response to several pro-inflammatory stimuli, the level of COX-2 expression can be rapidly induced to increase[18-20]. In our study, we found that COX-2 transcription remains at a very low level in normal pancreatic tissue. In contrast, COX-2 expression was increased rapidly after induction of pancreatitis by caerulein. COX-2 may serve as one of factors of at the early phase of inflammation. During the active inflammation, the synthesis of PGE_2 (an important inflammatory mediator), the increase of vaso-permeability, sequestration of inflammatory cells and pyrogen are likely resulted from COX-2.

It has been reported that a strong correlation between the number of intra-vascular neutrophils and MPO existed. Thus these parameters were measured to quantify the total neutrophil sequestration to the pancreas[21-23]. In our previous study, we found the positive correlation between COX-2 and MPO in AEP (r=0.5449, P<0.05). From this study, the elevation of plasma myeloperoxidase was present in the experiment, suggesting MPO can serve as an indicator of AEP.

There is increasing evidence that the vascular endothelium, which is directly exposed to various fluid mechanical forces generated by pulsatile blood flow, can discriminate among these stimuli and transduce them into genetic regulatory events, as COX-2 gene can be upregulated by steady laminar shear stress stimulation[25]. However little is known about the upregulation of COX-2 disturbing microcirculation. It is generally accepted that the dysfunction of pancreatic microcirculatory serves as an important causative factor for the development of acute pancreatitis. The morphology of pancreatic microcirculation revealed that pancreatic lobule is supplied by a single intralobular arteriole, which is considered end-artery[21,24-26]. This characteristic suggested that pancreatic lobules are susceptible to ischemic injury due to spasm of intralobular arterioles. In this study, we observed the responses of pancreatic microvascular after caerulein induction, which demonstrated that the enhanced COX-2 mRNA might involve in modulating the dynamical changes of the pancreatic microcirculation. The decrease of pancreatic capillary blood flow, the reduction of functional capillary density, and capillary perfusion irregular intermittent perfusion and capillary artery hypoperfusion were observed, especially at 8[th] h, which was coincident with the enhanced expression of COX-2 mRNA after AEP.

Based on the pathologic changes above, we postulate that COX-2 induce the inflammation of vascular endothelia, result in increase of vasopermeability, sequestration of leukocyte and water content in the pancreatic tissue. A functional role of the COX-2, mediating the changes of pancreatic microcirculation has several possible explanations: (1) it may be cooperated with inducible nitric oxide synthase (iNOS), and both mediators can activate platelets and leukocytes, promote the occurrence of microthrombus and affect microcirculatory stability[27]; (2) it may be in linkage with the overexpression of adhesion molecules (e.g. ICAM-1, PCAM-1). Adhesion molecules are known to regulate partly the disturbance of microvascular barrier both *in vivo* and *in vitro*[28,29]. Treatment with the monoclonal antibodies against ICAM-1, PECAM-1 to rats with gut barrier failure caused by intestinal ischemia and reperfusion (I/R) seemingly

most efficiently reduces the severity of I/R (i.e., enhanced capillary blood flow in the pancreas, reduced leukocyte rolling and stabilized capillary permeability)[30,31]; (3) it may be feedback control of COX-2 expression through peroxisome proliferator-activated receptor-γ (PPAR-γ). PPAR-γ expressed in macrophages has been postulated as a negative regulator of inflammation[9]. Additional investigation will be necessary to distinguish between these mechanisms of action.

REFERENCES

1 **Foitzik T**, Faulhaber J, Hotz HG, Kirchengast M, Buhr HJ. Endothelin receptor blockade improves fluid sequestration, pancreatic capillary blood flow and survival in severe experimental pancreatitis. *Ann Surg* 1998; **228**: 670-675

2 **Zhou ZG**, Chen YD. Influencing factors of pancreatic micrcirculatory impairment in acute pancreatitis. *World J Gastroenterol* 2002; **8**: 406-412

3 **Menger MD**, Plusczyk T, Vollmar B. Microcirculatory derangements in acute pancreatitis. *J Hepatobiliary Pancreat Surg* 2001; **8**: 187-194

4 **Dembinski A**, Warzecha Z, Ceranowicz P, Stachura J, Tomaszewska R, Konturek SJ, Sendur R, Dembinski M, Pawlik WW. Pancreatic damage and regeneration in the course of ischemia- reperfusion induced pancreatitis in rats. *J Physiol Pharmacol* 2001; **52**: 221-235

5 **Jaffray C**, Yang J, Carter G, Mendez C, Norman J. Pancraetic elastase activates pulmonary nuclear factor kappa B and inhibitory kappa B, mimicking pancreatitis -associated adult respiratory distress syndrome. *Surgery* 2000; **128**: 225-231

6 **Heuser M**, Popken O, Kleiman I, Post S. Detrimental effects of octreotide on intestinal microcirculation. *J Surg Res* 2000; **92**: 186-192

7 **Yamanaka K**, Saluja AK, Brown GE, Yamaguchi Y, Hofbauer B, Steer ML. Protective effects of prostaglandin E_1 on acute lung injury of caerulein-induced acute pancreatitis in rats. *Am J Physiol* 1997; **272**: G23-G30

8 **Caughey GE**, Cleland LG, Gamble JR, James MJ. Up-regulation of endothelial cyclooxygenase-2 and prostanoid synthesis by platelets. Role of thromboxane A_2. *J Biol Chem* 2001; **276**: 37839-37845

9 **Crofford LJ**, Wilder RL, Ristimaki AP, Sano H, Remmers EF, Epps HR, Hla T. Cyclooxygenase-1 and 2 expression in rheumatoid synovial tissues. Effects of interleukin-1β, phorbol ester, and corticosteroids. *J Clin Invest* 1994; **93**: 1095-1101

10 **Tamura M**, Sebastian S, Gurates B, Yang S, Fang Z, Bulun SE. Vascular endothelial growth factor upregulates Cydooxygenase-2 expression in human endothelia cells. *J Clin Endocrinol Metab* 2002; **87**: 3504-3507

11 **Inoue H**, Tanabe T, Umesono K. Feedback control of Cydooxygenase-2 expression through PPARγ. *J Biol Chem* 2000; **275**: 28028-28032

12 **Chen JX**, Berry LC Jr, Christman BW, Tanner M, Myers PR, Meyrick BO. NO regulates LPS -stimulated cydooxygenasegene expression and activity in pulmonary artery endothelium. *Am J Physiol Lung Cell Mol Physiol* 2001; **280**: L450-457

13 **Williams CS,** Dubois RN. Prostaglandin endoperoxide synthase: why two isoforms? *Am J Physilo* 1996; **270**: G393-400

14 **Crofford LJ**. Prostaglandin biology. *Gastroenterol Clin North Am* 2001; **30**: 863-876

15 **Colville-Nash PR**, Gilroy DW. COX-2 and the cyclopentenone prostaglandins-a new chapter in the book of inflammation? *Prostaglandins Other Lipid Media* 2000; **62**: 33-43

16 **Parfenova H**, Parfenov VN, Shlopov BV, Levine V, Falkos S, Pourcyrous M, Leffler CW. Dynamics of nuclear localization sites for COX-2 in vascular endothelial cells. *Am J Physiol* 2001; **81**: C166-C178

17 **Zabel-Langhennig A**, Holler B, Engeland K, Mossner J. Cydooxygenase-2 transcription is stimulated and amylase secretion is inhibited in pancreatic acinar cells after induction of acute pancreatitis. *Biochem Biophys Res Commun* 1999; **265**: 545-549

18 **Inoue H**, Umesono K, Nishimori T, Hirata Y, Tanabe T. Glucocorticiod- mediated suppression of the promoter activity of the Cydooxygenase-2 gene is modulated by expression of its receptor in vascular endothelial cells. *Biochem Biophys Res Commun* 1999; **254**: 292-298

19 **maszewska R**, Dembinski A, Warzecha Z, Ceranowicz P, Konturek SJ, Stachura J. The influence of epidermal growth factor on the course of ischemia-reperfusion induced pancreatitis in rats. *J Physiol Pharmacol* 2002; **53**: 183-198

20 **Calkins CM**, Barsness K, Bensard DD, Vasquez-Torres A, Raeburn CD, Meng X, McIntyre RC Jr. Toll-like receptor-4 signaling mediates pulmonary neutrophil sequestration in response to Gram-positive bacterial enterotoxin. *J Surg Res* 2002; **104**: 124-130

21 **Zhou ZG**, Gao XH, Wayand WU, Xiao LJ, Du Y. Pancreatic microcirculation in the monkey, with special reference to the blood drainage system of Langerhans islets: Light and scanning electron microscopic study. *Clin Anat* 1996; **9**: 1-9

22 **Peskar BM**, Maricic N, Gretzer B, Schuligoi R, Schmassmann A. Role of cyclooxygenase-2 in gastric mucosal defense. *Life Sci* 2001; **69**: 2993-3003

23 **Calkins CM**, Barsness K, Bensard DD, Vasquez-Torres A, Raeburn CD, Meng X, McIntyre RC. Toll-like receptor-4 signaling mediates pulmonary neutrophil sequestration in response to gram-positive bacterial enterotoxin. *J Surg Res* 2002; **104**: 124-130

24 **Dib M**, Zhao X, Wang XD, Andersson R. Role of mast cells in the development of pancreatitis- induced multiple organ dysfunction. *Br J Surg* 2002; **89**: 172-178

25 **Gimbrone MA**, Topper JN, Nagel T, Anderson KR, Garcia-Cardena G. Endothelial dysfunction, hemodynamic forces and atherogenesis. *Ann NY Acad Sci* 2002 **902**: 230-239

26 **Plusczyk T**, Bersal B, Westermann S, Menger M, Feifel G. ET-1 induces pancreatitis-like microvascular deterioration and acinar cell injury. *J Surg Res* 1999; **85**: 301-310

27 **Zhou ZG**, Zhang ZD, Yan LN, Shu Y, Cheng Z, Zhao JC, Lan P, Feng XM, Wang R. The feature of pancreatic microcirculatory impairment in caerulein induced acute pancreatitis. *Zhonghua Waike Zazhi* 1999; **37**: 138-140

28 **Gao HK**, Zhou ZG, Chen YQ, Han FH, Wang C. Expression of platelet endothelial cell adhesion molecule-1 between pancreatic microcirculation and peripheral circulation in rats with acute edematous pancreatitis. *Hepatobiliary Pancreat Dis Int* 2003; **2**: 463-466

29 **Zingarelli B**, Southan GJ, Gilad E, O'Connor M, Salzman AL, Szabo C. The inhibitory effects of mercaptoalkyguanidines on cyclo-oxygenase activity. *Br J Pharmacol* 1997; **120**: 357-366

30 **Sun Z**, Wang X, Lasson A, Bojesson A, Annborn M, Andersson R. Effects of inhibition of PAF, ICAM-1 and PECAM-1 on gut barrier failure caused by intestinal ischemia and reperfusion. *Scand J Gastroenterol* 2001; **36**: 55-65

31 **Frossard JL**, Saluja A, Bhagat L, Lee HS, Bhatia M, Hofbauer B, Steer ML. The role of intercellular adhesion molecule 1 and neutrophils in acute pancreatitis and pancreatitis -associated lung injury. *Gastroenterology* 1999; **116**: 694-701

Edited by Zhang JZ **Proofread by** Chen WW and Xu FM

PO Box 2345, Beijing 100023, China
Fax: +86-10-85381893
E-mail: wjg@wjgnet.com www.wjgnet.com

World J Gastroenterol 2004;10(14):2099-2102
World Journal of Gastroenterology
 ISSN 1007-9327

• BASIC RESEARCH •

Management of carbon tetrachloride-induced acute liver injury in rats by syngeneic hepatocyte transplantation in spleen and peritoneal cavity

Charalampos Pilichos, Despina Perrea, Maria Demonakou, Athena Preza, Ismini Donta

Charalampos Pilichos, Athena Preza, Third Department of Propaudeutic Surgery, University of Athens, Sotiria Hospital, Athens, Hellas
Despina Perrea, Ismini Donta, Laboratory of Experimental Surgery, University of Athens, Hellas
Maria Demonakou, Laboratory of Pathological Anatomy, Sismanogleion General Hospital, Athens, Hellas
Correspondence to: Dr. Charalampos Pilichos, Mpoumpoulinas 27-15341- Ag Paraskevi, Athens, Hellas (Greece). hpilichos@hotmail.com
Telephone: +30-210-6524097 **Fax:** +30-210-6524097
Received: 2004-01-02 **Accepted:** 2004-01-17

Abstract

AIM: Acute hepatitis may seldom have a fulminant course. In the treatment of this medical emergency, potential liver support measure must provide immediate and sufficient assistance to the hepatic function. The goal of our study was to study the adequacy of hepatocyte transplantation (HCTx) in two different anatomical sites, splenic parenchyma and peritoneal cavity, in a rat model of reversible acute hepatitis induced by carbon tetrachloride (CCl_4).

METHODS: After CCl_4 intoxication, 84 male Wistar rats used as recipients were divided in to four experimental groups accordingly to their treatment: Group A (n=24): intrasplenic transplantation of $10x10^6$ isolated hepatocytes, Group B (n=24): intraperitoneal transplantation of $20x10^6$ isolated hepatocytes attached on plastic microcarriers, Group C (n=18): intrasplenic injection of 1 mL normal saline (sham-operated controls), Group D (n=18): intraperitoneal injection of 2.5 mL normal saline (sham-operated controls). Survival, liver function tests (LFT) and histology were studied in all four groups, on d 2, 5 and 10 post-HCTx.

RESULTS: The ten-day survival (and mean survival) in the 4 groups was 72.2% (8.1±3.1), 33.3% (5.4±3.4), 0% (3.1±1.3) and 33.3% (5.4±3.6) in groups A, B, C, D, respectively ($P_{AB}<0.05$, $P_{AC}<0.05$, P_{BD}=NS). In the final survivors, LFT (except alkaline phosphatase) and hepatic histology returned to normal, independently of their previous therapy. Viable hepatocytes were identified within splenic parenchyma (in group A on d 2) and both in the native liver and the fatty tissue of abdominal wall (in group B on d 5).

CONCLUSION: A significantly better survival of the intrasplenically transplanted animals has been demonstrated. Intraperitoneal hepatocytes failed to promptly engraft. A different timing between liver injury and intraperitoneal HCTx may give better results and merits further investigation.

Pilichos C, Perrea D, Demonakou M, Preza A, Donta I. Management of carbon tetrachloride-induced acute liver injury in rats by syngeneic hepatocyte transplantation in spleen and peritoneal cavity. *World J Gastroenterol* 2004; 10(14): 2099-2102
http://www.wjgnet.com/1007-9327/10/2099.asp

INTRODUCTION

Acute hepatitis may seldom have a fulminant course. In the treatment of this medical emergency, potential liver support measure must provide immediate and sufficient assistance to the hepatic function. Hepatocyte transplantation (HCTx) is a mainly experimental and minimally invasive method for liver support, offering the opportunity for native liver regeneration in cases of reversible failure or serving as a "bridge" to whole liver transplantation in cases of irreversible damage. However, for the clinical implementation of this newly developed technique both theoretical and practical aspects have to be further elucidated.

Various anatomical sites for cell implantation such as native liver, spleen, peritoneal cavity, kidney, lung, pancreas and fat pads have been investigated by different teams since the introduction of the method, but their results are not conclusive due to the great methodological diversity[1-7]. The spleen is considered as the most privileged anatomical site for HCTx. It is accessible by means of laparotomy. It can entrap a limited, but a sufficient number of hepatocytes within its sinusoids, providing conditions very similar to natural cell microenvironment. This process has been described by Mito in the early 1980's, by the term "splenic hepatization"[8]. On the other hand, peritoneal cavity is very promising as it can be accessed by minimally invasive means and allows the injection of a greater number of cells. However, the major disadvantage of intraperitoneal route was the inability of injected cells to promptly engraft and thus to receive an adequate vascular supply. This led to cell death in three days following transplantation[9]. To overcome this limitation, Demetriou *et al*. introduced the technique of cell attachment on collagen-coated dextran-microcarriers, prior to transplantation[10]. Since then, most experimental studies have relied on this concept. Microcarrier-attached hepatocytes can survive for a long time, forming neovascularized aggregates[11].

The aim of our study was to study the adequacy of HCTx in two different anatomical sites, splenic parenchyma and peritoneal cavity, in a rat model of reversible acute hepatitis induced by carbon tetrachloride (CCl_4).

MATERIALS AND METHODS

Donors

Hepatocyte isolation Fifteen male Wistar rats (Institute Pasteur-Athens), weighing 300-450 g were used as donors of hepatocytes. For cell isolation, we used collagenase perfusion/incubation technique, which was previously described by our team[12]. Aliquots were taken for cell count (Neubauer hemocytometer) and determination of cellular viability (Trypan Blue Exclusion Test).

Recipients

Development of acute hepatitis model In preliminary experiments, we tested a wide range of CCl_4 doses (0.5-4 mL/kg) given intraperitoneally in 35 controls. Total bilirubin, SGOT,

SGPT and ALP levels were measured before and after CCl_4 administration and correlated with the histological severity of liver damage. A single dose of 1 mL/kg CCl_4, dissolved in olive oil in a ratio of 1:5 v/v, resulted in approximately 10% mortality of acute hepatic injury within 24 h. This dosage allowed liver support measures to be initiated before animal death and was used for all experiments reported herein.

Experimental groups

One hundred male Wistar rats (Institute Pasteur-Athens) weighing 300-450 g were used as candidate recipients. They were maintained in a 48-h dark/light cycle, had free access to food and water and were given CCl_4 at the above-mentioned dose (d 0). Twenty-four hours later (d 1), 84 survivors were divided into 4 groups accordingly to their subsequent therapy: Group A (n=24): intrasplenic transplantation of 10×10^6 isolated hepatocytes, Group B (n=24): intraperitoneal transplantation of 20×10^6 isolated hepatocytes attached on plastic microcarriers, Group C (n=18): intrasplenic injection of 1 mL normal saline (sham-operated controls), Group D (n=18): intraperitoneal injection of 2.5 mL normal saline (sham-operated controls).

Transplantation technique

All rats were transplanted under ketamine and midazolame anesthesia. For intasplenic HCTx, cell suspension was diluted in 1 mL of Hank' s solution and injected after laparotomy using a 27G needle. Leakage was prevented with suture at the point of injection. Prior to intraperitoneal HCTx, cells were attached onto gelatin-coated plastic beads (Sigma, 1.5 g/10 g of liver tissue) by incubation at 37 ℃ for 45 min. Cell suspension was diluted in 2.5 mL of Hank' s solution and subsequently injected using an 18G needle

Survival, liver function tests and histological study

Eighteen rats in groups A and B and nine rats in control groups C and D were observed for a 10-day period, in order to determine survival (survival rate and mean survival). Three animals from each group were sacrificed on d 2 and 5 respectively for biochemical and histological study. Final survivors were also sacrificed on day 10 for both biochemical and histological study. Sacrifice was achieved under general anesthesia according to the guidelines of the Hellenic National Research Council. Blood samples were taken directly from the left ventricle. Total bilirubin, SGPT, SGOT and alkaline phosphatase were measured in all groups. Liver, spleen and cell aggregates (when macroscopically visible) were taken for anatomical study. After fixation in buffered formaldehyde 40 g/L, they were stained with hematoxylin/eosin. The prepared sections were assessed systematically under code by one hepatopathologist, who was unaware of protocol features.

Determination of normal and baseline values

Normal and baseline values (24 h after CCl_4 administration) of liver function tests were measured in ten controls before and 24 h after CCl_4-intoxication.

Statistical analysis

For statistical analysis of mean survival and liver function tests we used Student' s t-test. For statistical analysis of 10-day survival rate we used chi-square test. Statistical significance level was set at P<0.05.

RESULTS

Number and viability of isolated hepatocytes

A mean of approximately 250×10^6 of liver cells was harvested from each donor, with a mean viability greater than 90%.

Survival rate

In all 4 groups, the 10-day survival rate was: 13/18 (72.2%), 6/18 (33.3%), 0/9 (0%) and 3/9/(33.3%) in groups A, B, C, D, respectively. Furthermore, the mean survival was 8.1±3.1 d, 5.4±3.4 d, 3.1±1.3 d and 5.4±3.6 d in groups A, B, C, D, respectively (Figures 1 and 2). Statistically significant difference between transplanted groups (A and B) and their respective controls (C and D) was proven only for the intrasplenic HCTx (P_{AC}<0.05, P_{BD}=NS). Differences in 10-day survival rate and mean survival between groups A and B were also statistically significant (P_{AB}<0.05). All animals with a decreased survival time died within six days after CCl_4 poisoning.

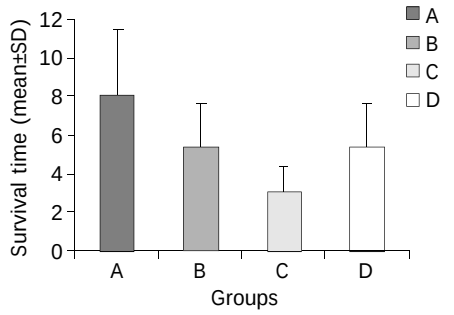

Figure 1 Mean survival in all four groups (P_{AC}<0.05, P_{BD}=NS, P_{AB}<0.05).

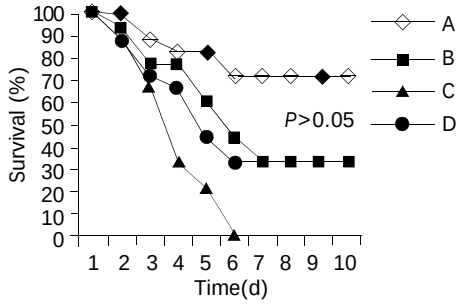

Figure 2 Survival curves in all four groups. Notice that all animal deaths occurred within the first 6 d after poisoning.

Table 1 Liver function tests during the 10-day observation period

		Day 2	Day 5	Day 10
Total Bilirubin (mg / dL)	A	0.53±0.05	0.33±0.05	0.35±0.10
	B	0.60±0.10	0.46±0.05	0.37±0.14
	C	0.86±0.10	0.76±0.10	[1]
	D	0.86±0.15	0.66±0.15	0.20±0.10
SGPT (IU / L)	A	273±76.2	67.5±32.1	29.2±11
	B	400.3±155	61.6±27.7	54.8±25.0
	C	710±29.3	90.3±23.1	[1]
	D	507.3±91.2	66±22.7	56.3±14.9
SGOT (IU / L)	A	380.6±63.4	68.3±24.1	84±13.3
	B	779.3±235.2	287.6±114	76.8±30.9
	C	1 088.3±131.7	610.6±148.6	[1]
	D	836.6±171.2	250.6±139.6	112±63.2
Alkaline Phosphatase (IU / L)	A	469.3±157.5	427.6±129.5	343.1±180.5
	B	88.6±50	58.6±39	564.3±142.7
	C	123.6±50.5	116.3±37.4	[1]
	D	104±31.1	129.3±41.7	792.3±246.5

All differences between final and baseline values were statistically significant. [1]All animals died before d 10. (Normal Values: Total Bilirubin: 0.18±0.07 mg / dL, SGPT: 44.1±24.8 IU / L, SGOT: 53.4±23.6 IU / L, Alk. Phosphatase: 86.8±49.6 IU / L -Baseline

Value: Total Bilirubin: 0.6±0.09 mg / dL, SGPT: 616.1±117.5 IU / L, SGOT: 1296.7±381.2 IU / L, Alk. Phosphatase: 91.4±63 IU / L).

Laboratory findings

After CCl_4 administration the rats responded with a marked increase in both serum aminotransferases, a moderate elevation in total bilirubin, while alkaline phosphatase was not affected. Table 1 summarizes the mean total bilirubin, SGPT, SGOT and alkaline phosphatase values during the whole period of the experimental observation.

On d10, in all experimental groups total bilirubin and aminotransferase levels were significantly lower than their pre-transplantation levels. In contrast, all final survivors presented significantly higher levels of alkaline phosphatase, independently of their previous therapy.

Histological findings

Twenty-four hours following CCl_4 intoxication, liver submassive necrosis affecting zone 3 of the hepatic lobule was the main histological finding. The type of cell injury leading to necrosis was more often ballooning degeneration and apoptosis. Normal hepatic histology was present in all final survivors. Viable hepatocytes were found within splenic parenchyma by d 2, forming structures similar to liver plates (Figure 3). Microcarrier-cell aggregates were macroscopically detected by d 5, within the native liver and the fatty tissue of the abdominal wall. The histological study of implants revealed presence of viable hepatocytes and formation of neo-vessels in the surrounding tissues (Figure 4).

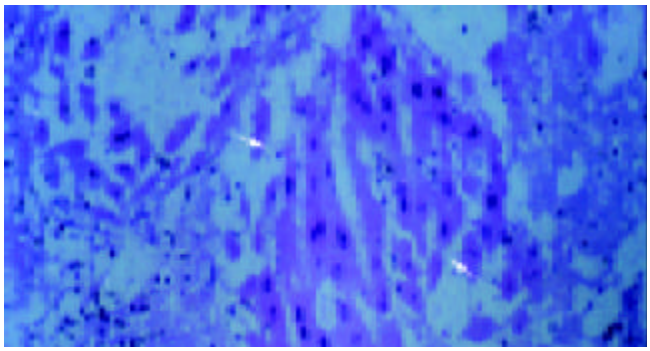

Figure 3 Viable hepatocytes within splenic parenchyma, forming structures similar to liver plates on d 2 (the so-called "splenic hepatization").

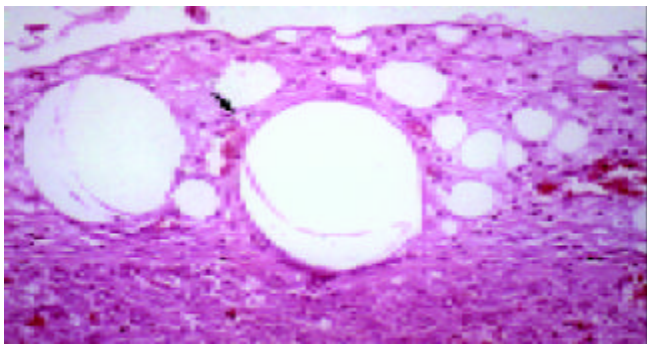

Figure 4 Microcarrier-cell aggregates within native liver parenchyma, Formation of neo-vessels in surrounding tissue on d 5.

DISCUSSION

To the best of our knowledge, this is the first experimental study, investigating two of the most popular anatomical sites for HCTx, in a model of chemically induced acute hepatic injury. In their original work, te Velde *et al*. compared and found equivalent intrasplenic and intraperitoneal HCTx, in a model of liver ischemia-induced failure[13]. However, liver ischemia based on liver devascularization in rodents is a model that induces massive hepatic necrosis within a few hours, but in contrast to hepatic failure in humans, the damage is always irreversible. Thus, we have chosen to work on CCl_4-induced acute hepatitis model, although it did not strictly meet the criteria of acute liver failure, because the induced liver damage was potentially reversible, mostly resembling the clinical course of the syndrome in humans and consequently was considered more realistic[14,15].

A significantly better survival of intrasplenically transplanted animals has been demonstrated, suggesting the superiority of the spleen as a site for cell implantation in this experimental model. Intraperitoneal hepatocytes failed to promptly engraft and provided a delayed and probably useless liver support, indicating that the right timing between induction of liver injury and HCTx seems to be of major importance. Actually, Demetriou *et al*. observed that when microcarrier-attached hepatocytes were transplanted 3 d prior to 90% hepatectomy in rats, they induced a marked improvement in long term survival, whereas when they were transplanted after hepatectomy they did not[16].

Furthermore, the rats succeeding to survive until d 6, remained alive for the whole 10-day period and their liver function tests and histology returned almost to normal, independently of their previous therapy. These survival data and laboratory findings are highly suggestive of the presence of a "crucial period" (extending from d 0 to d 6 in this experimental model), during which liver support measures must be initiated. Reversal of hepatic damage seems to be due initially to the direct action of engrafted hepatocytes during this "crucial period" and subsequently to the host liver recovery, taking place in all survivors beyond this period, independently of their initial treatment. Actually, the significant increase in alkaline phosphatase levels, occurring after d 5, could more possibly be attributed to the native liver regeneration than to a late cholestasis[17].

In conclusion, intrasplenic HCTx has been proved effective on providing liver support, after CCl_4-intoxication. In contrast, a certain inability of intraperitoneally transplanted hepatocytes for immediate engraftment and vascularization, even after attachment onto microcarriers was observed in this experimental model. A different timing between liver injury and HCTx might give better results and merits further investigation. Theoretically, the intraperitoneal route has many advantages, such as easy accessibility and great capacity for cells implantation. To our opinion research should be encouraged towards this direction. It seems highly possible that the recent advances in various fields, such as the development of new biomaterials and especially the introduction of humoral factors accelerating the process of neovascularization, may overcome the current limitations of the intraperitoneal HCTx[18,19].

REFERENCES

1 **Matas AJ,** Sutherland DE, Stefes MW, Mauer SM, Sowe A, Simmons RL, Najarian JS. Hepatocellular transplantation for metabolic deficiencies: decrease of plasma bilirubin in Gunn rats. *Science* 1976; **192:** 892-894

2 **Mito M,** Ebata H, Kusano M, Onishi T, Saito T, Sakamoto S. Morphology and function of isolated hepatocytes transplanted into rat spleen. *Transplantation* 1979; **28:** 499-505

3 **Sutherland DE,** Numata M, Matas AJ, Simmons RL, Najarian JS. Hepatocellular transplantation in acute liver failure. *Surgery* 1977; **82:** 124-132

4 **Ricordi C,** Flye MW, Lacy PE. Renal subcapsular transplantation of clusters of hepatocytes in conjunction with pancreatic islets. *Transplantation* 1988; **45:** 1148-1151

5 **Selden C,** Gupta S, Johnstone R, Hodgson HJ. The pulmonary vascular bed as a site for implantation of isolated liver cells in inbred rats. *Transplantation* 1984; **38:** 81-83

6 **Vroemen JP**, Buurman WA, van der Linden CJ, Visser R, Heirwegh KP, Kootstra G. Transplantation of isolated hepatocytes into the pancreas. *Eur Surg Res* 1988; **20**: 1-11

7 **Groth CG**, Arborgh B, Bjorken C, Sundberg B, Lundgren G. Correction of hyperbilirubinemia in the glucuronyltransferase-deficient rat by intraportal hepatocyte transplantation. *Transplant Proc* 1977; **9**: 313-316

8 **Mito M**, Ebata H, Kusano M, Onishi T, Hiratsuka M, Saito T. Studies on ectopic liver utilizing hepatocyte transplantation into the rat spleen. *Transplant Proc* 1979; **11**: 585-591

9 **Henne-Bruns D**, Kruger U, Sumpelmann D, Lierse W, Kremer B. Intraperitoneal hepatocyte transplantation: morphological results. *Virchows Arch A Pathol Anat Histopathol* 1991; **419**: 45-50

10 **Demetriou AA**, Whiting JF, Feldman D, Levenson SM, Chowdhury NR, Moscioni AD, Kram M, Chowdhury JR. Replacement of liver function in rats by transplantation of microcarrier-attached hepatocytes. *Science* 1986; **233**: 1190-1192

11 **Arkadopoulos N,** Rozga J, Petrovic L. Intraperitoneal transplantation of microcarrier-attached hepatocytes. In: Mito M, Sawa M ed. Hepatocyte transplantation. *Basel Karger* **1997**; 98-106

12 **Fotiadis C**, Pilichos H, Preza A, Papalois A, Demonakou M, Perrea D, Xekouki P, Poussios D, Karampela E, Papadopoulou A, Grigoriou T, Karayannakos P, Sechas M. Transplantation of cultured allogeneic hepatocytes without immunosuppression. *Transplant Proc* 2001; **33**: 2400-2403

13 **te Velde AA**, Bosman DK, Oldenburg J, Sala M, Maas MA, Chamuleau RA. Three different hepatocyte transplantation techniques for enzyme deficiency disease and acute hepatic failure. *Artif Organs* 1992; **16**: 522-526

14 **Sommer BG**, Sutherland DE, Simmons RL, Najarian JS. Hepatocellular transplantation for experimental ischemic acute liver failure in dogs. *J Surg Res* 1980; **29**: 319-325

15 **Chamuleau RAFM.** Hepatocyte transplantation for acute liver failure. In: Mito M, Sawa M ed. Hepatocyte transplantation. *Basel Karger* **1997**: 159-163

16 **Demetriou AA**, Reisner A, Sanchez J, Levenson SM, Moscioni AD, Chowdhury JR. Transplantation of microcarrier-attached hepatocytes into 90% partially hepatectomized rats. *Hepatology* 1988; **8**: 1006-1009

17 **Pelton JJ**, Hoffman JP, Eisenberg BL. Comparison of liver function tests after hepatic lobectomy and hepatic wedge resection. *Am Surg* 1998; **64**: 408-414

18 **Mooney DJ**, Kaufmann PM, Sano K, McNamara KM, Vacanti JP, Langer R. Transplantation of hepatocytes using porous, biodegradable sponges. *Transplant Proc* 1994; **26**: 3425-3426

19 **de Roos WK**, Borel Rinkes IH, Minnee P, Toet KH, Bouwman E, Kooistra T, Valerio D, Bruijn JA, Terpstra OT. Hepatocyte transplantation into solid supports in the rhesus monkey: the influence of acidic fibroblast growth factor on prevascularization and hepatocyte survival. *Transplant Proc* 1995; **27**: 633-634

Edited by Wang XL **Proofread by** Xu FM

PO Box 2345, Beijing 100023, China
Fax: +86-10-85381893
E-mail: wjg@wjgnet.com www.wjgnet.com

World J Gastroenterol 2004;10(14):2103-2108
World Journal of Gastroenterology
 ISSN 1007-9327

• BASIC RESEARCH •

Bridging PCR and partially overlapping primers for novel allergen gene cloning and expression insert decoration

Ai-Lin Tao, Shao-Heng He

Ai-Lin Tao, Shao-Heng He, Allergy and Inflammation Research Institute, Medical College, Shantou University, Shantou 515031, Guangdong Province, China
Supported by the Li Ka Shing Foundation, Hong Kong, China, No. C0200001 and Natural Science Foundation of Guangdong Province, No. 034617
Correspondence to: Professor Shao-Heng He, Allergy and Inflammation Research Institute, Medical College, Shantou University, 22 Xin-Ling Road, Shantou 515031, Guangdong Province, China. shoahenghe@hotmail.com
Telephone: +86-754-8900405 **Fax**: +86-754-8900192
Received: 2004-01-15 **Accepted:** 2004-03-02

Abstract

AIM: To obtain the entire gene open reading frame (ORF) and to construct the expression vectors for recombinant allergen production.

METHODS: Gene fragments corresponding to the gene specific region and the cDNA ends of pollen allergens of short ragweed (Rg, *Ambrosia artemisiifolia* L.) were obtained by pan-degenerate primer-based PCR and rapid amplification of the cDNA ends (RACE), and the products were mixed to serve as the bridging PCR (BPCR) template. The full-length gene was then obtained. Partially overlapping primer-based PCR (POP-PCR) method was developed to overcome the other problem, i.e., the non-specific amplification of the ORF with routine long primers for expression insert decoration. Northern blot was conducted to confirm pollen sources of the gene. The full-length coding region was evaluated for its gene function by homologue search in GenBank database and Western blotting of the recombinant protein Amb a 8 (D106) expressed in *Escherichia coli* pET-44 system.

RESULTS: The full-length cDNA sequence of Amb a 8(D106) was obtained by using the above procedure and deduced to encode a 131 amino acid polypeptide. Multiple sequence alignment exhibited the gene *D106* sharing a homology as high as 54-89% and 79-89% to profilin from pollen and food sources, respectively. The expression vector of the allergen gene *D106* was successfully constructed by employing the combined method of BPCR and POP-PCR. Recombinant allergen rAmb a 8(D106) was then successfully generated. The allergenicity was hallmarked by immunoblotting with the allergic serum samples and its RNA source was confirmed by Northern blot.

CONCLUSION: The combined procedure of POP-PCR and BPCR is a powerful method for full-length allergen gene retrieval and expression insert decoration, which would be useful for recombinant allergen production and subsequent diagnosis and immunotherapy of pollen and food allergy.

Tao AL, He SH. Bridging PCR and partially overlapping primers for novel allergen gene cloning and expression insert decoration. *World J Gastroenterol* 2004; 10(14): 2103-2108
http://www.wjgnet.com/1007-9327/10/2103.asp

INTRODUCTION

Atopic diseases such as asthma, rhinitis, eczema, pollen allergies and food allergies have been increasing in most industrialized countries of the world during the last 20 years[1]. In the past years, we have improved our ability to recognize certain aspects of the pathogenesis of inflammatory bowel diseases, but our ability to effectively treat food and pollen allergy remains limited. The limitations for developing effective treatment regimens are due to some still unresolved and ambiguous aspects of the cross-reactivity of food and pollen allergy[2]. Among the "cross-reactivity" food allergies, the so-called pollen-related food allergies are the most important. Patients with pollinosis have a high risk of developing a related food allergy, up to 70% of the patients are also allergic to fruits, vegetables or nuts[3,4]. Short ragweed (Rg, *Ambrosia artemisiifolia* L.) is an important source of airborne allergens all over the world and has become an immunodominant allergen in China. Allergen-specific immunotherapy (SIT) represents one of the few curative approaches towards allergy[5], for which a powerful method is to express the recombinant allergen proteins *in vitro*. Therefore, it is pivotal to obtain full-length allergen gene and to construct the expression vector. Generally, many full-length genes are acquired by prior acquisition of the specific fragments, and subsequently constructed in conception with computers by joining the amphi-end sequences obtained by rapid amplification of cDNA end (RACE)[6]. In the process, a frequently occurred problem is the existence of alternatives in the amplification template. That is to say, though the length of amplified sequences is consistent with anticipation, the nucleotide compositions in different sequences are dramatically different and the existence of polymorphism is usually observed[7-11]. Screening and detection of different clones obtained would account for the main expenditure of the prophase work of gene cloning. As for the expression vector construction, specific primers needed usually comprise two parts. One is the region for restriction recognition or the vector specific sequences for ligation-independent cloning (LIC), like newly developed pET-44 EK/LIC system. The other is the gene specific region for stringent polymerase chain reaction (PCR). The melting temperature (Tm) of such primers always goes beyond the ordinary limit of 72 ℃, and the amplification specificity hence is reduced. It would be more disturbing when the GC content of the open reading frame (ORF) ends greatly deviates from 50%, which would usually occur in the 5' end of the ORF. To obviate the aforementioned problems, we have developed the *partially overlapping primer*-PCR (POP-PCR) method to surmount the non-specificity problem for long primers. This was then combined with bridging PCR (BPCR), which was coined for the PCR assay on joining two fragments containing a region of sequence similarity[12,13], to conquer the difficulty in retrieving the full-length gene in cDNA pool that was originally used for gene fragments cloning. In the current study, we successfully constructed the expression vector and expressed the allergen protein from Rg pollens, and hallmarked the allergenicity on the purified fusion protein.

MATERIALS AND METHODS

Subjects

Eight selected sera of patients with a well-defined case history of Rg pollen allergy and specific IgE antibodies against Rg pollen allergen (higher than 3.5 kU_A/L) were taken in Allergy Clinics, Shenyang North Hospital, Shenyang, China and used in this study. Thirteen sera from non-allergic individuals were recruited from the First Affiliated Hospital of Medical College, Shantou University, Shantou, China and used as negative controls.

Preparation of PCR template

Pollens of Rg were harvested from Wuhan, one of the four pervasive areas of short ragweed in China, and immediately submerged in liquid nitrogen. Following powder-grinding, total RNA was extracted by using RNeasy Maxi kit (Qiagen Valencia, CA, USA) according to the manufacturer's instructions. Reverse transcription (2 μg total RNA per sample) was then performed by using ProtoScript first strand cDNA synthesis kit (New England Biolabs, Beverly, MA, USA) according to the manufacturer's instructions. Subsequently, the 5' end of the gene (gene fragment A, Figure 1) was obtained by RT-PCR with primer pair Sg1P5/S3D10 (Table 1). Whereas the 3' end (gene fragment B in Figure 1) was acquired by RACE (rapid amplification of the cDNA end) method[6]. The cDNA pool, along with fragment A and fragment B would be used for the subsequent PCR templates.

Full-length gene cloning: BPCR

The amplification products A and B were mixed in equal volume and diluted 15-fold in distilled water. Bridging PCR (BPCR) outlined in Figure 1 was carried out by using 5 μL of the above diluents as template in 25 μL of the reaction mixture containing 1.25 U HotstarTaq DNA polymerase (Qiagen), 1×PCR buffer (Qiagen), 0.2 mmol/L dNTP, 0.4 μmol/L each of the primer pair Sg1P5 and RAC3 (Table 1). Thermal cycling was performed in a Peltier thermal cycler PTC-200 (MJ Research, Watertown, MA, USA) as follows. After an initial step at 95 ℃ for 15 min as recommended to activate the enzyme, the reaction temperature was decreased to 66 ℃ at the rate of -0.1 ℃/s followed by an extension at 72 ℃ for 5 min, then 7 touchdown cycles were carried out at 94 ℃ for 45 s, at 68 ℃ for 30 s and at 72 ℃ for 30 s, with the annealing temperature decreased by 1 ℃ per cycle. Subsequently, the reaction mixture was subjected to 30 conventional cycles at 94 ℃ for 45 s, at 66 ℃ for 30 s, and at 72 ℃ for 2 min. Conventional PCR was also conducted as a control by using cDNA pool aliquot as template. As visualized on a 12 g/L agarose gel, the target bands were recovered with a QIAquick™ gel extraction kit (Qiagen), cloned into pGEM-T easy vector (Promega Company, Madison, WI, USA), and transformed into *E. coli* strain JM109 (Promega). Sequencing of the positive clones was performed by BioAsia Biotechnology Co., Ltd (Shanghai, China). Sequence BLAST was performed in GenBank database.

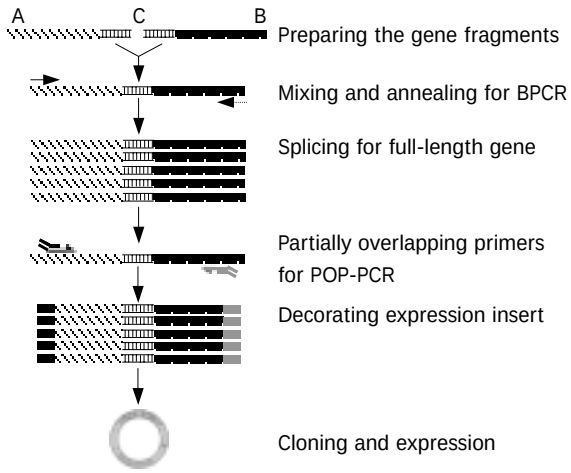

Figure 1 Experimental design and steps involved in bridging PCR (BPCR) and partially overlapping primer-based PCR (POP-PCR). Gene fragments A and B had the junction region C. Under specific temperature conditions, the fragments would anneal together to form the template molecule, thus triggering the amplification cascade. The partially overlapping primers at each site of the template ends contained two primers pre-mixed in a certain molar ratio that had sequence identity but with different lengths. All the short primers located at the outward overhang region. The sequences of all primers used are shown in Table 1.

Expression insert decoration: POP-PCR

To decorate the expression insert, primers were designed according to the sequence of the gene-coding region and the specific sequence of the expression vector as recommended by the manufacturer's instructions. The melting temperature (Tm) of all primers was calculated by using the software Omiga 2.0 (Oxford Molecular Ltd, Oxford, UK). Shorter overlapping primers were additionally designed for the long primers with the Tm beyond 72 ℃ (Table 1). The sequences of this kind of primers each were identical to the 5' terminal sequence of their corresponding longer ones. Pooling together the shorter and longer ones in different molar ratio formed the partially

Table 1 Primers used in bridging PCR (BPCR) and partially overlapping primer-PCR (POP-PCR)[1]

Code	Definition	Sequence (5'→3')	Tm (℃)
Sg1P5	For fragment A and BPCR	***ATGTCGTGGCAGGCGTACGT***	66.0
S3D10	For fragment A	***GGACAATGCAACATGCTTGTTGAGAGG***	70.4
S5D106	For fragment B	***GTGGAAAGAAGGGAGCAGGAGG***	66.4
RAC3	For fragment B and BPCR	***GCTGTCAACGATACGCTACGTAACGG***	68.4
DEN3	For ORF of D106	***TAATTAGAAACCCTGTTCGAGGAGATAGTCACC***	68.4
POP51	For POP-PCR	GACGACGACAAG***ATGTCGTGGCAGGCGTACGT***	80.8
POP52	For POP-PCR	GACGACGACAAG***ATGTCGTGGCA***	69.9
POP31	For POP-PCR	GAGGAGAAGCCCGGT***TTACATGCCCTGATCGATGAGAT***	80.7
POP32	For POP-PCR	GAGGAGAAGCCCGGT***TTACATGCC***	69.7

[1]Fragments A and B were derived from allergen gene D106. The relationship thereof and the PCR steps are shown in Figure 1. The underlined oligonucleotides were for the specific sequences of the expression vector. Oligonucleotides in italic bold were gene specific sequences. Primers POP51 and POP52, POP31 and POP32 formed the partially overlapping primers, respectively, which were corresponding to the 5' and 3' end of the target gene.

overlapping primers (Figure 1). Pilot assays were conducted to optimize the molar ratio of the two primers in the partially overlapping primer pairs for PCR. The optimal proportion was subsequently chosen for partially overlapping primer PCR (POP-PCR), by using the product recovered from BPCR as a template. As a control, the cDNA pool, originally used for fragment gene cloning, was also used as the PCR template in parallel. The PCR mixture and the initial step were similar to those for BPCR, but with some changes in denaturing temperature and extension time. Following the initial denaturing step, 12 touchdown cycles at the initiative annealing step at 72 ℃ for 45 s, and an extension at 72 ℃ for 5 min were performed, followed by 30 extenuation cycles, which were initiated at 95 ℃ for 45 s, at 72 ℃ for 1 min and at 72 ℃ for 30 s, with the annealing time decreased by 1 s per cycle, and ended by a final extension at 72 ℃ for 10 min. The annealing temperature was usually adjusted according to the Tm of the primer being used in the reaction. The target bands visualized on the gel were purified and sequenced as described above. However, the plasmids were cloned into *E. coli* strain NovaBlue Singles™ cells (Novagen, Madison, WI, USA), according to the manufacturer's instruction.

Northern blot

Northern blot was performed according to the manufacture's manual with a slight modification. Briefly, 20 μg RNAs from pollen and the mixture of calyx and pedicel was loaded on a formadehyde-containing gel. After running at 40 volts for 3 h or so, the RNA bands were electrically transferred onto Nytran SuPerCharge nylon transfer membranes (Schleicher & Schull BioScience, Inc. New Hampshire, USA). Before stained with methylene blue [0.2 g/L in 0.3 mol/L sodium acetate (pH 5.5)] to investigate the transferring efficiency, RNA was UV cross-linked onto the membrane. After destaining, BrightStar™ Psoralen-biotin (Ambion Inc., Austin, TX, USA) labeled probe D106 was applied for hybridization in the ULTRhyb™ hybridization buffer (Ambion Inc., USA). Subsequent washing was performed twice with a buffer containing 2×SSC (0.3 mol/L NaCl, 0.03 mol/L sodium citrate) and 1 g/L SDS, before its probe was detected by Phototope star detection kit (Ambion). Finally, the filter was exposed to Fuji medical X-ray film at room temperature for several min.

Protein expression

After confirmation of the in-frame insertion, the positive clones were incubated overnight at 37 ℃ on an orbital shaker. The plasmids therein were extracted by using QIAprep Miniprep kit (Qiagen) and transformed into *E. coli* strain BL21(DE3) (Novagen) for expression according to the manufacturer's instructions with a minor modification. Following overnight proliferation of the expression transformants, the cells were inoculated in liquid LB medium at the rate of 1%. After a further incubation for 4 h or so, expression of protein D106 was induced with 0.5 mmol/L isopropyl-*D*-thio-galactopyranoside (IPTG) for 2 h at 30 ℃ before harvest. The expression results were analyzed on 150 g/L SDS-PAGE.

Western blotting

After induced expression was confirmed, the recombinant allergen Amb a 8(D106) was purified with S·Tag thrombin purification kit (Novagen). Fifteen micrograms of fusion protein was resolved on 150 g/L SDS-PAGE and electrically transferred to PVDF membrane (Amersco, Solon, Ohio, USA). After the membrane was blocked overnight with 40 g/L BSA solution, Rg allergic serum (diluted 1:7) was added to each membrane strip for 8 h before addition of peroxidase conjugated goat anti-human IgE (Sigma-Aldrich, Inc., Saint Louis, MO, USA). The blotted band was visualized with DAB chromogenic substrate solution[14] (Amersco).

RESULTS

Fragment gene cloning

Gene fragments A and B corresponding to the 5'- and 3'-ends of the gene were enriched by RT-PCR and subsequently inserted into the vector. The sequence analysis demonstrated that fragments A and B, sized 363 bp and 431 bp respectively, contained a common region of 126 bp, which would provide the junction region for BPCR. The theoretical full-length gene joined contained the stop codon, poly (A) tail and primer sequences (Figure 2). Bridging the two fragments produced a novel theoretical full-length gene, which can be available under GenBank Accession No AY268426. BLAST with the amino acid sequence deduced from the full-length cDNA sequence of *D106* retrieved a large number of homologous proteins corresponding to pollen, food and contact allergens from different species, all of which belonged to profilin family. The BLAST data also showed that Amb a 8(D106) shared a homology of 54-89% with pollen allergens and of 79-89% with food allergens, which could help to cluster Amb a 8(D106) into both pollen and food allergen groups with short distances (Figure 3).

Figure 2 cDNA sequence of novel allergen gene *D106* from short ragweed pollens. The five shadowed regions represent the primer sites, Sg1p5, S5D106, S3D10, DEN3 and RAC3.

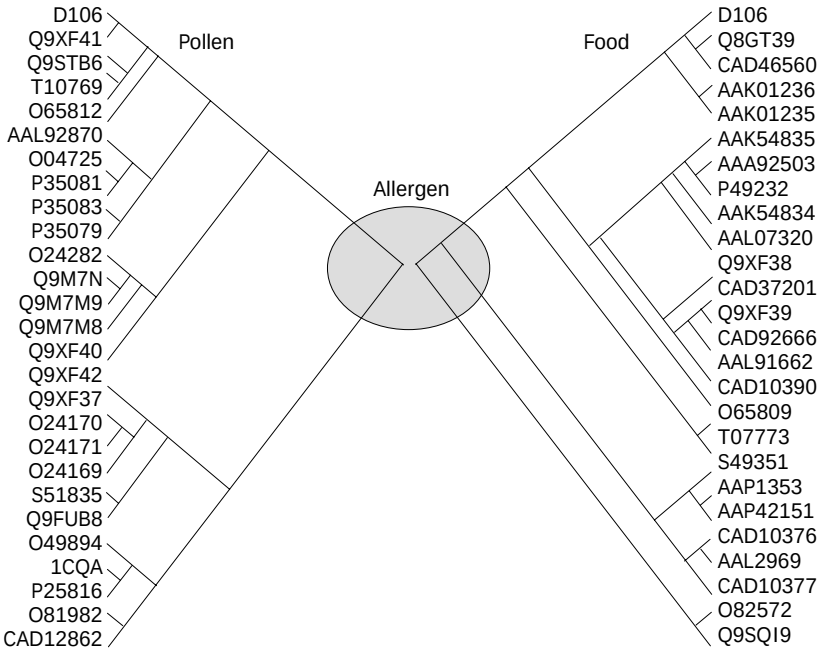

Figure 3 Phylogenetic relationships between newly obtained pollen allergen D106 (Amb a 8(D106)) and its cognates from GenBank as inferred from CLUSTAL W (1.82) alignment of the amino acid sequences. Amb a 8(D106) shared a homology as highly as 54-89% with different pollen allergens (from mugwort CAD12862 to apple Q9XF41) and as 79-89% with different food allergens (from peanut Q9SQI9 to peach Q8GT39).

Northern blot

To confirm the RNA derivation of cDNA of D106, Northern blot was performed. After blotting and UV-cross linking, methylene blue-staining of the membrane exhibited the sharp rRNA bands, suggesting the successful transferring and good quality of RNA. The sharp hybridization bands proved the pollen derivation of the cloned allergen cDNA (Figure 4). D106 could be detected both from pollen RNA and the RNA mixture from calyx and pedicel, which ruled out the PCR false derivation of D106.

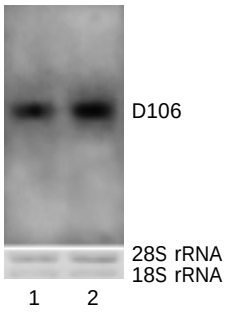

Figure 4 Northern blot profile confirming RNA derivation of cDNA of the newly obtained gene D106. Lane 1, total RNA from calyx and pedicel; Lane 2, total RNA from pollen. Both lanes exhibit obvious bands, suggesting the real RNA derivation of D106.

Enhanced amplification specificity

In order to clone the full-length gene coding region for expression vector construction, we first resorted to general PCR by using the cDNA pool as a template with the primers formerly used. However, no sharp bands of expected sizes were exhibited on the loaded agarose gel for general PCR, though a number of PCR conditions were applied. After the template was changed to the mixture of gene fragments A and B previously acquired, the bridging PCR (BPCR), as outlined in Figure 1, produced the optimal results with sharp bands and exact size observed (Figure 5). The gene sequence achieved was identical to that spliced from gene fragments A and B, indicating that the ORF of the target gene D106 was contained.

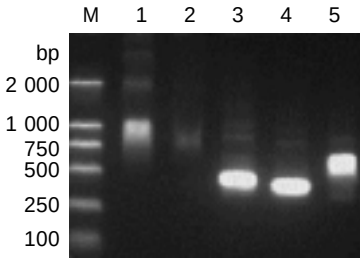

Figure 5 Agarose gel electrophoresis of PCR products. The PCR steps were depicted in Figure 1. Template in lanes 1, 2 and 5 is the mixture from gene fragments A and B; while template in lanes 3 and 4 is the BPCR product (lane 5). Lane 1, primer Sg1P5/RAC3; lane 2, primer POP51/POP31; lane 3, POP-PCR with primer POP51+POP52/POP31+POP32; lane 4, general PCR of the ORF of D106 with primer pair Sg1P5/DEN3; lane 5, BPCR of full-length D106 with primer Sg1P5/RAC3; M, molecular marker.

Decoration of expression insert

For comparison between conventional megaprimers and partially overlapping primers (POP), their amplification products were exhibited in parallel on the agarose gel (Figure 5). Longer primers and their relative shorter ones for POP-PCR listed in Table 1 were pre-mixed in a molar ratio of 1:1, 1:10, 1:50, 1:100. Hence 16 POP-pairs in different molar ratios were formed corresponding to both ends of the ORF of the gene, each of them was used for one reaction only. Comparison of the parallel PCR results showed that forward and reverse POPs in the molar ratios of 1:10 and 1:1 could produce the optimal amplification results, while conventional PCR exhibited the smear products with wrong sizes (Figure 5). The products recovered from target bands were successfully introduced into the expression vector pET-44 EK/LIC (Novagen) and transformed into *E. coli* strain NovaBlue Singles™ competent cells. Sequencing of the positive clones demonstrated that the

insert was in-frame and identical to those splices from gene fragments A and B and flanked by the vector specific sequence at both sides, indicating that the insertion was correct.

Protein expression and immunoblotting

Following proliferation of the clones selected, plasmids were extracted and successfully transformed into *E. coli* strain BL21 (DE3) for expression. SDS-PAGE analysis showed that the fusion protein was expressed mainly in a soluble form, with a molecular weight of 70 kDa as expected (Figure 6A). Immunobotting result showed that the purified fusion protein could bind to IgE in the sera of allergic patients (Figure 6B), suggesting the allergenicity and the correct expression of the allergen protein.

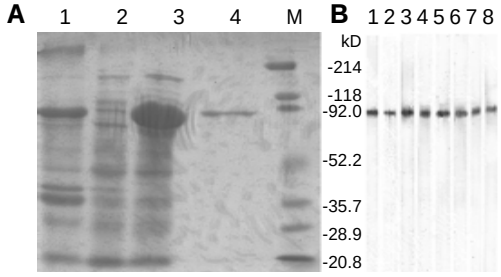

Figure 6 SDS-PAGE analysis (150 g/L) for expression (panel A) and immunoblot of fusion pollen allergen D106 (panel B). Panel A: 1. Lysate pellet of induced cells; 2. Cells without IPTG induction; 3. Supernatant of induced cell lysate; 4. Purified fusion pollen allergen D106; M. Broad range prestained SDS-PAGE standards (Bio-Rad, Hercules, CA, USA). Panel B: Fusion protein D106 was blotted with 8 serum samples from pollen allergic patients. Each strip represents one serum sample.

DISCUSSION

As industrialization developed, atopic diseases have been increasingly concerned in the past decades[1]. It is known that pollen-allergic patients frequently present allergic symptoms after ingestion of several kinds of plant-derived foods. The majority of these reactions were caused by cross-reactive structures that are present in pollens[2]. Allergic proteins containing these structures are often called 'panallergens'. Cloning the panallergen gene and expressing the recombinant protein would be one of the fewer prospective ways to pollen-food allergy diagnosis and immunotherapy[15]. This study aiming this goal successfully cloned an allergen gene D106 from short ragweed pollens and expressed the recombinant protein. Interestingly, the newly cloned gene showed a high homology not only with other pollen-derived profilins but also with food-derived profilins from numerous species. The allergenicity of the recombinant protein was primarily detected by its binding to the serum IgE from the Rg pollen allergic patients, of which 20% of the chief complaints expressed the food allergy of different kinds. Based on the homology results and the widely accepted rule-of-thumb that 30% or 35% identity over aligned regions could suffice for the structural or functional deduction[4,16,17], it is therefore tempting to speculate that the recombinant protein acquired in this study would be a useful tool both for pollen and food allergy study, and for diagnosis and immunotherapy.

The novel gene discovery by using suppression and subtractive hybridization (SSH)[18,19] and/or reverse genetic method[20] could clearly validate the overall strategy for the preparation of gene fragments. However, obtaining the full-length genes is needed for more investigations of gene functions. One of the pivotal steps in the process of obtaining the full-length genes is to generate the target genes from their fragments. The most commonly used methods for this at present were to screen the cDNA library[21-23], or back to the cDNA pool that was originally used for gene fragment detection[23]. Numerous polymorphic clones obtained would render these methods to time-consuming, expensive and liable to produce the microherterogeneity of the genes. In BPCR, only if an appropriate length region of sequence similarity existed, the two fragments could be spliced together. Obviously, the spliced sequence would be faithfully identical to that of the fragments originally used. Therefore no more screening work was needed. In order to anneal the two fragments and form a template molecule, it is a key point to optimize the annealing temperature according to the Tm of the junction regions of two gene fragments to be spliced, with the primers used in the reaction. Following this principle, BPCR would splice any two gene fragments with homology junction. Notably for the junction sequences either coming from the nature, or intentionally synthesized (see below), exact identity is not necessary but it does require a certain degree of homology to anneal the two fragment genes. Therefore, two heterogeneity genes could be spliced by BPCR method to form a novel chimeric gene or hybrid gene, which would be useful for gene function study and disease treatment.

Introducing restriction site and/or the specific sequences of vector to the primers is considered as a crucial step for exact insertion of exogenous gene into the vector, through which relatively long primers could be produced. It was well known that these longer primers would be easier to enhance the chance of non-specific amplification. To eliminate the potential non-specific amplification, partially overlapping primer technique was developed in the current study. According to the outward overhang sequence of the longer primers, the shorter identical sequence was synthesized and mixed in an appropriate molar ratio with the longer ones, thus forming the partially overlapping primer mixture. With this technique, increased amplification specificity was achieved, and the tedious screening process of target clones was avoided. According to the protocol of the partially overlapping primer, POP-PCR can be used for the amplification assays that are relevant to the addition of a length of extending sequence. It is therefore tempting to suggest that any genes that have no sequence similarities can be accommodated with the junction sequence and spliced together with repeated use and reciprocal combination of BPCR and POP-PCR to form a novel gene (or full-length gene). As this is concerned, a relatively more complicated procedure but with different efficiencies and proposes has been recently developed[24].

REFERENCES

1 **Miescher SM**, Vogel M. Molecular aspects of allergy. *Mol Aspects Med* 2002; **23**: 413-462
2 **Vieths S**, Scheurer S, Ballmer-Weber B. Current understanding of cross-reactivity of food allergens and pollen. *Ann N Y Acad Sci* 2002; **964**: 47-68
3 **Lorenz AR**, Scheurer S, Haustein D, Vieths S. Recombinant food allergens. *J Chromatogr B Biomed Sci Appl* 2001; **756**: 255-279
4 **Brusic V**, Petrovsky N, Gendel SM, Millot M, Gigonzac O, Stelman SJ. Computational tools for the study of allergens. *Allergy* 2003; **58**: 1083-1092
5 **Spangfort MD**, Mirza O, Ipsen H, Van Neerven RJ, Gajhede M, Larsen JN. Dominating IgE-binding epitope of Bet v 1, the major allergen of birch pollen, characterized by X-ray crystallography and site-directed mutagenesis. *J Immunol* 2003; **171**: 3084-3090
6 **Frohman MA**, Dush MK, Martin GR. Rapid production of full-length cDNAs from rare transcripts: amplification using a single gene-specific oligonucleotide primer. *Proc Natl Acad Sci U S A* 1988; **85**: 8998-9002
7 **Kruse S**, Kuehr J, Moseler M, Kopp MV, Kurz T, Deichmann

KA, Foster PS, Mattes J. Polymorphisms in the IL 18 gene are associated with specific sensitization to common allergens and allergic rhinitis. *J Allergy Clin Immunol* 2003; **111**: 117-122

8 **Karjalainen J**, Hulkkonen J, Pessi T, Huhtala H, Nieminen MM, Aromaa A, Klaukka T, Hurme M. The IL1A genotype associates with atopy in nonasthmatic adults. *J Allergy Clin Immunol* 2002; **110**: 429-434

9 **Cookson W**. Genetics and genomics of asthma and allergic diseases. *Immunol Rev* 2002; **190**: 195-206

10 **Vailes LD**, Sun AW, Ichikawa K, Wu Z, Sulahian TH, Chapman MD, Guyre PM. High-level expression of immunoreactive recombinant cat allergen (Fel d 1): Targeting to antigen-presenting cells. *J Allergy Clin Immunol* 2002; **110**: 757-762

11 **Hales BJ**, Hazell LA, Smith W, Thomas WR. Genetic variation of Der p 2 allergens: effects on T cell responses and immunoglobulin E binding. *Clin Exp Allergy* 2002; **32**: 1461-1467

12 **Mehta RK**, Singh J. Bridge-overlap-extension PCR method for constructing chimeric genes. *Biotechniques* 1999; **26**: 1082-1086

13 **Liu S**, Thaler DS, Libchaber A. Signal and noise in bridging PCR. *BMC Biotechnol* 2002; **2**: 13

14 **Reindl J**, Rihs HP, Scheurer S, Wangorsch A, Haustein D, Vieths S. IgE reactivity to profilin in pollen-sensitized subjects with adverse reactions to banana and pineapple. *Int Arch Allergy Immunol* 2002; **128**: 105-114

15 **Ferreira F**, Wallner M, Breiteneder H, Hartl A, Thalhamer J, Ebner C. Genetic engineering of allergens: future therapeutic products. *Int Arch Allergy Immunol* 2002; **128**: 171-178

16 **Rost B**. Twilight zone of protein sequence alignments. *Protein Eng* 1999; **12**: 85-94

17 **Hileman RE**, Silvanovich A, Goodman RE, Rice EA, Holleschak G, Astwood JD, Hefle SL. Bioinformatic methods for allergenicity assessment using a comprehensive allergen database. *Int Arch Allergy Immunol* 2002; **128**: 280-291

18 **Diatchenko L**, Lau YF, Campbell AP, Chenchik A, Moqadam F, Huang B, Lukyanov S, Lukyanov K, Gurskaya N, Sverdlov ED, Siebert PD. Suppression subtractive hybridization: a method for generating differentially regulated or tissue-specific cDNA probes and libraries. *Proc Natl Acad Sci U S A* 1996; **93**: 6025-6030

19 **Sers C**, Tchernitsa OI, Zuber J, Diatchenko L, Zhumabayeva B, Desai S, Htun S, Hyder K, Wiechen K, Agoulnik A, Scharff KM, Siebert PD, Schafer R. Gene expression profiling in RAS oncogene-transformed cell lines and in solid tumors using subtractive suppression hybridization and cDNA arrays. *Adv Enzyme Regul* 2002; **42**: 63-82

20 **Yu CJ**, Lin YF, Chiang BL, Chow LP. Proteomics and immunological analysis of a novel shrimp allergen, Pen m 2. *J Immunol* 2003; **170**: 445-453

21 **Ding H**, Griesel C, Nimtz M, Conradt HS, Weich HA, Jager V. Molecular cloning, expression, purification, and characterization of soluble full-length, human interleukin-3 with a baculovirus-insect cell expression system. *Protein Expr Purif* 2003; **31**: 34-41

22 **Erez N**, Milyavsky M, Goldfinger N, Peles E, Gudkov AV, Rotter V. Falkor, a novel cell growth regulator isolated by a functional genetic screen. *Oncogene* 2002; **21**: 6713-6721

23 **Forestier M**, Banninger R, Reichen J, Solioz M. Betaine homocysteine methyltransferase: gene cloning and expression analysis in rat liver cirrhosis. *Biochim Biophys Acta* 2003; **1638**: 29-34

24 **Gao X**, Yo P, Keith A, Ragan TJ, Harris TK. Thermodynamically balanced inside-out (TBIO) PCR-based gene synthesis: a novel method of primer design for high-fidelity assembly of longer gene sequences. *Nucleic Acids Res* 2003; **31**: e143

Edited by Wang XL **Proofread by** Xu FM

PO Box 2345, Beijing 100023, China
Fax: +86-10-85381893
E-mail: wjg@wjgnet.com www.wjgnet.com

World J Gastroenterol 2004;10(14):2109-2112
World Journal of Gastroenterology
 ISSN 1007-9327

• BASIC RESEARCH •

Cloning and expression of mouse peroxiredoxin I in IEC-6 Cells

Bo Zhang, Yong-Ping Su, Tao Wang, Feng-Chao Wang, Guo-Ping Ai, Hui Xu, Jun-Ping Wang, Yue-Sheng Huang, Jian-Xin Jiang

Bo Zhang, Yong-Ping Su, Tao Wang, Feng-Chao Wang, Guo-Ping Ai, Hui Xu, Jun-Ping Wang, Yue-Sheng Huang, Jian-Xin Jiang, Institute of Combined Injury of PLA, State Key Laboratory of Trauma, Burns and Combined Injury, Third Military Medical University, Chongqing 400038, China
Supported by the National Natural Science Foundation of China, No. 30230360
Correspondence to: Professor Yong-Ping Su, Institute of Combined Injury of PLA, Third Military Medical University, Gaotanyan Street 30, Chongqing 400038, China. suyping@yahoo.com
Telephone: +86-23-68752355 **Fax:** +86-23-68752279
Received: 2003-12-10 **Accepted:** 2004-02-01

Abstract

AIM: To clone and express mouse peroxiredoxin I in IEC-6 cells.

METHODS: Total RNAs were isolated from cultured IEC-6 cells, and the coding region of peroxiredoxin I was amplified by RT-PCR. After it was cloned into T-vector and sequenced, pSG5 was used to transiently express peroxiredoxin I in IEC-6 by liposome-mediated transfection, and the expression of peroxiredoxin I was evaluated by RT-PCR and Western blot.

RESULTS: A DNA fragment about 750 bp was amplified from total RNAs of IEC-6 cells using specific primers of peroxiredoxin I. The sequencing confirmed the coding region was successfully cloned into T-vector, which was completely coincident with the sequence in GeneBank. After the *Eco*RI-*Bam*HI fragment of T-vector containing peroxiredoxin I was inserted into pSG5, the recombinant plasmid was transferred to IEC-6 cells. RT-PCR assay showed that a DNA fragment of 930 bp could be amplified, which indicated the transcription of pSG5-Prx. Western blot confirmed the expression of peroxiredoxin I in IEC-6 cells.

CONCLUSION: Mouse peroxiredoxin I can be successfully expressed in IEC-6 cells.

Zhang B, Su YP, Wang T, Wang FC, Ai GP, Xu H, Wang JP, Huang YS, Jiang JX. Cloning and expression of mouse peroxiredoxin I in IEC-6 Cells. *World J Gastroenterol* 2004; 10(14): 2109-2112
http://www.wjgnet.com/1007-9327/10/2109.asp

INTRODUCTION

Peroxiredoxin (Prx) is a novel defined protein family which plays a critical role in reducing hydrogen peroxide with hydrogen derived from NAD(P)H[1-3]. The first member of this family was discovered as a 25 ku protein in yeast[4]. All Prx proteins contain a conserved cysteine residue in the *N*-terminal region that is the active site of catalysis. In mammal cells, there are six isoforms of peroxiredoxin, which can be devided into two subgroups, termed as 1-Cys Prx (VI) and 2-Cys Prx (I-V)[5,6]. The proteins of 2-Cys Prx subgroup contain another cysteine residue in the *C*-terminal portion of the molecule. Prx isoforms are distributed differently within cells and therefore with different functions. Prx I and II are localized to the cytosol[7,8], whereas Prx III has a mitochondrial-targeting signal and is localized in mitochondrion[9]. Prx IV is secreted out of cells because of its *N*-terminal sequence for secretion. Prx V is found in mitochondrion as long form of this protein, but it also exists in peroxisome as short form[10]. Same as Prx I and II, Prx VI is also found in cytosol[11].

Prx I, which belongs to 2-Cys subgroup, is also known as MSP23, PAG and NEEF-A[12-14]. Prx I is involved in redox regulation of the cell, such as reducing peroxides by reducing equivalents provided through the thioredoxin system but not from glutaredoxin. Prx I is found in abundance in the cytoplasm of cells as homodimers. Its cDNA was first cloned from mouse peritoneal macrophage encoding a protein of 23 ku. Now the antioxidative molecular mechanism of Prx I is elucidated by several researches on molecular structure has been performed. From the results of biochemical and physiological studies, Prx I has been implicated in a number of cellular functions, such as cell proliferation and differentiation, enhancement of the natural killer cell activity, and intracellular signaling, in addition to the antioxidant activity[15-17]. Further studies have shown that the expression of Prx I is increased in cancer cells, indicating it may be related to cancer development or progression[18]. We postulate that it may have an activity of anti-tumor development.

In our previous study, we found the expression of Prx I was up regulated by ionizing radiation in mouse intestinal epithelia[19]. This was coincident with the results of other researchers[20]. As a step to further study the biochemical functions of Prx I, we cloned the coding region of this gene and expressed it in IEC-6 cells. Our data showed that Prx I could be successfully expressed in this kind of cells.

MATERIALS AND METHODS

Materials

Male BALB/c mice, 58-62 d of age (weight 20-24 g), were purchased from Animal Center in Third Military Medical University, and housed in conventional cages with free access to drinking water and standard chow. Dulbecco's modified Eagle's medium (DMEM) and fetal bovine serum were purchased from Hyclone (Logan, USA). RNA PCR kit and T-vector were obtained from Takara (Dalian, China), and antibodies were from Santa Cruz (California, USA). Reagent for RNA isolation was from Roche Ltd. (Roche, USA). Plasmid pSG5 was a kindly gift from Dr. Chen Jian (Department of Biochemistry, Third Military Medical University). The specific primers were synthesized by Shanghai Shenyou Shengwu Jishu Corporation. Other chemicals not mentioned above were domestic made.

Isolation of total RNAs

Mouse intestinal epithelial cells were isolated as previously described[21]. After the cell pipette washed with cold PBS (0.01 mol/L, pH7.4), the cells were lysed with Tripure solution. All performs were according to the manufacturer's instructions. The quality of isolated RNAs was checked by electrophoresis.

RT-PCR

The coding region of Prx I was amplified by RT-PCR with forward primer, 5' CGAATTCGTTCTCACGGCTCTTTCTGTTT3' (P1) and backward primer, 5' AGGATCCTTCTGGCTGCTCAATGC TGC3' (P2). One microgram of total RNAs was added into each reaction. After the reverse transcription was performed at 50 ℃ for 30 min, the amplification was carried out with one denaturing cycle of 3 min at 94 ℃, then 28 cycles consisting of denaturation at 94 ℃ for 40 s, annealing at 58 ℃ for 40 s, and extension at 72 ℃ for 40 s, and one additional extension at 72 ℃ for 5 min. RT-PCR products were analyzed on 12 g/L agarose gel. To validate the transcription of recombinant plasmid, the mRNA of transfected IEC-6 cells was amplified by RT-PCR with primers P2 and P3 (5' AAAGCTGGATCGATCCTGAG3'). The procedure in details was performed according to the manufacturer' s instructions.

Construction of expression vector

The amplified DNA was separated by electrophorsis and purified from gels. Then 1μL of T-vector, 1μL of T4 DNA ligase and 2μL of 10×buffer were added to the purified RT-PCR product, and incubated at 16 ℃ overnight. Competent bacteria of *E.coli JM109* were transformed with the linkage product, and then spread on a LB agarose plate containing ampicillin and X-gal. The inserted DNA into T-vector of 3 random monoclonal colonies was sequenced, and the colony was termed as pT-Prx. To construct the recombinant expression vector, the *Eco*RI-*Bam*HI fragment of pT-Prx was inserted into vector pSG5, which could transfect IEC-6 cells.

Cell culture and transfection

IEC-6 cells were cultivated at 37 ℃ in an atmosphere containing 100 mL/L CO2 in air. The culture medium comprised of DMEM containing 100 mL/L fetal calf serum, penicillin (100 U/mL), and streptomycin (100 μg/mL). Exponentially growing cells were transferred to 100 mL culture dishes and cultured for 24 h to yield about 40% confluency at the time of transfection. Before transfection, 30 μg of DOTAP was diluted with 70 μL of HBS solution (20 mmol/L HEPES, 150 mmol/L NaCl, pH 7.4), and 5 μg of DNA was diluted to 0.1μg/μL with the same solution. The mixture of DNA and DOTAP was prepared by gently mixing them together and incubated for 15 min at room temperature. To prepare cells for transfection, IEC-6 cells were washed twice with serum-free medium. After the cells were incubated with the mixture of DNA and DOTAP in 2 mL of serum-free medium for 4 h, the cells were washed with serum-free medium, followed by further culture for 16 h. Transfection was repeated one more time. At the time of 24 h after the second transfection, the cells were collected for RNA and proteins isolation.

Immunoblotting

IEC-6 cells were collected and washed with ice-cold PBS (0.01 mol/L, pH7.4) after transfection. Total proteins were isolated with RPI solution. The extraction mixture was centrifuged at 12 000 *g* at 4 ℃ for 20 min. The supernatants were transferred to a clean tube and stored at -70 ℃ as aliquots. The protein concentration was determined using Bradford dye-binding assay with bovine serum albumin as a standard. Total proteins were separated on 120 g/L SDS-polyacrylamide gel, and then transferred to nitrocellulose membranes. After being blocked for 1 h with the Tris/NaCl (50 mmol/L Tris-HCl, 200 mmol/L NaCl, 0.5 g/L Tween-20, pH 7.4) containing 20 g/L BSA, the membranes were probed with the goat anti-mouse Prx I polyclonal antibody. Immunoreactive bands were visualized with solution containing 1 mg/mL DAB and 0.1 mL/L H_2O_2. The expression of Prx I was normalized by that of GAPDH.

RESULTS

Amplification of the cDNA of Prx I

Total RNAs were isolated with 3 main bands appeared on agarose gels electrophoresis (Figure 1A). Message RNAs were smeared on the gel. After 28 cycles of RT-PCR, the products were run on 12 g/L agarose gel. A DNA band about 750 bp was visualized which was coincident with the length of the PrxI cDNA and could be cloned in the next step (Figure 1).

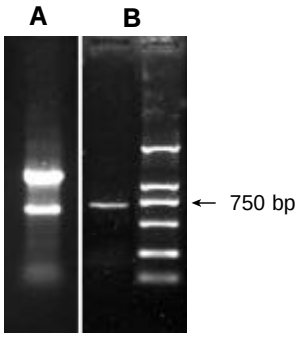

Figure 1 Amplification of Peroxiredoxin I by RT-PCR. A: total RNAs were isolated from mouse intestinal epithelia; three bands were visualized on agarose gel, which represented the main ribosome RNA of the cells. B: amplification of the coding region of peroxiredoxin I applying RT-PCR.

Cloning of Prx I

After the PCR product was ligated to T-vector, the linkage mixture transformed competent bacteria of JM109, and white colonies grew on LB plate containing ampicillin, X-gal and IPTG. Inserted DNA of 3 random colonies was sequenced, and the DNA was completely coincident with the sequence in GeneBank (data not shown). Then the inserted DNA of pT-Prx was digested with *EcoRI* and *BamHI*, purified, and inserted into

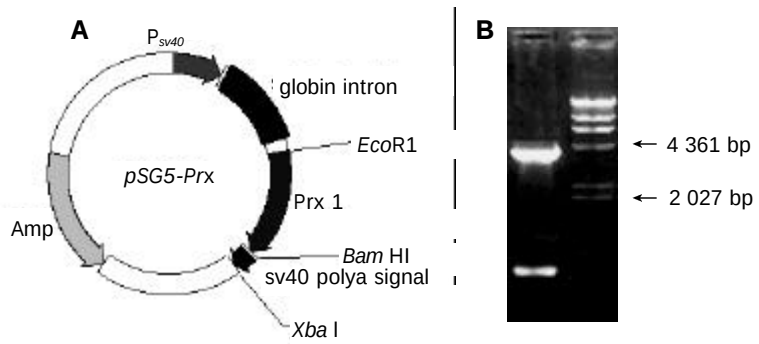

Figure 2 Recombinant expression vector pSG5-Prx. A: diagrams of the expression vector pSG5-Prx. B: electrophoresis map of this vector (*Eco*RI and *Bam*HI). λ / *Hin*dIII marker was loaded to estimate the relative molecular weight of the expression vector.

vector pSG5. The recombinant expression vector was termed as pSG5-Prx (Figure 2). This recombinant plasmid was directly applied in cell transfection.

Transcription of pSG5-Prx in IEC-6 Cells by RT-PCR

We transfected IEC-6 cells with pSG5-Prx using pSG5 as a control. The cells grew very well during the period of transfection. Total RNAs of transfected IEC-6 cells were isolated after the second transfection using TriPure solution. Transcription of the recombinant plasmid was detected by applying RT-PCR with primers P2 and P3. The result showed that 2 DNA bands were visualized on agarose gel. Because the beta-globin intron (Figure 2A) in the primary transcript was spliced, the length of RT-PCR product based on mature mRNA was about 817 bp. However, the length of the other DNA band was about 1 399 bp, which was the PCR product using the recombinant plasmid as template (Figure 3).

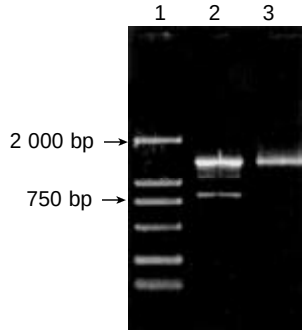

Figure 3 Detection of the transcription of recombinant vector pSG5-Prx by RT-PCR. Total RNAs isolated from transfected cells were applying for RT-PCR analysis with primers P2 and P3. Lane 1: DNA marker DL 2000, Lane 2: RT-PCR product, Lane 3: PCR product using purified recombinant vector as template.

Expression of Prx I in IEC-6 Cells

Total proteins of transfected IEC-6 cells were isolated after the second transfection and separated by SDS-PAGE. The blots were probed with specific antibodies against PrxI and GAPDH. Relative protein level was determined by quantitating the intensity of the bands with a densitometer. The ratio of the intensity of Prx I/GAPDH was automatically compared by Quantity One software (Bio-Rad Corp.). The result showed that the expression of Prx I was increased in pSG5-Prx transfected IEC-6 cells (50% more than the control cells) (Figure 4). This indicated that the recombinant plasmid could be transcripted and translated in IEC-6 cells.

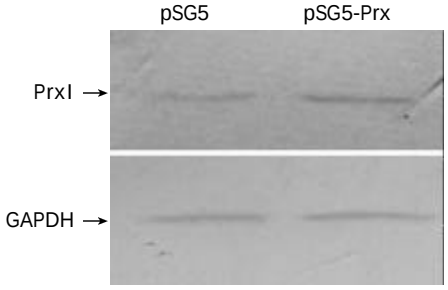

Figure 4 Immunoblotting of peroxiredoxin I of transfected and normal IEC-6 cell.

DISCUSSION

IEC-6 cell line was derived from normal rat intestinal epithelia. Its living condition for stable passage was successfully established after trials. The cell line was testified to be the small intestinal epithelial cell by electron microscopy and immunohistochemistry, and has been applied to some related research work[22]. It is rational to apply this cell line *in vitro* to mimic the intestinal epithelia *in vivo*.

To further study the biochemical and physiological function of Prx I, we cloned the coding region of this protein and over expressed it in IEC-6 cells in this study. The cDNA of Prx I was first cloned in 1994 applying differential hybridization technique, which was named as *MSP23*[23]. Treatment with diethylmaleate or glucose/glucose oxidase markedly enhanced the induction of its transcription, and the mount of its protein in the cells rapidly increased. Moreover, the cDNAs corresponding to the thiol-specific antioxidant (TSA), which encoded a protein termed as Prx, has been cloned and sequenced in yeast and mammalian cells[24]. From the results of biochemical and physiological studies, Prx I has been involved in association with a variety of diverse cellular functions including proliferation, differentiation, and immune response. However, the detailed pathophysiological functions of this protein remain unknown.

The most striking finding of Prx I was that it was increased in many kinds of tumor cells. Moreover, some researchers thought it might be a potential tumor marker[25]. Prx I was over-expressed in human breast cancer tissues compared to normal tissues[26]. Using comparative proteome analysis between human normal (BEAS 2B) and malignant (A549) lung epithelial cells, Chang *et al*.[27] found that Prx I was increased more than twofold reproducibly. Additionally, Prx I expression levels in follicular neoplasm and thyroiditis group were significantly higher than that of the control group, though papillary carcinoma group did not show statistical significance[25]. All these data suggested Prx I was involved in tumor development or progression, and it might be a new target for gene therapy of tumor cells.

It was suggested that Prx I was a radiation responsive gene. Lee *et al*.[28] demonstrated, when the irradiated testis was examined, Prx I was found to be transiently up-regulated. Its highly homologous gene Prx II was increased in tissues isolated from the patients who did not respond to radiation therapy. However, treatment with a Prx II antisense decreased the expression of Prx II, enhancing the radiation sensitivity of cells[29].

In this study, we found pSG5 was an efficient expression vector of mammal cells[30]. Though it has no screen marker, the expression of recombinant plasmid can be easily verified at mRNA level applying RT-PCR technology owing to the globin intron of this vector. Because of the existence of the vector DNA in the sample purified by applying Tripure solution, two kinds of RT-PCR product were displayed on agarose gel, which represented different PCR template. After the second transfection, most of the cells expressed the exogenous vector, and the protein was accumulated in these cells, which could be detected by immunoblotting. We will further study the biochemical and physiological role in radiation response of this protein.

REFERENCES

1 **Rhee SG,** Kang SW, Chang TS, Jeong W, Kim K. Peroxiredoxin, a novel family of peroxidases. *IUBMB Life* 2001; **52**: 35-41
2 **Fujii J,** Ikeda Y. Advances in our understanding of peroxiredoxin, a multifunctional, mammalian redox protein. *Redox Rep* 2002; **7**: 123-130
3 **Butterfield LH,** Merino A, Golub SH, Shau H. From cytoprotection to tumor suppression: the multifactorial role of peroxiredoxins. *Antioxid Redox Signal* 1999; **1**: 385-402
4 **Kim K,** Kim IH, Lee KY, Rhee SG, Stadtman ER. The isolation and purification of a specific "protector" protein which inhibits enzyme inactivation by a thiol/Fe(III)/O2 mixed-function

oxidation system. *J Biol Chem* 1988; **263**: 4704-4711

5 **Chang TS,** Jeong W, Choi SY, Yu S, Kang SW, Rhee SG. Regulation of peroxiredoxin I activity by Cdc2-mediated phosphorylation. *J Biol Chem* 2002; **277**: 25370-25376

6 **Rhee SG,** Chang TS, Bae YS, Lee SR, Kang SW. Cellular regulation by hydrogen peroxide. *J Am Soc Nephrol* 2003; **14**(8 Suppl 3): S211-215

7 **Lee TH,** Yu SL, Kim SU, Lee KK, Rhee SG, Yu DY. Characterization of mouse peroxiredoxin I genomic DNA and its expression. G*ene* 1999; **239**: 243-250

8 **Chung YM,** Yoo YD, Park JK, Kim YT, Kim HJ. Increased expression of peroxiredoxin II confers resistance to cisplatin. *Anticancer Res* 2001; **21**: 1129-1133

9 **Choi JH,** Kim TN, Kim S, Baek SH, Kim JH, Lee SR, Kim JR. Overexpression of mitochondrial thioredoxin reductase and peroxiredoxin III in hepatocellular carcinomas. *Anticancer Res* 2002; **22**: 3331-3335

10 **Seo MS,** Kang SW, Kim K, Baines IC, Lee TH, Rhee SG. Identification of a new type of mammalian peroxiredoxin that forms an intramolecular disulfide as a reaction intermediate. *J Biol Chem* 2000; **275**: 20346-20354

11 **Chen JW,** Dodia C, Feinstein SI, Jain MK, Fisher AB. 1-Cys peroxiredoxin, a bifunctional enzyme with glutathione peroxidase and phospholipase A2 activities. *J Biol Chem* 2000; **275**: 28421-28427

12 **Kawai S,** Takeshita S, Okazaki M, Kikuno R, Kudo A, Amann E. Cloning and characterization of OSF-3, a new member of the MER5 family, expressed in mouse osteoblastic cells. *J Biochem* 1994; **115**: 641-643

13 **Shau H,** Butterfield LH, Chiu R, Kim A. Cloning and sequence analysis of candidate human natural killer-enhancing factor genes. *Immunogenetics* 1994; **40**: 129-134

14 **Prosperi MT,** Apiou F, Dutrillaux B, Goubin G. Organization and chromosomal assignment of two human PAG gene loci: PAGA encoding a functional gene and PAGB a processed pseudogene. *Genomics* 1994; **19**: 236-241

15 **Yang KS,** Kang SW, Woo HA, Hwang SC, Chae HZ, Kim K, Rhee SG. Inactivation of human peroxiredoxin I during catalysis as the result of the oxidation of the catalytic site cysteine to cysteine- sulfinic acid. *J Biol Chem* 2002; **277**: 38029-38036

16 **Ishii T,** Itoh K, Sato H, Bannai S. Oxidative stress-inducible proteins in macrophages. *Free Radic Res* 1999; **31**: 351-355

17 **Neumann CA,** Krause DS, Carman CV, Das S, Dubey DP, Abraham JL, Bronson RT, Fujiwara Y, Orkin SH, Van Etten RA. Essential role for the peroxiredoxin Prdx1 in erythrocyte antioxidant defence and tumour suppression. *Nature* 2003; **424**: 561-565

18 **Crowley-Weber CL,** Payne CM, Gleason-Guzman M, Watts GS, Futscher B, Waltmire CN, Crowley C, Dvorakova K, Bernstein C, Craven M, Garewal H, Bernstein H. Development and molecular characterization of HCT-116 cell lines resistant to the tumor promoter and multiple stress-inducer, deoxycholate. *Carcinogenesis* 2002; **23**: 2063-2080

19 **Wei YJ,** Zhang B, Su YP, Liu XH, Wang FC, Ai GP. Effect of ionizing radiation on the expression of Prx I and Prx VI gene in murine intestinal epithelial cells. *Chongqing Med J* 2003; **32**: 1343-1345

20 **Chen WC,** McBride WH, Iwamoto KS, Barber CL, Wang CC, Oh YT, Liao YP, Hong JH, de Vellis J, Shau H. Induction of radioprotective peroxiredoxin-I by ionizing irradiation. *J Neurosci Res* 2002; **70**: 794-798

21 **Zhang B,** Su YP, Ai GP, Liu XH, Wang FC, Cheng TM. Differentially expressed proteins of gamma-ray irradiated mouse intestinal epithelial cells by two- dimensional electrophoresis and MALDI-TOF mass spectrometry. *World J Gastroenterol* 2003; **9**: 2726-2731

22 **Wood SR,** Zhao Q, Smith LH, Daniels CK. Altered morphology in cultured rat intestinal epithelial IEC-6 cells is associated with alkaline phosphatase expression. *Tissue Cell* 2003; **35**: 47-58

23 **Ishii T,** Yamada M, Sato H, Matsue M, Taketani S, Nakayama K, Sugita Y, Bannai S. Cloning and characterization of a 23-kDa stress-induced mouse peritoneal macrophage protein. *J Biol Chem* 1993; **268**: 18633-18636

24 **Chae HZ,** Rhee SG. A thiol-specific antioxidant and sequence homology to various proteins of unknown function. *BioFactors* 1994; **4**: 177-180

25 **Yanagawa T,** Ishikawa T, Ishii T, Tabuchi K, Iwasa S, Bannai S, Omura K, Suzuki H, Yoshida H. Peroxiredoxin I expression in human thyroid tumors. *Cancer Lett* 1999; **145**: 127-132

26 **Noh DY,** Ahn SJ, Lee RA, Kim SW, Park IA, Chae HZ. Overexpression of peroxiredoxin in human breast cancer. *Anticancer Res* 2001; **21**: 2085-2090

27 **Chang JW,** Jeon HB, Lee JH, Yoo JS, Chun JS, Kim JH, Yoo YJ. Augmented expression of peroxiredoxin I in lung cancer. *Biochem Biophys Res Commun* 2001; **289**: 507–512

28 **Lee K,** Park JS, Kim YJ, Soo Lee YS, Sook Hwang TS, Kim DJ, Park EM, Park YM. Differential expression of Prx I and II in mouse testis and their up-regulation by radiation. *Biochem Biophys Res Commun* 2002; **296**: 337-342

29 **Park SH,** Chung YM, Lee YS, Kim HJ, Kim JS, Chae HZ, Yoo YD. Antisense of human peroxiredoxin II enhances radiation-induced cell death. *Clin Cancer Res* 2000; **6**: 4915-4920

30 **Rose K,** Steinbuchel A. Construction and intergeneric conjugative transfer of a pSG5-based cosmid vector from Escherichia coli to the polyisoprene rubber degrading strain Micromonospora aurantiaca W2b. *FEMS Microbiol Lett* 2002; **211**: 129-132

Edited by Kumar M and Xu FM

PO Box 2345, Beijing 100023, China
Fax: +86-10-85381893
E-mail: wjg@wjgnet.com www.wjgnet.com

World J Gastroenterol 2004;10(14):2113-2115
World Journal of Gastroenterology
 ISSN 1007-9327

• BRIEF REPORTS •

Helicobacter pylori infection in patients with autoimmune thrombocytopenic purpura

Erdal Kurtoglu, Ertugrul Kayacetin, Aysegul Ugur

Erdal Kurtoglu, Department of Hematology, Selcuk University, Konya 42060, Turkey
Ertugrul Kayacetin, Department of Gastroenterology, Selcuk University, Konya 42060, Turkey
Aysegul Ugur, Department of Biochemistry, Selcuk University, Konya 42060, Turkey
Correspondence to: Dr. Erdal Kurtoglu, Feritpasa Mahallesi, Umit Bahadir Turk Sokak, No: 21/4 Girgic Apt, Konya 42060, Turkey. erdalkurtoglu@yahoo.com
Telephone: +90-332-323-2600 **Fax:** +90-332-324-4027
Received: 2004-02-02 **Accepted:** 2004-03-10

Abstract

AIM: To compare the prevalence of *Helicobacter pylori* (*H pylori*) infection in autoimmune thrombocytopenic purpura (AITP) patients with that of nonthrombocytopenic controls, and to evaluate the efficacy of the treatment in *H pylori*(+) and *H pylori*(-) AITP patients.

METHODS: The prevalence of gastric *H pylori* infection in 38 adult AITP patients (29 female and 9 male; median age 27 years; range 18-39 years) who consecutively admitted to our clinic was investagated.

RESULTS: *H pylori* infection was found in 26 of 38 AITP patients (68.5%). *H pylori* infection was found in 15 of 23 control subjects (65.2%). The difference in *H pylori* infection between the 2 groups was not significant. Thrombocyte count of *H pylori*-positive AITP patients was significantly lower than that of *H pylori*-negative AITP patients ($P<0.05$). Thrombocyte recovery of *H pylori*-positive group was less than that of *H pylori*-negative group ($P<0.05$).

CONCLUSION: *H pylori* infection should be considerecd in the treatment of AITP patients with *H pylori* infection.

Kurtoglu E, Kayacetin E, Ugur A. *Helicobacter pylori* infection in patients with autoimmune thrombocytopenic purpura. *World J Gastroenterol* 2004; 10(14): 2113-2115
http://www.wjgnet.com/1007-9327/10/2113.asp

INTRODUCTION

Autoimmune thrombocytopenic purpura (AITP) is an acquired bleeding disorder in which autoantibodies bind to platelet surface, leading to platelet destruction[1,2]. The mechanism triggering the production of platelet autoantibodies are poorly understood[2].

Helicobacter pylori (*H pylori*) is a spiral shaped bacterium that resides in the stomach mucosa. *H pylori* has been considered for years as the etiologic agent of gastritis, peptic ulcer, gastric cancer, and mucosa-associated lymphoid tissue (MALT) lymphoma[3-5]. More recently, *H pylori* has been found to be associated with a number of autoimmune disorders, such as rheumatoid arthritis[6], autoimmune thyroiditis[7], Sjogren' s syndrome[8], Schonlein-Henoch purpura[9], and AITP[10,11]. There are data consistent with an association between *H pylori* infection and AITP[12-14]. In addition a significant increase of platelet count following *H pylori* eradication has been reported in a proportion of AITP patients[12]. AITP in adults is most often chronic, and up to 25% of cases of chronic AITP are refractory to standard therapy[1]. However, although there is some evidence implicating *H pylori* in some autoimmune disorders, the association between AIPT and *H pylori* infection is speculative.

The aim of this study was to compare the prevalence of *H pylori* infection in AITP patients with that of nonthrombocytopenic controls and to evaluate the efficacy of the treatment in *H pylori*(+) and *H pylori*(-) AITP patients.

MATERIALS AND METHODS

Between May 2001 and October 2003 we investigated the presence of gastric *H pylori* infection in 38 adult AITP patients (29 females, 9 males, median age: 27 years, range: 18-39 years) consecutively admitted to our clinic. AITP was diagnosed on the basis of the presence of isolated thrombocytopenia ($<100\times10^9$/L) and megakaryocytic hyperplasia in bone marrow. Other causes of thrombocytopenia (drugs, pseudothrombocytopenia, hepatitis B and C virus infections, human immunodeficiency virus infection, malignancy) were excluded. Patients considered at bleeding risk who would require active treatment were also excluded. Age- and sex-matched 23 (18 females, 5 males, median age: 26 years, range: 18-35 years) nonthrombocytopenic patients without dyspeptic complaints were used as control group. None of the patients and controls had received antibiotics, proton pump inhibitors, and H_2-receptor blockers during 4 wk before the onset of AITP.

All patients underwent 1 mg/(kg.d) steroid therapy for 3 wk following diagnosis, and then the dose gradually tapered every week until withdrawal. Our second choice of therapy was intravenous immunoglobulin administration [400 mg/(kg.d) for 5 d], but we did not use it.

An agglutination method was used to detect anti-*H pylori* antibodies of IgG type in both patients and controls (Ridascreen®, R-Biopharm, Darmstadt, Germany). Hemogram analysis was done by Coulter®STKS (Coulter Corporation, Miami, Florida, USA).

Although demonstration of *H pylori* in gastric biopsies is the gold standard of *H pylori* detection, we prefered blood antibody detection due to following reasons. Endoscopy might cause unexpected bleeding in thrombocytopenic patients especially in those whose thrombocyte counts were less than 50×10^9/L. Urea breath test could not allow the detection of *H pylori* infection retrospectively. Both sensitivity and specificity of such kits were demonstrated in previous studies (95%<)[15].

Statistical analysis

Statistical analysis was performed using Kruskal-Wallis and Mann-Whitney *U* tests. Mean values were calculated for every variable in each group and compared between different groups. $P<0.05$ was considered as statistically significant.

RESULTS

There was no age or sex difference between controls and patients. *H pylori* infection was found in 26 of 38 patients with AITP (68.5%), and in 15 of 23 control subjects (65.2%). The difference between the 2 groups for *H pylori* infection was not significant (Table 1). Thrombocyte count of *H pylori*-positive AITP patients was lower than that of *H pylori*-negative AITP patients ($P<0.05$). Thrombocyte recovery of *H pylori*-positive group was less than that of *H pylori*-negative group (Table 2) ($P<0.05$).

Table 1 General characteristics of subjects in the study

Subjects	*n*	%	Mean age (range)	Sex (F/M)
H pylori-negative controls	8	(34.8)	25 (18-32)	6/2
H pylori-positive controls	15	(65.2)	27 (25-35)	12/3
H pylori-negative patients	12	(31.5)	29 (24-34)	8/4
H pylori-positive patients	26	(68.5)	26 (22-37)	21/5

Table 2 Platelet counts ($\times 10^9$/L) of AITP patients before and after steroid therapy

Parameters	*H pylori*-positive patients (*n*=26)	*H pylori*-negative patients (*n*=12)
Platelet counts ($\times 10^9$/L) (mean, range)	15 (10-22)[a]	29 (21-42)
Response to steroid (number, %)	17 (65)[a]	10 (83)
Post-treatment platelet counts ($\times 10^9$/L) (mean, range)	77 (61-112)	140 (124-180)

[a]$P<0.05$ *vs H pylori* negative patients.

DISCUSSION

AITP is an autoimmune disease caused by autoantibodies against platelets[16]. Several lines of direct and indirect evidences suggest that infectious agents may influence the occurence or the course of some autoimmune diseases[17]. The role of some bacterial or viral agents in the pathogenesis of AITP is well known. It has been demostrated that the mimicry of human antigens by infectious agents represents the mechanism underlying this phenomenon[18].

H pylori is a ubiquitous Gram-positive bacterium involved in the pathogenesis of gastric and duodenal ulcers. Recently, the involvement of *H pylori* has also been suggested in various autoimmune diseases[6-9]. *H pylori* has been shown to cause immunological responses to the production of large amounts of proinflammatory substances and mucosal damage through autoimmunity[19]. Previous *in vitro* studies suggested that *H pylori* has the potential to initiate autoreactivity through molecular mimicry. Recently, a role of *H pylori* in the pathogenesis of AITP has been suggested because significant increases in thrombocyte count were reported after eradication of *H pylori*[10,11]. Michel *et al*.[2] and Jargue *et al*.[14] found no evidence of an association between *H pylori* infection and AITP. But the role of *H pylori* in the pathogenesis of AITP is still controversial.

Regarding the association between *H pylori* and AITP, Gasbarrini *et al*.[11] reported that 61% of 18 AITP cases were infected with *H pylori*. Emilia *et al*.[10] then reported that 43% of 30 AITP patients were *H pylori* positive. Kohda *et al*.[18] found that *H pylori* was positive in 62.5% of 40 AITP patients in Japan. The prevalence of *H pylori* in our series was 68.5%. The prevelance of *H pylori* infection in healthy population of Italy, where Gasbarrini' s and Emilia' s studies were held, was about 63%[20]. In Japan the prevelance of *H pylori* infection was about 25-45%[21]. We found *H pylori* infection in 65.2% of healthy controls in Turkish population.

Steroid is considered as the most effective treatment for AITP in adults. But, most patients relapsed when steroids were withdrawn and only 10-30% of them maintained a long lasting remission[22]. Kohda *et al*.[18] and Michel *et al*.[2] found that there was no significant difference regarding thrombocyte counts between *H pylori*-positive and *H pylori*-negative AITP patients. In our series the thrombocyte count of *H pylori*-positive group was higher than that of *H pylori*-negative group at the initial presentation, and the difference between two groups was significant ($P<0.05$). Following treatment increase in the thrombocyte count of *H pylori*-positive patients was less than that of *H pylori*-negative patients. The difference was also significant ($P<0.05$).

Although the pathogenetic mechanism underlying *H pylori*-induced thrombocytopenia remains obscure, *H pylori* has been presumed to induce the formation of autoantibodies by way of a chronic immunological stimulus or cross mimicry between itself and platelets[23]. It has been demonstrated that autoantibodies against *H pylori* can also react with some extragastric tissues, such as glomerular capillary membrane, ductal cells of salivary glands, and renal tubular cells[24]. Platelets may also be a target of such antibodies although there is no proof for this cross reactivity.

In conclusion, *H pylori* infection should be searched in all AITP patients, and we suggest that *H pylori* should eradicated in *H pylori*-positive AITP patients.

REFERENCES

1 **George JN**, el-Harake MA, Raskob GE. Chronic idiopathic thrombocytopenic purpura. *N Engl J Med* 1994; **331**: 1207-1211

2 **Michel M**, Khellaf M, Desforges L, Lee K, Schaeffer A, Godeau B, Bierling P. Autoimmune thrombocytopenic purpura and Helicobacter pylori infection. *Arch Intern Med* 2002; **162**: 1033-1036

3 **Suzuki H**, Masaoka T, Nomura S, Hoshino Y, Kurabayashi K, Minegishi Y, Suzuki M, Ishii H. Current consensus on the diagnosis and treatment of *H pylori* associated gastroduodenal disease. *Keio J Med* 2003; **52**: 163-173

4 **Ando K**, Shimamoto T, Tauchi T, Ito Y, Kuriyama Y, Gotoh A, Miyazawa K, Kimura Y, Kawai T, Ohyashiki K. Ca eradication therapy for *Helicobacter pylori* really improve the thrombocytopenia in idiopathic thrombocytopenic purpura? Our experience and a literature review. *Int J Hematol* 2003; **77**: 239-244

5 **Veneri D**, Franchini M, Gottardi M, D'Adda M, Ambrosetti A, Krampera M, Zanetii F, Pizzolo G. Efficacy of Helicobacter pylori eradication in raising paltelet count in adult patients with idiopathic thrombocytopenic purpura. *Haematologia* 2002; **87**: 1177-1179

6 **Zentilin P**, Savarino V, Garnero A, Accardo S, Seriolo B. Is *Helicobacter pylori* infection a risk factor for disease severity in rheumatoid arthritis? *Gastroenterology* 1999; **116**: 503-504

7 **De Luis DA**, Varela C, de la Calle H. *Helicobacter pylori* infection is markedly increased in patients with autoimmune atropic thyroiditis. *J Clin Gastroenterol* 1998; **26**: 259-263

8 **Figura N**, Giordano N, Burroni D, Macchia G, Vindigni C, Gennari C, Bayeli PF. Sjogren's syndrome and *Helicobacter pycori* infection. *European J Gastroenterol Hepatol* 1994; **6**: 321-322

9 **Reinauer S**, Megahed M, Goertz G, Ruzicka T, Borchard F, Susanto F, Reinauer H. Schonlein-Henoch purpura associated with gastric *Helicobacter pylori* infection. *J Am Acad Dermatol* 1995; **33**: 876-879

10 **Emilia G**, Longo G, Luppi M, Gandini G, Morselli M, Ferrara L, Amarri S, Cogossi K, Torelli G. *Helicobacter pylori* eradication can induce platelet recovery in idiopathic thrombocytopenic purpura. *Blood* 2001; **97**: 812-814

11 **Gasbarrini A**, Franceschi F, Tartaglione R, Landolfi R, Pola P, Gasbarrini G. Regression of autoimmune thrombocytopenia after eradication of *Helicobacter pylori*. *Lancet* 1998; **352**: 878

12 **Hashino S**, Mori A, Suzuki S, Izumiyama K, Kahata K, Yonezumi M, Chiba K, Kondo T, Ota S, Toyashima N, Kato N, Tanaka J, Imamura M, Asaka M. Platelet recovery in patients with idiopathic thrombocytopenic purpura after eradication of *Helicobacter pylori*. *Int J Hematol* 2003; **77**: 188-191
13 **Hino M**, Yamane T, Park K, Tahubo T, Ohta K, Kitagawa S, Higuchi K, Arakawa T. Platelet recovery after eradication of *Helicobacter pylori* in patients with idiopathic thrombocytopenic purpura. *Ann Hematol* 2003; **82**: 30-32
14 **Jargue I**, Andreu R, Llopis I, De la Rubia J, Gomis F, Senent L, Jimenez C, Martin G, Martinez JA, Sanz GF, Ponce J, Sanz MA. Absence of platelet response after eradication of *Helicobacter pylori* infection in patients wtih chronic idiopathic thrombocytopenic purpura. *Br J Haematol* 2001; **115**: 1002-1003
15 **Feldman RA**, Deeks JJ, Evans SJ. For the *Helicobacter pylori* Serology Study Group Multi-laboratory comparison of eight commercially available *Helicobacter pylori* serology kits. *Eur J Clin Microbiol Infect Dis* 1995; **14**: 428-433
16 **McMillan R**. Autoantibodies and autoantigens in chronic immune thrombocytopenic purpura. *Semin Hematol* 2000; **37**: 239-248
17 **Benoist C**, Mathis D. Autoimmunity: the pathogen connection. *Nature* 1998; **394**: 227-228
18 **Kohda K**, Kuga T, Kogawa K, Kanisawa Y, Koike K, Kuroiwa G, Hirayama Y, Sato Y, Matsunaga T, Niitsu Y. Effect of *Helicobacter pylori* eradication on platelet recovery in Japanese patients with chronic idiopathic thrombocytopenic purpura and secondary autoimmune thrombocytopenic purpura. *Br J Hematol* 2002; **118**: 584-588
19 **Bamford KB**, Andersen L. Host response. *Current Opinion Gastroenterol* 1997; **13**(Suppl 1): 25-30
20 **Luzza F**, Imeneo M, Maletta M, Paluccio G, Nistico S, Perticone F, Foca A, Pallone F. Suggestion against an oral-oral rout of transmission for *Helicobacter pylori* infection: a seroepidemiological study ina rural area. *Dig Dis Sci* 1998; **43**: 1488-1492
21 **Asaka M**, Kimura T, Kudo M, Tadeka H, Miyazaki T, Miki K, Garaham DY. Relationship of *Helicobacter pylori* to serum pepsinogens in an asymptomatic Japanese population. *Gastroenterology* 1992; **102**: 760-766
22 **George JN**, Woolf SH, Raskob GE, Wasser JS, Aledort LM, Ballem PJ, Blanchette VS, Bussel JB, Cines DB, Kelton JG, Lichtin AE, McMillan R, Okerbloom JA, Regan DH, Warrier I. Idiopathic thrombocytopenic purpura: a practice guideline developed by explicit methods for the American Society of Hematology. *Blood* 1996; **88**: 3-40
23 **Gasbarrini A**, Franceschi F. Autoimmune diseases and *Helicobacter pylori* infection. *Biomed Pharmacother* 1999; **53**: 223-226
24 **Ko GH**, Park HB, Shin MK, Park CK, Lee JH, Youn HS, Cho MJ, Lee WK, Rhee KH. Monoclonal antibodies against *Helicobacter pylori* cross react with human tissue. *Helicobacter* 1997; **2**: 210-215

Edited by Wang XL **Proofread by** Chen WW and Xu FM

PO Box 2345, Beijing 100023, China
Fax: +86-10-85381893
E-mail: wjg@wjgnet.com www.wjgnet.com

World J Gastroenterol 2004;10(14):2116-2118
World Journal of Gastroenterology
 ISSN 1007-9327

• BRIEF REPORTS •

Curative effects of interferon-α and HLA-DRB1 -DQA1 and -DQB1 alleles in chronic viral hepatitis B

Guo-Qing Zang, Min Xi, Ming-Liang Feng, Yun Ji, Yong-Sheng Yu, Zheng-Hao Tang

Guo-Qing Zang, Min Xi, Yong-Sheng Yu, Zheng-Hao Tang, Department of Infectious Diseases, 6th People's Hospital of Shanghai Jiaotong University, Shanghai 200233, China
Ming-Liang Feng, Yun Ji, Shanghai Blood Center, Shanghai 200051, China
Supported by the Foundation of Shanghai Municipal Health Bureau, No. 01444
Correspondence to: Dr. Guo-Qing Zang, Department of Infectious Diseases, 6th People's Hospital of Shanghai Jiaotong University, Shanghai 200233, China
Telephone: +86-21-64369181
Received: 2003-11-26 **Accepted:** 2004-02-01

Abstract

AIM: To investigate the association between curative effects of interferon-α and partial human leucocyte antigen (HLA) II alleles in chronic viral hepatitis B.

METHODS: Sixty patients with chronic viral hepatitis B in Shanghai were treated with a standard course of treatment with interferon-α for 6 mo. HLA-DRB1, -DQA1, and -DQB1 alleles were detected by polymerase chain reaction-sequence specific primer (PCR-SSP) method.

RESULTS: Frequencies of HLA-DRB1*04 ($P<0.025$) and HLA-DQA1*0303 ($P<0.01$) in non-responders were significantly higher than those in partial and complete responders. Frequencies of HLA-DQA1*0505 ($P<0.025$) and HLA-DQB1*0301 ($P<0.005$) in partial and complete responders were significantly higher than those in non-responders.

CONCLUSION: Non-response to interferon-α therapy is positively correlated with HLA-DRB1*04 and HLA-DQA1*0303, and negatively correlated with HLA-DQA1*0505 and -DQB1*0301 in patient with chronic viral hepatitis B. HLA II genes of the identification alleles provide a method for evaluating outcome of interferon-α treatment.

Zang GQ, Xi M, Feng ML, Ji Y, Yu YS, Tang ZH. Curative effects of interferon-α and HLA-DRB1 -DQA1 and -DQB1 alleles in chronic viral hepatitis B. *World J Gastroenterol* 2004; 10(14): 2116-2118
http://www.wjgnet.com/1007-9327/10/2116.asp

INTRODUCTION

Chronic viral hepatitis B is a contagious disease with the higher infection and incidence rate in China, and approximately 0.3 million peoples died of chronic viral hepatitis B per year[1]. Currently, it is mainly treated with interferon-α, lamivudine, *etc*. However, the effect of treatment is varying in different patients. Normally, complete response rate is about 30-40%, complete curability is less than 10%. What is the determinant of interferon-α curative effect on different individuals? Reports from domestic and overseas showed that individuals had different endings after being infected by HBV and HCV[2-3] and different response after being treated with interferon-α[4]. Researches indicated that these phenomenons were correlated with HLA alleles[5]. HLA gene contributes to the host response against HBV. Individuals with different HLA alleles may differ in susceptibility or resistance to HBV[6-8]. Our study tried to analyze HLA-DRB1, -DQB1, -DQA1 alleles in chronic viral hepatitis B to be treated with interferon-α for 6 mo, and study the association between curative effects of interferon-α and partial HLA alleles, which will help to direct the treating process of anti-virus in clinic.

MATERIALS AND METHODS

Research subjects and prescription

Sixty patients with chronic viral hepatitis B were enrolled in this study. The diagnosis of all the cases was made according to the criteria established on the Viral Hepatitis Conference held in 2000[9]. All patients had abnormal serum transaminase levels. HBsAg, HBeAg, HBcAb in serum were detected by ELISA and HBV-DNA was detected by immunofluorescent semi-quantitative polymerase chain reaction. All patients' HAV, HCV, HDV and HEV in serum were negative, and did not have a history of using adrenal cortical hormone before. There were 41 male and 19 female patients with average age 35±8 years. They were all treated with 5.0 million units interferon-α daily for 2 wk and then every other day for an additional 22 wk. Liver function was detected every 2 wk. Hepatitis B viral marks were detected by Abbott Laboratories and HBV-DNA was determined by PCR at every 3-mo therapy.

Sampling and action

Five milliliter blood from each research subject was taken, and treated with EDTA for anti-coagulation. After mixed with 1 mL cell membrane cracking solution, the samples were centrifuged for 30 s, and then the supernatant was removed. Another 1 mL of cell membrane cracking solution was added after drying the test tube by bibulous paper. Centrifuged for 20 s and the top clear water was removed again. The cell mass at the bottom of the tube was vibrated and dissolved thoroughly. When mixed equally with 0.4 mL karyen cracking solution, separated out floccule DNA by adding 1 mL absolute ethanol. Supernatant was abandoned, and washed with 70% ethanol. After drying by blot paper, put it under room temperature to let ethanol volatilize. Then 0.1 double distilled water was added, and kept at -40 ℃ for testing.

Study method

HLA-DRB1, HLA-DQA1, and HLA-DQB1 alleles were detected by applying the PCR-SSP technique[10]. PCR buffer solution was vibrated and mixed. Taq enzyme was put on the icebox. Distilled water 67 μL and 1.8 μL of Taq enzyme were added to the PCR buffer solution and vibrated. Then the solution was aspirated and added to the monitor hole. And 19 μL of DNA samples were added to the spare mixing solution. Except negative contrast hole, the solution was added

to every hole. Color changed from yellow to pink. The reagent was sealed up, and sent to PCR apparatus for amplification. Sample solution 6 μL was electrophoresed on 20 g/L agarose gel for 12 min under 150 V, and observed the under ultraviolet light.

Statistical analysis

HLA-DRB1, -DQA1, and -DQB1 alleles frequencies for the partial and complete responders were compared with those of the non-responders using the χ^2 test. $P<0.05$ was considered statistically significant.

RESULTS

Based on the results of HBV markers and HBV-DNA after 6-mo therapy with interferon-α, patients were divided into 3 groups: (1) Complete response group: HBeAg and HBV-DNA were negative, while HBeAb was positive, and ALT was normal; (2) Partial response group: HBeAg and HBV-DNA level decreased, while ALT was normal; (3) Non-response group: HBeAg and HBV-DNA were stable. After inspection, it was found that the frequencies of HLA-DRB1*04($P<0.025$) and HLA-DQA1*0303($P<0.01$) in non-responders were significantly higher than those in partial and complete responders, and the frequencies of HLA-DQA1*0505($P<0.025$) and HLA-DQB1*0301($P<0.005$) in partial and complete responders were significantly higher than those in non-responders (Tables 1, 2 and 3).

Table 1 Comparison of frequency of HLA-DRB1 allele among non-responders and partial and complete responders

Allele	Partial and complete responders (n=34)	Non-responders (n=26)	χ^2
DRB1*10(+)	1	0	0.778
DRB1*11(+)	9	3	2.053
DRB1*4(+)[a]	1	6	2.053
DRB1*12(+)	9	7	0.002
DRB1*8(+)	4	5	0.644
DRB1*9(+)	15	11	0.020
DRB1*14(+)	4	4	0.167
DRB1*15(+)	8	10	1.564
DRB1*17(+)	1	2	0.700
DRB1*16(+)	3	0	2.415
DRB1*7(+)	4	0	3.277

[a]$P<0.025$.

Table 2 Comparison of HLA-DQA1 allele frequencies among non-responders and partial and complete responders

Allele	Partial and complete responders (n=32)	Non-responders (n=28)	χ^2
DQA1*0105(+)	1	0	0.890
DQA1*0505(+)[a]	12	3	5.714
DQA1*0303(+)[b]	0	6	7.619
DQA1*0601(+)	10	7	0.287
DQA1*0103(+)	9	7	0.075
DQA1*0302(+)	15	12	0.097
DQA1*0104(+)	4	4	0.041
DQA1*0102(+)	4	6	0.857
DQA1*0301(+)	1	4	2.435

[a]$P<0.025$, [b]$P<0.01$.

Table 3 comparison of frequencies of HLA-DQB1 allele among non-responders and partial and complete responders

Allele	Partial and complete responders (n=32)	Non-responders (n=28)	χ^2
DQB1*0502(+)	6	1	3.338
DQB1*0301(+)[a]	20	7	8.485
DQB1*0401(+)	1	3	1.382
DQB1*0303(+)	15	12	0.097
DQB1*0503(+)	3	4	0.431
DQB1*0601(+)	6	9	1.429

[a]$P<0.005$.

DISCUSSION

Different individuals infected with HBV show different complicated symptoms. This is not only due to virus itself, but immunity itself [11]. A great deal of evidences suggested that both cellular and humoral immunities were required for viral clearance. The latter is mainly subjected to major histocompatibility complex (MHC). HLA, the genetic offspring of MHC, is the first inherited system discovered to be associated with diseases definitely. Genes for HLA are located on the short arm of chromosome 6 with high polymorphism, and it is closely associated with immunoreactions of anti-HBV[12]. Some special HLA genes may have influence on the rate of HBV infection and strength of immunoreactions[13]. Patients who have successfully recovered from acute hepatitis B develop strong HLA classes I and II restricted T cell response, whereas these responses are weak or absent in patients with chronic hepatitis B[14]. Jiang *et al*.[15] found that HLA-DRB1*0301, -DQA1*0501 and -DQB1*0301 might be the susceptible genes, and HLA-DRB1*1101/1104 and -DQA1*0301 might be the resistant genes to chronic hepatitis B, and that host HLA class II gene was an important factor for determining the outcome of HBV infection. HLA spread on the cell surface through membrane protein with function of integrating with inner and outer antigen peptide and taking immune response when detected by $CD4^+$ (cluster of differentiation) or $CD8^+$ T cell on the surface of antigen presenting cells and target cells. Class II molecule, on the surface of antigen presenting cells, submits outer antigen including virus molecule group to the $CD4^+$ T cell, which stimulates the releasing of the cell gene to take the effect of adjusting $CD8^+$ cytotoxic T lymphocyte response and determine the antibody produce. Diepolder *et al*.[16] found that people carrying HLA-DR13 had stronger $CD4^+$ T cell response. That might be depended on the more accurate submission function of DR13, or associated with multiple peptide property of immunity adjusting gene chain near DR13. Thursz *et al*.[17] discovered that DRB1*1302 possessed high frequency of clearance of hepatitis B virus in the Gambia people. Cotrina *et al*.[5] also reported that predominance of the DRB1*1302 allele was observed in acute viral hepatitis B versus chronic viral hepatitis B in adult American. And the HLA-DRB1*0401 antigen was lower in the cases of chronic viral hepatitis B and C than that in the controls. Hohler *et al*.[18] reported that the MHC class II allele DRB1*1301-02 was associated with protection from chronic viral hepatitis B in African Americans. Furthermore Bhimma *et al*.[19] demonstrated that there was a high frequency of DQB1*0603 in subjects compared to controls in black children with hepatitis B virus-associated membranous nephropathy. Jiang *et al*.[20] recently found that the possibility of fulminant hepatitis was increased in chronic hepatitis B with HLA-DRB1*1001. Tibbs *et al*.[21] showed that the HLA-DQB1*0302 and HLA-DQA1*03 alleles confered protection from chronic HCV-infection in Northern European

Caucasoid. These studies showed that HLA-II molecules were associated with clearance and prognosis of chronic viral hepatitis.

Currently, factors for forecasting interferon treating effect are as follows: ALT level before treatment; level of HBV-DNA; gene types of hepatitis B virus; sex of patients; and the duration of virus infection, *etc*. Interferon can induce the expression of IL-12 (interleukin-12) β_2 subpopulation, which induce Th0 (help T cell) cell to differentiate into Th1 cell. Previous studies showed that Th1 type response was beneficial for the clearance of chronically infected viruses[7]. The balance of HBV differential antigen may influence the persistent HBV infection. Superiority of Th1 tends to occur acute hepatitis, while superiority of Th2 tends to occur persistent infection[22]. There were fewer reports about association between curative effects of interferon-α with partial HLA allele. Qian *et al*.[23] reported that the frequency of HLA-DRB1*07 in non-responders was higher than that in partial and complete responders in Guangdong Province of China, and the level of IL-4 and IFN-γ of each patient was higher than that of pre-treatment. It indicated that after treatment of chronic viral hepatitis B with IFN-γ, TH1 expression was relevant to the HLA-DRB1*07. Dincer *et al*.[24] reported that in the HCV patient treated with interferon-α for 6 mo, the frequency of HLA-DRB1*13 was significantly higher in the non-responder group compared to the responder group. Our study showed that the frequency of HLA-DRB1*04 and HLA-DQA1*0303 in non-responders were obviously higher than those in partial and complete responders, and the frequency of HLA-DQA1*0505 and HLA-DQB1*0301 in partial and complete responders were markedly higher than those in non-responders. HLA-II molecules might be used for the treatment prognosis of interferon -α in patients with chronic hepatitis B.

REFERENCES

1 World Health Organization, 1998. Hepatitis Bfact Sheet WHO/204. http://www.who.int/inf-fs/en/fact203.html

2 **van Hattum J**, Schreuder GM, Schalm SW. HLA antigens in patients with various courses after hepatitis B virus infection. *Hepatology* 1987; **7**: 11-14

3 **Tong MJ**, el-Farra NS, Reikes AR, Co RL. Clinical outcomes after transfusion-associated hepatitis C. *N Engl J Med* 1995; **332**: 1463-1466

4 **Miyaguchi S**, Saito H, Ebinuma H, Morizane T, Ishii H. Possible association between HLA antigens and the response to interferon in Japanese patients with chronic hepatitis C. *Tissue Antigens* 1997; **49**: 605-611

5 **Cotrina M**, Buti M, Jardi R, Rodriguez-Frias F, Campins M, Esteban R, Guardia J. Study of HLA-II antigens in chronic hepatitis C and B and in acute hepatitis B. *Gastroenterol Hepatol* 1997; **20**: 115-118

6 **Sobao Y**, Sugi K, Tomiyama H, Saito S, Fujiyama S, Morimoto M, Hasuike S, Tsubouchi H, Tanaka K, Takiguch M. Identification of hepatitis B virus-specific CTL epitopes presented by HLA-A*2402, the most common HLA class I allele in East Asia. *J Hepatol* 2001; **34**: 922-929

7 **Thimme R**, Chang KM, Pemberton J, Sette A, Chisari FV. Degenerate immunogenicity of an HLA-A2-restricted hepatitis B virus nucleocapsid cytotoxic T-lymphocyte epitope that is also presented by HLA-B51. *J Virol* 2001; **75**: 3984-3987

8 **Shen JJ**, Ji Y, Guan XL, Huang RJ, Sun YP. The association of HLA-DRB1*10 with chronic hepatitis B in Chinese patients. *Zhonghua Weishengwuxue He Mianyixue Zazhi* 1999; **19**: 58-59

9 China physic association infectious disease & verminosis association liver disease sub-association viral hepatitis prevention & cure project. *Zhonghua Ganzangbing Zazhi* 2000; **8**: 324-329

10 **Olerup O**, Zetterquist H. HLA-DR typing by PCR amplification with sequence-specific primers(PCR-SSP) in 2 hours: an alternative to serological DR typing in clinical practice including donor-recipient matching in cadaveric transplantation. *Tissue Antigens* 1992; **39**: 225-235

11 **Chen WN**, Oon CJ. Mutation "hot spot" in HLA class I restricted T cell epitope on hepatitis B surface antigen in chronic carriers and hepatocellular carcinoma. *Biochem Biophys Res Commun* 1999; **262**: 757-761

12 **McDermott AB**, Cohen SB, Zuckerman JN, Madrigal JA. Human leukocyte antigens influence the immune response to a pre-S/S hepatitis B vaccine. *Vaccine* 1999; **17**: 330-339

13 **McDermott AB**, Madrigal JA, Sabin CA, Zuckerman JN, Cohen SB. The influence of host factors and immunogenetics on lymphocyte responses to hepagene vaccination. *Vaccine* 1999; **17**: 1329-1337

14 **Zhang SL**, Liu M, Zhu J, Chai NL. Predominant Th_2 immune response and chronic hepatitis B virus infection. *Shijie Huaren Xiaohua Zazhi* 1999; **7**: 513-515

15 **Jiang YG**, Wang YM, Liu TH, Liu J. Association between HLA class II gene and susceptibility or resistance to chronic hepatitis B. *World J Gastroenterol* 2003; **9**: 2221-2225

16 **Diepolder HM**, Jung MC, Keller E, Schrant W, Gerlach JT, Gruner N, Zachoval R, Hoffmann RM, Schirren CA, Scholz S, Pape GR. A vigorous virus-specific CD4+ T cell response may contribute to the association of HLA-DR13 with viral clearance in hepatitis B. *Clin Exp Immunol* 1998; **113**: 244-251

17 **Thursz MR**, Kwiatkowski D, Allsopp CE, Greenwood BM, Thomas HC, Hill AV. Association between an MHC class II allele and clearance of hepatitis B virus in the gambia. *New Engl J Med* 1995; **332**: 1065-1069

18 **Hohler T**, Gerken G, Notghi A, Lubjuhn R, Taheri H, Protzer U, Lohr HF, Schneider PM, Meyer zum Buschenfelde KH, Rittner C. HLA-DRB1*1301 and *1302 Protect against chronic hepatitis B. *J Hepatol* 1997; **26**: 503-507

19 **Bhimma R**, Hammond MG, Coovadia HM, AdhiKari M, Connolly CA. HLA class I and II in black children with hepatitis B virus-associated membranous nephropathy. *Kidney Int* 2002; **61**: 1510-1515

20 **Jiang YG**, Wang YM. Association between HLA-DRB1*1001 and severity of chronic hepatitis B. *Zhonghua Ganzangbing Zazhi* 2003; **11**: 256

21 **Tibbs C**, Donaldson P, Underhill J, Thomson L, Manabe K, Williams R. Evidence that the HLA DQA1 *03 allele confers protection from chronic HCV-infection in northern european caucasoids. *Hepatology* 1996; **24**: 1342-1345

22 **Lee M**, Lee SK, Son M, Cho SW, Park S, Kim HI . Expression of Th1 and Th2 type cytokines responding to HBsAg and HBxAg in chronic hepatitis B patient. *J Korean Med Sci* 1999; **14**: 175-181

23 **Qian Y,** Zhang L, Hou JL. Association between non-response to interferon and HLA-DRB1*07 genes in chronic hepatitis Bindividuals. *Mianyixue Zazhi* 2002; **18**: 371-374

24 **Dincer D**, Besisik F, Oguz F, Sever MS, Kaymakoglu S, Cakaloglu Y, Demir K, Turkoglu S, Carin M, Okten A. Genes of major histocompatibility complex class II influence chronic C hepatitis treatment with interferon in hemodialysis patients. *Int J Artiforgans* 2001; **24**: 212-214

Edited by Kumar M and Chen WW **Proofread by** Xu FM

PO Box 2345, Beijing 100023, China
Fax: +86-10-85381893
E-mail: wjg@wjgnet.com www.wjgnet.com

World J Gastroenterol 2004;10(14):2119-2123
World Journal of Gastroenterology
 ISSN 1007-9327

• BRIEF REPORTS •

Expansion and activation of natural killer cells from PBMC for immunotherapy of hepatocellular carcinoma

Bao-Gang Peng, Li-Jian Liang, Qiang He, Jie-Fu Huang, Ming-De Lu

Bao-Gang Peng, Li-Jian Liang, Qiang He, Jie-Fu Huang, Ming-De Lu, Department of Hepatobiliary Surgery, First Affiliated Hospital of Sun Yat-sen University, Guangzhou 510080, Guangdong Province, China
Supported by the Natural Science Foundation of Guangdong Province, No. 021889
Correspondence to: Dr. Bao-Gang Peng, Department of Hepatobiliary Surgery, First Affiliated Hospital of Sun Yat-sen University, 58 Zhongshan Road 2, Guangzhou 510080, Guangdong Province, China. pengbaogang@163.net
Telephone: +86-20-87335546 **Fax:** +86-20-87750632
Received: 2003-11-26 **Accepted:** 2004-01-15

Abstract

AIM: To induce efficient expansion of natural killer (NK) cells from peripheral blood mononuclear cells (PBMCs) using a culture of anchorage-dependent Wilms tumor cell lines, and to provide a reliable supply for adoptive immunotherapy of hepatocellular carcinoma.

METHODS: Culture expansion of NK cells was achieved using PBMCs cultured with Wilms tumor cells. Cytotoxicity was measured using a standard ^{51}Cr release assay and crystal violet staining technique. The proportions of CD3+, CD4+, CD8+, CD16+, and CD56+ cells were determined by flow cytometry.

RESULTS: After PBMCs from healthy donors and hepatocellular carcinoma (HCC) were cultured with irradiated HFWT cells for 10-21 d, CD56+ CD16+ cells shared more than 50% of the cell population, and more than 80% of fresh HFWT cells were killed at an effector/target ratio of 2 over 24 h. NK-enriched lymphocyte population from HCC patients killed HCC-1 and 2 cells with sensitivities comparable to fresh TKB-17RGB cells. HCC cells proliferated 196-fold with the irradiated HFWT cells at 18 d. Stimulation by HFWT cells required intimate cell-cell interaction with PBMC. However, neither the soluble factors released from HFWT cells nor the fixed HFWT cells were effective for NK expansion. The lymphocytes expanded with IL-2 killed fresh HFWT target cells more effectively than the lymphocytes expanded with the 4-cytokine cocktail (IL-I β, IL-2, IL-4 and IL-6). IL-2 was the sole cytokine required for NK expansion.

CONCLUSION: Wilms tumor is sensitive to human NK cells and is highly efficient for selective expansion of NK cells from PBMCs.

Peng BG, Liang LJ, He Q, Huang JF, Lu MD. Expansion and activation of natural killer cells from PBMC for immunotherapy of hepatocellular carcinoma. *World J Gastroenterol* 2004; 10 (14): 2119-2123
http://www.wjgnet.com/1007-9327/10/2119.asp

INTRODUCTION

Natural killer (NK) cells are CD3- CD56+ and/or CD16+ cytotoxic lymphocytes that mediate first-line defense against various types of target cells without prior immunization[1,2]. The regulation mechanism of human natural killer (NK) cell growth has not been well characterized despite the importance of NK cells in immune response[3]. One reason is that the currently used culture system for human NK cells is relatively poor at inducing a strong growth response compared with culture systems for other lymphocytes, such as T cells.

Since K562 cells expressing scarcely MHC-class I on their surface are highly sensitive to natural killer (NK) cells, they have been widely used for the assay of NK killing activity[4-6]. When K562 cells are killed by NK cells *in vitro*, apparent growth response of NK cells follows. The stimulation by K562 requires direct cell-cell contact and is not reconstituted by cell-free supernatants. However, the stimulation is not necessarily sufficient for the NK selective expansion in peripheral blood mononuclear cells (PBMCs) of every subject. Reports from Perussia *et al*.[7] and Silva *et al*.[8,9] suggested that human B lymphoblastoid cell lines and leukapheresed peripheral blood stem cell grafts were also useful for human NK cell expansion. Sekine *et al*.[10] developed an alternative method for lymphocyte expansion from peripheral blood by cultivating cells with IL-2 and immobilized anti-CD3 monoclonal antibodies. Application of expensive anti-CD3, anti-CD16 bispecific antibodies may avoid the dilution of NK cells in the lymphocyte populations[11]. Coculture of NK cells with dendritic cells (DCs) resulted in significant enhancement of NK cell cytotoxicity and IFN-gamma production[12]. Coexpression of GM-CSF and B70 may enhance NK-mediated cytotoxicity, and then induce the antitumor immunity in hepatoma transplanted into nude mice[13].We consider that, for further use of the NK cells in adoptive immunotherapy of human tumors, clear separation of expanded NK cells and suspension cultured allogeneic EB virus-transformed cells that may have escaped from the killing by NK cells will be difficult.

In this study, we screened anchorage-dependent virus-free human tumor cell lines as an appropriate target in the NK cell expansion culture. We found that an anchorage-dependent cell line derived from Wilms tumor (HFWT) was sensitive to human NK cells.

MATERIALS AND METHODS

Cell lines and reagents

All the cell lines were from routine stock cultures in the RIKEN Cell Bank. Cell lines were maintained in basal medium containing 100 mL/L or 150 mL/L fetal bovine serum (FBS). Peripheral blood was taken from healthy volunteers and hepatocellular carcinomas (HCCs) were from patients who gave their informed consent. Recombinant human IL-1 β, -2, -4, -6, -7, -12, and -15 were purchased from Genzyme (Tokyo, Japan). Mouse anti-human-CD3, CD4, -CD8, CD56 and CD16 monoclonal antibodies were purchased from Nichirei Co., (Tokyo, Japan). ^{51}Cr was purchased from Nen Life Science Products Inc. (Boston, USA).

Flow cytometry

Suspended cells (1×10^6) were washed three times with PBS, incubated for 30 min with monoclonal antibodies, 30 min with

FITC-labeled goat anti-mouse IgG polyclonal antibody. The cells were again washed with PBS containing 40 mL/L FBS. They were re-suspended in the same buffer at a concentration of l×10^6/mL and were immediately analyzed by FACS (Becton-Dickinson, Co.). The proportion of CD3+, CD4+, CD8+, CD16+, and CD56+ cells was detected with corresponding monoclonal antibodies.

Fixation of HFWT cells

HFWT cells (1×10^5/mL, 1 mL) were plated in a 24-well plate and incubated overnight in a humidified 50 mL/L CO_2 incubator. The culture medium was replaced with PBS, and the cells were fixed with 0.5 mL of 40 g/L formaldehyde or 3:1 methanol-acetic acid mixture for 1 h, and then thoroughly washed with water.

HFWT cells were subjected to heat treatment at 100 ℃ for 2 s in a microwave oven after the replacement of the culture medium with PBS. The treated HFWT cell concentration was adjusted to 1×10^5 /well for the NK expansion experiments.

Expansion culture of NK cells

PBMCs were prepared from heparinized peripheral blood with the conventional preparation kit (Lymphopre, Nycomed Pharma A.S., Norway). The cells were washed once with PBS, then once with RHAM alpha medium supplemented with 50 mL/L autologous plasma, and centrifuged at 1 400 r/min (240 g) for 10 min at room temperature. Before addition of PBMCs to the NK cell expansion cultures, the confluent target tumor cells maintained in a 24-well plate were irradiated with 50 Gy of X-rays. The PBMCs (l×10^6 /mL, approximately 1 mL/well) were then cultured with the tumor cells (at this stage, the responder/stimulator ratio was adjusted to 10 in the culture medium, i.e. the RHAMα medium was supplemented just before adding 50 mL/L autologous plasma and a 4-cytokine cocktail of IL-l β (167 U/mL), IL-2 (67 U/mL), IL-4 (67 U/mL), and IL-6 (134 U/mL)). When IL-2 alone was used, the concentration was adjusted to 200 U/mL. IL-7, IL-12, and IL-15 were used at a concentration of 10 U/mL, 10 ng/mL, and 20 U/mL, respectively.

NK expansion culture was continued with appropriate changes of the medium, including addition of the indicated cytokines (at least half of the medium was changed every 2 d), until the adherent target cells disappeared. When K562 cells were the targets, this period was set at 7 d. The cell suspension was diluted to 5×10^5/mL and the culture continued. Whenever the cell suspension reached 5×10^6/mL, the dilution was repeated.

Cytotoxicity assay

A standard ^{51}Cr release assay was performed in the 4-h co-culture of the effector lymphocytes and the target K562 cells as described[14]. The crystal violet staining was also used[15]. Briefly, the target cells, 1×10^4/well suspended in 200 μL RHAM α medium containing 50 mL/L plasma from the lymphocyte donor (or 50 mL/L PPF whenever the plasma was in short supply), were seeded in a 96-well plate and were pre-cultured overnight. The cultured target cells were washed once with PBS, then the cultured lymphocytes suspended in 200 μL of RHAM α medium containing 50 mL/L autologous plasma (or 50 mL/L PPF) were added as effector cells to each well at the indicated effector/target (E/T) ratio. The cells were co-cultured for 4 or 24 h. Then, the wells were washed once gently with appropriate amounts of Dulbecco's PBS containing calcium and magnesium. The target cells remaining adhered were fixed for 1 h with 40 g/L formaldehyde (200 μL/well), and then stained with crystal violet solution (4 g/L in water, 100 μL/well) for 30 min at room temperature. The plate was washed with water and dried at room temperature. A 200 μL of 800 mL/L methanol was added into each well and the absorbance at 570 nm (A_{570}) of each well was determined. As a 100% control, the A_{570} of the target cells cultured in a separate plate was determined just before the addition of the effector cells.

Percentage of surviving target cells was defined as follows:

Surviving target cells (%)=(A-B)/(C-D)×100%

Where A is the A_{570} of the well containing the target cells and the effector cells, B is the A_{570} of the well containing only the effector cells which remained in the well after the washing with calcium- and magnesium-containing Dulbecco's PBS, C is the A_{570} of the 100% control target cells just before the addition of the effector cells, and D is the A_{570} of the well containing medium alone. The target cells cultured at an E/T ratio of 0 grew rapidly over the 24-h incubation period and, therefore, showed more than 100% survival.

RESULTS

Proportion of NK cells in the lymphocyte culture

Two hundred and forty kinds of human cell lines from RIKEN Cell Bank were screened for their expression of MHC-class I and class II surface molecules. Ten cell lines including leukemia cell line K562, HFWT (Wilms tumor), HMV-II (melanoma) and NB 19 (neuroblastoma) were found that weakly expressed MHC molecules of both.

Subsequently, PBMCs taken from healthy subjects were co-cultured with these cell lines after the target cells had been irradiated with 50 Gy of X-rays. HFWT cultures demonstrated a striking change in anchorage-dependent HFWT cells that were totally killed and disappeared after 13-14 d. CD3- CD56+ cells occupied 64.6%, 54.6%, and 75.9% of the lymphocyte population in the three experiments, respectively. However, K562 and HMV-II in experiments 2 and 3 only raised the proportion of CD3-CD56+ cells to 17.6% and 18.9%, respectively, though these proportions were higher than those (5.4-13.0%) in the control cultures containing no target cells. In contrast, irradiated TKB-17RGB cells increased CD3+CD56 T cells in the lymphocyte populations in the three experiments to 95.1%, 96.0%, and 84.8%, respectively as compared to 74.4%, 58.2% and 60.9% in controls.

Assay for NK cytotoxicity activity

Figure 1A depicts a typical dose-response curve for the 4-h ^{51}Cr release assay. The NK-enriched population lysed 31.3% and 76.5% of the fresh HFWT cells at E/T ratios of 2 and 8, respectively. A mirror image of this curve was observed in crystal violet staining (Figure 1B). The target cells showed 100% survival in crystal violet staining and 20% lysis in the ^{51}Cr release assay when E/T ratio was 1.

Effect of extending co-culture time to 24 h was also examined. The percentage of the surviving control target cells usually exceeded 100% (Figure 1C) at an E/T ratio of 0, but the shoulder portion of the dose-response curve in Figure 1B disappeared and fewer surviving target cells were observed at larger E/T ratios. Only 17.0% of the target cells remained at E/T ratio of 4, whereas 42.5% remained in the 4-h crystal violet staining. Therefore, for determination of killing activity, 24-h crystal violet staining had a higher sensitivity than 4-h crystal violet staining at low E/T ratios.

PBMCs grown on TKB-17RGB target cells could efficiently kill fresh TKB-17RGB cells but not fresh 17 RGB cells. Lymphocytes grown on the HFWT target cells could efficiently kill both fresh TKB-17RGB cells and fresh HFWT cells (Figure 2, 8 columns on the right), indicating that the lymphocytes contained nonspecific NK cells. The latter lymphocyte population, at an E/T ratio of 2 at 24 h, reduced TKB- 17R GB target cells to 60.5% and HFWT target cells to 18.5% compared to the control tumor cells (E/T ratio of 0) that proliferated to 175-180% of starting levels.

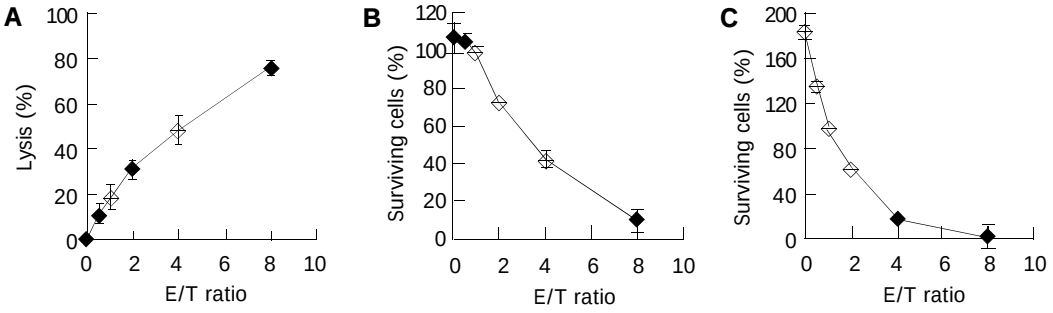

Figure 1 Dose-response relationships of ^{51}Cr release assay and the two crystal violet staining assays. PBMCs were detected after 15-d culture with irradiated HFWT cells. A: ^{51}Cr release assay, in which the effector lymphocytes and the fresh target cells pre-labeled with ^{51}Cr were incubated for 4 h. B and C: crystal violet staining, in which effector lymphocytes and fresh target HFWT cells were incubated for 4 and 24 h, respectively. Each point and bar represent mean and SD (3-6 replicates), respectively.

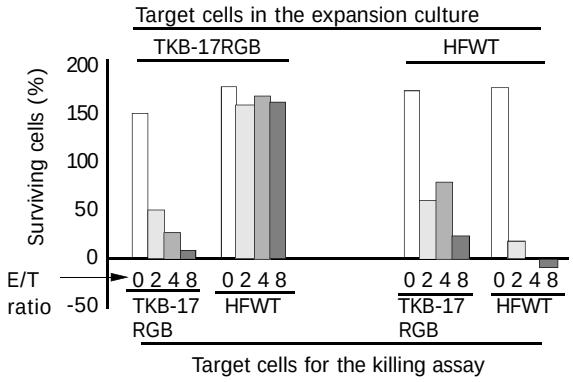

Figure 2 Killing by T cell- and NK-enriched lymphocytes. Lymphocytes derived from PBMC of the Subject-1 (taken from Experiment-1 of Table 1) were used in this 24-h crystal violet staining with various E / T ratios. Eight columns on left side are the results from assays of lymphocytes grown on irradiated TKB-17RGB cells (MHC class I positive). Major lymphocyte population was CD3+ CD56- (T cell-enriched, see Table 1). For the killing assay, fresh TKB-17RGB (left-end 4 columns) or cells (mid-left 4 columns) were submitted as the target. Right side 8 columns are the results from assays of lymphocytes grown on irradiated HFWT cells (MHC class I negative). Major lymphocyte population was CD3-CD56+ (NK-enriched, see Table 1). For the killing assay, fresh TKB-17RGB (mid-right 4 columns) or HFWT cells (right-end 4 columns) were used as the target. Each column represents the mean value of triplicate measurements.

Lymphocytes from PBMC of HCC patient were cultured on the irradiated cells and proliferated 196-fold at 18 d. This was about 6 times the proliferation of lymphocytes suspended with the irradiated K562 cells (data not shown) and the proliferation ceased after 14 d in the NK expansion culture. X-ray irradiated HCC-1 cells (MHC class I positive) and HCC-2 cells (MHC class I negative) obtained from the same hepatocellular carcinoma were used in place of HFWT cells, and neither of the two cell lines could support efficient growth of the lymphocytes from PBMC of HCC patient. NK-enriched lymphocyte population from HCC patient, however, killed HCC-1 and 2 cells with sensitivity comparable to fresh TKB- 17RGB cells (Figure 3). About half of the control HCC-2 cells detached spontaneously after 24-h incubation. The NK-enriched population derived from the patient and expanded on the irradiated HFWT cells could also kill fresh K562 cells with high efficiency (data not shown).

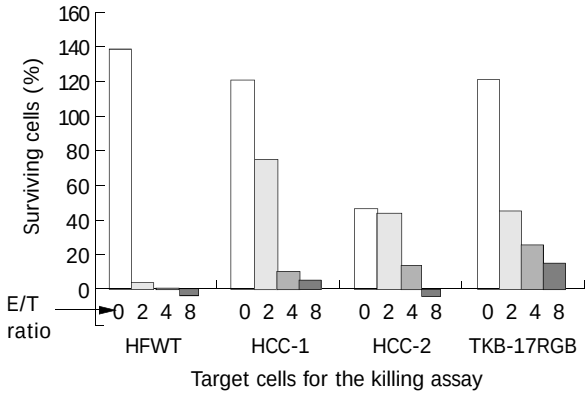

Figure 3 Killing activity of the NK-enriched population on MHC class I-positive and -negative cell lines. PBMCs of HCC patient were expanded on irradiated T cells and submitted to the 24-h crystal violet staining. Target cells were MHC class I-negative HFWT and HCC-2 cells, MHC class I-positive HCC- 1 and TKB-17 RGB cells. HCC-1 and HCC-2 cells were derived from the same human hepatocellular carcinoma tissue.

In a separate experiment, the effect on NK expansion of HFWT and MHC class I-non-expressing HCC-2 cells were compared using a medium containing IL-2 (Table 1). After 10 d of co-culture with PBMCs from Subject 1, irradiated HFWT cells induced 72.0% concentration of CD3- CD56+ cells, whereas irradiated HCC-2 cells induced only 18.5% concentration of CD3-CD56+ cells. CD16+CD56+ cells co-cultured with HFWT grew to 72.7% of the lymphocyte population, whereas CD16+CD56+ cells co-cultured with HCC-2 grew to 22.8% of the lymphocyte population. All the other tumor cell lines showed lower similar efficiency for NK cell expansion.

Cell-cell interaction between PBMC and HFWT cells

After PBMCs from Subject 1 were grown for 10 d in direct-contact co-culture, the final proportion of CD16+ CD56+ cells reached 71.7%, but in the case of PBMCs separated from HFWT cells with a membrane filter, the final proportion reached only

Table 1 Proportion of CD16+ CD56+ cells compared to other cell groups after NK cell expansion cultures

Irradiated target cells used for expansion culture	Cell proportion in lymphocyte populations (%)			
	CD3+CD56-	CD3-CD56+	CD3+CD56+	CD16+CD56+
HFWT	15.2	72.0	12.3	72.7
HCC-2	49.7	18.5	31.1	22.8

Table 2 Proportion of CD16+CD56+ after co-culture of PBMC with irradiated HFWT cells with and without separation by a membrane filter

PBMCs and HFWT co-culture conditions	Cell proportion in the final lymphocyte populations (%)		
	CD3+CD56-	CD3-CD56+	CD16+CD56+
Without separation	13.4	78.2	71.7
Separated by a membrane filter	83.4	5.3	3.9

3.9% (Table 2). Most of the lymphocytes in the latter culture were T lymphocytes. These results demonstrate that direct cell-cell interaction is crucial for NK expansion.

Cytokine requirements for NK cell induction

The highest increase in lymphocyte number from Subject-2 reached 401-fold after 15 d in the expansion culture. Lymphocytes derived from both Subject-2 and Subject-3 expanded with IL-2-containing medium killed fresh HFWT target cells more effectively than the lymphocytes expanded with the 4-cytokine cocktail (data not shown). Without the presence of target HFWT cells, lymphokine activated killer (LAK) cells grew slower than those cultured on the target cells. Unlike IL-2, IL-12 inhibited and IL-15 stimulated the growth of lymphocytes cultured on target HFWT cells. IL-7 (10 U/mL) was not effective on lymphocyte growth. Without addition of IL-2 to the culture medium, the irradiated HFWT cells themselves could not support survival of the lymphocytes for several days.

We compared the effects of HFWT and MHC class I-non-expressing HCC-2 cells on NK cell expansion using IL-2-containing medium. For 10 d in the culture of PBMC from Subject-1, irradiated HFWT cells induced 72.0% of CD3-CD56+ cells, but irradiated HCC-2 cells could induce only 18.5% of CD3-CD56+ cells. CD16+ CD56+ cells shared 72.7% in the former lymphocyte population and, in the latter, 22.8%.

DISCUSSION

Expansion of human NK cells from PBMCs has long been investigated but large-scale expansions for adoptive immunotherapy of human tumors deserve further investigation. LAK cells have been applied to tumor immunotherapy. However, LAK cell expansion in culture for more than 2 wk usually resulted in the loss of killer cell activity. T cells without killing activity formed a major part of the resulting lymphocyte populations[16]. Similar problems have been found in expansion cultures of tumor-infiltrating lymphocytes, in which cells bearing B cell, NK cell and macrophage markers disappeared early in the culture[17].

The K562 cell line in suspension culture has long been adopted as the common target cell line for determination of the killing activity of human NK cells by the standard ^{51}Cr release assay. For ecological reasons, a nonradioisotopic crystal violet staining assay was used in our experiments for determining the killing activity of CTLs against anchorage-dependent target tumor cells. The crystal violet staining assay is safe and amenable to coculturing effectors and targets for more than 4 h. Since HFWT cells disappeared completely during NK expansion culture described above, crystal violet staining using non-irradiated fresh T cells as the target, was considered as sensitive for assessment of the cytotoxic activity of the NK cells as the standard ^{51}Cr release assay.

The results demonstrated that an anchorage-dependent Wilms tumor cell line is a highly efficient target for selective expansion of human NK cells from PBMCs. After culturing PBMCs from healthy donors for 10-21 d, the number of lymphocytes increased extensively. More than 50% of the resulting population consisted of CD16+ CD56+ NK cells that could efficiently kill the MHC class I-non-expressing K562. Moreover, these expanded NK cells also appeared to kill MHC class I-expressing tumor cells (Figure 2, TKB-17 RGB target cells), suggesting the probablity of using these highly active NK cells for adoptive immunotherapy of human tumors.

We have already repeated more than 20 times the 2-week cultures for NK expansion from PBMCs on HFWT cells. Under microscopic examination, we observed that anchorage-dependent target HFWT cells always disappeared completely, the advantage of which was adoptive immunotherapy with NK cells when compared to the methods of NK cell proliferation with suspension-cultured target tumor cells such as K562 and B lymphoblastoid cell lines.

For NK expansion, direct contact of PBMCs with HFWT cells was required (Table 2), suggesting that factors released from target cells do not contribute to NK cells expansion. The need for direct cell-cell contact had been noted in experiments using K562 cells[18]. Growth stimulation through direct cell-cell contact might not be ascribed simply to molecules on the HFWT cell surface preserved after fixation, although Pierson *et al*.[19] reported that NK cells plated directly on ethanol/acetic acid-fixed M2-10B4, which leaves stromal ligands (cell membrane components and ECM) intact, resulted in increased NK cells expansion compared with medium alone. The variety of the fixation methods used in the present experiments conserved, at least partially, reactivity of the surface molecules. Therefore, some interactions between the surface molecules of HFWT cells may contribute to NK expansion. In any case, contact between PBMCs and live HFWT cells were found to be a key requirement.

NK cells are cytotoxic to tumor and virus-infected cells that have lost surface expression of MHC class I proteins. Target cell expressing MHC class I proteins inhibits NK cytotoxicity through binding to inhibitory NK cell receptors[20,21]. Therefore contrasting properties of NK cell inhibitory receptors compared to CTL T-cell receptors (MHC class I receptors that stimulate, rather than inactivate, the CTL cytotoxic response) are expected to provide complementarity in the cytotoxic response to tumor cells[22,23]. In humans, natural killer (NK) cell function is regulated by a series of receptors and coreceptors with either triggering or inhibitory activity[24].

HFWT cells were more effective targets for NK cell expansion than K562 cells. Since it has been reported that NK cells differentiate from CD34+ progenitor cells[25,26], HFWT cells must stimulate NK cells differentiation from the progenitor cells included in PBMC but not in the CD3-CD56+ subset. Further investigation needs to be conducted to identify the NK precursor cells to which HFWT cells transmit the proliferative signal.

Since the present NK cell expansion culture started as one of variation of the human CTL induction culture from PBMC, the present study has shown that IL-2 is the sole cytokine required for the NK expansion on the T cell layer[27]. In other reports, IL-15 was found to stimulate NK development from CD34+ hematopoietic progenitor cells[28-30]; IL-7 as a cofactor during myelopoiesis, is capable of activating monocytes/macrophages and NK cells[31]. IL-12 showed an inhibitory effect on NK cell growth[32,33]; TGF β was reported to be similarly inhibitory[34]. The present results suggest that expansion and activation of NK cells may provide an effective immunotherapy of hepatocellular carcinoma.

REFERENCES

1 **Souza SS,** Castro FA, Mendonca HC, Palma PV, Morais FR, Ferriani RA, Voltarelli JC. Influence of menstrual cycle on NK activity. *J Reprod Immunol* 2001; **50**: 151-159

2 **Luo DZ**, Vermijlen D, Ahishali B, Triantis V, Vanderkerken K, Kuppen PJ, Wisse E. Participation of CD45, NKR-P1A and ANK61 antigen in rat hepatic NK cell (pit cell) mediated target cell cytotoxicity. *World J Gastroenterol* 2000; **6**: 546-552

3 **Imai K,** Matsuyama S, Miyake S, Suga K, Nakachi K. Natural cytotoxic activity of peripheral-blood lymphocytes and cancer incidence: an 11-year follow-up study of a general population. *Lancet* 2000; **356**: 1795-1799

4 **Wong KH,** Simon JA. *In vitro* effect of gonadotropin-releasing hormone agonist on natural killer cell cytolysis in women with and without endometriosis. *Am J Obstet Gynecol* 2004; **190**: 44-49

5 **Malorni W,** Quaranta MG, Straface E, Falzano L, Fabbri A, Viora M, Fiorentini C. The Rac-activating toxin cytotoxic necrotizing factor 1 oversees NK cell-mediated activity by regulating the actin / microtubule interplay. *J Immunol* 2003; **171**: 4195-4202

6 **Guven H,** Gilljam M, Chambers BJ, Ljunggren HG, Christensson B, Kimby E, Dilber MS. Expansion of natural killer (NK) and natural killer-like T (NKT)-cell populations derived from patients with B-chronic lymphocytic leukemia (B-CLL): a potential source for cellular immunotherapy. *Leukemia* 2003; **17**: 1973-1980

7 **Perussia B,** Ramoni C, Anegon I, Cuturi MC, Faust J, Trinchieri G. Preferential proliferation of natural killer cells among peripheral blood mononuclear cells cocultured with B lymphoblastoid cell lines. *Nat Immun Cell Growth Regul* 1987; **6**: 171-188

8 **Silva MR,** Parreira A, Ascensao JL. Natural killer cell numbers and activity in mobilized peripheral blood stem cell grafts: conditions for *in vitro* expansion. *Exp Hematol* 1995; **23**: 1676-1681

9 **Porrata LF,** Inwards DJ, Lacy MQ, Markovic SN. Immunomodulation of early engrafted natural killer cells with interleukin-2 and interferon-alpha in autologous stem cell transplantation. *Bone Marrow Transplant* 2001; **28**: 673-680

10 **Sekine T,** Shiraiwa H, Yamazaki T, Tobisu K, Kakizoe T. A feasible method for expansion of peripheral blood lymphocytes by culture with immobilized anti-CD3 monoclonal antibody and interleukin-2 for use in adoptive immunotherapy of cancer patients. *Biomed Pharmacother* 1993; **47**: 73-78

11 **Malygin AM,** Somersalo K, Timonen T. Promotion of natural killer cell growth *in vitro* by bispecific (anti-CD3 x anti-CD16) antibodies. *Immunology* 1994; **81**: 92-95

12 **Yu Y,** Hagihara M, Ando K, Gansuvd B, Matsuzawa H, Tsuchiya T, Ueda Y, Inoue H, Hotta T, Kato S. Enhancement of human cord blood CD34+ cell-derived NK cell cytotoxicity by dendritic cells. *J Immunol* 2001; **166**: 1590-1600

13 **Kim KY**, Kang MA, Nam MJ. Enhancement of natural killer cell-mediated cytotoxicity by coexpression of GM-CSF / B70 in hepatoma. *Cancer Lett* 2001; **166**: 33-40

14 **Ucker DS,** Obermiller PS, Eckhart W, Apgar JR, Berger NA, Meyers J. Genome digestion is a dispensable consequence of physiological cell death mediated by cytotoxic T lymphocytes. *MoL Cell Biol* 1992; **12**: 3060-3069

15 **Liu SQ,** Saijo K, Todoroki K, Ohno T. Induction of human autologous cytotoxic T lymphocytes on formalin-fixed and paraffin-embedded tumour sections. *Nat Med* 1995; **1**: 267-271

16 **Zhang J,** Zhang JK, Zhuo SH, Chen HB. Effect of a cancer vaccine prepared by fusions of hepatocarcinoma cells with dendritic cells. *World J Gastroenterol* 2001; **7**: 690-694

17 **Haas GP,** Solomon D, Rosenberg SA. Tumor- infiltrating lymphocytes from nonrenal urological malignancies. *Cancer Immunol Immunother* 1990; **30**: 342-350

18 **Fink T,** Ebbesen P, Koppelhus U, Zachar V. Natural killer cell-mediated basal and interferon-enhanced cytotoxicity against liver cancer cells is significantly impaired under *in vivo* oxygen conditions. *Scand J Immunol* 2003; **58**: 607-712

19 **Pierson BA,** Gupta K, Hu WS, Miller JS. Human natural killer cell expansion is regulated by thrombospondin-mediated activation of transforming growth factor-beta 1 and independent accessory cell-derived contact and soluble factors. *Blood* 1996; **87**: 180-189

20 **Gumperz JE,** Parham P. The enigma of the natural killer cell. *Nature* 1995; **378**: 245-248

21 **Katz G,** Markel G, Mizrahi S, Arnon TI, Mandelboim O. Recognition of HLA-Cw4 but not HLA-Cw6 by the NK cell receptor killer cell Ig-like receptor two-domain short tail number 4. *J Immunol* 2001; **166**: 7260-7267

22 **Long EO,** Barber DF, Burshtyn DN, Faure M, Peterson M, Rajagopalan S, Renard V, Sandusky M, Stebbins CC, Wagtmann N, Watzl C. Inhibition of natural killer cell activation signals by killer cell immunoglobulin-like receptors (CD158). *Immunol Rev* 2001; **181**: 223-233

23 **Rolstad B,** Naper C, Lovik G, Vaage JT, Ryan JC, Backman-Petersson E, Kirsch RD, Butcher GW. Rat natural killer cell receptor systems and recognition of MHC class I molecules. *Immunol Rev* 2001; **181**: 149-157

24 **Bottino C,** Falco M, Parolini S, Marcenaro E, Augugliaro R, Sivori S, Landi E, Biassoni R, Notarangelo LD, Moretta L, Moretta A. NTB-A [correction of GNTB-A], a novel SH2D1A-associated surface molecule contributing to the inability of natural killer cells to kill Epstein-Barr virus-infected B cells in X-linked lymphoproliferative disease. *J Exp Med* 2001; **194**: 235-246

25 **Miller JS**, McCullar V, Punzel M, Lemischka IR, Moore KA. Single adult human CD34(+) / Lin- / CD38(-) progenitors give rise to natural killer cells, B-lineage cells, dendritic cells, and myeloid cells. *Blood* 1999; **93**: 96-106

26 **Mrozek E,** Anderson P, Caligiuri MA. Role of interleukin-15 in the development of human CD56+ natural killer cells from CD34+ hematopoietic progenitor cells. *Blood* 1996; **87**: 2632-2640

27 **Konjevic G,** Jovic V, Jurisic V, Radulovic S, Jelic S, Spuzic I. IL-2-mediated augmentation of NK-cell activity and activation antigen expression on NK- and T-cell subsets in patients with metastatic melanoma treated with interferon-alpha and DTIC. *Clin Exp Metastasis* 2003; **20**: 647-655

28 **Naora H,** Gougeon ML. Enhanced survival and potent expansion of the natural killer cell population of HIV-infected individuals by exogenous interleukin-15. *Immunol Lett* 1999; **68**: 359-367

29 **Carayol G,** Robin C, Bourhis JH, Bennaceur-Griscelli A, Chouaib S, Coulombel L, Caignard A. NK cells differentiated from bone marrow, cord blood and peripheral blood stem cells exhibit similar phenotype and functions. *Eur J Immunol* 1998; **28**: 1991-2002

30 **Lin SJ,** Yang MH, Chao HC, Kuo ML, Huang JL. Effect of interleukin-15 and Flt3-ligand on natural killer cell expansion and activation: umbilical cord *vs* adult peripheral blood mononuclear cells. *Pediatr Allergy Immunol* 2000; **11**: 168-174

31 **Appasamy PM**. Biological and clinical implications of interleukin-7 and lymphopoiesis. *Cytokines Cell Mol Ther* 1999; **5**: 25-39

32 **Liebau C,** Merk H, Schmidt S, Roesel C, Karreman C, Prisack JB, Bojar H, Baltzer AW. Interleukin-12 and interleukin-18 change ICAM-I expression, and enhance natural killer cell mediated cytolysis of human osteosarcoma cells. *Cytokines Cell Mol Ther* 2002; **7**: 135-142

33 **Satoh T,** Saika T, Ebara S, Kusaka N, Timme TL, Yang G, Wang J, Mouraviev V, Cao G, Fattah el MA, Thompson TC. Macrophages transduced with an adenoviral vector expressing interleukin 12 suppress tumor growth and metastasis in a preclinical metastatic prostate cancer model. *Cancer Res* 2003; **63**: 7853-7860

34 **Billiau AD**, Sefrioui H, Overbergh L, Rutgeerts O, Goebels J, Mathieu C, Waer M. Transforming growth factor-beta inhibits lymphokine activated killer cytotoxicity of bone marrow cells: implications for the graft-versus-leukemia effect in irradiation allogeneic bone marrow chimeras. *Transplantation* 2001; **71**: 292-299

Edited by Chen WW **Proofread by** Zhu LH and Xu FM

PO Box 2345, Beijing 100023, China
Fax: +86-10-85381893
E-mail: wjg@wjgnet.com www.wjgnet.com

World J Gastroenterol 2004;10(14):2124-2126
World Journal of Gastroenterology
 ISSN 1007-9327

• BRIEF REPORTS •

Intestinal colonization with *Candida albicans* and mucosal immunity

Xiao-Dong Bai, Xian-Hua Liu, Qing-Ying Tong

Xiao-Dong Bai, Department of Burn Surgery, General Hospital of Chinese People's Armed Police Force, Beijing 100039, China
Xian-Hua Liu, Central Laboratory, General Hospital of Chinese People's Armed Police Force, Beijing 100039, China
Qing-Ying Tong, Medical Affair Department, General Hospital of Chinese People's Armed Police Force, Beijing 100039, China
Supported by the National Natural Science Foundation of China, No. 30100197
Correspondence to: Dr. Xiao-Dong Bai, Department of Burn Surgery, General Hospital of Armed Police Force, 69 Yong Ding Road, Hai Dian District, Beijing 100039, China. baixiaotmu@yahoo.com.cn
Telephone: +86-10-88276632
Received: 2003-11-27 **Accepted:** 2004-01-08

Abstract

AIM: To observe the relationship between intestinal lumen colonization with *Candida albicans* and mucosal secretory IgA (sIgA).

METHODS: A total of 82 specific-pathogen-free mice were divided randomly into control and colonization groups. After *Candida albicans* were inoculated into specific-pathogen-free mice, the number of *Candida albicans* adhering to cecum and mucosal membrane was counted. The lymphocyte proliferation in Peyer's patch and in lamina propria was shown by BrdU incorporation, while mucosal sIgA (surface membrane) isotype switch in Peyer's patch was investigated. IgA plasma cells in lamina propria were observed by immunohistochemical staining. Specific IgA antibodies to *Candida albicans* were measured with ELISA.

RESULTS: From d 3 to d 14 after *Candida albicans* gavaging to mice, the number of *Candida albicans* colonizing in lumen and adhering to mucosal membrane was sharply reduced. *Candida albicans* translocation to mesenteric lymph nodes occurred at early time points following gavage administration and disappeared at later time points. Meanwhile, the content of specific IgA was increased obviously. Proliferation and differentiation of lymphocytes in lamina propria were also increased.

CONCLUSION: Lymphocytes in lamina propria play an important role in intestinal mucosal immunity of specific-pathogen-free mice when they are first inoculated with *Candida albicans*. The decreasing number of *Candida albicans* in intestine is related to the increased level of specific IgA antibodies in the intestinal mucus.

Bai XD, Liu XH, Tong QY. Intestinal colonization with *Candida albicans* and mucosal immunity. *World J Gastroenterol* 2004; 10(14): 2124-2126
http://www.wjgnet.com/1007-9327/10/2124.asp

INTRODUCTION

Candida albicans are the common opportunistic pathogens[1]; one of their infection routes is overgrowth and translocation in intestinal lumen. So, inhibition of the translocation of *Candida* is an important way to prevent the deadly systemic infection. With the development of the study on mucosal immunity, local antibody production of sIgA has attracted much attention in preventing pathogen[1] and bacterial translocation[2,3]. It has been reported that *Candida albicans* infection of vaginal and oral mucus membrane was specifically inhibited by anti-*Candida albicans* sIgA. But, the mechanism still remains unclear. In the present study, by using *Candidas*' colonization model, we observed lymphocytes proliferation and differentiation in gut-associated lymphatic tissue (GALT) and the relationship between specific IgA and change of *Candida albicans* in the intestine, and further explored the mechanism of host defense against opportunistic pathogen and the effect of specific IgA against *Candida albicans* in intestinal lumen.

MATERIALS AND METHODS

Candida albicans

Candida albican strain cmcc44104 provided by the Burn Institue of Southwest Hospital was amplified in the special selective culture medium. The *Candida albicans* suspension density was modulated to 1.5×10^9 cfu/mL, and stored below 4 ℃.

Grouping of animals

A total of 82 specific-pathogen-free mice (BALB/c) were provided by the Animal Center of Third Military Medical University, and randomly divided into the control and colonization groups. Mice in colonization group were gavaged 0.5 mL *Candida albicans*, and killed on days 3, 7 and 14 after gavage by cervical dislocation. The control animals were treated in a similar way with a vehicle alone, and killed on day 14 after sham-treatment. The mesenteric lymph nodes, cecum and ileum of the mice were taken out.

Candida albicans adhering to ileum

Ilea of 10 cm were rinsed in PBS (0.01 mol/L, pH 7.2) three times until the ilea were translucent, then weighed and homogenized. Homogenized suspension (0.1 mL) was applied on the surface of the selective culture medium at 37 ℃ for 72 h.

Adherence result (cfu/g)=Colony-forming units×dilution/Ileum weight (g).

Quantity of Candida albicans in cecum

Ceca were weighed and homogenized in 5 mL PBS, then the suspension was cultured in the selective medium at 37 ℃ for 72 h. *Candida albicans* quantity (cfu/g)=Colony-forming units×dilution/Cecum weight (g).

Translocation of Candida albicans

Mesenteric lymph nodes (MLN) were taken to be weighed and homogenized and the suspension was applied on the selective medium at 37 ℃ for 72 h.

Lymphocytes proliferation in Peyer's patch and lamina propria

Mice were intraperitoneally injected 5-bromo-2'-deoxyuridine

(BrdU, 10 μg/g bm) at 12 h before cervical dislocation, the intestine and Peyer's patch (PP) were taken for immunohistochemistry staining. BrdU-positive cells in PP and in lamina propria (LP) of intestinal villi were counted.

Number of IgA plasma cell in LP

IgA plasma cells were counted after immunohistochemical stain as 40 villi /per mice and 5 mice/per time-point.

Expression of IgA of Peyer's patch lymphocyte

Peyer's patch lymphocytes were isolated, pooled, washed in RPMI 1640. Then IgA of lymphocytes was measured by flow cytometry.

Specific IgA to Candida albicans in intestinal mucus

Intestinal mucus (0.1 mL) was homogenized in 0.5 mL cold PBS, then centrifuged at 5 000 r/min for 5 min, the supernatant was taken as 1:1 mucus onto 96-well plates and coated by *Candida albicans* as immobilized antigen, which had been fixed in 40 g/L formaldehyde overnight at 4 ℃ for 72 h. Then plates were washed three times with PBS, and blocked by 5 g/L BSA for 0.5 h, the mucus samples were applied to ELISA plates for 1 h below 37 ℃. After that, 96-well plates were washed with PBS, and goat anti-mouse IgA antibodies which coupled with horseradish-peroxidase were added to the wells, 100 μL/well and incubated at 37 ℃ for 1 h. Reaction was stopped by adding one drop of 2 mol/L H_2SO_4 and the result was shown by optical density (OD) at 492 nm.

Relative quantity of specific IgA[4]

The specific IgA positive mucus measured before were serially diluted from 1:1 to 1:16, the content of specific IgA to *Candida albicans* in 1:1 mucus was regarded as 1 U/mL. The mucus was applied to ELISA in order to produce a standard curve. Specific IgA activity to *Candida albicans* was counted as follows:

IgA(U/mg)=IgA relative quantity (U/mL)/Protein content in the mucus (mg/mL).

Statistic analysis

Data were analysed using analysis of variance (ANOVA).

RESULTS

Change of Candidas' adherence and translocation

In the colonization group, the total quantities of *Candida albicans* in intestine were larger on d 3 and 7 after gavage administration, about (34-39)×10^5 cfu/g, declined to 3.2×10^5 cfu/g on d 14. At the early phase after gavaging the mice, *Candida albicans* was found in the MLN, and then disappeared from day 7 to 14. Adherence also showed a declined tendency from the highest on day 3 to the lowest on d 14.

Proliferation of lymphocyte in PP and LP

BrdU incorporation of PP was found in both control and colonization group. BrdU-positive cells were mainly at the verge sites of PP; there were no obvious changes in the colonization group compared with that in the control group. On d 14 after gavaging, LP lymphocytes proliferation in colonization group was significantly higher than that in the control mice (Table 1).

IgA plasma cell in LP

IgA plasma cells increased at all times, the highest was on day 14 (Table 1).

Flow cytometry of mucosal sIgA

There was no difference between the control and the colonization group in the level of mucosal sIgA (Table 1).

Specific IgA to Candida albicans

Specific anti-*Candida albicans* IgA contents on day 14 in colonization group were higher than that in the control group (Table 2).

Table 2 Specific IgA to C*andida albicans* in intestinal mucus membrane

Group	*n*	Positive rate	Content (U/mg)
Colonization			
3 d	20	5/20	33±8
7 d	18	3/18	36±13
14 d	25	10/25	69±25[a]
Control	19	6/19	18.6±6.9

[a]*P*<0.05 *vs* control.

DISCUSSION

Candida albicans is an opportunistic pathogen, which could survive in the intestine and keep the balance of body. sIgA prevents the body from some pathogen infection such as typhoid fever and cholera[5,6], but its role in the balance between opportunistic pathogen and host is not clear yet[7,8]. So we investigated the relationship between *Candida albicans* colonization and the change of local intestinal mucosal immunity by using SPF mice model, in order to understand the mechanism of the balance. We have found that in the early period of *Candida albicans* colonization, *Candida albicans* adherence was serious, while the specific IgA content was lower. Accompanying the increase of specific IgA to *Candida albicans*, quantity of *Candida albicans* adherence and in the cecum decreased, there was negative correlation between specific IgA and quantity of *Candida albicans* adherence, that is to say that specific IgA was the important factor to keep the balance between opportunistic pathogen and host[9]. The colonization of *Candida albicans* could elicit a local mucosal immune reaction and finally limit *Candida albicans*' overgrowth[10,11].

Table 1 Proliferation and differentiation of lymphocytes

Group	Number of BrdU-positive cells sIgA in PP				Number of IgA plasma cells in LP
	n	PP	LP	Positive rates	
Colonization					
3 d	5	75±12	0.30±0.46	7.7±1.2	0.68±0.37
7 d	5	58±20	1.05±1.00	7.7±2.5	0.67±0.54
14 d	5	37±10	3.34±2.35[a]	ND	1.63±0.52[a]
Control	5	70±15	0.78±1.04	10.3±1.8	0.35±0.15

[a]*P*<0.05 *vs* control; PP: Peyer's patch; LP: Lamina propria; IgA plasma cells were counted after immunohistochemical stain as 40 villi/per mice and 5 mice/per time-point.

In the lamina propria, there was B lymphocyte clone that could secret specific IgA against *Candida albicans*[12], but the content was very lower. After *Candida albicans* were gavaged, stronger stimulation of *Candidas*' antigen induced specific B lymphocyte clone proliferation and differentiation, while the number of IgA plasma cell increased. Plenty of specific IgA against *Candida* secreted to the surface of intestinal mucus membrane and formed the antibody barrier. sIgA antibodies were thought to provide mucosal defense by immune exclusion[13]; this refers to their ability to prevent contact between pathogens and epithelial surfaces through agglutination in the intestinal lumen, entrapment of immune complexes in mucus, and clearance by peristalsis. We could draw the conclusion that though *Candida albicans* infection is more common recently, it is possible to prevent *Candida albicans* infection by setting up a specific sIgA antibody barrier in the host.

REFERENCES

1 **Lamm ME.** Interaction of antigens and antibodies at mucosal surface. *Annu Rev Microbiol* 1997; **51**: 311-340

2 **Shu Q,** Gill H. Immune protection mediated by the probiotic *Lactobacillus rhamnosus* HN001 (DR20) against *Escherichia coli* O157: H7 infection in mice. *FEMS Immunol Med Microbiol* 2002; **34**: 59

3 **Nakasaki H,** Mitomi T, Tajima T, Ohnishi N, Fujii K. Gut bacterial translocation during panteral nutrition in experimental rats and its countermeasure. *Am J Surg* 1998; **175**: 38-43

4 **Coogan MM,** Sweet SP, Challacombe SJ, Immunoglobulin A. IgA1 and IgA2 antibodies to *Candida albicans* in whole and parotid saliva in human immunodeficiency virus infection and AIDS. *Infect Immun* 1994; **62**: 892-896

5 **Apter FM,** Michetti P, Winner LS 3rd, Mack JA, Mekalanos JJ, Neutra MR. Analysis of the roles of antilipo-polysaccharide and anti-cholera toxin immunoglobulinA (IgA) antibodies in protection against *Vibrio cholerae* and cholera toxin by use of monoclonal IgA antibodies *in vivo*. *Infect Immun* 1993; **61**: 5279-5285

6 **Maury G,** Pilette C, Sibille Y. Secretory immunity of the airways. *Rev Mal Respir* 2003; **20**: 928-939

7 **Schmucker DL,** Owen RL, Outenreath R, Thoreux K. Basis for the age-related decline in intestinal mucosal immunity. *Clin Dev Immunol* 2003; **10**: 67-72

8 **Hirsh M,** Dyugovskaya L, Bashenko Y, Krausz MM. Reduced rate of bacterial translocation and improved variables of natural killer cell and T-cell activity in rats surviving controlled hemorrhagic shock and treated with hypertonic saline. *Crit Care Med* 2002; **30**: 861-867

9 **Wozniak KL,** Wormley FL Jr, Fidel PL Jr. *Candida*-specific antibodies during experimental vaginal *candidiasis* in mice. *Infect Immun* 2002; **70**: 5790-5799

10 **Belazi M,** Fleva A, Drakoulakos D, Panayiotidou D. Salivary IgA and serum IgA and IgG antibodies to *Candida albicans* in HIV-infected subjects. *Int J STD AIDS* 2002; **13**: 373-377

11 **Bai X,** Xiao G, Tian X. The relationship between postburn gene expression of modulators in gut associated lymph tissue and the change in IgA plasma cells. *Zhonghua Shaoshang Zazhi* 2000; **16**: 108-110

12 **Koga-Ito CY,** Unterkircher CS, Watanabe H, Martins CA, Vidotto V, Jorge AO. Caries risk tests and salivary levels of immunoglobulins to Streptococcus mutans and *Candida albicans* in mouthbreathing syndrome patients. *Caries Res* 2003; **37**: 38-43

13 **Ren JM,** Zou QM, Wang FK, He Q, Chen W, Zen WK. PELA microspheres loaded *H pylori* lysates and their mucosal immune response. *World J Gastroenterol* 2002; **8**: 1098-1102

Edited by Chen WW **Proofread by** Zhu LH and Xu FM

PO Box 2345, Beijing 100023, China
Fax: +86-10-85381893
E-mail: wjg@wjgnet.com www.wjgnet.com

World J Gastroenterol 2004;10(14):2127-2129
World Journal of Gastroenterology
 ISSN 1007-9327

• BRIEF REPORTS •

Multidetector CT in evaluating blood supply of hepatocellular carcinoma after transcatheter arterial chemoembolization

Yong-Song Guan, Xiao-Hua Zheng, Xiang-Ping Zhou, Juan Huang, Long Sun, Xian Chen, Xiao Li, Qing He

Yong-Song Guan, Xiao-Hua Zheng, Xiang-Ping Zhou, Juan Huang, Long Sun, Xian Chen, Xiao Li, Qing He, Department of Radiology, Huaxi Hospital, Sichuan University, Chengdu 610041, Sichuan Province, China
Supported by the Medical Science Research Foundation of Sichuan Province, No. 200054
Correspondence to: Dr. Yong-Song Guan, Department of Radiology, Huaxi Hospital, Sichuan University, 37 Guoxuexiang, Chengdu 610041, Sichuan Province, China. yongsongguan@yahoo.com
Telephone: +86-28-85421008 **Fax:** +86-28-85421008
Received: 2003-12-12 **Accepted:** 2004-01-15

Abstract

AIM: To assess the value of multidetector-row computed tomography (MDCT) in choosing retreatment methods of hepatocellular carcinoma (HCC) through evaluating the blood supply of low-density area of HCC after transcatheter arterial chemoembolization (TACE).

METHODS: Thirty-two patients with HCC after TACE treatment were examined by plain scanning and hepatic multidetector-row CT. The location of low-density area on plain scanning and the enhancement patterns on dynamic contrast-enhanced scanning were observed. At the same time, three-dimensional CT (3D CT) models of the volume rendering, curved multiplanar reformations, surface shaded display and maximum intensity projection reconstruction of the hepatic artery and portal vein were performed in 6 cases.

RESULTS: In CT plain scanning data, low density areas of 32 cases of HCC after TACE treatment were divided into three types: peripheral, one-side-located and mixed types. In contrast-enhanced CT scans, the blood supply of low-density area was classified into four types: arterial blood supply (20 cases), portal blood supply (5 cases), arterial combined with portal blood supply (5 cases) and poor blood supply (2 cases). In 6 cases, the relationship between the low-density area and branches of hepatic artery as well as portal vein was shown by 3D CT.

CONCLUSION: Hepatic MDCT is an effective method for evaluating the blood supply of low-density area and therapeutic effect of HCC after TACE treatment. Types of blood supply is helpful for the selection of retreatment.

Guan YS, Zheng XH, Zhou XP, Huang J, Sun L, Chen X, Li X, He Q. Multidetector CT in evaluating blood supply of hepatocellular carcinoma after transcatheter arterial chemoembolization. *World J Gastroenterol* 2004; 10(14): 2127-2129

http://www.wjgnet.com/1007-9327/10/2127.asp

INTRODUCTION

Hepatocellular carcinoma (HCC) is one of the most common malignant neoplasms. In China, HCC was the second cancer killer in rural areas, and ranked the third in urban areas and 110 000 patients were killed annually, accounting for 40% of the HCC deaths in the world[1]. The majority of HCC patients are treated with palliative approaches because surgery is sometimes limited by poor liver function. Transcatheter arterial chemoembolization (TACE) has been one of the most common and effective palliative therapies[2-11]. To evaluate the blood supply types of the low-density area of HCC pretreated by TACE and to explore its value in selecting appropriate retreatment, we studied MDCT and 3D CT image characteristics of 32 HCC cases pretreated with TACE.

MATERIALS AND METHODS

Patients

From January to November 2003, 32 consecutive patients with HCC who underwent TACE (28 men and 4 women, age range 15-61 years, mean age 37 years) were enrolled into this study. The diagnosis of HCC was based on the results of percutaneous needle biopsy (n=13) and operation (n=2) or test of serum alpha-fetoprotein level in combination with imaging appearance and follow-up images (n=17) according to the diagnostic criteria for HCC formulated by Chinese National Association of Anticancer Committee (1990).

TACE

TACE procedure was performed as follows: the focal segmental or sub-segmental artery was detected carefully by celiac arteriography, and variants were excluded by superior mesenteric arteriography and phrenic arteriography. When the tip of the catheter arrived at the appropriate focal artery, one or two anticancer agents were injected, followed by 8-15 mL iodized oil (Huaihai Pharmaceutical Factory, Shanghai, China) injected under fluoroscopic monitoring. Some patients were embolized with a gelatin sponge (1 mm ×1 mm ×10 mm) at the same time. TACE procedures were performed followed by MDCT within 4 to 6 wk.

MDCT

MDCT was performed with an MDCT scanner after TACE within 4 to 6 wk (Sensation16, Siemens Medical System, Germany). Multidetector row helical technique was applied to the scanning in cranial to caudal direction. Plain scanning of the liver was carried out. Then, after injection of the contrast media for hepatic arterial phase and portal venous phase image acquisition, enhanced scanning of 1.5 mm axial section was performed at 25 and 60 s, respectively. A total of 100 mL contrast medium (Ultravist 300, Schering Pharmaceutical Ltd., Guangzhou, China) was administered to each patient at a rate of 3.0 mL/s through a catheter placed in the peripheral vein of the antecubital fossa. Three dimensional CT models including the volume rendering technique, multiplanar reconstruction, shaded surface display and maximum intensity projection of the hepatic artery and portal vein were simultaneously completed in 6 cases.

Diagnostic criteria for low-density area

Diagnostic criteria for low-density area were the CT of 30 to 50 HU on non-enhanced CT.

Determination of low-density area and blood supply types

According to the location in CT plain scan, low-density area was divided into three types. The peripheral low-density area was the viable area around the portion that retained iodized oil. The one-side-located type was determined by the low-density area located in any one side of the lipiodol area .The mixed low-density area showed both peripheral and one-side-located types in which the lipiodol retention in the tumor was heterogeneous.

According to the showing time of low-density area on enhanced CT at biphasic MDCT, blood supply of low-density area was divided into four types. The arterial blood supply of low-density area could be enhanced early during contrast administration (during the hepatic arterial-dominant phase, HAP) as a hyperattenuating or a mixed attenuating area against a background of slightly enhanced liver parenchyma before the liver enhanced substantially from the portal venous delivery of contrast material. Furthermore, the area must be hypoattenuating during the portal venous-dominant phase (PVP). In the same way, the portal blood supplying low-density area could be enhanced during PVP as a hyperattenuating or a mixed attenuating area but hypoattenuating during HAP. If the low-density area was enhanced during both PVP and HAP, the type of arterial combined with portal blood supply was determined. The poor blood supply was defined as non-enhanced on biphasic MDCT.

Image analysis

MDCT of all the patients was retrospectively and blindly reviewed by two experienced radiologists. Image analysis included the presence/absence and patterns of low-density area at non-enhanced examination. After these results were recorded, the HAP and PVP images were reviewed. Lesions were categorized as hyperattenuating or hypoattenuating relative to adjacent liver parenchyma. If lesions exhibited in both hyper- and hypo-attenuating areas, they were categorized as having mixed attenuation.

RESULTS

Appearances and patterns of low-density area

Thirty-two patients with low-density area after TACE were divided into three types: sixteen patients were peripheral type; 5 were one-side location type and 11 were mixed type.

Types of blood supply

The appearances of the low-density area at each phase of imaging are shown in Table 1. According to the appearance of low-density area at biphasic MDCT, the cases of arterial blood supply, portal blood supply, arterial combined with portal blood supply and poor blood supply were 20, 5, 5, 2, respectively.

Table 1 Appearance of low-density area at biphasic MDCT

Phase of imaging	Appearance at MDCT (cases)		
	Hyperattenuating	Hypoattenuating	Mixed attenuating
HAP	17	7	8
PVP	4	22	6

HAP: hepatic arterial-dominant phase; PVP: portal venous-dominant phase.

DISCUSSION

Although surgery remains the best treatment of HCC, it is unsuitable for most of the cases who would be better treated with interventional therapy. However, as the blood supply of HCC includes regular, variant, extrahepatic and collateral arterial blood supply, the portal vein is involved in some patients[12,13]. Furthermore, the development of compensatory circulation after the occlusion of hepatic artery and the changes of the portal venous blood supply to tumor after TACE, will both result in incomplete tumor necrosis or recurrence[14-18].

MDCT is a breakthrough in medical imaging examination technology. Equipped with a multidetector array, MDCT can perform multislice data acquisition simultaneously, which greatly reduces the time of volume scanning. Image quality is improved due to increased image resolution and clarity. MDCT could therefore provide a technique of thin-slice and dynamic enhancement scanning of liver at hepatic arterial phase and portal venous phase. In addition, multiplanar reformations, 3D renderings, and high-quality CT angiographic displays have opened a new vista in clinical applications. Its performance has been improved in several problem-solving tasks and become extremely valuable in image interpretation[19,20].

The portion of tumor that retains iodized oil is necrotic. Pathologic specimens and the necrosis rate measured from CT image showed a good correlation between the portion of tumor that retained iodized oil and the portion of tumor necrotized. Lipiodol-negative but hypodense areas examined by X-ray proved to be necrotic or fibrotic with or without viable tumor islands. HCC with heterogeneous lipiodol uptake tended to recur at the site adjacent to the original tumors more frequently than HCC with homogeneous lipiodol uptake[21-23]. HCC images that revealed a dense retention of lipiodol within the whole tumor or revealed no enhancement on contrast enhanced CT had a significantly higher necrotic rate. A lipiodol-negative but hypodense area with enhancement on dynamic MDCT was low-density area[24-26]. According to the location, we divided it into three types: peripheral, one-side-located and mixed type. According to the time of enhancement of low-density area at biphasic MDCT, blood supply in low-density area was divided into four types: arterial blood supply, portal blood supply, arterial combined with portal blood supply and poor blood supply. The portal venous blood supply was mainly of tumor periphery distribution. After treatment of TACE, the portal venous blood supply to tumor periphery increased significantly, and some did have signs of enriched blood supply around the tumor[17].

Evaluating the blood supply of low-density area with HCC after TACE has clinical significance in choosing the method and route of retreatment. When MDCT pictures revealed the patient of arterial blood supply type, repeated treatment with TACE was suggested. If it is necessary, subsegmental TACE should be performed because of its superior capability of achieving complete lipiodol accumulation. TACE showed a strong antitumor effect because of the overflow of excess iodized oil into the portal veins[3]. Therefore, when the low-density area had two blood supply routes of arterial and portal veins, repeated treatment with TACE was also suggested. As portal venous blood supply to the tumor was affected by TACE treatment in portal blood supply group, interventional therapy via portal vein should be reasonable. Percutaneous ethanol injection and other non-vascular interventional therapy could be considered when the low-density area revealed poor blood supply[27,28].

In short, MDCT plays important roles in evaluating the efficacy of chemoembolization. It is a practical, effective, and safe method for assessing the therapeutic effect of TACE. Evaluation of the blood supply of low-density area in MDCT is of practical significance for making retreatment plans.

REFERENCES

1 **Ji XL**, Liu YX, Wang YH, Zhao H. Histopathological study of hepatocellular carcinoma after transcatheter hepatic

arterialembolization. *China Natl J New Gastroenterol* 1996; **2**: 79-81
2 **Fan J**, Ten GJ, He SC, Guo JH, Yang DP, Wang GY. Arterial chemoembolization for hepatocellular carcinoma. *World J Gastroenterol* 1998; **4**: 33-37
3 **Oi H**. Liver intervention. *Nippon Igaku Hoshasen Gakkai Zassh*i 2000; **60**: 826-832
4 **Okusaka T,** Okada S, Ueno H, Ikeda M, Yoshimori M, Shimada K, Yamamoto J, Kosuge T, Yamasaki S, Iwata R, Furukawa H, Moriyama N, Sakamoto M, Hirohashi S. Evaluation of the therapeutic effect of transcatheter arterial embolization for hepatocellular carcinoma. *Oncology* 2000; **58**: 293-299
5 **Kim P**, Prapong W, Sze DY, So SK, Razavi MK. Treatment of hepatocellular carcinoma with sub-selective transcatheter arterial oily chemoinfusion. *Tech Vasc Interv Radiol* 2002; **5**: 127-131
6 **Higashihara H**, Okazaki M. Transcatheter arterial chemoembolization of hepatocellular carcinoma: a Japanese experience. *Hepatogastroenterology* 2002; **49**: 72-78
7 **Achenbach T**, Seifert JK, Pitton MB, Schunk K, Junginger T. Chemoembolization for primary liver cancer. *Eur J Surg Oncol* 2002; **28**: 37-41
8 **Harris M**, Gibbs P, Cebon J, Jones R, Sewell R, Schelleman T, Angus P. Hepatocellular carcinoma and chemoembolization. *Intern Med J* 2001; **31**: 517-522
9 **Poyanli A**, Rozanes I, Acunas B, Sencer S. Palliative treatment of hepatocellular carcinoma by chemoembolization. *Acta Radiol* 2001; **42**: 602-607
10 **Zangos S**, Gille T, Eichler K, Engelmann K, Woitaschek D, Balzer JO, Mack MG,Thalhammer A, Vogl TJ. Transarterial chemoembolization in hepatocellular carcinomas: technique, indications, results. *Radiologe* 2001; **41**: 906-914
11 **Aguayo A**, Patt YZ. Nonsurgical treatment of hepatocellular carcinoma. *Semin Oncol* 2001; **28**: 503-513
12 **Zheng XH**, Guan YS. The boold supply of hepatocellular carcinoma. *Fangshexue Shijian* 2002; **17:** 549-550
13 **Huang J**, Zhou XP, Liu RB, Chen X, Xu CJ, Yan ZH, Xu JY. The spiral CT manifestations of the boold supply of primary hepatocellular carcinoma:correlation with pathologic findings. *Zhonghua Fangshexue Zazhi* 2000; **34**: 753-756
14 **Tanaka K**, Nakamura S, Numata K, Okazaki H, Endo O, Inoue S, Takamura Y, Sugiyama M, Ohaki Y. Hepatocellular carcinoma: treatment with percutaneous ethanol injection and transcatheter arterial embolization. *Radiology* 1992; **185**: 457-460
15 **Li C**, Guo Y, Tian G, Shi Z, Liu D, Zeng H, Jiang W, Li H, Zhou C. Extrahepatic arterial blood supply of hepatocellular carcinoma and interventional treatment. *Zhonghua Zhongliu Zazhi* 2002; **24**: 163-166
16 **Honda H**, Tajima T, Kajiyama K, Kuroiwa T, Yoshimitsu K, Irie H, Aibe H, Shimada M, Masuda K. Vascular changes in hepatocellular carcinoma: correlation of radiologic and pathologic findings. *Am J Roentgenol* 1999; **173**: 1213-1217
17 **Liu H**, Li D, Yang S, Wu Y, Luo J. Changes of blood supply from portal system after transcatheter arterial chemoembolization in huge hepatocellular carcinoma. *Hunan Yike Daxue Xuebao* 1998; **23**: 295-298
18 **Imaeda T**, Yamawaki Y, Seki M, Goto H, Iinuma G, Kanematsu M, Mochizuki R, Doi H, Saji S, Shimokawa K. Lipiodol retention and massive necrosis after lipiodol-chemoembolization of hepatocellular carcinoma: correlation between computed tomography and histopathology. *Cardiovasc Intervent Radiol* 1993; **16**: 209-213
19 **Mortele KJ**, McTavish J, Ros PR. Current techniques of computed tomography. Helical CT, multidetector CT, and 3D reconstruction. *Clin Liver Dis* 2002; **6**: 29-52
20 **Takahashi S**, Murakami T, Takamura M, Kim T, Hori M, Narumi Y, Nakamura H, Kudo M. Multi-detector row helical CT angiography of hepatic vessels: depiction with dual-arterial phase acquisition during single breath hold. *Radiology* 2002; **222**: 81-88
21 **Arnold MM**, Kreel L, Wallace AC, Li AK. Distribution of Lipiodol and evidence for tumor necrosis in hepatocellular carcinoma. *Am J Clin Pathol* 1992; **97**: 405-410
22 **Takayasu K**, Arii S, Matsuo N, Yoshikawa M, Ryu M, Takasaki K, Sato M, Yamanaka N, Shimamura Y, Ohto M. Comparison of CT findings with resected specimens after chemoembolization with iodized oil for hepatocellular carcinoma. *Am J Roentgenol* 2000; **175**: 699-704
23 **Choi BI**, Kim HC, Han JK, Park JH, Kim YI, Kim ST, Lee HS, Kim CY, Han MC. Therapeutic effect of transcatheter oily chemoembolization therapy for encapsulated nodular hepatocellular carcinoma: CT and pathologic findings. *Radiology* 1992; **182**: 709-713
24 **Kubota K**, Hisa N, Nishikawa T, Fujiwara Y, Murata Y, Itoh S, Yoshida D, Yoshida S. Evaluation of hepatocellular carcinoma after treatment with transcatheter arterial chemoembolization: comparison of Lipiodol-CT, power Doppler sonography, and dynamic MRI. *Abdom Imaging* 2001; **26**: 184-190
25 **Ikeya S**, Takayasu K, Muramatsu Y, Moriyama N, Hasegawa H, Hirohashi S. Evaluation of the efficacy of oil chemoembolization for hepatocellular carcinoma by computed tomography: a proposal for altering the criteria to indicate the efficacy. *Gan No Rinsho* 1990; **36**: 985-992
26 **Tan LL**, Li YB, Chen DJ, Li SX, Jiang JD, Li ZM. Helical dual-phase CT scan in evaluating blood supply of primary hepatocellular carcinoma after transcatheter hepatic artery chemoembolization with lipiodol. *Zhonghua Zhongliu Zazhi* 2003; **25**: 82-84
27 **Murakami R**, Yoshimatsu S, Yamashita Y, Sagara K, Arakawa A, Takahashi M. Transcatheter hepatic subsegmental arterial chemoembolization therapy using iodized oil for small hepatocellular carcinomas. Correlation between lipiodol accumulation pattern and local recurrence. *Acta Radiol* 1994; **35**: 576-580
28 **Palma LD**. Diagnostic imaging and interventional therapy of hepatocellular carcinoma. *Br J Radiol* 1998; **71**: 808-818

Edited by Chen WW and Zhu LH **Proofread by** Xu FM

PO Box 2345, Beijing 100023, China
Fax: +86-10-85381893
E-mail: wjg@wjgnet.com www.wjgnet.com

World J Gastroenterol 2004;10(14):2130-2133
World Journal of Gastroenterology
 ISSN 1007-9327

• BRIEF REPORTS •

Multiple gene differential expression patterns in human ischemic liver: Safe limit of warm ischemic time

Qi-Ping Lu, Ting-Jia Cao, Zhi-Yong Zhang, Wei Liu

Qi-Ping Lu, Ting-Jia Cao, Zhi-Yong Zhang, Wei Liu, Department of General Surgery, Wuhan General Hospital of Guangzhou Military Command, Wuhan 430070, Hubei Province, China
Supported by the National Natural Science Foundation of China, No. 30170928 and the Key Project of the Tenth-Five-year plan Foundation of PLA, No. 01MA040
Correspondence to: Qi-Ping Lu, Department of General Surgery, Wuhan General Hospital of Guangzhou Military Command, Wuhan 430070, Hubei Province, China
Telephone: +86-27-68878501
Received: 2004-02-11 **Accepted:** 2004-03-02

Abstract

AIM: To investigate the multiple gene differential expression patterns in human ischemic liver and to produce the evidence about the hepatic ischemic safety time.

METHODS: The responses of cells to hepatic ischemia and hypoxia at hepatic ischemia were analyzed by cDNA microarrary representing 4 000 different human genes containing 200 apoptotic correlative genes.

RESULTS: There were lower or normal expression levels of apoptotic correlative genes during the periods of hepatic ischemia for 0-15 min, the maintenance homostatic genes were expressed significantly higher at the same time. But at the hepatic ischemia for 30 min, the expression levels of maintenance homeostatic genes were down-regulated, the expressions of many apoptotic correlative genes and nuclear transcription factors were activated and up-regulated.

CONCLUSION: HIF-1, APAF-1, PCDC10, FBX5, DFF40, DFFA XIAP, survivin may be regarded as the signal genes to judge the degree of hepatic ischemic-hypoxic injure, and the apoptotic liver cell injury due to ischemia in different time limits. The safe limit of human hepatic warm ischemic time appears to be generally less then 30 min.

Lu QP, Cao TJ, Zhang ZY, Liu W. Multiple gene differential expression patterns in human ischemic liver: Safe limit of warm ischemic time. *World J Gastroenterol* 2004; 10(14): 2130-2133

http://www.wjgnet.com/1007-9327/10/2130.asp

INTRODUCTION

The safety limit of human hepatic warm ischemic time is closely correlated with the recovery of hepatic function and the patient's prognosis after liver transplantation, serious hepatic injury and hepatectomy[1-7]. Owing to the development in hepatic surgical operation techniques and perioperative period, numerous experts discovered that the safety limit of human hepatic warm ischemic time could be prolonged further. But the critical problem of what degree the safety limit should be generally controlled is drawing special attention of the whole hepatic surgery. The cell apoptosis we have found now is one of the main cell death forms influencing visceral functions after the liver got ischemic injury[8-12]. But because too many genes are involved in cell apoptosis, the expressions in differential ischemic safety time of the main controlling gene influencing the safety limit of human hepatic warm ischemic time remain unclear. For such a reason, by cDNA microarray, we investigated the multiple genes differential expression patterns in human ischemic liver for the purpose of producing some scientific evidence for the hepatic ischemic safety time.

MATERIALS AND METHODS

Tissue specimens

All the tissue specimens in question came from the hepatic tissues contributed by the unconscious patients dying of external brain injury whose other organic functions were normal (Table 1). Each group consisted of 5 specimens. The specimens were immediately stored in liquid N_2 after resection. All contributors had no hepatic disease, and the liver function remains normal before resection. The liver tissue construction was proved normal by pathologic examinations.

Table 1 Group division of tissue specimens

Group	Experiment group	Control group
Group 1	15 min ischemic tissue	Normal liver tissue
Group 2	30 min ischemic tissue	Normal liver tissue
Group 3	30 min ischemic tissue	15 min ischemic tissue

Chemicals and materials

TriZol and Script II reverse transcriptases were bought from American Life Technologies, Ltd. cDNA microarray containing 200 apoptotic correlative genes and biochip hybridization kit were from Shanghai Biotstar Gene chip, Ltd.

Total RNA extraction

Total RNA was extracted from human liver tissues in each group following the single step extraction (see details in the manual).

Probe preparation and hybridization

An equal volume of RNA was extracted from each group and 60 μg RNA was added into 50 μL reverse transcription system. The experiment group was labeled with Cy5-d CTP and the control group with Cy5-d CTP (see the way of labeling in the manual of the test kit). The chip was denatured and prehybridized for one time in advance. After denatured at 95 ℃ for 5 min, the probe mixture was added on the microarray and covered with a hyi slip. The slide was then placed in a constant temperature hybridization chamber for hybridization at 42 ℃ for 20 h. After hybridization, slides were washed 10 min in each of 2×SSC with 2 g/L GSDS, 0.1×SSC with 2 g/L GSDS, 0.1×SSC, then dried at room temperature. The hybridization in each group was replicated 3 times.

Fluorescent scanning and analysis

The chip was scanned by GenePix 4000B laser scanner at

2 wavelengths. The acquired image was analyzed by GenePix Pro 3.0 software. The intensity of each spot at the 2 wavelengths cut off the additional background signal represented the quantity of Cy3-dUTP and Cy5-dUTP respectively. Each ratio value of Cy3 to Cy5 was computed. The 2 overall intensities were normalized by a coefficient according to the ratio of the located 88 housekeeping genes, 43 negative control genes, 45 positive control genes and 3 blank locations. We defined two standards to screen out each differentially expressed gene. The ratio value >2 represented the level of the gene expression elevated significantly, the ratio value <0.5 represented the level of the significantly depressed gene expression. The data about the genes whose ratio value >2 or <0.5 were screened out in the comparisons of normal control group with 15 min ischemic group or 30 min ischemic group, then the variation of the ratio value was observed in the comparison of 15 min ischemic group with 30 min ischemic group and each "±0.5" change in the ratio value was set as a "+". All the data were input in the datasheet, and the biological functions of the target genes were analyzed.

RESULTS

Comparison of differential gene expressions between 15 min ischemic group and normal control group

Figure 1 (A and B) shows that the double-colored fluorescent labels in 15 min ischemic group and normal control group were overlapping. A total of 41 differentially expressed genes were identified by cDNA chip between the 15 min ischemic group and normal control group. Among them the ratio values of 33 genes were <0.5, consisting of 22 genes correlated directly with cell apoptosis regulation, 9 congenic genes of stress-response protein relevant to cell apoptosis, and 3 genes correlated to metabolism regulation, 1 correlated to cell circle regulation, 1 correlated to the cell interpretation and synthesis. In the meantime, there were 8 differential expression genes whose ratio values were >2, mainly about P43=mitochondrial elongation factor homolog (GenBank-ID: S75463), human ribosomal protein *S14* gene, complete cds (GenBank-ID: humrps 14), *H. sapiens* mRNA for squalene synthase (GenBank-ID: hssqusyn), human sodium/potassium ATPase beta-2 subunit (atpb2) mRNA, complete cds (GenBank-ID: humatpbii), *H. sapiens* mRNA for H+-ATP synthase subunit b (GenBank-ID: hsatpsyn), and no gene relevant to apoptosis was highly expressed.

Comparison of differential gene expressions between 30 min ischemic group and normal control group

Figure 1 (C and D) shows that the double-colored fluorescent labels in 30 min ischemic group and normal control group were overlapping. A total of 9 differentially expressed genes were identified by cDNA chip between the 30 min ischemic group and normal control group. The ratio values of 3 genes of which were <0.5, consisting of 2 genes correlated directly with cell apoptosis regulation (the congenic genes of survivin, AB028869 and X-linked inhibitor apoptosis protein, u45880 respectively), and 1 congenic gene (GenBank-ID: af004711) of TPKC1. In the meantime, there were 6 differential expression genes whose ratio values were >2, of which 3 were the regulation genes correlated directly with cell apoptosis: APAF1 (GenBank-ID: NM-001160), PDCD10 (GenBank-ID: NM-007210) and an unnamed gene (GenBank-ID: AL031714), 1 was the congenic gene (GenBank-ID: AF050127) of HIF1, the functions of last 2 genes' were not clear.

Comparison of differential gene expressions between 15 min ischemic group and 30 min ischemic group

In the 200 genes, 35 genes were not expressed at the two time limits. The expressions of 167 genes in 30 min ischemic group differed from in 15 min ischemic group. One hundred and nineteen genes were expressed following the rising tendency, of which ratio values of 7 genes were >"+++", 19 >"++", 39>"+", and 55 genes only expressed the rising tendency but their ratio values were ≤"+". There are 46 genes following the descending tendency, of which ratio values of 4 genes were >"+++", 5 >"++", 12>"+", and 25 genes only expressed the descending tendency but their ratio values were ≤ "+". In addition, 16 genes were expressed in 30 min ischemic group, but not in 15 min ischemic group, of which 11 genes were

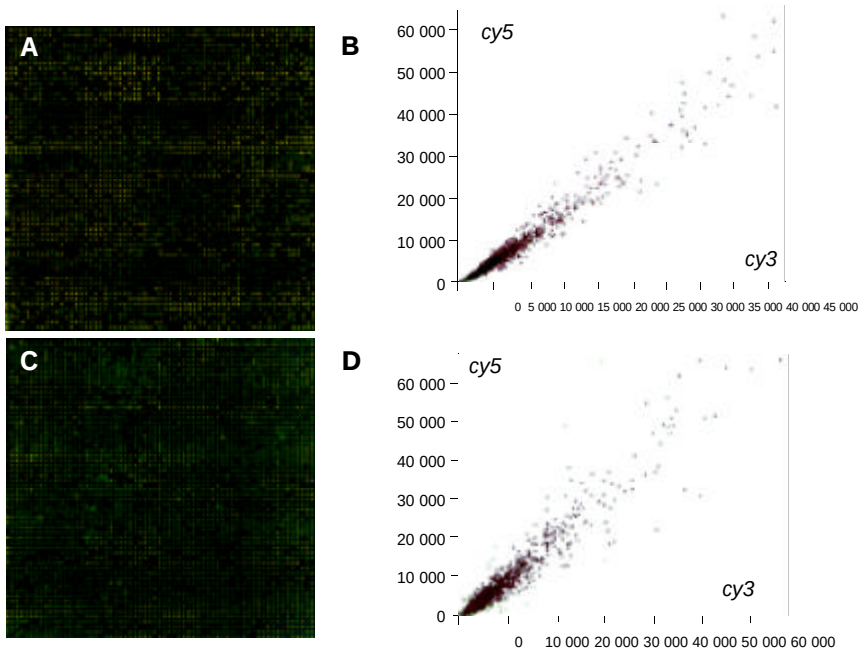

Figure 1 Double-colored fluorescent labels and scattered diagram of signal intensity of differential gene expressions in 15 min ischemic group and normal control group. Green: Down-regulation, Signal of cy3 is stronger; Red: Up-regulation, signal of cy5 is stronger. A, C: Double-colored fluorescent labels: In 15 min ischemic group and normal control group; B, D: Scatter diagram of signal intensity of differential gene expressions in 15 min ischemia group and normal control group.

correlated directly with cell apoptosis regulation, 5 genes were expressed in 15 min ischemic group, but not in 30 min ischemic group, of which only 1 gene was correlated directly with cell apoptosis regulation, namely XIAP (GenBank-ID: u45880).

DISCUSSION

Our data suggested that the apoptosis regulation gene at the hepatic ischemia for 0-30 min presented following features.

In hepatic ischemia for 0-15 min, the apoptosis regulation gene was expressed low or normally. The differentially expressed genes whose ratio values were >2 (namely, they were expressed following the rising tendency) were mainly the maintenance harmonious genes, such as genes regulate P43=mitochondrial elongation factor homolog (GenBank-ID: S75463), Human ribosomal protein S14 gene (GenBank-ID: humrps), *H. sapiens* mRNA for squalene synthase (GenBank-ID: hssqusyn), Na^+/K^+-ATPase activity α subunit (GenBank-ID: hsatpar) and β subunit(GenBank-ID: humatpbii), H^+-ATPase activity (GenBank-ID: hsatpsyn). But they were not highly expressed with the congenic genes correlated directly with cell apoptosis regulation.

In hepatic ischemia for 15-30 min, the expression of apoptosis regulation genes changed greatly. One hundred and nineteen genes were expressed following the rising tendency, of which 59 genes were relevant to the apoptosis regulation. Although some anti-apoptosis genes [such as the congenic gene of *bcl-2* (GenBank-ID: AJ006288), the congenic gene of inhibitor apoptosis protein IEX-IL (GenBank-ID: AF071596)] which were expressed the low level, the majority of the higher expressed genes were the apoptotic genes, for example, the congenic gene of apoptotic protease activating factor-1 (APAF-1, GenBank-ID: NM-001160); Homo sapiens F-box protein 5, FBX5 (GenBank-ID: NM-012177); DNA fragmentation factor, 40 ku, subunit, DFF40 (GenBank-ID: AF064019); DNA fragmentation factor, 45 ku, alpha subunit, DFFA (GenBank-ID: NM-004401); p53-induced protein; PIG11(GenBank-ID: NM-006034). Especially, APAF-1 was the only known human homologue of CED-4 and the nuclear element in the formation of apoptosis body[13-16]. Now it is thought as the key element regulating cell apoptosis, and the ratio value of its expression in 30 min hepatic ischemia was an additional "+++" than that in 15 min hepatic ischemia. Meanwhile the ratio value of the congenic gene of PDCD10 (GenBank-ID: NM-007217) was also "++". The significant rising of expression of the apoptotic genes showed that the unavoidable cell death after serious ischemic injury was a key expression of the serious cell injure. In 15 min hepatic ischemia, the congenic gene of the important X-linked inhibitor apoptosis protein, XIAP (GenBank-ID: u45880) changed from the normal expression to non-expression, following the obvious descending tendency. Compared with the normal group, the expression of the survivin congenic gene (GenBank-ID: AB028869) descended greatly with the ratio value <0.5. The codogenic genes (GenBank-ID: S75463, humrps, hssqusyn, hsatpar, humatpbii, hsatpsyn and so on) relevant to the internal circumstance and the organelle functions were expressed obviously in the period of 0-15 min hepatic ischemia, but in 15-30 min period their expression descended to "+"- "++". The congenic gene of human hypoxia-inducible factor 1 HIF-1 alpha gene (GenBank-ID: AF050127) was expressed apparently (increased to "+++"). Lots of the regulation genes of nucleus translation factors were expressed notably for example, the codogenic gene of EIF4G2 (eukaryotic translation-induction factor 4 gamma, 2 (EIF4G2) mRNA, GenBank-ID: NM-001418), NF-κB family, TNF receptor associated factor 6 (TRAF6) responsible for the existence and death of cells (GenBank-ID: hsu78798), increased to "++". The latter was a transmission factor participating in IL-1 signal transmission and activating the signal transmission about apoptosis of the nuclear factor NF-κB[17-20].

The data suggested that in 0-15 min hepatic ischemia, the gene regulation model inside of the cells was likely to better and maintain the harmonious of the internal circumstance to keep the wholeness of cell and organ functions even by controlling ion channel and organelle functions. At the same time, although acute ischemic-hypoxic injury changed the structure and functions of cells, the expression of each kind of genes relevant to apoptosis, according to the analysis of the level of gene regulation, remained on the low level, that is to say, the occurrence of apoptosis was not a main direction yet. With the time of ischemia and hypoxia passed, when hepatic ischemia lasted for 30 min, acute ischemic-hypoxic injury perhaps would lead to the significant rising of HIF-1, and the cell gene expression model responsible for the existence or death of the cells also was changed completely. The expressions of all kinds of regulation genes maintaining cells and the internal cellular circumstance descended obviously, while NF-κB and many genes relevant to apoptosis were activated evidently and notably expressed. Therefore, it is suggested that cell death is unavoidable when hepatic ischemia lasts for 30 min. It is true that some experts deduced that the time of the human hepatic ischemia could be prolonged beyond the safe limit according to clinical experience in the progress after liver operation. Yet when dynamic changes of gene expressions after liver suffered ischemic injury are analyzed, it is suggested that the safe limit of one time hepatic ischemia should be less than 30 min, namely, when key death genes such as *APAF-1, PDCD10, FBX5, DFF40, DFFA* are activated evidently and expressed significantly, and before the obvious descending of inhibitor apoptosis genes such as XIAP, survivin. In the meantime it is suggested that HIF-1, APAF-1, PCDC10, XIAP, survivin may be regarded as the signal gene to judge the degree of hepatic ischemic-hypoxic injury, and the apoptotic liver cell injury due to ischemia in different time limits.

REFERENCES

1 **Makuuchi M,** Mori T, Gunven P, Yamazaki S, Hasegawa H. Safety of hemihepatic vascular occlusion during resection of the liver. *Surg Gynecol Obstet* 1987; **164**: 155-158

2 **Mori T,** Makuuchi M, Kobayashi J, Sukigara M, Yamasaki S, Hasegawa H. Clinical studies on changes in serum transaminase, lactate dehydrogenase, total bilirubin and alkaline phosphatase levels after hepatectomy with and without the hemihepatic vascular occlusion technique. *Nippon Geka Gakkai Zasshi* 1985; **86**: 837-845

3 **Gotoh M,** Monden M, Sakon M, Kanai T, Umeshita K, Nagano H, Mori T. Hilar lobar vascular occlusion for hepatic resection. *J Am Coll Surg* 1994; **178**: 6-10

4 **Wu CC,** Yeh DC, Ho WM, Yu CL, Cheng SB, Liu TJ, P'eng FK. Occlusion of hepatic blood inflow for complex central liver resections in cirrhotic patients: a randomized comparison of hemihepatic and total hepatic occlusion techniques. *Arch Surg* 2002; **137**: 1369-1376

5 **Liu DL**, Jeppsson B, Hakansson CH, Odselius R. Multiple-system organ damage resulting from prolonged hepatic inflow interruption. *Arch Surg* 1996; **131**: 442-447

6 **Emond J**, Wachs ME, Renz JF, Kelley S, Harris H, Roberts JP, Ascher NL, Lim RC Jr. Total vascular exclusion for major hepatectomy in patients with abnormal liver parenchyma. *Arch Surg* 1995; **130**: 824-830

7 **Scheele J**. Anatomical and atypical liver resections. *Chirurg* 2001; **72**: 113-124

8 **Yin XM,** Ding WX. Death receptor activation-induced hepatocyte apoptosis and liver injury. *Curr Mol Med* 2003; **3**: 491-508

9 **Jaeschke H,** Lemasters JJ. Apoptosis versus oncotic necrosis in hepatic ischemia / reperfusion injury. *Gastroenterology* 2003; **125**: 1246-1257

10 **Sass G,** Soares MC, Yamashita K, Seyfried S, Zimmermann WH, Eschenhagen T, Kaczmarek E, Ritter T, Volk HD, Tiegs G. Heme oxygenase-1 and its reaction product, carbon monoxide, prevent inflammation-related apoptotic liver damage in mice. *Hepatology* 2003; **38**: 909-918
11 **Berberat PO,** Katori M, Kaczmarek E, Anselmo D, Lassman C, Ke B, Shen X, Busuttil RW, Yamashita K, Csizmadia E, Tyagi S, Otterbein LE, Brouard S, Tobiasch E, Bach FH, Kupiec-Weglinski JW, Soares MP. Heavy chain ferritin acts as an antiapoptotic gene that protects livers from ischemia reperfusion injury. *FASEB J* 2003; **17**: 1724-1726
12 **Topaloglu S,** Abbasoglu O, Ayhan A, Sokmensuer C, Kilinc K. Antiapoptotic and protective effects of roscovitine on ischemia-reperfusion injury of the rat liver. *Liver Int* 2003; **23**: 300-307
13 **Zou H,** Henzel WJ, Liu X, Lutschg A, Wang X. Apaf-1, a human protein homologous to C. elegans CED-4, participates in cytochrome c-dependent activation of caspase-3. *Cell* 1997; **90**: 405-413
14 **Pan G,** O'Rourke K, Dixit VM. Caspase-9, Bcl-XL, and Apaf-1 form a ternary complex. *J Biol Chem* 1998; **273**: 5841-5845
15 **Shulache VP**. Cytochrome c in the apoptotic and antioxidant cascades. *FEBS Lett* 1998; **423**: 275-280
16 **Hu Y,** Benedict MA, Wu D, Inohara N, Nunez G. Bcl-XL interacts with Apaf-1 and inhibits Apaf-1-dependent caspase-9 activation. *Proc Natl Acad Sci U S A* 1998; **95**: 4386-4391
17 **Matsumura T,** Degawa T, Takii T, Hayashi H, Okamoto T, Inoue J, Onozaki K. TRAF6-NF-kappaB pathway is essential for interleukin-1-induced TLR2 expression and its functional response to TLR2 ligand in murine hepatocytes. *Immunolog* 2003; **109**: 127-136
18 **Yoshida Y,** Yamashita U. Interleukin 1 signal transduction. *J UOEH* 2003; **25**: 237-248
19 **Takatsuna H,** Kato H, Gohda J, Akiyama T, Moriya A, Okamoto Y, Yamagata Y, Otsuka M, Umezawa K, Semba K, Inoue J. Identification of TIFA as an adapter protein that links tumor necrosis factor receptor-associated factor 6 (TRAF6) to interleukin-1 (IL-1) receptor-associated kinase-1 (IRAK-1) in IL-1 receptor signaling. *J Biol Chem* 2003; **278**: 12144-12150
20 **Kanamori M,** Kai C, Hayashizaki Y, Suzuki H. NF-kappaB activator Act1 associates with IL-1/Toll pathway adaptor molecule TRAF6. *FEBS Lett* 2002; **532**: 241-246

Edited by Wang XL **Proofread by** Chen WW and Xu FM

PO Box 2345, Beijing 100023, China
Fax: +86-10-85381893
E-mail: wjg@wjgnet.com www.wjgnet.com

World J Gastroenterol 2004;10(14):2134-2135
World Journal of Gastroenterology
 ISSN 1007-9327

• BRIEF REPORTS •

A report of 28 cases of 3-year follow-up after liver transplantation for advanced hepatocellular carcinoma

De-Chen Wang, Tong-Lin Zhang, Shi-Bing Song, Jiong Yuan, Dian-Rong Xiu, Xiao-Xia Yang

De-Chen Wang, Tong-Lin Zhang, Shi-Bing Song, Jiong Yuan, Dian-Rong Xiu, Xiao-Xia Yang, Department of General Surgery, Peking University Third Hospital, Beijing 100083, China
Correspondence to: Dr. De-Chen Wang, Department of General Surgery, Peking University Third Hospital, Beijing 100083, China. hepuzai@yahoo.com.cn
Telephone: +86-10-62017691 **Fax:** +86-10-62010334
Received: 2003-12-28 **Accepted:** 2004-01-08

Abstract

AIM: To investigate the therapeutic value of liver transplantation for advanced hepatocellular carcinoma (HCC).

METHODS: Twenty-eight patients with advanced HCC were treated by liver transplantation from August 2000 to October 2003 at Peking University Third hospital. All the patients were followed up to evaluate the result.

RESULTS: The longest follow-up duration was 3 years and 3 mo. Till the end of the follow-up period, 17 patients had already died and 11 were alive. Of those who died, 10 patients died of tumor recurrence, 4 died during the perioperative period, 2 died of variceal bleeding, and 1 died of biliary complication. According to life table method, the 1-, 2-, and 3-year survival rates were 87.5%, 52.5%,and 42.9%, respectively.

CONCLUSION: Liver transplantation provides a new treatment under the circumstance of lacking of an effective treatment for advanced HCC at present. Some patients can survive for a relatively long time free of tumor. In our country, if the patients can afford liver transplantation, advanced HCC without extrahepatic metastasis is an indication for liver transplantation at present.

Wang DC, Zhang TL, Song SB, Yuan J, Xiu DR, Yang XX. A report of 28 cases of 3-year follow-up after liver transplantation for advanced hepatocellular carcinoma. *World J Gastroenterol* 2004; 10(14): 2134-2135
http://www.wjgnet.com/1007-9327/10/2134.asp

INTRODUCTION

Hepatocellular carcinoma (HCC) is a common malignant tumor in China. The methods of treatment for advanced HCC are limited, and the prognosis is so poor. Peking University Third Hospital began to carry out liver transplantation since August 2000. Some of the patients suffered from advanced HCC. In our study, the result of treatment has been found to be somewhat accepted at present.

MATERIALS AND METHODS

Materials

Twenty-eight patients with advanced HCC were treated by liver transplantation from August 2000 to October 2003 at our hospital. Of them, twenty-six patients were male. The average age was 46.3 years, ranging from 20 to 63 years. All the patients suffered from cirrhosis caused by hepatitis B. Child-Pugh classes A, B, and C patients were 13, 8, and 7, respectively. The diagnosis was made by ultrasound, computed tomography, magnetic resonance imaging, arteriography and serum alpha-fetoprotein levels. Postoperative pathologic examination confirmed that all the patients had HCC. The patients with extrahepatic spread were excluded by ultrasound, chest film and bone scan. All the patients met the following criteria: solitary tumor $\geqslant$5 cm or with multiple nodules and total diameter >8 cm; and the mean diameter of single nodule was 10.3 cm, ranging from 3 cm to 20 cm. There were 12 patients with tumor involving bilateral hepatic lobes, 5 with positive porta hepatis nodes, and 18 with portal invasion.

Methods

All the patients underwent orthotopic liver transplantation (OLT) and were taken care of by the same medical team perioperatively. The donors were healthy male who had brain death with the age of 20-40 years. The initial 11 patients did not undergo formal chemotherapy postoperatively, and only the eighth patient underwent transarterial chemoembolization preoperatively (hot lipiodol 10 mL and cisplatin 100 mg). Seventeen patients underwent the formal intravenous chemotherapy postoperatively when the hepatic function was normal. The chemotherapy regime was: administration of adriamycin 40 mg, cisplatin 60 mg, calcium folinate-SF 200 mg and 5- Fluorouracil 1 000 mg on the first day, the same doses of calcium folinate-SF and 5- Fluorouracil from the second day to the fifth day. The course of chemotherapy was 5 d once a month, and there were 6 courses altogether. All the patients were followed up and the longest duration was 3 years and 3 mo.

Statistics

The survival rate was calculated according to the life table method. Patients who died of non-tumor and who stopped the follow-up in the intervals were listed into the lost.

RESULTS

Till the end of the follow-up period, 17 patients had already died, and 11 were alive. Of those dead patients (Table 1), 10 patients died of tumor recurrence, 4 died within perioperative period, 2 died of variceal bleeding, and 1 died of biliary complication. Among the patients who survived (Table 2), there were 1, 2, 2, and 3 patients survived for 8 mo, 1, 2, and 3 years free of tumor, respectively; and there were 1 and 2 patients survived for 8 mo and 1 year with tumor-recurrence, respectively. In the first year, 8 patients were lost, 3 were dead, and the 1-year survival rate was 87.5%. In the second year, 4 patients were lost, 6 were dead, and the 2-year survival rate was 52.5%. In the third year, 3 patients were lost, 1 was dead, and the 3-year survival rate was 42.9%.

Of the patients with single tumor of more than 10 cm, there was 1 patient who survived for more than 3 years. No patients with tumors involving many hepatic lobes could survive for more than 3 years, but there were 2 patients survived for more

than 2 years. There was 1 patient with positive portal lymph node survived for more than 3 years. Of the patients with portal invasion, 2 survived for more than 3 years, and 3 survived for more than 2 years. The cases were divided according to the different standards, and their survival time can be seen in Table 3.

Table 1 Causes and time of the death of patients

Cause	Peri-operatively	Variceal bleeding	Biliary complication	Tumor-recurrence		
				<1 yr	1-2 yr	>2 yr
Number	4	2[1]	1[2]	3	6	1

[1]2 years and 2 mo, and 6 mo after OLT, respectively, [2]6 mo after OLT.

Table 2 Survival time of the patients

Time	<1 yr	1-2 yr	2-3 yr	>3 yr
Number	1+1[1]	2+2[1]	2	3

[1]Survive with recurrence.

Table 3 Survival time of the different groups

Groups	<1 yr	12 yr	2-3 yr	>3 yr
Tumor diameter				
>10 cm	5	4	0	1
<10 cm	6	6	4	2
Portal invasion				
Yes	7	6	3	2
No	4	4	1	1

DISCUSSION

Among the surgical therapies of HCC, the dominant treatment is hepatic resection. A study showed that the 5-year survival rate is up to 50% after hepatic resection[1]. But HCC always occurs in the presence of liver cirrhosis, hepatic resection is limited by the poor hepatic function and the presence of portal hypertension. In general, Child' s C` stage is considered an absolute contraindication for any type of resection[1].

According to the principle of tumor surgery, replacing an allograft after total hepatectomy is an ideal curative resection of HCC[2]. Herrero *et al*. reported that in the patients with solitary HCC nodule less than 6 cm and those with 2-3 HCC nodules less than 5 cm in diameter,1- and 3-year recurrence free suvival rates were 87% and 79%, respectively[3]. In the study by Yao *et al*.[2], patients with HCC meeting the following criteria: solitary tumor $\leqslant$6.5 cm, or $\leqslant$3 nodules with the largest lesion $\leqslant$4.5 cm and total tumor diameter $\leqslant$8 cm, had survival rates of 90% and 75.2%, at 1 and 5 years after OLT, respectively. So they concluded that the current criteria for OLT based on tumor size might be modestly expanded while preserving excellent survival. Since OLT for early HCC is not fit for the situation of our country as well as the economic status, and the result of hepatic resection is good in our country, OLT is not accepted by the patients except that the patients having early HCC with serious cirrhosis can not tolerate hepatic resection.

The diagnosis of early HCC is achieved in around 30% of the cases[4]. As to the unresectable HCC, the chief therapy is a non-surgical treatment. But it always leads to poor prognosis for it is not a curative treatment. Now the generally accepted non-surgical treatment is transarterial chemoembolization. Lo *et al.* undertook a randomized controlled trial of transarterial chemoembolization for unresectable HCC[5]. The patients were excluded if they had 1 or more of the following criteria: poor hepatic function (presence of hepatic encephalopathy, ascites not controlled by diuretics, history of variceal bleeding within last three months, a serum total bilirubin level over 50 μmol/L, a serum total albumin level below 28 g/L, or a prothrombin time of more than 4 s over the control); extrahepatic metastasis; main portal vein thrombosis *etc*[5]. The chemoembolization group underwent transarterial chemoembolization, and the control group received only treatment for symptoms and complications. The estimated 1-, 2- and 3-year survival rates were 57%, 31% and 26% for the chemoembolization group, and 32%, 11%, and 3% for the control group, respectively.

There is no effective therapy for the patients with advanced HCC who do not meet the chemoembolization criteria, such as poor hepatic function and/or portal thrombosis, and they have poor prognosis even if there is no extrahepatic spread when the diagnosis of HCC is made. In the initial stage of OLT, the patients with advanced HCC were also treated by OLT in abroad, and the 3-year survival rate was 20-30%[1]. Due to the poor prognosis and the shortage of donor, OLT for advanced HCC was abandoned in foreign countries. From the year of 2000, our hospital began to perform OLT and chose advanced HCC for the initial trial just as peers at home and abroad. Till now, 28 patients with advanced HCC underwent OLT at our hospital. We can not conclude that the result is excellent through the 3-year follow-up. Many patients who underwent OLT did not meet the chemoembolization criteria, but the total survival rate was higher than that of the chemoembolization group reported by Lo *et al*. Some patients survived for a relatively long time free of tumor after OLT. Thus, liver transplantation provides a new treatment under the circumstance of lacking of an effective treatment for HCC at present, and some patients have a chance to lengthen their lives. But the expense of liver transplantation is very high. In our country, if the patients can afford liver transplantation, advanced HCC without extrahepatic metastasis is an indication for liver transplantation at present.

REFERENCES

1 **Frilling A**, Malago M, Broelsch CE. Current status of liver transplantation for treatment of hepatocellular carcinoma. *Dig Dis* 2001; **19**: 333-337
2 **Yao FY**, Ferrell L, Bass NM, Watson JJ, Bacchetti P, Venook A, Ascher NL, Roberts JP. Liver transplantation for hepatocellular carcinoma: expansion of the tumor size limits does not adversely impact survival. *Hepatology* 2001; **33**: 1394-1403
3 **Herrero JI**, Sangro B, Quiroga J, Pardo F, Herraiz M, Cienfuegos JA, Prieto J. Influence of tumor characteristics on the outcome of liver transplantation among patients with liver cirrhosis and hepatocellular carcinoma. *Liver transplantation* 2001; **7**: 631-636
4 **Varela M**, Sala M, Llovet JM, Bruix J. Treatment of hepatocellular carcinoma: is there an optimal strategy? *Cancer Treat Rev* 2003; **29**: 99-104
5 **Lo CM**, Ngan H, Tso WK, Liu CL, Lam CM, Poon RTP, Fan ST, Wong J. Randomized controlled trial of transarterial lipiodol chemoembolization for unresectable hepatocellular carcinoma. *Hepatology* 2002; **35**: 1164-1171

Edited by Kumar M and Xu FM

PO Box 2345, Beijing 100023, China
Fax: +86-10-85381893
E-mail: wjg@wjgnet.com www.wjgnet.com

World J Gastroenterol 2004;10(14):2136-2139
World Journal of Gastroenterology
 ISSN 1007-9327

• BRIEF REPORTS •

Clinical features, diagnosis, treatment and prognosis of multiple primary colorectal carcinoma

Hong-Zhi Wang, Xin-Fu Huang, Yi Wang, Jia-Fu Ji, Jin Gu

Hong-Zhi Wang, Xin-Fu Huang, Yi Wang, Jia-Fu Ji, Jin Gu, Department of Surgery, Beijing Cancer Hospital, School of Clinical Oncology, Peking University, Beijing 100036, China
Correspondence to: Hong-Zhi Wang, Department of Surgery, Beijing Cancer Hospital, School of Clinical Oncology, Peking University, Beijing 100036, China. doctorwhz@163.com
Telephone: +86-10-88135234 **Fax:** +86-10-68518676
Received: 2004-02-02 **Accepted:** 2004-02-18

Abstract

AIM: To investigate the clinical features, diagnosis, treatment and prognosis of multiple primary colorectal carcinomas (MPCC).

METHODS: A retrospective analysis of 37 patients with MPCC from 1974 to 1998 was carried out.

RESULTS: The incidence of MPCC was 2.74%(37/1 348) in patients with primary colorectal carcinomas, 15 cases of them were patients with synchronous carcinomas (SC) and 22 cases were diagnosed as metachronous carcinomas (MC). Most tumors were located in the right colon and rectum. Fifty-five percent (12/22) of MC were diagnosed within 3 years after tumor resection and 41%(9/22) of MC occurred after 8 years. Radical resections were performed in all patients except for 1 case. The 5-year survival rate of SC was 72.7%(8/11) and that of MC after the first cancer and second cancer was 71.4%(15/21) and 38.9%(7/18), respectively.

CONCLUSION: The results indicate the importance of complete preoperative examination, careful intraoperative exploration and periodic postoperative surveillance. Early diagnosis and radical resection can increase survival rate of MPCC.

Wang HZ, Huang XF, Wang Y, Ji JF, Gu J. Clinical features, diagnosis, treatment and prognosis of multiple primary colorectal carcinoma. *World J Gastroenterol* 2004; 10(14): 2136-2139

http://www.wjgnet.com/1007-9327/10/2136.asp

INTRODUCTION

Multiple primary colorectal carcinoma (MPCC) refers to two or more primary colorectal carcinomas detected in a single individual simultaneously or consecutively. It is named synchronous carcinoma (SC) and metachronous carcinoma (MC) respectively. The prognosis of colorectal carcinoma is good compared with other carcinomas of the digestive organs. Along with increasing incidence of colorectal carcinomas and prolonged survival after radical resection, patients with MPCC have increased gradually. Generally, SC does not affect prognosis if it is recognized and treated in time, but if ignored, it may turn into more advanced MC. Therefore, after colorectal cancer surgery, occurrence of metachronous carcinoma is regarded as an serious problem[1]. Due to influence of doctor's recognition degree, missed and error diagnosis or inaccurate treatment appears frequently. The purpose of this review was to discuss the prevalence, preoperative diagnosis, postoperative follow-up and survival, in order to strengthen the acquaintance of MPCC.

MATERIALS AND METHODS

A total of 1 348 cases of primary colorectal carcinomas were treated at the Department of Surgery, Beijing Cancer Hospital from January 1, 1974 to December 31, 1998. MPCC was diagnosed according to the following criteria proposed by Moertel[2]. Each tumor must have a definite pathologic picture of malignancy, metastasis or recurrence from another colorectal cancer was excluded, all cancers detected at the same time or within 6 mo were defined as SC, otherwise as MC, Tumors must be distinctly separated by at least 5 cm of an intact bowel wall from each other. MC must be more than 5 cm away from the normal anastomotic site of index cancer resection. MPCC originated from familial colonic polyposis or ulcerative colitis was excluded[2].

Tumor locations were divided into 3 groups: (1) right colon which included appendix, cecum, ascending colon, hepatic flexure, and transverse colon; (2) left colon which included splenic flexure, descending colon and sigmoid colon; (3) rectum, upper boundary of which was 15 cm from the dentate line. It was considered as lost follow-up if a patient failed to come back to the Outpatient Department or could not be contacted by letter or telephone for more than one year.

Independent *t*-test and χ^2-test were used to compare the factors in different groups. A P value less than or equal to 0.05 was considered statistically significant.

RESULTS

A total of 1 348 patients with colorectal carcinoma were treated during 25 years period. Fifteen cases had 2 SCs and 22 patients had 2(20 cases) or 4(1 case) or 5(1 case) MCs, respectively (Tables 1 and 2). No significant differences were noted among the groups in age and gender. The second MC appeared in 8-240 mo (mean: 68 mo), 55%(12/22) were diagnosed within 36 mo and 41%(9/22) after 96 mo. The interval of other one patient was 45 mo. Two patients had three times of MC, their interval was 15 years (one cancer), 19 years (two cancers) and 12 years (one cancer), 17 years (three cancers) respectively.

The distribution of MC and SC is shown in Table 2. Lesions were located at the adjacent intestinal segment in 6 of SC group (43%). In MC group, 20 patients had 2 lesions, 1 had 4 lesions and the other one had 5 lesions.

The clinical presentation was variable. All the 15 patients in SC group went to see doctors because of symptoms, such as bloody stool, abdominal pain, diarrhea, anemia and abdominal mass. The time of the development symptoms was more than 1 year. Thirteen cases (87%) were diagnosed by barium enema and/or colonoscopy before operation. And 2, 9 and 2 patients were staged as Dukes B, C and D, respectively. Other 2 patients of this group were diagnosed intraoperatively. In MC group,

3 of 22 cases (13.6%) were proved by routine postoperative colonoscopy (2: Dukes A, 1: Dukes B). Twenty-one patients went to see doctor owing to symptoms, 18(86%) were diagnosed preoperatively, 2 were diagnosed intraoperatively, and 1 was diagnosed by postoperative pathology.

Operation was the primary option. In SC group, 14 cases (93%) received radical resection. Among them, 5 cases received subtotal colectomy in combination with rectoileostomy, others received radical resection or combined radical resection of adjacent loop according to the cancer locations. One received by-pass due to severe local spread. In MC group, all the 22 cases with index cancer received radical resection. All secondary or third lesions except one underwent radical resection.

The histological types of all cancers are shown in Table 2. No significant differences were noted between the second cancer and SC with index cancer. There was a significant difference between the third cancer and index cancer.

The 5-year and 10-year survival rates are shown in Table 2. There was no significant difference between SC and index cancer of MC. The 5-year survival rate of the patients with secondary cancer could reach 39% after operation.

Table 1 Age and gender of patients with MPCC

	Group SC	Group MC
Number of patients	15	22
Age(yr)		
mean±SD	47±12	48±12
Range	27-71	30-68
P value		>0.1
Gender		
Male	11(73%)	16(73%)
Female	4(27%)	6(27%)
P value		>0.1

All statistical comparisons were with index cancer of MC by independent *t*-test or χ^2-test.

DISCUSSION

MPCC is not uncommon in clinic. The estimated incidence rates of SC and MC were 2.0-8.1% and 0.6-10.6% respectively[3-10]. Such a significantly different result of these series may be due to several reasons. For example, the definition varied to allow diagnosis of a second carcinoma at a range of 6 mo to 3 years after the diagnosis of the index tumor. The patient number, observation period and follow-up time all could influence the final results. Bulow *et al*.[9] followed up 501 patients younger than 40 years old with colorectal carcinoma for up to 41 years. In the first 10 years, only 12 cases developed MC. Since then, another 32 patients had developed MC in succession. Cali *et al*.[1] reported that the calculated incidence for MC was 0.35 percent per year and the cumulative incidence at 18 years was 6.3 percent according to a group of 5 476 patients. In another larger group of 141 945 patients with histologically confirmed primary colorectal tumors within 14 years (mean follow-up of 4.72 years), 3 402(2.4%) and 1 526(1.1%) cases were diagnosed with SC and MC respectively[8]. In our study, the incidence of MPCC was 2.74%(37/1348). The reported data showed that the occurrence of MPCC had a rising trend[11].

Chen *et al*.[12] reported that there was no difference in age of patients with SC, MC and single colorectal carcinoma. Oya *et al*.[13] found the index lesions of synchronous cases did not differ from single lesions in age, size, differentiation, and location. However the male: female ratio was higher and distant metastasis was more frequent in synchronous cases than in single cases. Welch[14] found that patients with synchronous tumors were older than those with single colon cancers or initial metachronous lesions. Our results showed that patients with SC or MC had similar age, gender, and location.

The time intervals between the diagnosis of index and metachronous cancers varied obviously. Kiefer *et al*. showed that early metachronous cancers (within 2 years) reached 40%[15]. But others[8] considered the "early" MC as an overlooked SC. The interval of MC could reach 41 years after the first tumor. Welch[14] pointed out that the median interval between metachronous tumors was 9 years. The symptom duration was shorter before discovery of the second metachronous tumors. The occurrence of the second MC was 55% within 3 years and 41% after 8 years from index cancer resection in our series. The longest was 20 years. Therefore, early follow-up examination (within 3 years) was very important.

Table 2 Location, types, and survival rate in two groups

	MC			SC
	Index cancer	2nd cancer	3rd cancer	
No. of tumors	22	22	5	30
Location				
Right colon	9(41%)	7(32%)	2(40%)	7(23%)
Left colon	7(32%)	8(36%)	2(40%)	15(50%)
Rectum	6(27%)	7(32%)	1(20%)	8(27%)
P value		>0.1	>0.1	>0.1
Types				
AC	20(91%)	19(86%)	3(60%)	18(64%)
Mucoid AC	2(9)	1(5)		7(25)
Canceration		1(5%)	2(40%)	3(11%)
(Adenoma / Polypus)				
Ring cell C		1(5)		
P value		>0.1	<0.01	>0.05
Survival Rate				
5-yr	71%(15 / 21)	39%(7 / 18)		73%(8 / 11)
10-yr	53%(10 / 19)	19%(3 / 16)		63%(5 / 8)
P value				>0.1

A: Adenoid; C: Carcinoma. All statistical comparisons were with index cancer of MC by independent *t*-test or χ^2-test.

The preoperative detection of SC not only can allow an appropriate surgical strategy to be carried out but also establish a logical policy for follow-up. It is stressed that a second tumor may present in large intestine during follow-up. Barium enema and/or colonoscopy should be given to patients in time. Examinations such as B-ultrasound, CT scan, CEA, fecal occult blood and fecal occult albumin may help to improve diagnosis, especially SC preoperatively. CEA, fecal occult blood and fecal occult albumin test were also used to detect the early stage colorectal cancer during mass screening for asymptomatic or follow-up for high risk populations[16]. However, many results were still unsatisfactory[5,12,17]. Finan *et al*.[5] diagnosed only 42% of 59 SC patients preoperatively. Chen *et al*.[12] reported that 66%(31/47) of SC were omitted during preoperative barium enema (46 patients) and/or colonoscopy (7 patients). But other report[18] showed that the sensitivity of colonoscopy reached 76.7%(56/73) for detecting SC and 82%(14/17) of missed lesions were smaller than 1 cm polyps. In our group, although preoperative diagnostic rate of SC reached 87%, but 85% were Dukes C or D. The reason why multiple lesions could not be identified preoperatively was that the occluded distal lesions made it difficult to detect the proximal lesions. Therefore, we could not be satisfactory for diagnosis of one colorectal cancer and should examine the whole large bowel carefully pre- or postoperatively.

It is important to palpate the whole colon and to check pathological specimens carefully before the end of operation so that misdiagnosis of SC can be avoided. Even now, miss-diagnosis is still existed. Chen's report[12] showed that there were still 13 patients without detection of SC by operative palpation in the 31 preoperative undiagnosed cases. Intraoperative colonoscopy should be advised if necessary. We think that this technique should not be used as a routine one and could be performed early (within 6 mo) after surgery.

It is an effective measure to follow up with barium enema or colonoscopy periodically for diagnosing MC earlier. A previous report[9] showed that surveillance colonoscopy once every three years after surgery, together with a fecal occult blood test, would be an efficient and appropriate way to detect MC. Some nonfamilial colorectal cancers have been reported to have microsatellite instability (MSI)[19-23]. A research[19] indicated the incidence of MC in MSI-positive group was significantly higher than that in MSI-negative. Logical analysis showed that MSI and coexistence of adenoma were significantly independent risk factors for the occurrence of MC. Studies[20,21] showed the analysis of MSI and testing for replication errors at microsatellite loci in tumors might be helpful in predicting the development of MC in sporadic carcinomas of the distal colon and rectum. Others[10,24] discovered the significant risk factor for developing MC was the presence of synchronous adenoma or carcinoma at the initial operation and the subsequent development of recurring metachronous adenomas. Therefore, colorectal cancer patients with MSI-positive and coexistence of adenoma should be given more rigorous surveillance. Togashi[25] monitored 341 colorectal cancer cases with colonoscopy about 4.6 times in 6.2 years after operation. Twenty-two MCs were detected in 19 cases (5.6%), of these 17 MCs (77%) were less than 1 cm, 14 MCs (64%) occurred within 5 years and 71%(10/14) were early stage cancers. In our study, 12 MCs (55%) were diagnosed in 3 years, 3 MCs were discovered by routine colonoscopy (Dukes A: 2 patients, Dukes B: 1 case) and 9 MCs were diagnosed after the development of symptoms (Dukes B, C, D: 3, 2, 4 respectively). These results might prove that colonoscopy was important after surgery. We suggest that regular postoperative colonoscopic examinations should be performed annually during the first 5 years, then once every 3 years.

The treatment of SC or MC is the same as single colorectal carcinoma, with removal of enough intestines and cleaning of local lymph node. It is suggested that subtotal colectomy with rectoileostomy should be performed for patients with far apart SC, combined with multiple adenomatoid polyps or a familial hereditary history if their general condition suits for operation. Fajobi *et al*.[7] recommended that SC in different lymph drainage areas seemed a justifiable indication for subtotal colectomy. Easson *et al*.[26] considered multiple colon cancer was an important factor for performing subtotal colectomy. While subtotal colectomy could eliminate the need for colonoscopic surveillance, however examining the rectum is still required.

Generally speaking, MPCC develops slowly and their prognosis is acceptable. Chen[12] reported that the 5 -year survivals of patients after radical resection for MPCC did not differ from that of patients with single colorectal cancer. The incidence rate was 54%, 60%, and 62% for "single", SC, MC respectively. Other reports[8,27] displayed similar conclusions. Adloff[3] found patients with SC or single lesions had similar 5-year survival, even when classified by Dukes' stage. Rennert *et al*.[8] reported that survival time of patients with the second tumor in the rectum was shorter than that of a single tumor in the same stage and site. Only the stage of the second tumor was found to influence survival time of patients with metachronous tumors. Welch's result[14] was quite worse. The overall uncorrected 5-year survival rate of MPCC was only 21 percent. In our study, there was no significant difference between SC and index cancer of MC in the 5-year or 10-year survival rate. The 5-year survival rate could reach 39% after second cancer resection. We consider early diagnosis with complete preoperative examination; careful intraoperative exploration and periodic postoperative surveillance and radical resection can increase the survival time of patients with MPCC.

REFERENCES

1 **Cali RL**, Pitsch RM, Thorson AG, Watson P, Tapia P, Blatchford GJ, Christensen MA. Cumulative incidence of metachronous colorectal cancer. *Dis Colon Rectum* 1993; **36**: 388-393

2 **Moertal CG**, Bargen JA, Dockerty MB. Multiple carcinomas of the large intestine a review of the literature and a study of 261 cases. *Gastroenterology* 1958; **34**: 85-98

3 **Adloff M**, Arnaud JP, Bergamaschi R, Schloegel M. Synchronous carcinoma of the colon and rectum: prognostic and therapeutic implications. *Am J Surg* 1989; **157**: 299-302

4 **Lasser A**. Synchronous primary adenocarcinomas of the colon and rectum. *Dis Colon Rectum* 1978; **21**: 20-22

5 **Finan PJ**, Ritchie JK, Hawley PR. Synchronous and 'early' metachronous carcinomas of the colon and rectum. *Br J Surg* 1987; **74**: 945-947

6 **Cunliffe WJ**, Hasleton PS, Tweedle DE, Schofield PF. Incidence of synchronous and metachronous colorectal carcinoma. *Br J Surg* 1984; **71**: 941-943

7 **Fajobi O**, Yiu CY, Sen-Gupta SB, Boulos PB. Metachronous colorectal cancers. *Br J Surg* 1998; **85**: 897-901

8 **Rennert G**, Robinson E, Rennert HS, Neugut AI. Clinical characteristics of metachronous colorectal tumors. *Int J Cancer* 1995; **60**: 743-747

9 **Bulow S**, Svendsen LB, Mellemgaard A. Metachronous colorectal carcinoma. *Br J Surg* 1990; **77**: 502-505

10 **Yamazaki T**, Takii Y, Okamoto H, Sakai Y, Hatakeyama K. What is the risk factor for Metachronous colorectal carcinoma? *Dis Colon Rectum* 1997; **40**: 935-938

11 **Levin B**. "Multiple primary carcinomas of the large intestine"-50 years later. *Cancer* 1998; **83**: 2425-2426

12 **Chen HS**, Sheen-Chen SM. Synchronous and "early" metachronous colorectal adenocarcinoma: analysis of prognosis and current trends. *Dis Colon Rectum* 2000; **43**: 1093-1099

13 **Oya M**, Takahashi S, Okuyama T, Yamaguchi M, Ueda Y. Synchronous colorectal carcinoma: clinico-pathological features and prognosis. *Jpn J Clin Oncol* 2003; **33**: 38-43

14 **Welch JP**. Multiple colorectal tumors. An appraisal of natural history and therapeutic options. *Am J Surg* 1981; **142**: 274-280

15 **Kiefer PJ**, Thorson AG, Christensen MA. Metachronous colorectal cancer. Time interval to presentation of a metachronous cancer. *Dis Colon Rectum* 1986; **29**: 378-382
16 **Zhang YL**, Zhang ZS, Wu BP, Zhou DY. Early diagnosis for colorectal cancer in China. *World J Gastroenterol* 2002; **8**: 21-25
17 **Tate JJ**, Rawlinson J, Royle GT, Brunton FJ, Taylor I. Pre-operative or postoperative colonic examination for synchronous lesions in colorectal cancer. *Br J Surg* 1988; **75**: 1016-1018
18 **Postic G**, Lewin D, Bickerstaff C, Wallace MB. Colonoscopic miss rates determined by direct comparison of colonoscopy with colon resection specimens. *Am J Gastroenterol* 2002; **97**: 3182-3185
19 **Shitoh K**, Konishi F, Miyakura Y, Togashi K, Okamoto T, Nagai H. Microsatellite instability as a marker in predicting metachronous multiple colorectal carcinomas after surgery: a cohort-like study. *Dis Colon Rectum* 2002; **45**: 329-333
20 **Masubuchi S**, Konishi F, Togashi K, Okamoto T, Senba S, Shitoh K, Kashiwagi H, Kanazawa K, Tsukamoto T. The significance of microsatellite instability in predicting the development of metachronous multiple colorectal carcinomas in patients with nonfamilial colorectal carcinoma. *Cancer* 1999; **85**: 1917-1924
21 **Horii A**, Han HJ, Shimada M, Yanagisawa A, Kato Y, Ohta H, Yasui W, Tahara E, Nakamura Y. Frequent replication errors at microsatellite loci in tumors of patients with multiple primary cancers. *Cancer Res* 1994; **54**: 3373-3375
22 **Thibodeau SN**, Bren G, Schaid D. Microsatellite instability in cancer of the proximal colon. *Science* 1993; **260**: 816-819
23 **Ionov Y**, Peinado MA, Malkhosyan S, Shibata D, Perucho M. Ubiquitous somatic mutations in simple repeated sequences reveal a new mechanism for colonic carcinogenesis. *Nature* 1993; **363**: 558-561
24 **Chen F**, Stuart M. Colonoscopic follow-up of colorectal carcinoma. *Dis Colon Rectum* 1994; **37**: 568-572
25 **Togashi K**, Konishi F, Ozawa A, Sato T, Shito K, Kashiwagi H, Okada M, Nagai H. Predictive factors for detecting colorectal carcinomas in surveillance colonoscopy after colorectal cancer surgery. *Dis Colon Rectum* 2000; **43**(10 Suppl): S47-53
26 **Easson AM**, Cotterchio M, Crosby JA, Sutherland H, Dale D, Aronson M, Holowaty E, Gallinger S. A population-based study of the extent of surgical resection of potentially curable colon cancer. *Ann Surg Oncol* 2002; **9**: 380-387
27 **Kaibara N**, Koga S, Jinnai D. Synchronous and metachronous malignancies of the colon and rectum in Japan with special reference to a coexisting early cancer. *Cancer* 1984; **54**: 1870-1874

Edited by Wang XL **Proofread by** Chen WW and Xu FM

PO Box 2345, Beijing 100023, China
Fax: +86-10-85381893
E-mail: wjg@wjgnet.com www.wjgnet.com

World J Gastroenterol 2004;10(14):2140-2144
World Journal of Gastroenterology
 ISSN 1007-9327

• BRIEF REPORTS •

Inhibition of growth and metastasis of human gastric cancer implanted in nude mice by *d*-limonene

Xiao-Guang Lu, Li-Bin Zhan, Bing-An Feng, Ming-Yang Qu, Li-Hua Yu, Ji-Hong Xie

Xiao-Guang Lu, Department of General Surgery, The Fourth Affiliated Hospital of Dalian Medical University, Dalian 116001, Liaoning Province, China
Li-Bin Zhan, Bing-An Feng, Ming-Yang Qu, Li-Hua Yu, Dalian Medical University Molecular Biological Laboratory for Chinese Traditional Medicine, Dalian 116027, Liaoning Province, China
Ji-Hong Xie, Dalian Medical Science Instituteg, Dalian 116001, Liaoning Province, China
Correspondence to: Dr. Xiao-Guang Lu, M.D. Department of General Surgery, Fourth Hospital of Dalian Medical University, Dalian 116001, Liaoning Province, China. dllxg@yahoo.com.cn
Telephone: +86-411-3039179 **Fax:** +86-411-4721582
Received: 2004-02-02 **Accepted:** 2004-02-21

Abstract

AIM: To investigate the effects and mechanism of *d*-limonene on the growth and metastasis of gastric cancer *in vivo*.

METHODS: Metastatic model simulating human gastric cancer was established by orthotopic implantation of histologically intact human tumor tissue into gastric wall of nude mice. One percent *d*-limonene was orally administered at dose of 15 ml/kg every other day for seven weeks. Eight weeks after implantation, tumor weight, inhibition rate, apoptotic index (AI), microvessel density (MVD), vascular endothelial growth factor (VEGF), variation of ultrastructure, and the presence of metastasis were evaluated, respectively, after the mice were sacrificed.

RESULTS: The tumor weight was significantly reduced in 5-FU group (2.55±0.28 g), *d*-limonene group (1.49±0.09 g) and combined treatment group (1.48±0.21 g) compared with the control group(2.73±0.23 g, $P<0.05$). In 5-FU group, *d*-limonene group, combined treatment group, the inhibition rates were 2.60%,47.58% and 46.84% and 0, respectively; AI was (3.31±0.33)%, (8.26±1.21)%, (20.99±1.84)% and (19.34±2.19)%, respectively; MVD was (8.64±2.81), (16.77±1.39), (5.32±4.26) and (5.86±2.27), respectively; VEGF expression was (45.77±4.79), (41.34±5.41), (29.71±8.92) and (28.24±8.55), respectively. The incidences of peritoneal metastasis also decreased significantly in 5-FU group(77.8%), *d*-limonene group (20.0%) and combined group (22.2%) compared with control group (100%) versus 62.5%,30% and 22.2%) ($P<0.05$). Liver metastasis was also inhibited and the incidences decreased significantly in 5-FU group, *d*-limonene group and combined group than that in control group (87.5% *vs* 55.5%, 20.0% and 22.2% respectively) ($P<0.05$). The incidence of ascites in control group, 5-FU group, *d*-limonene group and combined group was 25.0%, 22.2%, 0, 0, respectively and 12.5%, 11.1% 0, 0, with respect to the metastasis rate to other organs.

CONCLUSION: *d*-limonene has antiangiogenic and proapoptotic effects on gastric cancer, thereby inhibits tumor growth and metastasis. Combination of *d*-limonene with cytotoxic agents may be more effective.

Lu XG, Zhan LB, Feng BA, Qu MY, Yu LH, Xie JH. Inhibition of growth and metastasis of human gastric cancer implanted in nude mice by *d*-limonene. *World J Gastroenterol* 2004; 10 (14): 2140-2144
http://www.wjgnet.com/1007-9327/10/2140.asp

INTRODUCTION

d-limonene is a monoterpene compound. In recent years, it was used for prevention and cure of various animal tumor models induced by chemical carcinogen and was proved to have anti-cancer activities[1-7]. Our previous study also suggested that *d* -limonene can inhibit the growth of human gastric cancer cell *in vitro* through a mechanism of inducing the apoptosis of tumor cells[8]. To make a further understanding of the anti-cancer effects and mechanism of *d*-limonene *in vivo*, an orthotopic transplantation model of gastric cancer in nude mice was employed. The *d*-limonene emulsion was administrated to investigate its inhibition effects on the growth and metastasis of gastric cancer dynamically, which will be the theoretical basis for the clinical application of *d* -limonene.

MATERIALS AND METHODS

Materials

Experimental animals Forty male BALB/c nu/nu nude mice, purchased from Chinese Medical University, were raised under the SPF (specific pathogen free) condition for a week to adapt the surroundings before the initiation of the experiment.

Tumor tissues Gastric cancer cell line BGC-823 was obtained from Cell Research Institute (Shanghai, China). A 0.2 mL of cell suspension (2×10^6 cells) was subcutaneously injected into the anterior axilla of nude mice to form the entity of cancer. When the tumor grew to a diameter of 2-2.5 cm, the mouse was sacrificed to dissect the neoplasm and the capsule of tumor was removed and kept in saline containing 100 U /mL penicillin, 100 U/mL streptomycin (pH 7.2). Pieces of fresh tumor tissue (1 mm^3) near the margin were inoculated to another mouse by puncture method. The above procedure was repeated for 5 times and the last generation of the tumor tissue was be used for orthotopic transplantation.

Animal model Before transplantation, mice bearing tumor were killed. Then the tumor was dissected and put into saline containing penicillin (100 U/mL) and streptomycin (100 U/mL) aseptically. Pieces of intact, fish-meat-like tumor tissue of 3 mm^3 in diameter from margin were prepared after the removing of tumor capsule. Mice anesthetized by the thialisobumalnatrium (40 mg/kg) injected into abdominal cavity were sterilized with caseoiodine on skin of abdomen and a transverse incision was made in left upper quadrant. After the exposure of greater curvature of stomach, the serosa and muscular layer were incised. Then, tumor tissues were transplanted under serosa of stomach by means of suture and embedding. Stomach was brought into abdominal cavity; the incision in belly was sutured delaminatedly. The whole operation procedure followed the doctrine of aseptic manipulation.

Drugs and groups *d*-limonene with 97% purity (product

number: 183164) was purchased from Sigma Company (USA). It was prepared as 10 g/L lecithin emulsion by Dalian Medical Science Institute. Mice were randomly divided into 4 groups: control group, 5-FU group, *d*-limonene group, and *d*-limonene+5-FU group and administrated with saline (0.3 mL/d, gastric perfusion), 5-FU (30 mg/kg/d, intraabdominal injection), D-limonene (15 mL/kg/d, gastric perfusion), and 5-FU (30 mg/kg/d, intraabdominal injection)+ *d*-limonene (15 ml/kg.d, gastric perfusion), respectively for 7 wk. The body mass and abdominal circumstances were measured on the 7th, 14th, 21st, 28th, 35th, 42nd, 49th d after transplantation and the status of eating, drinking and defecation of mice were recorded. The dying mice were executed and necropsy was performed. In the 8th wk, all the mice were killed; the neoplasm was resected and weighted; and the occurrence of distant metastasis and ascites were examined.

Methods

The measurement of tumor weight and inhibition rate of tumor growth Mice were killed by dislocation of cervical vertebra, the tumor weight was measured and the tumor inhibition rate was calculated. inhibition rate=[(tumor weight of control group-tumor weigh of treated groups)/weight of control]×100%.

The occurrence of metastasis and ascites in nude mice The metastasis of gastric cancer was examined in abdominal cavity, peritoneum and liver. Tumor specimens were fixed in neutral formaldehyde, dehydrated by dimethylbenzene and embedded in paraffin for the hematoxylin and eosin (HE) staining and immunohistochemistry. The characters and volume of ascites were recorded.

Apoptotic index (AI) TUNEL method was used to detect the apoptosis of tumor cell. The sections were fixed and embedded as usual. TUNEL test kit was purchased from Roche Company. DNase I (1 mg/mL) was used to digesting the positive control specimen for 10 min before being put into TUNEL response mixture. Only label liquor was added into the negative control response mixture. Cells with brown or yellow nuclei were assumed as apoptotic cells. the number of apoptotic cells and total cancer cells were counted under light microscope at 400×magnification in 5 fields of vision and the average values were used for the calculation of apoptosis index (AI) according to the following formula: AI=(apoptotic cells/total cancer cells) ×100%.

Microvessel density assay The polyclonal antibody for factor □-related antigen (F□-RAg, Santa Cruz Biotechnology, Inc, USA) was selected to detect the microvessel density in paraffin embedded tumor sections by immunohistochemical method according to the manufacturer's instruction . Result determination: Sections were screened at 40× magnification under a light microscope to identify three regions with the highest MVD. Then, blood vessels stained brown by antibody for F□-RAg was counted at 200×magnification. For the determination of microvessels, first of all, the hemorrhage area and marginal region were eliminated. Those brown-stained endothelial cells or cell cluster that had interspaces with microvessel, cancer cells and connective tissue were regarded as a micro vessels. The average value of the three regions was regarded as MVD.

Imunohistochemical assay of VEGF Imunohistochemical staining was performed with mouse monoclonal antibody specific for human VEGF (C1, Santa Cruz Biotechnology, Inc, USA) in a dilution of 1:100 according to SP method specification. The presence of brown or yellow granules in plasma or nucleus was regarded as positive staining for VEGF protein expression. The sum of positive cells number was calculated in five fields per slide at 200× magnification under light microscope. Results were ratified by fluorescence microscope and colorful microscopic figure analysis system (OLYMPUS BX51TR, Image-Pro Plus , Analysis Software).

Statistical analysis

Tumor weight, AI, MVD and VEGF were expressed as the mean±SD. Comparison between groups was performed using analysis of variance; Differences of the metastasis in peritoneum, liver and other organs and the occurrence of ascites were examined by χ^2 test (P<0.05 was considered statistically significant).

RESULTS

The influence of d-limonene on the general condition of tumor-bearing mice

At the end of the 7th wk, two mice-bearing tumor from control group, one from 5-FU group and one from combined group died of exhaustion while none from *d*-limonene group. During the whole process of the experiment, only one mouse in 5-FU group was found with loose stools, and no passage of bloody stools was found in any groups. Compared with the control and 5-FU group in which mice were found emaciation, inactive and lassitude, mice in *d*-limonene group and combined group had better appetite and increased body mass although statistically had no difference.

Influence of d-limonene on orthotopic transplanted tumor weight and tumor inhibition rate

At necropsy, xenografts of gastric cancer were found in each groups of nude mice. The transplanted tumor entity was pink in color, ellipse or round in shape, with nodosity in surface and necrosis in central parts, and was confirmed as adenocarcinoma by pathological section. Compared with the control group, the tumor weight of mice in *d*-limonene group and combined group were decreased significantly (P<0.05). Moreover, the inhibition effects of *d*-limonene or the combined effects of *d*-limonene and 5-FU on the growth of gastric cancer were more significant than that of 5-FU (Table 1).

Effects of d -limonene on tumor cell morphology and ultrastructure

Morphologically, tumor cells in the control group were bigger, ellipse, with red plasma and big, deep stained nuclei. A clear imbalance ratio of nucleus to plasma was found also. No significant difference was observed between the control and 5-FU group. While in *d*-limonene group and combined group, relatively small tumor cells with vacuoles in plasma and clouding nucleus were observed in which the ratio of nucleus to plasma was relatively normal.

Table 1 Inhibition effects of *d*-limonene on growth of orthotopic transplanted gastric tumor (mean±SD)

Groups	*n*	Tumor mass (g)	Inhibition rate (%)	AI (%)	MVD (*n*)	VEGF(%)
Control	8	2.69±0.32	0	3.31±1.44	18.64±2.81	45.77±4.79
5-FU	9	2.62±0.35	2.60	8.26±1.21[a]	16.77±1.39	41.34±5.41
d-limonene	10	1.41±0.58[ac]	47.58[ac]	20.99±2.84[ac]	5.32±4.26[ac]	29.71±8.92[ac]
Combined	9	1.43±0.51[ad]	46.84[ac]	19.34±3.19[ac]	5.86±2.27[ac]	28.24±8.55[ac]

[a]P<0.05 *vs* control group; [c]P<0.05 *vs* 5-FU group.

The major morphological changes of cancer cells in D-limonene and combined group were the shrinkage of cell, the condensation of cytoplasm, the aggregation of ribosome and mitochondrion, the occurrence of nuclear fragmentation, the peripheral masses of condensed chromatin. Apoptotic bodies derived from the shedding of condensed masses were found to be degradated by surrounding phagocytes and formed vacuoles in cytoplasm. Fusiform shape, morphological irregular and karyomegaly cancer cells were observed in control and 5-FU group with tight binding between cells, imbalance ratio of nucleus to plasma and the maldistribution of chromatin. But no obviously changes in cell morphology were detected.

Effects of d-limonene on apoptosis of cancer cell

Results of TUNEL demonstrated that apoptotic cells with yellow nucleus were seen occasionally in control group and 5-FU group while piles of apoptotic cells were observed in *d*-limonene and combined group. There was a significantly difference in AI in *d*-limonene and combined group compared to the control and 5-FU group ($P<0.05$) (Table 1, Figures 1-4).

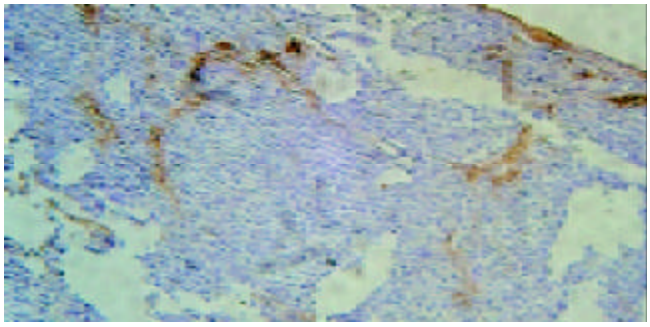

Figure 1 Control group FVIII-RAg with SP method. ×100.

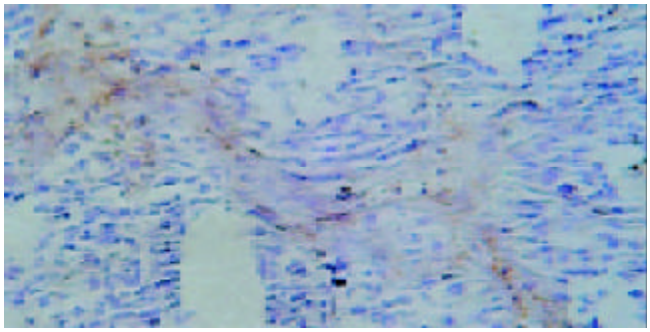

Figure 2 5-FU group FVIII-RAg with SP method. ×200.

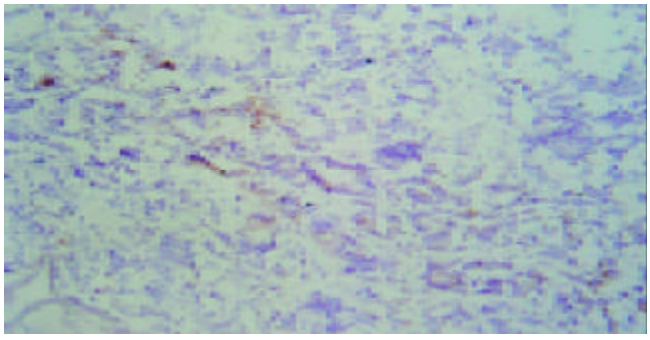

Figure 3 *d*-limonene group FVIII-RAg with SP method. ×100.

The influence of d-limonene on MVD of orthotopic transplanted tumor

Under light microscope, the intensive brown-staining microvessels on stomach wall was observed without integrated basement membrane in the control group. Compared with the control and 5-FU group, almost no microvessels was found in the tumor of *d*-limonene and combined group for the cancer cells were in dormancy status, and the MVD of those two groups was statistically lower than that of the control and 5-FU group (Table 1, Figures 5-8).

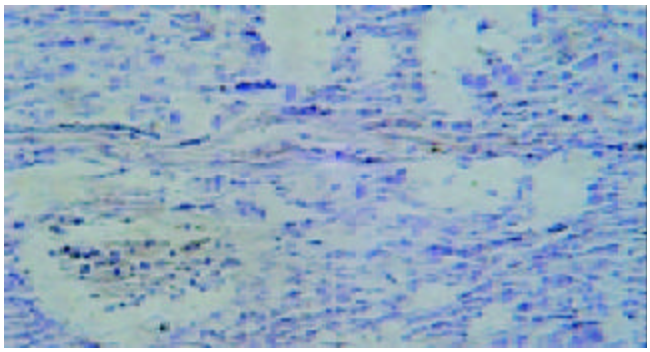

Figure 4 Combined group FVIII-RAg with SP method. ×100.

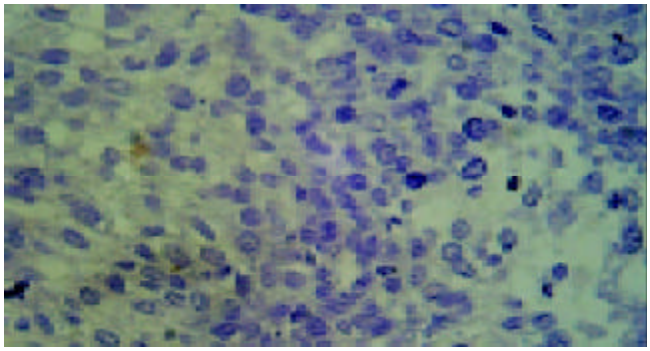

Figure 5 Control group TUNEL. ×400.

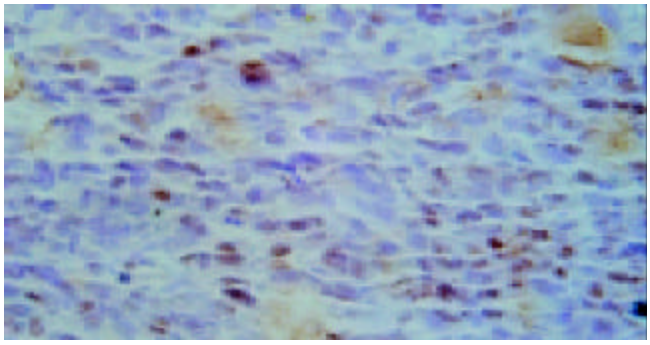

Figure 6 5-FU group TUNEL. ×400.

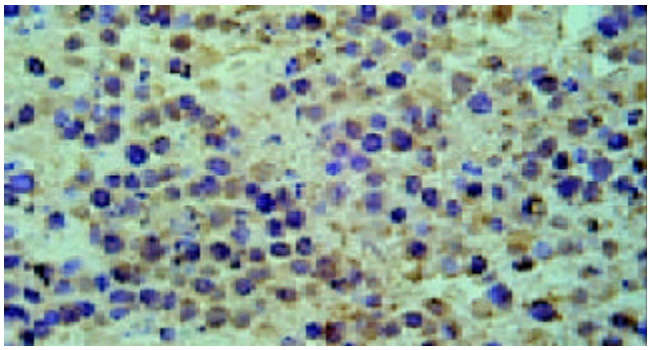

Figure 7 *d*-limonene group TUNEL. ×400.

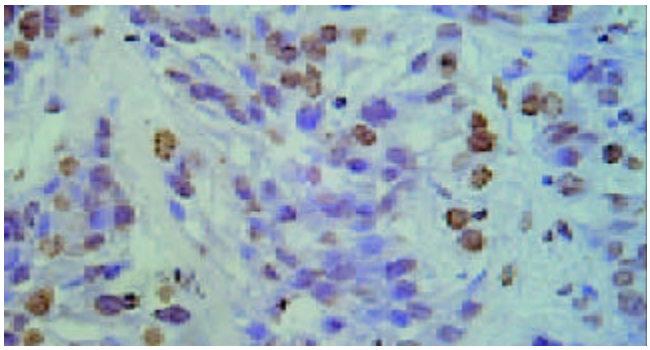

Figure 8 Combined group TUNEL. ×400.

Inhibitory effects of d-limonene on metastasis of gastric cancer

The metastasis rate of gastric cancer to peritoneum (regional lymph node) was to 100% in the control group and the metastasis rates in other groups are displayed in Table 2. the metastasis to liver, peritoneum and other organs of gastric cancer and the formation of ascites were significantly inhibited in *d*-limonene and combined groups ($P<0.05$) while no statistical inhibitory effects on the metastasis to liver and peritoneum were observed in 5-FU group ($P>0.05$, Table 2).

Table 2 The Inhibitory effects of *d*-limonene on orthtopic transplanted gastric cancer (%)

Group	*n*	Peritoneum metastasis	Liver metastasis	Ascites	Metastasis to other organs
Control	8	8(100.0)	7(87.5)	2(25.0)	1(12.5)
5-FU	9	7(77.8)	5(55.5)	2(22.2)	1(11.1)
D-limonene	10	2(20.0)[ac]	2(20.0)[ac]	0[ac]	0
Combined	9	3(33.3)[ac]	2(22.2)[ac]	0[ac]	0

[a]$P<0.05$ *vs* control group; [c]$P<0.05$ *vs* 5-FU group.

DISCUSSION

Gastric cancer is the most common malignant tumor in digestive system. The cure rate of gastric cancer was increased year by year with the progress of surgical technique, chemotherapy and other means. But a five-year survival rate is still wandered below 10%, especially in middle or late phase patients[10]. Thus, to find an effective adjuvant chemotherapy drug became the focus of gastric cancer therapy besides emphasizing surgical operation.

Limonene (1-methyl-4-isopropyl-cyclohexene) is the essential component in citrus oil. *d*-limonene, the most common isomer of limonene, is a kind of monoterpene component. It has the ability of anti-oxygenation, anti-inflammation and drainage for gallstone. The anti-cancer activity of *d*-limonene was found recently. Therefore, *d*-limonene has been applied to precaution and treatment in chemical-induced animal model, such as colon cancer, breast cancer, gastric cancer, pancreatic cancer and hepatic cancer with promising results[1-7]. Most of those studies focus in the chemoprophylaxis of tumor. Our results demonstrated that in *d*-limonene and combined group, the tumor weight of xenograft was decreased drastically, the metastasis to liver, peritoneum and the occurrence of ascites were inhibited significantly compared with the control group. Thus, an inhibition effect of *d*-limonene on the growth and metastasis of gastric cancer cells was ratified. Taking the results of TUNEL assay into consideration, we found the main mechanism underlying the inhibition effects of *d*-limonene was to induce the apoptosis of cancer cells.

At present, it is thought that a phenotype change from no-vascular period to angiogenesis stage exists during the growth of tumor. In no-vascular period, the velocity of cancer cells apoptosis and proliferation maintain a dynamic balance and the tumor may survive for months or even years without the presence of metastasis. But the alterations of some important factors, such as heredity cause, over-expression of proangiogenic factors originated from cancer cells or down-regulation anti-angiogenic factors expressed by body tissues or cancer cells, the switch for tumor angiogenesis thereby activating and leading to vascularization of tumor. Once the tumor vascular is formed, the growth speed of tumor will be increased and the invasive growth and metastasis will be induced.

Microvessel density (MVD), is usually used to evaluate the vascularization level of tumor[10]. A large amount of experiments and clinical research results showed that MVD had a close relationship with the prognosis of almost all malignant tumors, a higher MVD suggested the lower differentiation and the higher reoccurrence and metastasis incidence[11]. We demonstrated that compared with control and 5-FU group, tumor MVD in *d*-limonene and combined group was decreased significantly, suggesting a inhibitive effect of *d*-limonene on tumor angiogenesis.

Although the mechanisms involved in tumor angiogenesis have not been understood exactly, the effect of VEGF on vascularization has been conformed. VEGF, a specific mitogen for vascular endothelial cells was isolated from follicular cell plasma of cattle and considered as the most important angiogenic factor of metastatic tumor[12-14]. The expression of VEGF was found very low in normal adult tissues. Once initiated in pathologic status of tumor, the angiogenesis was induced and promoted drastically by VEGF and resulted in the increase of MVD. Among vascular growth factors, VEGF was the only one to stimulate the proliferation of tumor endothelial cell and to induce the vascularization of tumor directly[15]. As the newly formed vessels may provide tumor with oxygen, nutrition, the growth of tumor will be invasive and uncontrollable[16]. It was reported that the over expression of VEGF had close relationship with tumor metastasis and poor prognosis. The invasion of blood vessels and lymph nodes has been often observed in patients with enhanced VEGF expression, which will result in the rapidly malignant change of tumor, easily relapse and short survival period after surgical operation. Here we showed that relatively high level of VEGF in the tumor of control and 5-FU group, especially in the areas around vessels, while notably decreased expression of VEGF in *d*-limonene and combined group. Thus, a positive correlation of VEGF expressiono with increased MVD was ratified, suggesting the anti-angiogenic mechanism of *d*-limonene via down-regulation of VEGF. Moreover, we found that the anti-cancer target of 5-FU might not on the inhibition of neovascularization.

5-fluorouracil, an antimetabolite pyramine, has been used as traditional chemitherapeutic drug for more than 40 years. For the anti-cancer target of 5-FU lies in the inhibition of thymidylic acid synthetase to prevent DNA synthesis but not the interference of tumor angiogenesis[17], no satisfied cure effect was obtained in our experiment. As to *d*-limonene, preventing tumor angiogenesis and increasing tumor cells apoptosis are the main anti-cancer mechanisms, which may diminish the incidence of drug resistance mutation for its character of physiological cell death. The effectiveness, none-toxicity, and lower drug resistance of *d*-limonene were ratified for a better eating, activity and living ability in *d*-limonene and combined groups than in control group within the 7-wk experiment. No statistical difference in body weight was observed among four groups for increased tumor weight and the formation of ascites in control and 5-FU group.

Further studies need to elucidate the apoptotic mechamisms of *d*-limonene before its clinical application.

REFERENCES

1 **Uedo N,** Tatsuta M, Iishi H, Baba M, Sakai N, Yano H, Otani T. Inhibition by D-limonene of gastric carcinogenesis induced by N-methyl-N'-nitro-N-nitrosoguanidine in Wistar rats. *Cancer Lett* 1999; **137**: 131-136

2 **Broitman SA,** Wilkinson J 4th, Cerda S, Branch SK. Effects of monoterpenes and mevinolin on murine colon tumor CT-26 *in vitro* and its hepatic "metastases" *in vivo*. *Adv Exp Med Biol* 1996; **401**: 111-130

3 **Kaji I,** Tatsuta M, Iishi H, Baba M, Inoue A, Kasugai H. Inhibition by d-limonene of experimental hepatocarcinogenesis in Sprague-Dawley rats does not involve p21(ras) plasma membrane association. *Int J Cancer* 2001; **93**: 441-444

4 **Witschi H,** Uyeminami D, Moran D, Espiritu I. Chemoprevention of tobacco-smoke lung carcinogenesis in mice after cessation of smoke exposure. *Carcinogenesis* 2000; **21**: 977-982

5 **Stratton SP,** Dorr RT, Alberts DS. The state-of-the-art in chemoprevention of skin cancer. *Eur J Cancer* 2000; **36**: 1292-1297

6 **Guyton KZ,** Kensler TW. Prevention of liver cancer. *Curr Oncol Rep* 2002; **4**: 464-470

7 **Nakaizumi A,** Baba M, Uehara H, Iishi H, Tatsuta M. d-limonene inhibits N-nitrosobis (2-oxopropyl) amine induced hamster pancreatic carcinogenesis. *Cancer Lett* 1997; **117**: 99-103

8 **Lu XG**, Feng BA, Zhan LB, Yu ZH. D-limonene induces apoptosis of gastric cancer cells. *Zhonghua Zhongliu Zazhi* 2003; **25**: 325-327

9 **Sun X,** Mu R, Zhou Y, Dai X, Qiao Y, Zhang S, Huangfu X, Sun J, Li L, Lu F. 1990-1992 mortality of stomach cancer in China. *Zhonghua Zhongliu Zazhi* 2002; **24**: 4-8

10 **Fanelli M,** Locopo N, Gattuso D, Gasparini G. Assessment of tumor vascularization: immunohistochemical and non-invasive methods. *Int J Biol Markers* 1999; **14**: 218-231

11 **El-Assal ON,** Yamanoi A, Soda Y, Yamaguchi M, Igarashi M, Yamamoto A, Nabika T, Nagasue N. Clinical significance of microvessel density and vascular endothelial growth factor expression in hepatocellular carcinoma and surrounding liver: possible involvement of vascular endothelial growth factor in the angiogenesis of cirrhotic liver. *Hepatology* 1998; **27:** 1554-1562

12 **Seo Y,** Baba H, Fukuda T, Takashima M, Sugimachi K. High expression of vascular endothelial growth factor is associated with liver metastasis and a poor prognosis for patients with ductal pancreatic adenocarcinoma. *Cancer* 2000; **88**: 2239-2245

13 **Shi H,** Xu JM, Hu NZ, Xie HJ. Prognostic significance of expression of cyclooxygenase-2 and vascular endothelial growth factor in human gastric carcinoma. *World J Gastroenterol* 2003; **9**: 1421-1426

14 **Ren J,** Dong L, Xu CB, Pan BR. The role of KDR in the interactions between human gastric carcinoma cell and vascular endothelial cell. *World J Gastroenterol* 2002; **8**: 596-601

15 **Risau W.** What, if anything, is an angiogenic factor? *Cancer Metastasis Rev* 1996; **15**: 149-151

16 **Folkman J.** The influence of angiogenesis research on management of patients with breast cancer. *Breast Cancer Res Treat* 1995; **36:** 109-118

17 **Rose MG,** Farrell MP, Schmitz JC. Thymidylate synthase: a critical target for cancer chemotherapy. *Clin Colorectal Cancer* 2002; **1**: 220-229

Edited by Kumar M and Xu FM

PO Box 2345, Beijing 100023, China
Fax: +86-10-85381893
E-mail: wjg@wjgnet.com www.wjgnet.com

World J Gastroenterol 2004;10(14):2145-2146
World Journal of Gastroenterology
 ISSN 1007-9327

• BRIEF REPORTS •

Clinical evaluation of radiotherapy for advanced esophageal cancer after metallic stent placement

You-Tao Yu, Guang Yang, Yan Liu, Bao-Zhong Shen

You-Tao Yu, Guang Yang, Yan Liu, Bao-Zhong Shen, Department of Radiotherapy, Tumor Hospital of Harbin University, Harbin 150040, Heilongjiang Province, China
Correspondence to: Bao-Zhong Shen, Department of Radiotherapy, Tumor Hospital of Harbin University, Harbin 150040, Heilongjiang Province, China. shenbzh@hotmail.com
Telephone: +86-451-88513575 **Fax:** +86-451-86623347
Received: 2003-11-12 **Accepted:** 2004-01-08

Abstract

AIM: To evaluate the therapeutic effect of radiotherapy for esophageal cancer after expandable metallic stent placement.

METHODS: Ten cases of advanced esophageal cancer were evaluated, 7 having complete obstruction and 3 with digestive-respiratory fistula. Ten nitinol stents were placed at the site of stenosis. Patients were treated with a total dose of 1 200 cGy divided into 3 fractions of 400 cGy 4-7 d after stents placement.

RESULTS: All the 10 stents were placed successfully at one time. After radiotherapy for advanced esophageal cancer, the survival period of the cases ranged from 14 to 22 mo, with a mean survival of 17 mo. No re-stenosis occurred among all the 10 cases.

CONCLUSION: Stent placement combined with radiotherapy for esophageal cancer is helpful to prolong patients' survival and reduce occurrence of re-stenosis.

Yu YT, Yang G, Liu Y, Shen BZ. Clinical evaluation of radiotherapy for advanced esophageal cancer after metallic stent placement. *World J Gastroenterol* 2004; 10(14): 2145-2146
http://www.wjgnet.com/1007-9327/10/2145.asp

INTRODUCTION

Radiotherapy for esophageal cancer is a relatively effective treatment. However, esophageal obstruction and esophageal stenosis due to inoperable cancer, as serious complications of esophageal cancer, are directly life-threatening and contraindicatory to radiotherapy for esophageal cancer. Inserting membrane-covered esophageal stents as an effective conservative and palliative treatment to expand the stent at the stenosis site due to cancer and obstruct the digestive fistulas is a currently widely-used therapy, which can dramatically alleviate obstruction and enhance patients' quality of life by enabling oral ingestion in patients with obstruction due to late cancer[1-4]. With radiotherapy after membrane-covered esophageal stents placement for advanced esophageal cancer, we successfully overcame the contraindication of radiotherapy for esophageal cancer and achieved a quite satisfactory short-term effect[5,6].

MATERIALS AND METHODS

Materials

Ten cases of esophageal cancer (8 males, 2 females, aging from 58 to 85 years) were studied. Esophagoscopic examination indicated that 9 of the cases were squamous carcinoma and one was adenocarcinoma. Barium contrast radiography and meglucamine diatrizoate radiography showed that the site of stenosis due to cancer ranged from 6 to 12 cm in length, with an average length of 8 cm, and the width of the esophageal lumen at the site of stenosis was less than 2 mm, which had been hard for liquid diet to pass for more than 2 wk. Seven of the cases had complete obstruction and 3 had digestive-respiratory fistulas. Physical examination showed that 9 of them had no carcinomatous distant metastasis and 1 case had carcinomatous metastasis to unilateral lung.

Methods

Stent placement Stents to be placed were homemade or imported silicone-covered nitinol memory alloy mesh stents, 2 cm in diameter and 8, 10, 12 cm in length, respectively, and bell-mouthed at one or both ends. Patients should take gentamicin orally, 160 000 units each time, 4-5 times per day before the therapy and stop eating and drinking 2 h before the placement. In accordance with the stenosis length shown by esophageal radiography, the stent of proper length was selected, placed and released along the site of stenosis by endoesophageal stent introducer under the guidance of the peroral guide wires, leaving both ends of the stent surpassing 1-2 cm respectively. After replacement, patient was advised to drink adequate warm water, making the stent expand properly. One week after the placement, a reexamination was carried out through upper digestive tract fluoroscopy with barium to see how unobstructed the stent was and an X-ray plane film was taken to locate the stent, measure its length and width, fix reference point, set irradiation dose and draw the related dose curve.

Endoesophageal irradiation Irradiation was performed 4-7 d after the stent was properly placed. First, the balloon catheter was inserted to the site of the lesion. Second, air was pumped into the saccule to expand it and fix it inside the stent. Third, the location of the saccule was confirmed through fluoroscopy and spot film. And finally, irradiation was performed according to the mark of the reference point fixed through measurement with the total dose of 1 200 cGy divided into three 400 cGy doses.

RESULTS

In all the 10 cases, the stents were all placed successfully once and fixed properly. Of all the 10 stents, 7 (four 8 cm, two 10 cm and one 12 cm in length) were homemade and 3 (two 10 cm and one 8 cm in length) were imported and all could expand properly, through which contrast medium could pass smoothly after placement. Esophageal fistulas in three cases were obstructed immediately after insertion and the patients could begin to take semiliquid diet 4 h afterwards. Reexaminations were performed through radiography 4 d after insertion, and it indicated that the contrast medium could go through the stents smoothly, that the stents did not displace and the esophageal fistulas were obstructed. So, patients could take food normally without dysphagia. After stents placement, 3 cases had retrosternal

foreign body sensation and retrosternal pain, which disappeared within 4-6 d. After endoesophageal radiotherapy, the survival period of the cases ranged from 14 to 22 mo, with a mean survival period of 17 mo. Of all the 10 cases, no endogenous stenosis recurred during the survival period.

DISCUSSION

Radiotherapy for esophageal cancer after esophageal stent placement effectively solved this contraindication of endoesophageal therapy and the problem of stenosis recurrence after stent placement. Esophageal stent insertion enhanced the life quality of patients with advanced esophageal cancer in a quick and effective way in that it remarkably improved the patients' nutrition absorption and constitution by enabling them to take food orally and it completely eliminated the symptoms such as coughing while eating or drinking by effectively obstructing the digestive-respiratory fistulas, which also alleviated the patients' psychological pressure and greatly comforted them. It enlarged the indication scope of radiotherapy for esophageal cancer by turning the former contraindication into indication. The stent inserted expanded the stenosis site and made it possible for brachytherapeutic treatment and radioactive source to pass easily and eventually dramatically prolonged the patients' survival period[7,9-18]. No stenosis recurred in the 10 cases under our treatment during their survival period, which, in contrast to the 5% stenosis reoccurrence rate in other patients under our treatment who had stents placement without radiotherapy, marked a great decrease in occurrence of re-stenosis[8]. Radiotherapy for esophageal cancer prevented the stents from being obstructed by the overgrowth of tumor, alleviated the patients' sufferings and raised their life quality. After the stents were properly placed, radiography was performed and film was spotted, through which the width of the stents expansion was measured. According to the width after calculation, the esophagus was expanded by the stents, the diameter of the balloon catheter and the reference point were fixed, and the optimal internal irradiation dose curve was designed. A comparison of the dose curves indicated that, after the expansion of the stents, the irradiation dosage over the esophageal mucosa was decreased, with the dose gradient homogeneous and small, which prevented the esophageal mucosa from being unnecessarily harmed while effectively inhibited the overgrowth of esophageal mucosa and the surface tumor, and insured the pathological center to receive therapeutic dose of irradiation. Experiments showed that the refraction and diffraction of the irradiation ray against the metallic stents could be neglected when the radioactive source was more than 5 mm away from the metallic stents. Our results of the clinical research seem to indicate that radiotherapy for esophageal cancer after esophageal stents placement is very helpful in treatment of advanced esophageal cancer.

REFERENCES

1 **Knyrim K**, Wagner HJ, Bethge N. A controlled trial of an expansile metal stent for palliation of esophageal obstruction due to inoperable caner. *N Eng J Med* 1993; **329**: 1302-1303
2 **Nelson DB**, Axelrad AM, Fleischer DE, Koazarek RA, Silvis SE. Silicone-covered wallstent prototypes for palliation of malignant esophageal obstruction and digestive-respiratory fistulas. *Gastrointest Endosc* 1997; **45**: 31-37
3 **Decker P,** Lippler J, Decker D, Hirner A. Use of the Polyflex stent in the palliative therapy of esophageal carcinoma: results in 14 cases and review of the literature. *Surg Endosc* 2001; **15**: 1444-1447
4 **Morgan R,** Adam A. The radiologist's view of expandable metallic stents for malignant esophageal obstruction. *Gastrointest Endosc Clin N Am* 1999; **9**: 431-435
5 **Zhong J,** Wu Y, Xu Z, Liu X, Xu B, Zhai Z. Treatment of medium and late stage esophageal carcinoma with combined endoscopic metal stenting and radiotherapy. *Chin Med J* 2003; **116**: 24-28
6 **Funami Y**, Tokumoto N, Miyauchi H, Kuga K, Sato S. Improvement of oral ingestion in patients with inoperable esophageal cancer treated with radiotherapy, chemotherapy and insertion of a self-expanding nitionol stent. *Dis Esophagus* 1999; **12**: 289-292
7 **Bethge N**, Sommer A, Vakil N. Treatment of esophageal fistulas, with a new polyurethane-covered,self-expanding mesh stent: A prospective study. *Am J Gastroenterol* 1995; **90**: 2143-2146
8 **Schoefl R**, Winkelbauer F, Haefner M, Poetzi R, Gangl A, Lammer J. Two cases of fractured esophageal nitinol stents. *Endoscopy* 1996; **28**: 518-520
9 **Olsen E**, Thyregaard R, Kill J. Esophageal expanding stent in the management of patients with nonresectable malignant esophageal of cardiac neoplasm: a prospective study. *Endoscopy* 2001; **1**: 3-6
10 **Williamson JF**, Li Z. Monte Carlo aided dosimetry of the microselectron pulsed and high dose-rate ^{192}Ir sources. *Med Phys* 1995; **22**: 809-819
11 **Ciesielski B**, Reinstein LE, Wielopolski L, Meek A. Doseenhancement in buildup region by lead, aluminum and Lucite absorbers for 15 MV photon beam. *Med Phys* 1989; **16**: 609-613
12 **Kawrakow I**. Accurate condensed history Monte Carlo simulation of electron transport.I.EGSnrc, the new EGS4 version. *Med Phys* 2000; **27**: 485-498
13 **Knyrim K**, Wagner HJ, Bethge N, Keymling M, Vakil N. A controlled trial of an expansile metal stent for palliation of esophageal obstruction due to inoperable cancer. *N Engl J Med* 1993; **329**: 1302-1307
14 **Mayoral W,** Fleischer D, Salcedo J, Roy P, Al-Kawas F, Benjamin S. Nonmalignant obstruction is a common problem with metal stents in the treatment of esophageal cancer. *Gastrointest Endosc* 2000; **51**: 556-559
15 **Wang MQ,** Sze DY, Wang ZP, Wang ZQ, Gao YA, Dake MD. Delayed complications after esophageal stent placement for treatment of malignant esophageal obstructions and esophagorespiratory fistulas. *J Vasc Interv Radiol* 2001; **12**: 465-474
16 **Davies N,** Thomas HG, Eyre-Brook IA. Palliation of dysphagia from inoperable oesophageal carcinoma using Atkinson tubes or self-expanding metal stents. *Ann R Coll Surg Engl* 1998; **80**: 394-397
17 **Conio M,** Caroli-Bosc F, Demarquay JF, Sorbi D, Maes B, Delmont J, Dumas R. Self-expanding metal stents in the palliation of neo-plasms of the cervical esophagus. *Hepatogastroenterology* 1999; **46**: 272-277
18 **Sandha GS,** Marcon NE. Expandable metal stents for benign esophageal obstruction. *Gastrointest Endosc Clin N Am* 1999; **9**: 437-446

Edited by Chen WW **Proofread by** Zhu LH and Xu FM

PO Box 2345, Beijing 100023, China
Fax: +86-10-85381893
E-mail: wjg@wjgnet.com www.wjgnet.com

World J Gastroenterol 2004;10(14):2147-2149
World Journal of Gastroenterology
 ISSN 1007-9327

• BRIEF REPORTS •

Relationship between microvessel density and telomerase activity in hepatocellular carcinoma

Yun-Feng Piao, Min He, Yang Shi, Tong-Yu Tang

Yun-Feng Piao, Yang Shi, Tong-Yu Tang, Department of Gastroenterology, First Hospital of Jilin University, Changchun 130021, Jilin Province, China
Min He, Comprehensive Department of Infection, Changchun Infectious Hospital, Changchun 130021, Jinlin Province, China
Correspondence to: Dr. Yang Shi, Department of Gastroenterology, First Hospital of Jilin University, No.1 Xinmin Road, Changchun 130021, Jilin Province, China. shiyangwhy@163.com
Telephone: +86-431-5612242 **Fax:** +86-431-5612542
Received: 2004-02-21 **Accepted:** 2004-03-12

Abstract

AIM: To study the relationship between microvessel density (MVD), telomerase activity and biological characteristics in hepatocellular carcinoma (HCC).

METHODS: S-P immunohistochemical method and telomeric repeat amplification protocol (TRAP) were respectively used to analyze the MVD and telomerase activity in 58 HCC and adjacent normal tissues.

RESULTS: The MVD in HCC with metastasis, lower differentiation or without intact capsule was significantly higher than that in HCC with intact capsule, higher differentiation, or without metastasis. While MVD had no relationship with tumor size, hepatic virus infection and other clinical factors. Telomerase activity was related to differentiation degree, but not to tumor size or histological grade. MVD in HCC with telomerase activity was higher than that in HCC without telomerase activity.

CONCLUSION: MVD and telomerase activity may serve as diagnostic criteria of HCC in earlier stage. Meanwhile, there may be a cooperative effect between MVD and telomerase on the growth and metastasis of HCC.

Piao YF, He M, Shi Y, Tang TY. Relationship between microvessel density and telomerase activity in hepatocellular carcinoma. *World J Gastroenterol* 2004; 10(14): 2147-2149
http://www.wjgnet.com/1007-9327/10/2147.asp

INTRODUCTION

Primary hepatocellular carcinoma (HCC) is a common malignant solid tumor, which is rich of blood. It has many characteristics, such as fast infiltrating growth, metastasis in early stage, high grade malignancy, poorly therapeutic efficacy. So it is important to study the angiogenesis of HCC. At present, it has been proved that MVD can serve as a prognostic criterion for relapse, metastasis and survival rate of all kinds of carcinoma[1-6].

Telomerase is a reverse transcriptase. It can make up telomeres that lose 50-200 bp during each DNA replication so as to retain the telomere length and stabilize the cells. The expression of telomerase activity is important to cell proliferation, senescence, immortalization and carcinogenesis[7-9]. It is known that telomerase activity can be detected in many carcinomas, but not in most of normal tissues[10-16].

MVD and telomerase activity can act as specific markers for malignant tumors, and are used to analyze the biologic characteristics, infiltration, metastasis and prognosis of tumors. But the relationship between them has not been reported. In this study, S-P immunohistochemistry method and telomeric repeat amplification protocol (TRAP) were used to respectively detect MVD and telomerase activity, so as to study their relationship and other clinical factors.

MATERIALS AND METHODS

Tissue specimens

Fifty-eight HCC and adjacent normal tissues specimens were obtained from Hepatobiliary Surgery Department of Changchun Infectious Hospital from December 2000 to December 2002. They were all proved as primary HCC. These patients did not receive radiotherapy, chemotherapy, or other therapies. Of them, 35 cases had liver cirrhosis, 52 cases had chronic hepatitis, 6 cases had carcinoma emboli in portal vein, 48 cases had positive marker of HBV, 4 cases had positive anti-HCV antibody, and 4 cases had negative marker of hepatitis virus. Each specimen was divided into two parts. One was stained by immunohistochemical method, and routinely fixed in formalin, embeded in paraffin, and then cut into 4-5 μm thick sections. The other was frozen in liquid nitrogen and used to analyze telomerase activity by TRAP.

S-P Immunohistochemical method

UltraSensitiveTM S-P kit, anti-VIII factor related antigen monoantibody (anti-FVIII RAG), and positive control were purchased from Fuzhou Maixin Biotechnology Development Company. The sections were deparaffinized in xylene and rehydrated in a serial gradient of ethanol solutions. Then S-P immunohistochemical method was used according to its manual. At last, they were restained with hematoxylin and observed. The negative control included empty control with normal rabbit IgG instead of primary antibodies or with the second antibody only. MVD was determined in triplicate in the area of the most intense vascularization (hot spot) of each tumor, and the average count was recorded.

Activity of telomerase assayed by TRAP silver staining

About 50-100 mg tissue was split. Then the supernatant was collected for analysis. The telomerase activity was detected using a TRAP kit following instructions of the manufacturer (Beijing Tiangekangning Biotech Institute). The reaction system containing 25 μL TRAP agent, 0.2 μL *Taq* enzyme and 1 μL cell extract was incubated for 30 min at 25 ℃, then 0.5 μL of primer was added and PCR was conducted for 30 cycles with denaturing at 94 ℃ for 30 s, annealing at 60 ℃ for 30 s, extending at 72 ℃ for 30 s. Fifteen microliter PCR product was loaded onto a 90 g/L non-degenerative SDS gel, resolved through the SDS-PAGE, demonstrated by a reaction in 2 g/L silver nitrate for 15 min, and visualized by incubation in 30 g/L anhydrous sodium carbonate containing formaldehydes (1 mL/L). The activity of telomerase was indicated by the presence of a 6 bp-DNA ladder. The cell extract inactivated by incubation at 75 ℃ for 10 min was used as negative control.

Statistical analysis

Result were expressed as mean±SD. Student's *t* test and χ^2 test were used. $P<0.05$ was considered statistically significant.

RESULTS

Relationship between MVD and some clinical factors

Observed with light microscope, venous endothelium but not lymphatic vessel endothelium was brown (Figure 1).

Table 1 shows that MVD in HCC tissues with metastasis within vein or liver was significantly higher than that in HCC without metastasis ($P<0.05$), MVD in HCC without intact capsule was higher than that in HCC with intact capsule ($P<0.05$). There was no significant difference in MVD between big (>5 cm) and small (≤5 cm) tumors.

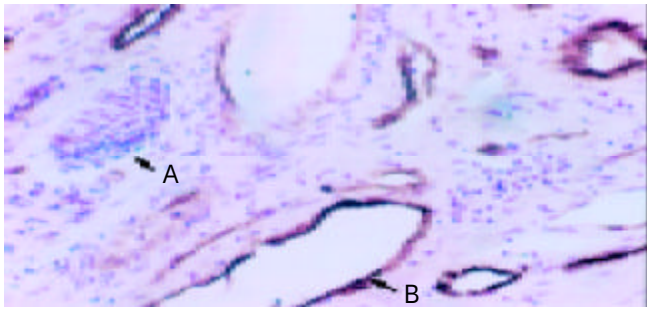

Figure 1 Immunohistochemical staining with anti-FVIII RAG (S-P, original magnification: ×400). A indicates the lymphatic vessel endothelium. B indicates the brown venous endothelium.

Table 1 Relationship between MVD and metastasis, capsular integrity, or size of tumor

Classification		Cases (*n*)	MVD(mean±SD)
Metastasis	+	36	39.3±9.6[a]
	-	22	32.2±5.6
Capsular	-	38	38.8±9.3[a]
	+	20	31.2±5.8
Integrity	>5 cm	42	37.3±8.8
Size	≤5 cm	16	36.9±8.7

[a]$P<0.05$, *vs* corresponding group.

In this study, the distribution of MVD was different in various regions. MVD was higher in HCC with lower differentiation than that in HCC with higher differentiation (Table 2). MVD in adjacent normal tissues (13.2±2.7) was mainly distributed in the area near the carcinoma tissues, especially around the pseudolobules with liver cirrhosis. It was reported that MVD in normal tissues was 11.8±0.2.

Table 2 MVD in HCC and adjacent normal liver tissues

Group	Cases (*n*)	MVD (mean±SD)
Adjacent normal tissue	58	13.2±2.7
HCC grade I	11	19.6±3.7
HCC grade II	22	29.7±6.1[a]
HCC grade III	16	48.4±10.7[a]
HCC grade IV	9	59.3±10.5[a]

[a]$P<0.05$ *vs* adjacent normal tissue.

Relationship between telomerase activity in HCC or adjacent normal tissues and some clinical factors

The results are shown in Figure 2. The positive rate of telomerase activity in HCC tissues (89.6%) was significantly higher than that in adjacent normal liver tissues (20.7%). The telomerase activity in HCC was related to differentiation grade of HCC, but was not related to HCC size, capsule integrity, number of liver nods, metastasis, or hepatitis virus infection. While the telomerase activity in adjacent normal liver tissues was related to capsule integrity, number of liver nods and hepatitis virus infection (Table 3).

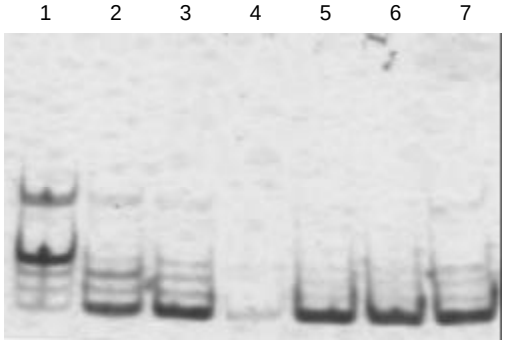

Figure 2 Telomerase activity of HCC tissues. Lane 1: Positive control. Lanes 2, 3: HCC tissue with low differentiation with a 6-bp interval ladder pattern. Lane 4: No ladder in a djacent normal tissues. Lanes 5, 6: HCC tissue with high differentiation with a 6-bp interval ladder pattern. Lane 7: HCC with moderate differentiation with a 6-bp interval ladder pattern.

Table 3 Relationship between telomerase activity in HCC or adjacent normal liver tissues and some clinical factors

Group		HCC				Adjacent normal tissues		
		Cases	Positive number	Positive rate(%)	*P*	Positive number	Positive rate(%)	*P*
Differentiation	High	11	6	54.4		0	0	
	Middle	38	37	97.4		5	13.2	
	Low	9	9	100	<0.05	7	77.8	<0.05
Size	≤5 cm	16	14	87.5		3	18.8	
	>5 cm	42	38	90.9	>0.05	9	21.4	>0.05
Capsule	-	20	16	80.0		1	5.0	
Integrity	+	38	36	94.7	>0.05	11	29.8	<0.05
Hepatitis virus	+	48	44	91.6		1	22.9	
Infection	-	10	8	80.0	>0.05	1	10.0	<0.05
Nod number	Mono-nod	15	12	80.0		1	6.7	
	Multi-nod	43	40	93.0	>0.05			<0.05
Metastasis	+	36	34	94.4		10	27.8	
	-	22	18	81.8	>0.05	2	9.1	<0.05

Relationship between telomerase activity and MVD in HCC or adjacent normal tissue

Among the 58 HCC and adjacent normal liver tissues, MVD in those with positive telomerase activity was significantly higher than that in those with negative activity (Table 4).

Table 4 Relationship between telomerase activity and MVD in HCC or adjacent normal liver tissues

Group	HCC	Adjacent normal tissue
Group with positive telomerase activity	49.3±7.8[a]	16.2±2.7[a]
Group with negative telomerase activity	31.2±5.8	11.9±1.4

[a]$P<0.05$ *vs* group with negative telomerase activity.

DISCUSSION

Carcinogenesis of HCC is a multi-factor, multi-step and complex process. Angiogenesis is necessary for solid tumors larger than 1 mm×1 mm. Or else the tumor would remain at dormancy phase and would not metastasize. As soon as it entered angiogenesis stage, the potency of metastasis exhibited at once[17-20].

MVD is an important marker of angiogenesis in tumor and is valuable in prognosis of various carcinomas. In this study, S-P immunohistochemical staining was used to analyze MVD in 58 HCC and corresponding adjacent normal tissues. FVIII in cytoplasma of various vascular endothelium cells is synthesized in endothelial cells. FVIII- RAG is specific to endothelial cells so that it could be differentiated blood vessel from lymphatic vessel. The role of vascular genesis, development and distribution in occurrence, development, infiltration, metastsis and advancement of tumors has been studied[21]. MVD in poorly differentiated HCC with metastasis in vein or liver, intact capsule was significantly higher than that in corresponding ones. This result was consistent with others, suggesting that HCC with higher MVD may obtain more nutrition from new blood vessels, so that it can grow faster and has the ability to infiltrate and metastasize. MVD might play a key role in development of HCC. There was no close relationship between MVD and tumor size, HBV infection. Maybe HBV infection is merely a carcinogenic factor, and is not related to the growth, infiltration and metastasis of HCC.

We also detected telomerase activity in 58 HCC and adjacent normal tissues by TRAP. Similar to Nouso's research, the expression of telomerase activity in HCC was negatively related to differentiation, but was not related to tumor size or histologic grade. Telomerase activity in adjacent normal tissues with middle or big size, multi-nods, unintegral capsule, positive HBsAg was higher than that in adjacent normal tissues without them, suggesting that there is some relationship between telomerase activity in adjacent normal tissue and prognosis of HCC. Hepatitis viruses, especially HBV, have been found to be an important factor in causing HCC. HBx, encoded by HBV, could block the function of p53, and make genome unstable. With the cell division, telomerase was activated. The cells with positive telomerase activity became immortalized and further developed to carcinoma cells. Histological examination in combination with detection of telomerase activity could increase the accuracy of diagnosis in early stage and improve the judgment on its prognosis.

In addition, there was some relationship between MVD and telomerase activity. Activation of telomerase could make liver cells immortalized, and MVD could offer nutrition for their growth and stimulate metastasis. These two factors would result in carcinogenesis at last.

In a word, MVD and telomerase activity have a key role in occurrence, development, infiltration and metastasis of HCC and have notable clinical values in diagnosing and treating HCC in early stage.

REFERENCES

1 **Du JR**, Jiang Y, Zhang YM, Fu H. Vascular endothelial growth factor and microvascular density in esophageal and gastric carcinomas. *World J Gastroenterol* 2003; **9**: 1604-1606
2 **Ding YB**, Chen GY, Xia JG, Zang XW, Yang HY, Yang L. Association of VCAM-1 overexpression with oncogenesis, tumor angiogenesis and metastasis of gastric carcinoma. *World J Gastroenterol* 2003; **9**: 1409-1414
3 **Moon WS**, Rhyu KH, Kang MJ, Lee DG, Yu HC, Yeum JH, Koh GY, Tarnawski AS. Overexpression of VEGF and angiopoietin 2: a key to vascularity of hepatocellular carcinoma? *Mod Pathol* 2003; **16**: 552-557
4 **Takahashi R**, Tanaka S, Kitadai Y, Sumii M, Yoshihara M, Haruma K, Chayama K. Expression of vascular endothelial growth factor and angiogenesis in gastrointestinal stromal tumor of the stomach. *Oncology* 2003; **64**: 266-274
5 **Poon RT**, Ng IO, Lau C, Yu WC, Yang ZF, Fan ST, Wong J. Tumor microvessel density as a predictor of recurrence after resection of hepatocellular carcinoma: a prospective study. *J Clin Oncol* 2002; **20**: 1775-1785
6 **Ng IO**, Poon RT, Lee JM, Fan ST, Ng M, Tso WK. Microvessel density, vascular endothelial growth factor and its receptors Flt-1 and Flk-1/KDR in hepatocellular carcinoma. *Am J Clin Pathol* 2001; **116**: 838-845
7 **Blackburn EH**. Structure and function of telomeres. *Nature* 1991; **350**: 569-573
8 **Morin GB**. The human telomere terminal transferase enzyme is a ribonucleoprotein that synthesizes TTAGGG repeats. *Cell* 1989; **59**: 521-529
9 **Shay JW**, Wright WE. Ageing and cancer: the telomere and telomerase connection. *Novartis Found Symp* 2001; **235**: 116-125
10 **Kim NW**, Piatyszek MA, Prowse KR, Harley CB, West MD, Ho PL, Coviello GM, Wright WE, Weinrich SL, Shay JW. Specific association of human telomerase activity with immortal cells and cancer. *Science* 1994; **266**: 2011-2015
11 **Mu J**, Wei LX. Telomere and telomerase in oncology. *Cell Res* 2002; **12**: 1-7
12 **Masutomi K**, Yu EY, Khurts S, Ben-Porath I, Currier JL, Metz GB, Brooks MW, Kaneko S, Murakami S, DeCaprio JA, Weinberg RA, Stewart SA, Hahn WC. Telomerase maintains telomere structure in normal human cells. *Cell* 2003; **114**: 241-253
13 **Testorelli C**. Telomerase and cancer. *J Exp Clin Cancer Res* 2003; **22**: 165-169
14 **Yokota T**, Suda T, Igarashi M, Kuroiwa T, Waguri N, Kawai H, Mita Y, Aoyagi Y. Telomere length variation and maintenance in hepatocarcinogenesis. *Cancer* 2003; **98**: 110-118
15 **Mariani E**, Meneghetti A, Formentini I, Neri S, Cattini L, Ravaglia G, Forti P, Facchini A. Telomere length and telomerase activity: effect of ageing on human NK cells. *Mech Ageing Dev* 2003; **124**: 403-408
16 **Tomita M**, Matsuzaki Y, Onitsuka T. Effect of mast cells on tumor angiogenesis in lung cancer. *Ann thorac Surg* 2000; **69**: 1686-1690
17 **Lichtenbeld HH**, van Dam-Mieras MC, Hillen HF. Tumour angiogenesis: pathophysiology and clinical significance. *Neth J Med* 1996; **49**: 42-51
18 **Paweletz N**, Knierim M. Tumor-related angiogenesis. *Crit Rev Oncol Hematol* 1989; **9**: 197-242
19 **Desai SB**, Libutti SK. Tumor angiogenesis and endothelial cell modulatory factors. *J Immunother* 1999; **22**: 186-211
20 **Saaristo A**, Karpanen T, Alitalo K. Mechanisms of angiogenesis and their use in the inhibition of tumor growth and metastasis. *Oncogene* 2000; **19**: 6122-6129
21 **Ruiter DJ**, Schlingemann RO, Rietveld FJ, de Waal RM. Monoclonal antibody-defined human endothelial antigens as vascular markers. *J Invest Dermatol* 1989; **93**(2 Suppl): 25S-32S

Edited by Wang XL and Chen WW **Proofread by** Xu FM

PO Box 2345, Beijing 100023, China
Fax: +86-10-85381893
E-mail: wjg@wjgnet.com www.wjgnet.com

World J Gastroenterol 2004;10(14):2150-2152
World Journal of Gastroenterology
 ISSN 1007-9327

• BRIEF REPORTS •

Treatment of severe *Clonorchiasis sinensis* by endoscopic nasobiliary drainage and oral praziquantel

Fa-Chao Zhi, Xu-Ming Liu, Ze-Quan Liu, Yan Lin, Shu-Jian Chen

Fa-Chao Zhi, PLA Institute for Digestive Medicine, Nanfang Hospital, First Military Medical University, Guangzhou 510515, Guangdong Province, China
Xu-Ming Liu, Ze-Quan Liu, Yan Lin, Shu-Jian Chen, Department of Digestive Diseases, Hexian Hospital, Panyu, Guangzhou 511400, Guangdong Province, China
Correspondence to: Fa-Chao Zhi, PLA Institute for Digestive Medicine, Nanfang Hospital, First Military Medical University, Guangzhou 510515, Guangdong Province, China. zfc@fimmu.com
Telephone: +86-20-61641534 **Fax:** +86-20-87280770
Received: 2003-11-13 **Accepted:** 2004-01-12

Abstract

AIM: To assess the therapeutic value of endoscopic nasobiliary drainage (ENBD) and oral praziquantel for severe *Clonorchiasis sinensis* infection.

METHODS: Of the 84 *Clonorchiasis sinensis*-infected patients enrolled, 58 were treated with ENBD (as observing group, ENBD group), 26 received operations (control group, operation group). Both of the two groups were comparable in terms of patient's age, body mass index. Before and one week after treatment, the average diameters of common bile ducts were measured by ultrasound, and serum bilirubin, ALP, γ-GT and ALT were detected by biochemical methods. After ENBD or operation, the patients took praziquantel for two days.

RESULTS: Compared with the patients in operation group, ENBD patients in ENBD group had higher recovery rates of abdominal pain and fever as well as jaundice, quicker remission, smaller trauma, fewer complications and lower cost.

CONCLUSION: ENBD combined with oral praziquantel is an effective and safe method for the treatment of severe *Clonorchiasis sinensis*.

Zhi FC, Liu XM, Liu ZQ, Lin Y, Chen SJ. Treatment of severe *Clonorchiasis sinensis* by endoscopic nasobiliary drainage and oral praziquantel. *World J Gastroenterol* 2004; 10(14): 2150-2152
http://www.wjgnet.com/1007-9327/10/2150.asp

INTRODUCTION

Oral praziquantel is effective for the treatment of mild *Clonorchiasis sinensis*. As the parasitism of *Clonorchiasis sinensis* metacercaria can take more than 50 years in human body[1], the therapy of *Clonorchiasis sinensis* is very difficult because of repeated infections. We have achieved effective results in treating 58 cases of severe *Clonorchiasis sinensis* infection from July 2000 to April 2003 by endoscopic nasobiliary drainage (ENBD) and oral praziquantel.

MATERIALS AND METHODS

Diagnostic criteria for severe Clonorchiasis sinensis

Criteria for severe *Clonorchiasis sinensis* are as follows: A history of eating raw fish; spawn can be detected in feces or bile; obstructive jaundice or cholecystitis, biliary calculus in common bile duct, and suppurative cholangitis. All the 58 cases were in line with the above diagnostic standards.

Patients and treatments

There were 58 cases in ENBD group including 55 males and 3 females (aged from 29 to 76 with a mean age of 46.5 years). All cases had a history of eating raw fish. Among them, 36 cases had common bile duct dilatation, intrahepatic bile duct and gallbladder distention (6 of the 36 cases also had gallstones in common bile duct); 23 cases had mild dilatation in common bile duct. Nineteen cases were companied with fever and increased leukocyte counts. *Clonorchiasis sinensis* metacercaria were detected in feces of 39 cases. Laboratory examination results were as follows: Total bilirubin 86-280 μmol/L with an average of 103 μmol/L, glutamic-pyruvic transaminase 60-360 U/L with an average of 98 U/L.

The 58 cases in ENBD group were treated according to the routine procedure[2]. The instruments included duodenoscope, ducts, knives, guide wires, meshes, *etc*. The papilla of Vater and bile duct were examined for *Clonorchiasis sinensis* metacercaria. Then, endoscopic retrograde cholangiopancreatography (ERCP) was performed to diagnose the severity of the disease. Patients with mild inflammation without constriction were treated by nasobiliary drainage. Patients with obvious constriction were treated by nasobiliary drainage after sphincterotomy. If the common bile duct was full of *Clonorchiasis sinensis* metacercaria and purulent discharge, the ducts were first washed, and then nasobiliary drainage was performed. For the patients with biliary calculus in common bile ducts, stones were taken out by sphincterotomy followed by nasobiliary drainage. All the 58 patients took praziquantel orally 8-48 h after procedures. The dose was 3.6 g/d three times daily for 2 d.

There were 26 patients with *Clonorchiasis sinensis* infection proved by operations (operation group) including 25 males and 1 female aged 36 to 75 years with a mean age of 48.5 years. Preoperative diagnosis was as follows: Fifteen patients with cholecystitis, 5 with gallstones in common bile duct and 6 with duodenal ampulla carcinoma. Fifteen cases underwent cholecystectomy, 5 cases underwent choledocholithotomy, and 20 cases received operations for common bile duct dilatation. All the 26 cases had T-tube drainage. Laboratory examination results were as follows: Total bilirubin 76-123 μmol/L with a mean of 94 μmol/L, glutamic-pyruvic transaminase 63-286 U/L with an average of 105 U/L.

The 26 cases were treated by exploratory laparotomy. The common bile duct was opened, and *Clonorchiasis sinensis* metacercaria and their purulent discharge were washed away with saline. Then, common bile duct was expanded with bougie. At last, T-tube was placed inside. Cholecystectomy followed by T-tube was performed for patients with cholecystolithiasis or cholecystitis. Choledocholithotomy followed by T-tube was performed for patients with gallstones in common bile ducts. All the 26 patients took praziquantel orally for 3-6 d after operation. The dose was 3.6 g/d three times daily for 2 d.

Table 1 Average diameter of common bile ducts, levels of serum total bilirubin, ALP, γ-GT and ALT one week after operation (mean±SD)

Group	Cases (*n*)	Therapy	Average diameter of common bile duct (mm)	Serum total bilirubin (μmol/L)	ALP (U/L)	γ-GT (U/L)	ALT (U/L)
ENBD	58	Before	16±3	89±11	286±63	166±38	132±32
		After	9.6±2.2[b]	29±9[b]	108±23[b]	86±22[b]	60±12[b]
Operation	26	Before	15.3±3.1	87±10	263±54	156±36	130±30
		After	9.5±2.1[d]	27±8[d]	98±25[d]	87±22[d]	57±11[d]

[b]$P<0.01$ *vs* markers before ENBD, [d]$P<0.01$ *vs* markers before operation.

Table 2 Therapeutic effects of two groups

Group	Cases (*n*)	Remission time of abdominal pain (d)	Complication (cases)	Average length of hospital stay (d)	Average cost (Yuan)
ENBD	58	1	13	9	6 503
Operation	26	6[b]	10	20[b]	16 300[b]

[b]$P<0.01$ *vs* ENBD group.

Observing parameters

The following parameters were measured before and one week after treatment. (1) Changes of the average diameter of common bile ducts, serum total bilirubin, ALP, γ-GT and ALT; (2) Complications, average length of hospital stay and the costs; (3) *Clonorchiasis sinensis* metacercaria in feces in follow-up patients.

Statistical analysis

All data were analysed by *t* test, and the significant level was set at $P<0.05$.

RESULTS

Therapeutic effects are shown in Tables 1 and 2. (1) ENBD group: Jaundice decreased in 72 h and disappeared in 3 wk. The average remission time of abdominal pain was 1 d after ENBD. Nineteen cases with fever returned to normal temperature 48 h after drainage. The dead polyp could be seen discharged from nasobiliary drainage 12 h after oral praziquantel. Peak time of dead polyp discharging was within 24-48 h after oral praziquantel and there was no dead polyp on the fifth day. (2) Operation group: The mean remission time of abdominal pain was 6 d after operation. Jaundice and fever began to decrease 2 d after operation. The dead polyp could be seen discharged from T-tube 12 h after oral praziquantel.

There were 8 cases with transient hyperamylasemia in ENBD group, who were cured in 48 h by fasting, anti-acid and anti-inflammation therapy. Two cases with bile duct retrograde infection after sphincterotomy accompanied with transient fever and chill were cured by anti-inflammation therapy. In all 58 cases, there was no case of bleeding and perforation, but 3 cases developed recurrent disease in 1-2 years and needed therapy again. In operation group, there were 8 cases with gallstone in common bile duct or cholangitis after operation, and 2 cases with intestinal adhesion.

Clonorchiasis sinensis metacercaria was found in feces of all the patients of the two groups 3, 6, 12, 18 and 24 mo after ENBD or operation. After oral praziquantel again, no *Clonorchiasis sinensis* metacercaria was found in feces.

DISCUSSION

Clonorchiasis sinensis is an amphixenosis parasitic disease threatening people's health. The average infectious rate was 21.1% in Pearl River Delta region, and up to 88.6% in certain areas. Oral praziquantel is the first-line therapy drug; its effectiveness can be 98.8%[3-5]. When *Clonorchiasis sinensis* infection is companied with obstructive jaundice[6,7], obstruction remission and bile drainage should be the most important treatment target. The traditional method of obstruction remission is operation, but operation has some shortcomings, such as big trauma, high costs and recurrence. With the development of endoscopic intervention, the therapy of *Clonorchiasis sinensis* with endoscopic bile duct drainage has bright prospect[8].

Our results showed that oral praziquantel after endoscopic nasobiliary drainage was a safe and effective way for the treatment of *Clonorchiasis sinensis* companied with obstructive jaundice. The two methods had equal effects (as shown in Tables 1 and 2), and no significant difference with regard to the remission time of jaundice and average diameter of common bile duct. However, endoscopic nasobiliary drainage did have some advantages, such as rapid remission of fever and abdominal pain, little trauma, rapid recovery, fewer complications, less length of hospital stay and less cost.

Sphincterotomy is required for patients with inflammatory papillary stenosis. Drainage is helpful for decreasing the re-stenosis after operation. Sphincterotomy is indicated in the following situations: Papilla opening is very small, stiff, and has no bile flow; it is difficult to inject contrast; contrast shows that inferior part of common bile duct is obviously narrow.

Generally, nasobiliary drainage should last 4-7 d and the bile duct should be washed by 5 g/L metronidazol 1-2 times daily. Once the drainage tube is out of place, it is not necessary to re-put drainage if there is no symptom of increasing stenosis, jaundice or fever. The causes of drainage dislocation included: Anterior extremity of nasobiliary drainage had no bents; the papilla opening was too big during sphincterotomy; some patients would pull out the nasobiliary drainage because of irritation and nausea; some patients had too much hiccupping and vomiting. Doctors should make more explanations to get patients' cooperation.

The main complication of endoscopic therapy was transient hyperamylasemia, which was associated with repeated pancreatic duct visualization during contrast imaging. This complication could be relieved by fasting, antacid and anti-inflammation therapy for 48 h. Once there was pancreatitis, the therapy was initiated for acute pancreatitis. In patients with moderate jaundice and good general condition, oral praziquantel could be taken 8 h after endoscopic drainage. Patients with

severe jaundice and severe impairment of hepatic function, should receive therapy to improve and protect hepatic function, and take oral praziquantel 2-3 d after drainage to decrease the damage to liver caused by the drugs.

On the whole, both ENBD and traditional operation are effective for the treatment of *Clonorchiasis sinensis* infection complicated with obstructive jaundice. However, ENBD has some advantages, such as rapid remission of fever and abdominal pain, little trauma, rapid recovery, fewer complications, less length of hospital stay and less cost.

REFERENCES

1 **Gao JS,** Liu YH, Wang XG,Yu DG, Shu Q. Experimental Observation of Praziguantel and Frichloro-benzodazole of Dog's Clonorchiosis. *Zhongguo Jishengchongbing Zazhi* 1998; **11**: 357-283

2 **Zhi FC,** Yan ZQ, Li XL, Zhu JX, Chen CL, Zhang XL, Zhou DY. Prospective study of diagnostic value of magnetic resonance cholangiopancreatography versus endoscopic retrograde cholangiopancreatography in cholangiopancreatic diseases. *Chin J Dig Dis* 2002; **3**: 124-126

3 **Huang XL.** 68 cases analysis of clonorchiasis. *Guangzhou Yixue* 2001; **32**: 45-50

4 **Yu SH,** Kawanaka M, Li XM, Xu LQ, Lan CG, Rui L. Epidemiological investigation on Clonorchis sinensis in human population in an area of South China. *Jpn J Infect Dis* 2003; **56**: 168-171

5 **Wang KX,** Zhang RB, Cui YB, Tian Y, Cai R, Li CP. Clinical and epidemiological features of patients with clonorchiasis. *World J Gastroenterol* 2004; **10**: 446-448

6 **Kim KH,** Kim CD, Lee HS, Lee SJ, Jeen YT, Chun HJ, Song CW, Lee SW, Um SH, Choi JH, Ryu HS, Hyun JH. Biliary papillary hyperplasia with clonorchiasis resembling cholangiocarcinoma. *Am J Gastroenterol* 1999; **94**: 514-517

7 **Lee SH,** Lee JI, Huh S, Yu JR, Chung SW, Chai JY, Hong ST. Secretions of the biliary mucosa in experimental clonorchiasis. *Korean J Parasitol* 1993; **31**: 13-20

8 **Zhi FC,** Li XL, Yang LC, He ZB, Cui XY, Qiu XL, lin Y, Liu XM, Liang NL, Zhu JX. Diagnosis and treatment for clonorchiasis sinensis by endoscopic retrograde cholangiopancreatography and sphincterotomy. *Zhonghua Xiaohua Zazhi* 2003; **23**: 279-281

Edited by Chen WW and Zhu LH **Proofread by** Xu FM

PO Box 2345, Beijing 100023, China
Fax: +86-10-85381893
E-mail: wjg@wjgnet.com www.wjgnet.com

World J Gastroenterol 2004;10(14):2153-2155
World Journal of Gastroenterology
 ISSN 1007-9327

• CASE REPORT •

Benign nontraumatic inflammatory stricture of mid portion of common bile duct mimicking malignant tumor: Report of two cases

Chiu-Yung Ho, Tseng-Shing Chen, Full-Young Chang, Shou-Dong Lee

Chiu-Yung Ho, Tseng-Shing Chen, Full-Young Chang, Shou-Dong Lee, Division of Gastroenterology, Department of Medicine, Taipei Veterans General Hospital, National Yang-Ming University School of Medicine, Taipei, Taiwan, China
Chiu-Yung Ho, Tao Yuang Veterans Hospital, Tao-Yuang, Taiwan, China
Correspondence to: Dr. Tseng-Shing Chen, Division of Gastroenterology, Department of Medicine, Taipei Veterans General Hospital, 201, Sec. 2, Shih-Pai Road, Taipei 112, Taiwan, China. tschen@vghtpe.gov.tw
Telephone: +886-2-2871-2121 **Fax:** +886-2-2873-9318
Received: 2004-03-06 **Accepted:** 2004-04-09

Abstract

Benign nontraumatic inflammatory stricture of the common bile duct (CBD) may result in obstructive jaundice, which can be misdiagnosed as a malignant tumor of the CBD preoperatively. Two cases with strictures of the mid portion of the common bile duct presenting with obstructive jaundice are reported herein. Preoperative radiological studies prompted us to confidently make the diagnosis of cholangiocarcinoma. However, the postoperative diagnosis on histological examination of the resected lesions was chronic inflammation and fibrosis. The complications of chronic duodenal ulcer are considered as the etiology of these two disorders.

Ho CY, Chen TS, Chang FY, Lee SD. Benign nontraumatic inflammatory stricture of mid portion of common bile duct mimicking malignant tumor: Report of two cases. *World J Gastroenterol* 2004; 10(14): 2153-2155
http://www.wjgnet.com/1007-9327/10/2153.asp

INTRODUCTION

Malignant bile duct strictures are mainly the result of cancer of the ampulla of Vater, pancreas, or bile duct, and account for most patients presenting with obstructive jaundice secondary to extra-hepatic bile duct stricture. Benign non-traumatic inflammatory strictures of the extra-hepatic bile duct are extremely rare with the exception of primary sclerosing cholangitis[1-3]. Most benign strictures reported in the literature are located in the hepatic hilum[4] or distal common bile duct (CBD). Here we report two cases of benign nontraumatic inflammatory strictures of the mid portion of the CBD with painless obstructive jaundice. They were confidently diagnosed as cholangiocarcinoma by radiological studies preoperatively.

CASE REPORT

Case 1

A 70 year-old male who had a 10-year history of hypertension and type 2 diabetes mellitus was presented to our hospital. He had tea-colored urine and yellowish skin discoloration for about 2 wk. No abdominal pain or body weight loss was reported. The physical examination was unremarkable except icteric sclera. A complete blood count was within normal limits. Serum total bilirubin/direct bilirubin (TB/DB) 5.6/2.9 mg/dL (normal 0.2-1.6/0-0.3 mg/dL), alanine aminotransferase (ALT) 127 U/L (normal 0-40 U/L), asparate aminotransferase (AST) 78 U/L (normal 5-45 U/L), alkaline phosphatase (ALK-P) 380 U/L (normal 10-100 U/L) and gamma-glutamyl transpeptidase (γ-GT) 333 U/L (normal 8-60 U/L) were noted. Abdominal sonography showed dilatation of the intrahepatic ducts and CBD. The contrast-enhanced abdominal CT scan disclosed similar findings. A PTCD tube was inserted and anterograde cholangiograms exhibited a segmental narrowing of the CBD about 2 cm below the insertion site of the cystic duct (Figure 1A). A segmental stricture about 1.5 cm in length over the CBD but below the cystic duct level and dilatation of the intrahepatic ducts were also demonstrated in the endoscopic retrograde cholangiopancreatogram (ERCP) (Figure 1B). The pancreatogram was normal. Three sets of bile fluid cytology were negative. Tumor markers CA19-9 and CEA were not elevated. A diagnosis of cholangiocarcinoma with CBD stricture was made. At surgery, stricture of the mid portion of the CBD was found. Cholecystectomy and choledocholithotomy with T-tube drainage were performed. Histological examination of the resected CBD showed chronic inflammation and fibrosis without malignant cells. No stone was detected in the gallbladder. Unfortunately, tea-colored urine and skin itching developed 3 years later. The laboratory evaluation revealed serum TB/DB 2.9/1.5 mg/dL, AST 111 U/L, ALT 125 U/L, ALK-P 427 U/L and γ-GT 676 U/L. Serum AMA, ASMA, IgG, IgM, IgA and ANA titers were within normal range. ERCP demonstrated segmental stricture of the common hepatic duct about 4 cm in length (Figure 1C) and choledochoduodenal fistula. The pancreatogram was normal. MR cholangiogram disclosed an annular mass lesion with enhancement at the proximal CBD, which caused segmental narrowing of the common hepatic duct and dilatation of the intrahepatic ducts (Figure 1D). Bile duct tumors such as cholangiocarcinoma were considered. At surgery, a firm and fixed tumor 4 cm ×3 cm in size at the CBD was palpated. The duodenal bulb was adhered to the tumor and a choledochoduodenal fistula was found. Segmental resection of the CBD, hepaticojejunostomy and enteroenterostomy, end-to-side, were performed. Histological examination of the resected CBD showed chronic cholangitis with focal atypical epithelium.

Case 2

A 55 year-old male without significant past medical history was admitted because of painless jaundice for 1 mo. A double-contrast barium study of the upper gastrointestinal tract 2 years earlier demonstrated chronic duodenal ulcer with bulb deformity and prepyloric constriction (Figure 2). On examination, there was only icteric sclera. A complete blood count was within normal limits. Serum TB/DB 4.2/2.5 mg/dL, ALT 404 U/L, AST 293 U/L, ALK-P 357 and γ-GT 333 U/L were noted. Abdominal sonography showed dilatation of the intrahepatic ducts and CBD. A contrast-enhanced abdominal CT scan disclosed dilatation of the intrahepatic ducts and proximal CBD associated with distention of the gallbladder. ERCP failed. The MRI revealed an annular lesion about 3.5 cm

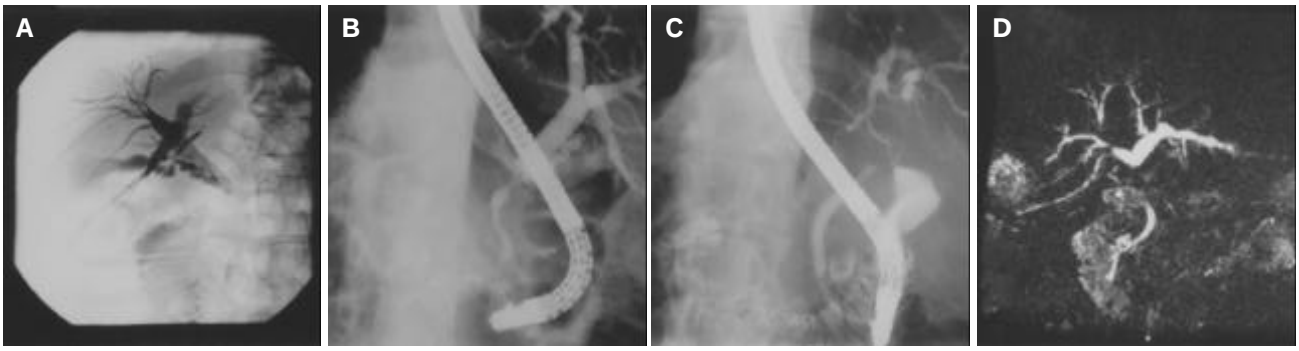

Figure 1 Segmental strictures of CBD demonstrated in percutaneous cholangiogram, ERCP and MR cholangiogram. A: Segmental narrowing of CBD below the insertion site of cystic duct in percutaneous cholangiogram; B: Segmental stricture of CBD with dilatation of intrahepatic bile ducts demonstrated in ERCP; C: Segmental stricture of CHD demonstrated in ERCP; D: Segmental narrowing of CHD and dilatation of the intrahepatic bile ducts demonstrated in MR cholangiogram.

in length in the mid portion of the CBD (Figure 3). Three sets of bile fluid cytology were negative. Tumor markers CA19-9 and CEA were not elevated. A diagnosis of cholangiocarcinoma was made. The patient had a laparotomy for resection of the tumor. A tumor over the middle third portion of the CBD with thickened wall was found. No stone was detected in the gallbladder or CBD. Resection of the tumor and Roux-en-Y choledochojejunostomy, end-to-side, was then performed. However, the postoperative histological examination of the lesion showed only chronic inflammation with marked fibrosis.

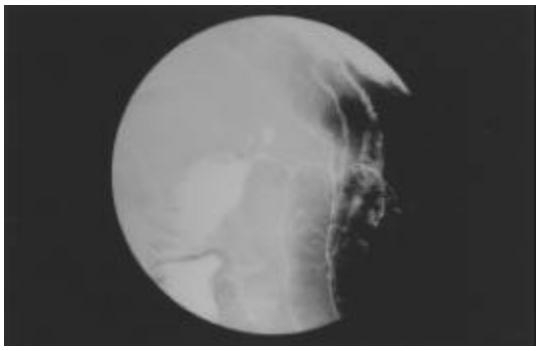

Figure 2 Chronic duodenal disease with bulb deformity and prepyloric constriction revealed in a double-contrast barium study.

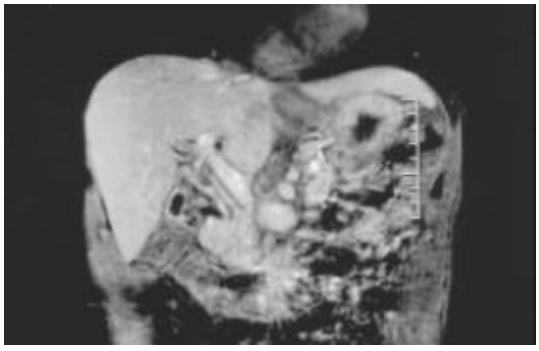

Figure 3 Annular lesion in the mid portion of CBD disclosed in MRI (coronal view).

DISCUSSION

The clinical presentation and preoperative radiological studies without tissue or cytological proof led us to the diagnosis of malignant bile duct strictures in these 2 cases. It has been agreed that any localized extra-hepatic bile duct obstruction coexisting with intra-hepatic bile duct dilatation should be considered as malignancies such as cancer of the ampulla of Vater, pancreas, or bile duct (cholangiocarcinoma) until proven otherwise[5]. This agreement arose because of the difficulty in obtaining a tissue diagnosis in patients with obstructive jaundice caused by a bile duct stricture. Application of improved diagnostic methods, such as thin-section spiral CT and magnetic resonance cholangiopancreatography, can potentially increase the diagnostic accuracy, but neither could reliably differentiate malignant from benign lesions[6,7]. Preoperative histological or cytological examination by means of biopsy or brush cytology was often difficult and liable to false-negative results with low sensitivity and could carry a potential risk of needle tract metastases[8-12]. The lack of a tissue or cytological evidence might result in some patients being inappropriately treated as malignant disease when a benign stricture was present and vice versa. In the study of Gerhards *et al*.[4] a false-positive preoperative diagnosis of malignancy resulted in a 15% resection rate of benign lesions in patients with suspicious hilar strictures. Careful review of all preoperative information and radiological images of our 2 cases yielded the initial diagnosis of a CBD tumor, although post-operative pathological examination revealed only inflammation and fibrosis. The decision to undertake resection of the strictures in these 2 cases was therefore not an error of judgment. Obviously, resection of the lesion and obtaining a tissue diagnosis are still the most reliable way to rule out malignancy. Therefore, resection of a benign stricture mimicking a malignant stricture in the extra-hepatic bile duct cannot be avoided completely. However, the lack of clinical constitutional symptoms such as body weight loss or abdominal pain and elevated tumor markers may implicate the possible benign entity of the disorder.

Benign, single, non-traumatic inflammatory strictures of the biliary tracts were infrequently reported with the exception of primary sclerosing cholangitis[1-3]. Indeed, many benign nontraumatic inflammatory strictures of the common bile duct have been generally considered to be a variant of primary sclerosing cholangitis although Standfield *et al*.[13] described 12 cases of benign strictures of unknown etiology, and differentiated them from the localized form of sclerosing cholangitis. Other inflammatory conditions of the CBD which are potential etiological factors included bacteria or virus infection, parasite infestation, abdominal trauma, congenital abnormality[14], chronic pancreatitis[15], inflammatory pseudotumors[16], complication of chemotherapy[17], complication of duodenal ulcer disease[18-20], and sclerosing therapy of bleeding duodenal ulcer[21]. Most benign segmental strictures of the extra-hepatic bile duct reported in the literature were located at the hilum or distal CBD. Few cases in the mid CBD have been reported.

The CBD strictures of these 2 patients were less likely due to biliary duct stones because the radiological studies and operative findings did not show the existence of stones. The normal pancreatogram excluded the possibility of chronic pancreatitis as the cause of mid CBD strictures. The radiological appearance, histological examination and the extremely rare incidence in this area made the diagnosis of primary sclerosing cholangitis less likely.

According to the clinical history and surgical findings, stricture of the CBD owing to fibrous encasement by chronic inflammatory changes due to an adjacent duodenal ulcer in these 2 cases was considered. Duodenal ulcer disease is a common disorder, and its associated complications such as hemorrhage, gastric outlet obstruction and perforation, are well known. However, the biliary complications of duodenal ulcer disease, such as biliary-enteric fistula or partial obstruction of the CBD were rare and less well-known[18-20], especially after the worldwide use of effective antisecretory agents, H_2-receptor antagonists and proton pump inhibitors.

In conclusion, benign non-traumatic inflammatory strictures affecting the common bile duct can be mistaken for malignant tumors. Their existence should be considered in the differential diagnosis of any biliary strictures. The radiological documentation of these 2 cases is of interest to draw attention to the rare complication of obstructive jaundice secondary to duodenal ulcer disease. A tissue diagnosis should be obtained whenever possible as radiology alone is often insufficient to make a firm diagnosis of malignancy in biliary strictures.

REFERENCES

1 **Golematis B**, Giannopoulos A, Papachristou DN, Dreiling DA. Sclerosing cholangitis of the bifurcation of the common hepatic duct. *Am J Gastroenterol* 1981; **75**: 370-732

2 **Smadja C**, Bowley NB, Benjamin IS, Blumgart LH. Idiopathic localized bile duct strictures: relationship to primary sclerosing cholangitis. *Am J Surg* 1983; **146**: 404-408

3 **Panes J**, Bordas JM, Buguera M, Cortes M, Rhodes J. Localized sclerosing cholangitis? *Endoscopy* 1985; **17**: 121-122

4 **Gerhards MF**, Vos P, van Gulik TM, Rauws EAJ, Bosma A, Gauma DJ. Incidence of benign lesions in patients resected for suspicious hilar obstruction. *Br J Surg* 2001; **88**: 48-51

5 **Longmire WP Jr**, McArthur MS, Bastounis EA, Hiatt J. Carcinoma of the extrahepatic biliary tract. *Ann Surg* 1973; **178**: 333-345

6 **Feydy A**, Vilgrain V, Denys A, Sibert A, Belghiti J, Vullierme MP. Helical CT assessment in hilar cholangiocarcinoma: correlation with surgical and pathologic findings. *Am J Roentgenol* 1999; **172**: 73-77

7 **Choi BI**, Han JK, Shin YM, Baek SY, Han MC. Peripheral cholangiocarcinoma: comparison of MRI with CT. *Abdom Imaging* 1995; **20**: 357-360

8 **Rabinovitz M**, Zajko AB, Hassanein T, Shetty B, Bron KM, Schade RR, Gavaler JS, Block G, Van Thiel DH, Dekker A. Diagnostic value of brush cytology in the diagnosis of bile duct carcinoma: a study of 65 patients with bile duct strictures. *Hepatology* 1990; **12**: 747-752

9 **Rustgi AK**, Kelsey PB, Guelrud M, Saini S, Schapiro RH. Malignant tumors of the bile ducts: diagnosis by biopsy during endoscopic cannulation. *Gastroint Endosc* 1989; **35**: 248-251

10 **Terasaki K**, Wittich GR, Lycke G, Walter R, Nowels K, Swanson D, Lucas D. Percutaneous transluminal biopsy of biliary strictures with a bioptome. *Am J Roentgenol* 1991; **156**: 77-78

11 **Cope C**, Marinelli DL, Weinstein JK. Transcatheter biopsy of lesions obstructing the bile ducts. *Radiology* 1988; **169**: 555-556

12 **Andersson R**, Andren-Sandberg A, Lundstedt C, Tranberg KG. Implantation metastases from gastrointestinal cancer after percutaneous puncture or biliary drainage. *Eur J Surg* 1996; **162**: 551-554

13 **Standfield NJ**, Salisbury JR, Howard ER. Benign non-traumatic inflammatory strictures of the extrahepatic biliary system. *Br J Surg* 1998; **76**: 849-852

14 **Baggott BB**, Long WB. Annular pancreas as a cause of extrahepatic biliary obstruction. *Am J Gastroenterol* 1991; **86**: 224-226

15 **Littenberg G**, Afroudakis A, Kaplowitz N. Common bile duct stenosis from chronic pancreatitis: a clinical and pathologic spectrum. *Medicine* 1979; **58**: 385-412

16 **Hadjis NS**, Collier NA, Blumgart LH. Malignant masquerade at the hilum of the liver. *Br J Surg* 1985; **72**: 659-661

17 **Herrmann G**, Lorenz M, Kirkowa-Reiman M, Hottenrott C, Hubner K. Morphological changes after intra-arterial chemotherapy of the liver. *Hepatogastroenterology* 1987; **34**: 5-9

18 **Neiman JH**. Obstructive jaundice caused by duodenal ulcer. *J Am Med Assoc* 1953; **152**: 141

19 **Glick S**. Benign non-traumatic stricture of the common bile duct owing to penetrating duodenal ulcer. *Br J Surg* 1971; **58**: 918-920

20 **Fuller JW**, Christensen JA, Sherman RT. Common bile duct obstruction secondary to peptic ulcer. *Ann Surg* 1975; **41**: 640-642

21 **Luman W**, Hudson N, Choudari CP, Eastwood MA, Palmer KR. Distal biliary stricture as a complication of scerlosant injection for bleeding duodenal ulcer. *Gut* 1994; **35**: 1665-1667

Edited by Wang XL **Proofread by** Chen WW and Xu FM